Research Article

Taxonomic notes on the genus *Chlorophorus* Chevrolat, 1863 (Coleoptera, Cerambycidae), with one new synonym and four newly recorded species from China

Zheng-Ju Fu[1], Lu Chen[1], Zhu Li[1]

1 *College of Plant Protection, Southwest University, Chongqing, China*
Corresponding author: Zhu Li (lizhu0526@swu.edu.cn)

Abstract

Chlorophorus fainanensis Pic, 1918 is redescribed. Four species, *C. coniperda* Holzschuh, 1992, *C. diversicolor* Holzschuh, 2016, *C. orbatus* Holzschuh, 1991 and *C. pinguis* Holzschuh, 1992 are newly reported from China. A new synonymy, *Chlorophorus arciferus* (Chevrolat, 1863) = *Chlorophorus semisinuatus* Pic, 1949, **syn. nov.** is proposed.

Key words: Cerambycinae, Clytini, longhorn beetle, new records, new synonym, taxonomy

Introduction

The genus *Chlorophorus* was established by Chevrolat in 1863 with the type species *Callidium annulare* Fabricius, 1787. It is distributed in the Old World, mainly in the Oriental and Palearctic regions. It is the largest genus in the tribe Clytini, consisting of 299 species/subspecies worldwide (Tavakilian and Chevillotte 2024). Numerous taxonomists have significantly contributed to the diversity of the genus. Pic (1908, 1916, 1920, 1924, 1931, 1943, 1949, 1950) described 34 species and Gressitt and Rondon (1970) described 11 species/subspecies from Laos. Holzschuh (1984, 1989, 1991a, 1991b, 1992, 1993, 1998, 2003, 2006, 2009, 2010, 2016, 2019) described 47 taxa and Viktora (2019, 2020, 2021, 2022, 2023) described 29 taxa since the 1980s, primarily originating from Laos, Thailand, Vietnam, Nepal, India and China.

Özdikmen (2011) conducted a study using especially Turkish species to propose a subgeneric arrangement with five subgenera. Current research indicates that the genus is polyphyletic (Lee and Lee 2020; Zamoroka 2021). Zamoroka (2021) proposed five new genera based on the three mitochondrial genes *12S rRNA*, *16S rRNA* and *COI* and two nuclear genes *18S rRNA* and *28S rRNA* of 15 species, leading to the genus *Sparganophorus* Zamoroka, 2021, to the subgenus *Viridiphorus* Zamoroka, 2021 and to the subgeneric status of *Humeromaculatus* Özdikmen, 2011 and *Perderomaculatus* Özdikmen, 2011. Based on the elytral pattern of all the taxa worldwide, Özdikmen (2022) proposed 36 subgenera for the world fauna. However, Lazarev (2024) synonymized *Sparganophorus* with *Humeromaculatus* and *Viridiphorus* with *Brevenotatus*, and he treated *Perderomaculatus* as

a subgenus. As Özdikmen (2022) indicated, it should be noted that the subgeneric arrangement of *Chlorophorus* remains far from its final solution. Waiting for a general agreement, the subgenera are not considered in this article.

Prior to our study, 83 species/subspecies had been recorded in China (Chen et al. 2019; Danilevsky, 2020; Tavakilian and Chevillotte 2024). In the present study, four newly recorded species are included, making a total of 87 species/subspecies recorded in China.

Material and methods

Pictures of adult morphology are composites taken using a digital camera Canon 7D with HELICON REMOTE (HeliconSoft, Ukraine). For detailed examination, male genitalia were extracted from specimens, cleared in 10% NaOH, and stored in ethanol 75%. The male genitalia were imaged using a Leica M205A stereomicroscope.

The following collection abbreviations are used in the text.

BMNH   The Natural History Museum, London, UK
BPBM   Bernice Pauahi Bishop Museum, Honolulu, USA
CCH   Collection Carolus Holzschuh, Vienna, Austria
MNHN   Muséum National d'Histoire Naturelle, Paris, France
OUMNH   Oxford University Museum of Natural History, Oxford, UK
SWU   Insect Collection of Southwest University, Chongqing, China
SYSU   Sun Yat-sen University, Guangzhou, China

Taxonomy

Chlorophorus fainanensis Pic, 1918
Figs 1–7

Chlorophorus fainanensis Pic, 1918: 4. TL: China, Taiwan. TD: MNHN.
Chlorophorus (*Humeromaculatus*) ? *fainanensis* Özdikmen 2022: 654, 690.

Specimens examined. Chⁱɴᴀ • 12♂♂ 5♀♀; Anhui Province, Huangshan City, Tangkou Town, Zhaixi Village, Huangshan Wild Monkey Valley; 10–14 VII. 2014; Qiu Jianyue and Xu Hao leg. (SWU).
**Distribution.** China (Anhui, Zhejiang, Taiwan); Japan.
Redescription. Male, body length: 11.6–15.4 mm; humeral width: 2.6–3.3 mm.
Female, body length: 11.1–14.0 mm; humeral width: 2.0–3.0 mm.

Body moderately slender, female slightly stouter than male. Body black, covered with sulphur-yellowish or olive-green pubescence; antennae black with pale grayish pubescence. Pronotum with three or four markings, vague and small markings or a pair of dots on the center of disc, and a spot before middle of each side. Scutellum covered by yellowish pubescence; each elytron marked with three black markings: 1) an externally open arc commencing on humerus and extending around to outer portion of disc just before end of basal fourth; 2) a wide transverse band in the middle; and 3) a narrower band at apical fourth. Legs dark reddish-brown covered with grayish pubescence.

Head narrow, irregularly punctured; frons wider; antennae filiform and slender, reaching the basal fourth of elytra. Third antennomere slightly longer than
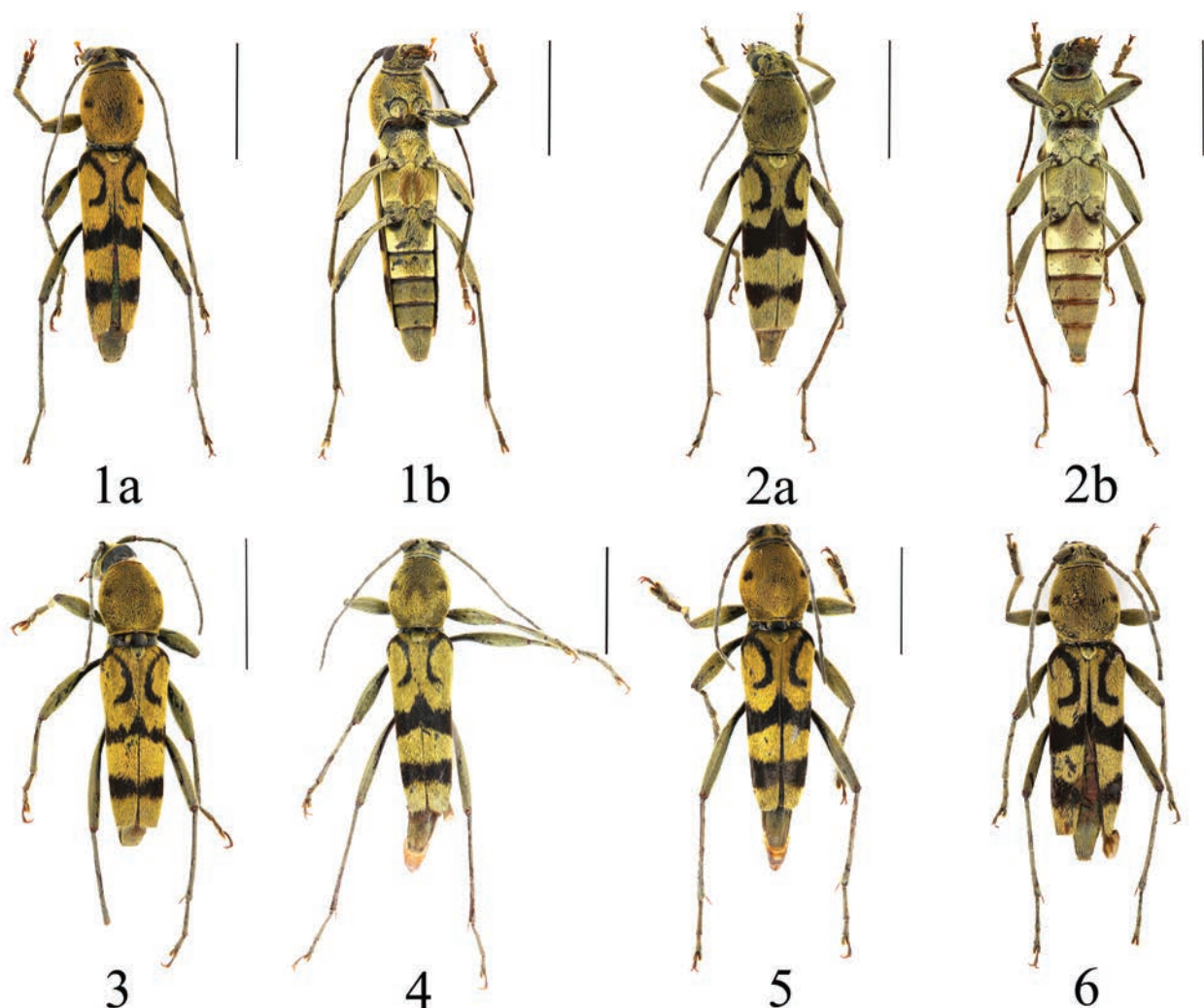
Figures 1−6. *Chlorophorus fainanensis* Pic, 1918 **1** male **a** dorsal habitus **b** ventral habitus **2** female **a** dorsal habitus **b** ventral habitus **3−5** males and **6** female from Anhui, adults, dorsal habitus. Scale bars for adult habitus: 5 mm.

scape and the fourth. Pronotum rounded at sides, widest before middle, l.2 times as long as wide at widest; apical margin distinctly narrower than base; disk slightly convex, coarsely punctate. Scutellum rounded apically, slightly longer than wide. Elytra 2.8 times as long as humeral width, parallel at side and narrowed towards apex; elytral apex truncate. Legs long and narrow; femora slightly club-shaped; mesofemora carinate internally; tibiae narrow and almost straight; metatarsomere 1 as long as remainder combined.

Male genitalia. Tergite VIII as long as broad, apex truncate and moderately emarginate, and with long setae (Fig. 7a, b); parameres elongate, base of each paramere transversely ridged ventrally, the ridge covered with setae (Fig. 7c−e); median lobe long and slender, curved in lateral view, median struts 2/5 times as long as entire median lobe, ventral plate longer than dorsal plate, the apex of ventral plate pointed; median foramen rounded (Fig. 7f, g).

Remarks. Gressitt (1951) synonymized *C. fainanensis* with *C. signaticollis* Laporte de Castelnau & Gory, 1841 (= *C. annulatus* (Hope, 1831)) and then Holz-schuh (2020) resurrected it. There is a lot of variation in the pronotal and elytral markings. The species is often confused with *C. annulatus*, *C. hainanicus* Gressitt, 1940 and *C. arciferus* (Chevrolat, 1863). It can be distinguished by the

Figure 7. *Chlorophorus fainanensis* Pic, 1918, male genitalia **a, b** tergite VIII with sternites VIII and IX **a** dorsal view **b** ventral view **c–e** tegmen **c** dorsal view **d** ventral view **e** lateral view **f, g** median lobe **f** ventral view **g** lateral view. Scale bars for genitalia: 1 mm.

preapical band on the elytra and different male genitalia: parameres 2/5 as long as the entire tegmen, neither 3/5 (*C. hainanicus* and *C. arciferus*), nor 1/4 (*C. annulatus*). It is native to Taiwan and distributed in the east of mainland China Zhejiang (Lin et al. 2023) and Anhui.

Chlorophorus arciferus (Chevrolat, 1863)
Figs 8–15

Amauraesthes arciferus Chevrolat, 1863: 330. TL: India. TD: BMNH.
Caloclytus arciferus Gahan 1906: 263.
Chlorophorus arciferus Aurivillius 1912: 403.
Clytanthus varius v. *pieli* Pic, 1924:15. TL: China, Jiangsu. TD: MNHN.
*Clytanthus verbasci* v. *rectefasciatus* Pic, 1937: 14. TL: Vietnam. TD: MNHN.
Chlorophorus semisinuatus Pic, 1949: 54. TL: India. TD: MNHN. syn. nov.
Chlorophorus (*Immaculatus*) *arciferus* Lazarev 2019: 147.
Chlorophorus (*Humeromagnomaculatus*) *arciferus* Özdikmen 2022: 655, 687, 691.

Specimens examined. CHINA • 13♂♂ 12♀♀; Xizang, Lingzhi City, Chayu County, Shangchayu Town, Shizhong Village; 1700 m; 26 VIII. 2017; Qiu Jianyue, Peng Chenli and Xu Hao leg. (SWU) • 4♂♂ 5♀♀; Xizang, Lingzhi City, Motuo County, Beibeng Township, Yarang Village; 800 m; 21 VIII. 2017; Qiu Jianyue, Peng Chenli and Xu Hao leg. (SWU).
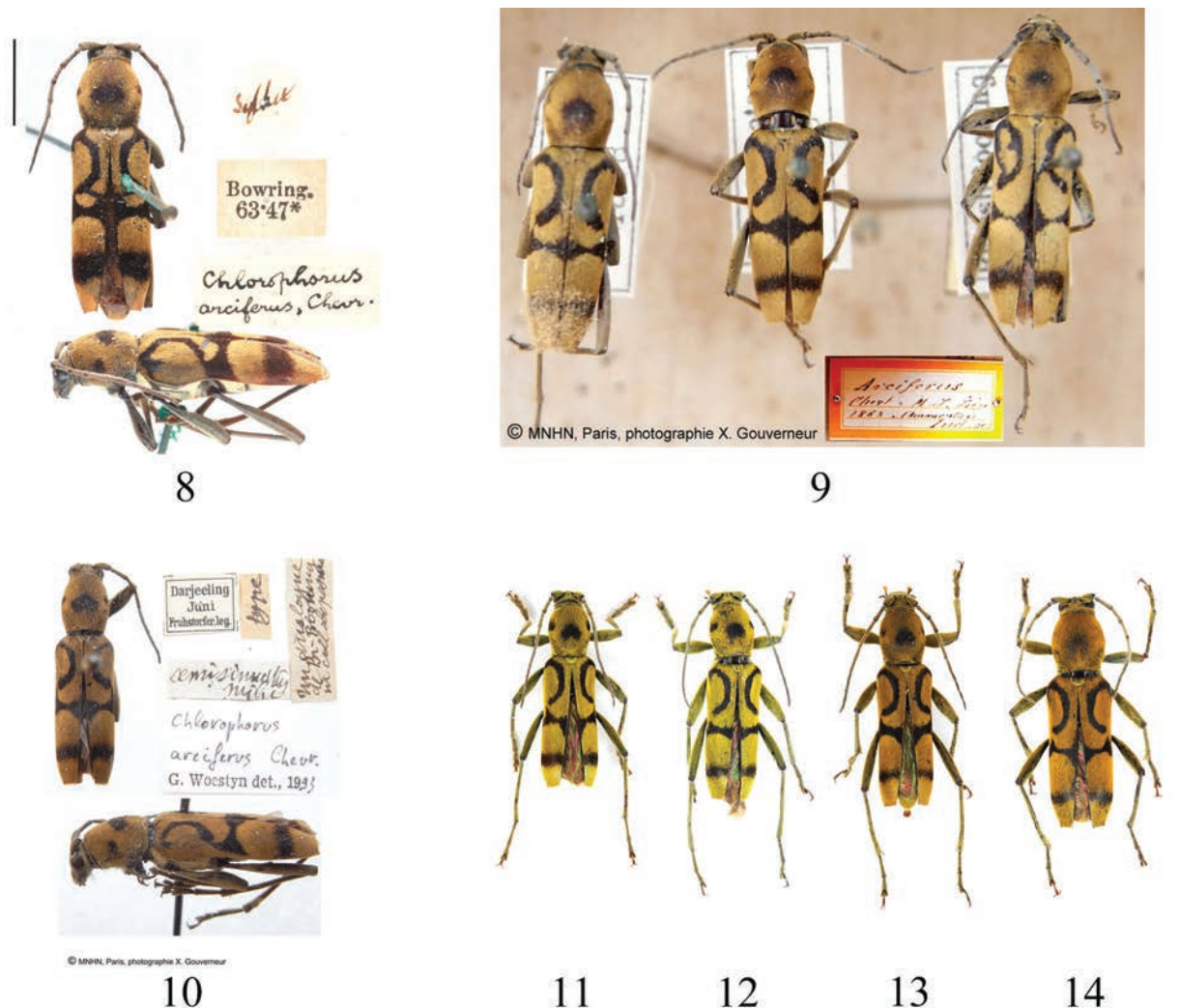
Figures 8−14. *Chlorophorus arciferus* (Chevrolat, 1863) **8** adult habitus (from BMNH photo J.-Y. Qiu and H. Xu) **9** adult habitus (from MNHN, photo X. Gouverneur) **10** holotype of *Chlorophorus semisinuatus* Pic, 1949 (from MNHN, photo X. Gouverneur) **11−13** males and **14** female from Xizang, adults, dorsal habitus. Scale bars for adult habitus: 5 mm.

Male genitalia. Tergite VIII rounded at apical margin. Sternite VIII truncate at apical margin and with long setae (Fig. 15a, b); Tegmen weakly arcuate in lateral view, paramere 3/5 the length of tegmen, dehiscent in apical 1/4, provided with short setae near apex (Fig. 15c−e); median lobe long and slender, curved in lateral view, median struts 2/5 times as long as entire median lobe, ventral plate longer than dorsal plate, the apex of ventral plate pointed; median foramen convex (Fig. 15f, g).

Remarks. Gressitt (1951) reported *C. varius pieli* from China (Shanghai, Zhejiang, Anhui, Sichuan) and treated *Clytanthus verbasci* v. *rectefasciatus* as a synonym of this taxon. Gressitt and Rondon (1970) synonymized *C. varius* v. *pieli* and *C. socius* with *C. arciferus*. However, according to Holzschuh (1991b), the figures provided in both Gressitt (1951, plate XI, fig. 5 with legend "*C. varius* v. *pieli* ?: Anhwei") and Gressitt and Rondon (1970, fig. 36h−i; 36h marked as *C. arciferus* and 36i as "ditto subsp ?") do not show *C. arciferus*; fig. 36h might represent *C. ictericus* Holzschuh, 1991 and fig. 36i *C. copiosus* Holzschuh, 1991. Hua (2002) reported *C. arciferus* from China (Anhui, Jiangxi, Zhejiang, Hainan, Sichuan), Laos, Bhutan, India and Nepal. But fig. 145 in Hua et al. (1993, pl. X) and fig. 334 in Hua et al. (2009, pl. XXIX) do not show *C. arciferus* either.

Figure 15. *Chlorophorus arciferus* (Chevrolat, 1863), male genitalia **a, b** tergite VIII with sternites VIII and IX **a** dorsal view **b** ventral view **c–e** tegmen **c** dorsal view **d** ventral view **e** lateral view **f, g** median lobe **f** ventral view **g** lateral view. Scale bars for genitalia: 1 mm.

So far, we have examined specimens only from Xizang, China (Figs 11–14). Therefore, the distribution of this species is not wide: it might be distributed in India, Nepal, China (Xizang) and adjacent areas.

Although based on the figures of *Clytanthus varius* v. *pieli*, Gressitt's (1951) specimen is not *C. arciferus*. However, we did not examine the type specimen. Therefore, both are still treated as synonyms of *C. arciferus*. Furthermore, we examined the pictures of the type of *Chlorophorus semisinuatus* Pic, 1949 (Fig. 10), and found that the external morphological characteristics of this species are the same as *C. arciferus* (Figs 8–9, 11–14), so *Chlorophorus arciferus* (Chevrolat, 1863) = *Chlorophorus semisinuatus* Pic, 1949, syn. nov.

Chlorophorus socius (Gahan, 1906)
Fig. 16

Caloclytus socius Gahan, 1906: 264. TL: India. TD: BMNH.
Chlorophorus socius Aurivillius 1912: 404.
Chlorophorus (*Brevenotatus*) *socius* Özdikmen 2022: 636, 689.

Specimen examined. *Holotype:* INDIA • 1♀; Darjeeling (BMNH).
Remarks. Gressitt and Rondon (1970) synonymized *Chlorophorus socius* with *C. arciferus* and then Holzschuh (1991b) resurrected it. According to Holzschuh (1991b), *C. socius* can be separated from *C. arciferus* by having a carinate femora.
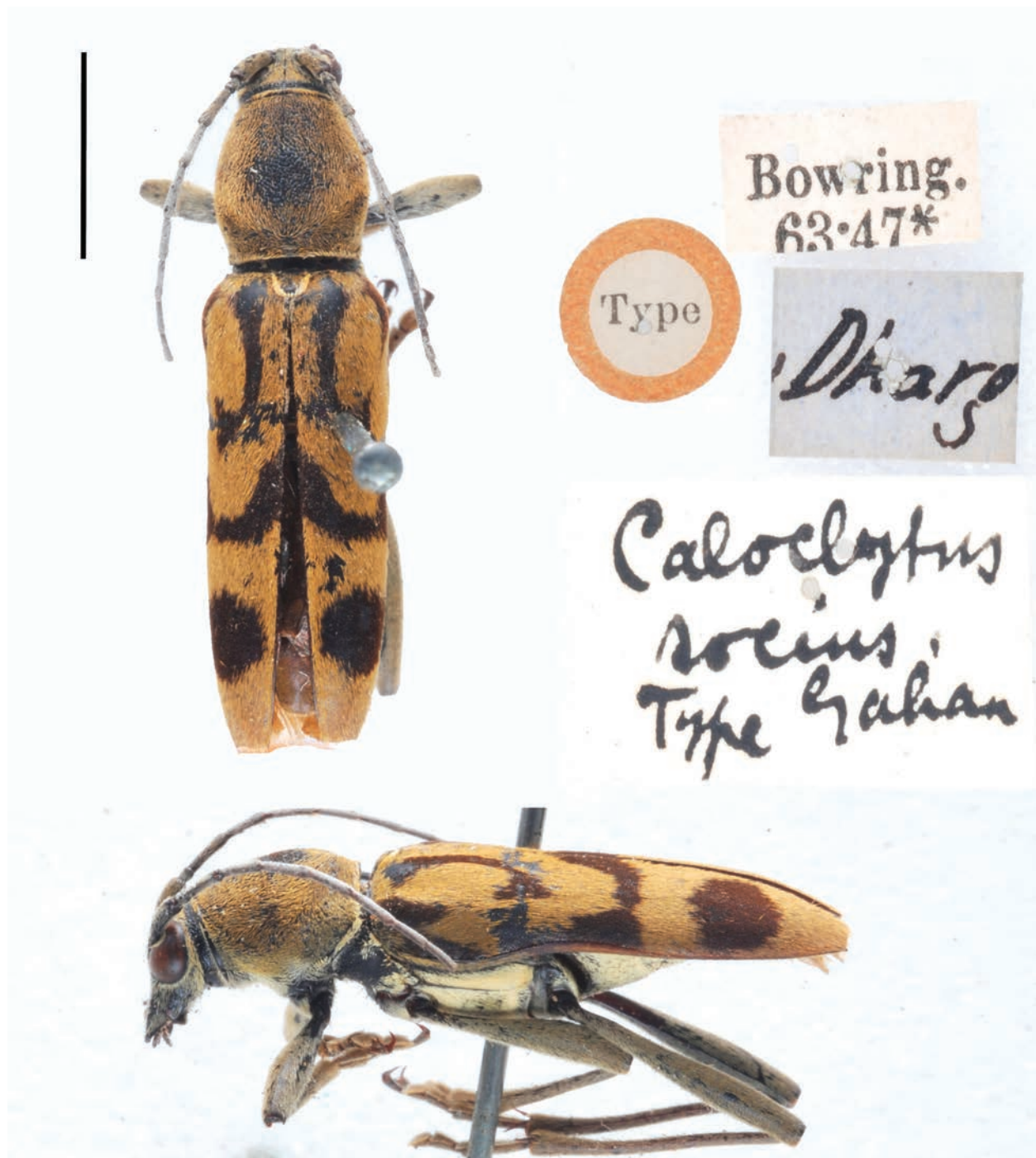
Figure 16. *Chlorophorus socius* (Gahan, 1906), holotype (photo J.-Y. Qiu and H. Xu). Scale bar: 5 mm.

Chlorophorus annulatus (Hope, 1831)
Figs 17, 18

Clytus annulatus Hope, 1831: 28. TL: Nepal. TD: OUMNH.
Clytus signaticollis Laporte de Castelnau & Gory, 1841: 103. TL: India. TD: OUMNH. Syn. by Holzschuh 2020: 49.
Anthoboscus signaticollis Chevrolat 1863: 303.
Clytanthus signaticollis Waterhouse 1874: xxviii.
Chlorophorus signaticollis Schwarzer 1925: 27.

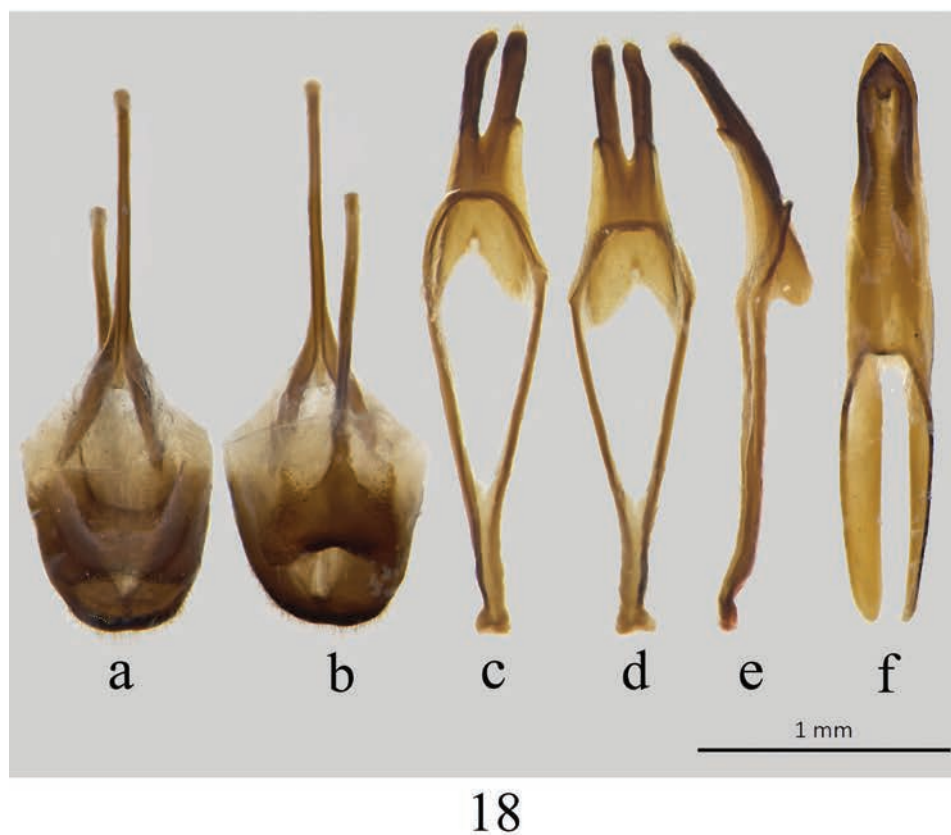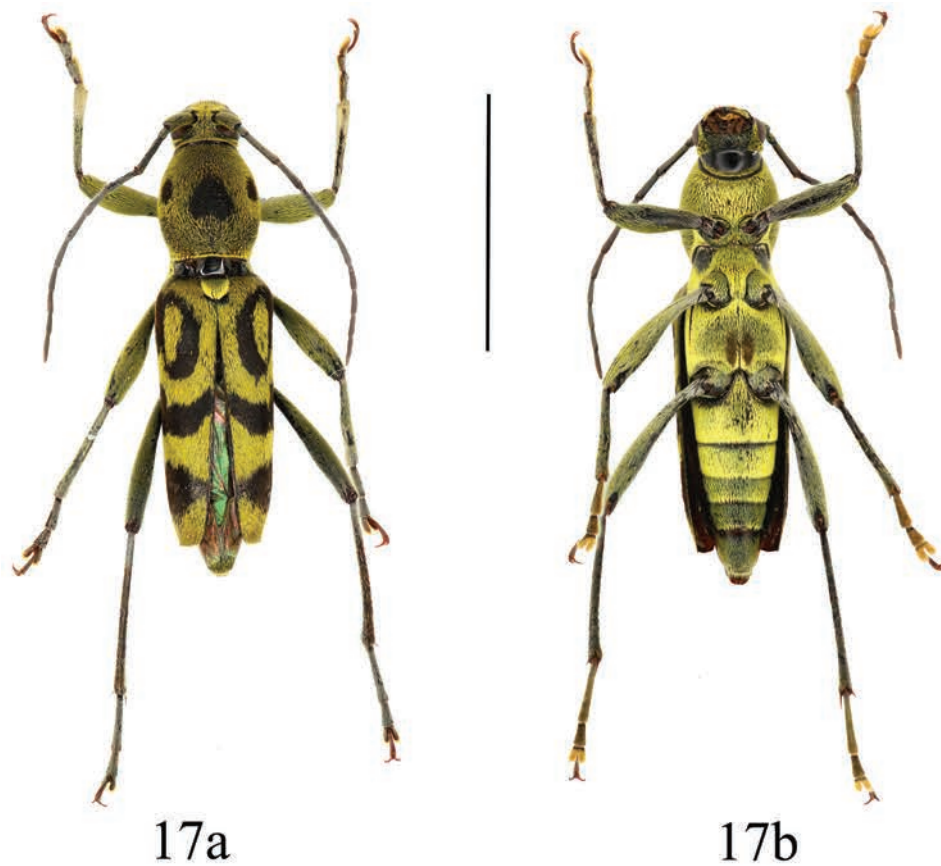**Figures 17, 18.** *Chlorophorus annulatus* (Hope, 1831) **17** adult habitus **a** dorsal habitus **b** ventral habitus **18** male genitalia **a, b** tergite VIII with sternites VIII and IX **a** dorsal view **b** ventral view **c–e** tegmen **c** dorsal view **d** ventral view **e** lateral view **f** median lobe, ventral view. Scale bars: 5 mm (for adult habitus); 1 mm (for genitalia).

Chlorophorus separatus Gressitt, 1940: 78. TL: China. TD: SYSU. Syn. by Holzschuh 2020: 49.

Chlorophorus nigroannulatus Pic, 1943: 1. TL: Vietnam. TD: MNHN. Syn. by Holzschuh 2020: 49.

Chlorophorus nigroannulatus v. *rufonotatus* Pic, 1943: 1. Syn. by Holzschuh, 2020: 49.

Rhaphuma signaticollis Ohbayashi 1963: 11.

Chlorophorus nigroannulatus Villiers and Chûjô 1966: 552[HN].

Chlorophorus viticis Gressitt & Rondon, 1970: 220, 225. TL: Laos. TD: BPBM. Syn. by Holzschuh 2020: 49.

Chlorophorus annulatus Holzschuh 1984: 358.

Chlorophorus (*Chlorophorus*) *signaticollis* Mitra et al. 2017: 81.

Chlorophorus (*Humeromaculatus*) *annulatus* Lazarev and Murzin 2019: 765.

Chlorophorus (*Immaculatus*) *signaticollis* Niisato in Danilevsky 2020: 231.

Chlorophorus (*Chlorophorus*) *annulatus* Özdikmen 2022: 641, 686, 690.

Specimens examined. CHINA • 16♂♂ 8♀♀; Yunnan Province, Pu'er City, Simao, Laiyang River; 11–13 V. 2018; Qiu Jianyue, Peng Chenli and Xu Hao leg. (SWU) • 25♂♂ 19♀♀; Yunnan Province, Pingbian County, Dawei Mountain; 25–27 V. 2018; Qiu Jianyue, Peng Chenli and Xu Hao leg. (SWU).

Remarks. This species is similar in elytral markings to *C. fainanensis*, but the male genitalia are distinctly different (Fig. 18).

New records for China

Chlorophorus coniperda Holzschuh, 1992
Fig. 19

Chlorophorus coniperda Holzschuh, 1992: 27, fig. 28. TL: Vietnam. TD: CCH.
Chlorophorus (*Humeromaculatus*) *coniperda* Özdikmen 2022: 652, 687.

Specimens examined. CHINA • 2♂♂ 1♀, Yunnan Province, Yuxi City, E'shan County; 3 V. 2021; Tian Lichao leg. (SWU) • 1♀; Yunnan Province, Xishuangbanna, Jinghong City, Dadugang; 28 IV. 2023; Tian Lichao leg. (SWU).

Distribution. China (Yunnan); Vietnam.

Chlorophorus diversicolor Holzschuh, 2016
Fig. 20

Chlorophorus diversicolor Holzschuh, 2016: 113, figs 7, 8. TL: Laos. TD: CCH.
Chlorophorus (*Humeromaculatus*) *diversicolor* Özdikmen 2022: 652, 687.

Specimens examined. CHINA • 2♂♂ 2♀♀, Yunnan Province, Pu'er City, Ning'er, Tongxin; 4 V. 2012; Tian Lichao and Huang Guiqiang leg. (SWU).

Distribution. China (Yunnan); Laos, Thailand.

Remarks. There is sexual dimorphism in this species in body color. Males are light reddish-brown while females are dark reddish-brown or blackish-brown.
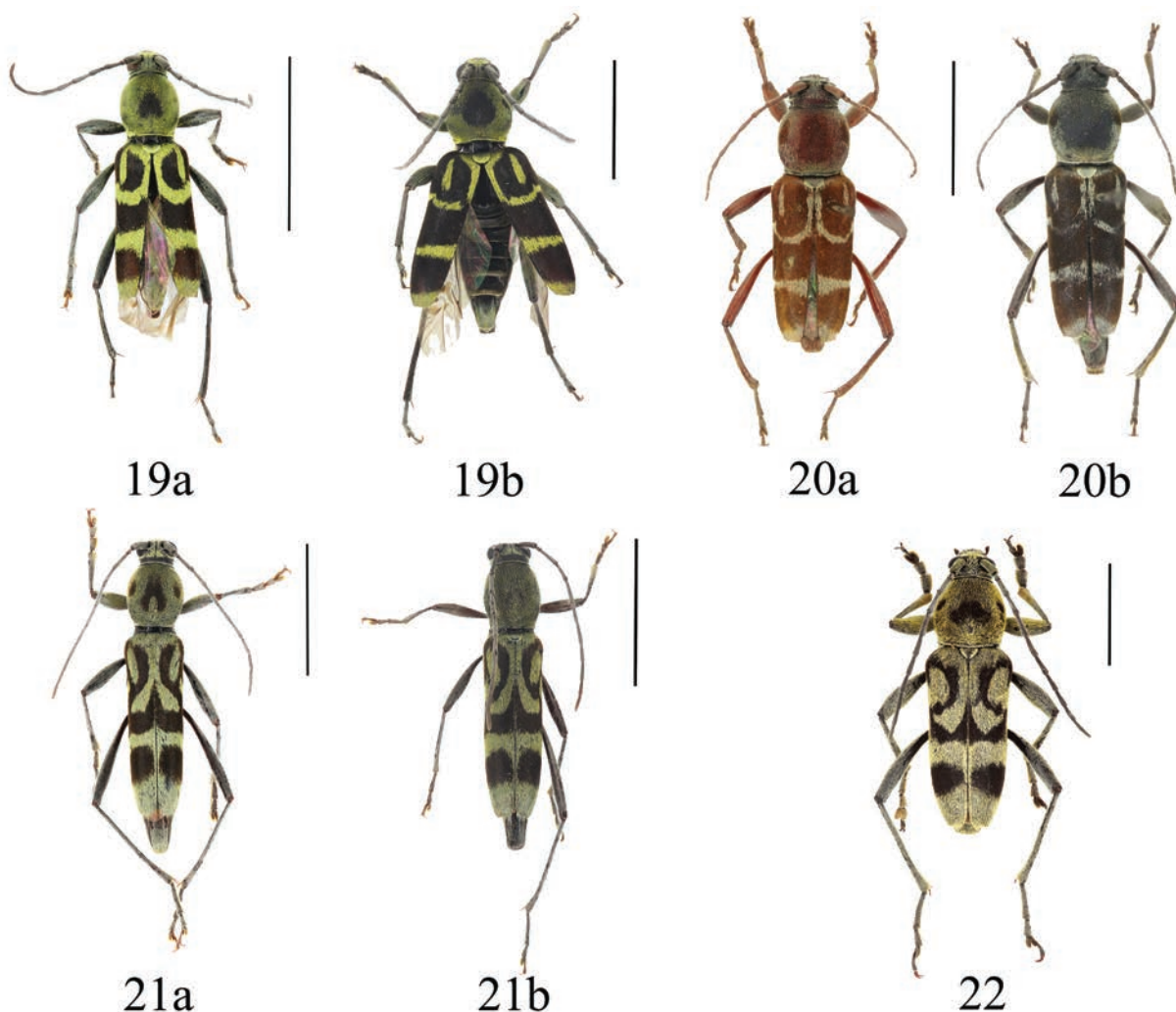
Chlorophorus orbatus Holzschuh 1991
Fig. 21

Chlorophorus orbatus Holzschuh, 1991a: 12, fig. 11. TL: Thailand. TD: CCH.
Chlorophorus (*Chlorophorus*) *orbatus* Özdikmen 2022: 641, 686.

Specimens examined. CHINA • 2♂♂; Yunnan Province, Xishuangbanna, Jinghong City, Dadugang; 4 V. 2013; Tian Lichao leg. (SWU).

Distribution. China (Yunnan); Thailand, India.

Remarks. This species is similar to *C. sappho* Gressitt & Rondon, 1970. *Chlorophorus sappho* can be distinguished from this species mainly by the larger body size; yellow body coloration; meso- and metafemora finely carinate externally; metatibia slightly sinuate and feebly carinate; and elytral apex toothed at the external edge.

Figures 19–22. 19 *Chlorophorus coniperda* Holzschuh, 1992 **a** male **b** female **20** *Chlorophorus diversicolor* Holzschuh, 2016 **a** male **b** female **21** *Chlorophorus orbatus* Holzschuh, 1991 **a** male **b** female **22** *Chlorophorus pinguis* Holzschuh, 1992. Scale bars for adult habitus: 5 mm.

Chlorophorus pinguis Holzschuh, 1992
Fig. 22

Chlorophorus pinguis Holzschuh, 1992: 21, figs 21, 63. TL: Vietnam. TD: CCH.
Chlorophorus (*Humeromagnomaculatus*) *pinguis* Özdikmen 2022: 655, 687.

Specimens examined. CHINA • 3♂♂ 2♀♀; Guangxi Province, Baise City, Leye County, Yachang Town; V. 2016; native collector leg. (SWU).
   Distribution. China (Guangxi); Vietnam.

Acknowledgments

Additional information

Conflict of interest

The authors have declared that no competing interests exist.

Ethical statement

No ethical statement was reported.

Funding

Author contributions

Data curation: ZJF, LC. Methodology: ZJF. Visualization: ZJF, LC. Writing original draft: ZJF. Writing-review and editing: ZL. All authors have read and agreed to the published version of the manuscript.

Author ORCIDs

Zhu Li ⓘ https://orcid.org/0000-0002-7322-5863

Data availability

All of the data that support the findings of this study are available in the main text.

References

Aurivillius C (1912) Cerambycidae: Cerambycinae. Coleopterorum Catalogus pars 39. In: Schenkling S (Ed.) Coleopterorum Catalogus. Volumen 22. Cerambycidae I. Junk, Berlin, 574 pp.

Chen L, Liu ZP, Li Z (2019) Subfamily Cerambycinae. In: Lin MY, Yang XK (Eds) Catalogue of Chinese Coleoptera Volume 9 Chrysomeloidea Vesperidae Disteniidae Cerambycidae. Science Press, Beijing, 98–216.

Chevrolat LA (1863) Clytides d'Asie et d'Océanie. Mémoires de la Société Royale des Sciences de Liège 18(4): 253–350.

Danilevsky ML (2020) Catalogue of Palaearctic Coleoptera Volume 6/1 Revised and Updated Second Edition Chrysomeloidea I (Vesperidae, Disteniidae, Cerambycidae). Koninklijke Brill, Leiden, XXVIII + 712 pp. https://doi.org/10.1163/9789004440333_002

Gahan CJ (1906) The Fauna of British India, including Ceylon and Burma. Coleoptera. – Vol. I (Cerambycidae). Taylor and Francis, London, XVIII + 329 pp.

Gressitt JL (1940) The Longicorn Beetles of Hainan Island, Coleoptera: Cerambycidae. The Philippine Journal of Science 72 (1–2): 1–239. [pls 1–8]

Gressitt JL (1951) Longicorn beetles of China. P. Lechevalier, Paris, 667 pp.

Gressitt JL, Rondon JA (1970) Cerambycid-beetles of Laos (Disteniidae, Prioninae, Philinae, Aseminae, Lepturinae, Cerambycinae). Pacific Insects Monograph 24: II–III + 1–314. [48 pls]

Holzschuh C (1984) Beschreibung von 24 neuen Bockkäfern aus Europa und Asien, vorwiegend aus dem Himalaya (Coleoptera, Cerambycidae). Entomologica Basiliensa 9: 340–372.

Holzschuh C (1989) Beschreibung von 20 neuen Bockkäfern aus Thailand, Vietnam und Taiwan (Coleoptera, Cerambycidae). Entomologica Basiliensa 13: 361–390.

Holzschuh C (1991a) 33 neue Bockkäfer aus der palaearktischen und orientalischen Region (Coleoptera, Cerambycidae). Schriftenreihe der Forstlichen Bundesversuchanstalt (FBVA-Berichte) 51: 5–34.

Holzschuh C (1991b) 45 neue Bockkäfer aus Asien, vorwiegend aus Thailand (Coleoptera: Disteniidae und Cerambycidae). Schriftenreihe der Forstlichen Bundesversuchanstalt (FBVA-Berichte) 51: 35–75.

Holzschuh C (1992) 57 neue Bockkäfer aus Asien, vorwiegend aus China, Thailand und Vietnam (Coleoptera: Cerambycidae). Schriftenreihe der Forstlichen Bundesversuchanstalt (FBVA-Berichte) 69: 5–63.

Holzschuh C (1993) Neue Bockkäfer aus Europa und Asien IV, 60 neue Bockkäfer aus Asien, vorwiegend aus China und Thailand (Coleoptera: Cerambycidae). Schriftenreihe der Forstlichen Bundesversuchanstalt (FBVA-Berichte) 75: 1–63.

Holzschuh C (1998) Beschreibung von 68 neuen Bockkäfern aus Asien, überwiegend aus China und zur Synonymie einiger Arten (Coleoptera: Cerambycidae). Schriftenreihe der Forstlichen Bundesversuchanstalt (FBVA-Berichte) 107: 1–65.

Holzschuh C (2003) Beschreibung von 72 neuen Bockkäfern aus Asien, vorwiegend aus China, Indien, Laos und Thailand (Coleoptera, Cerambycidae). Entomologica Basiliensa 25: 147–241.

Holzschuh C (2006) Neue Arten der Triben Molorchini und Clytini aus China und Laos (Coleoptera, Cerambycidae). Entomologica Basiliensa et Collectionis Frey 28: 277–302.

Holzschuh C (2009) Beschreibung von 59 neuen Bockkäfern und vier neuen Gattungen aus der orientalischen und palaearktischen Region, vorwiegend aus Laos, Borneo, und China (Coleoptera, Cerambycidae). Entomologica Basiliensa et Collectionis Frey 31: 267–358.

Holzschuh C (2010) Beschreibung von 66 neuen Bockkäfern und zwei neuen Gattungen aus der orientalischen Region, vorwiegend aus Borneo, China, Laos und Thailand (Coleoptera, Cerambycidae). Entomologica Basiliensa et Collectionis Frey 32: 137–225.

Holzschuh C (2016) Neue Clytini (Coleoptera: Cerambycidae) aus Laos und zur Synonymie einiger Arten. Zeitschrift der Arbeitsgemeinschaft Österreichischer Entomologen 68: 103–127.

Holzschuh C (2019) Beschreibung von dreizehn neuen Bockkäfern aus Asien (Coleoptera, Cerambycidae). Les Cahiers Magellanes (NS) 34: 79–95.

Holzschuh C (2020) Neue Synonymien, Neumeldungen für China und Beschreibung von acht neuen Bockkäfern aus Asien (Coleoptera, Cerambycidae). Les Cahiers Magellanes (NS) 36: 48–64.

Hope W (1831) Synopsis of the new species of Nepal Insects in the collection of Major General Hardwicke. Gray's Zoologica Miscellanea 1: 21–32.

Hua LZ (2002) List of Chinese Insects. Guangzhou, Sun Yat-sen University Press, 612 pp.

Hua LZ, Nara H, Yu CK (1993) Longicorn-Beetles of Hainan & Guangdong. Nantou, Muh-Sheng Museum of Entomology, 151 pp.

Hua LZ, Nara H, Samuelson GA, Lingafelter SW (2009) Iconography of Chinese Longicorn Beetles (1406 Species) in Color . Guangzhou, Sun Yat-sen University Press, 474 pp.

Laporte de Castelnau FL, Gory HL (1841) Monographie du Genre *Clytus*. P. Duménil. Histoire Naturelle et Iconographie des Insectes Coléoptères. Paris 3 [1836]: III + 124 pp. [+ 20 pls]

Lazarev MA (2019) Catalogue of Bhutan Longhorn beetles (Coleoptera, Cerambycidae). Humanity space International Almanac 8(2): 141–198.

Lazarev MA (2024) Taxonomic notes on longhorned beetles with the descriptions of several new taxa (Coleoptera, Cerambycidae). Humanity space International almanac 13(1): 21–38.

Lazarev MA, Murzin SV (2019) Catalogue of Nepal Longhorn beetles (Coleoptera, Cerambycidae). Humanity space International Almanac 8(6): 746–868.

Lee S, Lee S (2020) Multigene phylogeny uncovers oviposition-related evolutionary history of Cerambycinae (Coleoptera: Cerambycidae). Molecular Phylogenetics and Evolution 145: 106–707. https://doi.org/10.1016/j.ympev.2019.106707

Lin MY, Fang DD, Yang XK (2023) Cerambycidae. In: Yang XK, Zhang RZ (Eds) Insect Fauna of the Zhejiang, Vol. VII Coleoptera (III). China Science Publishing and Media Ltd, Beijing, 5–227.

Mitra B, Chakraborti U, Mallick K, Bhaumik S, Das P (2017) An updated list of cerambycid beetles (Coleoptera: Cerambycidae) of Assam, India. Records of the Zoological Survey of India 117(1): 78–90. https://doi.org/10.26515/rzsi/v117/i1/2017/117286

Ohbayashi K (1963) Systematic notes and descriptions of new forms in Cerambycidae from Japan. Fragmenta Coleopterologica (3): 11–12.

Özdikmen H (2011) The first attempt on subgeneric composition of *Chlorophorus* Chevrolat, 1863 with four new subgenera (Col.: Cerambycidae: Cerambycinae). Munis Entomology & Zoology 6(2): 535–539.

Özdikmen H (2022) A new attempt on the subgeneric composition of *Chlorophorus* Chevrolat, 1863 with descriptions of new subgenera (Cerambycidae: Cerambycinae). Munis Entomology & Zoology 17(2): 628–693.

Pic M (1908) Nouveaux Longicornes de la Chine méridionale. Matériaux pour servir à l'étude des Longicornes 7(1): 14–18.

Pic M (1916) Longicornes asiatiques. Matériaux pour servir à l'étude des Longicornes 10(1): 12–19.

Pic M (1920) Longicornes nouveaux de Chine [Col. Cerambycidae]. Bulletin de la Société Entomologique de France 1920: 197–198. https://doi.org/10.3406/bsef.1920.26638

Pic M (1924) Nouveautés diverses. Mélanges Exotico-Entomologiques 41: 1–32.

Pic M (1931) Cérambycides paléarctiques et prépaléarctiques. Bulletin de la Société Entomologique de France 1931: 257–259. https://doi.org/10.3406/bsef.1931.28479

Pic M (1937) Nouveautés diverses. Mélanges Exotico-Entomologiques 69: 1–36.

Pic M (1943) Coléoptères du globe (suite). L'Échange, Revue Linnéenne 59(491): 1–4.

Pic M (1949) Nouveaux Coléoptères exotiques et notes diverses. Miscellanea Entomologica 46: 49–55.

Pic M (1950) Coléoptères du globe (suite). L'Échange, Revue Linnéenne 66(520): 5–8.

Schwarzer B (1925) Sauters Formosa-Ausbeute (Cerambycidae. Col.). (Subfamilie Cerambycinae.). Entomologische Blätter 21(1): 20–30.

Tavakilian G, Chevillotte H (2024) Base de données Titan sur les Cérambycidés ou Longicornes. http://titan.gbif.fr/index.html [accessed 30 May 2024]

Viktora P (2019) New *Chlorophorus* species from Palaearctic, Oriental and Australian Region (Coleoptera, Cerambycidae, Cerambycinae, Clytini). Folia Heyrovskyana, (Series A) 27(1): 119–163.

Viktora P (2020) New Clytini from the Palaearctic, Oriental and Australian Regions (Coleoptera, Cerambycidae, Cerambycinae). Folia Heyrovskyana (Series A) 28(2): 102–158.

Viktora P (2021) New Clytini from the Palaearctic and Oriental Regions (Coleoptera, Cerambycidae, Cerambycinae). Folia Heyrovskyana (Series A) 29(2): 116–172.

Viktora P (2022) New Clytini from the Palaearctic and Oriental Regions (Coleoptera: Cerambycidae: Cerambycinae). Folia Heyrovskyana (Series A) 30(1): 161–230.

Viktora P (2023) Two new species of the genus *Chlorophorus* Chevrolat, 1863 from Vietnam (Coleoptera: Cerambycidae: Cerambycinae: Clytini). Studies and Reports of District Museum Prague-East, Taxonomical Series 19(1): 181–187.

Villiers A, Chûjô M (1966) Coleoptera of East Nepal Arranged by Michio Chûjô. 13. Famille Cerambycidae. Journal of the College of Arts and Sciences, Chiba University 4(4): 550–552.

Waterhouse CO (1874) Synonymical Notes on Longicorn Coleoptera. The Proceedings of the Entomological Society of London 1874: XXVIII–XXIX.

Zamoroka AM (2021) Is Clytini monophyletic? The evidence from five-gene phylogenetic analysis. Proceedings of the State Natural History Museum 37: 191–214. https://doi.org/10.36885/nzdpm.2021.37.191-214

![ZooKeys]

Research Article

A new species of *Opsariichthys* (Teleostei, Cypriniformes, Xenocyprididae) from Southeast China

Xin Peng[1*], Jia-Jun Zhou[2,3*], Hong-Di Gao[2], Jin-Quan Yang[1]

1   *Shanghai Universities Key Laboratory of Marine Animal Taxonomy and Evolution, Shanghai Ocean University, Shanghai 201306, China*
2   *Zhejiang Forest Resource Monitoring Center, Hangzhou 310020, China*
3   *Zhejiang Forestry Survey Planning and Design Company Limited, Hangzhou 310020, China*
Corresponding authors: Hong-Di Gao (*ghd1118@163.com*); Jin-Quan Yang (*jqyang@shou.edu.cn*)

Abstract

Opsariichthys iridescens **sp. nov.** is described from the Qiantang and Oujiang rivers in Zhejiang Province and a tributary of the Yangtze River adjacent to the Qiantang River. It is distinguished from congeners by the following combination of morphological features: no obvious anterior notch on the tip of the upper lip; 45–52 lateral-line scales; 18–21 pre-dorsal scales; two rows of pharyngeal teeth; a maxillary extending to or slightly beyond the vertical anterior margin of the orbit in adult males; a pectoral fin extending to the pelvic fin in adult males; nuptial tubercles on the cheeks and lower jaw of males, which are usually united basally to form a plate; uniform narrow pale pink cross-bars on trunk and two widening significantly on caudal peduncle. Its validity was also supported by its distinct Cyt *b* gene sequence divergence from all congeners and its monophyly recovered in a Cyt *b* gene-based phylogenetic analysis.

Key words: Cytochrome *b*, morphology, opsariichthine, phylogenetic analysis, principal component analysis (PCA), taxonomy

![OPEN ACCESS]

Introduction

The genus *Opsariichthys* Bleeker, 1863, are a group of small-sized cyprinid fishes endemic to East Asia that live in fast-flowing rivers or streams (Chen 1982; Chen and Chang 2005; Wang et al. 2019). The type species, *Opsariichthys uncirostris* (Temminck & Schlegel, 1846), was initially described from Japan and assigned to the genus *Leuciscus* Cuvier, 1816. Since the genus *Opsariichthys* was first established, its earliest members, such as *Zacco* Jordan & Evermann, 1902 and *Candidia* Jordan & Richardson, 1909, that belonged to the so-called opsariichthine group and have large and elongated anal fins and a series of nuptial tubercles on the jaws as common adult features (Chen 1982), have been placed in this genus, and a total of 27 species have been described over the last one hundred years or more (Fricke et al. 2024). Chen (1982) taxonomically defined the opsariichthine fishes and noted that *Opsariichthys* included

---

*   These authors contributed equally to this paper.

only two species, among which *O. uncirostris* was distributed in Japan and the other species, *O. bidens* Günther, 1873, was distributed in East Asia. Chen and Chu (1998) continued to follow this opinion.

Both morphological and molecular studies have shown that *Opsariichthys* and *Zacco* are closely related genera (Bănărescu 1968; Chen 1982; Huang et al. 2017; Wang et al. 2019; Zhang et al. 2023), and the traditional morphological features that distinguishes these two genera are that the former have a conspicuous notch on the tip of their upper lip and undulated jaws, while the latter has no obvious notch on the tip of their upper lip and relatively straight jaws (Jordan and Evermann 1902; Bănărescu 1968; Chen 1982; Chen and Chu 1998). However, recent molecular studies have revealed distinct genetic differentiation and multiple genetic lineages within *O. bidens* and *Z. platypus* (Temminck & Schlegel, 1846), which may correspond to different species based on traditional diagnostic features (Berrebi et al. 2005; Perdices et al. 2004; 2005). Furthermore, the genetic lineages of both species are paraphyletic (Perdices and Coelho 2006). These two species are sympatric in many places and are considered widespread in East Asia (Wang et al. 2019).

Subsequently, based on the results of morphological and phylogenetic studies, Chen et al. (2009) proposed new diagnostic key features of these two genera, suggesting that the nuptial tubercles on the cheeks of male *Opsariichthys* were separated and that the pale green lateral cross-bars were clear and independent, while the nuptial tubercles on the cheeks of male *Zacco* were united basally to form a plate and that the lateral pale green cross-bars were fused into fewer large patches. A phylogenetic study based on the mitochondrial genome by Huang et al. (2017) reaffirmed that the lateral cross-bars were a key diagnostic feature in the taxonomy of the opsariichthine group. This view has now been widely accepted. Based on this new classification, the following four new species are described: *O. songmaensis* Nguyen & Nguyen, 2000; *O. dienbienensis* Nguyen & Nguyen, 2000; *O. kaopingensis* Chen & Wu, 2009; and *O. duchuunguyeni* Huynh & Chen, 2013. Three species, viz., *O. acutipinnis* (Bleeker, 1871), *O. evolans* (Jordan & Evermann, 1902), and *O. macrolepis* (Yang & Hwang, 1964), formerly known as *Z. platypus*, are reinstated as valid *Opsariichthys* species. Three species, viz., *O. amurensis* Berg 1932, *O. minutus* Nichols, 1926, and *O. hainanensis* Nichols & Pope, 1927, that were once considered to be synonymous with *O. bidens* are also revalidated. Two species, *O. chengtui* (Kimura 1934) and *O. pachycephalus* (Günther 1868), are transferred from *Zacco* to *Opsariichthys*, while the taxonomic status of two other species, *O. bea* Nguyen 1987 and *O. hieni* Nguyen 1987, remains uncertain (Fricke et al. 2024). Therefore, *Opsariichthys* is currently considered to include 14 valid species, eight of which are distributed across mainland China. The valid species in mainland China are *O. acutipinnis*, *O. amurensis*, *O. bidens*, *O. chengtui*, *O. evolans*, *O. hainanensis*, *O. macrolepis*, and *O. minutus*, and with the exception of *O. bidens*, are all regionally distributed species.

While examining *Opsariichthys* specimens collected from Zhejiang Province and the tributaries of the Yangtze River adjacent to the Qiantang River, we found that some of the specimens did not belong to any described species. Further morphological and molecular analyses of these specimens support that they belong to a new species, which we describe here.

Materials and methods

Sample collection and morphological analysis

Sixteen specimens were collected from the Qiantang River system in Lin'an District, Hangzhou City, and Suichang County, Lishui City, Zhejiang Province, as well as from the Qiantang River region in She County, Huangshan City, Anhui Province. The right pectoral fins of these freshly collected specimens were preserved in 95% ethanol for molecular biology analyses. Meanwhile, specimens with left fins were fixed in 10% formalin for three days and then transferred to 70% ethanol for long-term preservation and subsequent morphological analyses. The specimens used in the present study were deposited at Shanghai Ocean University, Shanghai, China (SHOU). Two species (*O. bidens* and *O. evolans*) were used for deep morphological comparison with the new species because their sympatric distribution (Fig. 1). Data of other similar *Opsariichthys* species for comparison were cited from literatures (Yang and Huang 1964; Chen et al. 2009; Huynh and Chen 2013; Wang et al. 2019).

The morphometric measurements and meristic counts generally followed those of Chen et al. (2009) and Huynh and Chen (2013). Morphometric characteristics were measured with digital calipers and recorded to the nearest 0.1 mm. Counts and measurements were made on the left side of the specimen. The meristic abbreviations are as follows: D, dorsal fin; A, anal fin; P1, pectoral fin; P2, pelvic fin; LL, lateral-line scales; LLa, scales above the lateral line; LLb, scales below the lateral line; PreD, predorsal scales; and CPS, circum-peduncular scales. All the fish were measured for standard length (SL).
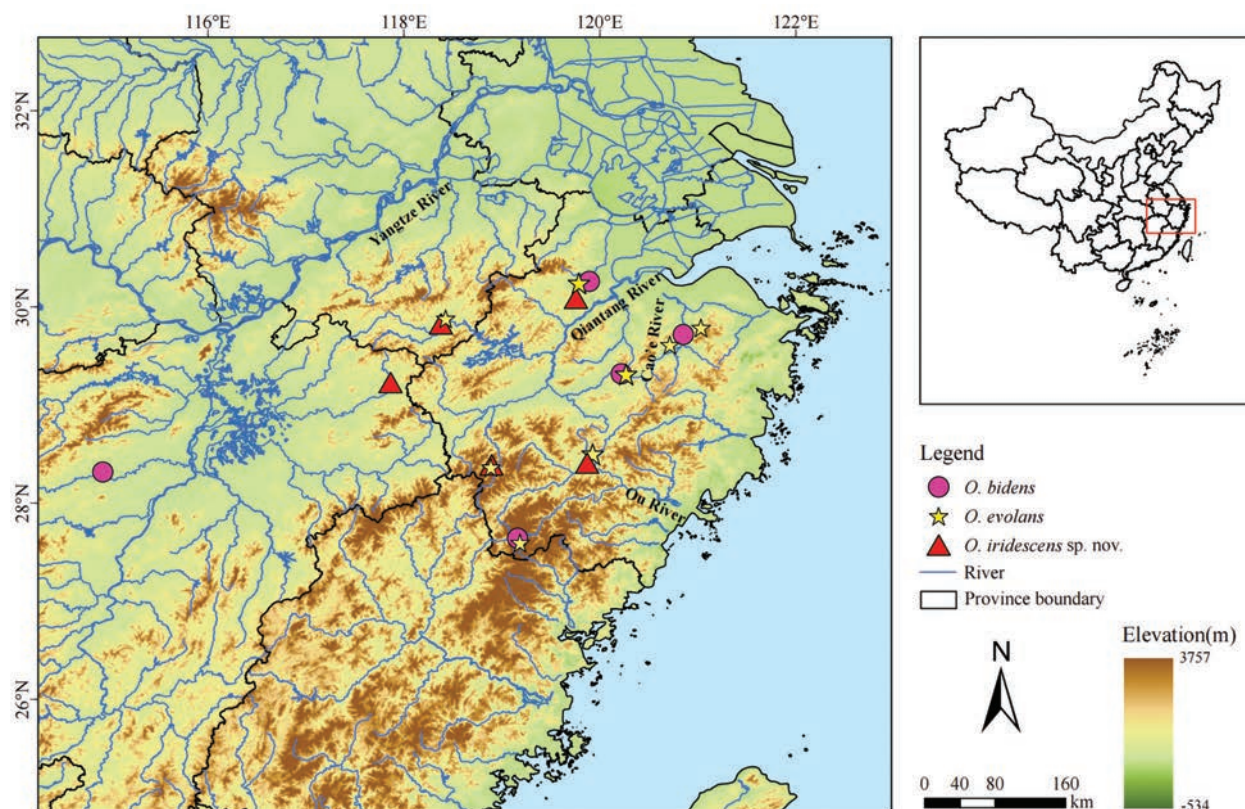

Figure 1. Map showing sampling sites of *O. iridescens* sp. nov. and its two sympatric species that were examined in the present study.

Based on the morphological data, principal component analysis (PCA) was performed on the three *Opsariichthys* species using R software. From the cumulative contribution of the principal components, the scores of the first principal component (PC1) and the second principal component (PC2) were plotted. Canonical discriminant analysis (CDA) and graphing were performed using SPSS version 23.0.

DNA extraction, PCR amplification, and sequencing

Genomic DNA was extracted using an animal genomic DNA extraction kit from Shanghai Sangon Biotech Co., Ltd. The cytochrome *b* gene (Cyt *b*) was amplified using polymerase chain reaction (PCR) with the primers L14724 (5'-GACTT-GAAAAACCACCGTTG-3') and H15915 (5'-CTCCGATCTCCGGATTACAAGAC-3') (Xiao et al. 2001). Each 25 μL of PCR reaction mixture contained 1 μL of DNA template, 1 μL of each primer, 12.5 μL of Taq PCR Mix (Sangon Biotech Co., Ltd., Shanghai, China), and 9.5 μL of ddH$_2$O. The PCR conditions were as follows: pre-denaturation at 95 °C for 3 min; denaturation at 94 °C for 30 s; annealing at 54 °C for 40 s; extension at 72 °C for 1 min; 35 cycles of extension at 72 °C for 5 min; and heat preservation at 4 °C. After the PCR reaction was completed, the products were detected by agarose (1.5%) electrophoresis and sequenced bidirectionally by Shanghai Sangon Biotech Co., Ltd. The sequencing results for the Cyt *b* sequences were manually corrected and assembled using SeqMan software from DNASTAR (Burland 2000).

Phylogenetic analysis

A total of 74 sequences were used, 45 of which were newly sequenced and 29 of which were obtained from GenBank. The specific sample information is shown in Table 1. MEGA v. 11.0 (Tamura et al. 2021) was used to align the sequences and calculate the nucleotide composition, variable sites, parsimony informative sites and genetic distances between species. Neighbor joining (NJ) analysis was also performed with MEGA v. 11.0 using the Kimura 2-parameter (K2P) model. Bootstrapping with 1,000 pseudo replicates was used to examine the robustness of the clades in the resulting tree. The best substitution model (TIM2+I+G) was selected for maximum likelihood (ML) analysis and Bayesian inference (BI) analysis using jModeltest v. 2.0 software (Darriba et al. 2012) with the Akaike information criterion (AIC). ML analysis was conducted using IQ-TREE v. 2.0 software (Minh et al. 2020), and node confidence was analyzed by bootstrap analysis with 1,000 repetitive samples. Mrbayes v. 3.2.6 software (Ronquist et al. 2012) was used to conduct the BI analysis, and posterior probability was used to indicate the credibility of each branch. The starting tree was set as a random tree. Four Markov chains were run simultaneously for two million generations, with three hot chains and one cold chain. The system tree was sampled every 100 generations to remove the top 25% of untrustworthy regions, and the process was stopped when the variance of convergence was less than 0.01. All trees were viewed and edited using FigTree v. 1.4.3 software (Rambaut 2016).

Table 1. The samples used in this study with their localities, voucher information, and GenBank accession numbers.

Genus	Species	Location	River	Voucher number	GenBank accession number
Opsariichthys	*O. iridescens* sp. nov.	Lin'an, Zhejiang	Qiantang River	ZJQT01-05	PP639122–PP639123, PP639130–PP639132*
		Huangshan, Anhui	Qiantang River	ZJXA01-03	PP639124–PP639126*
		Wuyuan, Jiangxi	Yangtze River	ZJLA01-03	PP639127–PP639129*
		Lishui, Zhejiang	Ou River	ZJOJ01-03	PP639133–PP639135*
	O. bidens	Lin'an, Zhejiang	Qiantang River	MKQT01-02	PP639101–PP639102*
		Dongyang, Zhejiang	Qiantang River	MKQT03	PP639103*
		Shengzhou, Zhejiang	Cao'e River	MKCE	PP639097*
		Yichun, Jiangxi	Gan River	MKJJ01-03	PP639098–PP639100*
		Fujian	Jiulong River	OBJLJ1-2	FJ602005–FJ602006
	O. evolans	Lin'an, Zhejiang	Qiantang River	CQQT01-02	PP639110–PP639111*
		Dongyang, Zhejiang	Qiantang River	CQQT03-07	PP639112–PP639116*
		Quzhou, Zhejiang	Qiantang River	ZP_QTJ_1-2	MH350437–MH350438
		Shangyu, Zhejiang	Cao'e River	CQCE01	PP639104*
		Shengzhou, Zhejiang	Cao'e River	CQCE02-06	PP639105–PP639109*
		Lishui, Zhejiang	Ou River	CQOJ01-02	PP639117–PP639118*
		Taiwan	Unknown	OETaiW1-2	KR698567–KR698568
	O. macrolepis	Hejiang, Sichuan	Yangtze River	ZP_CJU2_1	MH350702
	O. hainanensis	Hainan	Unknown	OHAND2	KJ940933
	O. chengtui	Chengdu, Sichuan	Yangtze River	–	KT725244
	O. acutipinnis	Huangshan, Anhui	Yangtze River	ZPQimen4	KM491719
	O. duchuunguyeni	Baise, Guangxi	Pear River	ZPPE_You1	KP101024
	O. pachycephalus	Taiwan	Unknown	OPTaiW1	KR698649
	O. kaopingensis	Taiwan	Unknown	–	AY958189
	O. minutus	Guangxi	Pear River	OMhap01	KR698540
	O. uncirostris	Japan	Unknown	OUJapan1	KR698682
	Opsariichthys sp. A	Huangshan, Anhui	Yangtze River	ZPTaiping2	KM491721
	Opsariichthys sp. B	Fujian	Min River	OEMinJ1	KR698572
	Opsariichthys sp. C	Hunan	Yangtze River	OEXiangJ5	KR698575
	Opsariichthys sp. D	Jiangxi	Yangtze River	ZA_FH2	MH350668
	Opsariichthys sp. E	Hunan	Yangtze River	OELI1	KR698563
Zacco	*Z. acanthogenys*	Shengzhou, Zhejiag	Qiantang River	JJQT01-03	PP639119–PP639121*
	Z. tiaoxiensis	Yuhang, Zhejiang	Tiaoxi River	TX01-03	PP639136–PP639138*
	Z. sinensis	Fengcheng, Liaoning	Yalu River	ZHYL01-03	PP639139–PP639141*
	Z. platypus	Japan	Miya River	ZPWJ1	LC019793
Parazacco	*P. spilurus*	Unknown	Unknown	PS1	KF971863
	P. fasciatus	Unknown	Unknown	PF1	AY958195
Nipponocypris	*N. temminckii*	Unknown	Unknown	NT1	EF452750
	N. sieboldii	Unknown	Unknown	NS1	AY958198
Candidia	*C. barbatus*	Taiwan	Fenggang River	CB1	AY958200
	C. pingtungensis	Taiwan	Gaoping River	CP1	KT725246
Aphyocypris	*A. chinensis*	Japan	Unknown	–	NC008650
	A. chinensis	China	Unknown	–	AF307452

Note: * Sequenced in this study.

Results

Taxonomic account

Family Xenocyprididae Günther 1868
Genus *Opsariichthys* Bleeker, 1863

***Opsariichthys iridescens* Peng, Zhou & Yang, sp. nov.**
https://zoobank.org/FADF08EA-9DBC-45A3-9D67-79274C1B3083
Figs 2, 3A, B

Type material. *Holotype* • SHOU202210001, male, adult, 91.0 mm standard length (SL), collected by Jia-Jun Zhou and Hui Cao in October 2022, in Lin'an District, Hangzhou City, Zhejiang Province (Qiantang River) (30.2368°N, 119.7196°E). *Paratypes* • SHOU202210002−SHOU202210010, 9 specimens, 79.1−96.0 mm standard length (SL), collected by Jia-Jun Zhou and Hui Cao in October 2022, from the same locality as the holotype; SHOU202106089, SHOU202106090, and SHOU202106125, 3 specimens, 85.7~110.7 mm standard length (SL), collected by Jia-Jun Zhou and Wei Sun in June 2021, in Suichang County, Lishui City, Zhejiang Province (Qiantang River) (28.5956°N, 119.2709°E); SHOU202106001−SHOU202106003, 3 specimens, 84.5~109.4 mm standard length (SL), collected by Yun-Feng Huang in June 2021, in Shexian County, Huangshan City, Anhui Province (Qiantang River) (29.8637°N, 118.4100°E).

Diagnosis. The new species, *Opsariichthys iridescens* sp. nov. can be clearly distinguished from its two sympatric congeners in the Qiantang River and nearby geographic regions (Tables 3, 4). It can be distinguished from *O. evolans* by the following features: (1) lateral-line scales 45−52 (vs 42−45); (2) scales above lateral-line nine or ten (vs 8); (3) pre-dorsal scales 18−21 (vs 15−17); (4) two rows of pharyngeal teeth (vs 3 rows); (5) maxillary extending to or slightly beyond the vertical of anterior margin of orbit in adult male (vs never extending to the vertical of anterior margin of orbit); (6) pectoral fin extending to pelvic fin in adult male (vs extending far beyond origin of ventral fin); (7) almost uniform narrow pale cross-bars on trunk and widening significantly on caudal peduncle (vs gradually widened, Fig. 3E, F); (8) lower jaw with one row of large tubercles usually united basally to form a plate in male (vs 1 row of moderate tubercles well separated). The new species can be clearly distinguished from *O. bidens* by the following features: (1) absence of distinct anterior notch on upper lip (vs presence of conspicuous anterior notch on upper lip); (2) two rows of pharyngeal teeth (vs 3 rows); (3) maxillary extending to or slightly beyond the vertical of anterior margin of orbit in adult male (vs extending to the vertical midpoint of the eye); (4) pectoral fin extending to pelvic fin in adult male (vs never extending); (5) almost uniform narrow pale cross-bars on trunk and widening significantly on caudal peduncle (vs gradually widened, Fig. 3C, D); (6) one row of large tubercles under lower jaw united basally to form a plate in male (vs 3 or 4 rows of moderate tubercles well separated).

Opsariichthys iridescens sp. nov. can be well separated from the congeners: *O. uncirostris* from Japan and Korea; *O. amurensis*, *O. minutus*, and *O. hainanensis* from mainland China; *O. dienbienensis* and *O. songmaensis* from Vietnam, like *O. bidens*, by the absence of distinct anterior notch on upper lip

Figure 2. *Opsariichthys iridescens* sp. nov. **A** holotype, SHOU202210001, preserved male specimen, 91.0 mm SL **B** paratype, SHOU202308012, preserved female specimen, 85.2 mm SL.

(vs the presence of distinct anterior deep notch on that). Besides *O. evolans*, the new species can be distinguished from the remaining congeneric species: *O. acutipinnis*, *O. chengtui*, and *O. macrolepis* from mainland China; *O. kaopingensis* and *O. pachycephalus* from Taiwan; *O. duchuunguyeni* from Vietnam, that have an absence of distinct anterior notch on upper lip as well as by the following combination of morphological features (Table 4): (1) lateral-line scales 45–52; (2) scales above lateral line nine or ten; (3) pre-dorsal scales 18–21; (4) circum-peduncular scales 16 or 17; (5) two rows of pharyngeal teeth; (6) maxillary extending to or slightly beyond vertical of anterior margin of orbit in adult male; (7) pectoral fin extending to pelvic fin in adult male; (8) almost uniform, narrow, pale cross-bars on trunk, widening significantly on caudal peduncle; (9) nuptial tubercles on cheeks and lower jaw united basally to form a plate in adult male.

Description. The morphometric and meristic data are listed in Tables 2, 3. Fig. 2A, B shows lateral views of the male and female fish.

Dorsal fin rays iii, 7; anal fin rays iii, 9; pectoral fin rays i,13–14; pelvic fin rays i,7–8; lateral-line scales 45–52; scales above lateral line nine or ten; scales below lateral line three or four; predorsal scales 18–21; circum-peduncular scales 16 or 17; and two rows of pharyngeal teeth.
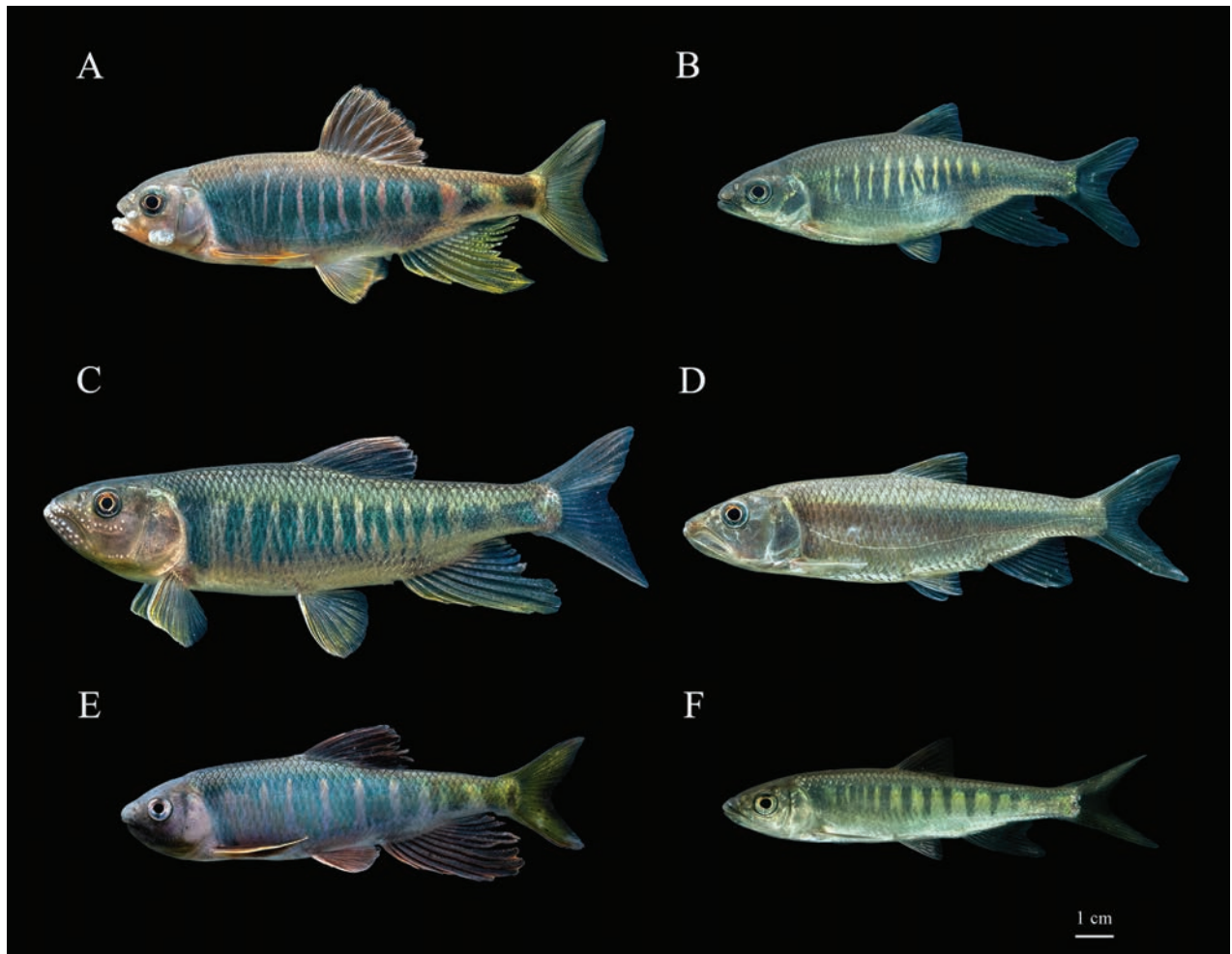
Figure 3. *Opsariichthys iridescens* sp. nov. **A** live male **B** live female; *Opsariichthys bidens* **C** live male **D** live female; *Opsariichthys evolans* **E** live male **F** live female.

Body elongated and laterally compressed, belly rounded. Body depth slightly shorter than head length. No maxillary or rostral barbels. Mouth subterminal and oblique, maxillary extending to or slightly beyond the vertical of anterior margin of orbit. Mouth lacking obvious anterior notch and jaws relatively straight. Eyes rather large, upper lateral. Interorbital width approximately equal to or slightly less than snout length. Distinct nuptial tubercles on head and anal fin rays of adult male, one row of 3–6 on each side of lower jaw, one row of three or four on cheek. One row of 4–6 large, rounded tubercles on snout, usually united basally to form a plate. Body with moderately cycloid scales. Lateral line complete, depressed downward above pectoral fin and extending along lower half of body to mid-lateral on caudal peduncle. Tiny scales on belly.

Pectoral fin reaching or extending slightly beyond pelvic fin origin when depressed in adult male, but not reaching the origin in female. Pelvic fin origin vertical or slightly behind dorsal fin origin, extending to anal fin origin when depressed in adult male, but not reaching the origin in female. Anal fin rays rather elongate, especially first to fourth branched rays longer in male, with the rear tip extending beyond vertical line of caudal fin base. Caudal fin forked, lower lobe almost equal to upper one.

Table 2. Morphometric measurements of *Opsariichthys bidens*, *O. evolans*, and *O. iridescens* sp. nov.

	O. bidens						O. evolans						O. iridescens sp. nov.						
	Male			**Female**			**Male**			**Female**			**Holotype Male**	**Male**			**Female**		
n	2			8			9			8			1	13			2		
Standard length (mm)	95.2~100.6			76.1~131.6			71.2~111.6			67.5~84.0			91.0	79.1~110.7			84.5~92.4		
% of SL	Min	Max	Mean	Min	Max	Mean	Min	Max	Mean	Min	Max	Mean		Min	Max	Mean	Min	Max	Mean
Body depth	24.6	26.8	25.7	20.1	25.2	22.5	22.1	25.5	24.2	22.0	24.8	23.8	24.0	23.7	28.6	26.0	23.3	24.7	24.0
Head length	30.0	30.1	30.0	29.8	31.1	30.5	23.4	26.5	24.8	24.2	26.6	25.3	27.2	25.8	27.9	27.1	26.5	27.2	26.9
Length of the caudal fin peduncle	17.3	18.2	17.7	14.6	20.0	16.5	16.3	19.3	17.6	16.2	19.5	17.9	18.5	17.1	20.1	18.7	17.6	18.1	17.9
Depth of the caudal fin peduncle	9.0	9.5	9.2	8.2	9.9	8.8	7.7	9.4	8.7	8.2	9.3	8.8	9.2	8.5	10.0	9.3	8.5	8.8	8.7
Dorsal fin length	18.7	18.9	18.8	14.1	17.4	15.8	19.3	26.0	23.3	17.8	24.9	20.9	17.2	17.0	19.8	18.2	16.5	16.8	16.7
Pectoral fin length	19.6	22.0	20.8	12.9	19.8	17.9	24.6	30.9	27.3	19.4	28.5	24.2	23.1	21.1	26.7	23.5	18.4	19.1	18.8
Pelvic fin length	15.3	16.2	15.7	11.7	14.8	13.6	16.8	22.2	19.3	13.9	19.7	17.3	15.5	14.2	17.8	15.5	12.8	14.5	13.7
Anal fin length	25.6	28.5	27.0	18.3	25.1	21.8	33.3	42.4	38.2	22.6	39.7	31.5	29.3	28.0	35.7	32.1	25.7	25.8	25.8
Dorsal fin base length	13.0	13.3	13.2	9.3	11.4	10.6	12.1	15.2	13.5	10.0	14.9	12.1	12.3	11.6	13.4	12.5	10.2	10.7	10.5
Pectoral fin base length	4.5	5.1	4.8	3.3	4.4	3.9	4.6	5.9	5.3	4.0	5.1	4.6	5.1	5.0	6.3	5.8	4.0	4.2	4.1
Pelvic fin base length	3.7	3.8	3.7	3.2	4.0	3.6	3.3	4.5	3.8	3.2	4.6	3.8	4.9	3.8	4.9	4.2	3.6	3.7	3.7
Anal fin base length	15.1	15.4	15.3	10.5	12.0	11.0	15.6	18.9	17.2	13.6	19.1	15.6	17.6	15.2	18.6	16.9	12.6	13.2	12.9
Predorsal length	53.2	53.3	53.2	51.8	56.2	53.8	48.4	50.0	48.9	48.3	50.5	49.2	51.1	49.0	55.2	51.9	51.3	54.0	52.7
Prepectoral length	26.8	27.0	26.9	27.5	29.6	28.9	23.6	25.7	24.5	23.9	27.7	25.0	24.5	24.5	26.8	25.6	26.5	26.8	26.7
Prepelvic length	50.1	52.0	51.1	51.6	54.8	53.0	46.1	49.5	47.3	46.4	50.2	48.3	46.3	46.3	49.9	48.0	49.8	50.0	49.9
Preanal length	68.9	69.3	69.1	71.2	73.9	72.6	46.6	68.6	65.1	66.6	71.5	69.1	63.1	63.1	70.4	66.2	69.4	71.2	70.3
% of HL																			
Snout length	29.3	32.1	30.7	29.6	33.7	32.1	25.7	33.4	29.0	27.6	31.5	29.3	31.4	28.8	35.6	31.5	29.7	30.8	30.3
Eye diameter	18.2	19.6	18.9	16.0	22.4	19.1	21.9	30.5	27.0	25.5	28.4	27.5	20.4	20.4	29.3	25.4	26.5	27.8	27.2
Interorbital width	31.7	31.9	31.8	28.2	31.4	29.7	29.5	34.7	31.4	26.1	34.4	30.7	34.3	32.0	37.1	34.8	30.9	32.5	31.7
Head depth	64.0	66.2	65.1	56.4	62.6	59.4	69.7	78.7	74.5	64.1	76.5	68.6	69.5	67.2	75.6	70.6	66.2	67.0	66.6
Head width	49.0	54.3	51.6	38.9	49.5	43.9	44.5	52.3	49.5	42.1	54.1	49.0	48.5	45.4	55.8	51.0	49.1	52.9	51.0

Coloration. In life, body brightly colored, males more colorful than females. Ten to thirteen irregular blue-green cross-bars separated by pale cross-bars on the flanks. In adult male, uniform narrow pale pink cross-bars on trunk and two on caudal peduncle widening significantly; upper and lateral sides of head grayish and transitioning to orange-red on ventral side and lower margin of cheek. Dorsal fin rays transparent and membrane black-grey with orange margin. Anal fin and caudal fin rays transparent, membrane pale yellow or colorless. Pectoral fins orange and pelvic fins yellow (Fig. 3A). In females, narrow bright yellow bars on trunk and always absent on caudal peduncle. Dorsal fin black-grey. Pectoral fin orange yellow. Pelvic fin, anal fin and caudal fin transparent and colorless (Fig. 3B). In 10% formalin-fixed specimens, dorsal and flank of head and body grayish brown; ventral surface of head and abdomen white to yellowish. Dorsal and caudal fin dark gray. Pectoral, pelvic and caudal fin grayish white (Fig. 2).

Table 3. Meristic counts of the three sympatric *Opsariichthys* species and its congeners that absence of distinct anterior notch on upper lip.

Species	D iii			A iii				P1 i				P2 i		
	7	8	M	8	9	10	M	13	14	15	M	7	8	M
O. iridescens sp. nov.	16	–	7.0	–	16	–	9.0	1	15	–	13.9	2	14	7.9
O. bidens	10	–	7.0	1	9	–	8.9	–	10	–	14.0	–	10	8.0
O. evolans	17	–	7.0	–	16	1	9.1	1	15	1	14.0	3	14	7.8
*O. acutipinnis**	9	–	7.0	–	9	–	9.0	–	1	8	14.9	–	9	8.0
*O. duchuunguyeni**	5	–	7.0	–	5	–	9.0	–	4	1	14.2	1	4	7.9
*O. kaopingensis**	118	–	7.0	3	115	–	9.0	5	147	72	14.3	210	14	8.1
*O. macrolepis**	30	–	7.0	–	30	–	9.0	–	30	–	14.0	15	15	7.5
*O. pachycephalus**	421	2	7.0	17	398	12	9.0	251	251	38	13.6	251	123	8.3

Species	CPS						LLa					LLb			
	16	17	18	19	20	M	8	9	10	11	M	3	4	5	M
O. iridescens sp. nov.	5	11	–	–	–	16.7	–	7	9	–	9.6	3	13	–	3.8
O. bidens	–	2	7	1	–	17.9	–	10	–	–	9.0	3	6	1	3.8
O. evolans	10	7	–	–	–	16.4	17	–	–	–	8.0	3	14	–	3.8
*O. acutipinnis**	–	–	2	6	1	18.9	2	7	–	–	8.8	1	8	–	3.9
*O. duchuunguyeni**	–	4	1	–	–	17.2	5	–	–	–	8.0	5	–	–	3.0
*O. kaopingensis**	–	1	1	1	1	18.5	–	95	17	–	9.2	104	7	–	3.1
*O. macrolepis**	–	15	15	–	–	17.5	30	–	–	–	8.0	30	–	–	3.0
*O. pachycephalus**	–	1	4	3	5	18.9	–	–	251	38	10.1	251	20	–	3.1

Species	PreD											
	13	14	15	16	17	18	19	20	21	22	23	M
O. iridescens sp. nov.	–	–	–	–	–	2	5	7	2	–	–	19.6
O. bidens	–	–	–	–	–	–	3	5	2	–	–	19.9
O. evolans	–	–	2	10	5	–	–	–	–	–	–	16.2
*O. acutipinnis**	–	–	1	5	3	–	–	–	–	–	–	16.2
*O. duchuunguyeni**	1	4	–	–	–	–	–	–	–	–	–	13.8
*O. kaopingensis**	–	–	–	–	7	47	60	–	–	–	–	18.6
*O. macrolepis**	–	–	–	–	12	9	9	–	–	–	–	17.9
*O. pachycephalus**	–	–	–	–	–	–	–	90	139	89	25	21.1

Species	LL														
	41	42	43	44	45	46	47	48	49	50	51	52	53	54	M
O. iridescens sp. nov.	–	–	–	–	1	2	1	4	4	1	1	2	–	–	48.6
O. bidens	–	–	–	–	2	6	2	–	–	–	–	–	–	–	46.0
O. evolans	–	1	7	3	6	–	–	–	–	–	–	–	–	–	43.8
*O. acutipinnis**	–	7	2	–	–	–	–	–	–	–	–	–	–	–	42.2
*O. duchuunguyeni**	5	–	–	–	–	–	–	–	–	–	–	–	–	–	41.0
*O. kaopingensis**	–	–	–	13	84	66	57	2	–	–	–	–	–	–	45.8
*O. macrolepis**	–	–	–	–	–	15	10	4	1	–	–	–	–	–	46.7
*O. pachycephalus**	–	–	–	–	–	–	–	2	59	121	129	137	120	108	51.7

M: mean of all listed values; *: data cited from the literature.

Distribution. The new species is only found in Qiantang and Oujiang River systems in Zhejiang Province and the tributaries of the lower Yangtze River adjacent to the Qiantang River.

Habitat. The new species lives in the headwaters of streams with moderate flow velocities and clear water with small to medium-sized pebbles and boulders in the substrate (Fig. 4).

Etymology. *Iridescens* is the Latin form of the word iridescent. Here, it refers to the unique body color, which is brighter than that of any known species in the genus. In this study, we propose the Chinese common name Hóng Cǎi Mǎ Kǒu Yú (虹彩马口鱼).

Table 4. Morphological differences among eight *Opsariichthys* species that absence of distinct anterior notch on upper lip.

Character	*O. iridescens* sp. nov.	*O. evolans*	*O. acutipinnis**	*O. chengtui**	*O. duchuunguyeni**	*O. kaopingensis**	*O. macrolepis**	*O. pachycephalus**
Lateral-line scales	45−52	42−45	42−43	60−67	41	44−48	46−49	48−54
Scales above the lateral line	9−10	8	8−9	11	8	9−10	8	10−11
Predorsal scales	18−21	15−17	15−17	25−26	13−14	17−19	17−19	20−23
Circum-peduncular scales	16−17	16−17	18−20	21−22	17	17−20	17−18	17−20
Pharyngeal teeth	2 rows	3 rows	3 rows	2 rows	3 rows	3 rows	2 rows	3 rows
Whether the maxillary extending the vertical of anterior margin of orbit	Extending to or slightly beyond	Not reaching to or slightly extending	Extending	Extending	Extending to or slightly beyond	Reaching or slightly beyond	Not reaching	Extending to or beyond the middle vertical of orbit
Whether the pectoral extends to the origin of the pelvic fin	Slightly extending	Extending far beyond	Never reaching	Never reaching	Not reaching or slightly extending	Never reaching	Not reaching or slightly extending	Never reaching
Features of the bright bars on the flanks	Uniform and narrow on the trunk and widening significantly on the caudal peduncle	Gradually widened	Gradually widened	Gradually widened	Gradually widened	Uniform on the trunk and wider on the caudal peduncle	Gradually widened	Gradually widened
The number of tubercles on the lower jaw of adult males	1 row, united basally to form a plate in males	1 row, well separated	1 row, well separated	1 row, well separated	2 rows, well separated	1 row, well separated	2 or 3 rows, well separated	1 row, well separated

*: data cited from literature.

Morphological analysis

PCA was performed on three *Opsariichthys* species based on the morphological data. Fig. 5 shows the principal component score plot. The cumulative contribution of PC1 and PC2 was 79.28%, which represents most of the information in the original data. The contribution rate of PC1 was 58.63%, and the eigenvalue was 23.34, which was the highest contribution to the model. The contribution rate of PC2 was 20.65%, and the eigenvalue was 4.09. In the principal component score plot, *O. evolans* was mainly clustered on the negative side of the origin of the PC1 axis, whereas the new species and *O. bidens* were mainly distributed on the origin of the PC1 axis and on the positive side, so that the three species could be clearly distinguished from each other.

Through typical discriminant analysis, a table of coefficients of typical discriminant functions related to the morphological data was obtained, and two typical discriminant functions were established. The eigenvalues of the two typical discriminant functions were 23.343 and 4.085, and their variance contribution rates were 85.1% and 14.9%, respectively. According to the two discriminant functions, the scores of different *Opsariichthys* species were calculated, and scatter plots of the scores of different *Opsariichthys* species were obtained by using these two discriminant functions as horizontal and vertical coordinates, respectively (Fig. 6). As shown in the scatter plot, none of the three species overlapped, suggesting that they are different species.

Figure 4. Image of the habitat of *Opsariichthys iridescens* sp. nov., near riverbed with stones.

Molecular phylogenetic analysis

In this study, a total of 72 Cyt *b* gene sequences from 27 species of the opsariichthine group were used, and two additional Cyt *b* sequences from *Aphyocypris chinensis* were used as outgroups. Based on the length heterogeneity of the sequences from GenBank, four sequences were compared to obtain a sequence length of 913 bp for *Z. platypus*, *Opsariichthys* sp. A, *O. acutipinnis*, and *O. duchuunguyeni*, and the remaining 68 opsariichthine group sequences were 1140 bp in length. The base frequencies (excluding outgroups) were A = 25.6%, C = 28.1%, G = 16.2%, and T = 30.1%. The content of A+T (55.7%) was significantly greater than that of G+C (44.3%), which was basically consistent with the characteristics of the mitochondrial genes of fish that have high A and T contents and low G and C contents. There were 672 conserved sites, accounting for 58.9% of the total number of sites; 468 mutated sites, accounting for 41.1% of the total number of sites; 74 single mutated sites, accounting for 6.5% of the total number of sites; and 394 parsimony informative sites, accounting for 34.6% of the total number of sites. The conversion ratio of the sequence was 3.03.

The phylogenetic tree of the opsariichthine group was reconstructed based on the NJ, BI, and ML analyses, and all three trees had a consistent topology despite the differences in support at some branches. Here, we only show the topology of the NJ tree while adding the self-expanding support of the BI and ML trees at the nodes. The topology of the NJ tree (Fig. 7) shows that *Opsariichthys* and *Zacco* form a monophyletic group and are sister groups to each other. The new monophyly species clustered in the *Opsariichthys* group, was located at the base of the genus, and formed a sister group with other *Opsariichthys* species with the support of 82/96/0.97 (NJ/ML/BI).

The genetic distances among the species of the opsariichthine group were calculated based on a K2P model. The genetic distances among the new species and the congeneric species and lineages ranged from 0.143 to 0.186, and those among the inter-genus species ranged from 0.144 to 0.193. Among them, the smallest
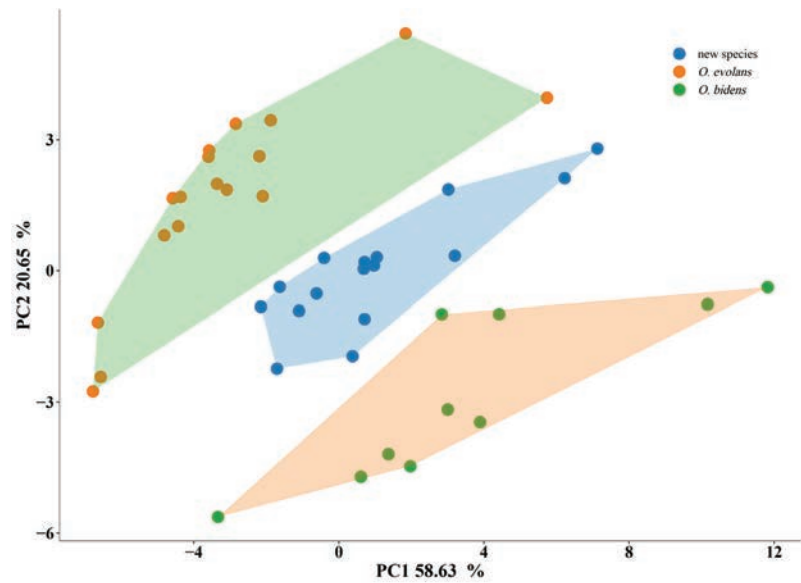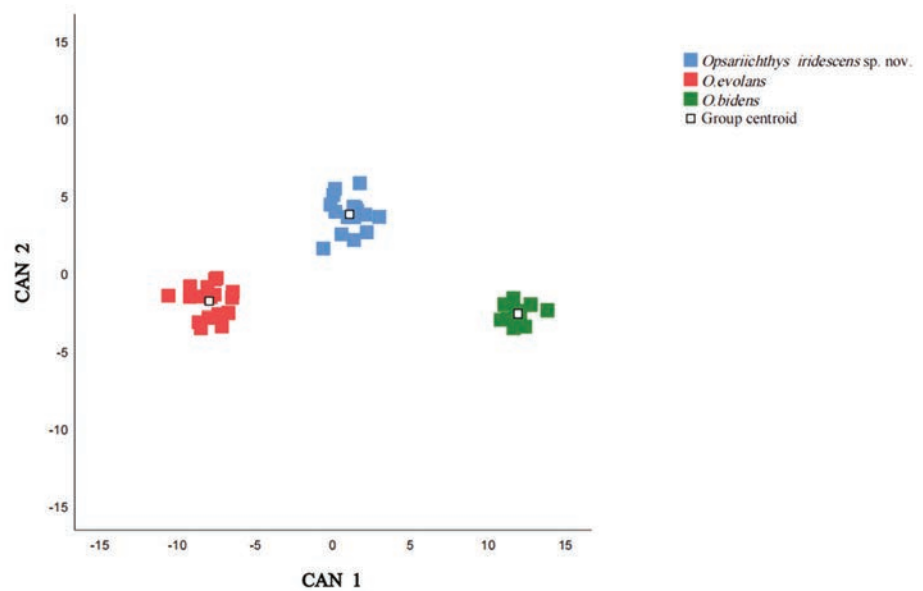
Figure 5. PCA score plots for PC1 and PC2.

Figure 6. Canonical discriminant score plot for the three species of *Opsariichthys*.

genetic distance from the new species was observed for *Opsariichthys* sp. D, with a value of 0.143, while the greatest genetic distance from the new species was observed for *Parazacco spilurus*, with a value of 0.193 (Table 5).

Diagnostic key to *Opsariichthys* species

1	Absence of distinct anterior notches on the upper lip; lateral jaws relatively straight	**2**
–	Presence of a distinct anterior notch on the upper lip; lateral jaws undulated	**9**
2	2 rows of pharyngeal teeth	**3**
–	3 rows of pharyngeal teeth	**5**

3 Fewer than 60 lateral-line scales...**4**

– More than 60 lateral-line scales ......***O. chengtui* (the upper Yangtze River)**

4 2 or 3 rows with 15–21 rather small, rounded tubercles in total that are well separated on the lower jaw in males; body with 11–13 greenish blue stripes of almost equal width in males.........***O. macrolepis* (the upper Yangtze River)**

– Single row of 3–6 rather large, rounded tubercles on the lower jaw of males, united basally to form a plate; 10–13 pale pink strips on the body of males, uniform and narrow on the trunk and widening significantly on the caudal peduncle ....***O. iridescens* sp. nov. (southeast China)**

5 Fewer than 42 lateral−line scales; 13 or 14 predorsal scales; 3 scales below the lateral line; very narrow body width; 2 rows with 12−15 rather large and rounded tubercles on the lower jaw in adult males ....
.... ***O. duchuunguyeni* (northern Vietnam)**

– More than 42 lateral-line scales; 15−17 predorsal scales; 4 scales below the lateral line modally; a rather narrow to thick body width; a series of 4−7 rounded tubercles on lower jaw in adult males..**6**

6 42−45 lateral-line scales; 15−17 predorsal scales; a rather narrow body width; maxillary that does not extend to or slightly reaches the vertical anterior margin of the orbit; pectoral fin reaching or extending far beyond the origin of the ventral fin **7**

– More than 45 lateral-line scales; 18−23 predorsal scales; rather thick body width; maxillary that extends to or far beyond the vertical anterior margin of the orbit; pectoral fin that does not extend beyond the origin of the ventral fin **8**

7 18−20 circum-peduncular scales; 15 pectoral fin rays modally; maxillary that extends to the vertical anterior margin of the orbit; a pectoral fin that does not extend to the origin of the ventral fin; 9 scales above the lateral line modally..***O. acutipinnis* (southern China)**

– 16 or 17 circum-peduncular scales; 14 pectoral fin rays modally; maxillary that does not extend to the vertical anterior margin of the orbit; pectoral fin that extends far beyond the origin of the ventral fin; 8 scales above the lateral line modally ....
....................***O. evolans* (northern Taiwan Island, eastern mainland China)**

8 More than 48 lateral-line scales (mode 50−54); 20−23 predorsal scales; 40 or 41 vertebrae; maxillary that extends to or beyond the vertical midline of the orbit in females; opercle and ventral side of head orange-red to pink-red in adult males ....
..............***O. pachycephalus* (northern, middle and western Taiwan Island)**

– 40−45 lateral-line scales (mode 45−47); 18 or 19 predorsal scales; 39 vertebrae; maxillary that extends to or slightly beyond the vertical anterior margin of orbit in females; opercle and ventral side of head bright yellow in adult males .... ***O. kaopingensis* (southern Taiwan Island)**

9 Fewer than 50 lateral-line scales; 8−10 scales above the lateral line......**10**

– More than 50 lateral-line scales; 10−12 scales above the lateral line.........
.... ***O. uncirostris* (Japan and Korea)**

10 45−50 lateral-line scales; rounded tubercles on lower jaw rather small and arranged in 3 rows in males...**11**

– 40−43 lateral-line scales; rounded tubercles on lower jaw rather large and arranged in 2 or 3 rows in males **13**

11   45−47 lateral-line scales; 8 or 9 scales above lateral line; 17−19 circum-peduncular scales; 40−42 vertebrae...**12**

–   46−50 lateral-line scales; 9 or 10 scales above lateral line; 19 or 20 circum-peduncular scales; 38 or 39 vertebrae ..... ***O. amurensis* (Amur River)**

12   19−21 predorsal scales; 9 scales above lateral line; 41 or 42 vertebrae ....***O. bidens* (northern and east China)**

–   16−18 predorsal scales; 8 scales above lateral line modally; 40 or 41 vertebrae .... ***O. minutus* (southern China)**

13   41−43 lateral-line scales (mode 42); 15 or 16 predorsal scales modally; rounded tubercles large or small arranged in 2 or 3 rows; rather small head; body strongly laterally compressed at position of anal fin origin 14

–   40 or 41 lateral-line scales (mode 41); 17 predorsal scales modally; rounded tubercles on lower jaw rather large and arranged in 2 rows; rather large head; body rather wide at anal fin origin ......***O. hainanensis* (Hainan Island)**

14   13−15 pectoral fin rays (mode 14); 16−19 caudal peduncle scales (mode 17); 15−18 predorsal scales (mode 16); 14−16 anterior scales before pelvic origin (mode 15); rounded tubercles on lower jaw rather large and arranged in 3 rows in males; body with 14 greenish blue cross-bars in males; maxillary that extends to vertical midline of orbit in females; snout length of approximately 32−33% in males; interorbital width of approximately 30% in males......................................***O. dienbienensis* (northern Vietnam)**

–   13 or 14 pectoral fin rays (mode 13); 18 caudal peduncle scales modally; 15−18 predorsal scales (mode 15); 13−15 anterior scales before the pelvic origin (mode 14); rounded tubercles on lower jaw rather small and arranged in 2 or 3 rows in males; body with 13 greenish blue cross-bars in males; maxillary does not extend to vertical midline of orbit in females; snout length of approximately 30% in males; interorbital width of approximately 27−28% in males................***O. songmaensis* (Ma River of Vietnam)**

Discussion

For a long time, the genus *Opsariichthys* was thought to include only one species, *O. bidens*, which was widely distributed in East Asia (Chen 1982; Chen and Chu 1998). With the help of modern molecular techniques, the nuptial tubercles on the cheeks of males and the lateral cross-bars on the body, which were first identified by Chen et al. (2009) and later confirmed by Huang et al. (2017), were found to be the key diagnostic features distinguishing this genus from its sister genus *Zacco*. Thus, the taxonomy of the two genera gradually became clearer. Therefore, based on the stripe features and phylogeny of this study, we ascribe *O. iridescens* sp. nov. to the genus *Opsariichthys*. In addition, based on geographic distribution, the results of morphological and PCA analyses also indicated the validity of the new species. With many independent rivers and diverse habitats, southeast mainland China is rich in freshwater fish species, and some species have a common distribution with northern Taiwan, including *O. evolans*, which was used for the comparison in this study. According to our investigations, in addition to the new species, only *O. bidens* and *O. evolans* are found in Zhejiang Province, north of the Wuyi Mountains, and are distinct from the other congeners. Based on our observations, all *Opsariichthys* species can be divided into two types: one with a large mouth, a conspicuous anterior notch on the upper lip, and undulated jaws;

Table 5. Nucleotide distances between the opsariichthine group species based on the K2P model.

|	1	2	3	4	5	6	7	8	9	10	11	12	13	14	15	16	17	18	19	20	21	22	23	24	25	26	27
O. iridescens sp. nov.																											
O. bidens	0.146																										
O. evolans	0.144	0.138																									
O. acutipinnis	0.146	0.126	0.055																								
O. chengtui	0.150	0.158	0.098	0.110																							
O. duchuunguyeni	0.186	0.155	0.128	0.128	0.117																						
O. hainanensis	0.152	0.144	0.089	0.109	0.106	0.141																					
O. kaopingensis	0.149	0.133	0.092	0.095	0.099	0.144	0.101																				
O. macrolepis	0.147	0.135	0.072	0.074	0.093	0.119	0.099	0.087																			
O. minutus	0.162	0.154	0.099	0.114	0.109	0.143	0.082	0.105	0.107																		
O. pachycephalus	0.144	0.148	0.099	0.115	0.101	0.144	0.106	0.051	0.101	0.094																	
O. uncirostris	0.170	0.074	0.156	0.144	0.163	0.184	0.152	0.145	0.148	0.159	0.155																
Opsariichthys sp. A	0.155	0.136	0.046	0.060	0.117	0.131	0.100	0.089	0.079	0.110	0.106	0.159															
Opsariichthys sp. B	0.147	0.142	0.062	0.061	0.088	0.120	0.097	0.100	0.069	0.100	0.098	0.158	0.068														
Opsariichthys sp. C	0.150	0.147	0.077	0.087	0.095	0.121	0.104	0.095	0.059	0.096	0.097	0.159	0.091	0.074													
Opsariichthys sp. D	0.143	0.147	0.076	0.091	0.100	0.115	0.097	0.096	0.053	0.103	0.105	0.165	0.092	0.072	0.052												
Opsariichthys sp. E	0.153	0.138	0.077	0.088	0.095	0.117	0.102	0.102	0.041	0.104	0.105	0.152	0.094	0.071	0.065	0.070											
Z. acanthogenys	0.147	0.164	0.164	0.171	0.164	0.188	0.167	0.160	0.157	0.183	0.162	0.178	0.173	0.166	0.162	0.164	0.170										
Z. platypus	0.146	0.154	0.157	0.150	0.156	0.173	0.172	0.155	0.155	0.176	0.166	0.167	0.162	0.165	0.164	0.170	0.172	0.085									
Z. sinensis	0.149	0.154	0.156	0.148	0.154	0.173	0.160	0.158	0.143	0.172	0.160	0.169	0.164	0.163	0.167	0.167	0.164	0.076	0.043								
Z. tiaoxiensis	0.144	0.164	0.165	0.165	0.163	0.184	0.171	0.152	0.153	0.187	0.162	0.177	0.164	0.170	0.162	0.170	0.168	0.046	0.081	0.080							
P. fasciatus	0.192	0.209	0.194	0.202	0.194	0.240	0.183	0.189	0.202	0.216	0.206	0.216	0.195	0.193	0.214	0.195	0.200	0.206	0.198	0.205	0.197						
P. spilurus	0.193	0.202	0.204	0.212	0.209	0.254	0.189	0.214	0.198	0.214	0.211	0.221	0.203	0.190	0.212	0.200	0.207	0.196	0.198	0.196	0.195	0.107					
N. sieboldii	0.182	0.184	0.192	0.194	0.187	0.221	0.174	0.181	0.188	0.205	0.188	0.192	0.184	0.190	0.192	0.186	0.190	0.168	0.171	0.187	0.172	0.165	0.163				
N. temminckii	0.171	0.180	0.186	0.185	0.185	0.207	0.184	0.181	0.191	0.200	0.194	0.190	0.179	0.191	0.192	0.181	0.197	0.161	0.163	0.169	0.161	0.176	0.165	0.126			
C. barbatus	0.172	0.196	0.182	0.186	0.181	0.213	0.185	0.194	0.188	0.195	0.198	0.213	0.185	0.166	0.182	0.173	0.193	0.166	0.164	0.171	0.169	0.168	0.163	0.141	0.130		
C. pingtungensis	0.187	0.207	0.198	0.204	0.209	0.229	0.209	0.202	0.196	0.218	0.209	0.210	0.200	0.196	0.199	0.183	0.200	0.180	0.172	0.190	0.180	0.178	0.183	0.159	0.154	0.097	
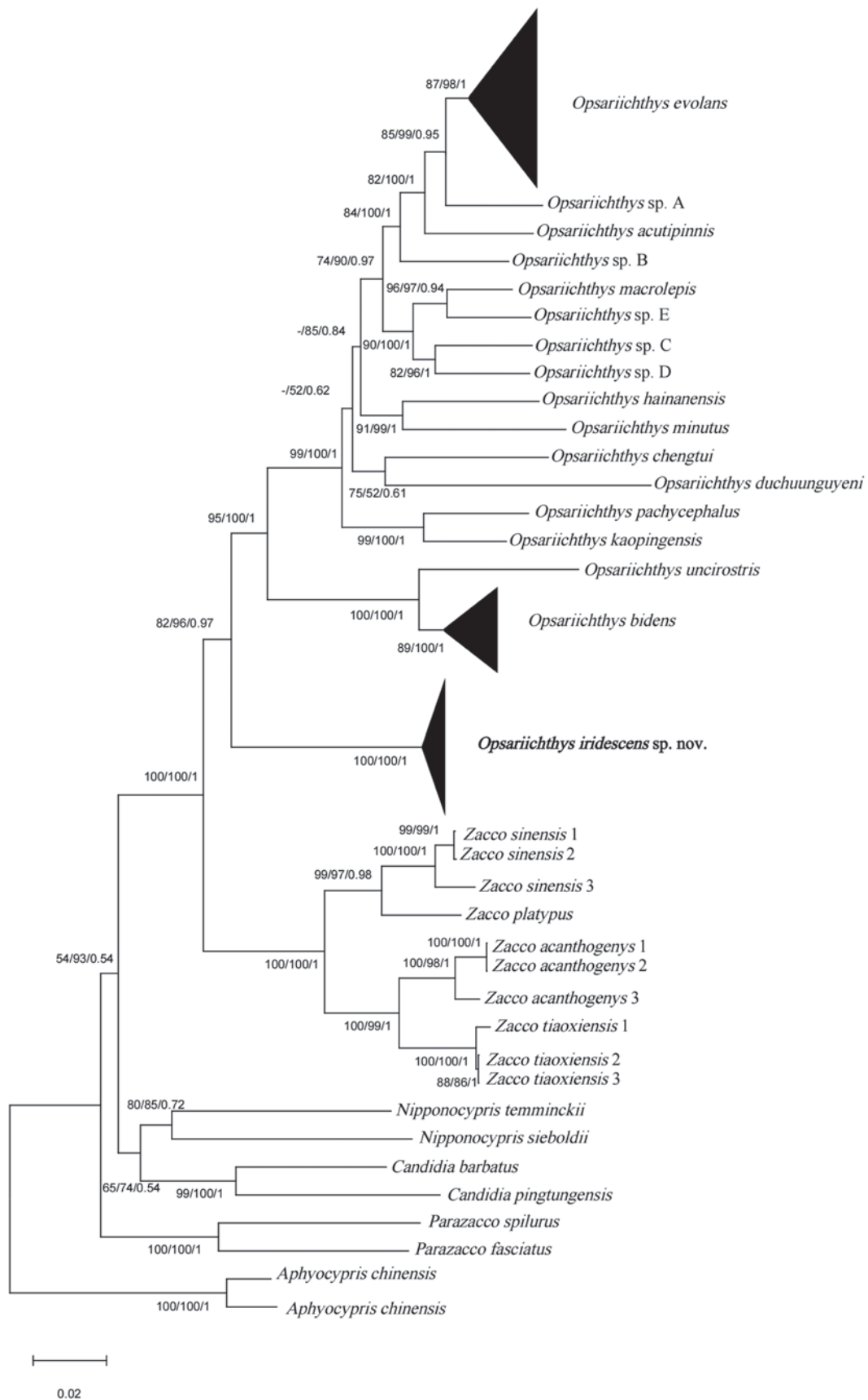
Figure 7. Phylogenetic relationships of opsariichthine derived from the NJ tree based on the Cyt *b* gene sequences; the values at the nodes correspond to the support values for the NJ/ML/BI methods. '-' indicates that the value is less than 50%.

and another with a small mouth, no distinct anterior notch on the upper lip, and relatively straight jaws. These two types are morphological adaptations to feeding habits, carnivores and omnivores, respectively. The new species belongs to the latter; however, the phylogenetic analysis in this study shows that the two types do not form monophyletic groups, indicating that mouth shape may be a derived evolutionary trait. In addition to the difference in scale numbers (Table 3), the new species also has several obvious morphological features that distinguish it from other species in the same group: 1) the nuptial tubercles on the cheeks and lower jaw of the adult males were united basally to form a plate, similar to the species of *Zacco*; 2) two rows of pharyngeal teeth; and 3) the narrow, pale, lateral cross-bars that are almost uniform in width on the trunk and widening significantly on the caudal peduncle (Table 4). In the diagnostic key for *Opsariichthys* species presented above the data for all but three species was obtained from published sources (Yang and Huang 1964; Chen et al. 2009; Huynh and Chen 2013; Wang et al. 2019).

Wang et al. (2019) used a 3% Cyt *b* gene genetic distance to delimit the opsariichthine fish species, identified 20 haplogroups of *Opsariichthys*, and reported that the species diversity of this genus was underestimated. The new species reported herein does not belong to any of the haplogroups in Wang et al. (2019), and its genetic distance from both congeneric and intergeneric species exceeds 14%, which is much greater than their 3% limit (see Table 5). Our phylogenetic results are consistent with the results of previous studies (Huang et al. 2017; Wang et al. 2019; Zhang et al. 2023) (Fig. 7). *Opsariichthys* and *Zacco*, which both have lateral cross-bars, are both monophyletic and form separate clades, which supports the use of stripes as key diagnostic features for distinguishing them. Moreover, *O. iridescens* sp. nov., as a monophyletic group, is located at the base of all *Opsariichthys* species. In conclusion, the genetic distance and phylogenetic analyses support morphological distinctiveness and the validity of the new species.

Comparative materials

O. evolans: SHOU2021060004-006, 3 specimens, 67.5–112.0 mm SL, She County, Qiantang River System, Anhui Province, China; SHOU2021060091, 1 specimen, 103.3 mm SL, Suichang County, Qiantang River System, Zhejiang Province, China; SHOU2021060145, 1 specimen, 83.5 mm SL, Qingyuan County, Ou River System, Zhejiang Province, China; SHOU202208005-006, 2 specimens, 71.4–77.5 mm SL, Shangyu District, Cao'e River System, Zhejiang Province, China; SHOU202208031-040, 10 specimens, 71.2–84.0 mm SL, Shengzhou City, Cao'e River System, Zhejiang Province, China.

O. bidens: SHOU202209008-012, 5 specimens, 76.1–100.6 mm SL, Qingyuan County, Ou River System, Zhejiang Province, China; SHOU202111001-005, 5 specimens, 99.6–131.6 mm SL, Shengzhou City, Cao'e River System, Zhejiang Province, China.

Acknowledgments

Additional information

Conflict of interest

The authors have declared that no competing interests exist.

Ethical statement

No ethical statement was reported.

Funding

Author contributions

Conceptualization: HDG. Data curation: XP. Funding acquisition: JQY. Investigation: JJZ. Resources: JJZ. Visualization: HDG. Writing – original draft: XP. Writing – review and editing: JQY.

Author ORCIDs

Jia-Jun Zhou https://orcid.org/0000-0003-1038-1540
Hong-Di Gao https://orcid.org/0009-0004-6891-3209
Jin-Quan Yang https://orcid.org/0000-0003-0387-1824

Data availability

All of the data that support the findings of this study are available in the main text.

References

Bănărescu P (1968) Revision of the genera *Zacco* and *Opsariichthys* (Pisces, Cyprinidae). Vestnik Ceskoslovenske Spolecnosti Zoologicke 32: 305–311.

Berrebi P, Boissin E, Fang F, Cattaneo-Berrebi G (2005) Intron polymorphism (EPIC-PCR) reveals phylogeographic structure of *Zacco platypus* in China: A possible target for aquaculture development. Heredity 94: 589. https://doi.org/10.1038/sj.hdy.6800660

Burland TG (2000) DNASTAR's Lasergene sequence analysis software. Methods in Molecular Biology (Clifton, N.J.) 132: 71–91. https://doi.org/10.1385/1-59259-192-2:71

Chen YY (1982) A revision of opsariichthine cyprinid fishes. Oceanologi Et Limnologia Sinica 13: 293–298. [In Chinese]

Chen IS, Chang YC (2005) The photographic guide of inland water fishes of Taiwan. VoI. I. Cypriniformes. Sheichuan Press, Keelung, 14–49. [In Chinese]

Chen YY, Chu XL (1998) Danioninae. In: Chen YY (Ed.) Fauna Sinica (Osteichtyes: Cypriniformes II). Science Press, Beijing, 40–49. [In Chinese]

Chen IS, Wu JH, Huang SP (2009) The taxonomy and phylogeny of the cyprinid genus *Opsariichthys* Bleeker (Teleostei: Cyprinidae) from Taiwan, with description of a new species. Environmental Biology of Fishes 86(1): 165–183. https://doi.org/10.1007/s10641-009-9499-y

Darriba D, Taboada GL, Doallo R, Posada D (2012) jModelTest 2: more models, new heuristics and parallel computing. Nature Methods 9(8): 772. https://doi.org/10.1038/nmeth.2109

Fricke R, Eschmeyer WN, Van der Laan R (2024) Eschmeyer's catalog of fishes: genera, species, references. http://researcharchive.calacademy.org/r-search/ichthyology/catalog/fishcatmain.asp [Electronic version accessed 2024]

Huang SP, Wang FY, Wang TY (2017) Molecular phylogeny of the *Opsariichthys* Group (Teleostei: Cypriniformes) based on complete mitochondrial genomes. Zoological Studies 56: 1–13. https://doi.org/10.1016/j.bse.2015.11.004

Huynh TQ, Chen IS (2013) A new species of cyprinid fish of genus *Opsariichthys* from Ky Cung-Bang Giang river basin, northern Vietnam with notes on the taxonomic status of the genus from northern Vietnam and southern China. Journal of Marine Science and Technology 21: 135–145.

Jordan DS, Evermann BW (1902) Notes on a collection of fishes from the island of Formosa. Proceedings of the United States National Museum 25(1289): 315–368. https://doi.org/10.5479/si.00963801.25-1289.315

Minh BQ, Schmidt HA, Chernomor O, Schrempf D, Woodhams MD, von Haeseler A, Lanfear R (2020) IQ-TREE 2: New models and efficient methods for phylogenetic inference in the genomic era. Molecular Biology and Evolution 37(5): 1530–1534. https://doi.org/10.1093/molbev/msaa015

Perdices A, Coelho MM (2006) Comparative phylogeography of *Zacco platypus* and *Opsariichthys bidens* (Teleostei, Cyprinidae) in China based on cytochrome *b* sequences. Journal of Zoological Systematics and Evolutionary Research 44: 330–338. https://doi.org/10.1111/j.1439-0469.2006.00368.x

Perdices A, Cunha C, Coelho MM (2004) Phylogenetic structure of *Zacco platypus*, (Teleostei, Cyprinidae) populations on the upper and middle Changjiang (=Yangtze) drainage inferred from cytochrome *b* sequences. Molecular Phylogenetics and Evolution 31: 192–203. https://doi.org/10.1016/j.ympev.2003.07.001

Perdices A, Sayanda D, Coelho MM (2005) Mitochondrial diversity of *Opsariichthys bidens* (Teleostei, Cyprinidae) in three Chinese drainages. Molecular Phylogenetics and Evolution 37: 920–927. https://doi.org/10.1016/j.ympev.2005.04.020

Rambaut A (2016) Figtree, a graphical viewer of phylogenetic trees. http://tree.bio.ed.ac.uk/software/gtree

Ronquist F, Teslenko M, van der Mark P, Ayres DL, Darling A, Höhna S, Larget B, Liu L, Suchard MA, Huelsenbeck, JP (2012) MrBayes 3.2: efficient Bayesian phylogenetic inference and model choice across a large model space. Systematic Biology 61(3): 539–542. https://doi.org/10.1093/sysbio/sys029

Tamura K, Stecher G, Kumar S (2021) MEGA11: Molecular Evolutionary Genetics Analysis Version 11. Molecular Biology and Evolution 38(7): 3022–3027. https://doi.org/10.1093/molbev/msab120

Wang X, Liu F, Yu D, Liu HZ (2019) Mitochondrial divergence suggests unexpected high species diversity in the opsariichthine fishes (Teleostei: Cyprinidae) and the revalidation of *Opsariichthys macrolepis*. Ecology and Evolution 9(5): 2664–2677. https://doi.org/10.1002/ece3.4933

Xiao WH, Zhang YP, Liu HZ (2001) Molecular systematics of Xenocyprinae (Teleostei: Cyprinidae): taxonomy, biogeography, and coevolution of a special group restricted in east Asia. Molecular Phylogenetics and Evolution 18(2): 163–173. https://doi.org/10.1006/mpev.2000.0879

Yang GR, Huang HJ (1964) Leuciscinae. In: Wu XW (Ed.) The Cyprinids fishes of China (I). Shanghai People's Press, Shanghai, 40–47. [In Chinese]

Zhang Y, Zhou JJ, Yang JQ (2023) A new species of genus *Zacco* from southern China (Cypriniformes: Cyprinidae). Journal of Shanghai Fisheries University 32(3): 544–552. https://doi.org/10.12024/jsou.20220703918 [In Chinese]

ZooKeys

Review of *Asaphes* Walker, 1834 (Hymenoptera, Chalcidoidea, Asaphesinae) from Xinjiang, China

Qin Li[1,2*], Tong-You Zhang[1,2], Gary A. P. Gibson[3], Shi-Lei Shan[1,2], Hui Xiao[4]

1 College of Life Science and Technology, Xinjiang University, 666 Shengli Road, Tianshan District, Urumqi, Xinjiang, 830046, China
2 Xinjiang Key Laboratory of Biological Resources and Genetic Engineering, 666 Shengli Road, Tianshan District, Urumqi, Xinjiang, 830046, China
3 Honorary Research Associate, Agriculture and Agri-Food Canada, Canadian National Collection of Insects, Arachnids and Nematodes, K. W. Neatby Bldg., 960 Carling Avenue, Ottawa, Ontario, K1A0C6, Canada
4 Key Laboratory of Zoological Systematics and Evolution, Institute of Zoology, Chinese Academy of Sciences, Beijing, 100101, China
Corresponding author: Hui Xiao (xiaoh@ioz.ac.cn)

Abstract

Four species of the cosmopolitan genus *Asaphes* Walker, 1834 (Hymenoptera: Chalcidoidea: Asaphesinae, family incerta sedis) are recorded from Xinjiang Uyghur Autonomous Region, China, bringing the number of known species in China to eight. In addition to *Asaphes suspensus* (Nees ab Esenbeck), 1834 and *A. vulgaris* Walker, 1834, *A. fuyunis* Li & Zhang, **sp. nov.** is newly described based on females and *A. californicus* Girault, 1917, previously known only from North and South America, is newly recorded from China. These four species are differentiated using an integrative taxonomic approach that includes COI barcode data and morphometrics, and are illustrated using macrophotography. Additionally, the 13 described world species of *Asaphes* are tabulated and females of the eight recognized Chinese species are keyed.

Key words: *Asaphes*, COI, integrative taxonomy, morphometrics, Xinjiang

Introduction

Asaphes Walker, 1834 is one of three genera recognized in Asaphesinae by Burks et al. (2022), the other two being *Hyperimerus* Girault, 1917 and *Coriotela* Burks & Heraty, 2020. Both *Asaphes* and *Hyperimerus* are cosmopolitan, whereas *Coriotela* is an extinct genus described from Eocene Baltic amber (Burks and Heraty 2020). The subfamily was historically treated in the family Pteromalidae (Hymenoptera: Chalcidoidea) as Asaphinae prior to Burks and Heraty (2020) providing the new name Asaphesinae when they discovered Asaphinae was a junior homonym of a trilobite family. Subsequently, Burks et al. (2022) removed Asaphesinae from Pteromalidae and treated it as family *incertae sedis* based on the molecular results of Cruaud et al. (2024). Most species of *Asaphes* are hyperparasitoids of aphids (Hemiptera: Aphididae), parasitizing primary hymenopteran parasitoids, including Aphidiinae (Braconidae), *Trechnites* spp. (Encyrtidae), and *Aphelinus* spp. (Aphelinidae) (Bouček 1988; Gibson and Vikberg 1998; de Boer et al. 2019; Kamel et al. 2020).

---

* These authors contributed to this work equally.

Prior to the present study, 12 valid world species of *Asaphes* were known (Noyes 2019), including six species from mainland China: *A. globularis* Xiao & Huang, 2000, *A. oculi* Xiao & Huang, 2000, *A. siciformis* Xiao & Huang, 2000, *A. suspensus* (Nees), 1834, *A. umbilicalis* Xiao & Huang, 2000, and *A. vulgaris* Walker, 1834 (Xiao and Huang 2000). Here, we increase the number of species from China to eight by describing one new species, *A. fuyunis* Li & Zhang, sp. nov., and a new record of *A. californicus* Girault, from Xinjiang Uyghur Autonomous Region of China. *Asaphes californicus* was previously reported only from North and South America (Gibson and Vikberg 1998, but our new record is based not only on morphological features using the available keys but also by COI molecular and morphometric evidence. A maximum likelihood (ML) tree by K2P distances based on COI sequences and morphometric evidence are provided to support the presence of the four *Asaphes* species in Xinjiang. Additionally, the 13 described world species of *Asaphes* are tabulated and females of the eight species recorded from China are keyed.

Materials and methods

Morphological studies

Specimens of the four herein treated species from China were collected by sweeping with a net in Xinjiang Uyghur Autonomous Region, 2020–2022, and preserved in 100% ethanol at -20 °C. All specimens are deposited in the Insect Collection of the College of Life Science and Technology, Urumqi, Xinjiang, China (**ICXU**). The **s**pecimens were air dried from ethanol, glued on triangular cards, and examined with a Nikon SMZ 745T stereomicroscope. Dried, point-mounted specimens of *A. californicus* from North America that were used for comparative studies were obtained from the Canadian National Collection of Insects, Arachnids and Nematodes, Ottawa, Canada (**CNC**), and are deposited in ICXU as voucher specimens. Images were taken with a Nikon DS-Fi3 camera connected to a Nikon SMZ 25 camera stereomicroscope. All images were stacked with NIS-Elements software and arranged in plates using Adobe Photoshop. All specimens were identified using Graham (1969), Kamijo and Takada (1973), Gibson and Vikberg (1998), Xiao and Huang (2000), and Narendran and van Harten (2007).

Morphological terms follow Bouček (1988) and Gibson (1997). Body length excludes the protruding parts of ovipositor sheaths and was measured in millimeters (mm); other measurements are given as ratios. Abbreviations of morphological terms used are:

ED	shortest distance between the inner margins of the eyes;	**mps**	multiporous plate sensilla,
EH	eye height;	**MV**	marginal vein;
EL	eye length;	**OOL**	shortest distance between eye margin and a posterior ocellus;
EW	eye width;		
Fu$_n$	antennal funicular 1, 2…;	**PMV**	postmarginal vein;
Gt$_n$	gastral tergite 1, 2…;	**POL**	shortest distance between posterior ocelli;
HL	head length;	**SMV**	submarginal vein;
HW	head width;	**STV**	stigmal vein.

Morphometrics

Forty morphometric variables of seventeen females (four of *A. californicus*, three of *A. fuyunis*, five of *A. suspensus*, and five of *A. vulgaris*) were included in the morphometrical analysis (Table 2). A Principal Components Analysis of the morphometric data in the ADEGENET package in R (Jombart et al. 2010) was conducted to distinguish the four species.

The following abbreviations are used for structures measured:

A_nL	length of anellus 1, 2…;	PDL	length of pedicel;
CL	length of clava;	PDW	width of pedicel;
CW	width of clava;	PFCL	combined length of pedicel and flagellum;
DL	length of dorsellum;		
DW	width of dorsellum;	PL	length of propodeum;
Fu_nL	length of funicle 1, 2…;	PRL	length of pronotum;
Fu_nW	width of funicle 1, 2…;	PRW	width of pronotum;
FRL	length of frenum;	PTL	length of petiole;
FWL	length of fore wing;	PTW	width of petiole;
FWW	width of fore wing;	PW	width of propodeum;
GL	length of gaster;	SCPL	length of scape;
Gt_nL	length of gastral tergite 1, 2…;	SCPW	width of scape;
GW	width of gaster;	SL	length of scutellum; -
IL	distance between the inner orbits in dorsal view;	SW	width of scutellum;
		TA	distance from dorsal margin of torulus to ventral margin of anterior ocellus;
MFL	length of metafemur;		
MFW	width of metafemur;	TC	distance from ventral margin of torulus to apical margin of clypeus;
ML	length of mesoscutum;		
MTAL	length of metatarsus;		
MTL	length of metatibia;		
MTW	width of metatibia;	TL	length of temple in dorsal view;
MW	width of mesoscutum;	UL	length of uncus of stigmal vein.

Acronyms for specimen depositories are as follows: **CNC**, Canadian National Collection of Insects, Arachnids and Nematodes, Ottawa, ON, Canada; **DZUC**, Department of Zoology, University of Calicut, Calicut, Kerala, India; **HOPE**, Hope Entomological Collection, Oxford, England; **ICXU**, Insect Collection of College of Life Science and Technology, Urumqi, Xinjiang, China; **IZCAS**, Institute of Zoology, Chinese Academy of Sciences, Beijing, China; **MZLU**, Lund Museum of Zoology, Lund, Scania, Sweden; **NHMUK** (formerly BMNH), Natural History Museum, London, England; **USNM**, US National Museum of Natural History, Washington, DC, USA.

DNA extraction, mtDNA COI amplification, and sequencing

Genomic DNA was extracted from either from individuals preserved in 100% ethanol at -20 °C (Chinese specimens) or dried, point-mounted specimens (*A. californicus*) through whole body extraction using a DNA extraction kit (TIANamp Genomic DNA Kit, China) following the manufacturer's protocol. In both processes the mixture of proteinase K and Buffer GA were the same

and both were held at a constant 56 °C temperature in a metal bath, but duration of the treatments differed. The specimens in ethanol were treated at for 5 h, whereas the dried, point-mounted specimens were treated for 12 h. PCR reaction mixture of 2 5µL was prepared with the following composition of 2× Taq Mix 12.5 µL, ddH$_2$O 5.5 µL, the forward primer 1 µL, the reverse primer 1 µL and DNA template 5 µL. The primers of mtDNA COI sequences for *Asaphes* were designed based on sequences of *Asaphes* and *Hyperimerus*, plus those of *Chlorocytus* Graham, 1956, *Dinarmus* Thomson, 1878 and *Mesopolobus* Westwood, 1833 (Pteromalidae: Pteromalinae) on GenBank (www.ncbi.nlm. nih.gov/Genbank) using the software DNAMAN 9.0.1.116 and SNAPGENE 4.1.9. DNAMAN 9.0.1.116 was used to proofread and analyze the specific single nucleotide polymorphism (SNP) site differences in the COI sequences and design specific primers for *Asaphes* by SNAPGENE 4.1.9. The forward primer and reverse primers, respectively, are: 5'- ACC TGT AAT AAT AGG AGG ATT TGG -3' and 5'- TAA TAG CTC CCG CTA AAA CTG GT-3'. Thermocycling conditions included an initial denaturing step at 95 °C for 4 min, followed by 42 cycles of 95° for 30 sec, 46° for 30 sec, 72° for 1 min and an additional extension at 72° for 10 min. Amplified products were secession on 1% agarose stained with Nucleic acid dye and visualized using a UV trans-illuminator. PCR products were purified and double stranded products were bidirectionally sequenced by Sangon Biotech.

Sequence data and phylogenetic analysis

Sequences from both directions were assembled and edited in BIOEDIT v. 7.0.5.3. The COI data set was chosen for phylogenetic analysis and was aligned using the Alignment (Align by Clustal W) multiple alignment program built in MEGA X with the default alignment parameters. Pairwise nucleotide sequence divergences were calculated using a Kimura 2-parameter (K2P) model of substitution (Kimura 1980) and construct the phylogenetic tree ML (Maximum likelihood) in MEGA X (Alajmi et al. 2020; Malagón-Aldana et al. 2022). The robustness of the node of the phylogenetic tree was estimated from 1,000 bootstrap replicates. Based on genetic distance and phylogenetic tree construction, molecular identification was conducted for further verify the results of morphological identification.

COI sequences of *A. vulgaris*, and Pteromalidae sp. as the out-group, were downloaded from NCBI. The details of the sequences are shown in the Table 1.

Table 1. Detailed information about NCBI-downloaded sequences of *A. vulgaris* and Pteromalidae sp.

GenBank accession	Morphospecies	Collectors	Collection site
ON704783.1	*Asaphes vulgaris*	Zhang, X	China, Ningxia, Yinchuan
KY912683.1	*Asaphes vulgaris*	Ye, Z., Vollhardt, I.M.G., Tomanovic, Z. and Traugott, M.	Austria, Tirol, Innsbruck
MT878057.1	Pteromalidae sp.	Woolley, V.C., Tembo, Y. and Ndakidemi, B., et al.	United Kingdom, Greenwich, London

Table 2. The main ratios measured for characters of female *Asaphes*.

No.	Ratio character	Number	Ratio character
1	FW/FH	21	PRW/PRL
2	EH/EW	22	MW/ML
3	ED/FW	23	SW/SL
4	TA/TC	24	ML/SL
5	SCPL/SCPW	25	SL/FRL
6	PDL/PDW	26	DW/DL
7	An_2L/An_1L	27	PW/PL
8	Fu_1L/Fu_1W	28	PTL/PTW
9	Fu_2L/Fu_2W	29	FWL/FWW
10	Fu_3L/Fu_3W	30	MV/ PMV
11	Fu_4L/Fu_4W	31	MV/STV
12	Fu_5L/Fu_5W	32	PMV/STV
13	Fu_6L/Fu_6W	33	SMV/ MV
14	CL/CW	34	STV/UL
15	PFCL/ FW	35	GL/GW
16	HL/HW	36	Gt_1L/ Gt_2L
17	EL/EW	37	FML/FMW
18	EL/TL	38	MTL/MTW
19	POL/OOL	39	FML/ MTL
20	IL/HL	40	MTL/MTAL

Results

Taxonomy

Asaphes Walker, 1834

Asaphes Walker, 1834: 151. Type species: *Asaphes vulgaris* Walker; by monotypy.
Isocratus Förster, 1856: 53, 58. Unnecessary replacement name according to Gahan and Fagan 1923: 18; incorrectly considered as preoccupied by *Asaphus* Brongniart.
Parectroma Brèthes, 1913: 91. Type species: *Parectroma hubrichi* Brèthes by monotypy. Synonymized by De Santis 1960: 113.

Diagnosis. *Asaphes* can be recognized by the following features: head with horseshoe-like occipital carina (Figs 1C, 2C) and with genal carina; antenna 14-segmented including one or two anelli (basal flagellomeres without mps), seven or six funiculars (with mps) and three distinct clavomeres plus tiny apical fourth clavomere (terminal button); torulus distinctly below midline of head near lower margin of eyes, with upper margin slightly above (Figs 1D, 4B) to distinctly below lower ocular line; left mandible bidentate and right mandible tridentate; pronotum transverse-quadrangular, ~ 1/2 as long as mesoscutum and rounded to abruptly angled to neck but without marginal rim (Fig. 1A, B); mesoscutum with compete notauli (Figs 1B, 2A, 3F); marginal vein subequal in

length or shorter than stigmal vein (Figs 1F, 2F, 3G, 4G); petiole tubular, divided into dorsal and ventral parts by lateral sulcus and with dorsal surface strongly sculptured, reticulate and/or with irregular longitudinal ribs (Figs 1E, 2E); gaster strongly sclerotized, non-collapsing (Figs 1A, B, I, 2E, 3A, H, K).

Comments. Graham (1990: 200) incorrectly listed *Notopodion* Dahlbom, 1857 as a junior synonym of *Asaphes*, which was followed by Gibson and Vikberg (1998) and Xiao and Huang (2000); rather, *Notopodion* is a synonym of *Podagrion* Spinola, 1811 (Torymidae) (Noyes 2019). Gibson and Vikberg (1998) provide a more comprehensive diagnosis of the genus as well as a subfamily diagnosis as then recognized, which was modified by Burks and Heraty (2020) and Burks et al. (2022). Burks et al (2022) considered the antenna of Asaphenesinae to be 14-segmented, including a small, terminal, fourth clavomere. While we follow their interpretation, because of its size the terminal clavomere, or "terminal button", is inconspicuous and the antenna superficially appears to be 13-segmetned with three distinct clavomeres (e.g., Fig. 1G, H). Most *Asaphes* species also have two basal flagellomeres without mps and six funiculars with mps, though the antenna of *A. umbilcatus* has only a single strongly transverse anellus and seven funiculars with mps (Xiao and Huang: fig. 6). Narendran and van Harten (2007) described the antennal formula of *A. ecarinatus* as 1: 1: 3: 7: 3 (i.e., 15-segmented), but their line drawing illustration of the flagellum appears to show a single basal flagellomere without mps, six funiculars with mps, and three clavomeres (i.e., 12-segmented). We did not examine type material to clarify these inconsistencies, but almost certainly the described antennal formula is incorrect, and the basal flagellomere likely is so strongly transverse that it is not clearly illustrated in the line drawing so that the antennal formula likely is 1:1:2:6:3, excluding the terminal button. The number of basal flagellomeres lacking mps requires close examination because even though Xiao and Huang (2000) key both *A. suspensus* and *A. vulgaris* as having "at most F1 without sensilla", the flagellum of both species have two anelli, i.e., lacking mps (Gibson and Vikberg 1998 figs 28, 30). As such, the number of basal flagellomeres without mps for the new species described by Xiao and Huang (2000) requires confirmation, including *A. globularis*, which has the basal four flagellomeres so strongly transverse as to possibly lack mps (Xiao and Huang 2000: fig. 16).

Asaphes can be differentiated from other genera classified in Pteromalidae prior to Burks et al. (2022) using such keys as Graham (1969), Bouček and Rasplus (1991), Bouček and Heydon (1997), Xiao and Huang (2000), or Huang and Xiao (2005).

Key to Chinese species of *Asaphes* based on females

1   Temple setose posteriorly; malar space ~ 1/3 length of eye height............
    ....***A. oculi* Xiao & Huang, 2000**
–   Temple bare posteriorly; malar space ~ 1/2 length of eye height **2**
2   Length of flagellum and pedicel combined slightly greater than head width; petiole slightly transvese, 0.8× as long as broad ....
    ....***A. siciformis* Xiao & Huang, 2000**
–   Length of flagellum and pedicel combined slightly less than head width; petiole at leastquadra-te and usually slightly longer than wide **3**

3   Mesoscutum with umbilicate punctuation (Xiao and Huang 2000: fig. 7); metacoxa dorsally bare.........................***A. umbilicalis* Xiao & Huang, 2000**

–   Mesoscutum with shallow engraved reticulation; metacoxa setose dorsally **4**

4   POL at most 2.2× OOL............................***A. globularis* Xiao & Huang, 2000**

–   POL at least 2.3× OOL **5**

5   Fore wing with speculum distinct (Gibson and Vikberg 1998: figs 68, 70).....**6**

–   Fore wing with speculum absent or indistinct (Gibson and Vikberg 1998: fig. 67) **7**

6   Head in dorsal view with distinct emargination between inner orbits and temples almost straight (Fig. 4D); hind leg with trochanter and femur similarly infuscate to black (Fig. 4A); fore wing speculum broad basally and narrowing toward stigmal vein (Fig. 4G; Gibson and Vikberg 1998: fig. 70); Gt_1 slightly longer than Gt_2....................................***A. vulgaris* Walker, 1834**

–   Head in dorsal shallowly emarginate between inner orbits and temples curved and rather strongly convergent (Fig. 1C); hind leg with trochanter paler than femur (Fig. 1A); speculum equal in width from parastigma to stigmal vein (Fig. 1F; Gibson and Vikberg 1998: fig. 68); Gt_1 usually shorter than Gt_2 (Fig. 1B) ....***A. californicus* Girault, 1917**

7   Legs more or less uniformly pale, yellowish to yellowish orange (Fig. 3A, B); stigmal vein 3.3−4.0 × length of uncus ...... **A. suspensus (Nees), 1834**

–   Legs reddish brown (Fig. 2A); stigmal vein 2.2−2.6 × length of uncus........ ....***A. fuyunis* Li & Zhang, sp. nov.**

Asaphes californicus Girault, 1917
Fig. 1

Asaphes californicus Girault, 1917: 1; Gibson and Vikberg 1998: 219−224.

Diagnosis. Female. Antenna (Fig. 1G) with pedicel at most 2.0−2.4× as long as wide; clava 2.4−2.5× as long as wide. Head in dorsal view (Fig. 1C) with shallow emargination between inner orbits and temple curved and rather strongly convergent; eye length 3.6−3.8× temple length (Fig. 1A); POL 0.3−0.6× OOL (Fig. 1C). Frenum smooth and shiny except finely carinate laterally (Fig. 1E); metapleuron bare; petiole at least quadrate and usually slightly longer (1.3×) than wide (Fig. 1E). Fore wing (Fig. 1F) with broad speculum. Legs with at least metafemur in part darker than light-colored metatrochanter (Fig. 1A). Gaster (Fig. 1B) 1.4× as long as wide; Gt_1L usually shorter (0.9×) than Gt_2L (Fig. 1B).

    Male. Color pattern similar to female except clava yellowish brown and legs entirely yellow (Fig. 1I). Structure similar to female, with combined length of pedicel and flagellum 0.9× head width; pedicel 2.1× as long as wide; all funicle segments slightly transverse (Fig. 1H) and with few mps; clava 2.4× as long as wide. Petiole (Fig. 1I) 1.4× as long as wide. Gaster (Fig. 1I, J) ovate, 1.8× as long as wide; Gt_1L almost equal to Gt_2L.

    Material examined. CHINA. Xinjiang • 2♀; Altay Prefecture, Altay City; 47°40'16"N, 88°01'16"E; 710 m; 12 Jul 2020; Qin Li research group • 1♂; Fuyun City; 46°56'10"N, 89°33'51"E; 848 m; 10 Jul 2020; Qin Li research group • 1♀;
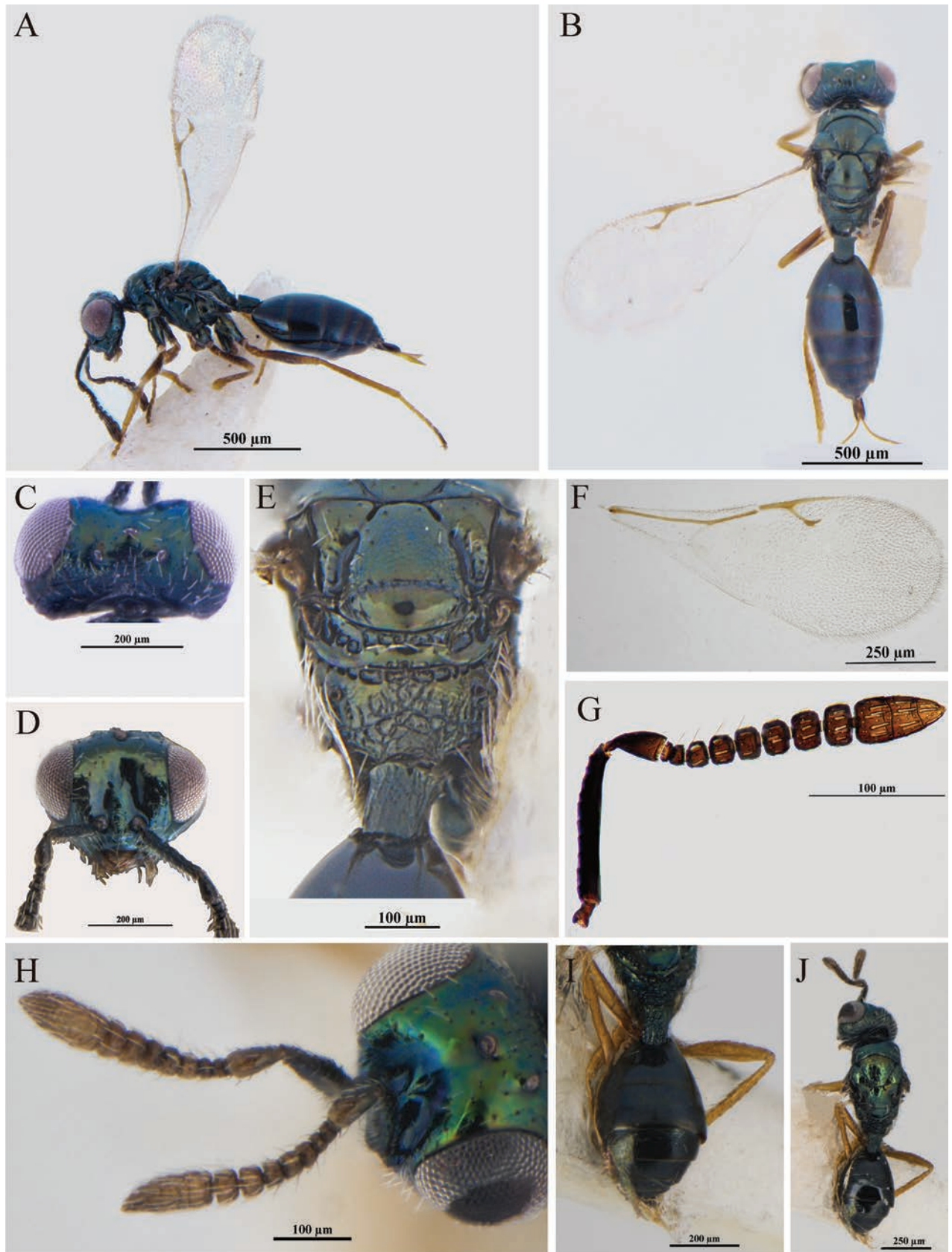
Figure 1. *A. californicus* Girault **A–D** female **A** body, lateral view **B** body, dorsal view **C** head, dorsal view **D** head, frontal view **E** scutellum, propodeum and petiole, dorsal view **F** fore wing **G** antenna **H–J** male **H** antenna **I** petiole and gaster, dorsal view **J** body, dorsal view.

Hotan Prefecture, Yutian County; 36°90'02"N, 81°40'58"E; 1432 m; 3 Aug 2021; Zhulidezi Aishan research group • 2♀; Ili Kazakh Autonomous Prefecture, Gongliu County; 43°22'60"N, 82°72'09"E; 1137 m; 10 Jul 2021; Qin Li research group.

CANADA. Alberta • 1♀1♂; Waterton; 49°06'N, 113°59'W; 1530 m; 11 Jul 1991; H. Goulet. Yukon Territory • 1♀; Alaska Hwy; 60°54'N, 137°09'W; 664 m; 7 Jul 2006; Goulet and Boudreault • 1♂; Alaska Highway E. of Hines Junction; 60°54.062'N, 137°09.791'W; 664 m; sweeping; 7 Jul 2006; Goulet and Boudreault • 1♀; Whitehorse; 60°43'N, 133°03'W; 814 m; 11 Jul 2006; Boudreault and Goulet.

USA. Alaska • 1♀; Wosnesenski Island; 55°12'N, 161°21'W; 11 Jul 2009; Boudreault and Goulet. California • 1♀1♂; Siskiyou County; 2 mi. W. Bartle along McCloud river; 17 Jul.1990; J.D. Pinto.

Distribution. China (Xinjiang) (new country record); Nearctic and Neotropical regions (Noyes 2019).

Hosts. *Asaphes californicus* is strictly a hyperparasitoid of aphids through Aphidiinae (Hymenoptera: Braconidae) and Aphelinidae (Hymenoptera) primary parasitoids (Gibson and Vikberg 1998).

Comments. *Asaphes californicus* was previously reported only from the Nearctic and Neotropical regions (Gibson and Vikberg 1998). It is reported here from Xinjiang, China for the first time.

Asaphes fuyunis **Li & Zhang, sp. nov.**
https://zoobank.org/07578F4B-1781-4CF2-918F-B118A2E0C58C
Fig. 2

Type material. *Holotype* • ♀ (ICXU); CHINA, Xinjiang, Altay Prefecture, Fuyun County, Turhong Township; 47°01'49"N, 89°01'40"E; 1360 m; 11 Jul 2020; Qin Li group. *Paratypes* • 3♀; same collection data as holotype.

Diagnosis. Female. Body (Fig. 2A) metallic green, with luster. Head in dorsal shallowly emarginate between inner orbits. Combined length of pedicel and flagellum subequal in width to head. Fore wing hyaline with speculum absent or indistinct; stigmal vein 2.2–2.6 × length of uncus. Legs reddish brown (Fig. 2A). Gt_1 and Gt_2 combined are approximately equal to the length of the gaster, with Gt_1 being longer than Gt_2 (Fig. 2E).

Description. Female. Body (Fig. 2A) length 1.75 mm. Head, mesosoma, and propodeum dark with green and bronze lusters under different angles of light (Fig. 2A–E); antenna dark brown (Fig. 2G) except scape and pedicel concolorous with mesosoma; gaster black or with only slight metallic lusters under some angles of light (Fig. 2A, E); fore wing hyaline with brown venation (Fig. 2F); legs with coxae concolorous with mesosoma, otherwise reddish brown except apical tarsomeres dark brown to black (Fig. 1A).

Head in frontal view (Fig. 2B) transverse-subtriangular, width 1.4× height, with genae distinctly converging ventrally; face with regular, raised reticulation and with dense, white setae; scrobal depression broad and deep, smooth and bare ventrally; clypeus smooth with truncate apical margin. Malar space ~ 1.1× eye height (Fig. 2B). Scape extending to level of vertex (Fig. 2A); pedicel 2.0× as long as wide; funiculars broadly joined, each transverse and with 1 line of mps, with fu_4 0.6× as long as wide; clava 1.9× as long as wide; combined length of pedicel and flagellum subequal in width to head. Head in lateral view with eye height
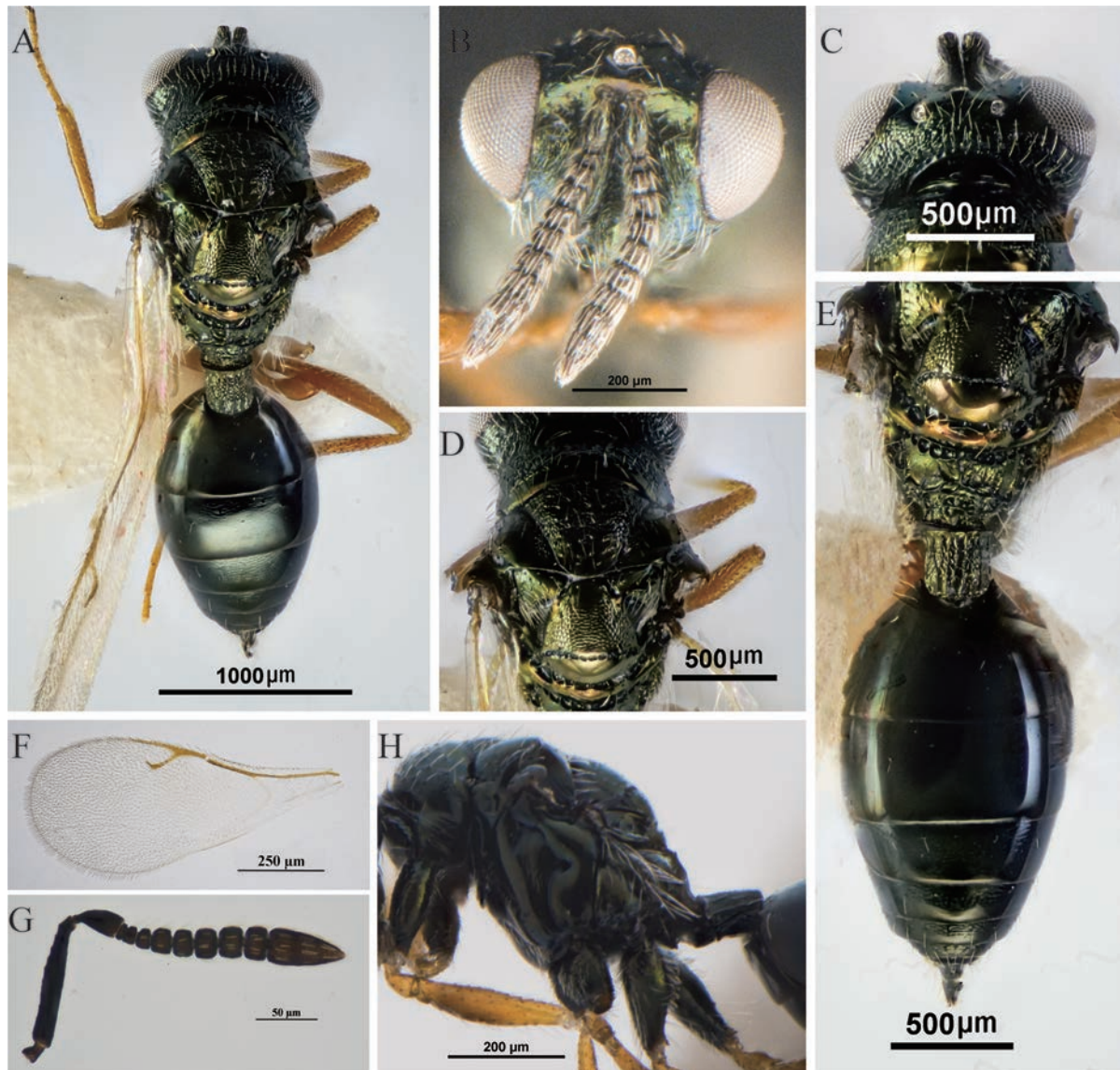
Figure 2. *A. fuyunis* Li & Zhang, sp. nov., holotype, female **A** body, dorsal view **B** head, frontal view **C** head, dorsal view **D** mesosoma; dorsal view **E** propodeum and gaster, dorsal view **F** fore wing **G** antenna **H** prepectus.

1.7× eye length and 2.5× malar space; malar sulcus absent. Head in dorsal view (Fig. 2C) 2.0× as wide as long; POL 2.6× OOL; gena length 0.5× eye length.

Mesosoma in dorsal view (Fig. 2D) slightly narrower than head width (0.9×); mesosoma compact and convex; pronotum narrower than mesoscutum (0.9×), and 0.6× as long as mesoscutum; collar abruptly margined anteriorly, posterior margin smooth and bare (Fig. 2D); mesoscutum 2.0× as long as broad, equal in length to scutellum; notauli deep and complete; scutellum (Fig. 2D, E) 0.8× as long as broad, with engraved, reticulate sculpture; frenum smooth and shiny, delineated anteriorly by continuous septate frenal line; propodeum (Fig. 2E) 0.8× as long as scutellum, without median carina or plicae, median area with coarse and irregular sculpture, and laterally with dense, whitish, long setae. Mesosoma in lateral view (Fig. 2H) with metapleuron bare. Fore wing (Fig. 2F) densely setose, without distinct speculum; proportions of length of marginal, postmarginal, and stigmal veins 19:24:16; stigmal vein 2.6× as long as uncus. Metacoxa setose both dorsally and ventrally (Fig. 2H).

Metasoma with petiole quadrate, subequal in length and breadth (Fig. 2A, E), dorsally with numerous irregular longitudinal ribs. Gaster (Fig. 2A, E) oval, 1.8× as long as wide; Gt_1 and Gt_2 smooth and combined length 0.5× length of gaster, Gt_1 1.2× as long Gt_2.

Male. Unknown.

Variation. No significant difference in measurement data.

Host. Unknown.

Etymology. The specific name is derived from the collection locality of its holotype.

Distribution. China (Xinjiang).

Comments. Females of this species have an unusually long malar space for members of *Asaphes*, being ~ 1.1× the height of an eye (Fig. 1B). Leg color is similar to some specimens of *A. suspensus* that have comparatively dark, yellowish orange legs as well as an indistinct fore wing speculum (Fig. 3G), but *A. suspensus* females have the malar space at most ~ 0.7× the height of an eye (Gibson and Vikberg 1998).

Asaphes suspensus **(Nees, 1834)**
Fig. 3

Chrysolampus suspensus Nees, 1834: 127; McMullen 1966: 236–239; Graham 1969: 82–83; Gibson and Vikberg 1998: 230–236; Xiao and Huang 2000: 194–195; Huang and Xiao 2005: 273–274.

Chrysolampus altiventris Nees, 1834: 127. Synonymized by Graham 1969: 82.

Pteromalus petioliventris Zetterstedt, 1838: 429. Synonymized by Graham 1969: 82.

Chrysolampus aphidiphagus Ratzeburg, 1844: 181. Synonymized by Graham 1969: 82.

Chrysolampus aphidicola Rondani, 1848: 19–21. Synonymized by Bouček 1974: 244.

Euplectrus lucens Provancher, 1887: 207. Synonymized by Gibson and Vikberg 1998: 231.

Asaphes rufipes Brues, 1908: 160. Synonymized by Gibson and Vikberg 1998: 231.

Megorismus fletcheri Crawford, 1909: 98. Synonymized by Gibson and Vikberg 1998: 231.

Asaphes americana Girault, 1914: 114. Synonymized by Gibson and Vikberg 1998: 231.

Pachycrepoides indicus Bhatnagar, 1952: 160–163. Synonymized by Gibson and Vikberg 1998: 231.

Asaphes sawraji Sharma & Subba Rao, 1959: 181. Synonymized by Bouček et al. 1979: 436.

Pachyneuron uniarticulata Mani & Saraswat, 1974: 96–98. Synonymized by Bouček et al. 1979: 436.

Material examined. Cʜɪɴᴀ, Xinjiang: Altay Prefecture, Qin Li group • 2♀; Altay City; 47°40'16"N, 88°01'16"E; 710 m; 12 Jul 2020 • 1♀; Fuyun County; 47°01'49"N, 89°53'46"E; 1360 m; 11 Jul 2020 • 1♀; Qinghe County; 46°41'31"N, 90°21'28"E;
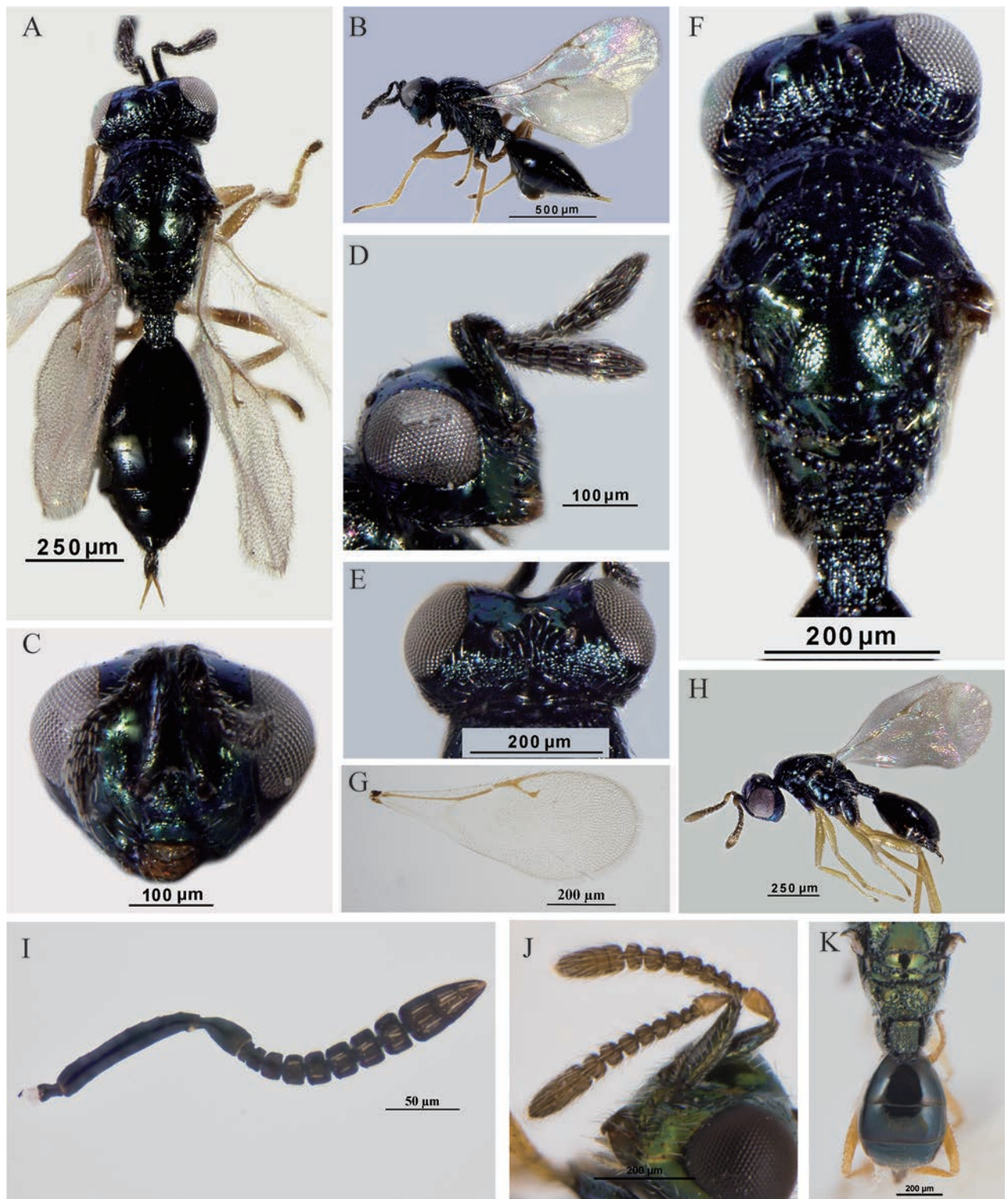
Figure 3. *A. suspensus* (Nees) **A–G, I** female **A** body, dorsal view **B** body, lateral view **C** head, frontal view **D** head, lateral view **E** head, dorsal view **F** head and mesosoma, dorsal view **G** fore wing **I** antenna **H, J, K** male **H** body, lateral view **J** antenna **K** propodeum and gaster, dorsal view.

1240 m; 10 Jul 2020 • 1♀; Qinghe County; 46°92'88"N, 90°01'62"E; 1427 m; 6 Jul 2021. Bayingol Mongolian Autonomous Prefecture, Hongying Hu group • 1♀1♂; Bohu County; 42°02'63"N, 86°66'48"E; 1053 m; 7 Aug 2010 • 1♀; Yuli County; 41°39'01"N, 86°25'01"E; 871 m; 5 Aug 2010 • 2♀; Bortala Mongolian

Autonomous Prefecture, Bole City; 44°87'72"N, 82°14'60"E; 405 m; 30 Jun 2021; Qin Li group. Changji Hui Autonomous Prefecture, Hongying Hu research group • 1♀; Mulei Kazakh Autonomous County; 43°98'32"N, 90°37'70"E; 1219 m; 30 Jul 2012 • 2♀4♂; Qitai County; 43°95'16"N, 89°52'85"E; 833m; 29 Jul 2012 • 1♀; Qitai County; 43°58'27"N, 89°78'10"E; 847 m; 29 Jul 2012. Ili Kazakh Autonomous Prefecture, Hongying Hu research group • 1♀; Huocheng County; 44°06'76"N, 80°85'81"E; 661 m; 22 Jun 2010 • 1♀; Tekes County; 43°23'25"N, 81°84'36"E; 1865 m; 27 Jul 2010. Ili Kazakh Autonomous Prefecture, Qin Li research group • 2♀; Gongliu County; 43°22'60"N, 82°72'09"E; 1137 m; 10 Jul 2021 • 2♀3♂; Huocheng County; 43°94'47"N, 80°87'04"E; 515 m; 5 Jul 2021 • 1♀; Tekes County; 43°22'19"N, 81°88'88"E; 1201 m; 8 Jul 2021 • 2♂; Kashgar Prefecture, Artux City; 39°69'49"N, 76°20'23"E; 1303 m; 22 Jun 2008; Hongying Hu research group • 1♀; Tarbagatay Prefecture, Wusu County; 44°00'43"N, 84°95'34"E; 1908 m; 25 Jul 2013; Hongying Hu research group • 1♂; Urumqi, Tianshan District; 43°77'49"N, 87°62'07"E; 928 m; 17 Apr 2007; Hongying Hu research group.

Diagnosis. Female. Antenna (Fig. 3I) with combined length of pedicel and flagellum less than head width; pedicel at most 1.6–1.8× as long as wide; funiculars subquadrate, broadly joined, and each with one line of sensilla; fu_4 0.8× as long as broad. Head in dorsal view (Fig. 3E) with shallow emargination between inner orbits; eye length 2.3–2.8× temple length. Frenum smooth and shiny (Fig. 3F); metapleuron bare. Metatibia 6.2–6.8× times as long as wide. Fore wing (Fig. 3G) with speculum indistinct; marginal vein 0.6–0.8× as long as postmarginal vein and stigmal vein 3.3–4.0× as long uncus. Legs (Fig. 3B) more or less uniformly light-colored, yellowish. Petiole (Fig. 3A, F) at least quadrate and usually slightly longer (1.1×) than wide. Gaster 1.9× as long as broad (Fig. 3A).

Male. Color pattern brighter than female, and pedicel and flagellum yellowish brown (Fig. 3H, J). Antenna (Fig. 3J) with combined length of pedicel and flagellum 0.9× head width; pedicel 1.8× as long as wide; funicle with all segments slightly transverse; clava 2.3× longer than wide. Petiole (Fig. 3K) 1.2× as long as wide, entirely reticulate with longitudinal carinae. Gaster (Fig. 3H, K) ovate, Gt_1L 1.1× as long as Gt_2L. Otherwise similar to female.

Distribution. China (Xinjiang, Beijing, Fujian, Guangdong, Hebei, Heilongjiang, Henan, Hunan, Jilin, Shaanxi, Shanxi, Sichuan, Tibet, Yunnan). Palearctic region and Nearctic region (Noyes 2019).

Hosts. Usually a hyperparasitoid of aphids through Aphidiinae (Hymenoptera: Braconidae) and Aphelinidae (Hymenoptera) primary parasitoids, and rarely parasites *Psylla* Geoffroy, 1762 (Hemiptera: Psyllidae) (Gibson and Vikberg 1998).

Comments. The morphological features of our specimens fit within the limits described for *A. suspensus* by Gibson and Vikberg (1998); they described the length of the pedicel as at most 2× as long as wide, whereas the pedicel of our measured specimens was at most 1.8× as long as wide.

Asaphes vulgaris **Walker, 1834**
Fig. 4

Asaphes vulgaris Walker, 1834: 152.
Eurytoma aenea Nees, 1834: 42. Synonymized by Graham 1969: 80.
Chrysolampus aeneus Ratzeburg, 1848: 2. Synonymized by Reinhard 1857: 76.

Chrysolampus aphidophila Rondani, 1848: 21–22. Synonymized by Bouček 1974: 244.

Asaphes vulgaris Walker; Morley 1910: 28; Gibson and Vikberg 1998: 236–239; Xiao and Huang 2000: 198; Huang and Xiao 2005: 275–276; Narendran and Harten 2007: 114–116.

Material examined. CHINA, Xinjiang: Altay Prefecture, Qin Li research group • 5♀; Altay City; 47°40'16"N; 88°01'16"E; 710 m; 12 Jul 2020 • 1♀; Fuyun County; 47°01'49"N, 89°53'46"E; 1360 m; 11 Jul 2020 • 1♀; Fuyun County; 47°01'73"N,
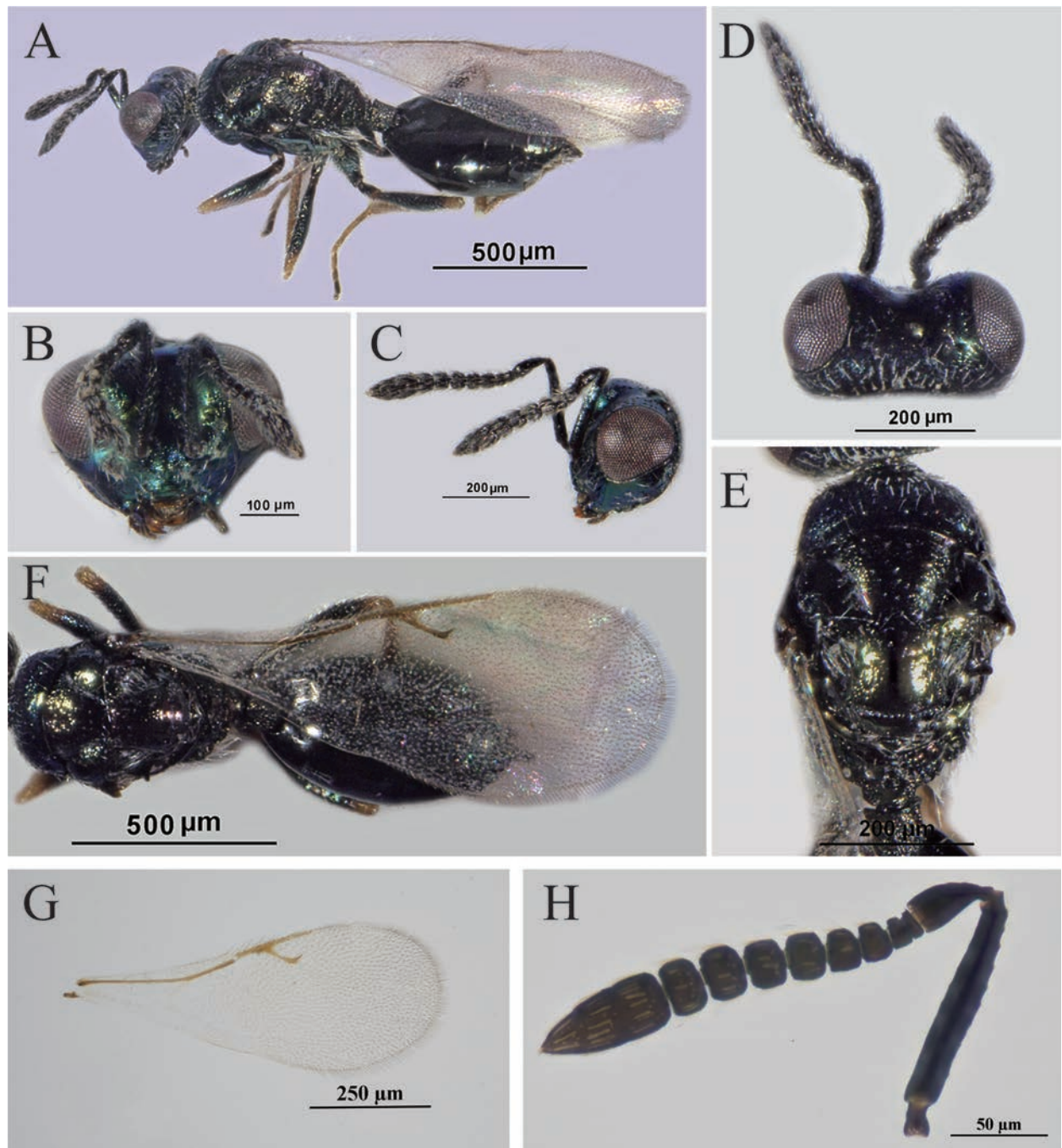
Figure 4. *A. vulgaris* Walker, female **A** body, lateral view **B** head, frontal view **C** head, lateral view **D** head, dorsal view **E** mesosoma, dorsal view **F** mesosoma, metasoma and wing, dorsal view **G** fore wing **H** antenna.

89°84'68"E; 1287 m; 22 Jun 2021 • 1♀; Fuyun County; 47°21'60"N, 89°84'43"E; 1141 m; 23 Jun 2021 • 1♀; Qinghe County; 46°43'35"N, 90°04'49"E; 1121 m; 21 Jun 2021 • 1♀; Bayingol Mongolian Autonomous Prefecture, Yuli County; 41°35'11"N, 86°29'45"E; 892 m; 5 Aug 2010; Hongying Hu group. Ili Kazakh Autonomous Prefecture, Qin Li research group • 3♀; Gongliu County; 43°22'60"N, 82°72'09"E; 1137 m; 10 Jul 2021 • 1♀; Huocheng County; 43°94'47"N, 80°87'04"E; 515 m; 5 Jul 2021.

Diagnosis. Female. Head in dorsal view (Fig. 4D) with comparatively deep emargination between inner orbits and straight temples; gena length (Fig. 4C) ~ 0.3−0.4× eye length. Antenna (Fig. 4C, H) with each funicular subquadrate, and segments loosely joined to each other. Pronotum (Fig. 4E) 2.3−2.8× wider than long. Hind leg (Fig. 4A) with trochanter and femur similarly infuscate to black; metatibia 7.7−7.8× longer than wide. Fore wing (Fig. 4G) with speculum distinct, broad basally and narrowed toward stigmal vein. Petiole (Fig. 4A) at least quadrate and usually slightly longer (1.1−1.3×) than wide. Gaster (Fig. 4A, F) 1.7−1.9× as long as broad; Gt_1L slightly longer (1.1×) than Gt_2L.

Male. Unknown.

Distribution. China (Xinjiang, Hebei, Sichuan, Yunnan, Tibet, Ningxia, Guangxi). Worldwide (Noyes 2019).

Hosts. In North America, *A. vulgaris* is a hyperparasitoid of aphids, including *Acyrthosiphon pisum* Harris and *Macrosiphum euphorbiae* Thomas (Hemiptera: Aphididae) through *Aphidius nigripes* Ashmead (Hymenoptera: Braconidae) (Gibson and Vikberg 1998).

Comments. Leg color of *A. vulgaris* females is similar to that of *A. californicus* except for trochanter color. Females of *A. vulgaris* have at least the meso- and metatrochanters infuscate to black, similar in color to the respective femora, whereas at least the metatrochanter of *A. californicus* females is mostly yellow, paler than the femur. In our study, gena length is 0.3−0.4× eye length, as described by Huang and Xiao (2005), which differs from the description of 0.5−0.6× eye length given by Gibson and Vikberg (1998); however, this may reflect a somewhat different method of measurement.

Morphometrics

The first two principal components (PCA1 and PCA 2) of the PCA analysis recovered 49.3% of the variation in the morphometric and meristic data set (Fig. 6) and loaded most heavily for the ratio of (Fu_4L/Fu_4W), (STVL/UL), (PFCL/ FW), (MV/ PMV) along PCA 1 and ratio of (PMV/STV), (IL/HL), (EL/TL), and (CL/CW) along PCA 2 (Table 5). The PCA data strongly support the results of the traditional morphology and molecular data.

Molecular results

We successfully obtained 22 DNA barcode (COI) sequences (see Table 3) from our specimens, in addition to the two sequences of *A. vulgaris* obtained from NCBI (Table 1), which support the presence of four species of *Asaphes* (Fig. 5) in Xinjiang, China. We identify these species as *A. californicus*, *A. fuyunis* sp. nov., *A. suspensus*, and *A. vulgaris*, although molecular evidence from western European specimens of *A. suspensus* is currently lacking to support our identification of this species from China. The two sequences identified as *A. vulgaris*
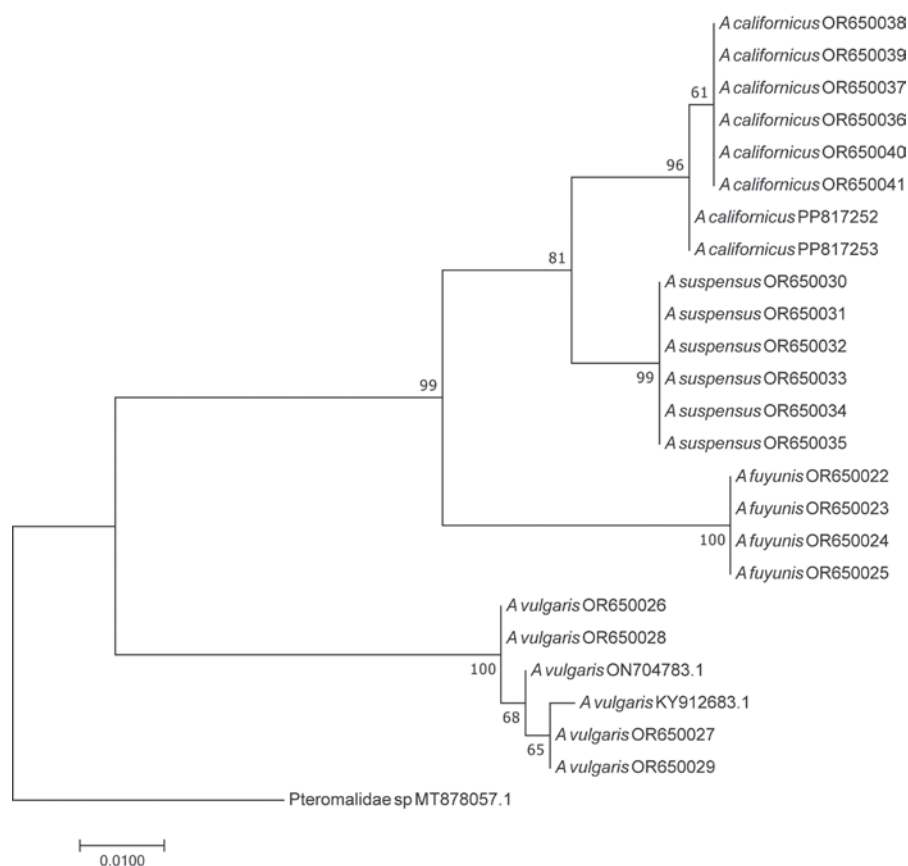
Figure 5. Maximum Likelihood (ML) tree by K2P distances based on COI sequences of *Asaphes*.

obtained from NCBI do support our identification of *A. vulgaris* from Xinjiang. Genetic Kimura-2 parameter (K2P) distances of the intraspecific and interspecific COI sequences were calculated in MEGA X (Table 4). The results indicate that intraspecific distances are 0.0% to 0.9% and interspecific distances between the four species varied from 2.3% to 11.3%.

Discussion

Individuals of *A. fuyunis*, *A. californicus*, *A. suspensus*, and *A. vulgaris* can be difficult to distinguish using traditional morphological features because of multiple variable characteristics, including the depth of the emargination between the inner orbits in dorsal view and leg color. Gibson and Vikberg (1998) described the emargination between the inner orbits of *A. vulgaris* as "relatively deeply" concave, and "relatively shallowly" concave in *A. suspensus* and *A. californicus* (cf. Figs 1C, 3E with 4D). Because this is a relative feature that differs somewhat depending on angle of view, it can be difficult to assess accurately. Gibson and Vikberg (1998) also reported that the trochanters and trochantelli of female *A. californicus* were almost always uniformly yellowish to yellowish brown, paler than the black meso- and metafemora, which matches our specimens from China (Fig. 1A), although with some variability in color of the metafemora. However, the accuracy of our morphological identifications is supported through an integrative taxonomic approach combining data from COI barcodes and morphometrics.

To assist future research of world *Asaphes*, we summarize the 13 described species with known distribution and habitat, and deposition of type material (Table 6).
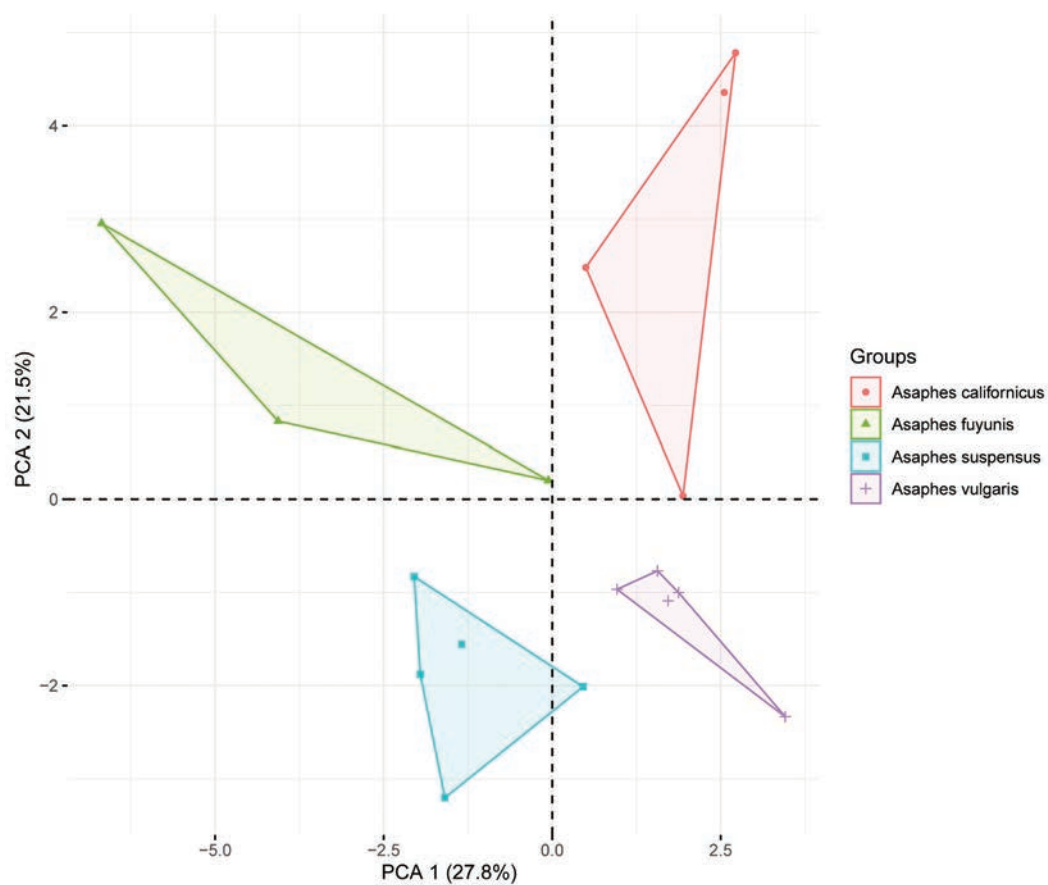
Figure 6. Principal component analysis (PCA) of *Asaphes* species.

Table 3. Information on sequenced specimens with GenBank accession of COI.

Specimen number	Morphospecies	GenBank accession number	Sex
1	*Asaphes fuyunis* 1	OR650022	F
2	*Asaphes fuyunis* 2	OR650023	F
3	*Asaphes fuyunis* 3	OR650024	F
4	*Asaphes fuyunis* 4	OR650025	F
5	*Asaphes californicus* 1	OR650036	M
6	*Asaphes californicus* 2	OR650037	M
7	*Asaphes californicus* 3	OR650038	F
8	*Asaphes californicus* 4	OR650039	F
9	*Asaphes californicus* 5	OR650040	F
10	*Asaphes californicus* 6	OR650041	F
11	*Asaphes californicus* 7	PP817252	F
12	*Asaphes californicus* 8	PP817253	F
13	*Asaphes suspensus* 1	OR650030	F
14	*Asaphes suspensus* 2	OR650031	F
15	*Asaphes suspensus* 3	OR650032	F
16	*Asaphes suspensus* 4	OR650033	M
17	*Asaphes suspensus* 5	OR650034	F
18	*Asaphes suspensus* 6	OR650035	F
19	*Asaphes vulgaris* 1	OR650026	F
20	*Asaphes vulgaris* 2	OR650027	F
21	*Asaphes vulgaris* 3	OR650028	F
22	*Asaphes vulgaris* 4	OR650029	F

Table 4. Kimura 2-parameter genetic distances calculated within and between each species of *Asaphes*. **1–4**, *A. fuyunis*, OR650022–OR650025. **5–10**, *A. californicus*, OR650036–OR650041; **11–12**, *A. californicus*, PP817252–PP817253. **13–18**, *A. suspensus*, OR650030–OR650035. **19–22**, *A. vulgaris*, OR650026–OR650029; **23.** *A. vulgaris*, ON704783.1; **24.** *A. vulgaris*, KY912683.1; **25.** MT878057.1 Pteromalidae sp.

	1	2	3	4	5	6	7	8	9	10	11	12	13	14	15	16	17	18	19	20	21	22	23	24	25
1																									
2	0.000																								
3	0.000	0.000																							
4	0.000	0.000	0.000																						
5	0.055	0.055	0.055	0.055																					
6	0.055	0.055	0.055	0.055	0.000																				
7	0.055	0.055	0.055	0.055	0.000	0.000																			
8	0.055	0.055	0.055	0.055	0.000	0.000	0.000																		
9	0.055	0.055	0.055	0.055	0.000	0.000	0.000	0.000																	
10	0.055	0.055	0.055	0.055	0.000	0.000	0.000	0.000	0.000																
11	0.055	0.055	0.055	0.055	0.003	0.003	0.003	0.003	0.003	0.003															
12	0.058	0.058	0.058	0.058	0.003	0.003	0.003	0.003	0.003	0.003	0.000														
13	0.058	0.058	0.058	0.058	0.026	0.026	0.026	0.026	0.026	0.026	0.023	0.023													
14	0.055	0.055	0.055	0.055	0.026	0.026	0.026	0.026	0.026	0.026	0.023	0.023	0.000												
15	0.055	0.055	0.055	0.055	0.026	0.026	0.026	0.026	0.026	0.026	0.023	0.023	0.000	0.000											
16	0.055	0.055	0.055	0.055	0.026	0.026	0.026	0.026	0.026	0.026	0.023	0.023	0.000	0.000	0.000										
17	0.055	0.055	0.055	0.055	0.026	0.026	0.026	0.026	0.026	0.026	0.023	0.023	0.000	0.000	0.000	0.000									
18	0.055	0.055	0.055	0.055	0.026	0.026	0.026	0.026	0.026	0.026	0.023	0.023	0.000	0.000	0.000	0.000	0.000								
19	0.104	0.104	0.104	0.104	0.099	0.099	0.099	0.099	0.099	0.099	0.096	0.096	0.099	0.099	0.099	0.099	0.099	0.099							
20	0.110	0.110	0.110	0.110	0.104	0.104	0.104	0.104	0.104	0.104	0.101	0.101	0.104	0.104	0.104	0.104	0.104	0.104	0.006						
21	0.104	0.104	0.104	0.104	0.099	0.099	0.099	0.099	0.099	0.099	0.096	0.096	0.099	0.099	0.099	0.099	0.099	0.099	0.000	0.006					
22	0.110	0.110	0.110	0.110	0.104	0.104	0.104	0.104	0.104	0.104	0.101	0.101	0.104	0.104	0.104	0.104	0.104	0.104	0.006	0.000	0.006				
23	0.107	0.107	0.107	0.107	0.101	0.101	0.101	0.101	0.101	0.101	0.099	0.099	0.101	0.101	0.101	0.101	0.101	0.101	0.003	0.003	0.003	0.003			
24	0.113	0.113	0.113	0.113	0.107	0.107	0.107	0.107	0.107	0.107	0.104	0.104	0.107	0.107	0.107	0.107	0.107	0.107	0.009	0.003	0.009	0.003	0.006		
25	0.101	0.101	0.101	0.101	0.099	0.099	0.099	0.099	0.099	0.099	0.096	0.096	0.087	0.087	0.087	0.087	0.087	0.087	0.084	0.090	0.084	0.090	0.087	0.093	

Table 5. Summary statistics of the principal component analysis of *Asaphes* species.

No.	Ratio Character	PCA 1	PCA 2	PCA 3	PCA 4	PCA 5
1	FW/FH	0.216603	3.1783295	5.282507068	0.35574012	0.11672155
2	EH/EW	2.87230488	0.01275921	2.403104213	2.77131137	8.66243702
3	ED/FW	0.064479	1.33391248	3.750109321	0.01440452	0.02641105
4	TA/TC	0.38712463	3.84482846	4.943076551	0.01412389	0.86188693
5	SCPL/SCPW	3.77417162	0.17398981	4.917479269	5.42866022	5.15896312
6	PDLL/PDLW	2.48648096	3.47521382	0.865723008	1.62566188	1.32165941
7	An_2L/An_1L	0.326642	0.07101507	3.637868218	0.12479640	0.03293327
8	Fu_1L/Fu_1W	0.54994757	3.14619133	0.678699525	0.10242453	4.41799084
9	Fu_2L/Fu_2W	0.54780303	0.91981684	6.491676859	4.87546358	0.57158251
10	Fu_3L/Fu_3W	2.55243666	1.5716729	0.021682635	0.00520423	1.24671401
11	Fu_4L/Fu_4W	10.73709122	0.03026482	3.00986227	0.53440516	0.46617328
12	Fu_5L/Fu_5W	4.27256446	0.01729463	0.171878122	6.27041051	7.96592789
13	Fu_6L/Fu_6W	5.31963583	0.02737012	0.462662143	5.37478061	7.93531917
14	CL/CW	0.02455471	5.55428663	4.020927977	6.27200768	0.73043984
15	PFCL/ FW	6.75428702	1.08591194	2.623988773	2.17895563	0.04085098
16	HL/HW	2.0032471	3.92372966	2.655545541	0.80496354	0.37575628
17	EL/EW	4.0012536	0.28429239	2.524285127	7.50944257	0.554169
18	EL/TL	0.11689347	7.48754868	0.021480775	0.51223903	6.31378767
19	POL/OOL	1.91102438	4.41288002	0.087581884	0.01816490	1.73381626
20	IL/HL	0.00495787	10.4068808	1.652372742	6.98858843	0.03276383
21	PW/PL	5.94539663	2.6230557	1.171565757	1.27406889	0.06924112
22	MW/ML	0.50006149	1.4715376	2.264067963	4.36335336	1.65929375
23	SW/SL	0.43666104	2.93931866	0.469217579	1.78127138	1.49050197
24	ML/SL	1.06564488	4.71355448	0.147326384	1.39131205	8.56569969
25	SL/FREL	0.03131094	0.30214966	0.762210045	14.6648713	5.19235602
26	DW/DL	5.35506306	1.0741069	1.789557847	0.51568116	11.02661261
27	PW/PL	2.01239276	1.79406094	9.730208122	0.06695963	0.157202
28	PTL/PTW	1.80838085	3.7644288	0.729981654	0.35903363	0.0955859
29	FWL/FWW	0.17121849	3.35181891	0.603319812	0.03354785	0.24197932
30	MV/ PMV	6.6232683	2.32960968	0.003427697	1.59581658	0.38893584
31	MV/STV	4.92799266	1.5431306	1.133819339	0.99042593	1.63080091
32	PMV/STV	0.13428142	13.4269751	0.456237813	0.68635732	0.15941343
33	SMV/ MV	3.59396951	0.25035778	2.226292291	6.41494374	0.27368141
34	STV/UL	7.66254386	0.81944172	0.313900134	4.92683749	1.32236046
35	GL/GW	0.01600313	0.43491547	9.055025395	0.07733081	2.85458356
36	Gt_1L/ Gt_2L	5.47504516	2.61689068	1.348141421	1.78054706	0.07476514
37	FML/FMW	0.15372799	1.95444963	5.602996723	5.19072632	3.09035096
38	MTL/MTW	2.11187438	3.25304848	4.255962542	0.86010845	1.1979344
39	FML/ MTL	1.70215655	0.36189028	7.626523209	0.74815528	2.27170915
40	MTL/MTAL	1.3495039	0.01706981	0.087706254	0.49690272	9.67068846

Based on our field studies and reports by Kamijo and Takada (1973) and Gibson and Vikberg (1998), it is highly likely that *Asaphes* mostly inhabit herbaceous areas such as cultivated fields, meadows, and potato fields. Interestingly, *Medicago sativa* (Fabaceae) was found in all our collecting sites of *A. vulgaris*. Therefore, we consider *A. vulgaris* to be most likely associated with *M. sativa*. Considering that *M. sativa* is an important economic green plant in Xinjiang and *A. vulgaris* is a hyper-parasitoid, our results also indicate that it is harmful.

Table 6. Described species of *Asaphes* with known distribution and habitat, and deposition of type material.

Species	Distribution	Habitat	Deposition of holotype or lectotype	References
A. brevipetiolatus	Nearctic, Finland	subalpine meadow, mix conifer forest	CNC	Gibson and Vikberg 1998
A. californicus	Nearctic, Neotropical, China (Xinjiang, new record)	clover field, weed land, *Calamagrostis pseudophragmites* (Poales: Poaceae)	USNM	Gibson and Vikberg 1998
A. ecarinatus	Yemen	unknown	DZUC	Narendran and van Harten 2007
A. fuyunis	China (Xinjiang)	miscellaneous grassland	ICXU	–
A. globularis	China (Tibet)	unknown	IZCAS	Xiao and Huang 2000
A. hirsutus	Nearctic, Mexico, western Palearctic	potato field, Ericaceae (Ericales), Boreal forest	CNC	Gibson and Vikberg 1998
A. oculi	China (Yunnan, Hebei)	unknown	IZCAS	Xiao and Huang 2000
A. petiolatus	Nearctic, western Palearctic	*Picea glauca* (Pinales: Pinaceae)	MZLU	Gibson and Vikberg 1998
A. pubescens	Japan	shrubs, orchards, gardens, Coniferous woods, Deciduous woods, mixed woods	unknown	Kamijo and Takada 1973
A. siciformis	China (Yunnan, Sichuan, Hebei)	unknown	IZCAS	Xiao and Huang 2000
A. suspensus	Nearctic, Palearctic	cultivated fields, meadows, road side shrubs, orchards, gardens, coniferous woods, deciduous woods, mixed woods	HOPE	Kamijo and Takada 1973; Gibson and Vikberg 1998
A. umbilicalis	China (Jilin)	unknown	IZCAS	Xiao and Huang 2000
A. vulgaris	cosmopolitan	potato field	NHMUK	Gibson and Vikberg 1998; Xiao and Huang 2000

Additional information

Conflict of interest

The authors have declared that no competing interests exist.

Ethical statement

No ethical statement was reported.

Author contributions

L.Q. proposed the project, participated in the design of the study, collected of samples, traditional classification and drafted the manuscript. Z.T.Y. collected of samples, traditional classification, sequence data analyses, phylogenetic analysis, and drafted the manuscript. G A P Gibson. provides U.S.A and Canada specimens and revised the draft of the manuscript S.S.L. classical morphometrics date analysis. X.Y. traditional classification, check specimens and revised the draft of the manuscript. All authors read and approved the final manuscript.

Author ORCIDs

Tong-You Zhang https://orcid.org/0009-0000-5425-3765
Gary A. P. Gibson https://orcid.org/0000-0002-8161-7445
Shi-Lei Shan https://orcid.org/0009-0002-0988-479X
Hui Xiao https://orcid.org/0000-0002-8979-3793

Data availability

All of the data that support the findings of this study are available in the main text.

References

Alajmi R, Haddadi R, Abdel-Gaber R, Alkuriji M (2020) Molecular phylogeny of *Monomorium pharaonis* (Hymenoptera: Formicidae) based on rRNA sequences of mitochondrial gene. Journal of Genetics 99: 1–7. https://doi.org/10.1007/s12041-020-1186-y

Bouček Z (1974) On the Chalcidoidea (Hymenoptera) described by C. Rondani. Redia 55: 241–285.

Bouček Z (1988) Australian Chalcidoidea (Hymenoptera): A Biosystematic Revision of Genera and Fourteen Families, with a Reclassification of Species (Fig wasp section). CAB International, Wallingford, Oxon, England/Cambrian News Ltd., Aberystwyth, Wales, 832 pp. https://doi.org/10.11646/zootaxa.1627.1.4

Bouček Z, Heydon SL (1997) Chapter 17. Pteromalidae. In: Gibson GAP, Huber JT, Woolley JB (Eds) Annotated Keys to the Genera of Nearctic Chalcidoidea (Hymenoptera). NRC Research Press, Ottawa, Canada, 541–692.

Bouček Z, Rasplus J-Y (1991) Illustrated key to West-Palearctic genera of Pteromalidae. Institut National de la Recherche Agronomique (INRA), Paris, France, 140 pp.

Bouček Z, Subba Rao BR, Farooqi SI (1979) A preliminary review of Pteromalidae (Hymenoptera) of India and adjacent countries. Oriental Insects 12: 433–468. https://doi.org/10.1080/00305316.1978.10432529

Brèthes J (1913) Himenópteros de la América Meridional. Anales del Museo Nacional de História Natural de Buenos Aires 24: 35–166.

Brues CT (1908) Notes and descriptions of North American parasitic Hymenoptera. VII. Bulletin of the Wisconsin Natural History Society 6: 160–163.

Burks RA, Heraty JM (2020) First described fossil representatives of the parasitoid wasp taxa Asaphesinae n. n. and Eunotinae (Hymenoptera: Chalcidoidea: Pteromalidae *sensu lato*) from Eocene Baltic amber. Journal of Natural History 54: 801–812. https://doi.org/10.1080/00222933.2020.1747653

Burks R, Mitroiu MD, Fusu L, Heraty JM, Janšta P, Heydon S, Papilloud NDS, Peters RS, Tselikh EV, Woolley JB, van Noort S, Baur H, Cruaud A, Darling C, Haas M, Hanson P, Krogmann L, Rasplus JY (2022 From hell's heart, I stab at thee! A determined approach towards a monophyletic Pteromalidae and reclassification of Chalci-

doidea (Hymenoptera). Journal of Hymenoptera Research 94: 13–88. https://doi.org/10.3897/jhr.94.94263

Crawford JC (1909) Notes on some Chalcidoidea. Canadian Entomologist 41: 98–99. https://doi.org/10.4039/Ent4198-3

Cruaud A, Rasplus JY, Zhang J, Burks R, Delvare G, Fusu L, Gumovsky A, Huber JT, Janšta P, Mitroiu MD, Noyes JS, van Noort S, Baker A, Böhmová J, Baur H, Blaimer BB, Brady S, Bubeníková K, Chartois M, Copeland R, Dale-Skey Papilloud N, Dal Molin A, Dominguez C, Gebiola M, Guerrieri E, Kresslein RL, Krogmann L, Lemmon E, Murray EA, Nidelet S, Nieves-Aldrey JL, Perry RK, Peters RS, Polaszek A, Sauné L, Torréns J, Triapitsyn S, Tselikh EV, Yoder M, Lemmon AR, Woolley JB, Heraty J (2024) The Chalcidoidea bush of life: evolutionary history of a massive radiation of minute wasps. Cladistics 40: 34–63. https://doi.org/10.1111/cla.12561

de Boer JG, Salis L, Tollenaar W, van Heumen LJM, Costaz TPM, Harvey JA, Kos M, Vet LEM (2019) Effects of temperature and food source on reproduction and longevity of aphid hyperparasitoids of the genera *Dendrocerus* and *Asaphes*. Journal of the International Organization for Biological Control 64: 277–290. https://doi.org/10.1007/s10526-019-09934-4

De Santis L (1960) Anotaciones sobre Calcidoideos Argentinos. II. (Hymenoptera). Revista de la Facultad de Agronomíía (3ª época) 36: 109–119.

Förster A (1856) Hymenopterologische Studien. II. Heft. Chalcidiae und Proctotrupii. Ernst ter Meer, Aachen, 152 pp.

Gahan AB, Fagan MM (1923) The type species of the genera of Chalcidoidea or chalcid-flies. Bulletin of the United States National Museum 124: 1–173. https://doi.org/10.5479/si.03629236.124.i

Gibson GAP (1997) Chapter 2. Morphology and terminology. In: Gibson GAP, Huber JT, Woolley JB (Eds) Annotated Keys to the Genera of Nearctic Chalcidoidea (Hymenoptera). NRC Research Press, Ottawa, Canada, 16–44.

Gibson GAP, Vikberg V (1998) The species of *Asaphes* Walker from America North of Mexico, with remarks on extralimital distributions and taxa (Hymenoptera: Chalcidoidea: Pteromalidae). Journal of Hymenoptera Research 7(2): 209–256. https://biostor.org/reference/522

Girault AA (1914) Descriptions of new chalcidflies. Proceedings of the Entomological Society of Washington 16: 109–119.

Girault AA (1917) Descriptiones Hymenopterorum Chalcidoidicarum variorum cum observationimus V. Private publication, Glendale, 16 pp.

Graham MWRdeV (1969) The Pteromalidae of north-western Europe (Hymenoptera: Chalcidoidea). Bulletin of the British Museum (Natural History) (Entomology), Supplement 16: 1–851. https://doi.org/10.5962/p.258046

Graham MWRdeV (1990) The identity of certain problematic *Dahlbom* genera of Chalcidoidea (Hymenoptera) some represented by original material in Zoologiska Institutionen, Lund, Sweden. Entomologist's Monthly Magazine 126(1516–1519): 197–200.

Huang DW, Xiao H (2005) Zoological of China. Vol. 42. Insecta. Hymenoptera (Pteromalidae). Science Press, Beijing, 272–281.

Jombart T, Devillard S, Balloux F (2010) Discriminant analysis of principal components: A new method for the analysis of genetically structured populations. BMC Genetics 11(1): 1–15. https://doi.org/10.1186/1471-2156-11-94

Kamel MBH, Kavallieratos NG, Starý P, Rakhshani E (2020) First record of *Diaeretus leucopterus* (Haliday) (Hymenoptera, Braconidae, Aphidiinae), the parasitoid of the aphid species, *Eulachnus agilis* (Kaltenbach) (Hemiptera, Aphididae) in North Africa.

Egyptian Journal of Biological Pest Control 30: 1–6. https://doi.org/10.1186/s41938-020-00249-6

Kamijo K, Takada H (1973) Studies on aphid hyperparasites of Japan, 2-aphid hyperparasites of the Pteromalidae occurring in Japan (Hymenoptera). Insecta Matsumura 2: 39–76. http://hdl.handle.net/2115/9773

Kimura MA (1980) A simple method for estimating evolutionary rates of base substitutions through comparative studies of nucleotide sequences. Journal of molecular evolution 16: 111–120. https://doi.org/10.1007/BF01731581

Malagón-Aldana LA, Jensen AR, Smith DR, Shinohara A, Vilhelmsen L (2022) Sawflies out of Gondwana: phylogenetics and biogeography of Argidae (Hymenoptera). Systematic Entomology 47(1): 231–258. https://doi.org/10.1111/syen.12527

Mani MS, Saraswat GG (1974) Part III. In: Mani MS, Dubey OP, Kaul BK, Saraswat GG (Eds) Descriptions of some new and new records of some known Chalcidoidea (Hymenoptera) from India. Memoirs of the School of Entomology, St. John's College, no. 3: 85–107.

McMullen RD (1966) New records of chalcidoid parasites and hyperparasites of *Psylla pyricola* Forster in British Columbia. Canadian Entomologist 98: 236–239. https://doi.org/10.4039/Ent98236-3

Morley C (1910) Catalogue of British Hymenoptera of the family Chalcididae. Longmans and Co., B. Quaritch, Dulau and Co., Ltd., London, 74 pp.

Narendran TC, van Harten A (2007) Five new species of Pteromalidae (Hymenoptera: Chalcidoidea) from Yemen. Journal of Experimental Zoology, India 10(1): 113–119.

Nees ab Esenbeck CG (1834) Hymenopterorum Ichneumonibus affinium monographiae, genera Europeaea et species illustrantes. Vol. 2. J. G. Cottae, Stuttgart and Tubingen, 448 pp. https://doi.org/10.5962/bhl.title.26555

Noyes JS (2019) Universal Chalcidoidea Database. http://www.nhm.ac.uk/chalcidoids.

Provancher L (1887) Additions et corrections a la Faune Hymenopterologique de la province de Québec. C. Darveau, Quebec, 477 pp. https://doi.org/10.5962/bhl.title.38326

Ratzeburg JTC (1844) Die Ichneumonen der Forstinsecten in forstlicher und entomologischer Beziehung, vol. 1. Berlin, 224 pp. https://doi.org/10.5962/bhl.title.11094

Ratzeburg JTC (1848) Die Ichneumonen der Forstinsecten in forstlicher und entomologischer Beziehung, vol 2. Berlin, vi + 238 pp.

Reinhard H (1857) Beiträgeb zur Geschichte und Synonymic der Pteromalinen. Berliner entomologische Zeitschrift 1: 70–80. https://doi.org/10.1002/mmnd.18570010112

Rondani C (1848) Osservazioni sopra parecchie species di esapodi afidicidi e sui loro nemici. Nuovi Annali delle Scienze Naurali e Rendiconto dei Lavori dell'Accademia delle Scienze dell'Istituto e della Society Agraria di Bologna 9: 5–37.

Sharma AK, Subba Rao BR (1959) Description of two new parasites of an aphid from North India (Aphidiidae: Ichneumonoidea and Pteromalidae: Chalcidoidea). Indian Journal of Entomology 20: 181–188.

Walker F (1834) Monographia Chalciditum. The Entomological Magazine 2: 148–179.

Xiao H, Huang DW (2000) A taxonomic study on *Asaphes* (Hymenoptera: Pteromalidae) from China, with descriptions of four new species. Entomologia Sinica 7(3): 193–202. https://doi.org/10.1111/j.1744-7917.2000.tb00407.x

Zetterstedt JW (1838) Sectio secunda. Hymenoptera. In: Zetterstedt JW (Eds) 1838–1840, Insecta lapponica descripta. Voss, Lipsiae, 417–476. https://doi.org/10.5962/bhl.title.8242

ZooKeys

Limnichthys koreanus, a new species of creediid fish (Teleostei, Acropomatiformes, Creediidae) from Korea

Yu-Jin Lee[1], Jin-Koo Kim[1]

1 Department of Marine Biology, Pukyong National University, Busan 48513, Republic of Korea
Corresponding author: Jin-Koo Kim (taengko@hanmail.net)

Abstract

Limnichthys koreanus **sp. nov.** is described on the basis of the holotype and 11 paratypes from subtidal waters of Seogwipo, Jeju Island, Korea. The new species had previously been regarded as the Northern Hemisphere population of the anti-equatorial *L. fasciatus*, but molecular analyses of mitochondrial COI and 16S genes recovers deep genetic divergences of 9.4% and 15.0% between the new species and topotypical specimens of *L. fasciatus*. *Limnichthys koreanus* **sp. nov.** is distinguished from all other species of *Limnichthys* based on the following combination of colouration and morphological characteristics: 38-40 vertebrae; 0–6 dorsal saddles joining mid-lateral stripe; small infraorbital sensory pores; a single median interorbital pore; and well-developed vomerine teeth. Summary characters for comparative congeneric species are provided.

Key words: benthic species, Jeju Island, sand burrower, taxonomy

Introduction

The family Creediidae consists of 18 species accommodated in eight globally distributed genera, most of which are concentrated in subtropical and tropical coastal waters of the Indo-Pacific Ocean (Nelson et al. 2016; GBIF Secretariat 2023; Fricke et al. 2024). Known colloquially as sand burrowers or sand lancers, creediids are small, slender, sand-dwelling fishes that camouflage and hide in the uppermost layer of sand in wait of passing prey before rapidly darting out and back into the sand in a boomerang fashion (Nelson 1985; Cozzi and Clark 1995). The creediid fishes have the following characteristics: less than 5–6 cm in length; prominent eyes positioned dorsally on the head; fleshy snout; no spines in the dorsal or anal fin rays (Nelson 1985). Studies on *Limnichthys* have compared their morphological phylogenetics and examined skeletal structures, new species, including feeding behavior, and early life history (Nelson 1978, 1979, 1985; Leis 1982; Shimada and Yoshino 1987; Pettigrew and Collin 1995; Yoshino et al. 1999; Pettigrew et al. 2000; Shibukawa 2010; Fricke and Golani 2012). The creediid genus *Limnichthys* is of particular taxonomic interest, with nearly all its species adopting anti-equatorial distribution. The possibility of the existence of cryptic populations has been discussed for a long time (Nelson 1978).

Although creediid species occur far from each other they are highly morphologically similar. Six species of *Limnichthys* are currently recognized as valid: *L. fasciatus* Waite, 1904; L. *marisrubri* Fricke & Golani, 2012; *L. nitidus* Smith, 1958; *L. orientalis* Yoshino, Kon & Odabe, 1999; *L. polyactis* Nelson, 1978; and *L. rendahli* Parrott, 1958. With the exception of *L. nitidus*, which occurs from tropical to temperate water of the Indo-Pacific Ocean, the other species of *Limnichthys* exhibit anti-equatorial distributions (Nelson 1985; GBIF Secretariat 2023). Notably, *L. fasciatus* exhibits a disjunct, anti-equatorial distribution in both hemispheres, but its status as a single, widespread species has not been properly investigated (Nelson, 1978). Morphological and molecular comparisons of specimens identified as *L. fasciatus* from Korea in the Northern Hemisphere indicate that they are different from topotypical examples of *L. fasciatus* from southeastern Australia. Accordingly, we describe *L. koreanus* sp. nov. on the basis of 12 specimens collected during a monitoring survey of subtropical fish species from the subtidal zone of Jeju Island, Korea. The new species is compared with congeneric species, and summary accounts and phylogenetic relationships for species of *Limnichthys* are discussed.

Materials and methods

Meristics, morphometrics, and specimen deposition

Methods for counting measuring follow Waite (1904), Nelson (1978), and Yoshino et al. (1999). Measurements were recorded to the nearest 0.1 mm using vernier calipers. Morphometric values are summarized in Tables 1, 2, expressed as percentages of the standard length (SL) and head length (HL). Images of specimens were taken using a digital camera (D750; Nikon, Japan). Detailed morphological characteristics were examined with a stereomicroscope (SZX-16; Olympus, Tokyo, Japan).

Osteological details were determined from X-ray images, cleared and stained specimens, and micro-CT data. Micro-CT scans were taken using Phoenix V-Tome-X C450 Volume Graphics® VGSTUDIO Max software and handled using Volume Graphics® myVGL viewer. We performed osteological staining with a paratype specimen (PKU 22428) using a modified version of the method detailed in Song and Parenti (1995). Vertebral counts were presented as a total number of abdominal to caudal vertebrae, which was followed by Nelson (1978). Terminology of skeletal bones followed by Lucena Rosa (1995).

Twelve specimens of the new species (35.8–45.3 mm TL, 33.4–40.0 mm SL) were collected from subtidal zones at depths of 1–5 m in Seogwipo, Jeju Island, Korea between July 2022 and December 2023 (Fig. 1). Specimens were vouchered in Pukyong National University (**PKU**) and National Marine Biodiversity Institute of Korea (**MABIK**) with register numbers (PKU 21427; PKU 21528–21530; PKU 22426–22428; PKU 22626–22627; PKU 63120–63122, MABIK PI00060703– MABIK PI00060705). Tissue samples were taken from the right side of the body, preserved in 99% ethanol, and deposited in the **PKU**. We followed the immersion specimen production manual of the **MABIK**, under the National Institute of Marine Biological Resources of the Ministry of Oceans and Fisheries. One specimen was anatomized to investigate the gonadal development. Comparative specimens were loaned and investigated from various

Table 1. Voucher number, institution, collected date, and GenBank number of specimens used in present study.

Species	Voucher Number	n	Institution	Collected location (country)	Date	GenBank number	
						COI	16S rRNA
Limnichthys koreanus	MABIK PI00060703 (PKU 63120)	1	National Marine Biodiversity Institute of Korea	Moseulpo, Jeju Island (South Korea)	2022.08.15	OR541978	OR543335
	MABIK PI00060704 (PKU 63121)	1			2022.08.15	OR541979	OR543336
	MABIK PI00060705 (PKU 63122)	1			2022.08.15	OR541980	OR543337
	PKU 21427	1	Pukyong National University		2022.07.13	OR541981	OR543338
	PKU 21528	1			2022.08.15	OR541982	OR543339
	PKU 21529	1			2022.08.15	OR541983	–
	PKU 21530	1			2022.08.15	–	OR543340
	PKU 22426	1			2023.07.17	–	–
	PKU 22427	1			2023.07.17	–	–
	PKU 22428	1			2023.07.17	–	–
	PKU 22626	1		Seongsanpo, Jeju Island (South Korea)	2023.12.16	PP708995	PP708997
	PKU 22627	1			2023.12.16	PP708996	PP708998
L. fasciatus	I.44122-031	1	Australian Museum	Central Coast, NSW (Australia)	2007.05.08	OR544519	–
	I.44627-025	1		Nelson Bay, NSW (Australia)	2008.04.08	OR544515	OR543322
	TCWC 17569.03	1	Texas A&M University	Central Coast, NSW (Australia)	2015.02.22	OR544522	OR543331
	CAS 109236*	3	California Academy of Science	Lord Howe Island, NSW (Australia)	1902.12.03 −1903.01.21	–	–
	CAS 38242	3		Lord Howe Island, NSW (Australia)	1973.02.09	–	–
	CAS 120473	7		Sydney, NSW (Australia)	1998.04.15		
	CAS 219288	1		Viti Levu (Fiji)	2002.02.10		
	NSMT-P-125200	1	National Museum of Nature and Science	Japan	–	LC753137	OR543330
	NSMT-P-125201	1		Japan	–	LC753135	OR543329
	NSMT-P-125202	1		Japan	–	OR546102	OR543328
L. cf. *nitidus*	CAS 228250	5	California Academy of Science	Hawaii Island (USA)	1993.04.15	–	–
	KAUM-I 124455		Kagoshima University	Amami Islands (Japan)	2018.12.16	OR544523	OR543332
	KAUM-I 143956			Amami Islands (Japan)	2020.07.03	OR544524	OR543333
L. orientalis	KPM-NI 51923		Kanagawa Prefectural Museum of Natural History	- (Japan)	2010.07.20	LC753149**	–
Trichonotus setiger	–		–		–	KU944772**	NC034345**
T. marleyi	–				–	JF494737**	–

* Paratypes specimens. ** Sequences were obtained from GenBank.

museums and institutions, including the Australian Museum, Sydney (**AMS**), the Kagoshima University Museum, Korimoto (**KAUM**), the Kanagawa Prefectural Museum of Natural History, Odawara (**KPM**), Fish Section and Center for Molecular Biodiversity Research, National Museum of Nature and Science, Tokyo (**NSMT**), the California Academy of Sciences, San Francisco (**CAS**), and the Biodiversity Research and Teaching Collections, Department of Wildlife and Fisheries Sciences, Texas A&M University (**TCWC**). Institutional codes follow Sabaj (2023).
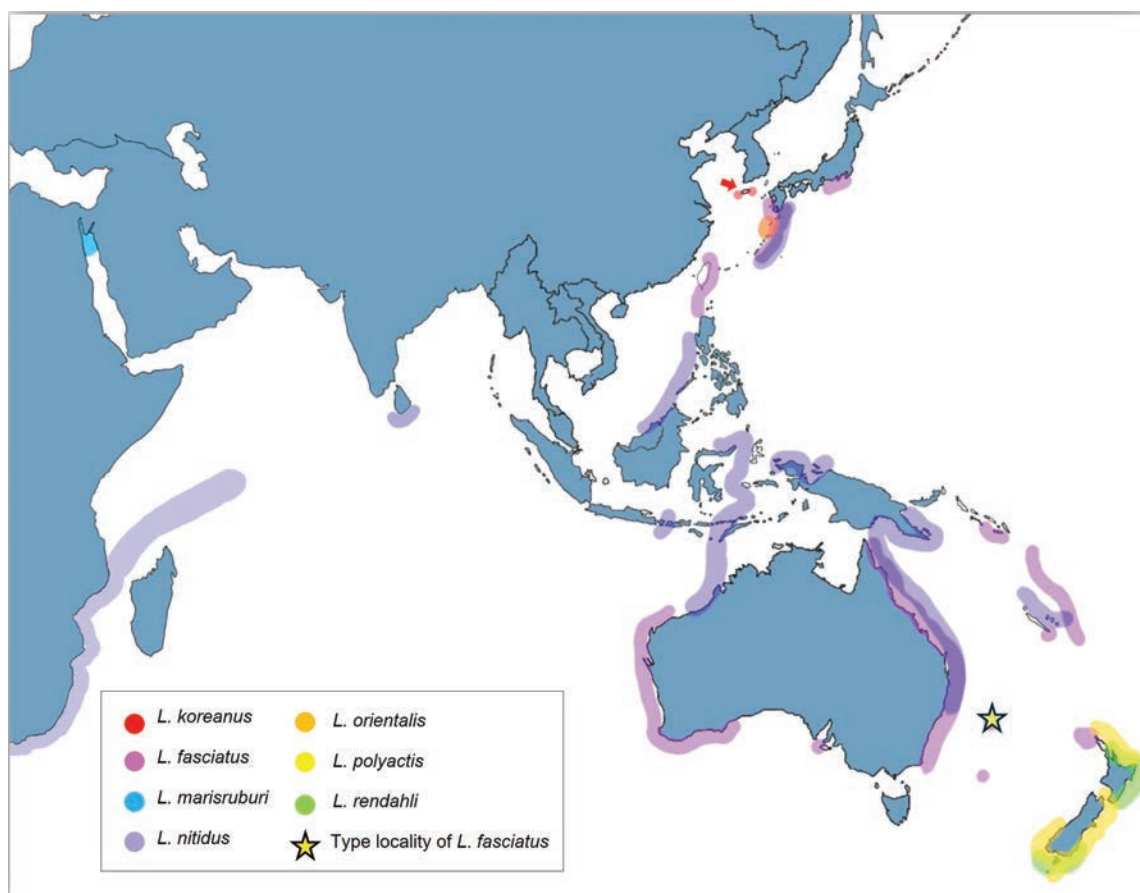
Figure 1. Map showing sampling sites and distribution of *Limnichthys* spp. Each color marks indicate each species: Red marks and arrow showing collected location of *Limnichthys koreanus* sp. nov.; pink marks showing *L. fasciatus*, which is anti-equatorial species, and yellow star mark showing the type locality of *L. fasciatus*; blue marks showing *Limnichthys marisrubri* in the Red Sea; purple marks showing *L. nitidus* in Indo-Pacific Ocean; orange marks showing *L. orientalis* in Japan; yellow marks showing *L. polyactis* in New Zealand; green marks showing *L. rendahli* in New Zealand.

Comparative materials of *L.* cf. *nitidus* used in this study were collected from Pacific Ocean (Japan, and Hawaii, USA), which is far from the type locality of the species (Mozambique, South Africa). Given that creediid fishes, in particularly those belonging to the genus *Limnichthys*, exhibit local endemism with the possibility of undescribed cryptic diversity, we refer to these non-topotypical comparative specimens as *L.* cf. *nitidus*. X-ray images and micro-CT images of syntypes and non-type material of *L. fasciatus* were examined, as well as skeletal sketch by Nelson (1978). See list of material examined below.

DNA extraction, amplification, and sequencing

Genomic DNA was extracted using tissues the AccuPrep Genomic DNA Extraction Kit (Bioneer, Daejeon, Republic of Korea). Mitochondrial cytochrome c oxidase subunit I (COI) and 16S ribosomal RNA (16S) were amplified from extracted gDNA using the polymerase chain reaction. Primer sets for 16S and COI follow by Palumbi (1996) and Ward et al. (2005) respectively. Polymerase chain reaction with a mixture (2 µL 10× buffer, 1.5 µL dNTPs, 2 µL primer set, 0.1 µL Taq polymerase, and 2 µL genomic DNA (gDNA) made up to 20 µL with distilled

water) was performed under the following conditions: initial denaturation step at 95 °C for 5 min followed by 35 cycles of denaturation at 95 °C for 30 s, annealing at 52–54 °C for 45 s, and extension at 72 °C for 45 s, with a final extension at 72 °C for 7 min. Amplification was conducted using a thermal cycler (MJ mini PCT-1148; Bio-Rad, Hercules, CA, USA). Sequences were read by BigDye Terminator v. 3.1 cycle sequencing kits (Applied Biosystems, Foster City, CA, USA) with an ABI PRISM 3730XL analyzer (96 capillary type; Applied Biosystems).

Molecular analysis

A total number of 5,750 bp in 16S and 7,564 bp in COI sequences were obtained. To analyze the relationships among sequences, alignment was performed using ClustalW (Thompson et al. 1994) in BioEdit 7 (Hall 1999). The final sequence lengths used in the analysis were 401 bp in 16S, and 417 bp in COI per individual. Genetic distances were calculated using Mega 11 (Tamura et al. 2021) with the Kimura 2-parameter (K2P) model (Kimura 1980). Neighbour-joining trees were constructed based on 1,000 bootstrap replications by maximum composite likelihood model using Mega 11 software (Tamura et al. 2004). Sequence data for other species in the genus *Limnichthys* (*Limnichthys orientalis*) and outgroup of two species [Trichonotidae: *Trichonotus marleyi* (JF494737 in COI); *T. setiger* (NC034345 in 16S; KU944772 in COI)] were obtained from the NCBI database. The accession numbers of all sequences are provided in Table 1.

Results

Taxonomy

Acropomatiformes Gill, 1893 (new Korean name: Ban-dit-bul-ge-reu-chi-mok)
Creediidae Waite, 1899 (new Korean name: Byeol-ba-ra-gi-gwa)
***Limnichthys* Waite, 1904 (new Korean name: Byeol-ba-ra-gi-sok) (Tables 2, 3, Figs 2–7)**

***Limnichthys koreanus* sp. nov.**
https://zoobank.org/462BD9BA-4E7A-44AC-96EB-52F8F972771D
Table 1, 2, Figs 2–7
New English name: Korean sand burrower; new Korean name: Tti-byeol-ba-ra-gi

Material examined. *Holotype*: Sᴏᴜᴛʜ Kᴏʀᴇᴀ • 45.95 mm TL, 39.5 mm SL; tidal pool on Jeju Island; 33°13'21.1"N, 126°14'30.9"E; 1 m; 15 August 2022; collector Yu-Jin Lee & Jin-Koo Kim; scoop net; MABIK PI00060703 (PKU 63120).
   Paratypes. Sᴏᴜᴛʜ Kᴏʀᴇᴀ • 44.5 mm TL, 38.4 mm SL; 15 August 2022; same data as holotype; MABIK PI00060704 (PKU 63121); Sᴏᴜᴛʜ Kᴏʀᴇᴀ • 45.3 mm TL, 40.0 mm SL; 15 August 2022; same data as holotype; MABIK PI00060705 (PKU 63122); Sᴏᴜᴛʜ Kᴏʀᴇᴀ • 1 ♀, 44.5 mm TL, 37.3 mm SL; 14 July 2022; same data as holotype; PKU 21427; Sᴏᴜᴛʜ Kᴏʀᴇᴀ • 38.5 mm TL, 34.5 mm SL; 15 August 2022; same data as holotype; PKU 21528; Sᴏᴜᴛʜ Kᴏʀᴇᴀ • 38.3 mm TL, 33.6 mm SL; 15 August 2022; same data as holotype; PKU 21529; Sᴏᴜᴛʜ Kᴏʀᴇᴀ • 35.8 mm TL, 33.4 mm SL; 15 August 2022; same data as holotype; PKU 21530;
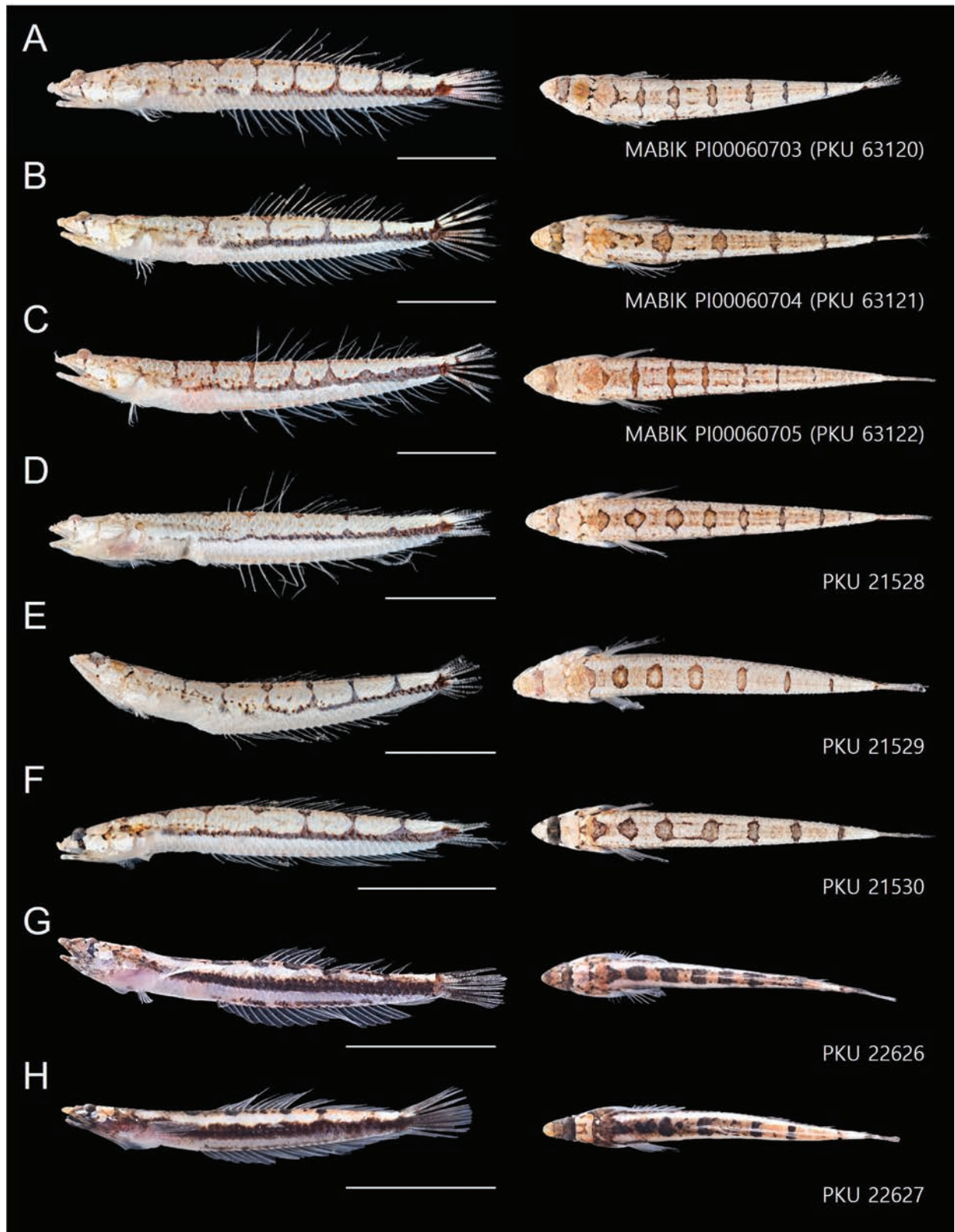
Figure 2. *Limnichthys koreanus* sp. nov. **A** holotype, MABIK PI00060703 (PKU 63120), 37.3 mm SL, Moseulpo **B** paratype, MABIK PI00060704 (PKU 63121), 38.4 mm SL, Moseulpo **C** paratype, MABIK PI00060705 (PKU 63122), 40.0 mm SL, Moseulpo **D** paratype, PKU 21528, 34.5 mm SL, Moseulpo **E** paratype, PKU 21529, 33.6 mm SL, Moseulpo **F** paratype, PKU 21530, 33.4 mm SL, Moseulpo **G** paratype, PKU 22626, 33.8 mm SL, Seongsanpo **H** paratype, PKU 22627, 35.7 mm SL, Seongsanpo. Scale bars indicate 10 mm. Left images showing lateral views; right images showing dorsal views. Voucher numbers are annotated in the bottom right corner of each image. Scale bars: 10 mm.
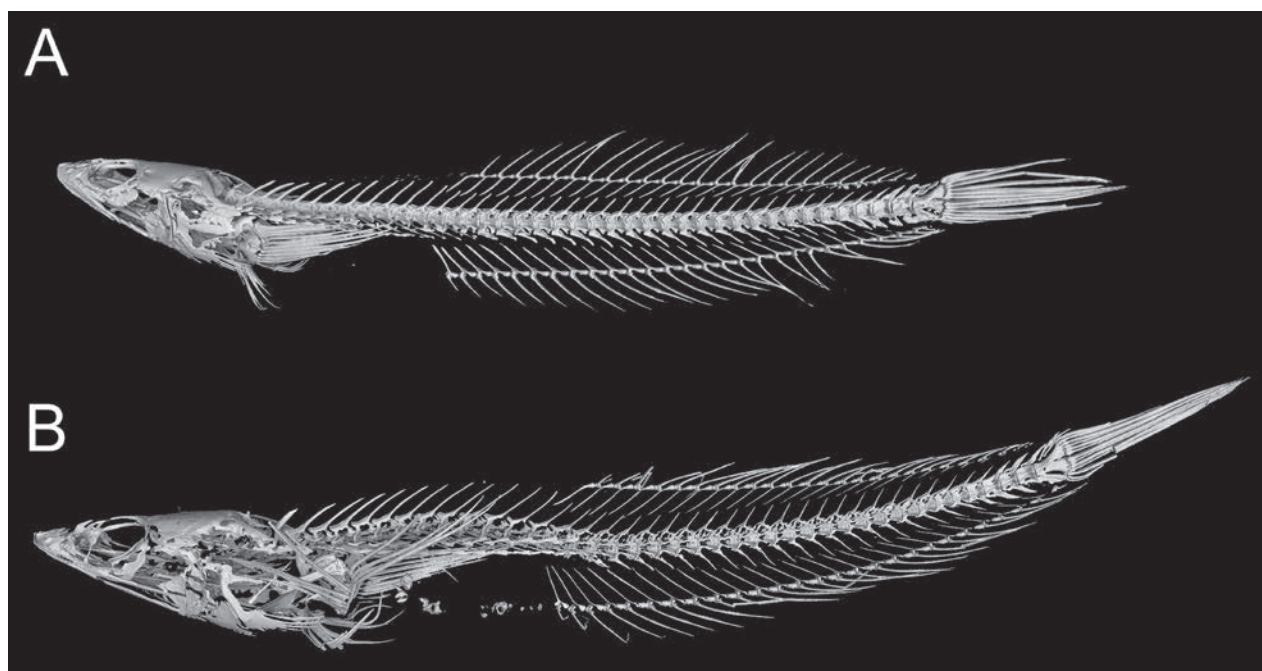
Figure 3. Radiographs of *Limnichthys* species using CT-scan **A** *Limnichthys koreanus* sp. nov., holotype, MABIK PI00060703 (PKU 63120), 37.3 mm SL, South Korea **B** *Limnichthys fasciatus*, syntype, AMS I.5858, 43 mm SL, preserved in Australian Museum.

South Korea • 42.4 mm TL, 38.5 mm SL; 17 July 2023; same data as holotype; PKU 22426; South Korea • 43.2 mm TL, 37.6 mm SL; 17 July 2023; same data as holotype; PKU 22427; South Korea • 44.1 mm TL, 39.4 mm SL; 17 July 2023; same data as holotype; staining specimen; PKU 22428; South Korea • 37.5 mm TL, 33.8 mm SL; tidal pool on Jeju Island; 33°27'37.0"N, 126°56'02.1"E; 5 m; 15 December 2023; hand net; PKU 22626; South Korea • 38.4 mm TL, 35.7 mm SL; tidal pool on Jeju Island; 33°27'37.0"N, 126°56'02.1"E; 5 m; 15 December 2023; collector Yu-Jin Lee & Jin-Koo Kim; hand net, depth PKU 22627.

Diagnosis. Combined number of dorsal and anal fin rays 52–55; vertebrae 38–40; lateral line scales 42–46; a single median interorbital pore; vomerine teeth well developed; pelvic girdle separated each other; dorsal saddle patterns 5–9; dorsal saddles joining mid-lateral stripe 0–6 (Fig. 3A, Table 2).

Description. Counts and measurements of type materials are shown in Table 1; holotype values indicate in parenthesis in table and description. Body elongated; cylindrical and posteriorly compressed. Head to body slope almost flat; head length 24.5–32% in SL (26.1%); head depth 7–10.6% (7.1%); snout length 3.8–5.7% (3.8%) in SL (Table 3). Eyes on dorsal of head, large, and bulging. Snout terminal; upper jaw projects more than lower jaw; upper and lower jaws with a single row of minute conical teeth; a pair of filament-like antennas on anterior upper jaw (or absent); cirri on lower jaw; lips fleshy; vomer with well-developed conical teeth (Fig. 4A); palatine teeth absent; pharyngeal teeth present; tongue slender and pointed. A single of median interorbital sensory pore (Fig. 5A); infraorbital sensory pores very smaller than posterior nostril (Fig. 5E); anterior nostril tubular. Branchiostegal rays 7. Opercular flap covered pectoral fin base. Pectoral fin not reaching anal fin origin; pectoral fin rays 12–13 (12); 6–7th pectoral fin rays longest. Pelvic fin ahead of pectoral fin; 3rd pelvic fin ray longest; pelvic fin not elongated; pelvic fin with I, 5; anterior process of pelvic girdle well separated (Fig. 6A) pelvic girdle with upper projecting process
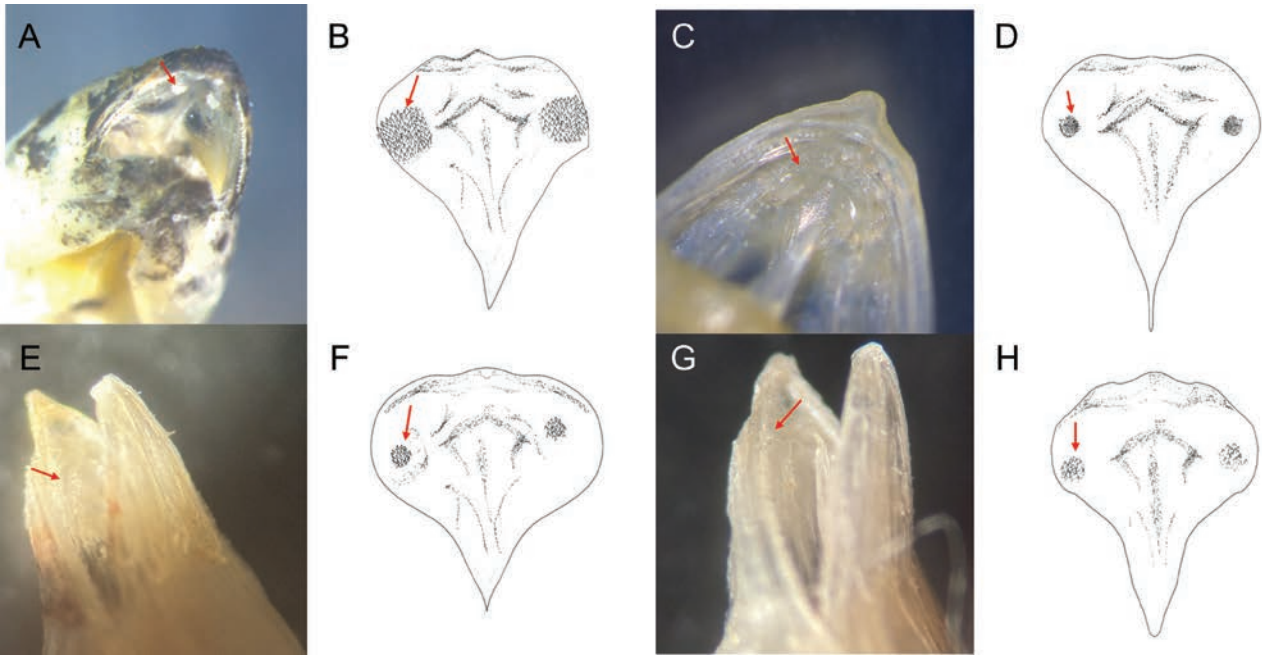
Figure 4. Vomerine teeth of *Limnichthys* spp. The red arrows indicate vomerine teeth. **A, B** *Limnichthys koreanus* sp. nov.; well-developed vomerine teeth; broad and bugling; conical teeth **C, D** *L. fasciatus,* weak-developed vomerine teeth; minute conical teeth **E, F** *L.* cf. *nitidus*; developed vomerine teeth; narrow and bugling; conical teeth **G, H** *L. orientalis*; slightly developed vomerine teeth; conical teeth.

Table 2. Comparison of counts in *Limnichthys* spp. Parentheses indicate counts of the holotype specimen.

	L. koreanus sp. nov.	*L. fasciatus* (Australia & Fiji)	*L. fasciatus* (Japan)	*L.* cf. *nitidus* (Japan & Hawaii Is.)	*L. marisrubri* (Red Sea)	*L. orientalis* (Japan)	*L. polyactis* (New Zealand)	*L. rendahli* (New Zealand)
References	In this study	In this study	In this study	In this study Nelson 1978	Fricke and Golani 2012	In this study Yoshino et al. 1999	Nelson 1978	Fricke and Golani 2012
Number of specimens	12	19	3	24	22	8	34	–
Counts								
Dorsal fin rays	25−27 (25)	24−27	26−27	22−25	22−24	21−23	28−32	29−33
Anal fin rays	26−28 (28)	26−29	27−28	26−28	24−26	24−25	31−34	30−32
Pectoral fin rays	12−13 (12)	11−14	12−13	11−12	13−15	10−11	12−13	13−16
Segment caudal fin rays	8−9 (8)	8	8	8	8	8	8	8
Lateral line scales	42−46 (43)	38−43	43−44	36−38	37−41	41−43	41−46	–
Teeth on vomer	Well-developed	Developed	Developed	Developed	–	Developed	Developed	–
Median interorbital pore	1	2	1	1	–	1	1	–
Total vertebrae	38−40 (40)	40−45	39−41	39−41	–	40−41	43−45	43−45
Number of epural	2	2	2	1	–	1	1	2
Midlateral stripe	Present	Present	Present	Present or absent	Present	Absent	Present	Present
Dorsal saddles (number)	5−9 (8)	7−9	7−9	8−12	11−14	6−11	7−9	6−8
Dorsal saddles joining midlateral stripe (number)	0−6 (4)	5−9	5−6	–	–	–	3−5	3−6

(Fig. 7A). Dorsal fin rays 25−27 (25); Origin of dorsal fin at 3−4th anal fin ray; posterior of dorsal and anal fin reaching precaudal (free from caudal). Anus ahead half of body. Anal fin rays 26−28 (28); anal fin length uniform. Caudal peduncle length very short. All fin rays not branched (only caudal fin branched). Segment of caudal
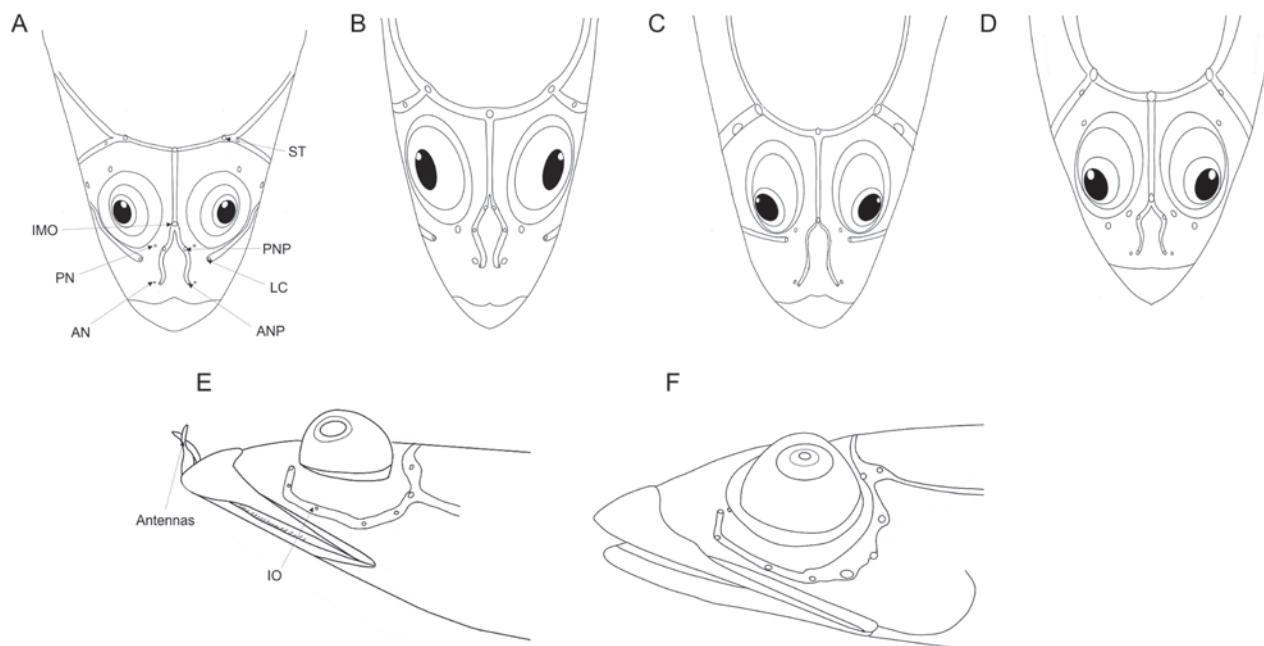
Figure 5. Dorsal and lateral view of head of *Limnichthys* spp. The photos show sensory canals and pores on head **A, E** *L. koreanus* sp. nov., sensory canals weak-developed, infraorbital sensory pores small; some species have anten-nas on snout **B, F** *L. fasciatus*; AMS I.44627; Nelson Bay, NSW; 28.7 mm SL; sensory canals well-developed; infraorbital sensory pores large **C** *L.* cf. *nitidus*; CAS 228250; Hawaii Island, USA; 20.24 mm SL; sensory canals well-developed **D** *L. orientalis*; KPM-NI 51923; Japan; 29.4 mm SL; sensory canals well developed. Abbreviations: AN, anterior nostril; ANP, anterior nasal pore; IMO, interorbital median pore; IO, infraorbital pores; LC, lachrymal pore; PN, posterior nostril; PNP, posterior nasal pore; ST, supratemporal pores.

fin rays 8–9 (8). Two epurals (Fig. 6B). Lateral line scales 42–46; lateral line scales trilobed (Fig. 8A); lateral line from opercular to precaudal gradually running down. Body covered with cycloid scales (Fig. 8B); no scales on frontal; scales on cheeks well developed. Gill rakers of first gill arch with small and low multi-spined stubs like patch; gill rakers 2+10.

Coloration when fresh. Body whitish pink. Dorsal and ventral edges pale or-ange, brown, or white. Dark stripe below eyes. Eyeballs dark brown or black. Oper-cular pinkish and slightly transparent. Dorsal saddle patterns 5–9, dark brown, dark orange, or black. Distinct horizontal bar on body. Number of dorsal saddle patterns joining with lateral bar 0–6. Pelvic, pectoral, and anal fins transparent. Darkish spots on dorsal fin rays. Caudal fin rays similar in color to body pattern.

Coloration when preserved. Body white. Head white with black or dark brown spots. Dark stripe below eyes. Lateral band black or dark brown. All fins transparent. Spots on dorsal and caudal fin rays. Dorsal or lateral patterns not clearly visible after fixation, depending on preservative solution.

Distribution. The species is presently known only from Jeju Island, Korea.

Biology and habitat. They inhabit relatively thick sand substrates (or may-be more like fine gravels), often hiding almost entirely in the sand in subtidal zone. They tended to dart out to catch prey (e.g. copepods) and then return to their original position. Females have mature eggs in their gonads from June to August. The eggs (522 per individual) are approximately 0.62–0.65 mm in diameter. In contrast, a specimen from December lacked developed gonads.

Etymology. The epithet of the new species, *koreanus*, refers to the type locality (Korea) where the species were collected.
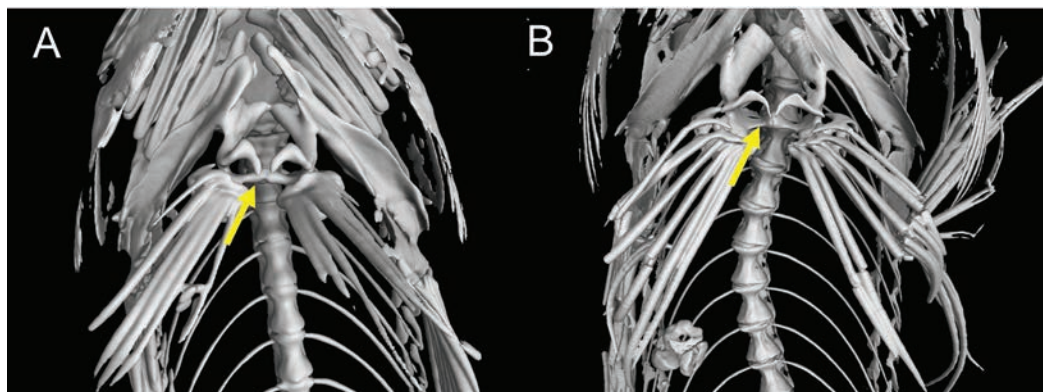
Figure 6. Separation of the anterior process of pelvic girdle **A** *Limnichthys koreanus* sp. nov., holotype, MABIK PI00060703, 39.5 mm SL, South Korea, pelvic girdle well-separated from each other **B** *Limnichthys fasciatus*, syntype, AMS I.5858, 43 mm SL, preserved in Australian Museum, pelvic girdle close to each other.

Table 3. Proportional measurements in *Limnichthys koreanus* sp. nov.

	Holotype (MABIK PI00060703)	Paratypes (*n* = 11)
Standard length (mm)	37.3	33.42−40.0
Morphometric characters		
In SL (%)		
Body depth	13.3	10.7−12.8
Head length	26.1	24.5−32.3
Head depth	7.1	7.6−10.6
Snout length	3.8	4.0−5.7
Orbital diameter	3.8	2.6−4.1
Interorbital length	2.1	1.8−2.6
Postorbital length	17.0	15.4−20.2
Upper jaw length	9.7	6.7−11.3
Predorsal length	46.6	44.2−50.5
Prepectoral length	26.8	23.8−30.0
Prepelvic length	23.2	22.3−26.0
Preanal length	41.4	41.9−45.9
Dorsal fin base length	44.0	41.4−49.5
Anal fin base length	52.0	52.9−60.8
In HL (%)		
Snout length	16.9	15.2−17.7
Orbital diameter	15.8	9.2−16.7
Interorbital length	4.7	4.4−6.7
Upper jaw length	34.1	24.6−37.7

Morphological comparisons. *Limnichthys koreanus* sp. nov. is clearly distinguished from the other species in the genus *Limnichthys* in having significantly developed vomerine teeth and number of total vertebrae (38−40) (Table 3; Fig. 4). The new species is most similar to *Limnichthys fasciatus*, but can be separated based on the following characters: well-developed vomerine teeth (significant bugling vs weak bugling in *L. fasciatus*); total vertebrae count (38−40 vs 40−45 in *L. fasciatus*); presence of spot pattern on dorsal- and caudal-fin rays (absent in *L. fasciatus*); size of the infraorbital sensory pore below the middle of the eyes (smaller than the posterior nostril [PN] vs similar or larger than the PN in *L. fasciatus*); a single of median interorbital pore
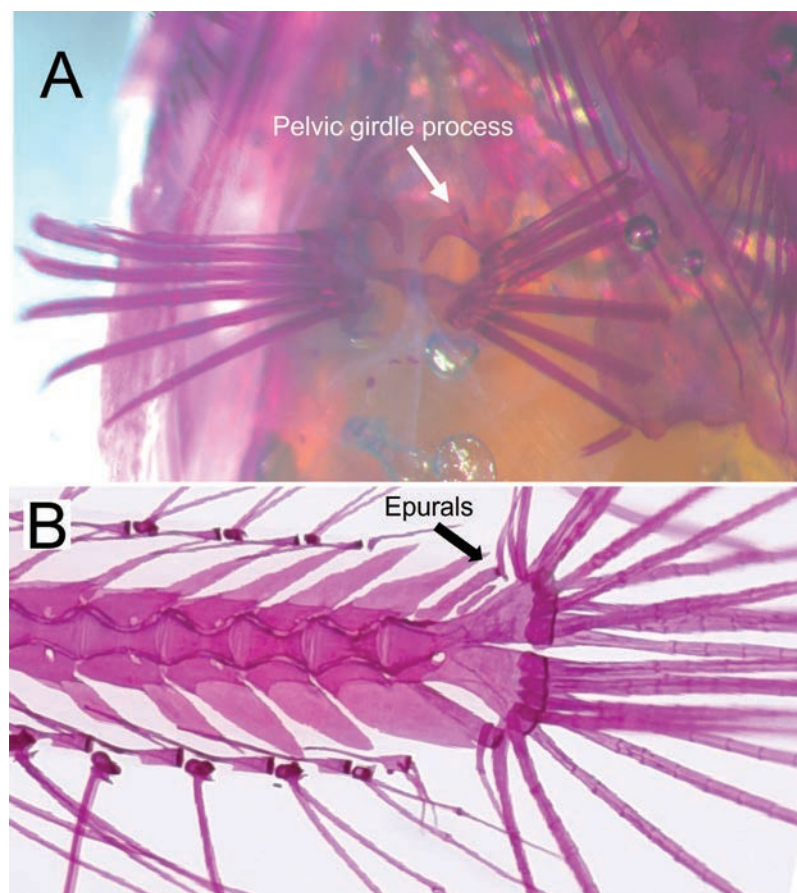
Figure 7. Photos showing detailed morphological traits in a staining specimen of *Limnichthys koreanus* sp. nov. **A** upper process of pelvic girdle **B** two epurals. Arrows indicate terms of parts.

(two in *L. fasciatus*) (Fig. 5); separation of the anterior process of pelvic girdle (nearby in *L. fasciatus*) (Fig. 6). Especially, *L. fasciatus* including paratype specimens in the south hemisphere has well-separated interorbital median pores (having two pores in *L. fasciatus* from Lord Howe Island, Fiji, and Sydney). Due to the proximity between the two interorbital median pores, they are often misidentified as one pore. *Limnichthys koreanus* further differs from *L.* cf. *nitidus*, *L. orientalis*, and *L. polyactis* in having: two instead of one epural; dorsal-fin rays (25−27 vs 22−25 in *L.* cf. *nitidus*; 21−23 in *L. orientalis*; 28−32 in *L. polyactis*); anal-fin rays (26−28 vs 26−28 in *L.* cf. *nitidus*; 24−25 in *L. orientalis*; 31−34 in *L. polyactis*), segement caudal-fin rays (8−9 vs 8); and presence of midlateral body stripe. *L. polyactis* is the endemic species which only distributed in New Zealand, and it is geographically separated from the other species (Fig. 1). *Limnichthys marisrubri* and *L. rendahli*, which have a single epural, are distinguished following characters: dorsal fin rays (25−27 vs 24−27 in *L. fasciatus* vs 22−24 in *L. marisrubri* vs 29−33 in *L. rendahli*), anal fin rays (26−28 vs 26−29 in *L. fasciatus* vs 24−26 in *L. marisrubri* vs 30−32 in *L. rendahli*).

Genetic comparisons. COI (510−614 bp) and 16S rRNA (442−508 bp) sequences were obtained from *L. koreanus* sp. nov. After alignment with National Center for Biotechnology Information (NCBI) sequences of other *Limnichthys* species (Fig. 9), we found significant genetic divergences of 9.4% and 15.0% for *L. fasciatus* in the COI and 16S rNA genes from near the type locality
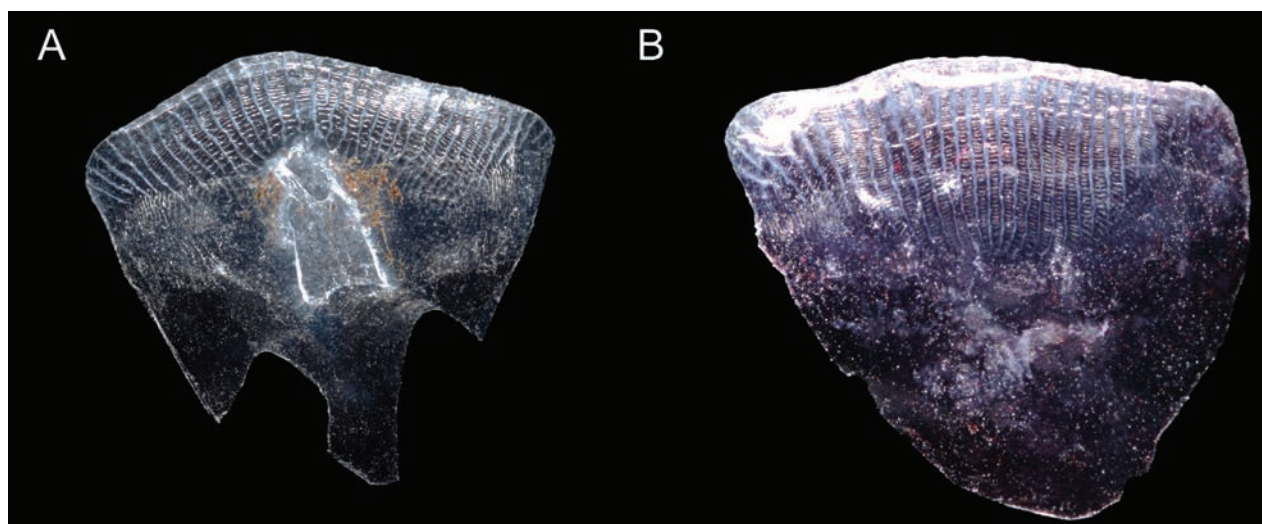
Figure 8. Two types of scales of *Limnichthys koreanus* sp. nov. **A** pored lateral line scales with trilobed shape **B** a scale on the body. Scales are cycloid.

(southeastern Australia), respectively. Furthermore, genetic distances of 16.2% and 18.4% were observed for *L.* cf. *nitidus*. Only COI gene sequences were obtained for *L. orientalis*, indicating a genetic distance of 20.9%.

Discussion

We discovered a new species, *Limnichthys koreanus* sp. nov., through morphological and molecular analysis of 12 specimens collected from the subtidal zone (at 1−2 m in depth) of Jeju Island, Korea between August 2022 and December 2023. *Limnichthys* species are remarkable because their morphological characteristics are strikingly similar despite high endemism. They commonly have dorsal saddle patterns, and the cirri on the lower jaw are well developed. Initially, this new species was considered a cryptic species of *L. fasciatus* because it appeared to have no morphological differences; it only exhibited a large genetic distance. However, we found significant morphological traits differing from type specimens as follows: the new species has fewer vertebrae; the infraorbital sensory pores below the middle of the eyes smaller than the posterior sensory pores; separation of the anterior process of both pelvic girdles; the highly developed vomerine teeth. Compared with the other species, the new species has spots (rarely absent) on the dorsal fin rays, in contrast to the transparent dorsal fin rays of *L. fasciatus*. The number of dorsal saddle patterns in the new species ranges from 5 to 9, whereas it ranges from 7 to 9 in *L. fasciatus*. Notably, differences in caudal fin ray segments were first discovered in this study. *Limnichthys* species typically have eight caudal fin ray segments and slightly developed vomerine teeth (Nelson 1985; Fricke and Golani 2012). However, our species has 8−9 branched caudal fin rays and well-developed vomerine teeth. Additionally, a previously unreported upper process of pelvic girdle was observed in the new species compared with previous skeletal sketches (Figs 6, 7).

In terms of genetic results, we considered that the individuals used for molecular analysis of *L. fasciatus* were far from the type locality (Lord Howe Island), located 600 km east of Australia. We representatively used three specimens from Nelson Bay and the central coast of New South Wales, the collected location of specimens are about 7−800 km away from each other.
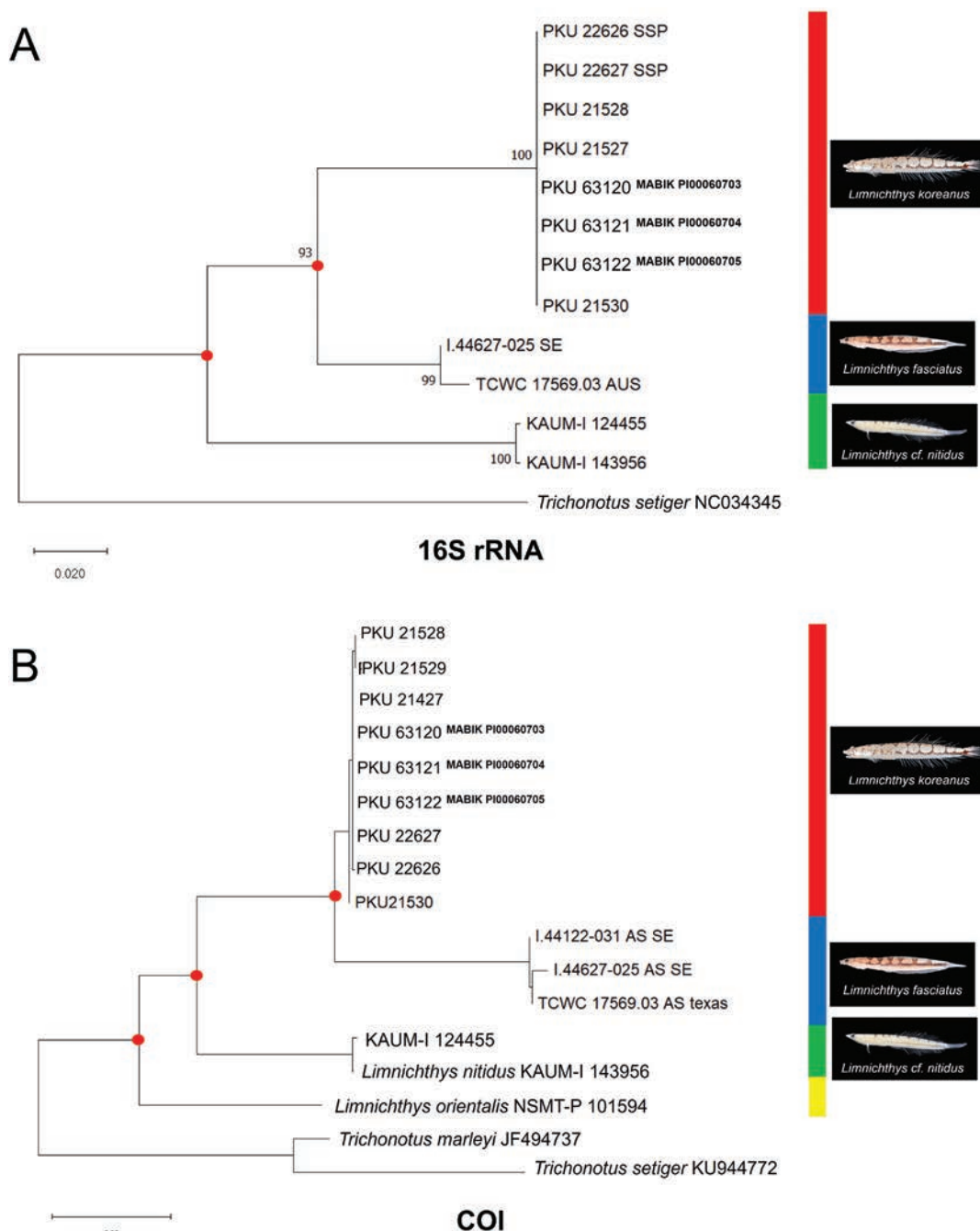
Figure 9. Neighbour-joining tree was constructed based on mtDNA 16S rRNA and COI gene. The tree showing genetic distances among *Limnichthys* species. Bootstrap values based on 1000 replicates were showed 100%, the values are omitted. The red box indicates *Limnichthys koreanus* sp. nov.; blue box indicates *L. fasciatus* from Southeastern Australia; green boxe indicates *L.* cf. *nitidus* from Japan; yellow box indicates *L. orientalis* from Japan; Trichonotidae species was used as outgroup.

We first confirmed that morphological characters of them were perfectly matched with type locality specimens (13 paratypes and 6 specimens from Lord Howe Island), and they have no genetic differences among the three specimens. Therefore, we treated them as truly *L. fasciatus*, which showed deep divergence from our species. Interestingly, we found cryptic diversity in the northwestern Pacific Ocean. *Limnichthys fasciatus* from Japan has similar morphological characteristics to *L. koreanus* sp. nov., but these species have significant genetic divergences. They are well separated from Australian specimens,

so they have possibility as a new species. *Limnichthys* species can be distinguished by their distribution, except for *L. nitidus*, and they might have high cryptic diversity and endemism (Fig. 1). *Limnichthys nitidus* is known for having cryptic complex like *L. fasciatus*. According to the original description and subsequent study, the *L. nitidus* complex was treated as subspecies, Indian Ocean species (*L. nitidus nitidus*) and West Pacific Ocean species (*L. nitidus donalsi*) by ichthyologists (Nelson 1978; Lucena Rosa 1995; Yoshino et al. 1999; Randall 2005). Fricke and Golani (2012) separated each species as *L. nitidus* (Indian Ocean species) and *L. donalsi* (Pacific species), but it is still unclear. For this reason, in this study, we referred to the species as *L.* cf. *nitidus*, indicating that it is likely *L. nitidus* but with some uncertainty in the exact identification. Based on ecological traits of *Limnichthys*, such as hiding in the sand and limited mobility, there is a possibility that each region can show high endemism. In the future study, we need molecular comparisons to clarify the genetic populations.

We also noted remarkably prominent color variation among individuals. Specimens of *L. koreanus* sp. nov. collected from western Jeju Island (Moseulpo) were more similar to *L. fasciatus* compared with specimens collected from eastern Jeju Island (Seongsanpo). Nevertheless, mtDNA analysis did not reveal infraspecies sequence variation. We hypothesize that the observed variation in body color of *L. koreanus* sp. nov. is influenced by differences in habitat substrates (bright in the west vs dark in the east), as suggested by Armbruster and Page (1996), who reported that benthic fish with dorsal saddle patterns can vary based on substrate characteristics such as color or particle size. In our study, *Limnichthys koreanus* sp. nov. was confirmed only in the west (Moseulpo) and east (Seongsanpo) areas of Jeju Island. Future research should investigate its habitat preferences relating to the size of sand (or gravel) for understanding their distribution pattern. All specimens of *L. koreanus* are adults; individuals collected from June to August exhibit maturity for spawning. They are mostly in maturation–mature stages, with an average egg diameter of 0.62–0.65 mm. Creediid fish lay pelagic eggs (Regan 1916; Leis 1982). Specimens were also collected from very shallow coastal waters at depths of 1–5 m. Therefore, spawning may occur near the collection site, highlighting the need for future studies of their spawning and reproductive habitats.

Key to species of four species of the genus *Limnichthys* from the West Pacific Ocean

1　Dorsal fin rays 25 or more; a single epural bone; dorsal saddles joining midlateral stripe absent **2**

–　Dorsal fin rays 25 or fewer; two epural bones; dorsal saddles joining midlateral stripe present **3**

2　Pectoral fin rays 11–12; anal fin rays 26–28; lateral line scales 36–38 ....*L.* cf. *nitidus*

–　Pectoral fin rays 10–11; anal fin rays 24–25; lateral line scales 41–43 ....*L. orientalis*

3　A single interorbital pore; total vertebrae 38–40; dorsal saddles joining midlateral stripe (s) 0–6; vomerine teeth well developed ....*L. koreanus* **sp. nov.**

–　A pair of interorbital pores; total vertebrae 40–45; dorsal saddles joining midlateral stripes 5–9; vomerine teeth slightly developed.......*L. fasciatus*

Comparative specimens

Limnichthys fasciatus: AMS I.5854; AMS I.5855; AMS I.5856; AMS I.5858, syntypes, 13 specimens, 29−43 mm SL, Lord Howe Island, NSW, Australia; AMS I.44627, 28.7 mm SL, Baronda Headland, south side, NSW, Australia; TCWC 17569, 41.1 mm TL, Forester Beach, Tasman Sea, NSW, Australia.

Limnichthys cf. *nitidus*: CAS 228250, 5 specimens, 18.44−20.73 mm SL, Hawaii Island, USA; KAUM-I 124455, 21.1 mm TL, 2018.12.16, 31°25'33.0"N, 130°07'11.4"E, south of Kome-jima island, Kataura, Kasasa, Minami-satsuma, Kagoshima, Japan, hand net, collected by Harutaka Hata; KAUM-I 143956, 1 specimen, 21.9 mm TL 2020.06.03, 27°52'03.6"N, 128°58'03.6"E, Daisuke Uyeno, Kagoshima, Japan, Hand net, collected by Ryuichi Nakagawa.

Acknowledgements

Additional information

Conflict of interest

The authors have declared that no competing interests exist.

Ethical statement

No ethical statement was reported.

Funding

Author contributions

Yu-Jin Lee wrote the text and made the figures. Jin-Koo Kim edited and approved the manuscript for publication.

Author ORCIDs

Yu-Jin Lee ⬤ https://orcid.org/0000-0002-9511-0610
Jin-Koo Kim ⬤ https://orcid.org/0000-0002-8499-406X

Data availability

The data underpinning the analysis reported in this paper are deposited at GBIF, the Global Biodiversity Information Facility, and are available at https://doi.org/10.15468/a436d4.

References

Armbruster JW, Page LM (1996) Convergence of a cryptic saddle pattern in benthic freshwater fishes. Environmental Biology of Fishes 45: 249–257. https://doi.org/10.1007/BF00003092

Cozzi J, Clark E (1995) Darting behavior of a sandburrower fish, *Limnichthys nitidus* (Creediidae), in the Red Sea. Environmental biology of fishes 44: 327–336. https://doi.org/10.1007/BF00008247

Fricke R, Golani D (2012) *Limnichthys marisrubri*, a new species of sand diver (Teleostei: Creediidae) from the Red Sea. Stuttgarter Beiträge zur Naturkunde A 5: 287–292.

Fricke R, Eschmeyer WN, Fong JD (2024) Eschmeyer's catalog of fishes. http://researcharchive.calacademy.org/research/ichthyology/catalog/fishcatmain.asp [Accessed on 03 July 2024]

Hall TA (1999) BioEdit: a user-friendly biological sequence alignment editor and analysis program for windows 95/98/ NT. Nucleic Acids Symposium Series 41: 95–98.

Kimura M (1980) A simple method for estimating evolutionary rates of base substitutions through comparative studies of nucleotide sequences. Journal of Molecular Evolution 16: 111–120. https://doi.org/10.1007/BF01731581

Leis JM (1982) Hawaiian creediid fishes (*Crystallodytes cookei* and *Limnichthys donaldsoni*): development of eggs and larvae and use of pelagic eggs to trace coastal water movement. Bulletin of Marine Science 32(1): 166–180.

Lucena Rosa IM (1995) Comparative osteology of the family Creediidae (Perciformes, Trachinoidei), with comments on the monophyly of the group. Iheringia Serie Zoologia 78: 45–66.

Nelson JS (1978) *Limnichthys polyactis*, a new species of blennioid fish from New Zealand, with notes on the taxonomy and distribution of other Creediidae (including Limnichthyidae). New Zealand Journal of Zoology 5(2): 351–364. https://doi.org/10.1080/03014223.1978.10428321

Nelson JS (1979) Some osteological differences between the blennioid fishes *Limnichthys polyactis* and *L. rendahli*, with comments on other species of Creediidae. New Zealand Journal of Zoology 6(2): 273–277. https://doi.org/10.1080/03014223.1979.10428364

Nelson JS (1985) On the interrelationships of the genera of Creediidae (Perciformes: Trachinoidei). Japanese Journal of Ichthyology 32: 283–293. https://doi.org/10.1007/BF02905432

Nelson JS, Grande TC, Wilson MVH (2016) Fishes of the World 5th edn. John Wiley and Sons, Hoboken, 454–455. https://doi.org/10.1002/9781119174844

Palumbi SR (1996) Nucleic acids II: the polymerase chain reaction. In: Hillis DM, Moritz C, Mable BK (Eds) Molecular Systematics, 2nd edn. Sinauer Associates, Sunderland, 205–247.

Parrott AW (1958) Fishes from the Auckland and Campbell Islands. Records of the Dominion Museum 3(2): 109–119.

Pettigrew JD, Collin SP (1995) Terrestrial optics in an aquatic eye: the sandlance, *Limnichthytes fasciatus* (Creediidae, Teleostei). Journal of Comparative Physiology A 177: 397–408. https://doi.org/10.1007/BF00187476

Pettigrew JD, Collin SP, Fritsches K (2000) Prey capture and accommodation in the sandlance, *Limnichthyes fasciatus* (Creediidae; Teleostei). Journal of Comparative Physiology A 186: 247–260. https://doi.org/10.1007/s003590050425

Randall JE (2005) Reef and shore fishes of the South Pacific. New Caledonia to Tahiti and the Pitcairn Islands, University of Hawai'i Press, Honolulu, 707 pp.

Regan CT (1916) Larval and post-larval fishes. British Antarctic ("Terra Nova") Expedition, 1910. British Museum of Natural History Report Zoology 1(4): 125–156. https://doi.org/10.5962/bhl.title.13214

Sabaj MH (2023) Codes for Natural History Collections in Ichthyology and Herpetology (online supplement). Version 9.5 (10 Nov 2023). American Society of Ichthyologists and Herpetologists, Washington, DC. https://asih.org

GBIF Secretariat (2023) GBIF Backbone Taxonomy. Checklist dataset. https://doi.org/10.15468/39omei [accessed via GBIF.org on 16 April 2024]

Shibukawa K (2010) *Myopsaron nelsoni* a new genus and species of sandburrowers (Perciformes: Trichonotidae: Creediinae) from the Ogasawara Islands, Japan. Bulletin of the National Museum of Nature and Science Series A, Japan 2010: 49–66.

Shimada K, Yoshino T (1987) A new creediid fish *Creedia bilineatus* from the Yaeyama Islands, Japan. Japanese Journal of Ichthyology 34(2): 123–127. https://doi.org/10.1007/BF02912405

Smith JLB (1958) The genus *Limnichthys* Waite, 1904 in African seas. Annals and Magazine of Natural History 1(4): 247–249. https://doi.org/10.1080/00222935808650944

Song J, Parenti LR (1995) Clearing and staining whole fish specimens for simultaneous demonstration of bone, cartilage, and nerves. Copeia 1995: 114–118. https://doi.org/10.2307/1446805

Tamura K, Nei M, Kumar S (2004) Prospects for inferring very large phylogenies by using the neighbor-joining method. Proceedings of the National Academy of Sciences 101: 11030–11035. https://doi.org/10.1073/pnas.0404206101

Tamura K, Stecher G, Kumar S (2021) MEGA11: molecular evolutionary genetics analysis version 11. Molecular Biology and Evolution 38: 3022–3027. https://doi.org/10.1093/molbev/msab120

Thompson JD, Higgins DG, Gibson TJ (1994) CLUSTAL W: improving the sensitivity of progressive multiple sequence alignment through sequence weighting, position-specific gap penalties and weight matrix choice. Nucleic Acids Research 22: 4673–4680. https://doi.org/10.1093/nar/22.22.4673

Waite ER (1904) Additions to the fish fauna of Lord Howe Island, No. 4. Records of the Australian Museum 5(3): 135–186. https://doi.org/10.3853/j.0067-1975.5.1904.1053

Ward RD, Zemlak TS, Innes BH, Last PR, Hebert PDN (2005) DNA barcoding Australia's fish species. Philosophical Transactions of the Royal Society B 360: 1847–1857. https://doi.org/10.1098/rstb.2005.1716

Yoshino T, Kon T, Obake S (1999) Review of the genus *Limnichthys* (Perciformes: Creediidae) from Japan, with description of a new species. Ichthyological Research 46: 73–83. https://doi.org/10.1007/BF02674950

ZooKeys

Progress or burden? Formal description of every apparently new species available in collections is neither necessary nor useful

Bernhard A. Huber[1], Hubert Szymański[2], Alice Bennett-West[3]

1   *Zoological Research Museum Alexander Koenig, LIB, Bonn, Germany*
2   *Włocławek, Poland*
3   *Clevedon, Somerset, UK*

Corresponding author: Bernhard A. Huber (*b.huber@leibniz-lib.de*)

Abstract

A new species of the Sub-Saharan spider genus *Quamtana* Huber, 2003 is described that has been collected in garden centers in Poland and the UK. Its closest known relative is probably *Q. lotzi* Huber, 2003, known from Free State Province in South Africa. Working on the premise that placing species in time and space is the fundamental task of taxonomy, and acknowledging that we cannot provide biologically meaningful spatial information for this species, we prefer open nomenclature to make this species known to science without formally describing it, using the unique provisional name *Quamtana* sp. ZFMK Ar 24490 aff. *lotzi*. We argue that the judicious use of open nomenclature can serve to improve the quality of species lists, reducing the noise in large-scale analyses of biodiversity data. We expand this argument to 'fragmentary' species descriptions in general, such as single-sex descriptions in large genera with many male-only and female-only descriptions. Not every taxonomic act allowed by the Code is necessarily beneficial. Under certain conditions, the informal description of a putatively new species may serve science better than a formal description based on inadequate material or data.

Key words: Alien species, Europe, new species, open nomenclature, Pholcidae, *Quamtana*, single-sex description, South Africa, species lists, taxonomy

Introduction

Species are often, and in many contexts, conveniently divided into two categories, the known and the unknown (Stork 1997; Reaka-Kudla 2001; Costello and Wilson 2010; Costello 2015; Huber and Chao 2019; Moura and Jetz 2021; Liu et al. 2022). This is not only an overly simplistic view of our knowledge of the earth's species diversity (Lawton 1993; Loxdale et al. 2016; Meier et al. 2022) but also a potentially misleading one. 'Known', i.e. formally described, species include a wide and continuous spectrum of taxa that range from well-studied model organisms to those of which we know little else than their names, and those whose names should not even exist because they are synonyms. Informed ignorance is a powerful research tool (Hortal et al. 2015), but in taxonomy, the level of ignorance hidden behind a scientific name is often not easily accessible except by a few specialists. Taxonomists are well aware of the fact

that focusing on formally undescribed taxa is only part of the job. In fact, more time and effort are often required to give meaning to names of species that are formally described but basically unknown than to formally describing a new species (e.g., Riedel et al. 2013; Kehlmaier et al 2019).

To some degree, this is a legacy of 250 years of taxonomic history, and of the rules (Codes) that the taxonomic community has chosen to adopt. These rules happen to conserve taxonomic decisions as long as certain formal criteria are followed, irrespective of scientific merit. However, the problem is not only historical. New species are still massively being formally described based on suboptimal or inadequate material or data. Countless species are being described from a single specimen, a single sex, or a single locality; from poorly preserved specimens; from photographs rather than physical specimens; from specimens without precise locality data; from specimens without any biologically meaningful type locality; etc. (e.g., Lim et al. 2012; Santos et al. 2016; Deng et al. 2019). From a theoretical point of view, there is nothing fundamentally wrong with this; this is how science works. Hypotheses (in this case, species) are proposed and further research can refine or reject these hypotheses. Every species description is necessarily incomplete in some respect, and what constitutes a reasonably 'complete' description varies with the taxonomic group, time, the needs of the end user, available research infrastructure, etc. (Durkin et al. 2020; Sharkey et al. 2021a, b). In addition, 'fragmentary' descriptions obviously can and usually do, provide useful information. Single-sex descriptions, for example, do not compromise the locality data nor the morphological, molecular, natural history etc. data provided about the known sex.

However, formal descriptions based on suboptimal or inadequate material or data can be harmful by introducing problems that interfere with scientific progress. For example, single-sex descriptions may become problematic if many male-only and female-only species are proposed within a taxon of superficially similar species; species with imprecise locality data may become problematic if the rough coordinates given in databases are used in biogeographic analyses; conservation efforts and ecological studies may be misled by problematic taxonomic decisions hidden behind the authority of a scientific name (Bortolus 2008; Maldonado et al. 2015; Ely et al. 2017; Nekola and Horsák 2022). At some point and under certain circumstances, the potential problems of a formal description may outweigh its advantages.

Our example to illustrate this point is a new species of daddy long-legs spider (Pholcidae) of the genus *Quamtana* Huber, 2003 that was recently discovered in several European garden centers. *Quamtana* is a Sub-Saharan genus, with a particularly high diversity in South Africa (Huber 2003). A few species have been found further north, reaching Central and East Africa. *Quamtana* spiders have been introduced to Europe before: two species were reported from German plant markets and greenhouses where they seemed to have established viable populations (Huber et al. 2015). Obviously, all these species have been introduced from Africa, probably with plants. They are not indigenous European species, and their natural distributions are unknown. Taxonomy is fundamentally about placing species in time and space, but in the case of *Quamtana* spiders in Europe, we lack biologically meaningful information on the spatial component. Our aim here is not to argue that formally describing such species is necessarily bad; it is obviously permitted by the relevant taxonomic Code (ICZN 1999). Instead, we favor the approach of 'open nomenclature' (Bengtson 1988;

Sigovini et al. 2016; Minelli 2019; Horton et al. 2021) for cases such as this, and claim that (1) all the relevant information available at this point can be provided without formally naming the species, and (2) informal descriptions of 'problematic' species helps improve the quality of formal species lists and databases.

Materials and methods

This study is primarily based on the examination of specimens deposited in Zoologisches Forschungsmuseum Alexander Koenig, Bonn, Germany (ZFMK). Further material is deposited in the private collections of the second and third authors. The taxonomic description follows the style of the only available revision of the genus (Huber 2003; based on Huber 2000). Measurements were done on a dissecting microscope with an ocular grid and are in mm unless otherwise noted; eye measurements are +/- 5 µm. Photos were made with a Canon EOS 2000D digital camera mounted on a Nikon SMZ18 stereo microscope or a Nikon Coolpix 995 digital camera mounted on a Leitz Dialux 20 compound microscope. CombineZP (https://combinezp.software.informer.com/) was used for stacking photos. Drawings are partly based on photos that were traced on a light table and later improved under a dissecting microscope, or they were directly drawn with a Leitz Dialux 20 compound microscope using a drawing tube. The cleared epigynum was stained with chlorazol black. Abbreviations used in figures only are explained in the figure legends. Abbreviations used in the text: **ALE** = anterior lateral eye(s); **AME** = anterior median eye(s); **a.s.l.** = above sea level; **L/d** = length/diameter; **PME** = posterior median eye(s).

Results

Order Araneae Clerck, 1757
Family Pholcidae C.L. Koch, 1850
Genus *Quamtana* Huber, 2003

Quamtana* sp. ZFMK Ar 24490 aff. *lotzi
Figs 1–5

Diagnosis. Small, long-legged pholcid (Fig. 1) with eight eyes and with median projection on male clypeus. Distinguished from most known congeners (except *Q. lotzi* Huber, 2003) by longer than wide male palpal patella (Fig. 2), by presence of distinct apophysis on male palpal coxa (Fig. 2), by presence of three rather than two modified hairs on each male cheliceral apophysis (Fig. 3A), and by distinctive ventral protrusion proximally on bulbal processes (bold arrow in Fig. 4D). From *Q. lotzi* and other congeners also by details of procursus shape (Fig. 4A–C; bifid prolateral-dorsal apophysis, long and slender prolateral-ventral spine; large rounded retrolateral-dorsal sclerite) and by details of genital bulb shape (Fig. 4D–G; two processes originating from common basis, one sclerotized, possibly containing sperm duct, other largely membranous, hooked at tip). Female distinguished from known congeners by large median epigynal pocket (Fig. 3B, E) rather than pair of pockets; female of *Q. lotzi* unknown.

Material examined. Poland – **Kuyavia-Pomerania** • 1 ♂, 1 ♀ abdomen, 2 juvs; Bydgoszcz; 53.123°N, 18.064°E; 50 m a.s.l.; in OBI market; 20 Jan. 2024;

H. Szymańksi leg.; ZFMK Ar 24490 • 1 ♂, 1 ♀ (abdomen transferred to ZFMK Ar 24490), in pure ethanol; same collection data as for preceding; ZFMK G161 • 1 ♂, 2 ♀, 6 juvs; Toruń; 53.024°N, 18.670°E; 65 m a.s.l.; in OBI market; 2 Mar. 2024; H. Szymański, D. Szymański, D. Szymański leg.; in private collection H. Szymańksi. Great Britain – **England** • 2 ♂; Almondsbury, garden center; 51.550°N, 2.577°W; 6 Nov. 2023; A. Bennett-West leg.; ZFMK Ar 24652 • 2 ♀; same collection data as for preceding; in private collection A. Bennett-West.

Description. Male (ZFMK Ar 24490). *Measurements.* Total body length 1.5, carapace width 0.54. Distance PME-PME 80 µm; diameter PME 75 µm; distance PME-ALE 20 µm; distance AME-AME 20 µm; diameter AME 35 µm. Leg 1 missing; tibia 2: 1.25, tibia 3: 0.75, tibia 4: 1.23.

Colour (in ethanol). Prosoma and legs mostly pale ochre, carapace with dark median mark including ocular area and clypeus; sternum monochromous; legs with darker rings on femora (subdistally) and tibiae (proximally and subdistally); abdomen pale gray, with dark internal marks dorsally and laterally, ventrally with indistinct rectangular darker mark in front of gonopore.

Body. Habitus as in Fig. 1A, B. Ocular area moderately raised. Carapace without thoracic groove. Clypeus with distinct median process ~60 µm long, ending in two tines. Sternum wider than long (0.42/0.38), unmodified. Abdomen globular, conical at spinnerets.

Chelicerae. As in Fig. 5A; with pair of proximal lateral processes weakly sclerotized and directed proximally and pair of distal apophyses close to median line, each with three modified (conical) hairs (Fig. 3A); without stridulatory files.

Palps. As in Fig. 2; coxa with distinct ventral apophysis; trochanter with short retrolateral process (~40 µm long); femur short, distally widening but otherwise unmodified; femur-patella joints slightly shifted toward prolateral side; patella very long; tibia-tarsus joints shifted toward retrolateral side; procursus (Fig. 4A–C) consisting of short proximal part and complex distal part hinged against proximal part; proximal part on prolateral-dorsal side with bifid apophysis with long hinged spine; distal part with large retrolateral-dorsal sclerite connected ventrally and prolaterally with membranous structures and simple flat ventral sclerite; genital bulb (Fig. 4D–G) with strong proximal sclerite and two distal processes, one sclerotized (putative embolus), the other one semitransparent and distally hooked; with ventral protrusion proximally on bulbal processes (bold arrow in Fig. 4D).

Legs. Without spines, without curved hairs, without sexually dimorphic short vertical hairs. Ventral hairs proximally on femora long, in particular on femur 2 (~350 µm long, proximal half of femur).

Supplementary information on other males: ZFMK G161: leg 1 length: 9.00 (2.40 + 0.25 + 2.45 + 3.10 + 0.80), tibia 2 missing, tibia 3: 0.98, tibia 4: 1.45; tibia 1 L/d: 41; retrolateral trichobothrium of tibia 1 at 11%; prolateral trichobothrium absent on tibia 1. Ventral hairs on femur 1 also long, but only in proximal fifth of femur, and shorter than on femur 2 (~300 µm); tarsus 1 with ~15 pseudosegments, distally distinct.

ZFMK Ar 24652: tibia 1: 2.75.

Female. In general, very similar to male (Fig. 1C) but clypeus unmodified, ventral hairs on leg femora shorter (up to ~150 µm). Tibia 1 missing. Epigynum (Fig. 3B–D) protruding, anterior plate triangular, with distinct median pocket in posterior position; posterior epigynal plate wide and simple. Internal genitalia (Fig. 3E, F) with anterior arc and pair of long pore plates in transversal position.
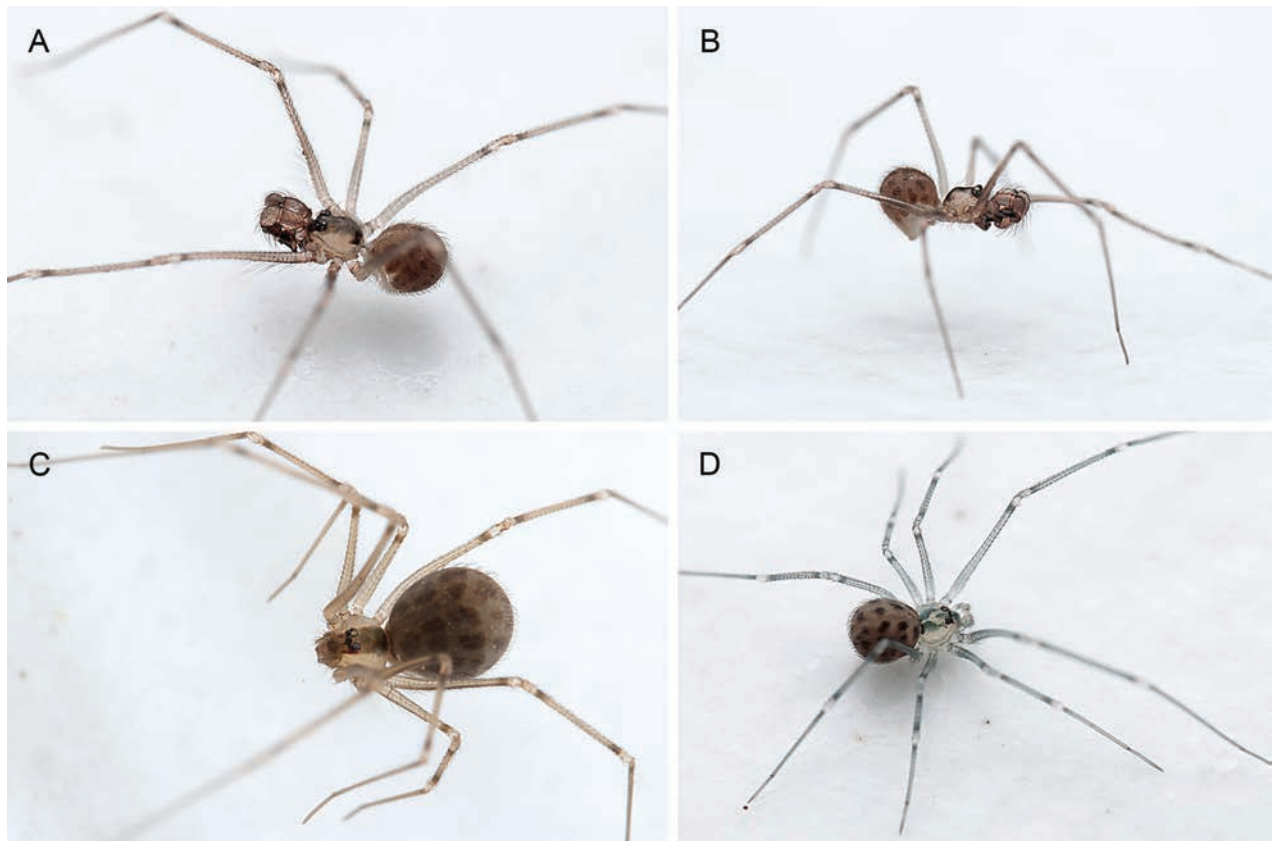
Figure 1. *Quamtana* sp. ZFMK Ar 24490 aff. *lotzi*; live specimens, from Poland, Bydgoszcz **A, B** male **C** female **D** juvenile (penultimate instar male).
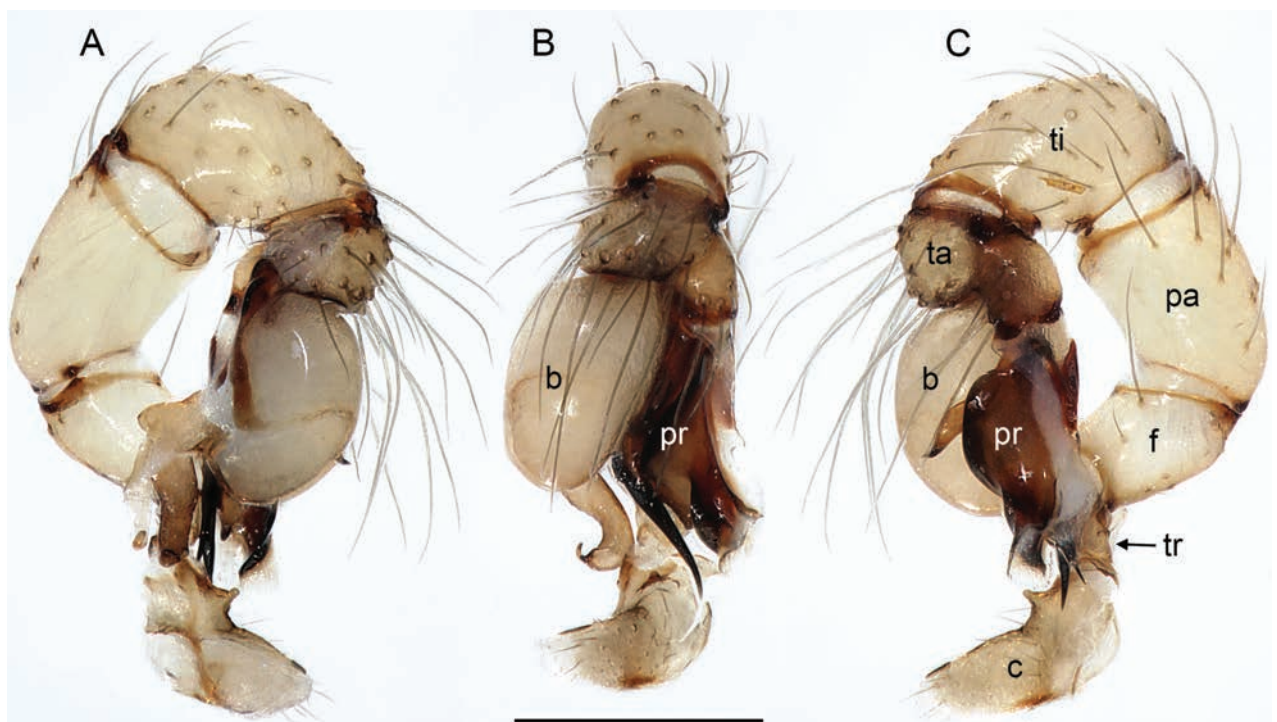
Figure 2. *Quamtana* sp. ZFMK Ar 24490 aff. *lotzi*; male from Poland, Bydgoszcz, ZFMK Ar 24490. Left palp, prolateral (**A**), dorsal (**B**), and retrolateral (**C**) views. Abbreviations: b, genital bulb; c, coxa; f, femur; pa, patella; pr, procursus; ta, tarsus; ti, tibia; tr, trochanter. Scale bar: 0.3 mm.
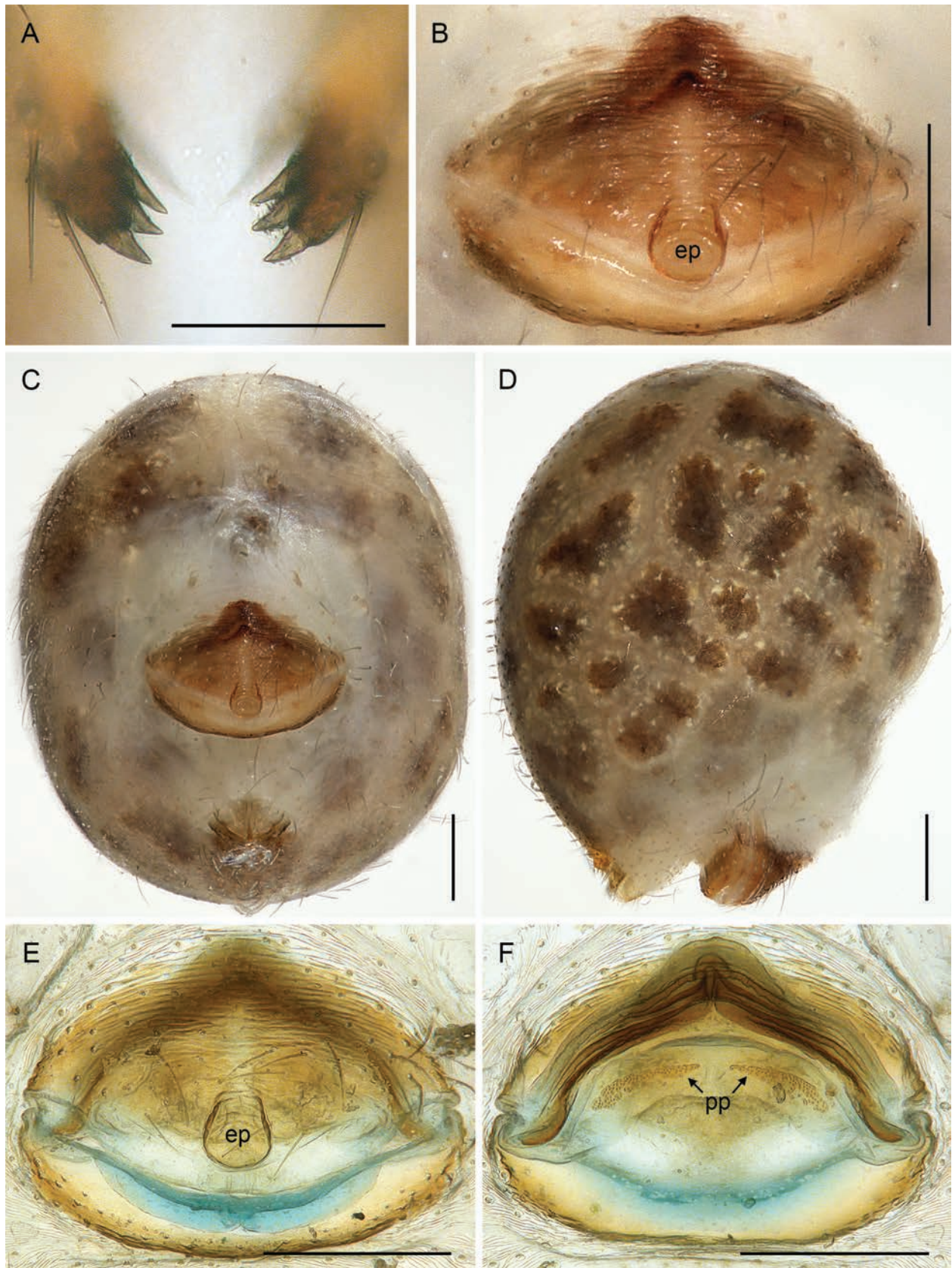
Figure 3. *Quamtana* sp. ZFMK Ar 24490 aff. *lotzi*; male and female from Poland, Bydgoszcz, ZFMK Ar 24490 **A** frontal male cheliceral apophyses, frontal view **B** epigynum, ventral view **C, D** female abdomen, ventral and lateral views **D, E** cleared female genitalia, ventral and dorsal views. Abbreviations: ep, epigynal pocket; pp, pore plates. Scale bars: 0.05 mm (**A**); 0.2 mm (**B–F**).
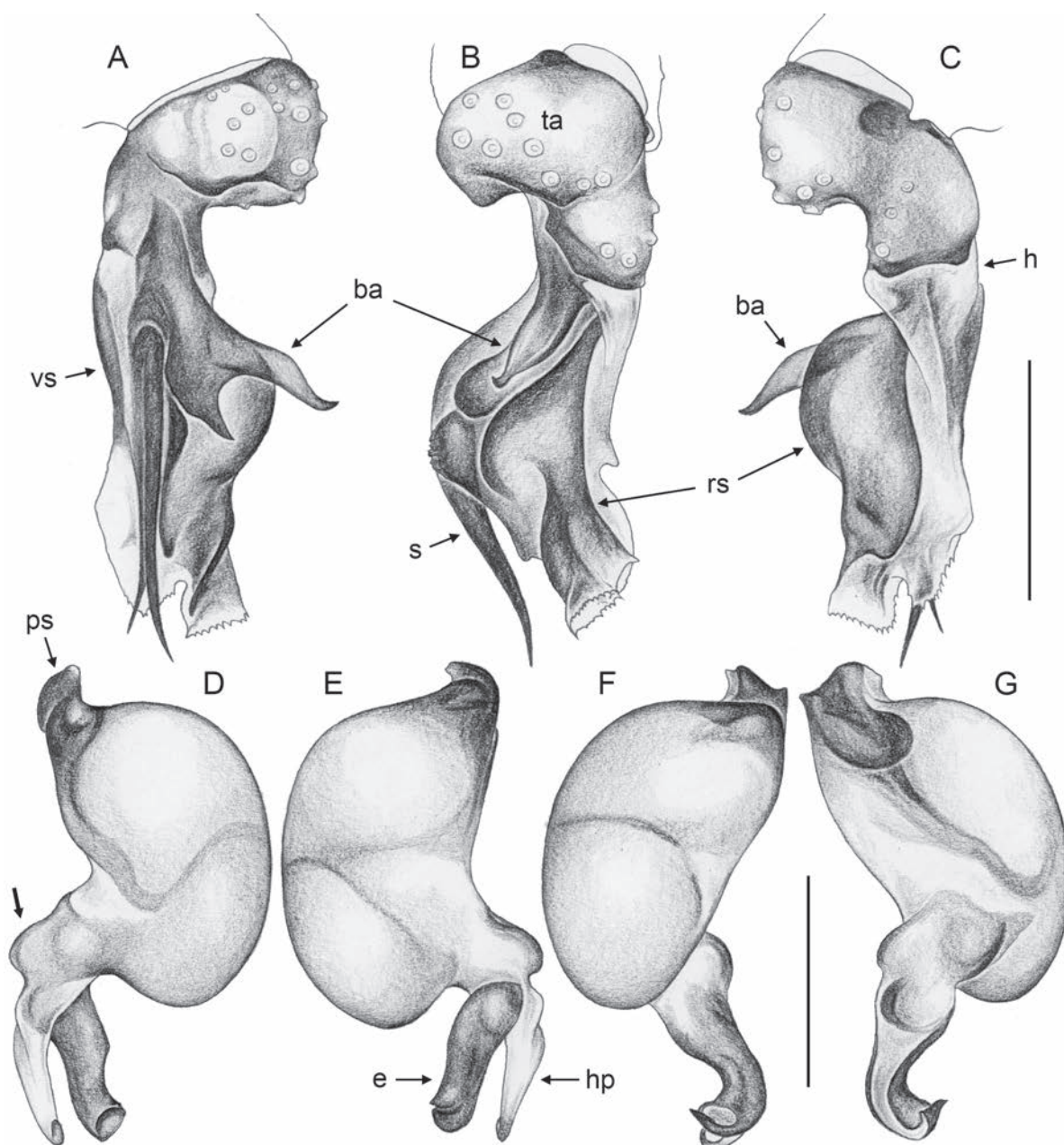
Figure 4. *Quamtana* sp. ZFMK Ar 24490 aff. *lotzi*; male from Poland, Bydgoszcz **A−C** left palpal tarsus and procursus, prolateral, dorsal, and retrolateral views, ZFMK Ar 24490 **D−G** left genital bulb, prolateral, retrolateral, dorsal, and ventral views, ZFMK G161; bold arrow in **D** points at ventral protrusion proximally on bulbal processes. Abbreviations: ba, bifid apophysis; e, putative embolus; h, hinge between proximal and distal parts of procursus; hp, hooked bulbal process; ps, proximal bulbal sclerite; rs, retrolateral-dorsal sclerite; s, hinged spine; ta, tarsus; vs, ventral sclerite. Scale bars: 0.2 mm.

Natural history. In the garden centers in Poland, the specimens were found in sections with xerophilic plants such as cacti and succulents, under bark, under stones and bricks, and under flowerpots. In the garden center in England, the specimens were found on the underside of shelving, also close to xerophilic plants and succulents.

Relationships. The present species shares with *Q. lotzi* a number of characters that are unique in *Quamtana*: (1) long male palpal patella (Fig. 2); (2) presence of distinct apophysis on male palpal coxa (Fig. 2); (3) presence of three rather than two modified hairs on each male cheliceral apophysis (Fig. 3A);
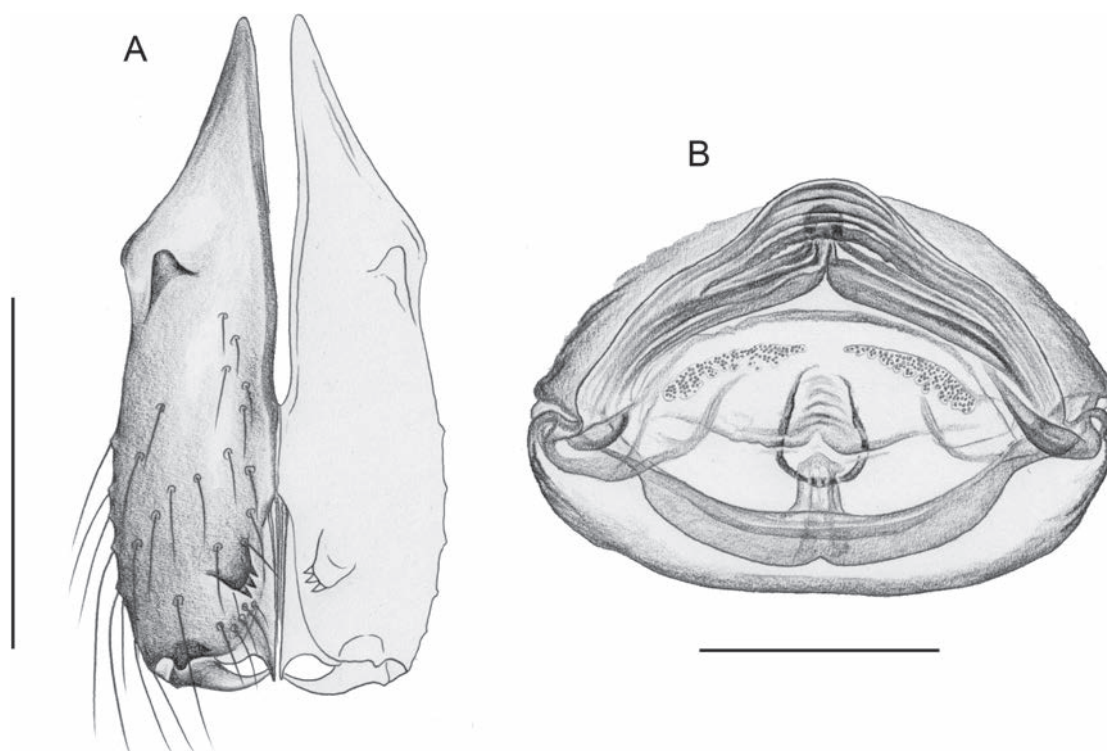
Figure 5. *Quamtana* sp. ZFMK Ar 24490 aff. *lotzi*; male and female from Poland, Bydgoszcz **A** male chelicerae, frontal view, ZFMK Ar 24490 **B** cleared female genitalia, dorsal view, ZFMK G161. Scale bars: 0.2 mm.

and (4) distinctive ventral protrusion proximally on bulbal processes (bold arrow in Fig. 4D). We suspect that most or all of these similarities are derived and that the two species are sister taxa.

Distribution and geographic origin. The species has so far only been found in garden centers in Poland and England. The plants in the Polish stores originate from several parts of the world, and they reach Poland via a nursery in the Netherlands. It is thus not possible to trace the spiders back via the plants. For England, we do not have any information regarding the origin of plants where specimens were found. The only clue regarding the origin we have is thus the putative sister species, *Q. lotzi*. This species is known from a single male specimen originating from the Koppiesdam Nature Reserve (27°13'S, 27°42'E; Huber 2003) in Free State, South Africa. We thus suspect that the present species may also originate from approximately this area.

Remark. The format of the provisional name above follows the suggestions in Horton et al. (2021). The two species of *Quamtana* previously reported from Germany (Huber et al. 2015) were not named according to such criteria that include unique registration numbers and facilitate integration into databases. We thus propose the following names for those two taxa: for "*Quamtana* sp. A" we propose "*Quamtana* sp. ZFMK Ar 12707 aff. *kabale*", for "*Quamtana* sp. B" we propose "*Quamtana* sp. ZFMK Ar 12704 aff. *mabusai*".

Discussion

Species represent a core unit of life, and taxonomy strives to discover, delimit, describe and name species according to scientific standards. Species names can be viewed as hypotheses that follow from the discovery, delimitation and

description process; unambiguous names are essential tools to communicate knowledge about the world's biodiversity across countries, time and scientific disciplines. Species (names) that are aggregated into species lists and databases affect views and decisions far beyond biological disciplines such as evolutionary and ecological research. They have potential impact on conservation, trade, agriculture, development, species invasions and health (Thomson et al. 2018; Garnett et al. 2020; Hobern et al. 2021; Sandall et al. 2023).

Taxonomic hypotheses, like hypotheses in any other field of science, range from poorly supported to well supported. Taxonomists are mostly well aware of which taxa in their specific group of interest are problematic and which can be regarded as solid and less likely to be rejected by further research. However, this information, even if published, is not visible in formal species names and is usually not visible in species lists. Instead, species lists usually contain every taxon name that meets the relevant criteria of the respective Code. While researchers in other biological disciplines can safely ignore published information that is arguably unreliable, formal taxonomic names are stubborn: once created they are here to stay, both individually and in lists, until they are formally rejected (Agatha et al. 2021).

Recent heated debates among taxonomists reflect this dilemma: while some argue that taxonomy has to follow new approaches to massively speed up species descriptions, others feel confronted with a mass of species they consider poorly supported but that they feel forced to include in species lists and to take into account in subsequent research (e.g., Sharkey et al. 2021a, 2021b, 2022 vs. Ahrens et al. 2021; Zamani et al. 2022a, b; Meier et al. 2022). A similar debate has been going on about species descriptions based on photographs, without physical vouchers (reviewed in Kasalo et al. 2021). A less controversial yet pervasive problem is synonyms. Depending on the taxonomic group, 20% and more of the species names in lists may be synonyms (Solow et al. 1995; Dubois 2008). Synonyms have been and are being created for a number of reasons. Some potential synonyms are indeed hard to avoid or to solve, for example, those resulting from different species concepts or delimitation criteria. Others appear avoidable. For example, genera with large numbers and percentages of male-only and female-only descriptions are likely to include synonyms. While the arachnological community, as an example, has long ago realized that describing new species based on juvenile specimens creates more problems than it solves, single sex descriptions continue to be produced massively. In the Asian funnel weaver genus *Draconarius* Ovtchinnikov, 1999, 155 of the currently 270 nominal species are known from a single sex (WSC 2024). Of these 155 single-sex descriptions (108 female-only, 47 male-only), 131 have been published since 2000. *Draconarius* is no exception; several other large spider genera have even higher numbers and higher percentages of male-only and female-only descriptions (WSC 2024). Taxonomists producing such descriptions are of course aware of the problem and correctly point out that it can be solved by further research. Until then, however, all these species will appear in lists and databases, with potential impacts far beyond the narrow niche of alpha taxonomy.

Informal species descriptions make knowledge available while keeping species lists and databases of formally described species as clean as possible. The idea of 'open nomenclature' is, of course, not new, and early proponents have argued that it should be seen as an essential tool in the taxonomist's repertoire

(e.g., Bengtson 1988). Not only is it a compromise between formal description and retention of information, but its "careful and judicious use … reflects scientific honesty" (Bengtson 1988). Recent proponents have emphasized the potential of open nomenclature, provided that its use becomes standardized and made compatible with modern biodiversity research (Sigovini et al. 2016; Minelli 2019; Horton et al. 2021). The basic motivation is certainly widely shared: to maximize efforts to prevent the publication of insufficient descriptions and redescriptions, and to improve the reliability of biological datasets and their utility in informing policy and management (Agatha et al. 2021; Horton et al. 2021).

Ryberg and Nilsson (2018) claimed that "an inflation in names that are difficult to interpret or apply may hamper taxonomy more than an inflation in species descriptions without valid names." What if Sharkey et al. (2021a) had published their tremendous amount of valuable data on wasp diversity in Costa Rica without producing more than 400 formal species names? What if proponents of species descriptions based on photographs instead of physical vouchers had published their discoveries of putative new species without binomials (as suggested by Löbl et al. 2016; Horton et al. 2021; and implemented in Kasalo et al. 2021)? What if taxonomists working on *Draconarius* spiders had produced formal single-sex descriptions for only one sex, while informally providing all the relevant information on 'species' known from the other sex only? For pholcid spiders, the first author has formally described over 900 species, but none are based on females only. Knowing one particular sex in all species (males in the case of Pholcidae, because they generally are easier to diagnose) minimizes the problem of creating different names for male-only and female-only 'species' when they are in fact the same species. In Pholcidae, apparent female-only species were not ignored but described informally (e.g., in Huber et al. 2023a, b). For a slightly different approach in dealing with the problem of matching sexes in spiders, also involving informal descriptions of putative new species, see Izquierdo and Ramírez (2017). Apart from keeping species lists clean, this may motivate future collectors to search for the missing sex and formally describe the species if, in fact, new.

It could be argued that informal names are not appropriately considered or entirely invisible in catalogs, species lists and databases and are consequently neglected in further research, legislation, conservation efforts, etc. However, whether this is a problem of open nomenclature or a problem of the species lists, catalogs, and legislation is open to debate. The WSC (2024) for example, includes a reference to the formally undescribed species of *Quamtana* from Germany mentioned above, duly separate from the list of formally described species, while other informally described species (e.g. those in Huber et al. 2023a, b; and those in Izquierdo and Ramírez 2017) are ignored. There is obviously not only a need for consistency but mainly for a way to incorporate available information into species lists and databases that allows the end user to decide which information is valuable for a particular purpose and which is not.

In sum, we work on the premise that placing species in time and space is the fundamental task of taxonomy, but we acknowledge that a fragmentary description (e.g., one without a meaningful space component, as in our case) can carry valuable information. We thus use open nomenclature to make this species known to science without formally describing it. All users of taxonomy might profit from a careful case-by-case evaluation by taxonomists of whether the available data justify formal species description or not. We extend this argument

to all species descriptions based on fragmentary data, as for example, on single-sex descriptions in species-rich taxa that already have many male-only and female-only species. Formal description of every putatively new species available in collections is not necessarily beneficial and potentially even harmful.

Acknowledgements

Additional information

Conflict of interest

The authors have declared that no competing interests exist.

Ethical statement

No ethical statement was reported.

Funding

Author contributions

BAH: concept, taxonomy, writing; HS and ABW: collecting, rearing, natural history.

Author ORCIDs

Bernhard A. Huber https://orcid.org/0000-0002-7566-5424
Hubert Szymański https://orcid.org/0000-0003-0549-8912

Data availability

All of the data that support the findings of this study are available in the main text.

References

Agatha S, Ganser MH, Santoferrara LF (2021) The importance of type species and their correct identification: A key example from tintinnid ciliates (Alveolata, Ciliophora, Spirotricha). The Journal of Eukaryotic Microbiology 68: e12865. https://doi.org/10.1111/jeu.12865

Ahrens D, Ahyong ST, Ballerio A, Barclay MVL, Eberle J, Espeland M, Huber BA, Mengual X, Pacheco TL, Peters RS, Rulik B, Vaz-De-Mello F, Wesener T, Krell FT (2021) Is it time to describe new species without diagnoses? -A comment on Sharkey et al. (2021). Zootaxa 5027(2): 151−159. https://doi.org/10.11646/zootaxa.5027.2.1

Bengtson P (1988) Open nomenclature. Palaeontology 31: 223−227.

Bortolus A (2008) Error cascades in the biological sciences: The unwanted consequences of using bad taxonomy in ecology. AMBIO, A Journal of the Human Environment 37(2): 114−118. https://doi.org/10.1579/0044-7447(2008)37[114:ECITBS]2.0.CO;2

Costello MJ (2015) Biodiversity: The known, unknown, and rates of extinction. Current Biology 25(9): R368−R371. https://doi.org/10.1016/j.cub.2015.03.051

Costello M, Wilson S (2010) Predicting the number of known and unknown species in European seas using rates of description. Global Ecology and Biogeography 20: 319–330. https://doi.org/10.1111/j.1466-8238.2010.00603.x

Deng J, Guo Y, Cheng Z, Lu C, Huang X (2019) The prevalence of single-specimen/locality species in insect taxonomy: An empirical analysis. Diversity 11: 106. https://doi.org/10.3390/d11070106

Dubois A (2008) A partial but radical solution to the problem of nomenclatural taxonomic inflation and synonymy load. Biological Journal of the Linnean Society 93: 857–863. https://doi.org/10.1111/j.1095-8312.2007.00900.x

Durkin L, Jansson T, Sanchez M, Khomich M, Ryberg M, Kristiansson E, Nilsson RH (2020) When mycologists describe new species, not all relevant information is provided (clearly enough). MycoKeys 72: 109–128. https://doi.org/10.3897/mycokeys.72.56691

Ely CV, de L Bordignon SA, Trevisan R, Boldrini II (2017) Implications of poor taxonomy in conservation. Journal for Nature Conservation 36: 10–13. https://doi.org/10.1016/j.jnc.2017.01.003

Garnett ST, Christidis L, Conix S, Costello MJ, Zachos FE, Bánki OS, Bao, Y, Barik SK, Buckeridge JS, Hobern D, Lien, A, Montgomery N, Nikolaeva S, Pyle RL, Thomson SA, van Dijk PP, Whalen A, Zhang, Z-Q, Thiele KR (2020) Principles for creating a single authoritative list of the world's species. PLoS Biology 18(7): e3000736. https://doi.org/10.1371/journal.pbio.3000736

Hobern D, Barik SK, Christidis L, Garnett ST, Kirk P, Orrell TM, Pape T, Pyle RL, Thiele KR, Zachos FE, Bánki O (2021) Towards a global list of accepted species VI: The Catalogue of Life checklist. Organisms Diversity and Evolution 21: 677–690. https://doi.org/10.1007/s13127-021-00516-w

Hortal J, de Bello F, Diniz-Filho JAF, Lewinsohn TM, Lobo JM, Ladle RJ (2015) Seven shortfalls that beset large-scale knowledge of biodiversity. Annual Review of Ecology, Evolution, and Systematics 46: 523–549. https://doi.org/10.1146/annurev-ecolsys-112414-054400

Horton T, Marsh L, Bett BJ, Gates AR, Jones DOB, Benoist NMA, Pfeifer S, Simon-Lledó E, Durden JM, Vandepitte L, Appeltans W (2021) Recommendations for the standardisation of open taxonomic nomenclature for image-based identifications. Frontiers in Marine Science 8: 620702. https://doi.org/10.3389/fmars.2021.620702

Huber BA (2000) New World pholcid spiders (Araneae: Pholcidae): a revision at generic level. Bulletin of the American Museum of Natural History 254: 1–348. https://doi.org/10.1206/0003-0090(2000)254<0001:NWPSAP>2.0.CO;2

Huber BA (2003) Southern African pholcid spiders: revision and cladistic analysis of *Quamtana* gen. nov. and *Spermophora* Hentz (Araneae: Pholcidae), with notes on male-female covariation. Zoological Journal of the Linnean Society 139: 477–527. https://doi.org/10.1046/j.0024-4082.2003.00082.x

Huber BA, Chao A (2019) Inferring global species richness from megatransect data and undetected species estimates. Contributions to Zoology 88: 42–53. https://doi.org/10.1163/18759866-20191347

Huber BA, Neumann J, Rehfeldt S, Grabolle A, Reiser N (2015) Back in Europe: *Quamtana* spiders (Araneae: Pholcidae) in Germany. Arachnologische Mitteilungen 50: 51–56. https://doi.org/10.5431/aramit5007

Huber BA, Meng G, Král J, Ávila Herrera IM, Izquierdo MA, Carvalho LS (2023a) High and dry: integrative taxonomy of the Andean spider genus *Nerudia* (Araneae: Pholcidae). Zoological Journal of the Linnean Society 198: 534–591. https://doi.org/10.1093/zoolinnean/zlac100

Huber BA, Meng G, A Váldez-Mondragón, Král J, Ávila Herrera IM, Carvalho LS (2023b) Short-legged daddy-long-leg spiders in North America: the genera *Pholcophora* and *Tolteca* (Araneae, Pholcidae). European Journal of Taxonomy 880: 1–89. https://doi.org/10.5852/ejt.2023.880.2173

ICZN (1999) International Commission on Zoological Nomenclature: International code of zoological nomenclature. Fourth edition, adopted by the international union of biological sciences. International Trust for Zoological Nomenclature, London.

Izquierdo MA, Ramírez MJ (2017) Taxonomic revision of the jumping goblin spiders of the genus *Orchestina* Simon, 1882, in the Americas (Araneae: Oonopidae). Bulletin of the American Museum of Natural History 410: 1–362. https://doi.org/10.1206/0003-0090-410.1.1

Kasalo N, Deranja M, Adžić K, Sindaco R, Skejo J (2021) Discovering insect species based on photographs only: The case of a nameless species of the genus *Scaria* (Orthoptera: Tetrigidae). Journal of Orthoptera Research 30: 173. https://doi.org/10.3897/jor.30.65885

Kehlmaier C, Zhang X, Georges A, Campbell PD, Thomson, S, Fritz U (2019) Mitogenomics of historical type specimens of Australasian turtles: clarification of taxonomic confusion and old mitochondrial introgression. Scientific Reports 9: 5841. https://doi.org/10.1038/s41598-019-42310-x

Lawton JH (1993) On the behaviour of autecologists and the crisis of extinction. Oikos 67(1): 3–5. https://doi.org/10.2307/3545089

Lim GS, Balke M, Meier R (2012) Determining species boundaries in a world full of rarity: singletons, species delimitation methods. Systematic Biology 61(1): 165–169. https://doi.org/10.1093/sysbio/syr030

Liu J, Slik F, Zheng S, Lindenmayer DB (2022) Undescribed species have higher extinction risk than known species. Conservation Letters 15: e12876. https://doi.org/10.1111/conl.12876

Löbl I, Cibois A, Landry B (2016) Describing new species in the absence of sampled specimens: A taxonomist's own-goal. The Bulletin of Zoological Nomenclature 73: 83–86. https://doi.org/10.21805/bzn.v73i1.a2

Loxdale HD, Davis BJ, Davis RA (2016) Known knowns and unknowns in biology. Biological Journal of the Linnean Society 117(2): 386–398. https://doi.org/10.1111/bij.12646

Maldonado C, Molina CI, Zizka A, Persson C, Taylor CM, Albán J, Chilquillo E, Rønsted N, Antonelli A (2015) Estimating species diversity and distribution in the era of Big Data: to what extent can we trust public databases? Global Ecology and Biogeography 24: 973–984. https://doi.org/10.1111/geb.12326

Meier R, Blaimer BB, Buenaventura E, Hartop E, von Rintelen T, Srivathsan A, Yeo D (2022) A re-analysis of the data in Sharkey et al.'s (2021) minimalist revision reveals that BINs do not deserve names, but BOLD Systems needs a stronger commitment to open science. Cladistics 38: 264–275. https://doi.org/10.1111/cla.12489

Minelli A (2019) The galaxy of the non-Linnaean nomenclature. History and Philosophy of the Life Sciences 41: 31. https://doi.org/10.1007/s40656-019-0271-0

Moura MR, Jetz W (2021) Shortfalls and opportunities in terrestrial vertebrate species discovery. Nature Ecology & Evolution 5: 631–639. https://doi.org/10.1038/s41559-021-01411-5

Nekola JC, Horsák M (2022) The impact of empirically unverified taxonomic concepts on ecological assemblage patterns across multiple spatial scales. Ecography 2022: e06063. https://doi.org/10.1111/ecog.06063

Reaka-Kudla ML (2001) Known and unknown biodiversity, risk of extinction and conservation strategy in the sea. In: Bendell-Young L, Gallaugher P (Eds) Waters in Peril. Springer, Boston, MA, 19–33. https://doi.org/10.1007/978-1-4615-1493-0_2

Riedel A, Sagata K, Suhardjono YR, Tänzler R, Balke M (2013) Integrative taxonomy on the fast track - towards more sustainability in biodiversity research. Frontiers in Zoology 10: 15. https://doi.org/10.1186/1742-9994-10-15

Ryberg M, Nilsson RH (2018) New light on names and naming of dark taxa. MycoKeys 23(30): 31–39. https://doi.org/10.3897/mycokeys.30.24376

Sandall EL, Maureaud AA, Guralnick R, McGeoch MA, Sica YV, Rogan MS, Booher DB, Edwards R, Franz N, Ingenloff K, Lucas M, Marsh CJ, McGowan J, Pinkert S, Ranipeta A, Uetz P, Wieczorek J, Jetz W (2023) A globally integrated structure of taxonomy to support biodiversity science and conservation. Trends in Ecology and Evolution 38(12): 1143–1153. https://doi.org/10.1016/j.tree.2023.08.004

Santos CMD, Amorim DS, Klassa B, Fachin DA, Nihei SS, De Carvalho CJB, Falaschi RL, Mello-Patiu CA, Couri MS, Oliveira SS, Silva VC, Ribeiro GC, Capellari RS, Lamas CJE (2016) On typeless species and the perils of fast taxonomy. Systematic Entomology 41: 511–515. https://doi.org/10.1111/syen.12180

Sharkey MJ, Janzen DH, Hallwachs W, Chapman EG, Smith MA, Dapkey T, Brown A, Ratnasingham S, Naik S, Manjunath R, Perez K, Milton M, Hebert P, Shaw SR, Kittel RN, Solis MA, Metz MA, Goldstein PZ, Brown JW, Quicke DLJ, van Achterberg C, Brown BV, Burns JM (2021a) Minimalist revision and description of 403 new species in 11 subfamilies of Costa Rican braconid parasitoid wasps, including host records for 219 species. ZooKeys 1013: 1–665. https://doi.org/10.3897/zookeys.1013.55600

Sharkey M, Brown B, Baker A, Mutanen M (2021b) Response to Zamani et al. (2020): The omission of critical data in the pursuit of "revolutionary" methods to accelerate the description of species. ZooKeys 1033: 191–201. https://doi.org/10.3897/zookeys.1033.66186

Sharkey MJ, Tucker EM, Baker AM, Smith A, Ratnasingham S, Manjunath R, Hebert P, Hallwachs W, Janzen D (2022) More discussion of minimalist species descriptions and clarifying some misconceptions contained in Meier et al. 2021. ZooKeys 1110: 135. https://doi.org/10.3897/zookeys.1110.85491

Sigovini M, Keppel E, Tagliapietra D (2016) Open nomenclature in the biodiversity era. Methods in Ecology and Evolution 7: 1217–1225. https://doi.org/10.1111/2041-210X.12594

Solow AR, Mound LA, Gaston KJ (1995) Estimating the rate of synonymy. Systematic Biology 44: 93–96. https://doi.org/10.2307/2413485

Stork NE (1997) Measuring global biodiversity and its decline. In: Reaka-Kudla ML, Wilson DE, Wilson EO (Eds) Biodiversity ii: Understanding and Protecting our Biological Resources. J. Henry Press, Washington, DC, 41–68.

Thomson SA, Pyle RL, Ahyong ST, Alonso-Zarazaga M, Ammirati J, Araya JF, et al. (2018) Taxonomy based on science is necessary for global conservation. PLoS Biology 16(3): e2005075. https://doi.org/10.1371/journal.pbio.2005075

WSC (2024) World Spider Catalog. Version 25.0. Natural History Museum Bern. [accessed on 1 Mar. 2024] https://doi.org/10.24436/2

Zamani A, Fric ZF, Gante HF, Hopkins T, Orfinger AB, Scherz MD, Bartoňová AS, Dal Pos D (2022a) DNA barcodes on their own are not enough to describe a species. Systematic Entomology 47: 385. https://doi.org/10.1111/syen.12538

Zamani A, Dal Pos D, Fric ZF, Orfinger AB, Scherz MD, Bartoňová AS, Gante HF (2022b) The future of zoological taxonomy is integrative, not minimalist. Systematics and Biodiversity 20: 1. https://doi.org/10.1080/14772000.2022.2063964

ZooKeys

Research Article

Carcinoplax mistio Ng & Mitra, 2019 (Crustacea, Decapoda, Goneplacidae): additional records and genetic differentiation of allied taxa

Mani Prema[1,2], Chien-Hui Yang[3], Samuthirapandian Ravichandran[1,4], Peter K. L. Ng[5]

1   Centre of Advanced Study in Marine Biology, Faculty of Marine Sciences, Annamalai University, Parangipettai–608 502, India
2   Centre for Marine Living Resources and Ecology, Ministry of Earth Sciences, Kochi – 682508, Kerala, India
3   Institute of Marine Biology and Center of Excellence for the Oceans, National Taiwan Ocean University, 2 Pei-Ning Road, Keelung 202231, Taiwan
4   Department of Zoology, Government Arts & Science College, Nagercoil – 629 004, India
5   Lee Kong Chian Natural History Museum, Faculty of Science, National University of Singapore, 2 Conservatory Drive, Singapore 117377, Singapore
Corresponding author: Chien-Hui Yang (chyang@ntou.edu.tw)

OPEN ACCESS

Abstract

The goneplacid crab, *Carcinoplax mistio* Ng & Mitra, 2019, was originally described from West Bengal, India, in the northern Indian Ocean. Additional material of *C. mistio* from off Tamil Nadu in the southeast of India revealed a high degree of size-associated variation in the structures of the anterolateral tooth of the carapace, chelipeds, and male and female pleons. In addition to an in-depth morphological examination of *C. mistio*, this study also records the natural coloration of the species and conducts a genetic comparison (with mitochondrial COI and 16S rRNA genes) with its close relatives, *C. haswelli* (Miers, 1884) and *C. purpurea* Rathbun, 1914. Molecular comparison of *C. mistio* with its morphologically closest congener, *C. haswelli* from northern Australia and the western Pacific, corroborates their status as separate species. The genetic sequence of *C. mistio*, however, is similar to that of *C. purpurea* from the West Pacific, although these two species can easily be distinguished by distinct carapace and ambulatory leg characters. The present study provides some possible explanations for the genetic and morphological incongruence observed between *C. mistio* and *C. purpurea* and highlights the need for a detailed molecular study for *Carcinoplax* H. Milne Edwards, 1852, to appreciate the evolution of various morphological characters in the genus.

Key words: Brachyura, COI, genetic and morphological incongruence, goneplacid crab, Goneplacoidea, India, systematics, 16S rRNA

Introduction

The goneplacid crab genus, *Carcinoplax* H. Milne Edwards, 1852, comprises 26 species from the Indo-West Pacific (Castro 2007, 2009; Ng and Kumar 2016; Ng and Mitra 2019; Ng and Castro 2020). Six species of *Carcinoplax* are known from India: *C. longimanus* (De Haan, 1833); *C. longipes* (Wood-Mason, in Wood-Mason & Alcock, 1891); *C. indica* Doflein, 1904; *C. specularis* Rathbun, 1914; *C. fasciata* Ng & Kumar, 2016; and *C. mistio* Ng & Mitra, 2019 (see Trivedi et al. 2018; Ng and Mitra 2019).

While describing *C. mistio* from West Bengal, India, Ng and Mitra (2019) compared it with two close congeners, *C. sinica* Chen, 1984, and *C. purpurea* Rathbun, 1914, noting that *C. mistio* has a combination of diagnostic characters of other species. *Carcinoplax sinica* has since been synonymised with *C. haswelli* (Miers, 1884) (cf. Ng et al. 2022). Ng and Mitra (2019) had only three specimens of *C. mistio* available for study, so they were unable to assess allometric variation, which can be pronounced in some species of *Carcinoplax* (Guinot 1989; Castro 2007). A good series of *C. mistio* was recently collected from Tamil Nadu, southeast coast of India, allowing the present evaluation of morphological variation in the species. The present study also takes the opportunity to document the natural coloration of *C. mistio* and compare the genetics of allied *C. mistio*, *C. haswelli* and *C. purpurea*.

Material and methods

Material

The material used for morphological examination is deposited in the Zoological Survey of India, Kolkata (**ZSIK**); and Centre of Advanced Study in Marine Biology, Annamalai University, Parangipettai, Tamil Nadu (**CASAU**). Details of all specimens examined are provided in the material examined subsection of the systematic account below. Measurements provided, in millimetres (**mm**), are of the maximum carapace width (inclusive of spines) and length (taken at the midline from the tips of the frontal margin to the median part of the posterior margin), respectively. The terminology used follows Davie et al. (2015) and Ng and Mitra (2019). Abbreviations used in this study are as follows: **coll.** = collector; **juv.** = juvenile; **G1 =** male first gonopod; and **G2** = male second gonopod; **ovig.** = ovigerous.

Molecular analysis

In addition to *C. mistio*, *C. haswelli* and *C. purpurea*, four other species of *Carcinoplax* [*C. ischurodous* (Stebbing, 1923), *C. longimanus*, *C. nana* Guinot, 1989 and *C. tomentosa* Sakai, 1969], are also included for the molecular analysis. *Goneplax rhomboides* (Linnaeus, 1758) was selected as the outgroup. The samples for molecular analyses were from the Zoological Reference Collection of the Lee Kong Chian Natural History Museum, National University of Singapore (ZRC), and National Taiwan Ocean University (NTOU) (Table 1).

Crude genomic DNA was extracted from the muscles of the pleon using a DNeasy® Blood and Tissue Kit (Qiagen, Hilden, Germany) following the protocol of the manufacturer. Molecular markers were selected as the mitochondrial COI and 16S rRNA genes, while the sequences amplification using LCO1490/HCO2198 (~657 bp, Folmer et al. 1994) and 16Sar/16S1472 (~550 bp) (Simon et al. 1994; Crandall and Fitzpatrick 1996), respectively. PCR reactions, cycling profiles, product checking and sequencing procedures followed those used in Ng et al. (2018). The output sequences were edited for contig assembly by SeqMan Pro™ (Lasergene®; DNASTAR, Madison, WI, USA), then blasted on the GenBank (National Center for Biotechnology Information, NCBI) to check for any potential contamination. EditSeq (Lasergene®; DNASTAR) was used to

Table 1. Material, sampling localities and GenBank accession numbers of *Carcinoplax* and outgroup used in this study. "#" sequences downloaded from GenBank. N.C. - no sequence available.

Species (code)	Locality	Voucher Nos.	GenBank Accession Nos.	
			COI	16S rDNA
C. haswelli (1)	Gulf of Tonkin	ZRC 2011.0607	OP163291	PQ163823
C. haswelli (2)	Off Singapore	ZRC 1984.5693	OP163292	N.C.
C. ischurodous			MZ434779#	MZ424933#
C. longimanus (1)	Taiwan	NTOU B00138	OP163293	PQ163824
C. longimanus (2)			MZ434781#	MZ424935#
C. longimanus (3)			MZ434783#	MZ424936#
C. mistio (1)	India	ZRC 2022.0812 (male)	OP163294	PQ163825
C. mistio (2)	India	ZRC 2022.0812 (female)	OP163295	PQ163826
C. nana	Philippines	ZRC 2019.0361	OP163296	PQ163827
C. purpurea (1)	Taiwan	ZRC 2001.0017	OP163297	PQ163828
C. purpurea (2)	Taiwan	NTOU B00139	OP163298	PQ163829
C. purpurea (3)	Philippines	ZRC 2006.0216	OP163299	PQ163830
C. tomentosa	Taiwan	NTOU B00140	OP163300	PQ163831
Goneplax rhomboides			MG935224#	JN591672#

translate into the corresponding amino acid sequences to avoid the inclusion of pseudogenes for the COI dataset (Song et al. 2008). Sequence alignment and nucleotide pairwise distance for each of the two datasets were calculated based on the Kimura 2-parameter model (K2P, Kimura 1980) by MEGA v.11 (Tamura et al. 2021). The maximum-likelihood (ML) tree was constructed based on the combined sequences (COI+16S rDNA) using MEGA v.11 by 1000 bootstrap replicates (Felsenstein 1985). We failed to get a complete 16S rDNA sequence on *C. haswelli* (ZRC 1984.5693), and the missing sequence was filled up by the fifth nucleotide "N" for the combined dataset.

Systematic account

Superfamily Goneplacoidea MacLeay, 1838
Family Goneplacidae MacLeay, 1838
Genus *Carcinoplax* H. Milne Edwards, 1852

***Carcinoplax mistio* Ng & Mitra, 2019**
Figs 1–3

Carcinoplax (*purpurea*)? – Stephensen 1946: 166, 208, fig. 44 (not *Carcinoplax purpurea* Rathbun, 1914).
Carcinoplax purpurea – Guinot 1967: 276 (list); Titgen 1982: 252 (list) (not *Carcinoplax purpurea* Rathbun, 1914).
Carcinoplax sinica – Guinot 1989: 285, fig. 14A, B, pl. 5 figs A, B, B1, C, C1, D, E, E1; Apel 2001: 101; Naderloo and Sari 2007: 449; Naderloo 2017: 69, text-fig. 11.2d, e, fig. 12.1 (not *Carcinoplax sinica* Chen, 1984) [= *Carcinoplax haswelli* Miers, 1884)].
Carcinoplax mistio Ng & Mitra, 2019: e2019004, figs 1, 2, 6A, 7A, G, H, 8A–G, 9A, B.
Carcinoplax haswelli – Sureandiran et al. 2024: figs 2–7 (not *Carcinoplax haswelli* Miers, 1884).
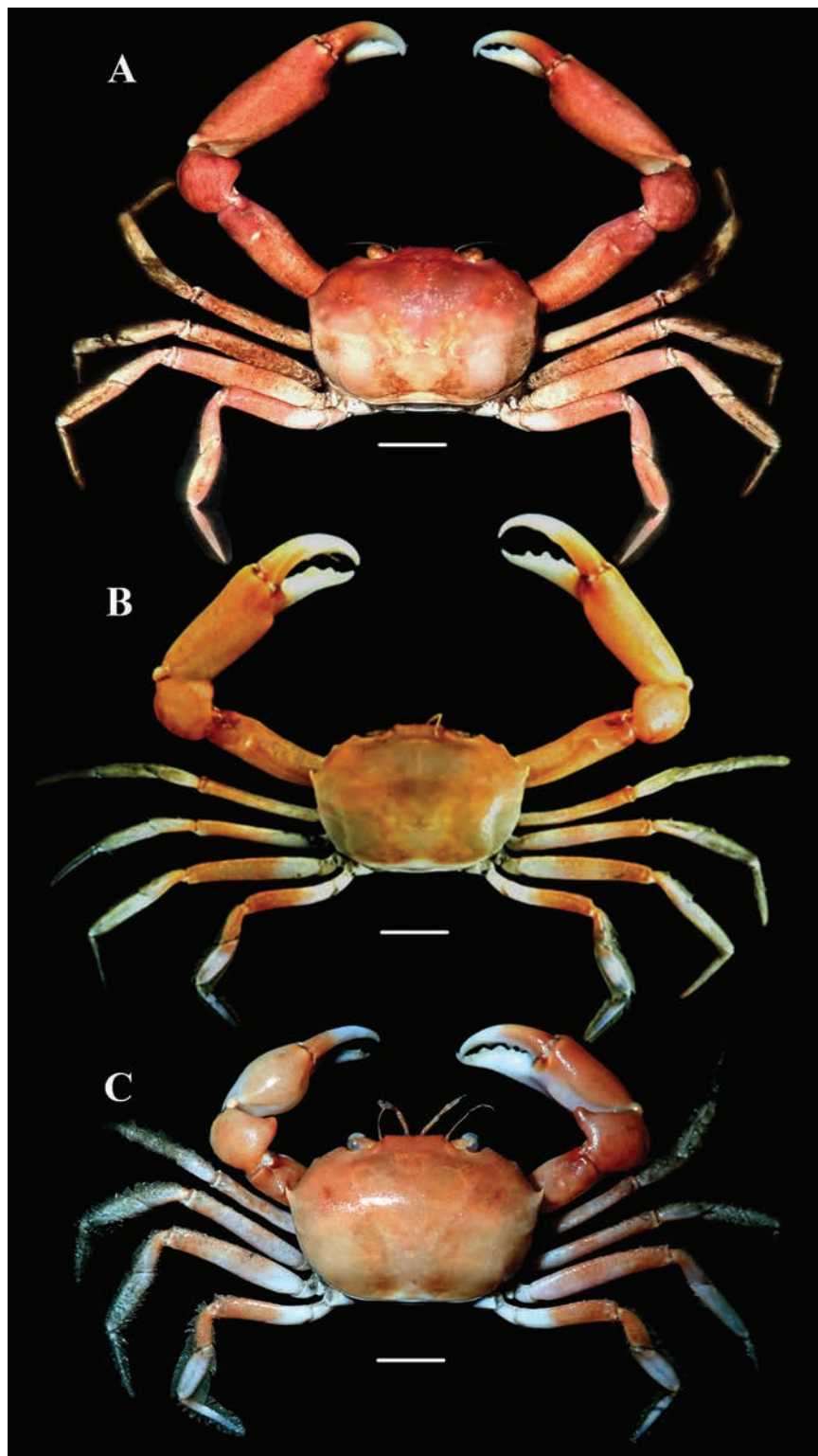
Figure 1. Colour in life and overall dorsal view of *Carcinoplax mistio* Ng & Mitra, 2019 **A** male (33.3 × 23.4 mm) (CASAU CR-1037) **B** male (29.2 × 20.5 mm) (CASAU CR-1036) **C** female (33.5 × 24.0 mm) (CASAU CR-1040). Scale bars: 1.0 cm (**A–C**).

Material examined. *Holotype.* India • ♂ (29.2 × 19.0 mm); northern Bay of Bengal, Fresargunj Fishing Harbour; 24 Feb. 2017; coll. local fishermen by trawl; ZSIK C7123/2. **Paratypes.** India • 1 ♀ (36.4 × 24.2 mm); same collection data as for holotype; ZSIK C7124/2 • 1 ♀ (36.7 × 27.5 mm); northern Bay of Bengal, Fresargunj Fishing Harbour; 28 Jul. 2018; ZSIK.

Other material. INDIA • 4 ♂♂ (35.1 × 30.0 mm, 29.2 × 22.3 mm, 25.1 × 18.2 mm, 23.2 × 29.2 mm), 5 ♀♀ (37.1 × 31.0 mm, 36.2 × 30.1 mm, 32.1 × 25.2 mm, 31.0 × 25.2 mm, 26.1 × 24.0 mm); southern Bay of Bengal, eastern Tamil Nadu, Pazhayar Fishing Port; 11°21'N, 79°50'E; depth 50−100 m; 2016−2020; coll. M. Prema & S. Ravichandran; CASAU CR-1031 • 1 ♂ (29.7 × 19.6 mm), 1 ♀ (43.2 × 29.2 mm); same collection data as for preceding; 2016−2020; CASAU CR-1032 • 2 ♂♂ (37.6 × 25.8 mm, 32.0 × 21.3 mm), 7 ♀♀ (37.9 × 24.5 mm, 37.0 × 25.1 mm, 34.0 × 22.9 mm, 32.3 × 21.6 mm, 31.2 × 21.1 mm, 29.5 × 19.6 mm, 27.6 × 25.6 mm,); same collection data as for preceding; 18 Mar. 2018; CASAU CR-1033 • 1 ♂ (26.4 × 18.0 mm), 1 juv. ♀ (19.7 × 13.4 mm); same collection data as for preceding; Mar. 2018; CASAU CR-1034 • 4 ♂♂ (36.0 × 23.8 mm, 33.0 × 22.7 mm, 32.5 × 22.2 mm, 31.5 × 21.4 mm), 1 ovig. ♀ (39.0 × 26.6 mm), 1 ♀ (36.1 × 23.4 mm); same collection data as for preceding; 2020−2021; CASAU CR-1035 • 3 ♂♂ (29.2 × 20.8 mm, 29.2 × 20.5 mm, 27.6 × 19.4 mm); same collection data as for preceding; 12 Jan. 2022; CASAU CR-1036 • 1 ♂ (33.× 23.4 mm); same collection data as for preceding; CASAU CR-1037 • 2 ♀♀ (37.3 × 24.6 mm, 35.9 × 23.7 mm); same collection data as for preceding; 26 Mar. 2023; CASAU CR-1038 • 2 ♂♂ (26.2 × 18.1 mm, 24.8 × 16.4 mm), 2 ♀♀ (32.2 × 22.0 mm, 29.5 × 19.4 mm); same collection data as for preceding; 11 Feb. 2024; CASAU CR-1039 • 7 ♀♀ (37.9 × 26.0 mm, 36.2 × 24.3 mm, 34.7 × 22.5 mm, 33.5 × 24.0 mm, 30.5 × 20.5 mm, 29.2 × 20.1 mm, 25.1 × 17.1 mm); same collection data as for preceding; 11 Feb. 2024; CASAU CR-1040.

Diagnosis. Modified from Ng and Mitra (2019). Carapace broad, dorsal surface gently convex; antero-lateral surfaces generally with small, rounded, densely packed granules, sometimes appearing almost smooth; post-orbital region with small, rounded granules; second anterolateral teeth relatively short in larger specimens, slightly sharp in smaller specimens; gastro-cardiac groove shallow but visible (Figs 1, 2A, B, 3A). Chelipeds unequal, male carpal spine more rounded, that on female more elongate (Figs 1, 2G−I, J−L, 3B−D). Ambulatory legs long, slender; articles laterally flattened, smooth; margins lined with setae (Fig. 1). G1 relatively slender, laterally flattened, tip elongate, tapering, lined with numerous short spines (Fig. 3G−K). G2 longer than G1, distal segment long, curved, tip weakly bifurcated (Ng and Mitra 2019: fig. 8D).

Habitat. The present specimens of *C. mistio* were collected from 50−100 m depth, off the coastal waters of Tamil Nadu state, Bay of Bengal, India. The three type specimens were obtained from West Bengal, also from a fishing port but without depth data (Ng and Mitra 2019).

Coloration in life. Carapace orange, cheliped fingers and upper surface of ambulatory legs white (Fig. 1A−C), merus of ambulatory leg generally orange (Fig. 1), and sternopleonal surfaces pale white.

Distribution. Northern Indian Ocean: Bay of Bengal (West Bengal and off Tamil Nadu coast, India; Ng and Mitra 2019; present study); north-western Arabian Sea (Gujarat, India; Sureandiran et al. 2024); and Persian Gulf (Guinot 1989; Naderloo 2017).

Remarks. The present specimens of *C. mistio* agree well with the type account (Ng and Mitra 2019). The large series of specimens, however, allowed us to document size-related morphological variation. The largest specimens of *C. mistio* collected in this study have a carapace width of 37.6 mm (male, CASAU CR-1033) and 43.2 mm (female, CASAU CR-1032), respectively; both are larger than the type specimens and are the largest known specimens of the species.
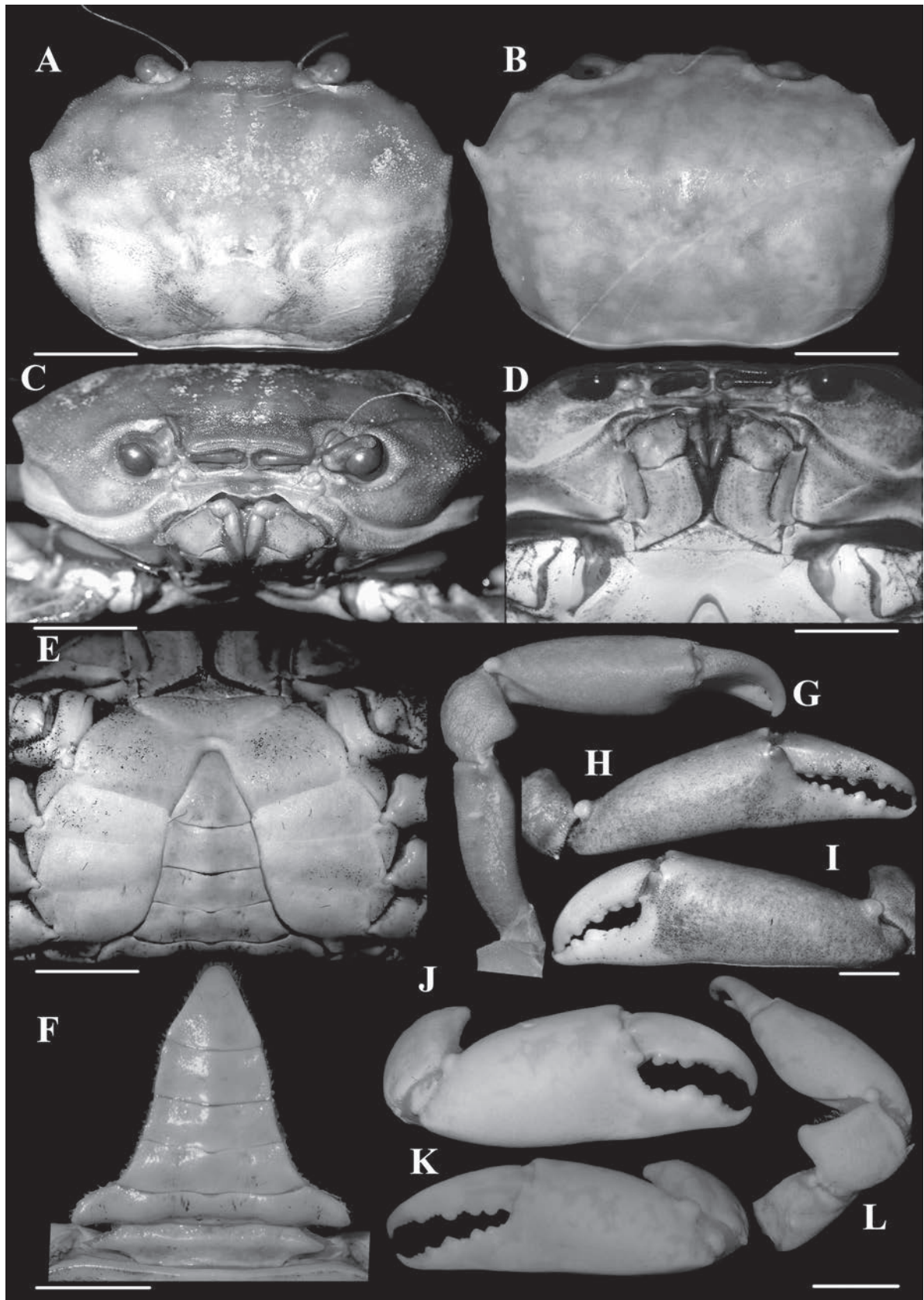
Figure 2. *Carcinoplax mistio* Ng & Mitra, 2019 **A, C, D, E−I** male (33.3 × 23.4 mm) (CASAU CR-1037) **B, J−L** male (24.8 × 16.4 mm) (CASAU CR-1039) **A, B** dorsal view of carapace **C** frontal view of cephalothorax **D** third maxillipeds **E** thoracic sternites 3−6, pleonal somites and telson **E** pleonal somites and telson **G−L** dorsal and outer views of chelae. Scale bars: 5.0 mm (**A−L**).

In the types as well as in the smaller males (e.g., 26.4 × 18.0 mm, CASAU CR-1034; 24.8 × 16.4 mm, CASAU CR-1039) and most of the larger specimens of the present collection, the second anterolateral tooth of the carapace is prominent, being sharp and curved (Figs 1B, 2B). In the largest males (e.g., 35.1 × 30.0 mm, CASAU CR-1031; 33.3 × 23.4 mm, CASAU CR-1037), this tooth is relatively lower (Figs 1A, 2A) and comparable to the condition in *C. purpurea*. In *C. purpurea*, however, the second anterolateral tooth is even lower and more like a rounded tubercle (cf. Ng and Mitra 2019: fig. 6C, D). As such, the form of the second anterolateral tooth is not a reliable diagnostic character for *C. mistio* at all body sizes, being sometimes size dependent, though it is usually sharp and longer. The cheliped of the largest males is elongate, with the merus and fingers extremely long (Fig. 1A, B, 2G–I), a condition like that of *C. longimanus* (see Guinot 1989). In the smaller holotype male of *C. mistio* as well as in smaller males, the chelipeds are relatively shorter (Fig. 2J–L). Sexual dimorphism is apparent as all females have relatively shorter cheliped fingers (Figs 1C, 3B–D).

The cheliped carpal spine of male *C. mistio* specimens examined, including the holotype male, is relatively more rounded and relatively shorter (Figs 1A, B, 2G, H, J, L) (versus the cheliped carpal spine being relatively less rounded, more elongate and curved in most of the females; Figs 1C, 3B, D). In the holotype male of *C. mistio*, the carpal spine is relatively short and rounded (Ng and Mitra 2019: fig. 1A, F) and as such, its length is a sexually dimorphic character (Ng and Mitra 2019: fig. 2A, D, F) that is not size dependent. This is similar to the condition of the cheliped carpal spine that was reported for *C. haswelli* (as *C. sinica*, cf. Ng and Mitra 2019: fig. 4E).

The lateral margins of pleonal somite 6 of large males is gently convex, gradually converging towards the telson, which is similar to that of the holotype of *C. mistio* (Fig. 2E, F; see Ng and Mitra 2019: fig. 7A). In the large male of *C. mistio* (33.3 × 23.4 mm, CASAU CR-1037), pleonal somite 6 is proportionately broader, width-to-length ratios 2.1 (versus pleonal somite 6 width-to-length ratios in two smaller males (26.2 × 18.1 mm, 24.8 × 16.4 mm, CASAU CR-1040) being 1.96 and 1.98, respectively). The pleon of large females in the present collection is similar to that reported for the paratype *C. mistio* (36.4 × 24.2 mm, ZSIK C7124/2) (cf. Ng and Mitra 2019: fig. 9A), but in a smaller specimen (26.1 × 24.0 mm, CASAU CR-1031), the pleon is relatively wider than in the paratype. Among the 28 female specimens studied, only one was ovigerous (39.0 × 26.6 mm, CASAU CR-1035). In juvenile females (e.g., 19.7 × 13.4 mm, CASAU CR-1034), the pleon is not expanded, lacking setae on pleopods, and the operculum of the vulva is poorly developed.

The proportions of the male telson vary regardless of size with the width-to-length ratios of three males (33.3 × 23.4 mm, CASAU CR-1037; 26.2 × 18.1 mm, 24.8 × 16.4 mm, CASAU CR-1040) are 0.76, 0.88 and 0.67, respectively. Overall, the male telson is slightly broader with the lateral margins being more concave (Fig. 2E, F) than in *C. haswelli* (cf. Ng and Mitra 2019: fig. 7D–F).

The mesial margin of the distal two-thirds of the G1 is gently concave in large specimens of *C. mistio* (Fig. 3G) and almost straight in smaller ones (Fig. 3I), but the tip is always elongate and tapering (Fig. 3G–J). Ng and Mitra (2019) observed that the G1s of the holotype (29.2 × 19.0 mm, ZSIK C7123/2) were distally damaged. Sureandiran et al. (2024) reported "*Carcinoplax haswelli*" based on one male specimen from Gujarat in western India, but all their figures of the G1 and the carapace (see Sureandiran et al. 2024: figs 2–7), actually correspond to *C. mistio*.
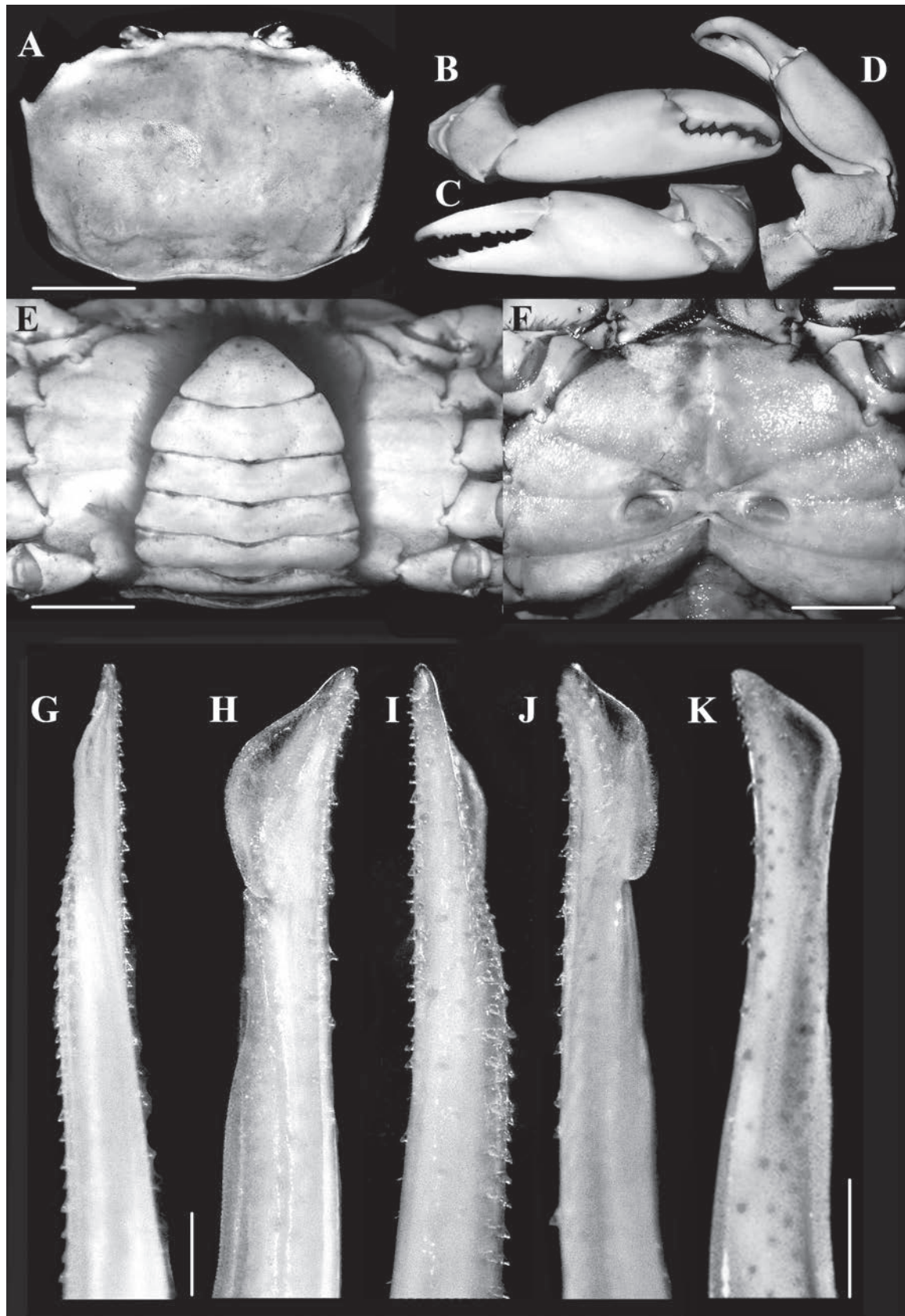
Figure 3. *Carcinoplax mistio* Ng & Mitra, 2019 **A–F** female (33.5 × 24.0 mm) (CASAU CR-1040); **G– J** male (33.3 × 23.4 mm) (CASAU CR-1037) **K** male (25.1 × 18.2 mm); **A** dorsal view of carapace **B–D** dorsal and outer views of chelae **E** pleon and telson **F** thoracic sternites with position of vulvae **G** dorsal view of left G1 **H** dorso-lateral view of left G1 **I** ventral view of left G1 **J** ventro-lateral view of left G1 **K** lateral view of left G1. Scale bars: 5.0 mm (**A–F**); 1.0 mm (**G–K**).

The genetic comparisons for seven species of *Carcinoplax*, including *C. mistio*, are interesting (Fig. 4). The intraspecific divergences of COI (657 bp) and 16S rRNA (552 bp) genes for four morphologically distinct species of *Carcinoplax* are less than 1.5%: *C. haswelli* (COI 0.2%), *C. mistio* (COI 0%, 16S 0.2%), *C. purpurea* (COI 0.5–1.1%, 16S 0%), and *C. longimanus* (COI 0.2–0.8%, 16S 0.0–0.4%) (Table 2). As for the interspecific divergences of the three species under study here (Table 2), that between *C. haswelli* and *C. mistio* is high (COI 10.3–10.5%, 16S 3.5–3.7%), as is that between *C. haswelli* and *C. purpurea* (COI 9.9–10.5%, 16S 3.5%) (Table 2, Fig. 4), corroborating their status as separate species. The genetic divergence between *C. mistio* and *C. purpurea*, however, was unexpectedly low (COI 0.3–0.8%, 16S 0.0–0.2%) and within the range normally considered for conspecificity (Fig. 4) when compared with the other four species of *Carcinoplax* (COI 12.4–21.1%, 16S 6.5–12.1%) (Table 2, Fig. 4). The morphological differences between *C. mistio* and *C. purpurea*, however, are substantial. In *C. mistio*, the carapace is proportionally wider, appearing more rectangular in shape with the posterolateral margins distinctly converging posteriorly (Figs 1A–C, 2A, B, 3A; see Ng and Mitra 2019: figs 1A, 2A, 6A, B) (versus carapace more quadrate with the posterolateral margins subparallel in *C. purpurea*; see Ng and Mitra 2019: figs 3A, 6C, D); the second (last) anterolateral tooth is usually sharp and curved (Figs 1B, C, 2B, 3A) (versus low and rounded in *C. purpurea*; see Ng and Mitra 2019: figs 3A, 6C, D); and the ambulatory legs are long and slender (Fig. 1A–C; see Ng and Mitra 2019: figs 1A, 2A, 7G, H) (versus distinctly shorter and stouter in *C. purpurea*; see Ng and Mitra 2019: figs 3A, 7I, J). Noteworthy is that the G1s of *C. mistio* and *C. purpurea* are similar (Fig. 3G–J; see Ng and Mitra 2019: fig. 8E, F, H, I). The characters of the G1 are more conservative in goneplacid evolution than carapace and pereopod differences, which are more plastic. Significant morphological differentiation but with low genetic variation has previously been reported in *Armases angustipes* (Dana, 1852) (Sesarmidae, Marochi et al. 2017), *Carcinus maenas* (Linnaeus, 1758) (Carcinidae, Silva et al. 2010), and *Pachygrapsus marmoratus* (Fabricius, 1787) (Grapsidae, Deli et al. 2015). There are many possible explanations for this observed discordance, ranging from incomplete lineage sorting to retention of ancestral genotypes, etc. (see Meier et al. 2006; Tang et al. 2012; Nabholz 2023).

A detailed molecular study of *Carcinoplax* will be necessary to appreciate the evolution of the various morphological characters in the genus as currently defined (sensu Castro 2007). *Carcinoplax* currently contains 26 species, all from the Indo-West Pacific, with many species morphologically similar and often occurring sympatrically, although several species span both oceans (see Castro 2007, 2009; Ng and Castro 2020). As the present study indicates, genetic and morphological incongruence may be more common in *Carcinoplax* than expected, and wide-ranging taxa may well prove to be species-complexes (see Ng and Castro 2020). Currently, *C. mistio* is known from the northern Indian Ocean, ranging from the Bay of Bengal to the Persian Gulf. *Carcinoplax purpurea* is only known for certain from the western Pacific (Castro 2007). There is also a record of *C. purpurea* from Madagascar by Castro (2007: 639), but it was based on a badly preserved male specimen, and it more likely belongs to either *C. monodi* Guinot, 1989, or *C. haswelli*. *Carcinoplax haswelli*, however, occurs in the western Pacific, Southeast Asia and eastern Indian Ocean (north-western Australia) (Ng et al. 2022).
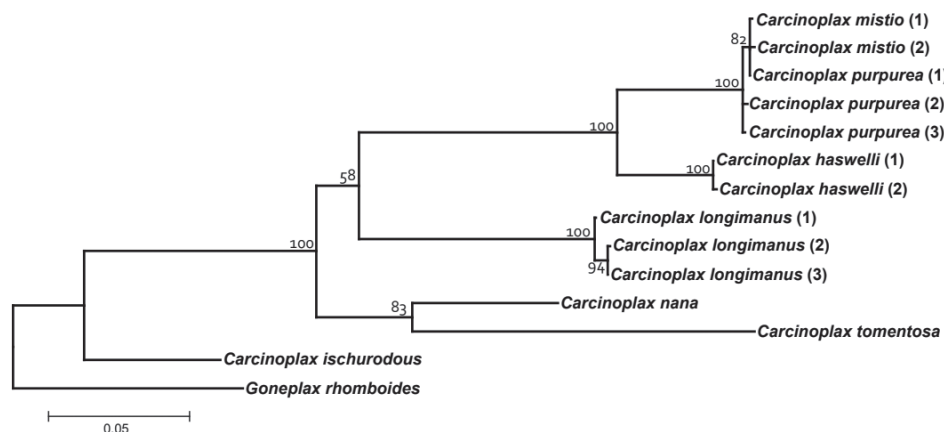
Figure 4. Maximum likelihood phylogenetic tree for seven species of *Carcinoplax* based on the mitochondrial COI+16S rRNA genes dataset. *Goneplax rhomboides* (Linnaeus, 1758) was chosen as outgroup. Bootstrap value is represented above the branches. Values < 50 are not shown.

Table 2. Pairwise distance based on Kimura-2-parameter (K2P) model of partial mitochondrial COI (within and under the diagonal) and 16S rDNA (value in the brackets and above the diagonal) sequences among *Carcinoplax* species. *Goneplax rhomboides* (Linnaeus, 1758) was treated as an outgroup.

	Carcinoplax haswelli	*C. ischurodous*	*C. longimanus*	*C. mistio*	*C. nana*	*C. purpurea*	*C. tomentosa*	*Goneplax rhomboides*
Carcinoplax haswelli	0.002	0.102	0.098–0.101	0.035–0.037	0.105	0.035	0.134	0.128
C. ischurodous	0.199–0.202		0.078–0.083	0.095–0.097	0.080	0.095	0.093	0.071
C. longimanus	0.172–0.178	0.176–0.178	0.002–0.008 [0.0–0.004]	0.082–0.088	0.078–0.084	0.082–0.086	0.084–0.087	0.113
C. mistio	0.103–0.105	0.190	0.159–0.164	0.0 [0.002]	0.093–0.095	0.0–0.002	0.118–0.121	0.113–0.116
C. nana	0.165–0.167	0.154	0.124–0.127	0.179		0.093	0.065	0.105
C. purpurea	0.099–0.105	0.192–0.195	0.159–0.169	0.003–0.008	0.181–0.184	0.005–0.011 [0.0]	0.118	0.113
C. tomentosa	0.173–0.175	0.209	0.203–0.211	0.203	0.160	0.200–0.203		0.105
Goneplax rhomboides	0.187–0.189	0.122	0.204–0.205	0.198	0.172	0.195–0.203	0.219	

Acknowledgements

Additional information

Conflict of interest

The authors have declared that no competing interests exist.

Ethical statement

No ethical statement was reported.

Author contributions

MP and SR collected the samples. MP prepared the photographs. CHY conducted the molecular works and prepared Fig. 4. MP and CHY prepared the draft and PN finalized the manuscript.

Author ORCIDs

Mani Prema https://orcid.org/0000-0003-2694-3034
Chien-Hui Yang https://orcid.org/0000-0002-4594-3622
Samuthirapandian Ravichandran https://orcid.org/0000-0002-8632-5062
Peter K. L. Ng https://orcid.org/0000-0001-5946-0608

Data availability

All of the data that support the findings of this study are available in the main text.

References

Apel M (2001) Taxonomie und Zoogeographie der Brachyura, Paguridea und Porcellanidae (Crustacea: Decapoda) des Persisch-Arabischen Golfes. PhD Thesis, Johann Wolfgang Goethe-Universität, Biologie und Informatik, Frankfurt am Main, Germany.

Castro P (2007) A reappraisal of the family Goneplacidae MacLeay, 1838 (Crustacea, Decapoda, Brachyura) and revision of the subfamily Goneplacinae, with the description of ten new genera and eighteen new species. Zoosystema 29(4): 609–773.

Castro P (2009) Two new species of *Carcinoplax* H. Milne Edwards, 1852, and *Pycnoplax* Castro, 2007, from the western Pacific, and a description of the female of *Thyraplax truncata* Castro, 2007 (Crustacea, Decapoda, Brachyura, Goneplacidae). Zoosystema 31(4): 949–957. https://doi.org/10.5252/z2009n4a9

Crandall Jr KA, Fitzpatrick JE (1996) Crayfish molecular systematics: using a combination of procedures to estimate phylogeny. Systematic Biology 45: 1–26. https://doi.org/10.1093/sysbio/45.1.1

Davie PJF, Guinot D, Ng PKL (2015) Anatomy and functional morphology of Brachyura. In: Castro P, Davie PJF, Guinot D, Schram FR, von Vaupel Klein JC (Eds) Treatise on Zoology – Anatomy, Taxonomy, Biology. The Crustacea (Vol. 9C–I): Decapoda: Brachyura (Part 1). Brill, Leiden, 11–163. https://doi.org/10.1163/9789004190832_004

Deli T, Bahles H, Said K, Chatti N (2015) Patterns of genetic and morphometric diversity in the marbled crab (*Pachygrapsus marmoratus*, Brachyura, Grapsidae) populations across the Tunisian coast. Acta Oceanologica Sinica 34: 49–58. https://doi.org/10.1007/s13131-015-0687-7

Felsenstein J (1985) Confidence limits on phylogenies: and approach using the bootstrap. Evolution 39: 783–791. https://doi.org/10.2307/2408678

Folmer O, Black M, Hoeh W, Lutz R, Vrijenhoek R (1994) DNA primers for amplification of mitochondrial cytochrome c oxidase subunit I from diverse metazoan invertebrates. Molecular Marine Biology and Biotechnology 3: 294–299.

Guinot D (1967) La faune carcinologique (Crustacea, Brachyura) de l'Ocean Indien occidental et de la Mer Rouge. Catalogue remarques biogéographiques et bibliographie. Mémoires de l'Institut fundamental d'Afrique noire 77: 235–352.

Guinot D (1989) Le genre *Carcinoplax* H. Milne Edwards, 1852 (Crustacea, Brachyura: Goneplacidae). In: Forest J (Ed) Resultats des campagnes MUSORSTOM, Volume 5. Mémoires du Muséum National d'Histoire Naturelle 144: 265–345.

Kimura M (1980) A simple method for estimating evolutionary rate of base substitutions through comparative studies of nucleotide sequences. Journal of Molecular and Evolution 16: 111–120. https://doi.org/10.1007/BF01731581

Marochi MZ, Masunari S, Schubart CD (2017) Genetic and morphological differentiation of the semiterrestrial crab *Armases angustipes* (Brachyura: Sesarmidae) along the Brazilian coast. The Biological Bulletin 232(1): 30–44. https://doi.org/10.1086/691985

Meier R, Shiyang K, Vaidya G, Ng PKL (2006) DNA taxonomy and DNA identification in Diptera: a tale of high intraspecific variability and low identification success. Systematic Biology 55(5): 715–728. https://doi.org/10.1080/10635150600969864

Nabholz B (2023) Incomplete lineage sorting explains the low performance of DNA barcoding in a radiation of four species of Western European grasshoppers (Orthoptera: Acrididae: *Chorthippus*). Biological Journal of the Linnean Society 141(1): 33–50. https://doi.org/10.1093/biolinnean/blad106

Naderloo R (2017) Atlas of crabs of the Persian Gulf. Cham, Springer, 440 pp. https://doi.org/10.1007/978-3-319-49374-9

Naderloo R, Sari A (2007) Subtidal crabs of the Iranian coast of the Persian Gulf: new collections and biogeographic considerations. Aquatic Ecosystem Health Management 10: 341–349. https://doi.org/10.1080/14634980701514620

Ng PKL, Castro P (2020) A revision of *Carcinoplax abyssicola* (Miers, 1885) and seven related species of *Carcinoplax* H. Milne Edwards, 1852, with the description of two new species and an updated key to the genus (Crustacea, Decapoda, Brachyura, Goneplacidae). Zoosystema 42(17): 239–284. https://doi.org/10.5252/zoosystema2020v42a17

Ng PKL, Kumar AB (2016) *Carcinoplax fasciata*, a new species of deep-water goneplacid crab from southwestern India (Crustacea: Decapoda: Brachyura: Goneplacoidea). Zootaxa 4147(2): 192–200. https://doi.org/10.11646/zootaxa.4147.2.6

Ng PKL, Mitra S (2019) *Carcinoplax mistio*, a new species of goneplacid crab from the Indian Ocean (Decapoda: Brachyura: Goneplacoidea). Nauplius 27: e2019004. https://doi.org/10.1590/2358-2936e2019004

Ng PKL, Ho P-H, Lin C-W, Yang C-H (2018) The first record of an eastern Pacific invasive crab in Taiwanese waters: *Amphithrax armatus* (Saussure, 1853) (Brachyura: Majoidea: Mithracidae), with notes on the taxonomy of the genus. Journal of Crustacean Biology 38(2): 198–205. https://doi.org/10.1093/jcbiol/rux109

Ng PKL, Clark PF, Ahyong ST (2022) The identity of *Homoioplax haswelli* (Miers, 1884) (Crustacea: Decapoda: Brachyura). Zoological Studies 61: 6. https://doi.org/10.6620/ZS.2022.61-06

Silva IC, Alves MJ, Paula J, Hawkins SJ (2010) Population differentiation of the shore crab *Carcinus maenas* (Brachyura: Portunidae) on the southwest English coast based on genetic and morphometric analyses. Scientia Marina 74(3): 435–444. https://doi.org/10.3989/scimar.2010.74n3435

Simon C, Frati F, Beckenbach A, Crespi B, Liu H, Flook P (1994) Evolution, weighting and phylogenetic utility of mitochondrial gene sequences and a compilation of conserved polymerase chain reaction primers. Annals of the Entomological Society of America 87: 625–701. https://doi.org/10.1093/aesa/87.6.651

Song H, Buhay JE, Whiting MF, Crandall KA (2008) Many species in one: DNA barcoding overestimates the number of species when nuclear mitochondrial pseudogenes are coamplified. Proceedings of the National Academy of Sciences of the United States of America 105: 13486–13491. https://doi.org/10.1073/pnas.0803076105

Stephensen K (1946) The Brachyura of the Iranian Gulf. With an appendix: The male pleopoda of the Brachyura. Danish Scientific Investigations in Iran 4: 57–237.

Sureandiran B, Dave TH, Suyani NK, Karuppasamy K (2024) First record of goneplacid crab, *Carcinoplax haswelli* (Decapoda: Brachyura: Goneplacidae) from the Indian Ocean. Journal of the Marine Biological Association of the United Kingdom 104: e37. https://doi.org/10.1017/S0025315424000328

Tamura K, Stecher G, Kumar S (2021) MEGA 11: Molecular Evolutionary Genetics Analysis version 11. Molecular Biology and Evolution 38: 3022–3027. https://doi.org/10.1093/molbev/msab120

Tang Q-Y, Liu S-Q, Yu D, Liu H-Z, Danley PD (2012) Mitochondrial capture and incomplete lineage sorting in the diversification of balitorine loaches (Cypriniformes, Balitoridae) revealed by mitochondrial and nuclear genes. Zoologica Scripta 41: 233–247. https://doi.org/10.1111/j.1463-6409.2011.00530.x

Titgen RH (1982) The systematics and ecology of the Decapods of Dubai, and their zoogeographic relationships to the Arabian Gulf and the Western Indian Ocean. PhD Thesis, Texas A&M University, USA.

Trivedi JN, Trivedi DJ, Vachhrajani KD, Ng PKL (2018) An annotated checklist of marine brachyuran crabs (Crustacea: Decapoda: Brachyura) of India. Zootaxa 4502(1): 1–83. https://doi.org/10.11646/zootaxa.4502.1.1

Morphological and molecular characterisation of *Mordellistena peloponnesensis* Batten, 1980 (Coleoptera, Mordellidae), with first records from Italy and Turkey

Dávid Selnekovič[1], Ján Kodada[1], Nilay Gülperçin[2], Serdar Tezcan[3], Enrico Ruzzier[4,5]

1 Department of Zoology, Faculty of Natural Sciences, Comenius University in Bratislava, Ilkovicočova 6, Bratislava, SK-842 15, Slovakia
2 Natural History Application and Research Centre, Ege University, 35040, Izmir, Turkey
3 Department of Plant Protection, Faculty of Agriculture, Ege University, 35040, Izmir, Turkey
4 Department of Science, Università Roma Tre, viale G. Marconi 446, 00146 Rome, Italy
5 National Biodiversity Future Center (NBFC), 90133 Palermo, Italy
Corresponding author: Dávid Selnekovič (david.selnekovic@uniba.sk)

Abstract

Mordellistena peloponnesensis Batten, 1980, previously known from Cyprus and Greece, is reported from Italy and Turkey for the first time. The species is redescribed based on type specimens and additional material from its entire known distributional range. Eighteen DNA barcoding sequences of *M. peloponnesensis* from Greece, Cyprus, and Italy were generated, and genetic variability across the sampling localities was examined. Three mitochondrial haplotypes were detected within *M. peloponnesensis*. Specimens from mainland Italy share the same haplotype as those from Rhodes and Cyprus, whereas Sardinian specimens exhibit a distinct haplotype. The third haplotype is represented by one specimen from Cyprus. The DNA barcoding sequences of *M. peloponnesensis* were compared with those of the morphologically allied *M. gemellata* Schilsky, 1898, and *M. pyrenaea* Ermisch, 1966, to reveal the phylogenetic relationships between the species.

Key words: Distribution, DNA barcoding, haplotype, Mediterranean, morphology, tumbling flower beetles

Introduction

Mordellistena A. Costa, 1854, is the largest genus within Mordellidae Latreille, 1802, with more than 150 species known to occur in Europe (Selnekovič and Kodada 2019; Horák 2020; Selnekovič et al. 2021a; Selnekovič et al. 2023; Ruzzier and Di Giulio 2024). Due to their high diversity and the limited number of experts studying this group in the past, current sampling efforts continuously yield new data on the distribution of tumbling flower beetles in Europe (e.g., Ruzzier 2013; Selnekovič and Ruzzier 2019; Ruzzier et al. 2020; Selnekovič et al. 2021b; Selnekovič and Kodada 2022). *Mordellistena peloponnesensis* Batten, 1980 was initially described based on specimens collected in southern mainland Greece and the Peloponnese (Batten 1980) and later was reported also from Cyprus (Horák 2008, 2020). During collecting trips in Sardinia and mainland Italy between 2021

and 2023, we collected 13 specimens that morphologically correspond to *M. peloponnesensis*. In addition, subsequent examination of specimens from the collections of the National Museum in Prague, the University of Ege in Izmir as well as the E. Ruzzier collection provided additional specimens of *M. peloponnesensis* from Italy (Apulia and Sicily) and Turkey.

Our records significantly expand the known distribution of *M. peloponnesensis*, representing the northernmost and westernmost occurrences of the species. The study of extensive material, including type series, allowed us to provide a redescription of the species and a differential diagnosis to separate it from the morphologically allied species of the *M. gemellata* species group. We also explored the genetic variability of *M. peloponnesensis* across the sampled localities, showing that individuals from the Italian mainland share the same mitochondrial haplotype with individuals from Rhodes and Cyprus, whereas the Sardinian specimens exhibit a distinct, well-separated haplotype. The COI barcoding sequences generated during this study represent the first available DNA sequences for the species.

Material and methods

For this study, 108 individuals of *M. peloponnesensis* from Cyprus, Greece, Italy, and Turkey were examined, including 18 paratypes. Material is deposited in the following institutions and private collections: Finnish Museum of Natural History, Helsinki, Finland (**MZH**); Hungarian Natural History Museum, Budapest, Hungary (**HNHM**); Lodos Entomological Museum, Izmir, Turkey (**LEMT**); Museum für Naturkunde der Humboldt-Universität, Berlin, Germany (**MNB**); National Museum, Prague, Czechia (**NMPC**); Naturalis Biodiversity Centre, Leiden, The Netherlands (**NBCL**); Senckenberg Naturhistorische Sammlungen, Dresden, Germany (**SNSD**); collection of Dávid Selnekovič, Bratislava, Slovakia (**DSBS**); collection of Enrico Ruzzier, Mirano, Italy (**ERPC**), and collection of Marion Mantič, Hlučín-Bobrovníky, Czechia (**MMCZ**).

Specimens of *M. peloponnesensis* were compared with the type series of other species that are morphologically associated with the *M. gemellata* group: *M. algeriensis* Ermisch, 1966 (SNSD), *M. aureotomentosa* Ermisch, 1977 (SNSD), *M. elbrusicola* Ermisch, 1969 (SNSD), *M. gemellata* Schilsky, 1899 (MNB), *M. maroccana* Ermisch, 1966 (SNSD), *M. microgemellata* Ermisch, 1965 (SNSD), *M. pyrenaea* Ermisch, 1966 (SNSD), *M. rhenana* Ermisch, 1956 (SNSD), *M. wankai* Ermisch, 1966 (SNSD), and *M. zoltani* Ermisch, 1977 (HNHM).

Individuals used for DNA isolation were killed in 96.3% ethanol and stored at -20 °C. DNA isolation and amplification procedures followed those provided by Selnekovič et al. (2023). The COI gene was amplified by PCR using standard primer pairs LCO1940 and HCO2198 (Folmer et al. 1994) or LEP-F1 and LEP-R1 (Hebert et al. 2003). After DNA isolation, the specimens were soaked for several hours in 5% acetic acid at room temperature, dissected, and mounted on cards. The dissected genitalia were cleared in lactic acid for several days, then dehydrated in 96.3% ethanol and mounted on slides in Euparal (Paradox Co., Cracow, Poland). After examination, the genitalia were mounted on the card with the respective specimen using dimethyl hydantoin formaldehyde (Entomopraxis, Barcelona, Spain).

Specimens were observed under an M205 C stereomicroscope (Leica, Wetzlar, Germany) with magnification up to 120× and diffused LED light (6400 K). Photographs of habitus were taken with an EOS 5D Mark II camera (Canon, Tokyo,

Japan) attached to an Axio Zoom.V16 stereoscope (Zeiss, Oberkochen, Germany); photographs of genitalia were taken with an Axio Imager.M2 microscope (Zeiss, Oberkochen, Germany). The images were stacked using Zerene Stacker v.1.4 software (https://zerenesystems.com/cms/stacker) and edited in Adobe Photoshop CC (https://www.adobe.com/products/photoshop.html) and DxO Photolab 5 (https://www.dxo.com/dxo-photolab/). Measurements were made with an ocular micrometre in the M205 C stereomicroscope and are given in the text as the range, followed by the arithmetic mean and standard deviation enclosed in parentheses. The measured characters are abbreviated in the text as follows:

EL   elytral length from scutellar apex to elytral apices along suture;
EW   maximum elytral width;
HL   head length from anterior clypeal margin to occipital carina along midline;
HW   maximum head width;
LPrL   maximum left paramere length;
PL   pronotal length along midline;
PW   maximum pronotal width;
PygL   maximum pygidial length;
RPrL   maximum right paramere length;
TL   combination of head, pronotal and elytral lengths

Nucleotide sequences were trimmed and assembled into contigs using ChromasPro v.2.1.10 (Technelysium Pty Ltd, South Brisbane, Queensland, Australia). The final alignment was performed manually in Mesquite v.3.81 (Maddison and Maddison 2023), and it is available in the Suppl. material 1. The uncorrected pairwise distances (p-distances) were calculated using the MEGA11 software (Tamura et al. 2021). Maximum likelihood analysis (ML) was performed using IQ-TREE (Nguyen et al. 2015). Three partitions were defined based on the codon positions. The best substitution models (TNe, F81+F, HKY+F) were identified by the built-in ModelFinder according to the BIC criterion. Node support values were obtained from 1000 ultrafast bootstrap replicates and tested with the aBayes test (Anisimova et al. 2011). The resulting trees were subsequently rooted in FigTree v.1.4.4 (https://github.com/rambaut/figtree). *Natirrica humeralis* (Linnaeus, 1758) was selected as the outgroup, as preliminary phylogenetic analyses indicate that the genus *Natirrica* is a sister group to *Mordellistena*. A haplotype network was created using the pegas 1.3 library (Paradis 2010).

All voucher specimens used in this study, along with respective BOLD Sample and Process IDs and GenBank accession numbers, are listed in the linked data table (Suppl. material 2). Trace files and additional information about voucher specimens are available within a dataset on BOLD (dx.doi.org/10.5883/DS-MPELOP).

Results

Mordellistena (s. str.) *peloponnesensis* Batten, 1980
Figs 1, 2

Mordellistena peloponnesensis Batten, 1980: 42–44. Type locality: "Skála, Pelopónnesos, Greece".
Mordellistena (s. str.) *peloponnesensis*: Horák (2008, 2020).

Type material examined. *Paratypes.* GREECE • 3 males; Lakonia, Skala env. [same as holotype]; 9 Jul. 1978; R. Batten leg.; NBCL, RMNH.INS.1485999 [genitalia illustrated], RMNH.INS.1486000, RMNH.INS.1486001 • 4 males; Arkadhia, Tripolis env.; 5 Jul. 1977; R. Batten leg.; NBCL, RMNH.INS.1485986, RMNH. INS.1485987, RMNH.INS.1485988, RMNH.INS.1485989 • 1 male; Messinia, 2 km N. of Kardamili; 6 Jul. 1977; R. Batten leg.; NBCL, RMNH.INS.1485985 • 2 males; Messinia, Pilos env.; 8 Jul. 1978; R. Batten leg.; NBCL, RMNH. INS.1485996, RMNH.INS.1485997 • 1 male; Korinthia, Neméa env.; 10 Jul. 1978; R. Batten leg.; NBCL, RMNH.INS.1485990 • 1 male; same data as preceding; HNHM • 1 male; Ilia, 4 km E. of Pirgos; 6 Jul. 1977; R. Batten leg.; NBCL, RMNH.INS.1485991 • 1 female; Fthiotis, 20 km S. of Lamia; 4 Jul. 1977; R. Batten leg.; NBCL, RMNH.INS.1485992 • 1 female; Aitolia, 5 km W of Navpaktos; 8 Jul. 1977; R. Batten leg.; NBCL, RMNH.INS.1485993 • 1 male; Aitolia, 11 km S of Agrinion; 8 Jul. 1977; R. Batten leg.; NBCL, RMNH.INS.1485998 • 1 female; Arta, 12 km NW of Arta; 8 Jul. 1977; R. Batten leg.; NBCL, RMNH.INS.1485994 • 1 male; Lakonia, 10 km N Sparti; 7 Jul. 1978; R. Batten leg.; NBCL, RMNH. INS.1485995 • 1 male, 1 female; Attica; E. Reitter leg.; syntypes of *Mordellistena gemellata* Schilsky, 1898; MNB • 1 female; "Parnass"; syntype of *Mordellistena gemellata* Schilsky, 1898; D. Krüper leg.; MNB.

Additional material examined. CYPRUS • 2 males, 3 females; Choirokoitia; 34.795833°N, 33.337500°E; alt. 186 m; 15 Jul. 2009; M. Mantič leg.; forest steppe, on flowers; MMCZ • 2 males; Pegeia, Coral Bay; 34.858333°N, 32.364167°E; alt. 9 m; 21 May 2017; M. Mantič leg.; forest steppe by sea, on flowers; MMCZ • 1 male, 6 females; Foinikaria, Germasogeia Reservoir; 34.755278°N, 33.093333°E; alt. 68 m; 27 Apr. 2018; D. Selnekovič leg.; secondary grassland, on *Daucus*; DSBS, DSBS15, DSBS16 • 1 male, 1 female; Kouklia env.; 34.666474°N, 32.628931°E; alt. 34 m; 9 May 2022; D. Selnekovič leg.; xeric grasslands on slopes, on *Ferula*; DSBS, DSBS609, DSBS610 • 1 male; Potamiou env.; 34.818289°N, 32.797439°E; alt. 677 m; 10 May 2022; D. Selnekovič leg.; road verge, orchards, on *Daucus* and *Tordylium*; DSBS, DSBS611 • 1 female; Pissouri; 34.653149°N, 32.715005°E; alt. 29 m; 12 May 2022; D. Selnekovič leg.; crop fields, slopes with xeric vegetation, on *Ferula* and *Tordylium*; DSBS • 3 males, 4 females; Avdimou env.; 34.675610°N, 32.758667°E; alt. 33 m; 13 May 2022; D. Selnekovič leg.; road verge, crop fields, on *Daucus* and *Ferula*; DSBS • 2 females; Kyrenia, Bellapais; 13 Jul 1939; H. Lindberg leg.; MZH, http://id.luomus.fi/GAC.38997. GREECE • 6 specimens; Crete, Paralia Kouma; 35.352222°N, 24.298889°E; alt. 1 m; 16 Jul. 2012; M. Mantič leg.; sand beech, on flowers; MMCZ • 7 specimens; Crete, Paralia Preveli; 35.152778°N, 24.473333°E; alt. 7 m; 5 Jun. 2018; M. Mantič leg.; forest steppe, on flowers; MMCZ • 4 specimens; Crete, Lavris, 4 km W of Panormos; 35.417778°N, 24.648611°E; alt. 21 m; 1 Jun. 2018; M. Mantič leg.; forest steppe, on flowers; MMCZ • 1 female; Crete, Panormos env.; 35.416667°N, 24.689444°E; alt. 27 m; 30 May 2018; M. Mantič leg.; forest steppe, on flowers; MMCZ • 1 female; Crete, Orino Gorge, 1.8 km NW of Koutsoras; 35.045278°N, 25.932778°E; alt. 97 m; 19 May 2023; M. Mantič leg.; stram valley, on flowers; MMCZ • 4 specimens; Crete, Ierapetra; 35.014167°N, 25.768333°E; alt. 20 m; 16 May 2023; M. Mantič leg.; olive groves, on flowers; MMCZ • 1 male; Crete, Chochlakies; 35.146389°N, 26.246389°E; alt. 106 m; 10 Jun. 2023; M. Mantič leg.; olive groves, on flowers; MMCZ • 1 male; Crete, Kournas, Kourna lake; 30 Jun. 2002; A. Přidal leg.; NMPC • 1 male; Crete,

Knossos; 1934; Mařan and Štěpánek leg.; NMPC • 2 specimens; Rhodes, Kalythiés env.; 36.326339°N, 28.187810°E; alt. 43 m; 26 May 2023; D. Selnekovič leg.; olive orchard, on *Ammi majus* and *Helichrysum* sp.; DSBS, DSBS715B, DSBS716 • 4 males, 1 female; Rhodes, Afantou env.; 36.311961°N, 28.189384°E; alt. 9 m; 26–30 May 2023; D. Selnekovič leg.; ruderal community, on *Daucus* sp.; DSBS • 3 males, 3 females; Rhodes, Kolympia; 36.259536°N, 28.131744°E; alt. 49 m; 28 May 2023; D. Selnekovič leg.; olive orchard, on *Daucus* and *Ammi majus*; DSBS, DSBS623 to DSBS626 • 11 specimens; Rhodes, Kolympia; 36.252222°N, 28.168056°E; alt. 15 m; 21 May 2011; M. Mantič leg.; forest steppe, on Apiaceae; MMCZ • 2 females; Rhodes, Kalythiés env.; 36.3202469°N, 28.1867823°E; alt. 14 m; 1 Jun. 2023; D. Selnekovič leg.; ruderal grassland with olive trees and shrubs, on *Daucus* sp.; DSBS. Italy • 4 males, 1 female; Campania, Naples, Camaldoli, 40.852285°N, 14.202138°E; alt. 142 m; 3 Jul. 2023; D. Selnekovič leg.; ruderal habitat, on *Daucus carota*; DSBS, DSBS558, DSBS598, DSBS599 • 5 males; Sardinia, Sassari; 40.712163°N, 8.549854°E; alt. 207 m; 27 Jun. 2021; D. Selnekovič leg.; urban area, ruderal community along olive orchard and parking lot, on *Daucus carota*; DSBS, DSBS700 to DSBS704 • 3 males; Puglia, Foggia, Vieste; 41.902976°N, 16.086091°E; alt. 60 m; 3 Jun. 2021; E. Ruzzier leg.; road verge, on *Daucus carota*; ERPC • 1 male; Sicilia, Caltagirone; NMPC. Turkey • 1 male, 1 female; Mugla, Bodrum, Aspat; 24 May 2008; N. Gulpercin leg.; LEMT • 1 female; Mugla, Bodrum, Aspat; 7 Jun. 2008; S. Tezcan leg.; LEMT.

Differential diagnosis. *Mordellistena peloponnesensis* is characterised by antennomeres 1–4 being narrower than the following ones and by the presence of two short lateral ctenidia on the posterior tibia that are perpendicular to the dorsal edge of the tibia. This combination of characters is unique to the *M. gemellata* species group as defined by Ermisch (1956). Within this group, *M. peloponnesensis* (Fig. 1) is further distinguished by its black integument, including mouth parts and appendages, pale brownish to yellowish pubescence on the dorsal surface of the body, short antennal segments 5–10 (1.2–1.5× longer than wide), relatively large body size (TL 3.26–4.87 mm), long and narrow elytra (2.2–2.5× longer than wide), male tibia expanded at the base with a group of extended setae, and the characteristic shape of parameres (Fig. 1B, C).

The species most closely resembling *M. peloponnesensis* in terms of size, body shape, elytral length and width, and pubescence color are *M. algeriensis* Ermisch, 1966 (Algeria, Italy, and Tunisia), *M. gemellata* Schilsky, 1898 (Portugal, Spain), and *M. pyrenaea* Ermisch, 1966 (France, Spain). These species can be differentiated from *M. peloponnesensis* by distinct paramere shapes [see Selnekovič and Kodada (2022) for *M. algeriensis*; Ermisch (1966) for *M. pyrenaea*; and Ermisch (1963a) for *M. gemellata*]. Of these, *M. algeriensis*, recently reported from Sardinia (Selnekovič and Kodada 2022), is the only species with a range that partially overlaps with *M. peloponnesensis*. It differs from *M. peloponnesensis* not only in paramere shape but also in size: *M. algeriensis* has an EL/RPrL ratio of 5.89–6.42 and an EL/LPrL ratio of 5.21–5.54, while *M. peloponnesensis* has corresponding ratios of 6.84–8.61 and 5.65–7.38. Additionally, *M. algeriensis* can be distinguished by its subquadrate antennal segments 5–10 (~1.0× longer than wide), whereas in *M. peloponnesensis*, these segments are 1.2–1.5× longer than wide. *Mordellistena aureotomentosa* Ermisch, 1966, described from Morocco, differs from *M. peloponnesensis* by its conspicuously light-yellowish and dense pubescence on the pronotum and
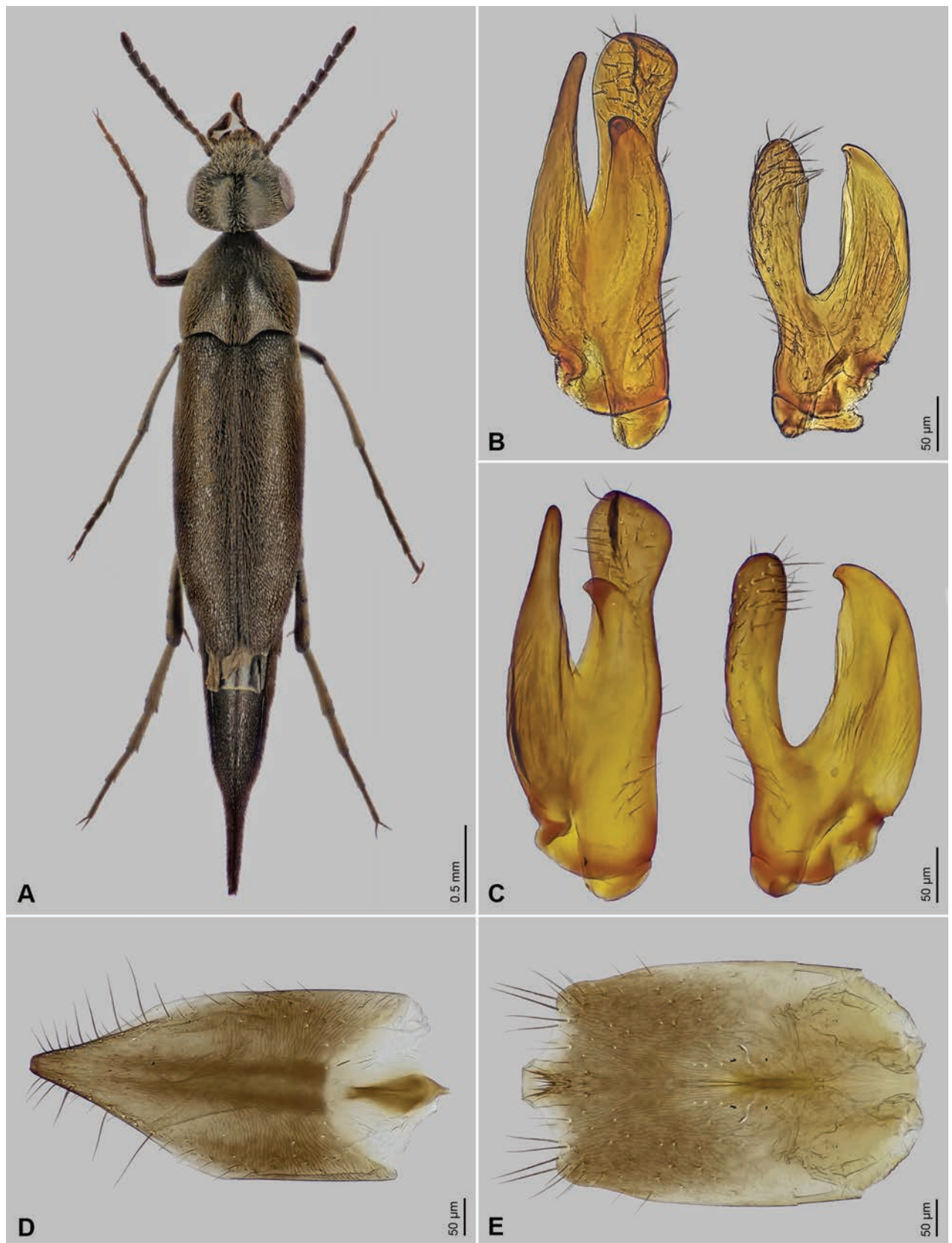
Figure 1. *Mordellistena peloponnesensis* Batten, 1980 **A** habitus, male, Rhodes, Greece, DSBS623 **B** parameres, paratype from Skala (type locality), RMNH.INS.1485999 **C** parameres, specimen from Italy, DSBS558 **D** female sternite VIII, DSBS610 **E** male sternite VIII, DSBS558.

elytra, and smaller, differently shaped parameres (Ermisch 1966). *Mordellistena maroccana* Ermisch, 1966, found in Morocco and Tunisia, differs from *M. peloponnesensis* in the distinctly shorter and broader elytra: the elytral length/width ratio in *M. maroccana* is 2.0, while in *M. peloponnesensis* it is 2.2−2.5.

Redescription. Measurements (in mm; ♂♂ *N* = 13, ♀♀ *N* = 10): TL: ♂♂ 3.26−4.52 (3.91 ± 0.45), ♀♀ 3.98−4.87 (4.41 ± 0.32); HL: ♂♂ 0.61−0.80 (0.72 ± 0.07), ♀♀ 0.72−0.85 (0.79 ± 0.05); HW: ♂♂ 0.65−0.84 (0.76 ± 0.07), ♀♀ 0.72−0.94 (0.84 ± 0.07); PL: ♂♂ 0.75−1.06 (0.91 ± 0.12), ♀♀ 0.88−1.19 (1.04 ± 0.10); PW: ♂♂ 0.73−1.06 (0.91 ± 0.12), ♀♀ 0.86−1.17 (1.05 ± 0.09); EL: ♂♂ 1.91−2.68 (2.28 ± 0.27), ♀♀ 2.35−2.82 (2.58 ± 0.17); EW: ♂♂ 0.77−1.14 (0.95 ± 0.12), ♀♀ 0.97−1.25 (1.12 ± 0.09); RPrL: 0.25−0.32 (0.30−0.02); LPrL: 0.31−0.41 (0.36 ± 0.03).

Body elongate (Fig. 1A), wedge-shaped, widest behind anterior third of elytra in males, around elytral mid-length in females. Dorsum moderately convex, venter strongly so. Entire body surface uniformly black, except for reddish-brown anteclypeus and tips of mandibles. Vestiture consisting of decumbent lanceolate setae; yellowish to brownish with purple sheen on dorsal surfaces, darkened towards elytral apices; yellowish on ventral surfaces, darkened along posterior margins of ventrites 3−5.

Head approximately as long as wide, HW/HL ratio: ♂♂ 1.02−1.12 (1.07 ± 0.03), ♀♀ 0.95−1.11 (1.07 ± 0.04), moderately convex dorsally, with highest point behind middle of eye length (lateral aspect); occipital carina rounded; integument weakly microreticulate, with small round setiferous punctures. Eyes broadly oval, approx. 1.4× longer than wide; posteriorly reaching to occipital margin; finely faceted; interfacetal setae longer than facet diameter. Anterior clypeal edge weakly convex. Labrum transverse, densely setose, anterior margin weakly convex. Antenna weakly serrate (Fig. 1A); antennomeres 1−4 shorter and narrower than following antennomeres; scape weakly conical, little longer than wide; pedicel cylindrical, approx. 1.5× longer than wide; antennomere 3 smallest, conical, as long as wide; antennomere 4 conical, approx. 1.7× as long as 3; antennomeres 5−10 in male 1.4−1.5×, in female 1.2−1.4× longer than wide, antennomere 5 longest; antennomere 11 oval, approx. 1.8× longer than wide; all antennomeres covered with decumbent trichoid sensilla, additionally, antennomeres 5−10 each with several long and erect trichoid sensilla apico-mesially. Galea moderately long, with spatulate sensilla and trichoid sensilla apically. Maxillary palpomere 2 subcylindrical, weakly expanded distally, similarly formed in both sexes except for distinctly longer trichoid sensilla on ventral surface in male; terminal maxillary palpomere scalene triangular, little wider in male than in female, mesial angle just behind mid-length; numerous decumbent and several erect trichoid sensilla over entire surface; apical sensory area with numerous short sensilla.

Pronotum approximately as long as wide, PL/PW ratio: ♂♂ 0.93−1.09 (1.00 ± 0.04), ♀♀ 0.96−1.02 (1.00 ± 0.02), widest before middle, strongly convex; surface microreticulate, densely covered with lanceolate setae, punctures larger than those on head; anterior edge convex in middle, anterior angles broadly rounded; lateral carinae strongly sinuate in lateral aspect; posterior edge sinuate, posterior angles rectangular in lateral aspect. Scutellar shield triangular, densely setose. Elytra moderately long and narrow, EL/EW ratio: ♂♂ 2.23−2.52 (2.40 ± 0.08), ♀♀ 2.18−2.42 (2.30 ± 0.07); apices separately rounded; surface microreticulate, densely covered with decumbent lanceolate setae, punctures coarser than those on pronotum. Hindwing fully developed. Metanepisternum

approx. 4× longer than maximum width, narrowed posteriorly. Protarsomeres cylindrical, each little narrower than preceding one; protarsomere 1 as long as two following tarsomeres combined; penultimate protarsomere truncate distally, with apical edge weakly concave; each protarsal claw with three denticles; male protarsus with longer and thicker seta on ventral surface than female one. Mesotibia approx. 0.8× as long as mesotarsus. Mesotarsomeres cylindrical, each little narrower than preceding one; first mesotarsomere as long as two following tarsomeres combined. Metatibia with short subapical ctenidium and two lateral ctenidia nearly perpendicular to dorsal tibial edge, proximal ctenidium located around mid-length of tibia, distal one at around third quarter; outer terminal spur ca. 0.5× as long as inner one. Metatarsomere 1 with three ctenidia; metatarsomere 2 with two ctenidia; metatarsomeres 3 and 4 without lateral ctenidia.

Abdominal ventrite 5 with narrowly rounded apical edge. Pygidium long, conical, bent ventrad, narrowly truncate at apex, approx. 0.5× as long as elytra. Male sternite VIII with sinuate posterior edge, postero-lateral angles and medial portion moderately produced, with long trichoid sensilla (Fig. 1E); female sternite VIII produced at middle of posterior edge, with long trichoid sensilla around lateral edges (Fig. 1D), anterior median strut short, clavate. Phallobase forming sheath around penis; tubular part short; anterior struts approx. 5× as long as tubular part; dorsal apodeme strongly sclerotised. Parameres as in Fig. 1B, C: left paramere longer than right one, EL/LPrL ratio: 5.65–7.38 (6.33 ± 0.58), dorsal process dilated and obliquely subtruncate apically, with numerous trichoid sensilla, ventral process slightly shorter than dorsal one, tapering towards apex, median process short and wide, with cluster of sensilla campaniformia located along its dorsal edge; left paramere with dorsal process rather narrow, rounded apically, with trichoid and campaniform sensilla, ventral process slightly shorter than dorsal one, wide, bent dorsad, EL/RPrL ratio: 6.84–8.61 (7.67 ± 0.65). Penis long, narrow, weakly expanded before apex.

Secondary sexual dimorphism. Females on average slightly larger than males. Males somewhat slenderer than females. Second maxillary palpomere with longer setae in males than in females. Terminal maxillary palpomere slightly narrower in females. Male protibia bears several elongate setae in proximal half, female protibia uniformly setose. Male protarsomeres with numerous thick setae ventrally.

DNA sequences. Eighteen sequences of the COI gene barcoding region were generated and submitted to BOLD (www.boldsystems.org) and GenBank (www.ncbi.nlm.nih.gov/genbank/). Details on voucher specimens as well as accession numbers are listed in the Suppl. material 2.

Distribution. Cyprus, Greece (mainland, Crete, Rhodes), Italy (southern part of the Italian peninsula, Sardinia, Sicily), Turkey (Fig. 2D).

Habitat and co-occurring species. Five individuals of *M. peloponnesensis* from Sardinia were sampled in June 2021 from the inflorescences of *Daucus carota* L. (Apiaceae) in ruderal vegetation separating a parking lot from a small olive orchard in the urban area of Sassari. Three individuals from Vieste were collected on the inflorescences of *D. carota* in ruderal vegetation along a road. Five individuals from the vicinity of Naples were sampled in July 2023 on the inflorescences of *D. carota* in a ruderal habitat along a footpath on Camaldoli Hill. This area featured young secondary forest, orchards, and dry grassland communities. The following species co-occur with *M. peloponnesensis* in Italy: *M. episternalis* Mulsant, 1856, *M. minima* A. Costa, 1854, *M. pseudorhenana*
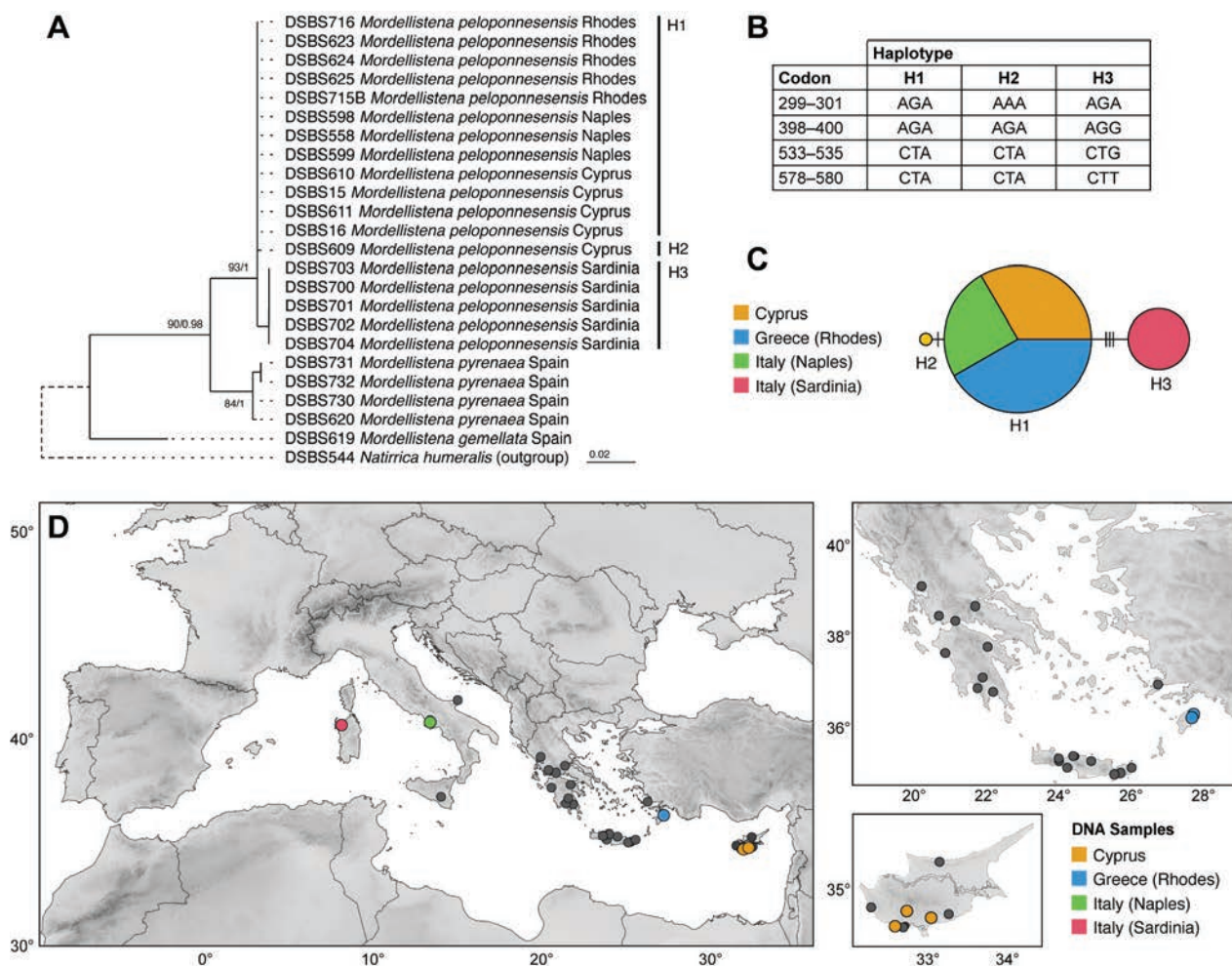
Figure 2. A results of maximum likelihood analysis of 658 bp COI fragment; support values are given as: bootstrap values / aBayes test values **B** differences between haplotypes of *Mordellistena peloponnesensis* Batten, 1980. Codons are marked as the nucleotide positions within 658 bp COI fragment **C** TCS haplotype network based on eighteen sequences of 658 bp COI fragment in *M. peloponnesensis*; colours represent sampling localities; vertical lines represent number of substitutions **D** distribution of *M. peloponnesensis*; left: entire range, right: details on Greece, Turkey, and Cyprus. Localities of DNA samples are marked with coloured dots matching those in the haplotype network; localities without DNA samples are marked with black dots.

Ermisch, 1977, *M. purpurascens* A. Costa, 1854, *M. tarsata* Mulsant, 1856, *Mediimorda bipunctata* (Germar, 1827), *Variimorda basalis* (A. Costa, 1854), and *Stenalia* sp. In similar ruderal habitats along roadsides, secondary grasslands, and olive orchards, specimens of *M. peloponnesensis* were also collected on the islands of Rhodes (Greece) and Cyprus.

DNA analyses

We generated 18 sequences of the COI barcoding region of *M. peloponnensis* from individuals originating from Cyprus, Greece (Rhodes) and Italy (mainland Italy and Sardinia). We recognised three haplotypes within the species: H1 shared by 12 individuals from Cyprus, Italy (Naples), and Greece (Rhodes); H2 represented by a single individual from Cyprus; and H3 shared by five individuals from Italy (Sardinia) (Fig. 2C). H2 differs from H1 at one position in the COI

barcoding region (H1—codon 299–301: AGA; H2—codon 299–301: AAA), and H3 differs from H1 at three positions (H1—codon 398–400: AGA, codon 533–535: CTA, codon 578–580: CTA; H3—codon 398–400: AGG, codon 533–535: CTG, codon 578–580: CTT) (Fig. 2B).

We compared the sequences of *M. peloponnesensis* with those of the morphologically allied *M. pyrenaea* (four individuals from Spain) and *M. gemellata* (one individual from Spain). The divergence between *M. peloponnesensis* and *M. gemellata* is 7.94–8.09%, and between *M. peloponnesensis* and *M. pyrenaea* it is 3.34–4.00%. The intra-species divergence within *M. peloponnesensis* reaches a maximum value of 0.61%. Maximum likelihood analysis revealed a separate clade for each species (Fig. 2A).

Discussion

Mordellistena peloponnesensis was described by Batten in 1980 based on specimens from various localities in southern mainland Greece and Peloponnese. Since its description, no further specific data have been published, except for its occurrence in Cyprus, as noted in the Catalogue of Palaearctic Coleoptera (Horák 2008, 2020). New data from the islands of Rhodes and Crete, Cyprus, as well as the previously unrecorded distribution of the species in Italy (southern part of the Italian peninsula, Sardinia, Sicily) and Turkey, significantly contribute to understanding this species' distribution. The records from Italy represent the northernmost and westernmost known occurrences of the species.

DNA sequences of *M. peloponnesensis* are currently available from the vicinity of Naples and Sardinia in Italy, from the island of Rhodes in Greece, and Cyprus. Analysis has shown that individuals from mainland Italy share the same haplotype as individuals from Rhodes and Cyprus. In contrast, individuals from Sardinia possess a distinct haplotype, separated by three nucleotide substitutions. Phylogenetic analysis suggested that the most closely related species is *M. pyrenaea*, known from Spain and France, with an interspecific divergence of 3.34–4.00%. The analysis did not include other morphologically similar species (*M. algeriensis*, *M. aureotomentosa*, *M. maroccana*, *M. elbrusicola* Ermisch, 1969, *M. microgemellata* Ermisch, 1965) for which DNA sequences were not available.

A parallel outcome from the examination of the type material is the identification of two syntypes of *M. gemellata* from Greece (Attica and Parnassus) as *M. peloponnesensis*. Likewise, two specimens from Kyrenia, Cyprus, originally identified and reported by Ermisch (1963b) as *M. gemellata*, are now confirmed to belong to *M. peloponnesensis*. This finding indicates that there are no verified specimens of *M. gemellata* from either Greece or Cyprus, and that the species is reliably documented only from Spain and Portugal (Schilsky 1898; Horák 2008). Additionally, we were unable to confirm a reported record of *M. gemellata* from Estonia (Silfverberg 2004), however, given the species' known distribution, this record is likely erroneous.

Acknowledgements

for generously providing us with material from his private collection. We extend our appreciation to Robert Naczi and Murray Andrew Johnston for their insightful comments and suggestions during the review process.

Additional information

Author ORCIDs

Dávid Selnekovič ⓘ https://orcid.org/0000-0002-9228-1174
Ján Kodada ⓘ https://orcid.org/0000-0002-1355-4323
Nilay Gülperçin ⓘ https://orcid.org/0000-0002-9309-6528
Serdar Tezcan ⓘ https://orcid.org/0000-0003-1980-9291
Enrico Ruzzier ⓘ https://orcid.org/0000-0003-1020-1247

Data availability

All of the data that support the findings of this study are available in the main text or Supplementary Information.

References

Anisimova M, Gil M, Dufayard J, Dessimoz C, Gascuel O (2011) Survey of branch support methods demonstrates accuracy, power, and robustness of fast likelihood-based approximation schemes. Systematic Biology 60(5): 685–699. https://doi.org/10.1093/sysbio/syr041

Batten R (1980) Notes on *Mordellistena gemellata* group: two new species and a case of synonymy (Coleoptera, Mordellidae). Entomologische Berichten 40: 41–46.

Ermisch K (1956) Mordellidae. In: Horion A (Ed.) Faunistik der Mitteleuropäischen Käfer. Band 5: Heteromera. Entomologische Arbeiten aus dem Museum G. Frey Tutzing bei München, München, 269–328.

Ermisch K (1963a) Beitrag zur Mordelliden-Fauna Portugals (Coleopt. Heteromera, Mordellidae). Notulae entomologicae 43: 14–21.

Ermisch K (1963b) Die Mordelliden der Insel Cypern (Coleoptera, Heteromera, Mordellidae). Notulae entomologicae 43: 49–67.

Ermisch K (1966) Neue westpaläarktische *Mordellistena*-Arten (Coleoptera – Heteromera – Mordellidae). Entomologische Blätter 62: 30–39.

Folmer O, Black M, Hoeh W, Lutz R, Vrijenhoek R (1994) DNA primers for amplification of mitochondrial cytochrome c oxidase subunit I from diverse metazoan invertebrates. Molecular Marine Biology and Biotechnology 3(5): 294–299.

Hebert PDN, Cywinska A, Ball SL, deWaard JR (2003) Biological identifications through DNA barcodes. Proceedings of the Royal Society B 270: 313–321. https://doi.org/10.1098/rspb.2002.2218

Horák J (2008) Family Mordellidae Latreille, 1802. In: Löbl I, Smetana A (Eds) Catalogue of Palaearctic Coleoptera. Volume 5. Tenebrionoidea. Apollo Books, Stenstrup, 87–105.

Horák J (2020) Family Mordellidae Latreille, 1802. In: Iwan D, Löbl I (Eds) Catalogue of Palaearctic Coleoptera. Volume 5. Tenebrionoidea. Revised and Updated Second Edition. Brill, Leiden-Boston, 79–104. https://doi.org/10.1163/9789004434998

Maddison WP, Maddison DR (2023) Mesquite: a modular system for evolutionary analysis. Version 3.81. http://www.mesquiteproject.org

Nguyen L, Schmidt HA, Haeseler A von, Minh BQ (2015) IQ-TREE: A fast and effective stochastic algorithm for estimating maximum-likelihood phylogenies. Molecular Biology and Evolution 32: 268–274. https://doi.org/10.1093/molbev/msu300

Paradis E (2010) pegas: an R package for population genetics with an integrated–modular approach. Bioinformatics 26: 419–420. https://doi.org/10.1093/bioinformatics/btp696

Ruzzier E (2013) Taxonomic and faunistic notes on Italian Mordellidae (Coleoptera Tenebrionoidea) with redescription of *Falsopseudotomoxia argyropleura* (Franciscolo, 1942) n. comb. Bollettino della Società Entomologica Italiana 145(3): 103–115. https://doi.org/10.4081/BollettinoSEI.2013.103

Ruzzier E, Di Giulio A (2024) Taxonomic considerations of selected Western Palaearctic Mordellidae Latreille, 1802 (Coleoptera, Tenebrionoidea). ZooKeys 1207: 151–165. https://doi.org/10.3897/zookeys.1207.119398

Ruzzier E, Morin L, Glerean P, Forbicioni L (2020) New and interesting records of Coleoptera from Northeastern Italy and Slovenia (Alexiidae, Buprestidae, Carabidae, Cerambycidae, Ciidae, Curculionidae, Mordellidae, Silvanidae). The Coleopterists Bulletin 74(3): 523–531. https://doi.org/10.1649/0010-065X-74.3.523

Schilsky J (1898) Die Käfer Europa's. XXXV. Bauer & Raspe, Nuremberg, Germany, 51 pp.

Selnekovič D, Kodada J (2019) Taxonomic revision of *Mordellistena hirtipes* species complex with new distribution records (Insecta, Coleoptera, Mordellidae). ZooKeys 854: 89–118. https://doi.org/10.3897/zookeys.854.32299

Selnekovič D, Kodada J (2022) First record of *Mordellistena algeriensis* Ermisch, 1966 in Italy (Coleoptera: Mordellidae). Fragmenta entomologica 54(1): 151–154. https://doi.org/10.13133/2284-4880/711

Selnekovič D, Ruzzier E (2019) New distributional records for sixteen Mordellidae species from the Western Palearctic (Insecta, Coleoptera, Mordellidae). ZooKeys 894: 151–170. https://doi.org/10.3897/zookeys.894.39584

Selnekovič D, Goffová K, Kodada J, Improta R (2021a) Revealing the identity of *Mordellistena minima* and *M. pseudorhenana* (Coleoptera: Mordellidae) based on re-examined type material and DNA barcodes, with new distributional records and comments

on morphological variability. The Canadian Entomologist 153: 343–367. https://doi.org/10.4039/tce.2021.3

Selnekovič D, Goffová K, Kodada J (2021b) First records of *Mordellochroa humerosa* (Rosenhauer, 1847) from Slovakia (Coleoptera, Mordellidae). Check List 17(3): 1015–1020. https://doi.org/10.15560/17.3.1015

Selnekovič D, Goffová K, Šoltýs J, Kováčová E, Kodada J (2023) *Mordellistena platypoda*, a new species of tumbling flower beetle from the island of Ischia in Italy (Coleoptera, Mordellidae). ZooKeys 1148: 41–63. https://doi.org/10.3897/zookeys.1148.86845

Silfverberg H (2004) Enumeratio nova Coleopterorum Fennoscandiae, Daniae et Baltiae. Sahlbergia 9: 1–111.

Tamura K, Stecher G, Kumar S (2021) MEGA11: Molecular Evolutionary Genetics Analysis Version 11. Molecular Biology and Evolution 38: 3022–3027. https://doi.org/10.1093/molbev/msab120

Supplementary material 1

Aligned sequences of COI barcoding region

Authors: Dávid Selnekovič, Ján Kodada, Nilay Gülperçin, Serdar Tezcan, Enrico Ruzzier
Data type: fas

Explanation note: Aligned sequences of 658 bp region of COI used in the present study.

Link: https://doi.org/10.3897/zookeys.1214.133348.suppl1

Supplementary material 2

List of DNA voucher specimens and sequence accession numbers

Authors: Dávid Selnekovič, Ján Kodada, Nilay Gülperçin, Serdar Tezcan, Enrico Ruzzier
Data type: xlsx

Explanation note: Linked table containing data on DNA vouchers used in the present study.

Link: https://doi.org/10.3897/zookeys.1214.133348.suppl2

Research Article

Sinocyclocheilus xiejiahuai (Cypriniformes, Cyprinidae), a new cave fish with extremely small population size from western Guizhou, China

Cui Fan[1*], Man Wang[2,3*], Jia-Jia Wang[1], Tao Luo[4], Jia-Jun Zhou[5], Ning Xiao[6], Jiang Zhou[1]

1   *School of Karst Science, Guizhou Normal University, Guiyang 550001, Guizhou, China*
2   *Institute of Hydrobiology, Chinese Academy of Sciences, Wuhan 430072, Hubei, China*
3   *University of Chinese Academy of Sciences, Beijing 100049, China*
4   *School of Life Sciences, Guizhou Normal University, Guiyang 550025, Guizhou, China*
5   *Zhejiang Forest Resource Monitoring Center, Hangzhou 310020, Zhejiang, China*
6   *Guiyang Healthcare Vocational University, Guiyang 550081, Guizhou, China*
Corresponding authors: Jiang Zhou (*zhoujiang@ioz.ac.cn*); Ning Xiao (*armiger@163.com*)

Citation: Fan C, Wang M, Wang
J-J, Luo T, Zhou J-J, Xiao N, Zhou J
(2024) *Sinocyclocheilus xiejiahuai*
(Cypriniformes, Cyprinidae), a new
cave fish with extremely small
population size from western
Guizhou, China. ZooKeys 1214:
119–141. https://doi.org/10.3897/
zookeys.1214.127629

Abstract

This study describes a new species, *Sinocyclocheilus xiejiahuai* **sp. nov**., discovered within a cave located in Hongguo Town, Panzhou City, Guizhou Province, southwestern China, with the type locality in the Nanpanjiang River basin. Phylogenetic trees reconstructed based on mitochondrial genes show that the new species represents an independent evolutionary lineage with large genetic differences, 1.9%–13.8% in mitochondrial Cyt *b*, from congeners. Morphologically, this species can be differentiated from the 79 species currently classified under the genus *Sinocyclocheilus* by several characteristics: absence of horn-like structures and indistinct elevation at the head-dorsal junction, absence of irregular black markings on the body lateral and scaleless, eyes large, eye diameter 13% of head length, dorsal-fin rays, iii, 6½, last unbranched ray strong, with serrations along posterior margin, pectoral-fin rays, i, 13, anal-fin rays, iii, 5, pelvic-fin rays, i, 7, lateral line pores 74, gill rakers well developed, nine on first gill arch, pectoral fins short, tip not reaching to pelvic-fin origin. The number of *Sinocyclocheilus* species has been increased from 79 to 80 since the description of this new species.

Key words: Cavefish, new species, morphology, phylogeny, taxonomy

Introduction

The genus *Sinocyclocheilus* Fang, 1936 (Cypriniformes: Cyprinidae) is endemic to China, and is currently found only in the Yangtze, Pearl, Lancangjiang, and Yuanjiang rivers (Xu et al. 2023). Based on recent taxonomic and phylogenetic studies, the genus *Sinocyclocheilus* includes 79 valid species (Shan et al. 2000; Zhao and Zhang 2009; Zhang et al. 2016; Luo et al. 2023; Xu et al. 2023; Shao et al. 2024), most of which are classified into five species groups, i.e., *S. angularis* species group includes 21 valid species, *S. cyphotergous* species group includes 20 valid species, *S. microphthalmus*

---
*   These authors contributed equally to this work.

species group includes three valid species, *S. jii* species group includes five valid species, and *S. tingi* species group includes 26 valid species (Zhao and Zhang 2009; Wen et al. 2022; Luo et al. 2023; Xu et al. 2023; Shao et al. 2024) (Table 1). The *S. angularis*, *S. cyphotergous*, and *S. microphthalmus* species groups have stygobite morphology, and the *S. jii* and *S. tingi* species groups a mixture of stygobite and stygophile morphology (Zhao and Zhang 2009). There are 25 species currently recorded for the *S. tingi* species group, of which 18, four, two, and one are distributed in the Nanpanjiang, Yuanjiang, Jinshajiang, and Lancangjiang rivers, respectively, and the new species is distributed in the Beipanjiang River (Fig. 1) (Zhao and Zhang 2009; Luo et al. 2023; Xu et al. 2023).

During our biodiversity survey in southwestern Guizhou Province, China, in October 2019, a specimen of *Sinocyclocheilus* with normal eyes, scaleless and absence of irregular black markings on the body lateral was collected in a completely dark cave. This specimen was identified to the *S. tingi* species group based on morphological characters. Subsequent morphological examination and molecular evidence suggest that this specimen represents an undescribed species of the *S. tingi* species group within the genus *Sinocyclocheilus*. However, between 2019 and 2023, we conducted 16 more surveys in this cave again, none of which revealed any new individuals. Considering the conservation of the species and the rescue of diversity, here we formally describe the species as *Sinocyclocheilus xiejiahuai* sp. nov. based on the single-numbered specimen. Although there is only one specimen of this species, the significance of its discovery is as important as that of the publication of *Sinocyclocheilus sanxiaensis* in terms of zoogeography and conservation biogeography (Jiang et al. 2019).

Materials and methods

Sampling and preservation

The single specimen of the genus *Sinocyclocheilus* were collected in southwestern Guizhou Province, China during a cave fish diversity survey in southern China in October 2019. Gill muscle tissue was preserved in 95% alcohol at -20 °C for molecular analysis. All specimens were fixed in 7% buffered formalin and then transferred to 75% ethanol for long-term storage. Specimen were preserved at Guizhou Normal University, Guiyang City, Guizhou Province, China.

Morphological comparison and statistical analysis

The new species can be placed in the *S. tingi* species group based on morphology and can be clearly distinguished from species in the *S. angularis*, *S. cyphotergous*, and *S. microphthalmus*, *S. jii* species groups, e.g., absence of horn-like structures and indistinct elevation at the head-dorsal junction; pectoral fins short, not reaching to pelvic-fin origin; and with serrations along posterior margin of the last unbranched fin of the dorsal fin (Zhao et al. 2009). Therefore, this study focused on morphological comparisons with 26 species within the *S. tingi* species group (Table 2).

Table 1. List of 79 currently recognized species of the genus *Sinocyclocheilus* endemic to China and references. Recognized species modified from Jiang et al. (2019) and Xu et al. (2023).

ID	Species	Species group	Province	Rivers	Literature obtained
1	*S. altishoulderus* (Li & Lan, 1992)	*S. angularis* group	Guangxi	Hongshui River	Li and Lan 1992
2	*S. anatirostris* Lin & Luo, 1986	*S. angularis* group	Guangxi	Hongshui River	Lin and Luo 1986
3	*S. angularis* Zheng & Wang, 1990	*S. angularis* group	Guizhou	Beipanjiang River	Zheng and Wang 1990
4	*S. aquihornes* Li & Yang, 2007	*S. angularis* group	Yunnan	Nanpanjiang River	Li et al. 2007
5	*S. bicornutus* Wang & Liao, 1997	*S. angularis* group	Guizhou	Beipanjiang River	Wang and Liao 1997
6	*S. brevibarbatus* Zhao, Lan & Zhang, 2009	*S. angularis* group	Guangxi	Hongshui River	Zhao et al. 2009
7	*S. broadihornes* Li & Mao, 2007	*S. angularis* group	Yunnan	Nanpanjiang River	Li and Mao 2007
8	*S. convexiforeheadus* Li, Yang & Li, 2017	*S. angularis* group	Yunnan	Nanpanjiang River	Yang et al. 2017
9	*S. hyalinus* Chen & Yang, 1994	*S. angularis* group	Yunnan	Nanpanjiang River	Chen et al. 1994
10	*S. longicornus* Luo, Xu, Wu, Zhou & Zhou, 2023	*S. angularis* group	Guizhou	Nanpanjiang River	Xu et al. 2023
11	*S. jiuxuensis* Li & Ran, 2003	*S. angularis* group	Guangxi	Hongshui River	Li et al. 2003c
12	*S. flexuosdorsalis* Zhu & Zhu, 2012	*S. angularis* group	Guangxi	Hongshui River	Zhu and Zhu 2012
13	*S. furcodorsalis* Chen, Yang & Lan, 1997	*S. angularis* group	Guangxi	Hongshui River	Chen et al. 1997
14	*S. mashanensis* Wu, Liao & Li, 2010	*S. angularis* group	Guangxi	Hongshui River	Wu et al. 2010
15	*S. rhinocerous* Li & Tao, 1994	*S. angularis* group	Yunnan	Nanpanjiang River	Li and Tao 1994
16	*S. simengensis* Li, Wu, Li & Lan, 2018	*S. angularis* group	Guangxi	Hongshui River	Wu et al. 2018
17	*S. tianeensis* Li, Xiao & Luo, 2003	*S. angularis* group	Guangxi	Hongshui River	Li et al. 2003d
18	*S. tianlinensis* Zhou, Zhang, He & Zhou, 2004	*S. angularis* group	Guangxi	Nanpanjiang River	Zhou et al. 2004
19	*S. tileihornes* Mao, Lu & Li, 2003	*S. angularis* group	Yunnan	Nanpanjiang River	Mao et al. 2003
20	*S. xingyiensis* Luo, Tang, Deng, Duan & Zhang, 2023	*S. angularis* group	Guizhou	Nanpanjiang River	Luo et al. 2023
21	*S. zhenfengensis* Liu, Deng, Ma, Xiao & Zhou, 2018	*S. angularis* group	Guizhou	Beipanjiang River	Liu et al. 2018
22	*S. anshuiensis* Gan, Wu, Wei & Yang, 2013	*S. microphthalmus* group	Guangxi	Hongshui River	Gan et al. 2013
23	*S. longshanensis* Li & Wu, 2018	*S. microphthalmus* group	Yunnan	Nanpanjiang River	Li et al. 2018
24	*S. microphthalmus* Li, 1989	*S. microphthalmus* group	Guangxi	Hongshui River	Li 1989
25	*S. aluensis* Li & Xiao, 2005	*S. tingi* group	Yunnan	Nanpanjiang River	Li et al. 2005; Zhao and Zhang 2013
26	*S. angustiporus* Zheng & Xie, 1985	*S. tingi* group	Guizhou; Yunnan	Nanpanjiang River	Zheng and Xie 1985; Zhao and Zhang 2009
27	*S. anophthalmus* Chen & Chu, 1988	*S. tingi* group	Yunnan	Nanpanjiang River	Chen et al. 1988a
28	*S. bannaensis* Li, Li & Chen, 2019	*S. tingi* group	Yunnan	Lancangjiang River	Li et al. 2019
29	*S. grahami* (Regan, 1904)	*S. tingi* group	Yunnan	Jinshajiang River	Zhao and Zhang 2009
30	*S. guishanensis* Li, 2003	*S. tingi* group	Yunnan	Nanpanjiang River	Li et al. 2003a
31	*S. huaningensis* Li, 1998	*S. tingi* group	Yunnan	Nanpanjiang River	Li et al. 1998
32	*S. huizeensis* Cheng, Pan, Chen, Li, Ma & Yang, 2015	*S. tingi* group	Yunnan	Jinshajiang River	Cheng et al. 2015
33	*S. lateristriatus* Li,1992	*S. tingi* group	Yunnan	Nanpanjiang River	Li 1992
34	*S. longifinus* Li, 1998	*S. tingi* group	Yunnan	Nanpanjiang River	Li et al. 1998
35	*S. macrocephalus* Li,1985	*S. tingi* group	Yunnan	Nanpanjiang River	Li 1985
36	*S. macroscalus* Li, 1992	*S. tingi* group	Yunnan	Nanpanjiang River	Li 1992
37	*S. maculatus* Li, 2000	*S. tingi* group	Yunnan	Nanpanjiang River	Zhao and Zhang 2009; Li et al. 2000a
38	*S. maitianheensis* Li,1992	*S. tingi* group	Yunnan	Nanpanjiang River	Li 1992
39	*S. malacopterus* Chu & Cui, 1985	*S. tingi* group	Yunnan	Nanpanjiang River	Chu and Cui 1985
40	*S. oxycephalus* Li, 1985	*S. tingi* group	Yunnan	Nanpanjiang River	Li 1985
41	*S. purpureus* Li, 1985	*S. tingi* group	Yunnan	Nanpanjiang River	Li 1985

ID	Species	Species group	Province	Rivers	Literature obtained
42	*S. qiubeiensis* Li, 2002	*S. tingi* group	Yunnan	Nanpanjiang River	Li et al. 2002b
43	*S. qujingensis* Li, Mao & Lu, 2002	*S. tingi* group	Yunnan	Nanpanjiang River	Li et al. 2002c
44	*S. robustus* Chen & Zhao, 1988	*S. tingi* group	Guizhou	Nanpanjiang River	Chen et al. 1988b
45	*S. tingi* Fang, 1936	*S. tingi* group	Yunnan	Nanpanjiang River	Zhao and Zhang 2009
46	*S. wenshanensis* Li, Yang, Li & Chen, 2018	*S. tingi* group	Yunnan	Yuanjiang River	Yang et al. 2018
47	*S. wumengshanensis* Li, Mao, Lu & Yan, 2003	*S. tingi* group	Yunnan	Yuanjiang River	Li et al. 2003a
48	*S. xichouensis* Pan, Li, Yang & Chen, 2013	*S. tingi* group	Yunnan	Yuanjiang River	Pan et al. 2013
49	*S. yangzongensis* Chu & Chen, 1977	*S. tingi* group	Yunnan	Nanpanjiang River	Zhao and Zhang 2009
50	*S. yimenensis* Li & Xiao, 2005	*S. tingi* group	Yunnan	Yuanjiang River	Li et al. 2005
51	*S. brevis* Lan & Chen, 1992	*S. cyphotergous* group	Guangxi	Liujiang River	Chen and Lan 1992
52	*S. cyphotergous* (Dai, 1988)	*S. cyphotergous* group	Guizhou	Hongshui River	Huang et al. 2017
53	*S. donglanensis* Zhao, Watanabe & Zhang, 2006	*S. cyphotergous* group	Guangxi	Hongshui River	Zhao et al. 2006
54	*S. dongtangensis* Zhou, Liu & Wang, 2011	*S. cyphotergous* group	Guizhou	Liujiang River	Zhou et al. 2011
55	*S. gracilicaudatus* Zhao & Zhang, 2014	*S. cyphotergous* group	Guangxi	Liujiang River	Wang et al. 2014
56	*S. guiyang* Shao, Cheng, Lu, Zhou & Zeng, 2024	*S. cyphotergous* group	Guizhou	Yangtze River	Shao et al. 2024
57	*S. huanjiangensis* Wu, Gan & Li, 2010	*S. cyphotergous* group	Guangxi	Liujiang River	Wu et al. 2010
58	*S. hugeibarbus* Li, Ran & Chen, 2003	*S. cyphotergous* group	Guizhou	Liujiang River	Li et al. 2003b
59	*S. lingyunensis* Li, Xiao & Lu, 2000	*S. cyphotergous* group	Guangxi	Hongshui River	Li et al. 2000
60	*S. longibarbatus* Wang & Chen, 1989	*S. cyphotergous* group	Guizhou; Guangxi	Liujiang River	Wang and Chen 1989
61	*S. luopingensis* Li & Tao, 2002	*S. cyphotergous* group	Yunnan	Nanpanjiang River	Li et al. 2002a
62	*S. macrolepis* Wang & Chen, 1989	*S. cyphotergous* group	Guizhou; Guangxi	Liujiang River	Wang and Chen 1989
63	*S. macrophthalmus* Zhang & Zhao, 2001	*S. cyphotergous* group	Guangxi	Hongshui River	Zhang and Zhao 2001
64	*S. multipunctatus* (Pellegrin, 1931)	*S. cyphotergous* group	Guizhou; Guangxi	Liujiang River; Hongshui River; Wujiang River	Zhao and Zhang 2009
65	*S. punctatus* Lan & Yang, 2017	*S. cyphotergous* group	Guizhou; Guangxi	Liujiang River; Hongshui River	Lan et al. 2017
66	*S. ronganensis* Luo, Huang & Wen, 2016	*S. cyphotergous* group	Guangxi	Liujiang River	Luo et al. 2016
67	*S. sanxiaensis* Jiang, Li, Yang & Chang, 2019	*S. cyphotergous* group	Hubei	Yangtze River	Jiang et al. 2019
68	*S. xunlensis* Lan, Zhan & Zhang, 2004	*S. cyphotergous* group	Guangxi	Liujiang River	Lan et al. 2004
69	*S. yaolanensis* Zhou, Li & Hou, 2009	*S. cyphotergous* group	Guizhou	Liujiang River	Zhou et al. 2009
70	*S. yishanensis* Li & Lan, 1992	*S. cyphotergous* group	Guangxi	Liujiang River	Li and Lan 1992
71	*S. brevifinus* Li, Li & Mayden, 2014	*S. jii* group	Guangxi	Hejiang River	Li et al. 2014
72	*S. guanyangensis* Chen, Peng & Zhang, 2016	*S. jii* group	Guangxi	Guijiang River	Chen et al. 2016
73	*S. guilinensis* Ji, 1985	*S. jii* group	Guangxi	Guijiang River	Zhao and Zhang 2009
74	*S. huangtianensis* Zhu, Zhu & Lan, 2011	*S. jii* group	Guangxi	Hejiang River	Zhu et al. 2011
75	*S. jii* Zhang & Dai, 1992	*S. jii* group	Guangxi	Guijiang River	Zhang and Dai 1992
76	*S. gracilis* Li, 2014	No assignment	Guangxi	Guijiang River	Li and Li 2014
77	*S. luolouensis* Lan, 2013	No assignment	Guangxi	Hongshui River	Lan et al. 2013
78	*S. pingshanensis* Li, Li, Lan & Wu, 2018	No assignment	Guangxi	Liujiang River	Wu et al. 2018
79	*S. wui* Li & An, 2013	No assignment	Yunnan	Mingyihe River	Li and An 2013

We measured 32 morphometric data points (Suppl. material 1) from a total of nine specimens of three species, referenced from Xu et al. (2023). Principal component analysis (PCA) of corrected morphometric measurements and two-dimensional scatter plots were used to explore the relative contribution of specific variables to morphological variation. Prior to PCA analysis, all included measurements were normalized using ratios to standard length (standard length is the ratio to full length) followed by log transformation (Shao et al. 2024). PCA analyses were performed in SPSS 21.0 (SPSS, Inc., Chicago, IL, USA).
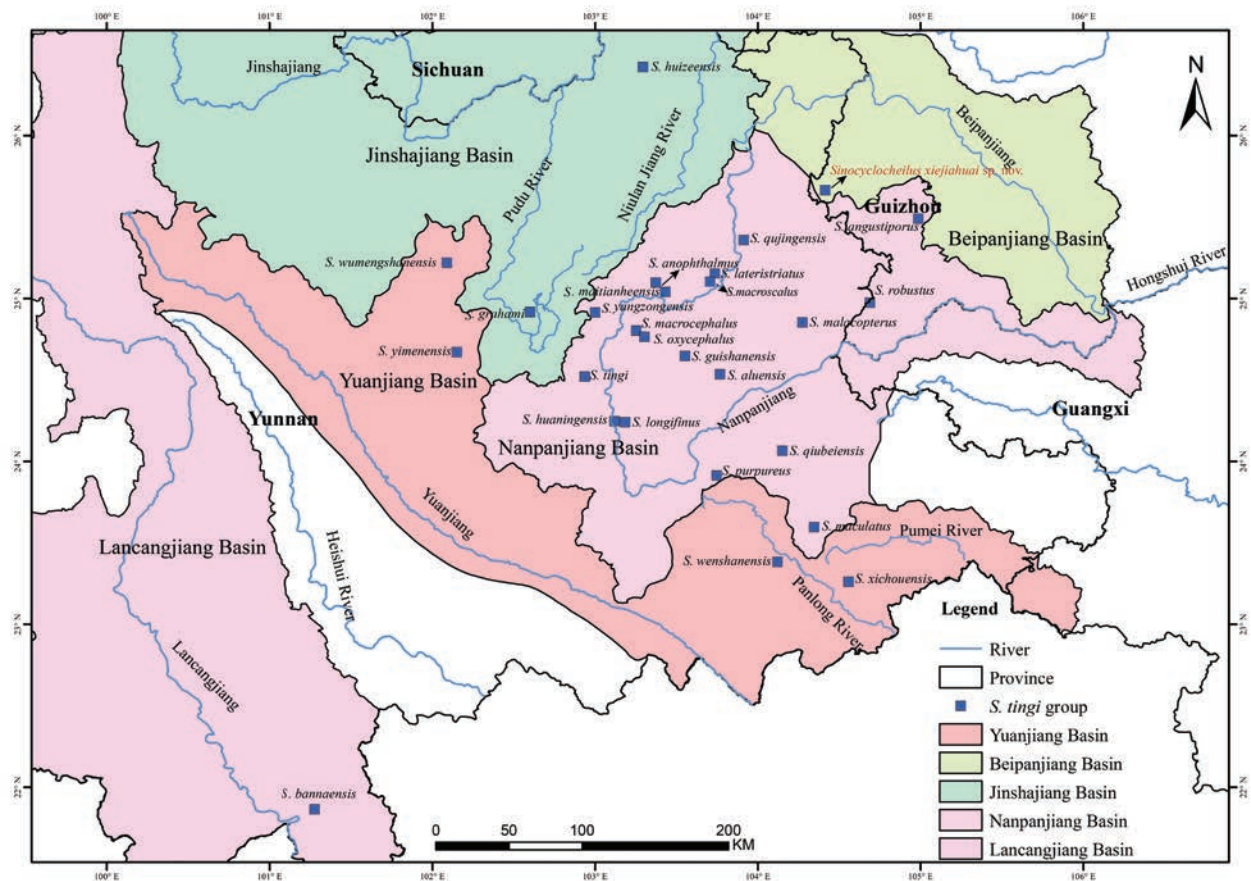
Figure 1. Sampling collection localities and distribution of the *Sinocyclocheilus xiejiahuai* sp. nov. and 26 species of the *S. tingi* species group of the genus *Sinocyclocheilus* in southwest China. The base maps are from Standard Map Service website (http://211.159.153.75/).

Table 2. Comparison of the diagnostic features of the new species described here with those selected for the 26 species of the *S. tingi* group and four unassigned species (last four) within the genus Sinocyclocheilus. Grey shading indicates clear difference in character compared to that of *Sinocyclocheilus xiejiahuai* sp. nov.

Species	Body lateral markings	Gill rakers	Dorsal-fin rays	Pectoral-fin rays	Anal-fin rays	Pelvic-fin rays	Caudal-fin rays	Lateral-line scales/pores	Tip of pectoral fin reaching to ventral fin	Tip of pelvic-fin rays reaching to anus	Source
S. xiejiahuai sp. nov.	Absent	9	iii, 6½;	i, 13	iii, 5	i, 7	17	74	No	No	This study
S. aluensis	Present	5–7	iii, 7	i, 13–16	ii, 5	i, 7–9	15–17	71–75	No	No	Li et al. 2005
S. angustiporus	Present	7–9	iv,7	i, 14–16	iii, 5	i, 8	15–16	68–80	NA	No	Zhao and Zhang 2009
S. anophthalmus	Absent	7–9	iv,8	i, 15–16	iii, 5	i, 8	16	52–56	Yes	No	Chen et al. 1988a
S. grahami	Present	5–8	iii, 7	i, 15–17	iii, 5	i, 8–9	16	61–69	No	No	Zhao and Zhang 2009
S. guishanensis	Present	5–6	iii, 7	i, 13–16	iii, 5	i, 7–8	15–16	73–80	No	No	Li et al. 2003a
S. huaningensis	Present	6	iii, 7	i, 16	iii, 5	i, 8	16	59–67	No	Yes	Li et al. 1998
S. huizeensis	Present	5–6	iii, 7	i, 15–16	iii, 5	i, 10	18	70–73	No	No	Cheng et al. 2015
S. bannaensis	Present	5	iii, 8	i, 9	ii, 5	i, 9	16	47	Yes	No	Li et al. 2019
S. maculatus	Present	14–17	iii, 7	i, 14–15	iii, 5	i, 7~8	16	81–88	No	No	Zhao and Zhang 2009
S. maitianheensis	Present	7–8	iii, 7	i, 14–15	iii, 5	i, 9	18	70–82	No	Yes	Li 1992
S. malacopterus	Present	7–9	iii, 7	i, 14–18	iii, 5	i, 9	15–16	67–81	No	No	Chu and Cui 1985

S. longifinus	Absent	NA	iii, 7	i, 16	ii, 5	i, 8	17	70–72	Yes	Yes	Li et al. 1998
S. longshanensis	Present	15–18	iii, 7	i, 14–15	ii, 5	i, 7–8	16	59–62	No	No	Li et al. 2018
S. macrocephalus	Absent	12	iv, 7	i, 15–17	iii, 5	i, 8	16	72–78	No	No	Li 1985
S. lateristriatus	Present	7–10	iv, 7	i, 15–16	iii, 5	i, 8	17	75–91	No	No	Li 1992
S. purpureus	Present	7–8	iv, 6–7	i, 16	iii, 5	i, 8	NA	63–67	No	No	Li 1985
S. qiubeiensis	Present	6–7	iii, 7	i, 14–17	iii, 5	i, 8–9	16	67–81	No	No	Li et al. 2002b
S. qujingensis	Absent	6–8	iii, 7	i, 16	iii, 5	i, 8	16	70–79	No	No	Li et al. 2002c
S. robustus	Present	9	iv, 7	i, 13–16	iii, 5	i, 7–8	16	72	No	No	Chen et al. 1988b
S. wumengshanensis	Present	5–6	iii, 7	16	ii, 5	i, 8	16	67–76	Yes	Yes	Li et al. 2003a
S. xichouensis	Present	6	iii, 6–7	i, 14–16	iii, 5	i, 8–9	NA	74–88	Yes	No	Pan et al. 2013
S. tingi	Present	7–9	iv, 7	i, 14–16	iii, 5	i, 6–8	16	62–73	No	No	Zhao and Zhang 2009
S. yangzongensis	Absent	8–11	iii, 7	i, 16	iii, 5	i, 9	16	71–81	No	No	Zhao and Zhang 2009
S. yimenensis	Present	5–7	iii, 7	i, 14–15	ii, 5	i, 8	16-17	70–79	No	No	Li et al. 2005
S. oxycephalus	Present	6–7	iv, 7	i, 16	iii, 5	i, 8	17	74–78	No	No	Li 1985
S. wenshanensis	Present	7–9	iii, 7	i, 13–15	ii, 5	i, 7–8	14–15	67–72	No	Yes	Yang et al. 2018
S.macroscalus	Present	9-10	iv, 7	i, 15–16	iii, 5	i, 8	NA	70-79	No	No	Li 1992
S. gracilis	Absent	12	NA	NA	NA	NA	NA	NA	No	No	Li and Li 2014
S. pingshanensis	Absent	10–12	iii, 7	i, 13–15	ii, 5	i, 7–8	16	75–78	Yes	No	Wu et al. 2018
S. luolouensis	Present	10	iii, 7	i, 13–14	iii, 5	i, 7–8	16–17	40–49	Yes	Yes	Lan et al. 2013
S. wui	Absent	7	iii, 7	i, 14–15	ii, 5	i, 7–8	14–15	79–81	No	No	Li and An 2013

DNA extraction and sequencing

We sequenced the mitochondrial genomes of 13 species of the genus *Sinocyclocheilus*. Total genomic DNA was extracted from each sample of 95% ethanol-preserved tissue using the Cetyltrimethylammonium Bromide method. For mitogenome sequencing, genomic DNA was fragmented to an appropriate size of 150–500 bp using a Covaris Ultrasonicator. A 400 bp DNA library was constructed based on the Whole Genome Shotgun and the library size. Sequencing was performed on an Illumina NovaSeq 6000 platform using a paired-end 150 bp protocol, generating an average of ~ 5.4 Gb of raw data. The raw data were cleaned using SOAPnuke v. 1.3 (Chen et al. 2018) based on the following criteria: removal of reads with more than 5% N-base content, reads with 50% low-quality bases, and reads with adapter contamination. The process yielded ~ 5.3 Gb of clean data. Mitogenome assembly was performed on the clean data using SPAdes v. 3.13 (parameter: -k 127) (Bankevich et al. 2012), and the assembled contigs were used for BLASTN analysis (BLAST 2.2.30+, parameter: e[-5]) using a reference mitogenome (*Sinocyclocheilus rhinocerous*: KR069119) to identify possible assembly errors. Assembled mitogenomes were annotated for genes using MITOS (Bernt et al. 2013). For mitochondrial cytochrome b (Cyt *b*) and NADH dehydrogenase subunit 4 (ND4) genes, PCR amplifications and sequencing followed Xu et al. (2023).

Phylogenetic reconstruction and divergence time estimate

In total, we collected 43 mitochondrial genomes and 76 mitochondrial gene fragments (36 Cyt*b*, 34 ND4, five 16S, three ND5, and three CO1) for phylogenetic reconstruction and estimation of divergence times.

Following Wen et al. (2022), we selected *Carassius auratus*, *Cyprinus carpio*, *Schizothorax yunnanensis*, *Onychostoma simum*, *Barbus barbus*, *Puntius ticto*, *Neolissochilus hexagonolepis*, *Garra orientalis*, *Myxocyprinus asiaticus*, and *Danio rerio* as outgroup species (Table 3). All sequences were assembled and aligned using the MUSCLE (Edgar 2004) module in MEGA v. 7.0 (Kumar et al. 2016) with default settings. The best-fit model was obtained based on the Bayesian information criterion computed with PartitionFinder v. 2.1.1 (Lanfear et al. 2017) (Suppl. material 2).

Phylogenetic reconstruction and divergence time estimation were performed in BEAST v. 2.4.7 (Bouckaert et al. 2014). In the absence of a reference fossil calibration, we refer to Wen et al. (2022) and Yang et al. (2016): (1) *Sinocyclocheilus* originated at 43.96 million years (Ma) (sigma = 2.8); (2) the most recent common ancestor of *Sinocyclocheilus* occurred at 32.13 Ma (sigma = 2.8); (3) the divergence of the *S. angularis* species group and the *S. tingi* + *S. cyphotergous* species groups occurred at ~ 26.3 Ma (sigma = 4.2). BEAST analyses were run for 40 million generations under an uncorrelated relaxed clock model and a Yule tree prior, sampled every 5000 generations. All calibrations were performed using a normal prior and monophyly. Convergence of the run parameters was checked using Tracer v. 1.7.1 (Rambaut et al. 2018) to ensure that the effective sample size of all parameters was greater than 200. A maximum clade credibility tree was generated using Treeannotator v. 2.4.1 (Bouckaert et al. 2014) by applying a burn-in of 25%. Uncorrected *p*-distances (1000 replicates) based on Cyt *b* gene were calculated in MEGA v. 7.0 (Kumar et al. 2016).

Results

Phylogenetic analyses, genetic divergence, and divergence time

The length of the aligned sequence was 15671 base pairs (bp), including 16S (1718 bp), 12S (954 bp), tRNAs (1587 bp), ATP6 (684 bp), ATP8 (165 bp), COI (1551 bp), COII (691 bp), COIII (786 bp), Cyt *b* (1142 bp), ND1 (975 bp), BD2 (1045 bp), ND3 (349 bp), ND4 (1381 bp), ND4L (297 bp), ND5 (1824 bp) and ND6 (522 bp). Information on the evolutionary models used for phylogenetic reconstruction is shown in Suppl. material 2.

The phylogenetic tree reconstructed using BEAST shows that the living *Sinocyclocheilus* can be divided into five major clades, Clades I−V, and is highly resolved (BPP = 1.00) (Fig. 2A). The phylogenetic relationship between the four clades is (Clade I+(Clade II+(Clade III + (Clade IV+ Clade V)))) (Fig. 2A). New species clustered in Clade V, close to *S. lateristriatus*, had a genetic distance of 1.9% at the level of the mitochondrial Cyt *b* (Suppl. material 3).

Divergence time analyses indicate that *Sinocyclocheilus* originated 40.22 Ma (95% highest probability density (HPD): 35.58−44.92 Ma), with its most recent common ancestor occurring at 34.83 (95%HPD: 30.87−38.8 Ma). Divergence of the remaining four clades (Clades II−IV) occurred in the Oligocene to Early Miocene, ~ 23.64−28.93 Ma (95% HPD: 19.39−32.92 Ma). The divergence of the new species from its close relatives occurred at the Pliocene/Pleistocene boundary at ~ 2.56 Ma (95% HPD: 0.87−4.89 Ma), which is older than the divergence of the other sister species (Fig. 2A).

Table 3. Localities, voucher information, and GenBank numbers for all samples used.

ID	Species	Location (* type localities)	Voucher number	Mitogenome	Cyt *b*	ND4/16S/ND5/ CO1
1	S. altishoulderus	Mashan County, Guangxi	–	NC_013186		
2	S. anatirostris	–	GZNU20210531002	NC_069226		
3	S. angularis	Panzhou City, Guizhou*	GZNU20180420001	MZ636514		
4	S. angularis	Baotian Town, Panzhou City, Guizhou	GZNU20180420001	PQ157935		
5	S. angustiporus	Xingren County, Guizhou	GZNU20190504001	MZ636515		
6	S. anophthalmus	–	–	NC_023472		
7	S. anshuiensis	Lingyun County, Guangxi	–	KR069120		
8	S. aquihornes	Shuanglongjian town, Qiubei County, Yunnan*	S28	–	**PQ155086**	**PQ155094**
9	S. bicornutus	XingrenCounty, Guizhou	–	KX528071		
10	S. brevibarbatus	–	GX0064–L20–13	–	MT373106	MW548423
11	S. brevifinus	–	–	–	OQ718395	
12	S. brevis	–	GX0155	–	MT373105	MW548424
13	S. cyphotergous	Luodian County, Guizhou*	GZNU20150819010	OQ319607		
14	S. convexiforeheadus	Wenliu Township, Qiubei County, Yunnan*	S30	–	**PQ155090**	**PQ155091**
15	S. donglanensis	Donglan County, Guangxi	CA139		AB196440	MW548425
16	S. furcodorsalis	Tian'e County, Guangxi	–	GU589570		
17	S. gracilicaudatus	–	–	–	OQ718398	
18	S. grahami	Kunming City, Yunnan	–	GQ148557		
19	S. guanyangensis	–	GX0173	–	MT373108	MW548426
20	S. guilinensis	–	GX0073–L17–2	–	MT373104	MW548427
21	S. guishanensis	Guishan, Shilin County, Yunnan	XH5401	–	AY854722	AY854779
22	S. huangtianensis	–	GX0175	–	MT373109	MW548428
23	S. huaningensis	Huaning County, Yunnan	XH3701	–	AY854718	AY854775
24	S. huanjiangensis	–	GX0124		MT373103	MW548429
25	S. hugeibarbus	Libo County, Guizhou*	GZNU20150120005	MW014319		
26	S. huizeensis	Huize County, Yunnan	hrfri2018046	MH982229		
27	S. hyalinus	Alugudong, Luxi County, Yunnan	XH4701	–	AY854721	AY854778
28	S. jii	Gongcheng County, Guangxi	YNUSJ201308060038	MF100765		
29	S. jiuxuensis	Jiuxu Town, Hechi City, Guangxi	XH8501	–	AY854736	AY854793
30	S. lateristriatus	Maojiachong, Zhanyi County, Yunnan	XH1102	–	AY854703	AY854760
31	S. lingyunensis	–	–	MW411665		
32	S. longibarbatus	Libo County, Guizhou*	GZNU2019102022	NC_056194		
33	S. longihornes	Hongguo Town, Panzhou City, Guizhou*	GZNU20210503016	–	MZ634123	MZ634125
34	S. longshnaensis	Shupi Township, Qiubei County, Yunnan*	S22	–	**PQ155085**	**PQ155093**
35	S. macrocephalus	Heilongtan, Shilin County, Yunnan	XH0103		AY854683	AY854740 DQ845925
36	S. macrolepis	Nandan County, Guangxi	XH8201		AY854729	AY854786
37	S. macrophthalmus	Xiaao, Duan County, Guangxi	XH8401		AY854733	AY854790 HM536754 HM536835 HM536889
38	S. maculatus	Weiwei Township, Yanshan County, Yunnan	8	–	EU366193	EU366183
39	S. malacopterus	Wulong Township, Shizong County, Yunnan*	S43	–	**PQ155088**	**PQ155095**
40	S. maitianheensis	Jiuxiang,Yiliang County, Yunnan	XH2301		AY854710	AY854767
41	S. mashanensis	–	GX0026–L18–12		MT373107	MW548430
42	S. microphthalmus	Lingyun County, Guangxi	NNNU201712001	MN145877		
43	S. multipunctatus	Huishui County, Guizhou	–	MG026730		
44	S. oxycephalus	Shilin County, Yunnan	YNUSO20160610002	MG686610		
45	S. purpureus	Luoping County, Yunnan	IHB:2006638	MW548264		
46	S. punctatus	–	–	MW014318		
47	S. purpureus	Zhonghe Ying Township, Kaiyuan, Yunnan*	S20	–	**PQ155083**	**PQ155097**
48	S. qiubeiensis	Songming, Yunnan	IHB:2006624	NC_063104		
49	S. qiubeiensis	Qiubei County, Yunnan*	S21	–	**PQ155084**	**PQ155098**

ID	Species	Location (* type localities)	Voucher number	Mitogenome	Cyt *b*	ND4/16S/ND5/CO1
50	*S. qujingensis*	Huize County, Yunnan	hrfri2018044	MH937706		
51	*S. rhinocerous*	Luoping County, Yunnan	–	KR069119		
52	*S. ronganensis*	Rong'an County, Guangxi	–	KX778473		
53	*S. sanxiaensis*	Guojiaba Town, Zigui County, Hubei*	KNHM 2019000001	OP745534		
54	*S. simengensis*	–	–		OQ718406	
55	*S. tingi*	Fuxian Lake, Yunnan	YNUST201406180002	MG323567		
56	*S. wenshanensis*	Xigu Town, Wenshan, Yunnan	YNUSW20160703016	MW553076		
57	*S. wenshanensis*	Dehou Town, Wenshan City, Yunnan*	S45	–	**PQ155089**	**PQ155100**
58	*S. wumengshanensis*	Xuanwei County, Yunnan	YNUSM20160817008	MG021442		
59	*S. xunlensis*	Huanjiang, Guangxi	IHB:04050268		EU366187	EU366184 HM536752 HM536833 HM536887
60	*S. xiejiahuai* sp. nov.	Hongguo Town, Panzhou City, Guizhou*	S46	**PQ165088**		
61	*S. xingyiensis*	XingyiCity, Guizhou, China*	–		ON573218	
62	*S. xichouensis*	Xingjie Town, Xichou County, Yunnan*	S37	–	**PQ155087**	**PQ155099**
63	*S. yangzongensis*	Yangzonghai Lake, Yunnan	XH6101		AY854725	AY854782 DQ845926
64	*S. yimenensis*	Yimen, Yunnan	IHB:2006646		EU366191	EU366180
65	*S. yishanensis*	Liujiang County, Guangxi	–	MK387704		
66	*S. zhenfengensis*	Zhenfeng County, Guizhou*	GZNU20150112021	MW014317		
67	*S. zhenfengensis*	Zhenfeng County, Guizhou*	S17	–	**PQ155082**	**PQ155096**
68	*S. tianlinensis*	Longping Township, Tianlin County, Guangxi*	S10	–	**PQ155081**	**PQ155092**
69	*S. tianlinensis*	Longping Township, Tianlin County, Guangxi*	GZNU20210531003	**PQ214929**		
Outgroup						
70	*Carassius auratus*	–	–	AB111951		
71	*Cyprinus carpio*	–	–	JN105357		
72	*Schizothorax yunnanensis*	–	–	KR780749		
73	*Onychostoma simum*	–	–	KF021233		
74	*Barbus barbus*	–	–	AB238965		
75	*Puntius ticto*	–	–	AB238969		
76	*Neolissochilus hexagonolepis*	–	–	KU380329		
77	*Garra orientalis*	–	–	JX290078		
78	*Myxocyprinus asiaticus*	–	–	AY526869		
79	*Danio rerio*	–	–	KM244705		

Morphological analyses

A total of five principal component factors with eigenvalues greater than two were extracted based on principal component analysis of the morphometric data (Suppl. material 3). These together accounted for 94.48% of the total variance, with the first principal component (PC1) and second principal component (PC2) accounting for 32.98% and 25.84% of the total variance. In the scatter plot of PC1 versus PC2, the new species *Sinocyclocheilus xiejiahuai* sp. nov. was distinguishable from *S. lateristritus* and *S. qujingensis* on the PC1 axis (Fig. 3). Major morphometric characters loaded on the PC1 axis included body depth, anal-fin length, prepectoral length, pectoral-fin base length, caudal peduncle length, caudal peduncle depth, head width, snout length, eye diameter, interorbital width, distance between anterior nostrils, mouth width, rostral barbel length, and maxillary barbel length (Table 4).
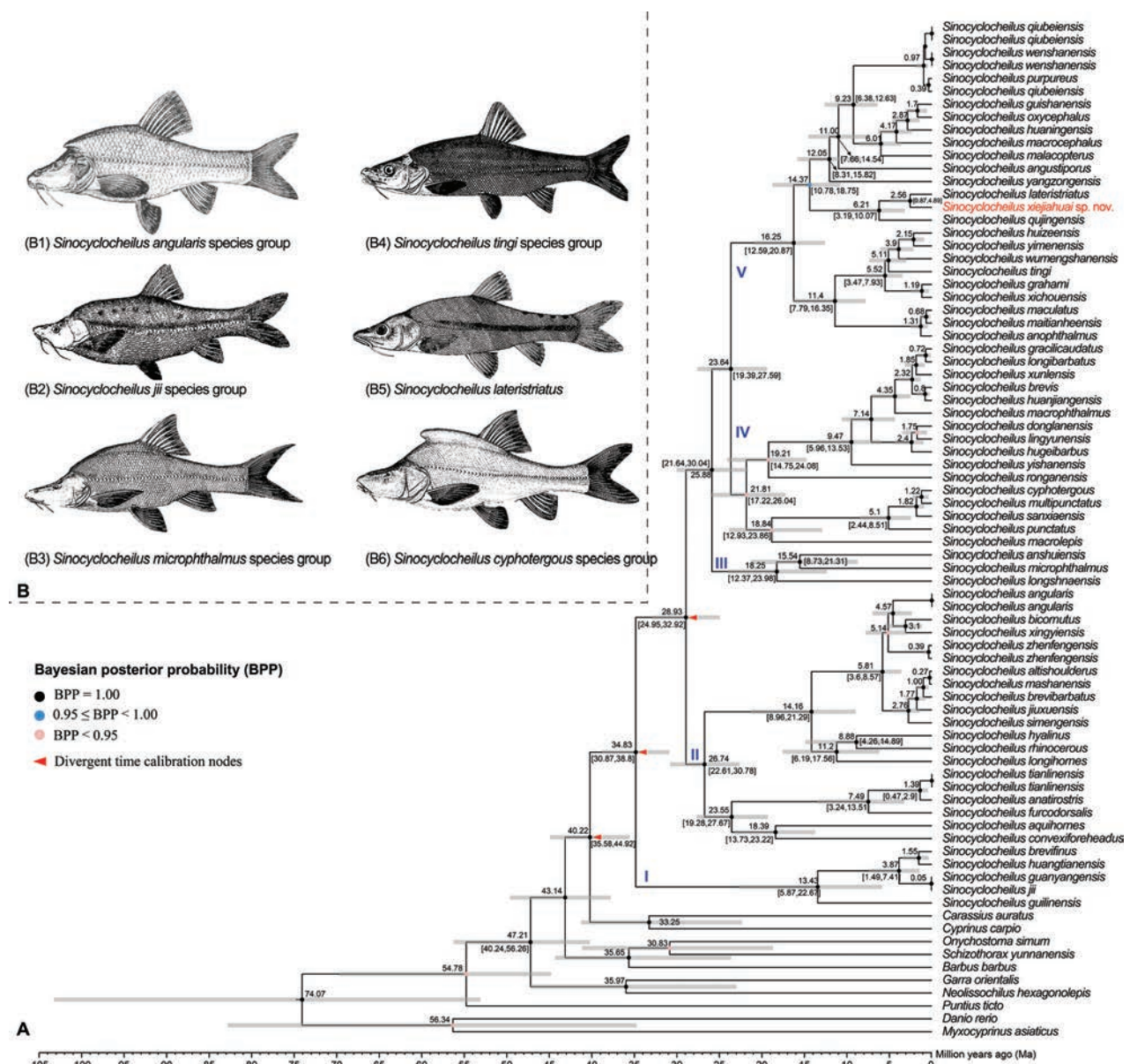
Figure 2. A time tree based on mitochondrial genes assessment **B** type species for five species groups. Species photos B1, B3, B4, and B6 from Shan et al. (2000), B2 from Zhang and Dai (1992), and B5 from Li (1992).

Morphological comparison

Based on morphology and phylogeny, the new species *Sinocyclocheilus xiejia-huai* sp. nov. was assigned to the *S. tingi* group, and a detailed morphological comparison is shown in Table 2.

Sinocyclocheilus xiejiahuai sp. nov. can be distinguished from the 24 species belonging to the *S. angularis* and *S. microphthalmus* groups by the absence of horn-like structures and indistinct elevation at the head-dorsal junction, pectoral fins tip not reaching to pelvic-fin origin (vs presence of horn-like structures and pectoral fins long and not reaching to pelvic-fin origin); from the five species belonging to the *S. jii* species group by with serrations along posterior margin of the last unbranched fin of the dorsal fin (vs absent) (Zhao et al. 2009), and from the 21 species belonging to the *S. cyphotergous* species group by pectoral fins tip not reaching to pelvic-fin origin (vs usually reaching to pelvic-fin origin).
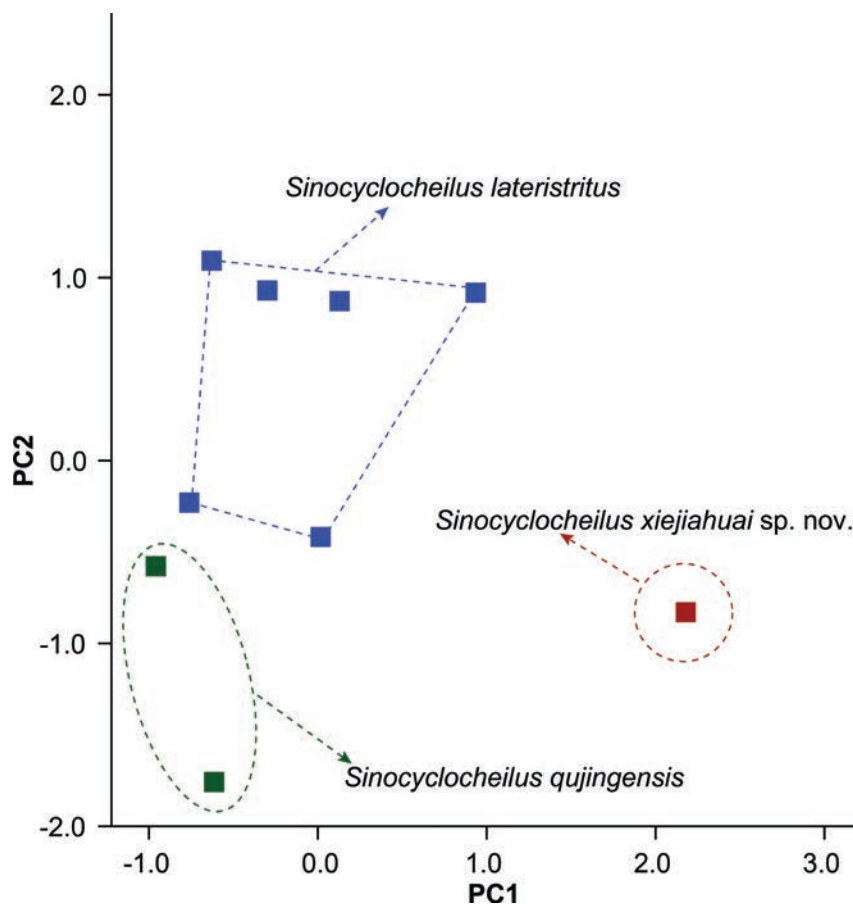
Figure 3. Plot of principal component analysis, scores of *Sinocyclocheilus xiejiahuai* sp. nov., *S. lateristritus*, and *S. qujingensis* based on morphometric data**.**

For the 26 species of the *S. tingi* group, new species can be distinguished by a series of morphological characters. By lacking irregular markings on the body lateral, the new species can be distinguished from *S. aluensis*, *S. angustiporus*, *S. bannaensis*, *S. grahami*, *S. guishanensis*, *S. huaningensis*, *S. huizeensis*, *S. lateristriatus*, *S. longshanensis*, *S. macrocephalus*, *S. maculatus*, *S. maitianheensis*, *S. malacopterus*, *S. oxycephalus*, *S. purpureus*, *S. robustus*, *S. wumengshanensis*, *S. xichouensis*, *S. tingi*, *S. yimenensis*, and *S. wenshanensis*. New species differs from *S. anophthalmus* by eyes present (vs absent) and lateral line pores 74 (vs 52–56); from *S. longifinus*, *S. qujingensis*, and *S. yangzongensis* by six branched dorsal-fin rays (vs 7) and seven branched pelvic-fin rays (vs 8 or 9). The new species can be further distinguished from *S. qujingensis* and *S. yangzongensis* by 13 branched pectoral-fin rays (vs 16), and from *S. longifinus* by the tip of the pectoral fin not reaching to pelvic-fin origin (vs reaching to pelvic-fin origin).

For the four species not placed in any species group, new species differed from *S. luolouensis* by eye normal (vs eyes reduced) and pectoral fins tip not reaching to pelvic-fin origin (vs .beyond pelvic-fin origin) (Lan et al. 2013), from *S. gracilis* by having nine rakers on the first gill arch (vs 12) and body depth of 13% of standard length (vs 21.0–23.8%), from *S. pingshanensis* and *S. gracilis* by with serrations along posterior margin of the last unbranched fin of the dorsal fin (vs absent) and nine rakers on the first gill arch (vs 10–12), and from *S. wui* by three unbranched anal-fin rays (vs 2), 13 branched pectoral-fin rays (vs 14–15), and 17 branched caudal-fin rays (vs 14–15).

Table 4. PCA loadings of five principal components extracted from 34 morphometric data of *S. xiejiahuai* sp. nov. and its related species.

	PC1	PC2	PC3	PC4	PC5
Standard length	0.389	0.508	-0.188	-0.616	0.164
Body depth	0.645	0.419	-0.614	-0.089	0.031
Predorsal length	0.351	0.531	-0.586	0.406	-0.159
Dorsal-fin base length	-0.476	0.765	-0.010	-0.267	0.106
Dorsal-fin length	-0.303	0.877	-0.217	-0.020	0.004
Pre-anal length	-0.383	0.026	-0.791	0.005	0.336
Anal-fin base length	-0.473	0.259	-0.066	0.155	0.648
Anal-fin length	-0.640	0.612	0.265	0.221	0.034
Prepectoral length	-0.820	0.378	-0.159	-0.275	-0.134
Pectoral-fin base length	0.683	0.056	0.499	-0.489	-0.080
Pectoral-fin length	-0.031	0.280	0.695	-0.075	-0.505
Prepelvic length	-0.544	0.741	0.325	0.096	0.030
Pelvic-fin base length	0.588	-0.293	-0.060	0.043	-0.662
Pelvic-fin length	-0.243	0.880	0.029	0.175	-0.363
Caudal peduncle length	0.602	-0.479	0.583	0.112	0.211
Caudal peduncle depth	0.725	0.363	-0.429	-0.356	-0.103
Head length	0.261	0.774	0.511	-0.039	0.180
Head depth	0.571	0.583	-0.409	-0.291	-0.219
Head width	0.727	0.353	-0.257	0.512	-0.004
Snout length	0.625	0.386	0.457	0.259	0.197
Eye diameter	0.643	0.702	0.060	-0.233	0.041
Interorbital width	0.755	0.532	0.057	-0.001	0.191
Prenostril length	0.852	0.336	0.008	0.063	0.348
Distance between posterior nostrils	0.561	-0.141	0.460	-0.393	0.278
Upper jaw length	-0.535	0.436	0.524	0.176	0.084
Lower jaw length	-0.562	0.649	0.151	0.248	0.072
Mouth width	0.731	0.415	-0.384	0.202	0.022
Rostral barbel length	0.639	0.369	0.403	0.477	-0.010
Maxillary barbel length	0.634	-0.022	0.719	0.192	-0.146
Distance from the pectoral-fin origin to the pelvic-fin origin	0.459	-0.352	-0.581	0.445	-0.073
Distance from the pelvic-fin origin to the anal-fin origin	0.456	-0.582	0.054	0.046	0.460
Eigenvalues	6.887	10.361	1.049	0.689	0.979
Percentage of total variance	32.981	25.837	17.032	7.820	6.814
Cumulative percentage	32.981	58.817	75.850	83.669	90.483

Taxonomic account

Sinocyclocheilus xiejiahuai Luo, Fan, Xiao & Zhou, sp. nov.

https://zoobank.org/B3636299-814D-4EE8-92F4-CA48078A7581

Fig. 4, Table 5

Material examined. *Holotype*. GZNU20230304001, total length 242.8 mm (TL), standard length 201.8 mm (SL), • Hongguo Town, Panzhou City, Guizhou Province, China; 25.6576°N, 104.4044°E; ca 1852 m a.s.l.; collected on October 2, 2021.

Diagnosis. *Sinocyclocheilus xiejiahuai* sp. nov. can be distinguished from all other congeners by the following combination of characters: (1) absence of horn-like structures and indistinct elevation at the head-dorsal junction;

Figure 4. Lateral view of adult holotype GZNU20230304001 of *Sinocyclocheilus xiejiahuai* sp. nov. in preservative **A** left side **B** right side.

(2) absence of irregular black markings on the body lateral and scaleless; (3) eyes large, eye diameter 13% of head length; (4) dorsal-fin rays, iii, 6½, last unbranched ray strong, with serrations along posterior margin; (5) pectoral-fin rays, i, 13; (6) anal-fin rays, iii, 5; (7) pelvic-fin rays, i, 7; (8) lateral line pores 74; (9) gill rakers well developed, nine on first gill arch; (10) pectoral fins short, tip not reaching to pelvic-fin origin (Table 5).

Description. Body fusiform, moderately elongate and compressed. Dorsal profile convex from nape to dorsal-fin, greatest body depth at dorsal-fin insertion, ventral profile slightly concave, tapering gradually toward the caudal-fin, greatest body depth slightly anterior to dorsal-fin insertion.

Head short, compressed laterally, length longer than maximum head width, depth longer than maximum head width. Eyes present, eye diameter 13% of head length (HL), interorbital distance larger than distance between posterior nostrils. Snout short, U-shaped, and projecting beyond lower jaw in dorsal view, length 37% of HL. Mouth subterminal, with slightly projecting upper jaw.

Two pairs of nostrils, anterior and posterior nostrils close set, nares at 2/3 between snout tip and anterior margin of eye, anterior nares possessing an anterior rim with a posterior fleshy flap forming a half-tube. Two pairs of barbels, rostral barbels short, not reaching the anterior edge of operculum when extended backwards, maxillary barbel slightly long compared to rostral barbel, beyond the anterior edge of operculum when extended backwards (Table 5).

Dorsal fin rays iii, 6½, pectoral fin rays i,13, pelvic fin rays i, 7, anal fin rays iii, 5, and 13 branched caudal fin rays. Dorsal fin long, 24% of SL, less than head length, distal margin truncated, origin posterior to pelvic fin insertion, situated slightly anterior to midpoint between snout tip and the caudal fin base, last unbranched ray strong, softening toward tip, with serrations along posterior margin, first

Table 5. Morphological characteristics and measurements of *Sinocyclocheilus xiejiahuai* sp. nov., *S. qujingensis*, and *S. lateristritus*.

	S. xiejiahuai sp. nov. (*n* = 1)	*S. lateristritus* (*n* = 2)		*S. qujingensis* (*n* = 6)	
	Range	Range	Mean ± SD	Range	Mean ± SD
Total length	240.0	73.2–87.5	80.8 ± 5.2	53.3–140.1	96.7 ± 61.4
Standard length	201.0	59.3–71.0	64.9 ± 4.1	43.3–98.1	70.7 ± 38.7
Body depth	56.7	13.0–18.4	15.3 ± 1.9	9.9–19.2	14.6 ± 6.6
Predorsal length	108.6	30.9–39.4	34.1 ± 3.0	22.3–50.0	36.1 ± 19.6
Dorsal-fin base length	24.7	8.5–9.6	9.2 ± 0.4	5.9–12.3	9.1 ± 4.5
Dorsal-fin length	40.0	12.7–16.7	15.2 ± 1.5	10.2–19.4	14.8 ± 6.4
Pre-anal length	140.4	42.0–49.2	45.5 ± 2.4	30.9–68.9	49.9 ± 26.9
Anal-fin base length	17.4	5.2–6.8	5.8 ± 0.5	4.0–8.4	6.2 ± 3.1
Anal-fin length	28.4	9.8–13.3	11.6 ± 1.2	7.3–16.3	11.8 ± 6.4
Prepectoral length	53.0	17.1–19.7	18.4 ± 0.9	12.7–27.2	19.9 ± 10.3
Pectoral-fin base length	8.9	2.1–3.1	2.5 ± 0.5	1.4–3.0	2.2 ± 1.2
Pectoral-fin length	32.9	8.9–16.0	13.0 ± 2.9	7.2–17.5	12.3 ± 7.3
Prepelvic length	98.1	29.9–36.0	33.3 ± 2.1	21.8–49.1	35.5 ± 19.3
Pelvic-fin base length	8.9	2.0–3.3	2.5 ± 0.5	1.8–4.2	3.0 ± 1.7
Pelvic-fin length	25.5	8.9–13.5	11.0 ± 1.6	6.5–13.7	10.1 ± 5.1
Caudal peduncle length	49.5	12.3–16.6	14.0 ± 1.6	8.4–22.6	15.5 ± 10.1
Caudal peduncle depth	24.7	6.4–8.5	7.1 ± 0.7	4.6–9.2	6.9 ± 3.2
Head length	57.1	16.4–21.0	19.2 ± 1.6	11.8–26.3	19.0 ± 10.3
Head depth	40.3	11.3–15.2	12.5 ± 1.4	8.1–16.1	12.1 ± 5.6
Head width	33.1	7.8–11.2	9.3 ± 1.2	5.6–13.6	9.6 ± 5.7
Snout length	21.0	4.7–6.8	6.3 ± 0.8	3.3–8.7	6.0 ± 3.8
Eye diameter	6.7	1.8–2.4	2.1 ± 0.2	1.2–2.4	1.8 ± 0.9
Interorbital width	18.6	4.4–6.4	5.5 ± 0.7	3.4–7.1	5.2 ± 2.6
Prenostril length	13.1	2.3–3.5	3.0 ± 0.4	1.7–3.5	2.6 ± 1.3
Distance between posterior nostrils	12.9	2.9–4.8	3.6 ± 0.7	2.4–4.8	3.6 ± 1.7
Upper jaw length	13.7	4.8–5.7	5.3 ± 0.4	3.2–7.6	5.4 ± 3.1
Lower jaw length	12.1	4.4–5.4	4.9 ± 0.4	3.0–6.8	4.9 ± 2.7
Mouth width	17.2	4.4–6.1	5.0 ± 0.7	3.1–6.8	5.0 ± 2.6
Rostral barbel length	24.6	4.8–9.8	7.1 ± 1.6	2.2–9.5	5.9 ± 5.2
Maxillary barbel length	30.2	5.3–12.0	8.0 ± 2.8	2.5–11.8	7.1 ± 6.6
Distance from the pectoral-fin origin to the pelvic-fin origin	42.2	11.4–14.2	12.7 ± 0.9	8.7–20.1	14.4 ± 8.0
Distance from the pelvic-fin origin to the anal-fin origin	38.4	9.5–10.8	9.9 ± 0.5	6.2–16.4	11.3 ± 7.2

branched ray longest, shorter than HL, tip reaching to the vertical of the anus. Pectoral fin developed, distal margin rounded, length slightly small than HL, 16% of SL, tips beyond 2/3 of the distance between pectoral-fin origin and pelvic-fin origin, tips not reaching to pelvic fin-origin. Pelvic fin moderately developed, distal margin rounded, length 14% of SL, and tips not reaching to anus. Anal fin short, 15% of SL, distal margin truncated, origin close to the anus, tips not reaching to caudal fin base. Caudal peduncle well developed, length 52.4 mm, depth 23.4 mm, and without adipose crests along both dorsal and ventral sides. Caudal fin slight forked, upper lobe equal in length to the lower one, tips rounded.

Body non-scale, lateral line pores 74. Complete lateral line, slightly curved, curved downward at the anus position, originating from posterior margin of operculum and extending to end of caudal peduncle.

Coloration. In 7% formalin solution, the specimen was grayish brown overall, with each fin pale yellow.

Geographical distribution and habitat. *Sinocyclocheilus xiejiahuai* sp. nov. is the only vertical cave found at an altitude of 2276 m in Hongguo Town, Panzhou City, Guizhou Province, China, some distance away. The discovery site is within the Beipanjiang River Basin (Fig. 1). There is no light in the cave. Individuals were distributed in a small pool ~ 25 m from the cave entrance. The pool is ~ 1.8 m wide and 80 cm deep, and the water temperature at the time of collection was ~ 16 °C and pH 7.4. Inside the cave, the species of *S. xiejiahuai* sp. nov. is symbiotic with *S. longicornus* (*S. angularis* group) and *Triplophysa panzhouensis*. The arable land outside the cave is mainly cultivated with maize, wheat, and potatoes.

Etymology. The specific name *xiejiahuai* is in honor of Professor Jia-Hua Xie (谢家骅), for his contribution to zoological research in China. Before retiring from Guizhou Normal University, he described *S. angustiporus*, the first species distributed in Guizhou within the *S. tingi* species group, and his work has been an important contribution to the study of zoology in Guizhou, especially the conservation of critically endangered species. We propose the common English name "Xie's Golden-lined Fish" and the Chinese name "Xiè Shì Jīn Xiàn Bā (谢氏金线鲃)."

Discussion

Based on previous records, the genus *Sinocyclocheilus* (Fang, 1936) was recorded with 79 species (Zhao and Zhang 2009; Xu et al. 2023; Luo et al. 2023; Shao et al. 2024), all of which are endemic to southwestern China, and the description of the new species in this study increases it to 80 species. Up to now, there are 27 species in the *tingi* group, mainly distributed in eastern Yunnan and western Guizhou. *Sinocyclocheilus xiejiahuai* sp. nov. is the third species of the *S. tingi* species group discovered in Guizhou with *S. angustiporus* and *S. robutus*. Although the description of this new species is based on a single specimen and some measurements may not be sufficient, the fin characteristics (see morphological comparisons above) and genetic differences support the validity of this new species. The new species is phylogenetically close to *S. lateristriatus* and *S. qujingensis* (Fig. 2), with genetic distances of 1.9% and 3.1% (Suppl. material 3), which was greater than that between sister species of the same genus, e.g., 1.2% between *S. yimenensis* and *S. huizeensis* (Suppl. material 2).

The new species co-inhabits a cave with *S. longicornus*, and is the first report of the sympatric distribution of the *S. tingi* and *S. angularis* groups. Furthermore, our phylogenetic tree suggests that *S. longshnaensis* should be assigned to the *S. microphthalmus* species group.

Our reconstructed divergence times are similar to those of Wen et al. (2022) who discussed the origin and early diversification of the genus *Sinocyclocheilus*. Time-tree-based results suggest that *Sinocyclocheilus* originated in the late Eocene, with its most recent common ancestor/Clade I occurring at 34.83 Ma, and that divergence of the remaining clades was centered in the Oligocene to early Miocene, ca 19.39–32.92 Ma (Fig. 2). The origin and early divergence events are well-coupled with the rapid uplift of the Qinghai-Tibetan Plateau during the Oligocene-middle Miocene (Ding et al. 2022). Middle Miocene Climate Optimum (17–14 Ma), the monsoon climate brings precipitation to promote the development of caves in the karst region (Farnsworth et al. 2019), which increases the ecological opportunities for the formation of cave fishes within the *Sinocyclocheilus*. We also observed that *Sinocyclocheilus xiejiahuai* sp. nov., *S. lateristriatus*, and *S. qujingensis* are distributed in the Nanpanjiang River basin in close phylogenetic and geographic proximity, and this congruence may indicate that the formation of these species, and even of species in the *S. tingi* group, is related to historical drainage changes resulting from the uplift of the Yunnan-Guizhou Plateau since the Late Miocene (Zhang et al. 2020). Thus, geographic isolation from historical drainage changes has shaped the formation of species diversity in the *S. tingi* species group (Mao et al. 2021,2022; Zhao and Zhang 2009; Wen et al. 2022).

This new species is presently restricted to its type locality. Given that its habitat borders the urban area of Panzhou, which is experiencing rapid urbanization, there is a significant risk of habitat disturbance and destruction in the near future. In the last five years, we have conducted a total of 16 field surveys at the type locality, and no new individuals have been detected except for the first one, suggesting that the population size of this species is very small. The Chinese government listed all species of *Sinocyclocheilus* endemic to China as second-class of the national protected animals on 5 February 2021 (National Forestry and Grassland Administration & National Park Administration, 2021). Therefore, the new species has strict legal protection in China, and the local government should strengthen publicity about the protection of this species to avoid it being caught and trafficked. In addition to the small population size, the following threats to the habitat of the new species include declining water levels in caves, pesticide use, domestic waste, and as potential land for urban construction. Therefore, we suggest the species may be eligible for listing as Endangered (B1ab (i, ii, iii) + 2ab (i, ii, iii)) in the IUCN Red List of Threatened Species.

Acknowledgments

Additional information

Conflict of interest

The authors have declared that no competing interests exist.

Ethical statement

No ethical statement was reported.

Funding

Author contributions

Jiang Zhou and Tao Luo conceived and designed the research; Cui Fan, Man Wang, Jia-Jun Zhou, and Tao Luo, conducted field surveys and collected samples; Tao Luo and Cui Fan performed molecular work; Cui Fan, Man Wang, and Ning Xiao processed the English language of the manuscript; Jiang Zhou provided financial support. All authors read and approved the final version of the manuscript.

Author ORCIDs

Cui Fan https://orcid.org/0009-0002-8039-649X
Man Wang https://orcid.org/0000-0001-6201-1811
Jia-Jia Wang https://orcid.org/0009-0007-8637-5469
Tao Luo https://orcid.org/0000-0003-4186-1192
Jia-Jun Zhou https://orcid.org/0000-0003-1038-1540
Jiang Zhou https://orcid.org/0000-0003-1560-8759

Data availability

All of the data that support the findings of this study are available in the main text or Supplementary Information.

References

Bankevich A, Nurk S, Antipov D, Gurevich AA, Dvorkin M, Kulikov AS, Lesin VM, Nikolenko SI, Pham S, Prjibelski AD, Pyshkin AV, Sirotkin AV, Vyahhi N, Tesler G, Alekseyev MA, Pevzner PA (2012) SPAdes: A New Genome Assembly Algorithm and Its Applications to Single-Cell Sequencing. Journal of Computational Biology 19(5): 455–477. https://doi.org/10.1089/cmb.2012.0021

Bernt M, Donath A, Jühling F, Externbrink F, Florentz C, Fritzsch G, Pütz J, Middendorf M, Stadler PF (2013) MITOS: Improved de novo metazoan mitochondrial genome annotation.Molecular Phylogenetics and Evolution 69(2): 313–319. https://doi.org/10.1016/j.ympev.2012.08.023

Bouckaert R, Heled J, Kühnert D, Vaughan T, Wu CH, Xie D, Suchard MA, Rambaut A, Drummond AJ (2014) BEAST 2: a software platform for Bayesian evolutionary analysis. PLoS Computational Biology 10(4): e1003537. https://doi.org/10.1371/journal.pcbi.1003537

Chen JX, Lan JH (1992) Description of a new genus and three new species of fishes from Guangxi, China (Cypriniformes: Cyprinidae, Cobitidae). Acta Zootaxonomica Sinica 17(1): 104–109. [In Chinese]

Chen YR, Chu XL, Luo ZY, Wu JY (1988a) A new blind Cyprinid fish from Yunnan, China with a reference to the evolution of its characters. Acta Zootaxonomica Sinica 34(1): 64–70. [In Chinese]

Chen JX, Zhao ZF, Zheng JZ, Li DJ (1988b) Description of three new barbine species from Guizhou, China (Cypriniformes, Cyprinides). Acta Academiae Medicinae Zunyi 11(1): 1–4(92–93). [In Chinese]

Chen YR, Yang JX, Zhu CG (1994) A new fish of the genus *Sinocyclocheilus* from Yunnan with comments on its characteristic adaptation (Cypriniformes: Cyprinidae). Acta Zootaxonomica Sinica 19(2): 246–252. [In Chinese]

Chen YR, Yang JX, Lan JH (1997) One new species of blind cavefish from Guangxi with comments on its phyogenetic status (Cypriniformes: Cyprinidae: Barbinae). Acta Zootaxonomica Sinica 22(2): 219–223. [In Chinese]

Chen YQ, Peng CL, Zhang E (2016) *Sinocyclocheilus guanyangensis*, a new species of cavefish from the Li-Jiang basin of Guangxi, China (Teleostei: Cyprinidae). Ichthyological Exploration of Freshwaters 27(1): 1–8. [In Chinese]

Chen Y, Chen Y, Shi C, Huang Z, Zhang Y, Li S, Li Y, Ye J, Yu C, Li Z, Zhang X, Wang J, Yang H, Fang L, Chen Q (2018) SOAPnuke: a MapReduce acceleration-supported software for integrated quality control and preprocessing of high-throughput sequencing data. Gigascience 7(1): gix120. https://doi.org/10.1093/gigascience/gix120

Cheng C, Pan XF, Chen XY, Li JY, Ma L, Yang JX (2015) A new species of the genus *Sinocyclocheilus* (Teleostei: Cypriniformes), from Jinshajiang Drainage, Yunnan, China. Cave Research 2(4): 1–4.

Chu XL, Cui GH (1985) A revision of Chinese cyprinid genus *Sinocyclocheilus* with ref erence to the interspecific relationships. Acta Zootaxonomica Sinica 10(4): 435–441. [In Chinese]

Ding L, Kapp P, Cai F, Garzione CN, Xiong Z, Wang H, Wang C (2022) Timing and mechanisms of Tibetan Plateau uplift. Nature Reviews Earth & Environment 3(10): 652–667. https://doi.org/10.1038/s43017-022-00318-4

Edgar RC (2004) MUSCLE: Multiple sequence alignment with high accuracy and high throughput. Nucleic Acids Research 32(5): 1792–1797. https://doi.org/10.1093/nar/gkh340

Fang PW (1936) *Sinocyclocheilus tingi*, a new genus and species of Chinese barbid fishes from Yunnan. Sinensia 7: 588–593.

Farnsworth A, Lunt DJ, Robinson SA, Valdes PJ, Roberts WHG, Clift PD, Markwick P, Su T, Wrobel N, Bragg F, Kelland SJ, Pancost RD (2019) Past East Asian monsoon evolution controlled by paleogeography, not CO2. Science Advances 5(10): eaax1697. https://doi.org/10.1126/sciadv.aax1697

Gan X, Wu TJ, Wei ML, Yang J (2013) A new blind barbine species, *Sinocyclocheilus anshuiensis* sp. nov. (Cypriniformes: Cyprinidae) from Guangxi, China. Zoological Research 34(5): 459–463.

Huang J, Gluesenkamp A, Fenolio D, Wu Z, Zhao Y (2017) Neotype designation and redescription of *Sinocyclocheilus cyphotergous* (Dai) 1988, a rare and bizarre cavefish species distributed in China (Cypriniformes: Cyprinidae). Environmental Biology of Fishes 100(11): 1483–1488. https://doi.org/10.1007/s10641-017-0658-2

Jiang WS, Li J, Lei XZ, Wen ZR, Han YZ, Yang JX, Chang JB (2019) *Sinocyclocheilus sanxiaensis*, a new blind fish from the Three Gorges of Yangtze River provides insights into speciation of Chinese cavefish. Zoological Research 40(6): 552–557. https://doi.org/10.24272/j.issn.2095-8137.2019.065

Kumar S, Stecher G, Tamura K (2016) MEGA7: Molecular evolutionary genetics analysis version 7.0 for bigger datasets. Molecular Biology and Evolution 33(7): 1870–1874. https://doi.org/10.1093/molbev/msw054

Lan JH, Zhang CG, Zhao YH (2004) A new speces of the genus *Sinocyclocheilus* from China (Cyprinformes, Cyprinidae, Barbinae). Acta Zootaxonomica Sinica 29(2): 377–380. [In Chinese]

Lan JH, Gan X, Wu TJ, Yang J (2013) Cave Fishes of Guangxi, China. Science Press, Beijing. [In Chinese]

Lan YB, Qin XC, Lan JH, Xiu LH, Yang J (2017) A new species of the genus *Sinocyclocheilus* (Cypriniformes, Cyprinidae) from Guangxi, China. Journal of Xinyang Normal University (Natural Science Edition) 30(1): 97–101. https://doi.org/10.3969/j.issn.1003-0972.2017.01.021 [In Chinese]

Lanfear R, Frandsen PB, Wright AM, Senfeld T, Calcott B (2017) PartitionFinder 2: New methods for selecting partitioned models of evolution for molecular and morphological phylogenetic analyses. Molecular Biology and Evolution 34(3): 772–773. https://doi.org/10.1093/molbev/msw260

Li WX (1985) Four species of *Sinocyclocheilus* from Yunnan. Zoological Research 6(4): 423–427. [In Chinese]

Li GL (1989) On a new fish of the genus *Sinocyclocheilus* from Guangxi China (Cypriniformes: Cyprinidae: Barbinae). Acta Zootaxonomica Sinica 14(1): 123–126. [In Chinese]

Li WX (1992) Description on three species of *Sinocyclocheilus* from Yunnan, China. Acta Hydrobiologica Sinica 16(1): 57–61. [In Chinese]

Li WX, An L (2013) A new species of Sinocyclocheilus from Kunming, Yunnan—*Sinocyclocheilus wui* sp. nov. Journal of Jishou University 34(1): 82–84. [Natural Science Edition] [In Chinese]

Li WX, Lan JH (1992) A new genus and three new species of Cyprinidae from Guangxi, China. Journal of Zhanjiang Fisheries College 12(2): 46–51.

Li J, Li XH (2014) *Sinocyclocheilus gracilis*, a new species of hypogean fish from Guangxi, South China (Teleostei: Cypriniformes: Cyprinidae). Ichthyological Exploration of Freshwaters 24(3): 249–256.

Li WX, Mao WN (2007) A new species of the genus *Sinocyclocheilus* living in cave from Shilin, Yunnan, China (Cypriniformes, Cyprinidae). Acta Zootaxonomica Sinica 32(1): 226–229. [In Chinese]

Li WX, Tao JN (1994) A new species of Cyprinidae from Yunnan—*Sinocyclocheilus rhinocerous*, sp. nov. Joumal of Zhanjiang Fisheries College 14(1): 1–3. [In Chinese]

Li WX, Wu DF, Chen AL (1998) Two new species of *Sinocyclocheilus* from Yunnan, China. (Cypriniformes: Cyprinidae). Journal of Zhanjiang Ocean University 18(4): 1–5. [In Chinese]

Li WX, Zong ZG, Nong RB, Zhao CH (2000a) A New Species of *Sinocyclocheilus* from Yunnan—*Sinocyclocheilus maculatus* Li, sp. nov. Journal of Yunnan University 22(1): 79–80. [In Chinese]

Li WX, Xiao H, Zan RG, Luo ZF, Li HM (2000b) A new species of *Sinocyclocheilus* from Guangxi, China. Zoological Research 21(2): 155–157. [In Chinese]

Li WX, Mao WN, Lu ZM, Tao JN (2002a) Two new species of Cyprinidae from Yunnan. Journal of Yunnan University 24(5): 385–387. [In Chinese]

Li WX, Liao YP, Yang HF (2002b) Two new species of *Sinocyclocheilus* from Eastern Yunnan, China. Journal of Yunnan Agricultural University 17(2): 161–163. [In Chinese]

Li WX, Mao WL, Lu ZM (2002c) A new species of *Sinocyclocheilus* from Yunnan' China. Journal of Zhanjiang Ocean University 22(3): 1–2. [In Chinese]

Li WX, Mao WN, Lu ZM, Yan WZ (2003a) The two new species of *Sinocyclocheilus* from Yunnan, China. Journal of Jishou University 24(2): 63–65. [Natural Science Edition] [In Chinese]

Li WX, Ran JC, Chen HM (2003b) A new species of cave *Sinocyclocheilus* in Guizhou and its adaptation comment. Journal of Jishou University 24(4): 61–63. [Natural Sciences Edition] [In Chinese]

Li WX, Lan JC, Chen XY (2003c) A new species of cave *Sinocyclocheilus* from Guangxi— *Sinocyclocheilus jiuxuensis* Li et Ran, sp. nov. Journal of Guangxi Normal University 21(4): 83–85. [In Chinese]

Li WX, Xiao H, Zan RG, Luo ZY, Ban CH, Fen JB (2003d) A new species of *Sinocyclocheilus* from caves in Guangxi. Journal of Guangxi Normal University 21(3): 80–81. [In Chinese]

Li WX, Xiao H, Jin XL, Wu DJ (2005) A new species of *Sinocyclocheilus* from Yunnan, China. Southwest China Journal of Agricultural Sciences 18(1): 90–91. [In Chinese]

Li WX, Yang HF, Han F, Tao CP, Hong Y, Chen H (2007) A new species in cave of blind *Sinocyclocheilus* from Yunnan, China (Cypriniformes: Cyprinidae). Journal of Guangdong Ocean University 27(4): 1–3.

Li J, Li XH, Mayden RL (2014) *Sinocyclocheilus brevifinus* (Teleostei: Cyprinidae), a new species of cavefish from Guangxi, China. Zootaxa 3873(1): 37–48. https://doi.org/10.11646/zootaxa.3873.1.3

Li GH, Wu JJ, Leng Y, Zhou R, Pan XF, Han F, Li SY, Liang X (2018) A new species *Sinocyclocheilus longshanensis* sp. nov. from Yunnan. Chinese Agricultural Science Bulletin 34(5): 153–158. [In Chinese]

Li WX, Li QQ, Chen HY (2019) A new species of *Sinocyclocheilus* from Yunnan, China: *Sinocyclocheilus bannaensis*. Journal of Jishou University (Natural Science Edition) 40(1): 61–63. http://doi.org/10.13438/j.cnki.jdzk.2019.01.015 [In Chinese]

Lin RD, Luo ZF (1986) A new blind barbid fish (Pisces, Cyprinidae) from subteeranean water in Guangxi, China. Acta Hydrobiologica Sinica 10(4): 380–382. [In Chinese]

Liu T, Deng HQ, Ma L, Xiao N, Zhou J (2018) *Sinocyclocheilus zhenfengensis*, a new cyprinid species (Pisces: Teleostei) from Guizhou Province, Southwest China. Journal of Applied Ichthyology 34(4): 945–953. https://doi.org/10.1111/jai.13629

Luo FG, Huang J, Liu X, Luo T, Wen YH (2016) *Sinocyclocheilus ronganensis* Luo, Huang et Wen sp. nov., a new species belonging to *Sinocyclocheilus* Fang from Guangxi (Cypriniformes: Cyprinidae). Nanfang Nongye Xuebao 47(4): 650–655. https://doi.org/10.3969/j:issn.2095-1191.2016.04.650 [In Chinese]

Luo Q, TangQ, DengL, Duan Q, Zhang R (2023) A new cavefish of *Sinocyclocheilus* (Teleostei: Cypriniformes: Cyprinidae) from the Nanpanjiang River in Guizhou, China. Journal of Fish Biology 104(2): 1–23. https://doi.org/10.1111/jfb.15490

Mao WN, Lu ZM, Li WX, Ma HB, Huang G (2003) A new species of *Sinocyclocheilus* (Cyprinidae) from cave of Yunnan, China. Journal of Zhanjiang Ocean University 23(3): 1–2.

Mao TR, Liu YW, Meegaskumbura M, Yang J, Ellepola G, Senevirathne G, Fu CH, Gross JB, Pie MR (2021) Evolution in *Sinocyclocheilus* cavefish is marked by rate shifts, reversals, and origin of novel traits. BMC Ecology and Evolution 21(1): 1–14. https://doi.org/10.1186/s12862-021-01776-y

Mao T, Liu Y, Vasconcellos MM, Pie MR, Ellepola G, Fu C, Meegaskumbura M (2022) Evolving in the darkness: Phylogenomics of *Sinocyclocheilus* cavefishes highlights

recent diversification and cryptic diversity. Molecular Phylogenetics and Evolution 168: 107400. https://doi.org/10.1016/j.ympev.2022.107400

National Forestry and Grassland Administration, National Park Administration (2021) Announcement of the State Forestry and Grassland Administration and the Ministry of Agriculture and Rural Development (No. 3, 2021) (List of Wildlife under State Key Protection) [2021-02-05] https://www.forestry.gov.cn/main/5461/20210205/122418 860831352.html

Pan XF, Li L, Yang JX, Chen XY (2013) *Sinocyclocheilus xichouensis*, a new species of golden-line fish from the Red River drainage in Yunnan, China (Teleostei: Cypriniformes). Zoological Research 34(4): 368−373.

Rambaut A, Drummond AJ, Xie D, Baele G, SuchardMA (2018) Posterior Summarization in Bayesian Phylogenetics Using Tracer 1.7. Systematic Biology 67(5): 901−904. https://doi.org/10.1093/sysbio/syy032

Shan X, Lin R, Yue P, Chu X (2000) Barbinae. In: Yue P (Ed.) Fauna Sinica, Osteichthyes. Cypriniformes III. Science Press, Beijing. [In Chinese]

Shao WH, Cheng GY, Lu XL, Zhou JJ, Zeng ZC (2024) Description of a new troglobitic *Sinocyclocheilus* (Pisces, Cyprinidae) species from the upper Yangtze River Basin in Guizhou, South China. Zoosystematics and Evolution 100 (2): 515−529. https://doi.org/10.3897/zse.100.119520

Wang DZ, Chen YY (1989) Ddscriptions of three new species of Cyprinidae from Guizhou Province, China (Cypriniformes: Cyprinidae). Academiae Medicinae Zunyi 12(4): 29−34. [In Chinese]

Wang DZ, Liao JW (1997) A new species of *Sinocyclocheilus* from Guizhou, China (Cypriniformes: Cyprinidae: Barbinae). Acta Academiae Medicinae Zunyi 20(2/3): 1−3. [In Chinese]

Wang D, Zhao YH, Yang JX, Zhang CG (2014) A new cavefish species from Southwest China, *Sinocyclocheilus gracilicaudatus* sp. nov. (Teleostei: Cypriniformes: Cyprinidae). Zootaxa 3768(5): 583−590. https://doi.org/10.11646/zootaxa.3768.5.5

Wen H, Luo T, Wang Y, Wang S, Liu T, Xiao N, Zhou J (2022) Molecular phylogeny and historical biogeography of the cave fish genus *Sinocyclocheilus* (Cypriniformes: Cyprinidae) in southwest China. Integrative Zoology 17(2): 311−325. https://doi.org/10.1111/1749-4877.12624

Wu TJ, Liao ZP, Gan X, Li WX (2010) Two new species of *Sinocyclocheilus* in Guangxi, China (Cypriniefrmes, Cyprinidae). Journal of Guangxi Normal University (Natural Science Edition) 28(4): 116−120. https://doi.org/10.16088/j.issn.1001-6600.2010.04.008 [In Chinese]

Wu ZL, Li CQ, Lan C, Li WX (2018) Two new species of *Sinocyclocheilus* from Guangxi, China. Journal of Jishou University 39(3): 55−59. [Natural Science Edition] [In Chinese]

Xu C, Luo T, Zhou J-J, Wu L, Zhao X-R, Yang H-F, Xiao N, Zhou J (2023) *Sinocyclocheilus longicornus* (Cypriniformes, Cyprinidae), a new species of microphthalmic hypogean fish from Guizhou, Southwest China. ZooKeys 1141: 1−28. https://doi.org/10.3897/zookeys.1141.91501

Yang JX, Chen XL, Bai J, Fang DM, Qiu Y, Jiang WS, Yuan H, Bian C, Lu J, He Y, Pan XF, Zhang YL, Wang XA, You XX, Wang YS, Sun Y, Mao DQ, Liu Y, Fan GY, Zhang H, Chen XY, Zhang XH, Zheng LP, Wang JT, Cheng L, Chen JM, Ruan ZQ, Li J, Yu H, Peng C, Ma XY, Xu JM, He Y, Xu ZF, Xu P, Wang J, Yang HM, Wang J, Whitten T, Xu X, Shi Q (2016) The *Sinocyclocheilus* cavefish genome provides insights into cave adaptation. BMC Biology 14(1): 1−13. https://doi.org/10.1186/s12915-015-0223-4

Yang HF, Li QQ, Li WX (2017) A new species cave blind fish of the *Sinocyclocheilus* from Yunnan Province: *Sinocyclocheilus convexiforeheadus*. Journal of Jishou University 38(2): 58–60. [Natural Science Edition] [In Chinese]

Yang HF, Li CQ, Chen YY, Li WX (2018) A new species of *Sinocyclocheilus* from Yunnan: *Sinocyclocheilus wenshanensis*. Journal of Yunnan University (Natural Science Edition) 39(3): 507–512. [In Chinese]

Zhang CG, Dai DY (1992) A new species of the *Sinocyclocheilus* from Guangxi, China (Cypriniformes: Cyprinidae). Acta Zootaxonomica Sinica17(3): 377–380. [In Chinese]

Zhang CG, Zhao YH (2001) A new fish of *Sinocyclocheilus* from Guangxi, China with a comment on its some biological adaptation (Cypriniformes: Cyprinidae). Acta Zootaxonomica Sinica 26(1): 102–107. [In Chinese]

Zhang CG, Zhao YH, Xing YC, Zhou W, Tang WQ (2016) Species diversity and distribution of inland fishes in China. Science Press, Beijing. [In Chinese]

Zhang DR, Hui H, Yu GH, Song XQ, Liu S, Yuan SQ, Xiao H, Rao DQ (2020) Shared response to changes in drainage basin: Phylogeography of the Yunnan small narrow-mouthed frog, *Glyphoglossus yunnanensis* (Anura: Microhylidae). Ecology and Evolution 10(3): 1567–1580. https://doi.org/10.1002/ece3.6011

Zhao YH, Zhang CG (2009) Endemic fishes of *Sinocyclocheilus* (Cypriniformes: Cyprinidae) in China species diversity, cave adaptation, systematics and zoogeography. Science Press, Beijing. [In Chinese]

Zhao YH, Zhang CG (2013) Validation and re-description of *Sinocyclocheilus aluensis* Li et Xiao, 2005 (Cypriniforms: Cyprinidae). Zoological Research 34(4): 374–378.

Zhao YH, Watanabe K, Zhang CG (2006) *Sinocyclocheilus donglanensis*, a new cavefish (Teleostei: Cypriniformes) from Guangxi, China. Ichthyological Research 53(2): 121–128. https://doi.org/10.1007/s10228-005-0317-z

Zhao YH, Lan JH, Zhang CG (2009) A new cavefish species, *Sinocyclocheilus brevibarbatus* (Teleostei: Cypriniformes: Cyprinidae), from Guangxi, China. Environmental Biology of Fishes 86(1): 203–209. https://doi.org/10.1007/s10641-008-9338-6

Zheng JZ, Wang J (1990) Description of a new species of the genus *Sinocyclocheilus* from China (Cypriniformes: Cyprinidae). Acta Zootaxonomica Sinica 15(2): 251–254. [In Chinese]

Zheng CY, Xie JH (1985) One new carp of the genus *Sinocyclocheilus* (Barbinae, Cyprinidae) from Guizhou Province, China. Transactions of the Chinese Ichthyological Society 4: 123–126.

Zhou J, Zhang CG, He AY (2004) A new species of the genus *Sinocyclocheilus* from Guangxi, China (Cypriniformes, Cyprinidae). Acta Zootaxonomica Sinica 29(3): 591–594. [In Chinese]

Zhou J, Li XZ, Hou XF, Sun ZL, Gao L, Zhao T (2009) A new species of *Sinocyclocheilus* in Guizhou, China. Sichuan Journal of Zoology 28(3): 321–323. [In Chinese]

Zhou J, Liu Q, Wang HX, Yang LJ, Zhao DC, Zhang TH, Hou XF (2011) Description on a new species of *Sinocyclocheilus* in Guizhou. Sichuan. Journal of Zoology 30(3): 387–389. [In Chinese]

Zhu DG, Zhu Y (2012) A new species of the genus *Sinocyclocheilus* (Cypriniformes, Cyprinidae) from Guangxi, China. Acta Zootaxonomica Sinica 37(1): 222–226. [In Chinese]

Zhu DG, Zhu Y, Lan JH (2011) Description of a new species of Barbinae, *Sinocyclocheilus huangtianensis* from China (Teleostei: Cyprinidae). Zoological Research 32(2): 204–207.

Supplementary material 1

Morphometric data for nine *S. tingi* group species

Authors: Cui Fan, Man Wang, Tao Luo, Jia-Jun Zhou, Ning Xiao, Jiang Zhou
Data type: docx

Link: https://doi.org/10.3897/zookeys.1214.127629.suppl1

Supplementary material 2

The best model obtained using PartitionFinder v. 2.1.1 evaluated under the Bayesian information criterion

Authors: Cui Fan, Man Wang, Tao Luo, Jia-Jun Zhou, Ning Xiao, Jiang Zhou
Data type: docx

Link: https://doi.org/10.3897/zookeys.1214.127629.suppl2

Supplementary material 3

Uncorrected p-distance (%) between 69 species of the genus *Sinocyclocheilus* based on mitochondrial genes

Authors: Cui Fan, Man Wang, Tao Luo, Jia-Jun Zhou, Ning Xiao, Jiang Zhou
Data type: xlsx

Link: https://doi.org/10.3897/zookeys.1214.127629.suppl3

Three new species of *Pseudopoda* Jäger, 2000 (Araneae, Sparassidae, Heteropodinae) from Qizimeishan National Nature Reserve of Hubei, China

Jian Chang[1], He Zhang[2,3], Jie Liu[2], Yang Zhu[2], Changyong Liu[4], Kuai Chen[4], Changhao Hu[1,5]

1   *The State Key Laboratory of Biocatalysis and Enzyme Engineering of China, College of Life Science, Hubei University, Wuhan 430062, Hubei, China*
2   *Hubei Key Laboratory of Regional Development and Environmental Response, Faculty of Resources and Environmental Science, Hubei University, Wuhan 430062, Hubei, China*
3   *Guo Shoujing Innovation College, Xingtai University, Xingtai 054001, Hebei, China*
4   *Qizimeishan National Nature Reserve Administration, Xuan'en 445500, Hubei, China*
5   *Hubei Broad Nature Technology Service Co., Ltd., Wuhan 430079, Hubei, China*
Corresponding author: Changhao Hu (changhaohu1998@gmail.com)

Abstract

The Qizimeishan National Nature Reserve is situated in the southwestern region of Hubei Province, adjacent to the northeastern edge of the Yunnan-Guizhou Plateau. A survey of spiders of this reserve was conducted recently, leading to the discovery of three new species of the genus *Pseudopoda* Jäger, 2000: *P. arcuata* Zhang, J. Liu & Hu, **sp. nov.** (♀), *P. qizimeishanensis* Zhang, J. Liu & Hu, **sp. nov.** (♂, ♀) and *P. weimiani* Zhang, J. Liu & Hu, **sp. nov.** (♂, ♀). Diagnoses, descriptions, photos, and a distribution map are provided.

Key words: Biodiversity, high-altitude niche, huntsman spiders, morphology, taxonomy, Yunnan-Guizhou Plateau

Introduction

The Qizimeishan National Nature Reserve is located in Xuan'en County, southwest Hubei, with a total area of 345.5 km² and the highest peak about 2010 m above sea level (Liu et al. 2006). It mainly protects the middle subtropical mountain evergreen broad-leaved forest and the subalpine sphagnum marshes wetland areas. The reserve is rich in wildlife resources and has been listed as a key area of biodiversity in the country by the China Biodiversity Conservation Action Plan (Xu et al. 2006).

The genus *Pseudopoda* Jäger, 2000 is the largest genus of the family Sparassidae Bertkau, 1872, with 256 known species (World Spider Catalog 2024). Currently, 155 *Pseudopoda* species are known in China and five in Hubei (Quan et al. 2014; Zhang et al. 2023; Gong et al. 2023; Wen et al. 2024). Recently, a series of taxonomic works on the genus was published: Wen et al. (2024) described one new species from Hubei; Wu et al. (2024) described three new species from China, Laos, and Thailand; Gong et al. (2023) described a new species from Hubei; Deng et al. (2023) described four new species from Chongqing; and Zhang et al. (2023) described 99 new species from East, South and South-

east Asia. *Pseudopoda* species are small to large spiders, living primarily in the leaf litter and less commonly on vegetation (Jäger et al. 2015).

A survey of spiders in the Qizimeishan National Nature Reserve carried out by colleagues of the Hubei University from June to July 2023 yielded three new species of *Pseudopoda*, which are described herein.

Material and methods

Specimens were examined using an Olympus SZX7 stereo microscope. Photographs were taken with a Leica M205C stereo microscope, and final multifocal images were produced with Helicon Focus (version 7.7.0). The male palps were examined and photographed after dissection. The epigynes were examined after being dissected from the spider's body. All morphological measurements were calculated using a Leica M205C stereo microscope. Eye diameters were taken at the widest point. Legs and palps measurements were given as total length (femur, patella, tibia, metatarsus [absent in palp], tarsus). The terminologies used in text and figure legends follow Quan et al. (2014). Spination follows that given in Davies (1994). All measurements were in millimetres (mm). The specimens examined in this study were deposited in the Centre for Behavioural Ecology and Evolution (CBEE), College of Life Sciences, Hubei University in Wuhan.

Abbreviations in text and figures: **AB**, anterior bands; **ALE**, anterior lateral eyes; **AME**, anterior median eyes; **C**, conductor; **CH**, clypeus height; **CO**, copulatory opening; **dRTA**, dorsal retrolateral tibial apophysis; **DS**, dorsal shield of prosoma; **E**, embolus; **EF**, epigynal field; **EP**, embolic projection; **FD**, fertilization duct; **Fe**, femur; **FW**, first winding; **LL**, lateral lobes; **Mt**, metatarsus; **OS**, opisthosoma; **Pa**, patella; **PLE**, posterior lateral eyes; **PME**, posterior median eyes; **Pp**, palp; **RTA**, retrolateral tibial apophysis; **S**, spermathecae; **Sp**, spermophor; **ST**, subtegulum; **T**, tegulum; **Ti**, tibia; **vRTA**, ventral retrolateral tibial apophysis; **I, II, III, IV**, legs I to IV.

Result

Taxonomy

Family Sparassidae Bertkau, 1872
Subfamily Heteropodinae Thorell, 1873

Genus *Pseudopoda* Jäger, 2000

Type species. *Pseudopoda prompta* (O. Pickard-Cambridge, 1885).

Diagnosis. Male *Pseudopoda* species can be diagnosed by the following combination of characters: 1) embolus at least in its basal part broadened and flattened; 2) conductor membranous (absent in some species); and 3) retrolateral tibial apophysis arising proximally or mesially from the tibia. Females can be diagnosed by the following combination of characters: 1) epigyne with lateral lobes extending distinctly beyond epigastric furrow, and covering median septum in most species; 2) first winding membranous, and with bent margins in most species; and 3) first winding or first winding and lateral lobes covering the internal duct system (Jäger, 2000; Jiang et al. 2018; Zhang et al. 2023; Wu et al. 2024).

Distribution. East, South and Southeast Asia.

Pseudopoda arcuata Zhang, J. Liu & Hu, sp. nov.

https://zoobank.org/79C05FD8-0C12-4853-A41E-E336BF9B01DD

Figs 2, 3, 10

Type material. *Holotype* • female: China, Hubei Province: Enshi Tujia and Miao Autonomous Prefecture, Xuan'en County, Qizimeishan National Nature Reserve, Chunmuying Town, Shaiping Village; 29°57'47.52"N, 109°45'20.60"E; elev. 1822 m; 31 July 2023; Changhao Hu & Mian Wei leg. (CBEE, QZMS00602). *Paratype* • 1 female, Enshi Tujia and Miao Autonomous Prefecture, Xuan'en County, Qizimeishan National Nature Reserve, Chunmuying Town, Huoshao-bao; 30°1'27.03"N, 109°45'23.23"E; elev. 1919 m; 13 July 2023; Changhao Hu & Mian Wei leg. (CBEE, QZMS00582).

Etymology. The specific epithet is a Latin word meaning "arc-shaped", referring to the arc-shaped LL; adjective.

Diagnosis. The female of *P. arcuata* Zhang, J. Liu & Hu, sp. nov. resembles that of *P. allantoides* Zhang, Jäger & Liu, 2023 (cf. fig. 2A–C vs. fig. 8A–C in Zhang et al. 2023) by having curved anterior and posterior margins of LL, but can be recognised by: 1) S extending horizontally; and 2) FD arising anteriorly from S (vs. S extending longitudinally, FD arising medially from S in *P. allantoides*).

Female: *Measurements:* Small-sized. Body length 6.0, DS length 3.0, width 2.8; OS length 2.9, width 2.0. *Eyes:* AME 0.13, ALE 0.19, PME 0.22, PLE 0.23, AME–AME 0.11, AME–ALE 0.07, PME–PME 0.21, PME–PLE 0.28, AME–PME 0.19, ALE–PLE 0.26, CH AME 0.23, CH ALE 0.19. *Spination:* Pp 131, 101, 2121, 1014; Fe I–III 323, IV 321; Pa I–IV 000; Ti I–II 2221, III–IV 2126; Mt I–II 2024, III–IV 2026. *Measurements of palp and legs:* Pp 3.4 (1.1, 0.8, 0.4, –, 1.1), I 9.3 (2.5, 1.1, 2.6, 2.2, 0.9), II 12.1 (3.2, 1.4, 3.6, 2.8, 1.1), III 7.3 (2.0, 0.7, 2.1, 1.7, 0.8), IV 9.2 (2.9, 0.9, 2.2, 2.3, 0.9). Leg formula: II-I-IV-III. Promargin of chelicerae with three teeth, retromargin with four teeth, cheliceral furrow with c. 28 denticles.

Epigyne (Fig. 2A–C): As in diagnosis. EF 2 times wider than long, without obvious AB. Anterior and posterior margins of LL almost parallel and strongly curved. FW covering the whole S. S with enlarged terminal. FD narrow and long, laterad.

Colouration (Fig. 3A, B): DS yellow, with black marks. Fovea black. Legs with black spots. Dorsal OS brown, with black spots, ventral OS dark yellow, with several black spots, with a brown patch in front of spinnerets.

Male: Unknown.

Distribution. China (Hubei Province) (Fig. 10).

Pseudopoda qizimeishanensis Zhang, J. Liu & Hu, sp. nov.

https://zoobank.org/DE4E69FA-D226-4043-A461-1E00BDCCB3B7

Figs 1, 4–6, 10

Type material. *Holotype* • male: China, Hubei Province: Enshi Tujia and Miao Autonomous Prefecture, Xuan'en County, Changtanhe Dong Autonomous Township, Qizimeishan National Nature Reserve, Qizimeishan Mountain; 30°1'45.19"N, 109°43'45.42"E; elev. 1270 m; 6–11 July 2023; Changhao Hu & Mian Wei leg. (CBEE, QZMS00902). *Paratypes* • 8 males and 10 females, with same data as for holotype (CBEE, QZMS02441–QZMS02458).

Figure 1. *Pseudopoda qizimeishanensis* Zhang, J. Liu & Hu, sp. nov. (photos by Mian Wei) **A** male **B** female.
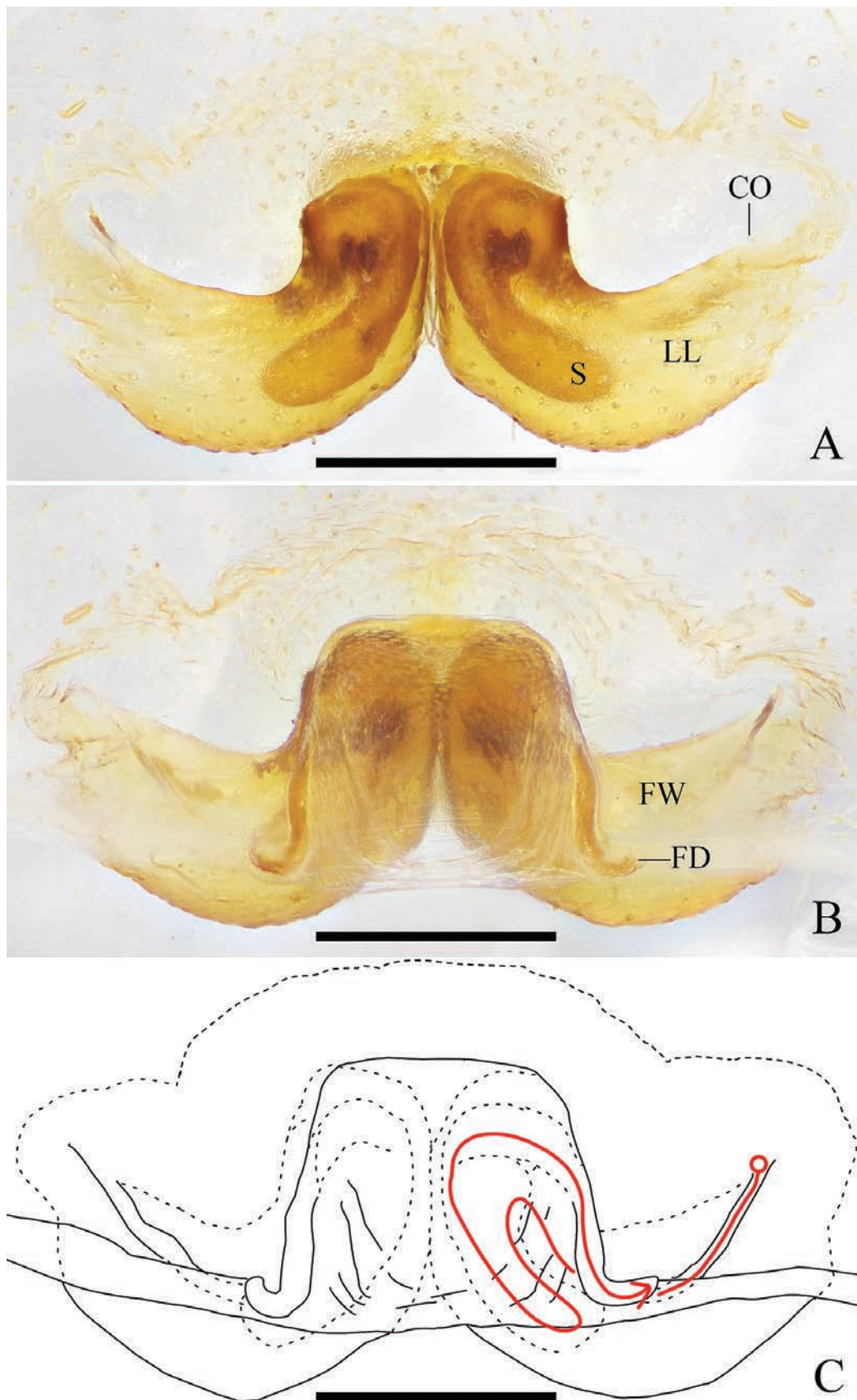
Figure 2. *Pseudopoda arcuata* Zhang, J. Liu & Hu, sp. nov., female **A** epigyne, ventral **B** vulva, dorsal **C** vulva, dorsal; red line represents schematic course of internal duct system. Abbreviations: CO, copulatory opening; FD, fertilization duct; FW, first winding; LL, lateral lobes; S, spermathecae. Scale bars: 0.2 mm.

Figure 3. *Pseudopoda arcuata* Zhang, J. Liu & Hu, sp. nov., female habitus (**A** dorsal **B** ventral). Scale bars: 2 mm.

Etymology. The specific epithet is derived from the type locality, the Qizimeishan Mountain; adjective.

Diagnosis. The male of *P. qizimeishanensis* Zhang, J. Liu & Hu, sp. nov. resembles that of *P. baoshanensis* Zhang, Jäger & Liu, 2023 (cf. fig. 4A–C vs. fig. 26A–C in Zhang et al. 2023) by having the expanded E, but can be recognised by: 1) RTA long, arising basally from Ti; 2) T without prolaterad outgrowth; and 3) tip of E pointing 11 o'clock (vs. RTA short, arising medially from Ti, T with prolaterad outgrowth, tip of E pointing 7 o'clock in *P. baoshanensis*). The female of *P. qizimeishanensis* Zhang, J. Liu & Hu, sp. nov. resembles that of *P. nanyueensis* Tang & Yin, 2000 (cf. fig. 5A–C vs. figs 2, 3 in Tang and Yin 2000) by: 1) anterior margins of LL V-shaped; 2) anterior margins of LL parallel to posterior margins of LL, but can be recognised by: S long, with wrinkles, almost parallel to anterior margins of LL (vs. S without wrinkles, extending horizontal in *P. nanyueensis*).

Male: *Measurements:* Medium-sized. Body length 14.9, DS length 7.7, width 6.6; OS length 6.8, width 4.8. *Eyes:* AME 0.29, ALE 0.42, PME 0.25, PLE 0.39, AME–AME 0.26, AME–ALE 0.17, PME–PME 0.46, PME–PLE 0.59, AME–PME 0.37, ALE–PLE 0.39, CH AME 0.72, CH ALE 0.66. *Spination:* Pp 131, 101, 2111; Fe I–II 323, III 322, IV 321; Pa I–III 101, IV 000; Ti I–II 2226, III–IV 2126; Mt I–II 2024, III 3025, IV 3036. ***Measurements of palp and legs:*** Pp 10.1 (3.3, 1.7, 1.9, –,
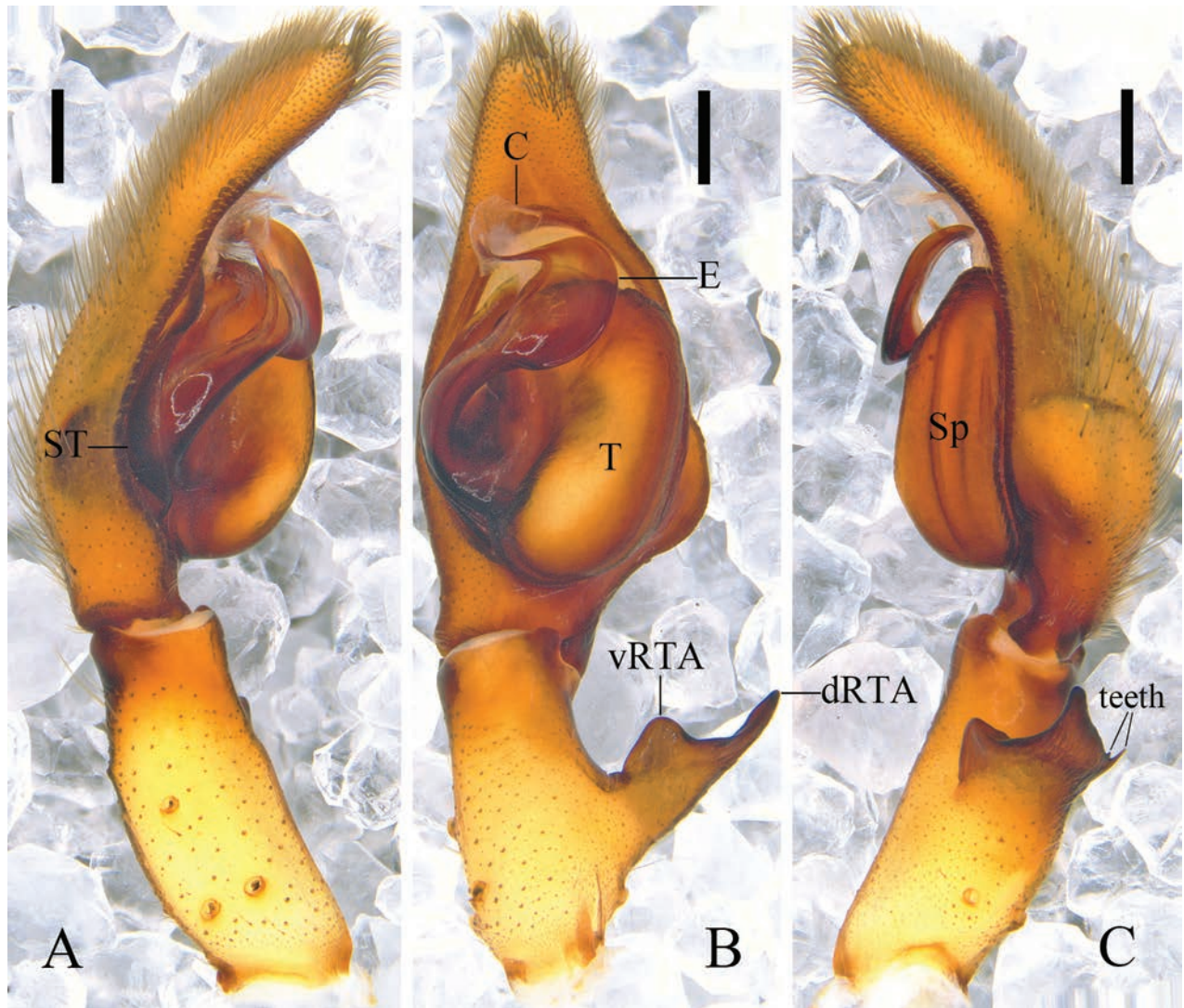
Figure 4. *Pseudopoda qizimeishanensis* Zhang, J. Liu & Hu, sp. nov., left male palp (**A** prolateral **B** ventral **C** retrolateral). Abbreviations: C, conductor; dRTA, dorsal retrolateral tibial apophysis; E, embolus; Sp, spermophor; ST, subtegulum; T, tegulum; vRTA, ventral retrolateral tibial apophysis. Scale bars: 0.5 mm.

3.2), I 33.2 (9.3, 3.0, 9.0, 8.9, 3.0), II 34.8 (9.9, 2.8, 9.5, 9.5, 3.1), III 26.6 (7.7, 2.2, 7.3, 7.0, 2.4), IV 29.5 (8.5, 2.2, 7.7, 8.6, 2.5). Leg formula: II-I-IV-III. Promargin of chelicerae with three teeth, retromargin with four teeth, cheliceral furrow with c. 26 denticles.

Palp (Fig. 4A–C): As in diagnosis. C membranous, arising from T at 11 o'clock position. E expanded and plate-like, arising from T at 9 o'clock position; embolic tip curved. RTA arising basally from Ti; vRTA triangular; dRTA long, with two thin teeth in retrolateral view.

Colouration (Fig. 6A, B): DS yellow, with black spots. Ventral legs with black spots. Dorsal OS brown, ventral OS with black spots, spinnerets yellow, with two parallel longitudinal lines of lighter dots.

Female: *Measurements:* Medium-sized. Body length 16.9, DS length 7.9, width 7.1; OS length 8.6, width 6.6. *Eyes:* AME 0.33, ALE 0.51, PME 0.31, PLE 0.42, AME–AME 0.32, AME–ALE 0.27, PME–PME 0.58, PME–PLE 0.64, AME–PME 0.44, ALE–PLE 0.41, CH AME 0.60, CH ALE 0.58. *Spination:* Pp 131, 101, 2121, 1014; Fe I–II 323, III 322, IV 321; Pa I–IV 101; Ti I–IV 2026; Mt I 1014, II–III 2024,
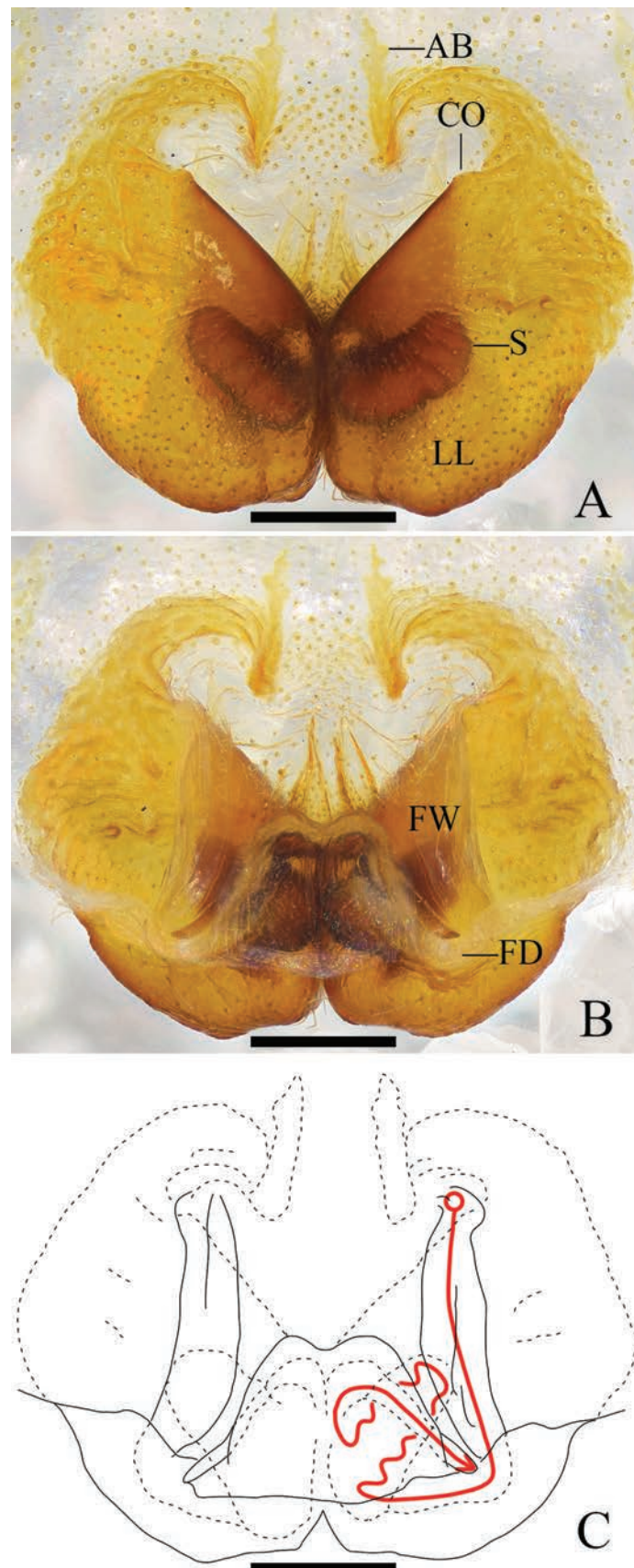
Figure 5. *Pseudopoda qizimeishanensis* Zhang, J. Liu & Hu, sp. nov., female **A** epigyne, ventral **B** vulva, dorsal **C** vulva, dorsal; red line represents schematic course of internal duct system. Abbreviations: AB, anterior bands; CO, copulatory opening; FD, fertilization duct; FW, first winding; LL, lateral lobes; S, spermathecae. Scale bars: 0.5 mm.
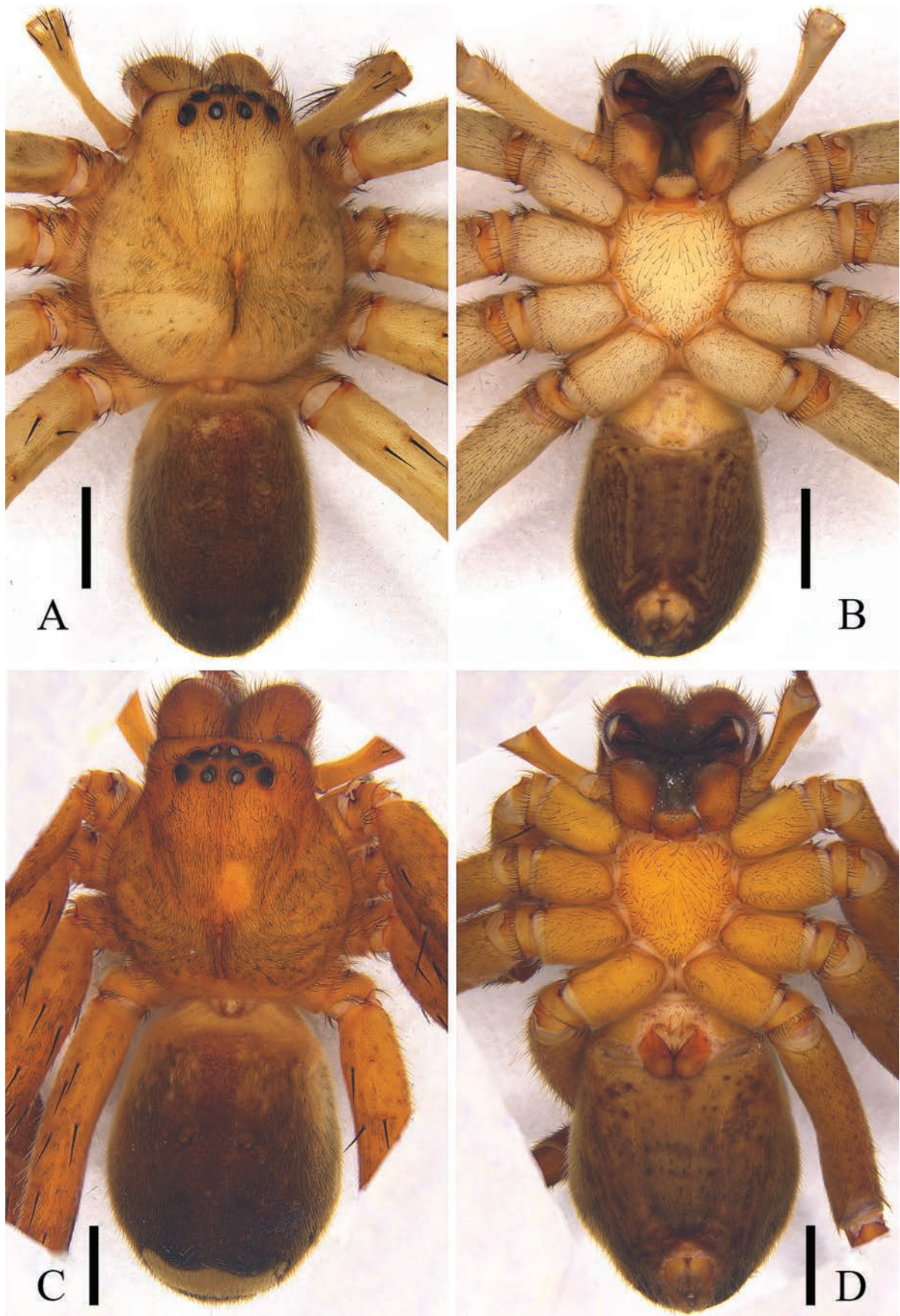
Figure 6. *Pseudopoda qizimeishanensis* Zhang, J. Liu & Hu, sp. nov. **A, B** male habitus (**A** dorsal **B** ventral) **C, D** female habitus (**C** dorsal **D** ventral). Scale bars: 2 mm.

IV 3025. ***Measurements of palp and legs:*** Pp 9.2 (2.8, 1.1, 2.1, −, 3.2), I 25.6 (7.0, 2.9, 7.0, 6.4, 2.3), II 26.9 (7.9, 2.8, 7.2, 6.8, 2.2), III 22.3 (7.0, 2.7, 5.4, 5.2, 2.0), IV 24.6 (7.6, 2.3, 5.9, 6.5, 2.3). Leg formula: II-I-IV-III. Promargin of chelicerae with three teeth, retromargin with four teeth, cheliceral furrow with c. 26 denticles.

Epigyne (Fig. 5A−C): As in diagnosis. EF as wide as long, with obvious AB. Anterior margins of LL V-shaped. S long and anterolaterally pointed, with wrinkles. FW covering entire S. FD narrow.

Colouration (Fig. 6C−D): As in males, but darker and with a transverse white patch in posterior part of dorsal OS.

Distribution. China (Hubei Province) (Fig. 10).

Pseudopoda weimiani Zhang, J. Liu & Hu, sp. nov.
https://zoobank.org/F77D7DED-DBF0-4CB9-907B-051ABD35FD04
Figs 7−10

Type material. *Holotype* • male: Сʜɪɴᴀ, Hubei Province: Enshi Tujia and Miao Autonomous Prefecture, Xuan'en County, Qizimeishan National Nature Reserve, Changtanhe Dong Autonomous Town Qizimeishan Mountain; 30°1'45.19"N, 109°43'45.42"E; elev. 1270 m; 6−11 July 2023; Changhao Hu & Mian Wei leg. (CBEE, QZMS00732). *Paratypes* • 2 males and 11 females, with same data as for holotype (CBEE, QZMS02459−QZMS02466, QZMS02779, QZMS04305−QZMS04308) • 1 male, Enshi Tujia and Miao Autonomous Prefecture, Xuan'en County, Qizimeishan National Nature Reserve, Changtanhe Dong Autonomous Town, Liangxihe Village; 29°58'46.33"N, 109°42'11.27"E; elev. 827 m; 29 June 2023; Changhao Hu & Mian Wei leg. (CBEE, QZMS00632) • 1 female, Enshi Tujia and Miao Autonomous Prefecture, Xuan'en County, Qizimeishan National Nature Reserve, Shadaogou Town, Longtan Village; 29°41'42.96"N, 109°39'46.03"E; elev. 637 m; 17 July 2023; Changhao Hu & Mian Wei leg. (CBEE, QZMS00622) • 1 female, Enshi Tujia and Miao Autonomous Prefecture, Xuan'en County, Qizimeishan National Nature Reserve, Shadaogou Town, Baishuihe Village; 29°55'25.78"N, 109°44'9.49"E; elev. 843 m; 23−24 July 2023; Changhao Hu & Mian Wei leg. (CBEE, QZMS03877).

Etymology. This species is named after one of the collectors: Mian Wei; noun in genitive case.

Diagnosis. The male of *P. weimiani* Zhang, J. Liu & Hu, sp. nov. resembles that of *P. hongqi* Deng, Zhong, Irfan & Wang, 2023 (cf. fig. 7A−C vs. figs 5−10 in Deng et al. 2023) by: 1) RTA unbranched; 2) E wide; and 3) EP distinct, but can be recognised by: 1) RTA short and smooth; and 2) EP twisted (vs. RTA long and gradually narrowing toward the tip, EP without a twist, terminal not exceeding E in *P. hongqi*). The female of *P. weimiani* Zhang, J. Liu & Hu, sp. nov. resembles that of *P. taipingensis* Zhang, Jäger & Liu, 2023 (cf. fig. 8A−C vs. fig. 237A−C in Zhang et al. 2023) by: 1) anterior margins of LL almost straight; and 2) S "八"-shaped, but can be recognised by: 1) posterior margins of LL almost straight and parallel to anterior margins; and 2) S with an obvious turning in ventral view (vs. posterior margins of LL W-shaped, S with distinct tube-like structures in *P. taipingensis*).

Male: *Measurements:* Small-sized. Body length 7.1, DS length 3.6, width 3.2; OS length 3.3, width 2.1. *Eyes:* AME 0.15, ALE 0.24, PME 0.17, PLE 0.26, AME−AME 0.13, AME−ALE 0.07, PME−PME 0.22, PME−PLE 0.28, AME−PME 0.24, ALE−PLE 0.22, CH AME 0.34, CH ALE 0.32. *Spination:* Pp 131, 101, 2111; Fe I−II

Figure 7. *Pseudopoda weimiani* Zhang, J. Liu & Hu, sp. nov., left male palp (**A** prolateral **B** ventral **C** retrolateral). Abbreviations: C, conductor; E, embolus; EP, embolic projection; RTA, retrolateral tibial apophysis; Sp, spermophor; ST, subtegulum; T, tegulum. Scale bars: 0.5 mm.

323, III–IV 322; Pa I–III 101, IV 100; Ti I–II 2228, III–IV 2126; Mt I–II 2024, III 3025, IV 3036. ***Measurements of palp and legs:*** Pp 5.1 (1.7, 0.6, 1.1, −, 1.7), I 18.8 (4.9, 1.4, 5.9, 4.8, 1.8), II 19.8 (5.5, 1.5, 6.2, 5.1, 1.5), III 14.6 (4.3, 1.0, 4.4, 3.6, 1.3), IV 17.5 (5.0, 1.1, 4.8, 4.8, 1.8). Leg formula: II-I-IV-III. Promargin of chelicerae with three teeth, retromargin with four teeth, cheliceral furrow with c. 26 denticles.

Palp (Fig. 7A–C): As in diagnosis. C membranous, arising from 12 o'clock position of T. E wide, arising from 9 o'clock position of T; EP plate-like and twisted; embolic tip with a small sharp tooth. RTA short, with smooth margin, arising medially from Ti.
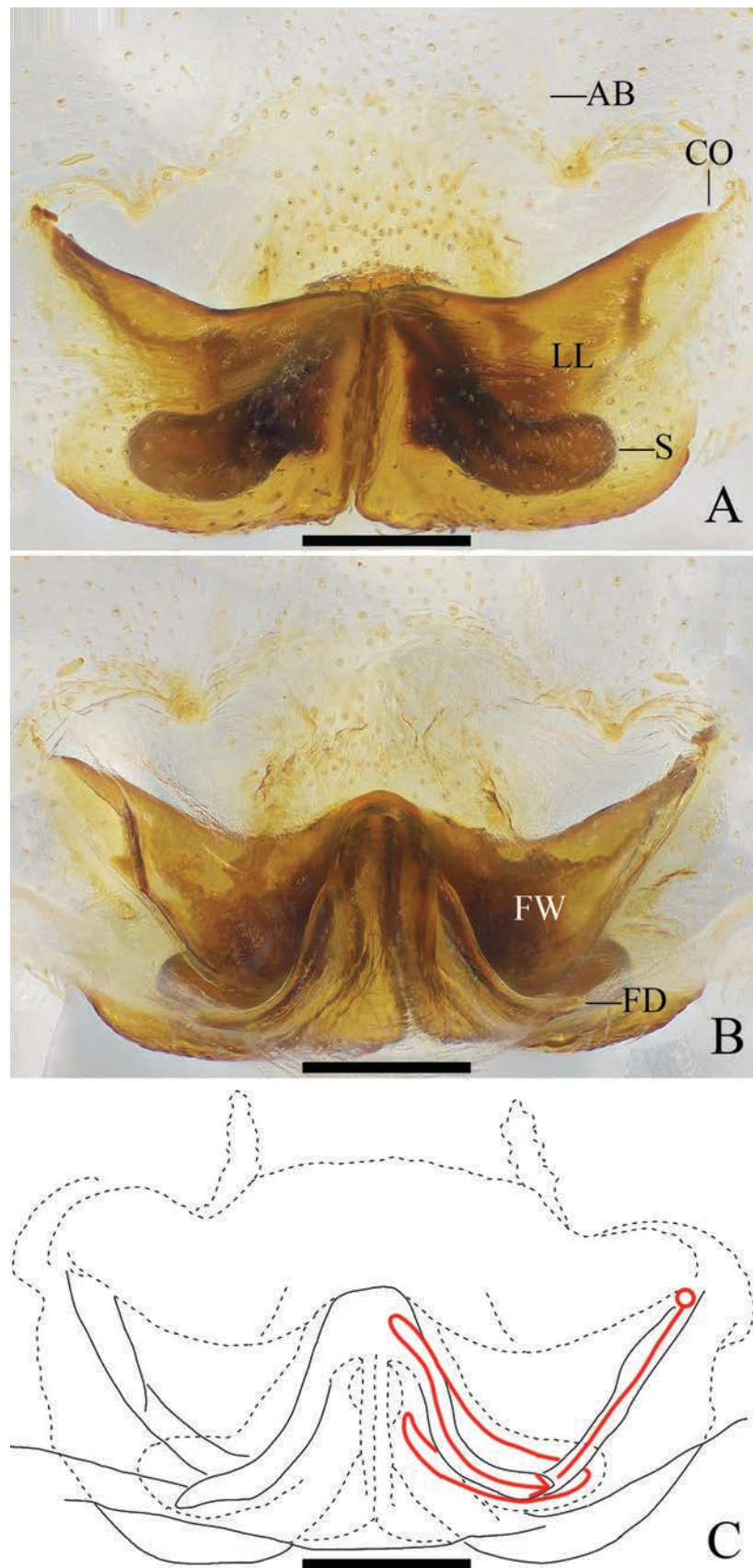
Figure 8. *Pseudopoda weimiani* Zhang, J. Liu & Hu, sp. nov., female **A** epigyne, ventral **B** vulva, dorsal **C** vulva, dorsal; red line represents schematic course of internal duct system. Abbreviations: AB, anterior bands; CO, copulatory opening; FD, fertilization duct; FW, first winding; LL, lateral lobes; S, spermathecae. Scale bars: 0.2 mm.
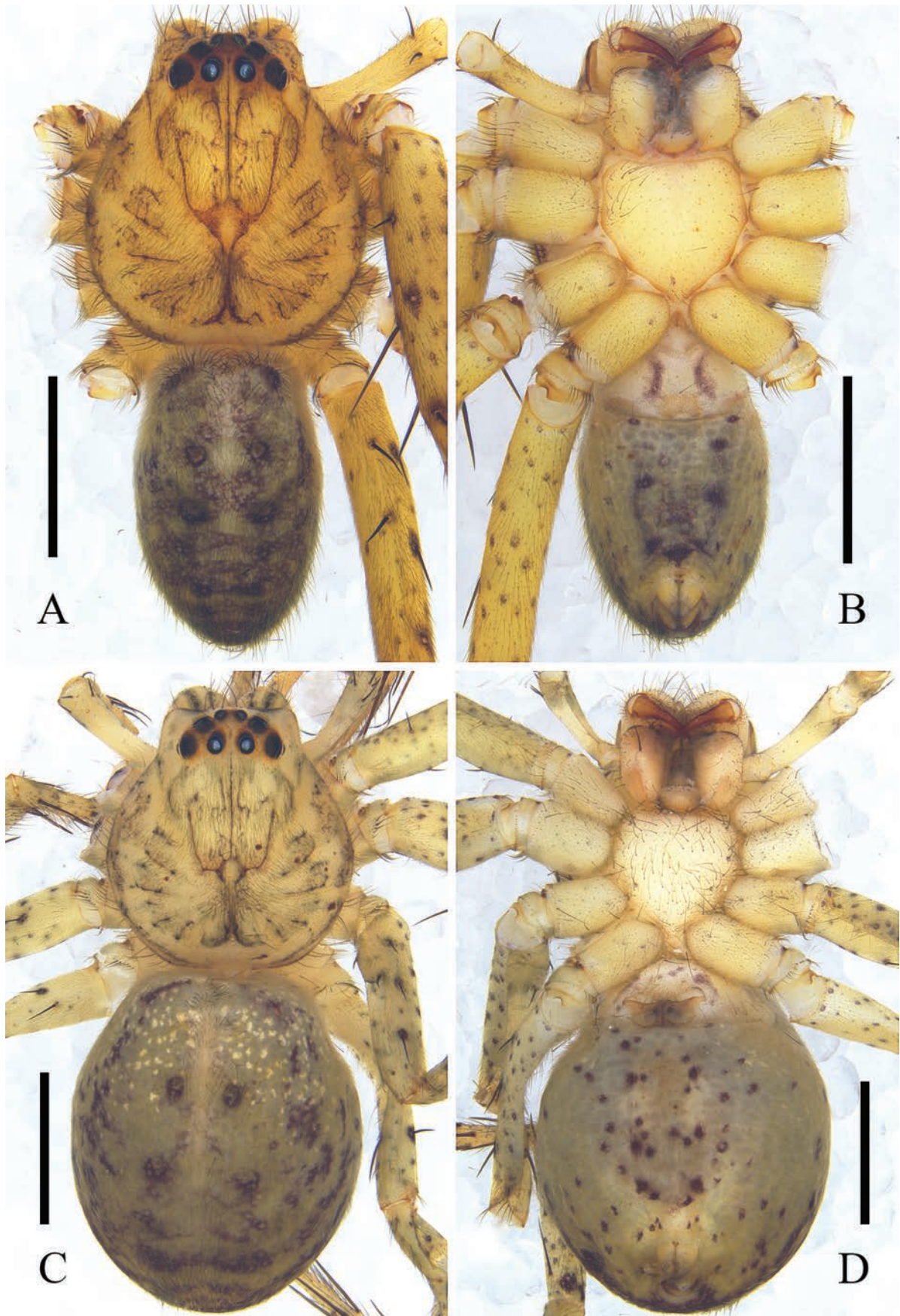
Figure 9. *Pseudopoda weimiani* Zhang, J. Liu & Hu, sp. nov. **A, B** male habitus (**A** dorsal **B** ventral) **C, D** female habitus (**C** dorsal **D** ventral). Scale bars: 2 mm.
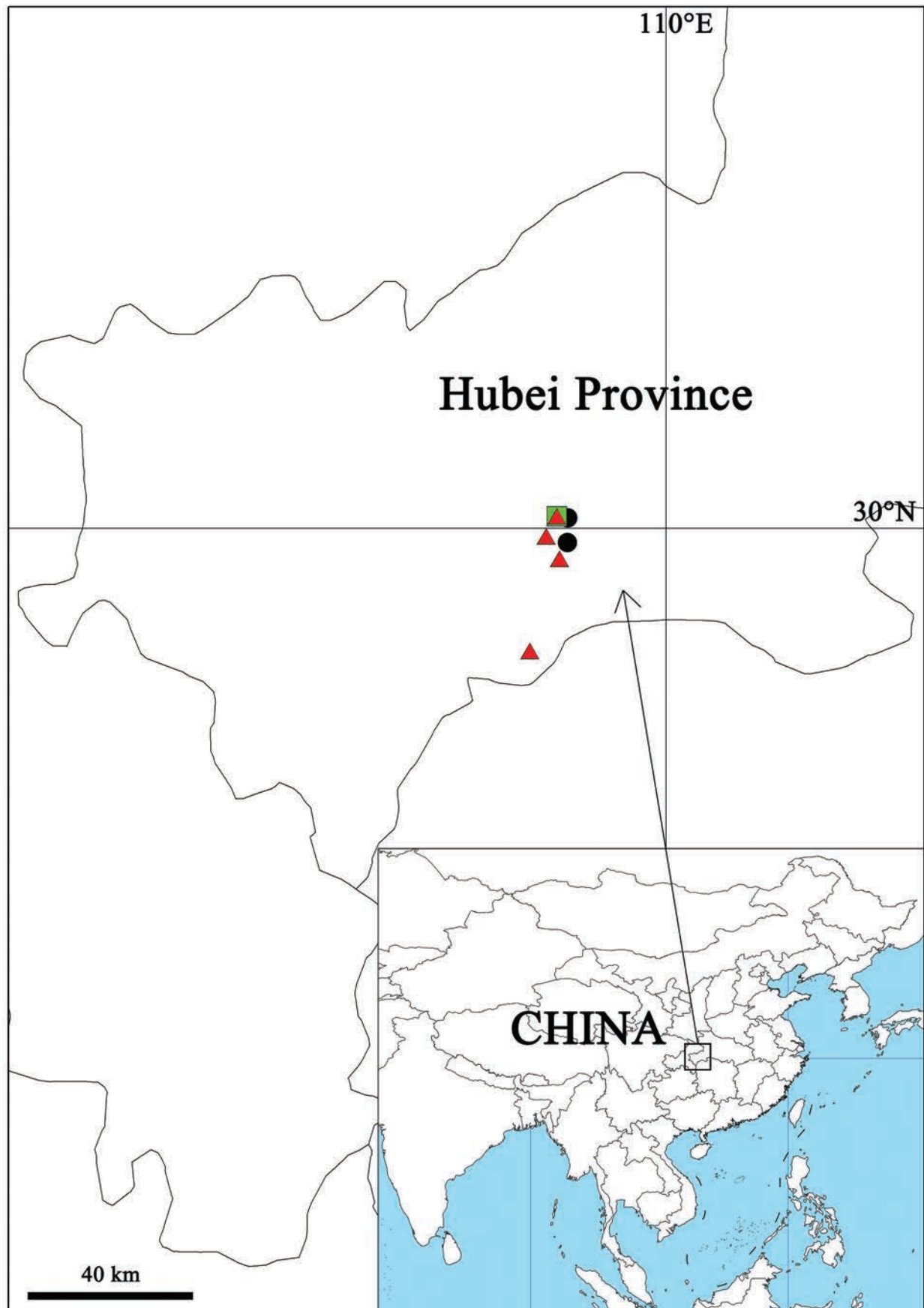
Figure 10. Distribution map of the three new species of *Pseudopoda*. Black circles: *P. arcuata* Zhang, J. Liu & Hu, sp. nov.; green square: *P. qizimeishanensis* Zhang, J. Liu & Hu, sp. nov.; red triangles: *P. weimiani* Zhang, J. Liu & Hu, sp. nov.

Colouration (Fig. 9A, B): DS yellow, with black marked and black margin. Fovea black. Legs with black spots. OS light brown, with several reddish-brown marks, regularly arranged.

Female: ***Measurements:*** Small-sized. Body length 8.2, DS length 3.6, width 3.4; OS length 4.5, width 3.9. ***Eyes:*** AME 0.15, ALE 0.18, PME 0.23, PLE 0.25, AME−AME 0.15, AME−ALE 0.11, PME−PME 0.22, PME−PLE 0.31, AME−PME 0.25, ALE−PLE 0.30, CH AME 0.32, CH ALE 0.26. ***Spination:*** Pp 131, 101, 2121, 1014; Fe I−II 323, III−IV 322; Pa I−III 101, IV 100; Ti I−II 2228, IV 2126; Mt I−II 2024, III 3025, IV 3036. ***Measurements of palp and legs:*** Pp 4.8 (1.5, 0.7, 1.0, −, 1.6), I 12.0 (3.2, 1.2, 3.4, 3.0, 1.2), II 13.9 (3.9, 1.0, 4.1, 3.6, 1.3), III 10.5 (3.2, 0.9, 2.8, 2.5, 1.1), IV 12.3 (3.8, 0.9, 3.1, 3.3, 1.2). Leg formula: II-IV-I-III. Promargin of chelicerae with three teeth, retromargin with four teeth, cheliceral furrow with c. 26 denticles.

Epigyne (Fig. 8A−C): As in diagnosis. EF wider than long, with indistinct AB. LL much wider than long, anterior margins of LL almost straight, posterior margins almost parallel to anterior margins of LL. Terminal of S twisted, posterolaterally pointed. FW covering anterior part of S. FD long and narrow.

Colouration (Fig. 9C, D): As in males, but with some bright dots in anterior part of dorsal OS.

Distribution. China (Hubei Province) (Fig. 10).

Discussion

The genus *Pseudopoda* is widely distributed across China, with 155 species accounting for approximately 61% of the world's total. The majority of these species are found in the southwestern regions, particularly on the Yunnan-Guizhou Plateau, which harbors 84 species – more than 54% of the Chinese species – highlighting the region's rich biodiversity and varied topography (Jäger 2001; Jäger and Vedel 2007; Yang et al. 2009; Zhang et al. 2013, 2017; Jiang et al. 2018; Zhang et al. 2019; Yang et al. 2022; Zhang et al. 2023). The distribution of *Pseudopoda* spiders in China is closely linked to the country's mountainous areas, where species have adapted to specific altitudinal niches. The Qizimeishan National Nature Reserve, part of the northeastern extension of the Yunnan-Guizhou Plateau, features a diverse landscape with elevations ranging from 650 m to over 2010 m (Liu et al. 2006). This variation in altitude creates a variety of microclimates and habitats that support a wide array of species. However, research on the spiders of this area remains limited.

Furthermore, *Pseudopoda* is particularly diverse in high-altitude regions (Jäger, 2001, 2015; Zhang et al. 2023), with approximately 79% of the world's species found at elevations above 1000 m. In the current study, we report three new *Pseudopoda* species, all of which were collected at elevations above 1000 m, except for *P. weimiani* Zhang, J. Liu & Hu, sp. nov., which was also found at elevations between 600 and 900 m. Finally, the limited dispersal ability of these spiders, likely due to the absence of ballooning behavior, results in small, localized populations, making these species highly susceptible to habitat changes (Bell et al. 2005; Zhang et al. 2021). Consequently, conservation efforts and taxonomic studies should prioritize the Qizimeishan National Nature Reserve to protect its unique and valuable spider fauna.

Acknowledgements

Additional information

Conflict of interest

The authors have declared that no competing interests exist.

Ethical statement

No ethical statement was reported.

Funding

Author contributions

Writing – original draft: JC, CH. Writing – review and editing: HZ, JL, YZ, CL, KC, CH.

Author ORCIDs

Jian Chang https://orcid.org/0009-0001-9840-7348
He Zhang https://orcid.org/0000-0002-1478-9837
Jie Liu https://orcid.org/0000-0001-7744-9744
Yang Zhu https://orcid.org/0009-0002-2934-6809
Changhao Hu https://orcid.org/0009-0007-5591-3121

Data availability

All of the data that support the findings of this study are available in the main text.

References

Bell JR, Bohan DA, Shaw EM, Weyman GS (2005) Ballooning dispersal using silk: world fauna, phylogenies, genetics and models. Bulletin of Entomological Research 95(2): 69–114. https://doi.org/10.1079/BER2004350

Davies VT (1994) The huntsman spiders *Heteropoda* Latreille and *Yiinthi* gen. nov. (Araneae: Heteropodidae) in Australia. Memoirs of the Queensland Museum 35(1): 75–122.

Deng MQ, Zhong Y, Irfan M, Wang LY (2023) Four new species of the spider genus *Pseudopoda* Jäger, 2000 (Sparassidae) from Yintiaoling Natural Reserve of Chongqing, China. Zootaxa 5257(1): 5–16. https://doi.org/10.11646/zootaxa.5257.1.3

Gong LJ, Zeng MY, Zhong Y, Yu HL (2023) A new species of *Pseudopoda* (Araneae, Sparassidae) from China, with the description of different and distinctive internal ducts of the female vulva. ZooKeys 1159: 189–199. https://doi.org/10.3897/zookeys.1159.97463

Jäger P (2000) Two new Heteropodine genera from southern continental Asia (Araneae: Sparassidae). Acta Arachnologica 49(1): 61–71. https://doi.org/10.2476/asjaa.49.61

Jäger P (2001) Diversität der Riesenkrabbenspinnen im Himalaya – die Radiation zweier Gattungen in den Schneetropen (Araneae, Sparassidae, Heteropodinae). Courier Forschungsinstitut Senckenberg 232: 1–136.

Jäger P (2015) Conductor-less and vertically niched: new species of the genus *Pseudopoda* (Araneae: Sparassidae: Heteropodinae) from Myanmar. Arachnology 16(9): 333–350. https://doi.org/10.13156/arac.2015.16.9.333

Jäger P, Vedel V (2007) Sparassidae of China 4. The genus *Pseudopoda* (Araneae: Sparassidae) in Yunnan Province. Zootaxa 1623: 1–38. https://doi.org/10.11646/zootaxa.1623.1.1

Jäger P, Li SQ, Krehenwinkel H (2015) Morphological and molecular taxonomic analysis of *Pseudopoda* Jäger, 2000 (Araneae: Sparassidae: Heteropodinae) in Sichuan Province, China. Zootaxa 3999(3): 363–392. https://doi.org/10.11646/zootaxa.3999.3.3

Jiang TY, Zhao QY, Li SQ (2018) Sixteen new species of the genus *Pseudopoda* Jäger, 2000 from China, Myanmar, and Thailand (Sparassidae, Heteropodinae). ZooKeys 791: 107–161. https://doi.org/10.3897/zookeys.791.28137

Liu SX, Qu JP, Jiang YF, Wang ZX, Gao EH, Lei Y (2006) Hubei Qizimeishan Nature Reserve scientific survey and research report. Hubei Science and Technology Press, Wuhan, 370 pp.

Quan D, Zhong Y, Liu J (2014) Four *Pseudopoda* species (Araneae: Sparassidae) from southern China. Zootaxa 3754(5): 555–571. https://doi.org/10.11646/zootaxa.3754.5.2

Tang G, Yin CM (2000) One new species of the genus *Pseudopoda* from south China (Araneae: Sparassidae). Acta Laser Biology Sinica 9: 274–275.

Wen LL, Li CC, Zhong Y (2024) One new species of *Pseudopoda* Jäger, 2000 from Shennongjia, Central China (Araneae, Sparassidae). Biodiversity Data Journal 12(e130445): 1–9. https://doi.org/10.3897/BDJ.12.e130445

World Spider Catalog (2024) World Spider Catalog. Version 25.0. Natural History Museum Bern. http://wsc.nmbe.ch [accessed on 20 July 2024]

Wu YR, Zhong R, Zhu Y, Jäger P, Liu J, Zhang H (2024) Description of three new species of the spider genus *Pseudopoda* Jäger, 2000 (Araneae, Sparassidae) from China, Laos and Thailand, and the female of *P. kavanaughi* Zhang, Jäger & Liu, 2023. ZooKeys 1202: 287–301. https://doi.org/10.3897/zookeys.1202.116007

Xu WH, Ouyang ZY, Huang H, Wang XK, Miao H, Zheng H (2006) Priority analysis on conserving China's terrestrial ecosystems. Acta Ecologica Sinica 2006(01): 271–280.

Yang ZZ, Chen YQ, Chen YL, Zhang YG (2009) Two new species of the genus *Pseudopoda* from Yunnan, China (Araneae: Sparassidae). Acta Arachnologica Sinica 18: 18–22.

Yang ZZ, Wu YY, Li ZM, Zhang BS (2022) Two new species of the genus *Pseudopoda* Jäger, 2000 and first description of the male of *Pseudopoda physematosa* (Araneae, Sparassidae) from Yunnan Province, China. Zootaxa 5188(4): 347–360. https://doi.org/10.11646/zootaxa.5188.4.3

Zhang F, Zhang BS, Zhang ZS (2013) New species of *Pseudopoda* Jäger, 2000 from southern China (Araneae, Sparassidae). ZooKeys 361: 37–60. https://doi.org/10.3897/zookeys.361.6089

Zhang H, Jäger P, Liu J (2017) One new *Pseudopoda* species group (Araneae: Sparassidae) from Yunnan Province, China, with description of three new species. Zootaxa 4318(2): 271–294. https://doi.org/10.11646/zootaxa.4318.2.3

Zhang H, Jäger P, Liu J (2019) Establishing a new species group of *Pseudopoda* Jäger, 2000 with the description of two new species (Araneae, Sparassidae). ZooKeys 879: 91–115. https://doi.org/10.3897/zookeys.879.35110

Zhang H, Zhong Y, Zhu Y, Agnarsson I, Liu J (2021) A molecular phylogeny of the Chinese *Sinopoda* spiders (Sparassidae, Heteropodinae): implications for taxonomy. PeerJ 9(e11775): 1–26. https://doi.org/10.7717/peerj.11775

Zhang H, Zhu Y, Zhong Y, Jäger P, Liu J (2023) A taxonomic revision of the spider genus *Pseudopoda* Jäger, 2000 (Araneae: Sparassidae) from East, South and Southeast Asia. Megataxa 9(1): 1–304. https://doi.org/10.11646/megataxa.9.1.1

ZooKeys

Research Article

Redescription of *Microphysogobio tungtingensis* (Nichols, 1926) with the description of a new species of the genus (Cypriniformes, Gobionidae) from southern China

Zhi-Xian Sun[1,2], Wen-Qiao Tang[1], Ya-Hui Zhao[2]

1 *Shanghai Universities Key Laboratory of Marine Animal Taxonomy and Evolution, Shanghai Ocean University, Shanghai, 201306, China*
2 *Key Laboratory of Zoological Systematics and Evolution, Institute of Zoology, Chinese Academy of Sciences, Beijing, 100101, China*
Corresponding authors: Ya-Hui Zhao (*zhaoyh@ioz.ac.cn*); Wen-Qiao Tang (*wqtang@shou.edu.cn*)

Citation: Sun Z-X, Tang W-Q, Zhao Y-H (2024) Redescription of *Microphysogobio tungtingensis* (Nichols, 1926) with the description of a new species of the genus (Cypriniformes, Gobionidae) from southern China. ZooKeys 1214: 161–186. https://doi.org/10.3897/zookeys.1214.127061

Abstract

Although *Microphysogobio tungtingensis* (Nichols, 1926) has been treated valid since it was described, its morphology remains vague, especially when comparing it with another similar species, *M. elongatus* (Yao & Yang, 1977). In this study, the types of both species were examined and also compared with several lots of specimens from a wide geographical range: there is no significant difference in morphology between them. Additionally, molecular evidence supported by mitochondrial gene sequence also showed low genetic distance in between. Thus, it is suggested that *M. elongatus* is a junior synonym of *M. tungtingensis*. While revising these two species, a new species, *Microphysogobio punctatus* sp. nov., was discovered that has a similar distribution with them both. However, it can be distinguished from its congeners by having a globular or oval shaped posterior air-bladder chamber which length 58.6%–82.8% of eye diameter; a narrow upper jaw cutting edge which less than half mouth width; a slender caudal peduncle with depth 34.6%–48.5% of length; and a six-branched-ray anal fin. This new species also has numerous small black spots on all fins which is also unique. The new species is morphologically and molecularly close to *M. bicolor* (Nichols, 1930).

Key words: East Asia, freshwater fish, Gobionidae, morphology, phylogeny, taxonomy

Introduction

The species of *Microphysogobio* Mori, 1934 are small gobionid fishes widely distributed in East Asia from northern Vietnam to eastern Russia, and eastern China is their main distribution region (Sun et al. 2022b; Fricke et al. 2024). They usually occur in the middle and upper reaches of the river system, preferring the sand and gravel mixed benthic habitats. Upon now, thirty-one *Microphysogobio* species were considered valid in the world, and approximately twenty-four of which were discovered in China (Sun et al. 2022a, 2022b; Fricke et al. 2024). The species in this genus has a three-lobe lower lip with developed papillae, horny sheaths on upper and lower jaw cutting margin and also a small posterior air-bladder chamber (Sun et al. 2021).

Microphysogobio tungtingensis was described by Nichols (1926a) based on one specimen collected near the lake Tungting, from Huping, Hunan (nowadays the Lake Dongting, Hubin Township in Yueyang City, Hunan Province), in the middle reaches of the Yangtze River basin. However, a more recent taxonomic study misidentified *M. tungtingensis* as a species that has only five branched anal-fin rays (vs six in holotype) based on three non-types (Luo et al. 1977). The subsequent taxonomic studies (Yue 1998; Huang et al. 2017, 2018; Sun and Zhao 2022) followed Luo et al. (1977). In fact, the branched anal-fin ray count in the genus *Microphysogobio* is conservative, and so it can be used as a key character in its taxonomy (Sun and Zhao 2022). Another species, *Microphysogobio elongatus*, originally described by Yao and Yang (in Luo et al. 1977) based on five syntypes collected in Guangxi Zhuang Autonomous Region, has a similar morphology with *M. tungtingensis*, and also a nearby distribution in the adjacent river basin (Luo et al. 1977; Yue 1998; Huang et al. 2017). This species, however, also has six branched anal-fin rays just as the holotype of *M. tungtingensis*. Therefore, a study needs to take a close look at both species and the validity of *M. elongatus*.

Although several new species were reported in recent studies (Huang et al. 2016, 2017, 2018; Sun et al. 2022b), the diversity of *Microphysogobio* is greatly underestimated. During the revision on *M. tungtingensis* and the so-called *M. elongatus*, we noticed several lots of specimens from Guangxi Zhuang Autonomous Region that were wrongly identified as *M. tungtingensis*. After thorough field investigations, with the morphological comparisons and molecular phylogenetic analyses, we describe them as a new species herein.

Materials and methods

Specimen collection, examination, and preservation

All examined specimens were collected by hand net, fish trap, or bought from the local markets. Detailed information on the specimens is listed in the section Comparative material. Specimens used for morphological study were fixed in 10% formalin solution for three days, followed by 70% ethanol alcohol for long-term preservation. Specimens used for molecular phylogenetic study were fixed in 95% ethanol. The holotype of the new species was deposited at the Institute of Zoology, Chinese Academy of Sciences, Beijing, China (**ASIZB;** abbreviation follows Leviton et al. 1985), paratypes were deposited at ASIZB, Institute of Hydrobiology, Chinese Academy of Sciences, Wuhan, China (**IHB**), and Laboratory of Ichthyology, Shanghai Ocean University, Shanghai, China (**SHOU**). The holotype of *M. tungtingensis* is stored at American Museum of Natural History, New York, the United States (**AMNH**). The syntypes of *M. elongatus* are stored at IHB. Other comparative materials are also deposited at ASIZB, IHB, and SHOU.

Morphological study

Measurements were taken point-to-point with a digital caliper to 0.01 mm on the left side of the specimens, and counts were also made on the left side of specimens. In order to make a more accurate measurement for lips structure,

photographs of the lip papillae system were taken and images were analyzed with ImageJ v. 1.52 software. Once the scale was settled, the distance between two points was measured with a straight line (Lunghi et al. 2019). Counts and measurements followed Sun et al. (2021). In order to get a general perception on external morphologic differences, 30 different measurable traits, $\log_{10}$-standardized to eliminate the allometries, were input into Past v. 4.03 (Hammer et al. 2001) for principal component analysis (PCA).

Molecular phylogenetic analyses

Molecular phylogenetic studies were based on the mitochondrial Cytochrome-*b* (Cyt-*b*) sequences. DNA was extracted from the pelvic fin on the right side of the fish. Cyt-*b* was amplified using the primers cytbF1 (5'-TGACTTGAAGAAC-CACCGTTGTA-3') and cytbR1 (5'-CGATCTTCGGATTACAAGACCGATG-3') following Huang et al. (2016). Sequencing reactions were performed according to the operating instructions of BigDye Terminator v. 3.1 (BDT), with 1 µL of primer (3.2 pmol/µL), 1 µL of template DNA, 2 µL of BigDye® Terminator v. 3.1, and 6 µL of double distilled water (dd H2O) for a total reaction volume of 10 µL. The thermo-cycling conditions were initial denaturation for 2 min at 96 °C, denaturation for 10 s at 96 °C, annealing for 10 s at 50 °C, and extension for 1 min at 60 °C. After 30 cycles, a final extension was performed at 60 °C for 3 min and the polymerase chain reaction (PCR) products were preserved at 4 °C. Sequencing was conducted by Beijing TsingKe Biotech Co., Ltd. (China).

The sequencing results were assembled using SeqMan II, and other sequences were acquired from the NCBI database. The voucher ID of each individual and GenBank accession No. are given in Table 1. Forty-three Cyt-*b* sequences of *Microphysogobio* species were included in the molecular phylogenetic analyses. *Pseudogobio guilinensis* was used as outgroup. Nucleotide sequence alignment was conducted using MEGA v. 6.0 (Tamura et al. 2013) with ClustalW. ModelFinder (Kalyaanamoorthy et al. 2017) was used to select the best-fit model using Bayesian information criterion (BIC). The Bayesian inference (BI) phylogenies were inferred using MrBayes v. 3.2.6 (Ronquist et al. 2012) under the HKY+F+G4 model (two parallel runs, 1 000 000 generations), with the initial 25% of sampled data discarded as burnin. Maximum likelihood (ML) phylogenetic analysis was conducted using MEGA 6.0 under the HKY+G+I model (10 000 bootstrap replications). Trees were visualized by using TVBOT (https://www.chiplot.online/tvbot.html; Xie et al. 2023). Each sequence was labeled with its own taxonomic nomenclature and the evolutionary divergence of sequence pairs between and within groups (i.e., species) was estimated using the Kimura 2-parameter model (Kimura 1980). In addition, two independent methods, i.e., Poisson tree process (PTP) and assemble species by automatic partitioning (ASAP), which rely on different operational criteria, were applied to infer molecular species delineation for *Microphysogobio* (Kapli et al. 2017; Puillandre et al. 2020). The rooted phylogenetic trees (both BI and ML) were uploaded to the PTP online server (http://species.h-its.org/ptp/). Aligned sequences were uploaded to the ASAP online server using the Jukes-Cantor (JC69) model (https://bioinfo.mnhn.fr/abi/public/asap/). The delineation results were visualized on the trees, respectively.

Table 1. Voucher code, sampling localities, haplotypes, and accession numbers of *Microphysogobio* species and outgroup for molecular analyses.

Voucher Code	Species	Locality	Drainage	Haplotype	Accession no.	Source
ASIZB 240450	*Microphysogobio punctatus* sp. nov.	Lingchuan County, Guangxi Zhuang Aut. Reg. China	R. Lijiang, Pearl River Basin	H1	–	This study
ASIZB 240452	*M. punctatus* sp. nov.	Lingchuan County, Guangxi Zhuang Aut. Reg. China	R. Lijiang, Pearl River Basin	H2	–	This study
ASIZB 240451	*M. punctatus* sp. nov.	Lingchuan County, Guangxi Zhuang Aut. Reg. China	R. Lijiang, Pearl River Basin	H3	–	This study
ASIZB 240554	*M. punctatus* sp. nov.	Yongfu County, Guangxi Zhuang Aut. Reg. China	R. Luoqingjiang, Pearl River Basin	H4	–	This study
ASIZB 240555	*M. punctatus* sp. nov.	Yongfu County, Guangxi Zhuang Aut. Reg. China	R. Luoqingjiang, Pearl River Basin	H5	–	This study
ASIZB 240539	*M. punctatus* sp. nov.	Yongfu County, Guangxi Zhuang Aut. Reg. China	R. Luoqingjiang, Pearl River Basin	H6	–	This study
ASIZB 240548	*M. punctatus* sp. nov.	Guanyang County, Guangxi Zhuang Aut. Reg. China	R. Xiangjiang, middle Yangtze River Basin	H7	–	This study
ASIZB 240549	*M. punctatus* sp. nov.	Guanyang County, Guangxi Zhuang Aut. Reg. China	R. Xiangjiang, middle Yangtze River Basin	H8	–	This study
ASIZB 240543	*M. punctatus* sp. nov.	Guanyang County, Guangxi Zhuang Aut. Reg. China	R. Xiangjiang, middle Yangtze River Basin	H9	–	This study
ASIZB 240544	*M. punctatus* sp. nov.	Guanyang County, Guangxi Zhuang Aut. Reg. China	R. Xiangjiang, middle Yangtze River Basin	H8	–	This study
ASIZB 220619	*M. bicolor*	Yanshan County, Jiangxi Prov. China	R. Xinjiang, middle Yangtze River Basin	H10	OM803135	Sun and Zhao 2022
ASIZB 220620	*M. bicolor*	Yanshan County, Jiangxi Prov. China	R. Xinjiang, middle Yangtze River Basin	H11	OM803136	Sun and Zhao 2022
ASIZB 220630	*M. bicolor*	Wuyuan County, Jiangxi Prov. China	R. Raohe, middle Yangtze River Basin	H12	OM803140	Sun and Zhao 2022
ASIZB 220646	*M. bicolor*	Wuyuan County, Jiangxi Prov. China	R. Raohe, middle Yangtze River Basin	H13	OM803141	Sun and Zhao 2022
MYUVN1	*M. yunnanensis*	Dien Bien Prov. Vietamn	R. Lixianjiang, Red River Basin	H14	MK133329	Huang et al. 2018
MLURJ1	*M. luhensis*	Luhe County, Guangdong Prov. China	Rongjiang River Basin	H15	KT877355	Huang et al. 2018
MKAND1	*M. kachekensis*	Nankai Town, Hainan Prov. China	Nandujiang River Baisn	H16	KM999930	Huang et al. 2016
ASIZB 240446	*M. tungtingensis*	Xiangtan City, Hunan Prov. China	R. Xiangjiang, middle Yangtze River Basin	H17	–	This study
ASIZB 240445	*M. tungtingensis*	Xiangtan City, Hunan Prov. China	R. Xiangjiang, middle Yangtze River Basin	H18	–	This study
ASIZB 240430	*M. tungtingensis*	Yuelu District, Hunan Prov. China	R. Xiangjiang, middle Yangtze River Basin	H19	–	This study
ASIZB 240431	*M. tungtingensis*	Yuelu District, Hunan Prov. China	R. Xiangjiang, middle Yangtze River Basin	H20	–	This study
ASIZB 240462	*M. elongatus*	Yongfu County, Guangxi Zhuang Aut. Reg. China	R. Luoqingjiang, Pearl River Basin	H17	–	This study
ASIZB 240461	*M. elongatus*	Yongfu County, Guangxi Zhuang Aut. Reg. China	R. Luoqingjiang, Pearl River Basin	H17	–	This study
ASIZB 240463	*M. elongatus*	Yongfu County, Guangxi Zhuang Aut. Reg. China	R. Luoqingjiang, Pearl River Basin	H21	–	This study
ASIZB 240553	*M. elongatus*	Yangshuo County, Guangxi Zhuang Aut. Reg. China	R. Lijiang, Pearl River Basin	H17	–	This study
MELQZ1	*M. elongatus*	Quanzhou County, Guangxi Zhuang Aut. Reg. China	R. Xiangjiang, middle Yangtze River Basin	H17	KU356199	Huang et al. 2017
MFUMJ1	*M. fukiensis*	Shaowu City, Fujian Prov. China	R. Futunxi, Minjiang River Basin	H22	KM999927	Huang et al. 2016
MFUMJ2	*M. fukiensis*	Shaowu City, Fujian Prov. China	R. Futunxi, Minjiang River Basin	H23	KM999928	Huang et al. 2016
MFUMJ3	*M. fukiensis*	Xinquan Town, Fujian Prov. China	R. Tingjiang, Hanjiang River Basin	H24	KM999929	Huang et al. 2016
ASIZB 220771	*M. fukiensis*	Guangze County, Fujian Prov. China	R. Futunxi, Minjiang River Basin	H25	OM803150	Sun and Zhao 2022
ASIZB 220772	*M. fukiensis*	Guangze County, Fujian Prov. China	R. Futunxi, Minjiang River Basin	H26	OM803151	Sun and Zhao 2022
ASIZB 220802	*M. fukiensis*	Wuyishan City, Fujian Prov. China	R. Jianxi, Minjiang River Basin	H27	OM803152	Sun and Zhao 2022

Voucher Code	Species	Locality	Drainage	Haplotype	Accession no.	Source
ASIZB 220803	*M. fukiensis*	Wuyishan City, Fujian Prov. China	R. Jianxi, Minjiang River Basin	H27	OM803153	Sun and Zhao 2022
20170925BB05	*M. kiatingensis*	Chengdu City, Sichuan Prov. China	Upper Yangtze River Basin	H28	MG797640	Zou et al. 2018
MZHGC1	*M. zhangi*	Gongcheng County, Guangxi Zhuang Aut. Reg. China	R. Gongchenghe, Pearl River Basin	H29	KT877354	Huang et al. 2017
MZHGL1	*M. zhangi*	Guilin City, Guangxi Zhuang Aut. Reg. China	R. Lijiang, Pearl River Basin	H30	KU356194	Huang et al. 2017
MZHQZ1	*M. zhangi*	Quanzhou County, Guangxi Zhuang Aut. Reg. China	R. Xiangjiang, middle Yangtze River Basin	H31	KU356196	Huang et al. 2017
ASIZB 220682	*M. zhangi*	Yanshan County, Jiangxi Prov. China	R. Xinjiang, middle Yangtze River Basin	H32	OM803145	Sun and Zhao 2022
ASIZB 220715	*M. zhangi*	Wuyuan County, Jiangxi Prov. China	R. Raohe, middle Yangtze River Basin	H33	OM803148	Sun and Zhao 2022
MABC01	*M. alticorpus*	Chiayi County, Taiwan Prov. China	Bazhang River Basin	H34	KM031524	Jean et al. 2014
MXIML1	*M. xianyouensis*	Xianyou County, Fujian Prov. China	Mulanxi River Basin	H35	KM999931	Huang et al. 2016
ASIZB 220826	*M. oujiangensis*	Jinyun County, Zhejiang Prov. China	R. Panxi, Oujiang River Basin	H36	OM803130	Sun et al. 2022b
MBDH01	*M. brevirostris*	Taoyuan City, Taiwan Prov. China	R. Dahan, Tamshui River Basin	H37	KP168487	Chang et al. 2016
Outgroup						
PG-YS01	*Pseudogobio guilinensis*	Yangshuo County, Guangxi Zhuang Aut. Reg. China	R. Lijiang, Pearl River Basin		KX096699	He et al. 2017

Results

Taxonomic account

Microphysogobio tungtingensis (Nichols, 1926)
Figs 1, 2; Table 2

Pseudogobio tungtingensis Nichols, 1926: 4 (original description); Nichols (1943): 180.
Microphysogobio tungtingensis: Bănărescu and Nalbant (1966): 201 (partim: Huping on lake Tungting, Hunan).
Abbottina elongata: Yao and Yang in Luo et al. (1977): 524.
Microphysogobio elongatus: Yue (1998): 362 (partim: Guilin, Liujiang, and Ningming in Guangxi); Zhang and Zhao (2016): 74; Xiao and Lan (2023): 154.
Microphysogobio kiatingensis: Xiao and Lan (2023): 152.

Material examined. *Holotype*. • AMNH 8447, 51.3 mm standard length (SL); Huping (= Hubin), Tungting Lake (= Lake Dongting), Hunan (= Hunan Province), China; collected by Clifford H. Pope; 1921.

Additional material examined. • ASIZB 240436−44, 9 specimens, 50.8−73.0 mm SL; Changsha City, Hunan Province, from the confluence of the Jinjianghe River and the Xiangjiang River (28.13403751°N, 112.95238278°E, 29 m a.s.l.); collected by Mr. Tao Jiang, 22 October 2022 • ASIZB 240430−2, 3 specimens, 58.9−69.4 mm SL; Ximaowu Village, Yisuhe Township, Xiangtan County, Xiangtan City, Hunan Province, from the Juanshui River (27.73808121°N, 112.88006622°E, 36 m a.s.l.); collected by Mr. Tao Jiang; 7 December 2022 • ASIZB 240386−92, 7 specimens, 70.9−84.7 mm SL; Longxia Village, Hukou Township, Chaling County, Zhuzhou City, Hunan Province, from the Mishui River (26.56112501°N, 113.60761060°E, 144 m a.s.l.); collected by Zhixian Sun; 1 October 2020 • ASIZB

Figure 1. *Microphysogobio tungtingensis*, holotype, AMNH 8447, 51.4 mm SL **A** lateral view **B** dorsal view **C** ventral view; photographed by Dr. Thomas Vigliotta.

240395–404, 10 specimens, 54.6–74.5 mm SL; Yuelu District, Changsha City, Hunan Province, from the Jinjianghe River (28.12234231°N, 112.90897867°E, 29 m a.s.l.); collected by Mr. Tao Jiang; 8–17 June 2023 • ASIZB 240445–9, 5 specimens, 43.1–59.4 mm SL; Yuelu District, Changsha City, Hunan Province, from the Jinjianghe River (28.12234231°N, 112.90897867°E, 29 m a.s.l.); collected by Mr. Tao Jiang; 25 November 2023 • IHB 587820, 1 specimen, 65.9 mm SL; Guilin City, Guangxi Zhuang Autonomous Region, from the Lijiang River; July 1958 • IHB 587249, 587254, 587876, 3 specimens, 74.3–79.0 mm SL; Liujiang District, Liuzhou City, Guangxi Zhuang Autonomous Region, from the Liujiang River; July 1958 • IHB 587915, 1 specimen, 64.2 mm SL; Ningming County, Chongzuo City, Guangxi Zhuang Autonomous Region, from the Mingjiang River • ASIZB 240340–5, 240461–77, 23 specimens, 61.3–75.3 mm SL; Shangtai Village, Yongfu Township, Yongfu County, Guilin City, Guangxi Zhuang Autonomous Region, from the Xihe River (25.01610083°N, 109.98018869°E, 140 m a.s.l.); collected by Zhixian Sun, Chen Tian and Dong Sheng; 2 January 2024 • ASIZB 185300–5, 6 specimens, 59.4–81.4 mm SL; Jiangzhou District, Chongzuo City, Guangxi Zhuang Autonomous Region, from the Zuojiang River; 14 March 2003 • ASIZB 185204–5, 2 specimens, 59.4–61.3 mm SL; Sanjiang Dong Autonomous County, Liuzhou City, Guangxi Zhuang Autonomous Region, from the Liujiang River; 8 March 2003 • ASIZB 240393–4, 2 specimens, 72.9–74.9 mm SL; Yangshuo County, Guilin City, Guangxi Zhuang Autonomous Region, from the Lijiang River; collected by Zhixian Sun; 8 July 2019 • ASIZB 240427–8, 2 specimens, 54.6–67.9 mm SL; Pingle County, Guilin City, Guangxi Zhuang Autonomous Region, from the Lijiang
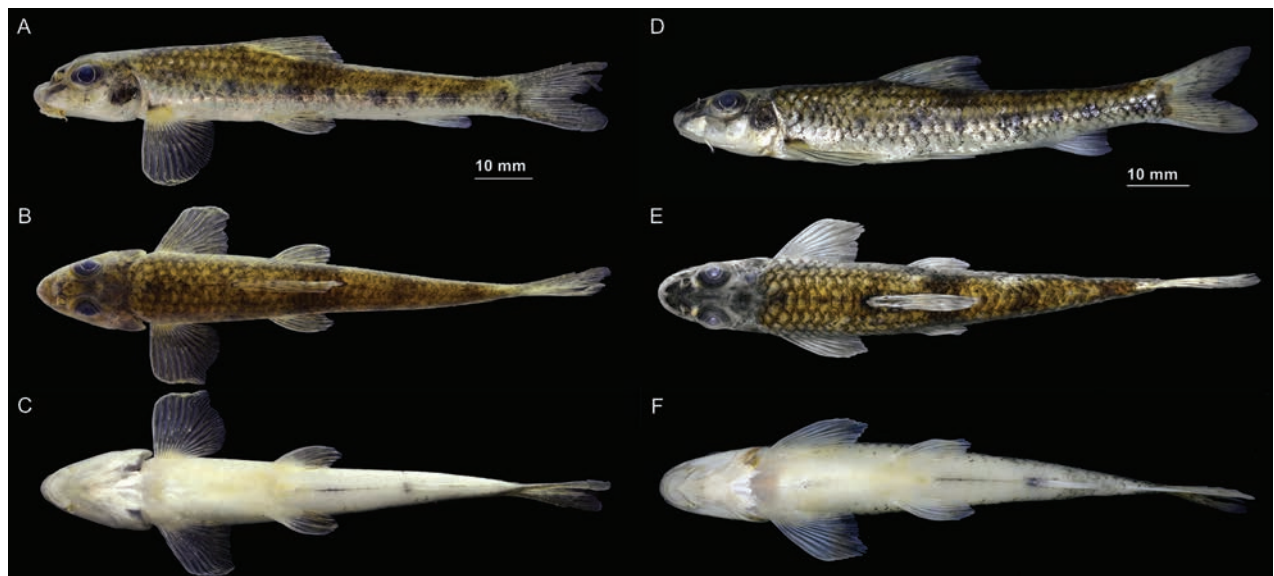
Figure 2. Lateral (**A**), dorsal (**B**), and ventral (**C**) views of *Microphysogobio tungtingensis*, ASIZB 240560, 81.8 mm SL, from the Jinjianghe River, a tributary of the Xiangjiang River, in Yuelu District, Changsha City, Hunan Province; Lateral (**D**), dorsal (**E**), and ventral (**F**) views of *M. elongatus* (= *M. tungtingensis*), ASIZB 240426, 72.3 mm SL, from the Lijiang River, the Pearl River Basin, in Pingle County, Guilin City, Guangxi Autonomous Region.

River; collected by Zhixian Sun; 16 January 2020 • ASIZB 240426, 1 specimen, 72.3 mm SL; Pingle County, Guilin City, Guangxi Zhuang Autonomous Region, from the Lijiang River; collected by Zhixian Sun; 10 January 2021.

Diagnosis. Posterior chamber of air-bladder small, elongated oval shaped, length 9.2%−11.8% of head length, and 30.4%−34.9% of eye diameter; upper jaw cutting-edge narrow, width less than half mouth width; lateral-line scales 36−39 (mode and mean 37); circumpeduncular scales 12; branched anal-fin rays 6; midventral region of body scaleless only before pectoral-fin base end.

Redescription. Body elongated, thoracic region flattened, abdomen rounded, caudal peduncle short, compressed laterally. Dorsal body profile rising from nostrils to dorsal-fin origin, dropping along dorsal-fin base, then gradually sloping to caudal-fin base. Maximum body depth at dorsal-fin origin, body depth 14.7%− 20.1% of standard length. Head elongated, length larger than body depth; snout blunt, with concavity on top of snout before nostrils; eye diameter 29.3%−38.9% of head length, located at dorsal half of head; interorbital region flattened, width smaller than eye diameter (28.6%−50.5% of eye diameter). Anus positioned at anterior one-third of distance from pelvic-fin insertion to anal-fin origin.

Mouth horseshoe-shaped and inferior, with one pair of maxillary barbels rooted at extremity of upper lip, barbel length shorter than eye diameter (35.2%−71.7% of eye diameter); upper and lower jaws with thin horny sheaths on cutting margins, upper jaw cutting edge width smaller than half mouth width (17.8%−43.2% of mouth width). Lips thick, well developed, with pearl-like papillae; central portion of anterior papillae arranged in one row with 2−4 well developed papillae, size slightly larger than other lateral side papillae; lateral portions of anterior papillae in several rows; medial pad on lower lip heart-shaped, or bisected into two oval-shape pads, rarely grooved on surface; lateral lobes on lower lip covered with multiple developed papillae, posteriorly disconnected from each other behind medial pad and laterally connected with upper lip anterior papillae at mouth corner (Fig. 3A, B).

Table 2. Morphometric measurements of *Microphysogobio tungtingensis* and *M. elongatus*. Numbers in the brackets indicate number of specimens.

| Characters | *Microphysogobio tungtingensis* (*n* = 35) | | | | *Microphysogobio elongatus* (*n* = 41) | | | | |
| | Holotype | Holotype + other specimens | | | Syntypes (*n* = 5) | | Syntypes + other specimens | | |
		Range	Mean	SD	Range	Mean	Range	Mean	SD
Branched dorsal-fin rays	7	7	7		7	7	7	7	
Branched anal-fin rays	6	6	6		6	6	6	6	
Branched pectoral-fin rays	13	11−13	12		11−12	12	11−12	12	
Branched pelvic-fin rays	7	7	7		7	7	7	7	
Lateral line scales	39	36−39	37		37−38	37	36−38	37	
Scales above lateral line	3.5	3.5	3.5		3.5	3.5	3.5	3.5	
Scales below lateral line	2	1.5−2	2		1.5−2	2	1−2	2	
Pre-dorsal scales	9	8−10	9		9−10	10	8−11	10	
Circumpeduncular scales	12	12	12		12	12	12	12	
Standard Length (mm)	51.3	43.1−84.7			64.2−79.0	72.1	54.6−81.4		
As percentage of SL									
Body depth	15.7	14.7−20.1	17.3	1.5	15.5−17.4	16.3	15.5−19.3	17.1	0.9
Head length	22.2	21.4−26.1	23.6	1.1	22.2−24.5	23.1	21.5−25.3	23.5	0.9
Dorsal-fin length	22.9	20.3−24.3	23.0	1.0	20.7−23.3	22.3	20.7−25.7	23.6	1
Dorsal-fin base length	14.8	11.6−14.8	13.3	0.7	12.5−13.4	13	12.0−14.1	13.1	0.5
Pectoral-fin length	21.2	19.0−23.7	21.2	1.2	20.4−23.6	22	19.4−25.0	22.4	1.3
Pectoral-fin base length	4.6	4.6−6.3	5.5	0.4	5.1−5.7	5.4	4.2−6.2	5.3	0.5
Pelvic-fin length	16.8	14.1−19.5	16.6	1.0	15.9−17.3	16.7	15.9−19.7	17.5	0.9
Pelvic-fin base length	3.5	3.3−4.9	4.1	0.4	3.4−4.0	3.7	3.3−4.7	4	0.4
Anal-fin length	15.0	12.7−17.7	15.0	1.1	13.5−16.0	14.5	13.5−18.1	15.7	1.1
Anal-fin base length	7.6	3.6−8.6	7.0	0.8	5.7−7.3	6.5	5.7−8.9	7	0.7
Pre-dorsal length	42.5	41.0−46.2	43.8	1.3	42.2−43.5	42.8	40.3−45.6	43.4	1.1
Pre-pectoral length	23.7	22.5−26.4	24.8	0.9	24.0−25.5	24.4	22.9−26.4	24.7	1
Pre-pelvic length	47.0	47.0−51.9	48.3	1.2	47.1−49.3	48.3	46.4−51.4	48.8	1.2
Pre-anal length	76.5	74.6−81.2	77.8	1.5	74.2−80.1	77.4	74.2−80.2	77.5	1.4
Caudal peduncle length	17.1	13.2−18.2	15.5	1.1	14.8−17.0	15.5	14.3−18.1	16	0.9
Caudal peduncle depth	7.7	7.4−9.4	8.3	0.4	7.8−8.4	8.1	7.6−9.3	8.4	0.4
Head Length (mm)	11.4	9.9−19.4			16.7	15.0−18.2	12.2−18.9		
As percentage of HL									
Head depth	57.9	46.9−60.7	54.9	3.3	53.7−56.9	55.2	48.8−59.1	54.6	2.3
Head width	65.8	49.5−65.8	59.9	3.2	52.7−58.8	55.5	52.7−62.9	58.3	2.4
Eye diameter	30.9	29.3−37.3	33.2	1.6	32.2−35.1	33.7	30.7−38.9	34.9	2.2
Interorbital width	20.8	13.4−25.2	19.3	2.9	18.5−23.2	21	16.6−23.2	19.8	1.7
Snout length	38.6	33.4−45.8	38.9	2.9	34.3−40.2	37.3	30.4−40.2	36	2
Anterior papillae length	28.4	22.3−32.0	27.3 (31)	2.6	26.4−36.9	31	25.2−36.9	28.6	2.6
Anterior papillae width	22.7	17.4−36.3	26.9 (31)	4.5	22.2−28.9	24.6	14.3−28.9	21.5	3.6
Central anterior papillae width	5.7	5.1−8.5	6.7 (31)	0.9	5.3−7.3	6.4	4.5−9.2	6.9	1.3
Upper jaw cutting edge width	7.8	4.7−9.1	6.7 (31)	1.3	6.2−7.1	6.6 (3)	4.4−7.7	5.9 (37)	0.8
Medial pad width	10.2	7.5−12.1	10.0 (31)	1.0	8.8−13.1	11.6	7.0−13.4	10.8	1.2
Mouth depth	15.1	14.7−22.7	17.9 (31)	2.0	17.7−21.2	19.1	15.2−21.2	18	1.3
Mouth width	18.0	18.0−28.6	22.4 (31)	2.7	18.8−24.2	20.9	16.9−27.2	21.2	2.5
Barbel length	20.6	12.0−23.2	16.5 (31)	2.9	15.3−24.8	18.3	14.7−24.8	17.7	2.2

Body covered with moderately small cycloid scales. Lateral line complete, almost straight in lateral center, slightly bent down under dorsal origin. Lateral line scales 36 (20 specimens), 37 (37), 38 (17), 39 (2); scales above lateral line 3.5 (76); scales below lateral line 1 (1), 1.5 (25), 2 (50); pre-dorsal scales 8 (7), 9 (33), 10 (35), 11 (1); circumpeduncular scales 12 (76). Midventral region of body scaleless only before pectoral-fin base end.

Dorsal fin with three unbranched and seven (76 specimens) branched rays; distal margin slightly concave, origin nearer to snout than caudal-fin base. Pectoral fin with one unbranched and 11 (12), 12 (50), 13 (14) branched rays; tip of

Figure 3. Lip papillae patterns of *Microphysogobio* species: **A** *M. tungtingensis*, ASIZB 240560 **B** *M. elongatus* (= *M. tungtingensis*), ASIZB 240426 **C** *M. punctatus* sp. nov., holotype, ASIZB 240329 **D** *M. punctatus* sp. nov., ASIZB 240300 **E** *M. microstomus*, SHOU 20231209017 **F** *M. zhangi*, holotype, ASIZB 204677 **G** *M. vietnamica*, ASIZB 240571 **H** *M. bicolor*, ASZIB 220638.

adpressed not reaching anterior margin of pelvic-fin base. Pelvic fin with one unbranched and seven (76) branched rays, inserted below 2nd or 3rd branched dorsal-fin ray; tip of adpressed reaching midway to anal-fin origin. Anal fin with three unbranched and six (76) branched rays; origin nearer to caudal-fin base than to pelvic-fin insertion. Caudal fin deeply forked, with nine branched rays on upper lobes and eight branched rays on lower lobes, lobes pointed.

Total vertebrae 4+34 (holotype). Gill rakers rudimentary. Pharyngeal teeth "5–5" (in one row). Air-bladder small, anterior chamber enveloped in thick fibrous capsule; posterior chamber small, elongated oval shaped, length less than half eye diameter (length 30.4%–34.9% of eye diameter), 9.2%–11.8% of head length.

Coloration in life. Dorsal side of head and body yellowish grey, mid-lateral side shallow yellowish grey, and ventral side grayish white. Dorsal side of body with four distinct black crossbars (1st and 2nd at dorsal-fin base origin and ending respectively, 3rd at vertical position above anal-fin base origin, 4th on caudal peduncle respectively). Lateral side with seven or eight small black blotches; margin of scales above lateral line slightly black pigmented, lateral-line scales without obvious black spots, margin of first row below lateral line slightly black pigmented. One fluorescent green strip extend above lateral line. Interorbital region without black crossbar. Operculum and suborbital region with two distinct

black blotches (one between anterior margin of eye and upper lip, the other expanded from posterior orbit to opercular) and one small black blotch exist between 2nd and 3rd suborbital plate. One black blotch above pectoral-fin base. Fins translucent, with small black pigments on some fin rays; dorsal-fin rays with some black spots; pectoral fin, pelvic fin with tiny black spots and lines; anal fin without spots; caudal-fin rays with two rows of black spots.

Coloration in preservation. Dorsal side of head and body brownish yellow, mid-lateral side shallow brownish yellow, and ventral side grayish white. Dorsal side of body with four distinct black crossbars in same position as live individual. Lateral side with seven or eight small dark grey blotches; margin of scales above lateral line slightly black pigmented, lateral-line scales without obvious black spots, margin of first row below lateral line slightly black pigmented. The fluorescent green strip faded. Interorbital region without black crossbar. Operculum and suborbital region with two distinct black blotches in same position as live individual, and one small black blotch exist between 2nd and 3rd suborbital plate. One black blotch above pectoral-fin base. Fins pale, with small black pigments on some fin rays; dorsal-fin rays with some black spots; pectoral fin, pelvic fin with tiny black spots and lines; anal fin without spots; caudal-fin rays with two rows of black spots. The black pigments on fin rays faded after long-time preserve.

Sexual dimorphism. No significant sexual dimorphism observed.

Distribution. *Microphysogobio tungtingensis* is distributed in the Xiangjiang River system and the Lake Dongting of the middle Yangtze River basin. It is also found distributed in the Xijiang River system, which belongs to the Pearl River basin (Fig. 4).
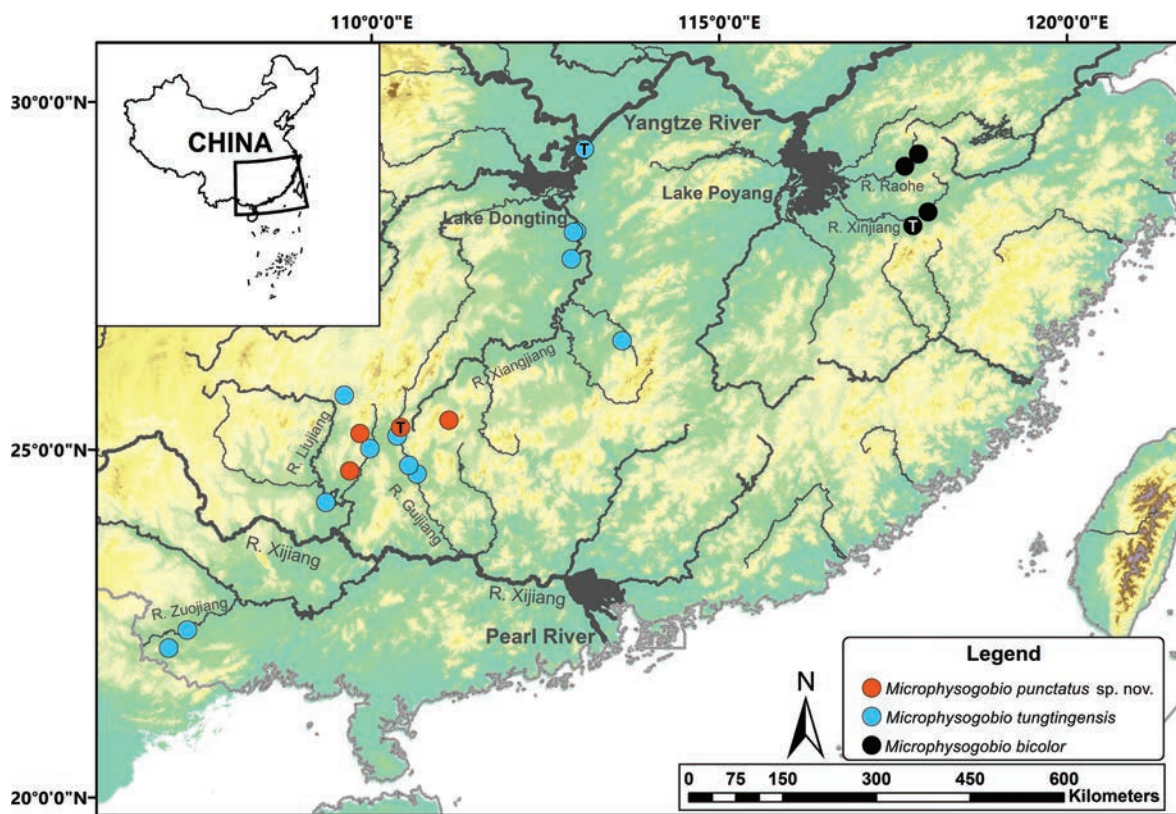

Figure 4. The distribution of the *Microphysogobio punctatus* sp. nov., *M. tungtingensis* and *M. bicolor*. "T" in circles indicates the type locality of each species.

Habitat and biology. *Microphysogobio tungtingensis* inhabits the slow flowing water of rivers. It usually appears in areas with sandy bottoms with gravel and pebbles like other congeners. It can also be found in the water body with muddy bottom.

Etymology. The name, *tungtingensis*, refers to its type locality, Lake Dongting. Chinese common name for this species is "洞庭小鳔鮈".

Microphysogobio punctatus sp. nov.

https://zoobank.org/F4C9B518-70FC-4A3B-928C-A305F9511A78
Figs 5, 6; Table 3

Microphysogobio kiatingensis: Wen (2006): 226.
Microphysogobio tungtingensis: Xiao and Lan (2023): 156.

Type material. *Holotype.* • ASIZB 240329, 75.4 mm SL; Lingchuan County, Guilin City, Guangxi Zhuang Autonomous Region, from the Huangshahe River, a tributary of the Lijiang River (25.3202379°N, 110.42292216°E, 166 m a.s.l.); collected by Zhixian Sun, Chen Tian, and Weihan Shao, 31 December 2023. *Paratypes.* • ASIZB 240330–5 (6 specimens), 240450–60 (11 specimens), 53.4–78.9 mm SL; IHB-T-A0000009, 1 specimen, 73.7 mm SL; SHOU 20231231061, 1 specimen, 73.8 mm SL; same collection information as holotype.

Additional material examined. • ASIZB 240528–38, 11 specimens, 56.0–75.2 mm SL; Guanyang County, Guilin City, Guangxi Zhuang Autonomous Region, from the Guanjiang River, a tributary of the Xiangjiang River; collected by Zhixian Sun; 5 December 2020 • ASIZB 240505–10, 6 specimens, 53.9–73.1 mm SL; Guanyang County, Guilin City, Guangxi Zhuang Autonomous Region, from the Guanjiang River, a tributary of the Xiangjiang River; collected by Zhixian Sun; 20 January 2021 • ASIZB 240511–27, 17 specimens, 47.4–78.2 mm SL; Guanyang County, Guilin City, Guangxi Zhuang Autonomous Region, from the Guanjiang River, a tributary of the Xiangjiang River; collected by Zhixian Sun; 31 December 2021 • ASIZB 240539–42, 4 specimens, 58.1–70.7 mm SL; Yongfu County, Guilin City, Guangxi Zhuang Autonomous Region, from the Luoqingjiang River; collected by Junhao Huang and Zhuocheng Zhou; 27 November 2020 • ASIZB 240300–14, 240423–8, 21 specimens, 65.0–76.0 mm SL; IHB-YF-2024010201–3, 3 specimens, 71.3–76.9 mm SL; SOU 20240102121–3, 3 specimens, 69.2–74.0 mm SL; Shebian Village, Longjiang Township, Yongfu County, Guilin City, Guangxi Zhuang Autonomous Region, from the Xihe River, a tributary of the Luoqingjiang River (25.22972694°N, 109.83651085°E, 205 m a.s.l.); collected by Zhixian Sun, Chen Tian and Dong Sheng; 2 January 2024.

Diagnosis. This new species can be distinguished from its congeners by a combination of the following characteristics: Posterior chamber of air-bladder small, globular or oval shaped, length 15.8%–26.4% of head length, and 58.6%–82.8% of eye diameter; upper jaw cutting-edge narrow, width less than half mouth width; caudal peduncle slender, depth 34.6%–48.5% of length; lateral-line scales 37–40 (mode 38, mean 39); circumpeduncular scales 12; branched anal-fin rays 6; midventral region of body scaleless only before pectoral-fin base end; all fins with numerous small black spots.

Figure 5. *Microphysogobio punctatus* sp. nov., holotype, ASIZB 240329, 75.4 mm SL **A** lateral view **B** dorsal view **C** ventral view; photos were taken after fixed by formalin.

Description. Body elongated, thoracic region flattened, abdomen rounded, caudal peduncle slender, compressed laterally. Dorsal body profile rising from nostrils to dorsal-fin origin, dropping along dorsal-fin base, then gradually sloping to caudal-fin base. Maximum body depth at dorsal-fin origin, body depth 14.6%–19.5% of standard length. Head elongated, length larger than body depth; snout blunt, with moderate concavity on top of snout before nostrils; eye diameter 30.7%–38.5% of head length, positioned at dorsal half of head; interorbital region flattened, width smaller than eye diameter (39.2%–67.9% of eye diameter). Anus positioned at anterior one-third of distance from pelvic-fin insertion to anal-fin origin.

Mouth horseshoe-shaped and inferior, with one pair of maxillary barbels rooted at extremity of upper lip, barbel length shorter than eye diameter (26.4%–79.3% of eye diameter, 54.4% in average); upper and lower jaws with thin horny sheaths on cutting margins, upper jaw cutting edge width smaller than half mouth width (22.0%–46.8% of mouth width, 35.2% in average). Lips thick, well developed, with pearl-like papillae; central portion of anterior papillae arranged in one row, usually consists 2–6 papillae, tightly contact with each other (occasionally separated, Fig. 3C), size slightly larger than other lateral
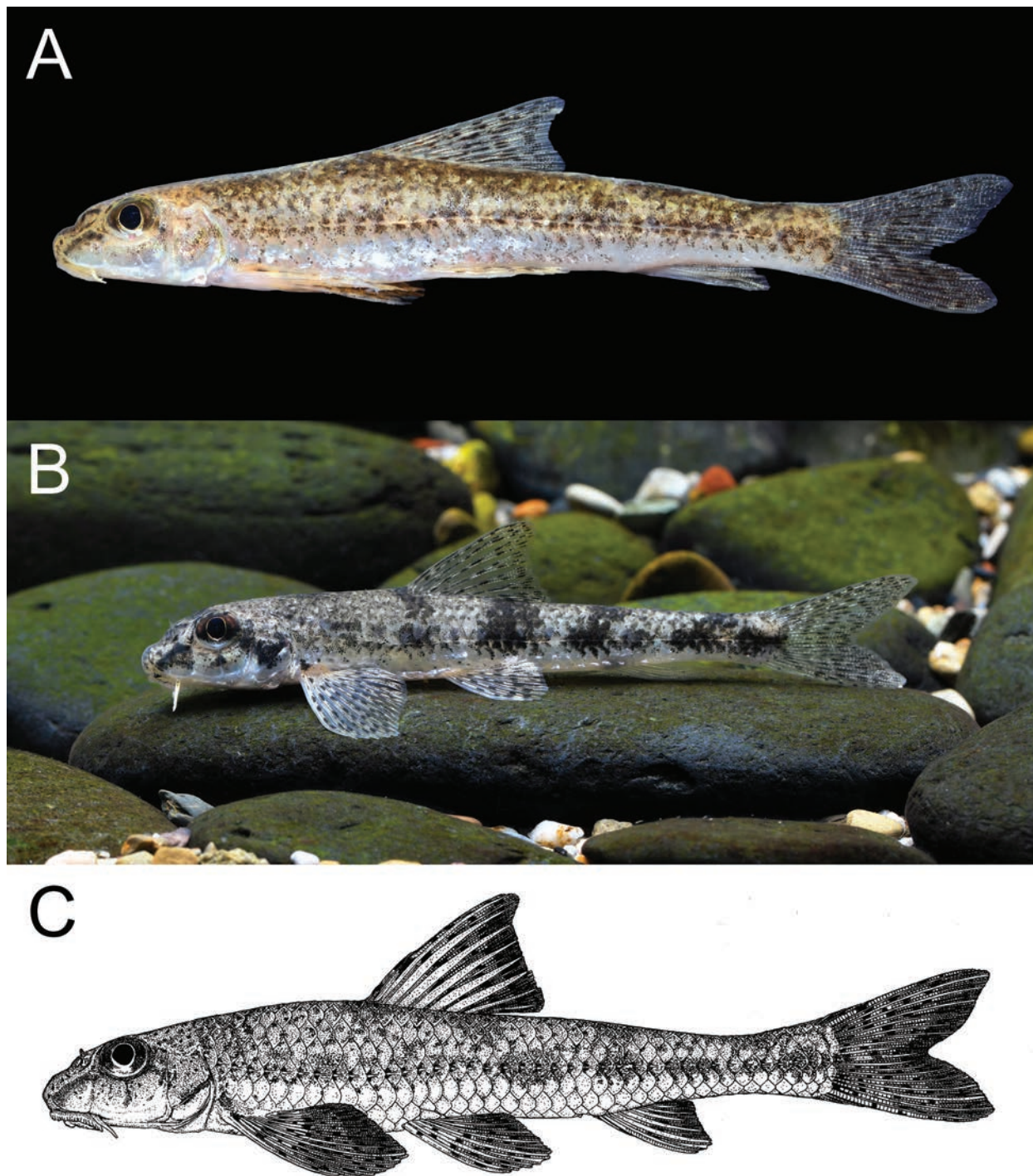
Figure 6. A Freshly caught *Microphysogobio punctatus* sp. nov. from its type locality, uncatalogued **B** live individual from Luzhai County, Liuzhou City, Guangxi Autonomous Region in Luoqingjiang River, collected and photographed by Dr. Fan Li **C** original drawing by Zhi-Xian Sun based on individual collected from Yongfu County, Guilin City, Guangxi Autonomous Region in Xihe River.

side papillae; lateral portions of anterior papillae in several rows; medial pad on lower lip heart-shaped, shallow grooved on surface; lateral lobes on lower lip covered with multiple developed papillae, posteriorly disconnected from each other behind medial pad and laterally connected with upper lip anterior papillae at mouth corner (Fig. 3C, D).

Table 3. Morphometric measurements of *Microphysogobio punctatus* sp. nov. and *M. bicolor*.

| Characters | *Microphysogobio punctatus* sp. nov. (*n* = 85) | | | | *Microphysogobio bicolor* (*n* = 26) | | | |
| | Holotype | Holotype + Paratypes + Other Specimens | | | Holotype | Holotype + Other Specimens | | |
		Range	Mean	SD		Range	Mean	SD
Branched dorsal-fin rays	7	7	7		7	7	7	
Branched anal-fin rays	6	6	6		5	5	5	
Branched pectoral-fin rays	12	11−13	12		12	11−12	12	
Branched pelvic-fin rays	7	7	7		7	7	7	
Lateral line scales	37	37−40	39		37	36−38	37	
Scales above lateral line	3.5	3.5−4	3.5		3.5	3.5	3.5	
Scales below lateral line	2	2	2		2	2	2	
Pre-dorsal scales	10	9−11	10		9	9−10	10	
Circumpeduncular scales	12	12	12		12	12	12	
Standard Length (mm)	75.4	47.4−78.9			58.7	39.1−84.5		
As percentage of SL								
Body depth	16.4	14.6−19.5	17.1	1.0	19.0	15.7−24.3	19.0	2.2
Head length	22.1	20.7−25.4	23.1	0.9	22.1	22.1−26.1	23.8	0.8
Dorsal-fin length	23.3	21.9−28.2	24.4	1.4	22.9	20.6−24.7	22.6	1.1
Dorsal-fin base length	12.1	11.5−15.5	13.4	0.8	12.8	11.7−14.8	13.5	0.7
Pectoral-fin length	21.9	21.0−28.3	23.6	1.5	22.5	18.7−23.1	21.0	1.3
Pectoral-fin base length	5.2	4.4−6.4	5.4	0.4	5.3	4.8−6.4	5.5	0.4
Pelvic-fin length	17.9	16.2−20.8	18.6	0.9	18.0	14.3−18.1	16.4	1.0
Pelvic-fin base length	4.1	3.4−4.9	4.0	0.3	3.4	3.4−5.7	4.4	0.5
Anal-fin length	16.4	14.3−20.3	17.0	1.0	14.4	12.8−16.2	14.6	0.7
Anal-fin base length	6.6	6.1−8.9	7.3	0.5	5.3	5.3−7.6	6.8	0.5
Pre-dorsal length	42.6	40.4−46.3	43.2	1.1	44.4	41.2−46.1	43.8	1.2
Pre-pectoral length	23.2	21.9−26.8	24.1	0.8	23.6	23.6−29.7	26.4	1.5
Pre-pelvic length	45.7	44.0−51.2	47.5	1.3	46.5	46.5−58.4	52.1	3.3
Pre-anal length	73.9	71.5−78.1	74.7	1.5	77.3	75.5−90.0	81.0	3.3
Caudal peduncle length	18.5	16.2−21.0	18.4	0.9	17.5	15.8−19.3	17.3	1.0
Caudal peduncle depth	7.5	6.4−9.0	7.6	0.5	9.4	7.9−9.9	8.6	0.6
Head Length (mm)	16.7	10.6−19.2			13.0	9.1−22.0		
As percentage of HL								
Head depth	59.9	52.2−62.4	56.5	2.1	65.2	50.4−65.2	55.9	3.5
Head width	59.9	50.9−63.7	57.5	2.6	66.0	55.9−66.0	61.0	2.7
Eye diameter	31.8	30.7−38.5	33.6	1.7	31.5	26.0−33.9	30.2	1.9
Interorbital width	23.8	19.4−30.9	24.6	2.2	21.8	21.0−34.5	27.8	4.2
Snout length	35.6	31.7−43.2	37.6	2.5	32.4	32.4−43.4	38.0	2.5
Anterior papillae length	28.8	26.5−38.2	32.3	2.8	25.4	25.4−38.1	30.8	3.0
Anterior papillae width	28.3	17.6−36.1	27.2	4.1	22.5	21.8−39.9	29.8	4.6
Central anterior papillae width	9.8	4.3−11.0	6.7	1.4	4.9	4.4−11.0	6.2	1.5
Upper jaw cutting edge width	11.4	5.7−11.8	8.7	1.5	6.1	6.1−11.7	8.3	1.5
Medial pad width	13.5	9.6−19.4	12.9	1.5	10.1	9.7−14.1	11.7	1.2
Mouth depth	18.9	15.1−23.4	19.9	1.6	16.4	15.4−23.8	18.9	2.2
Mouth width	24.4	17.9−30.1	24.7	2.6	18.3	18.3−33.1	24.6	3.3
Barbel length	15.4	8.9−25.6	18.2	4.1	11.3	11.3−22.7	17.5	3.2

Body covered with moderately small cycloid scales. Lateral line complete, almost straight in lateral center, slightly bent down under dorsal origin. Lateral line scales 37 (6 specimens), 38 (38), 39 (29), 40 (12); scales above lateral line 3.5 (72), 4 (13); scales below lateral line 2 (85); pre-dorsal scales 9 (23), 10 (60), 11 (2); circumpeduncular scales 12 (85). Midventral region of body scaleless only before pectoral-fin base end.

Dorsal fin with three unbranched and seven (76 specimens) branched rays; distal margin slightly concave, origin nearer to snout than caudal-fin base. Pectoral fin with one unbranched and 11 (2), 12 (57), 13 (26) branched rays; tip of adpressed almost reaching or slightly extending anterior margin of pelvic-fin base. Pelvic fin with one unbranched and seven (85) branched rays, inserted below 2nd or 3rd branched dorsal-fin ray; tip of adpressed reaching or extending midway to anal-fin origin. Anal fin with three unbranched and six (85) branched rays; origin almost equal-distant from caudal-fin base to pelvic-fin insertion. Caudal fin deeply forked, with nine branched rays on upper lobes and eight branched rays on lower lobes, lobes pointed.

Gill rakers rudimentary. Pharyngeal teeth "5–5" (in one row). Air-bladder small, anterior chamber enveloped in thick fibrous capsule; posterior chamber small, globular or oval shaped, length less than eye diameter (58.6%–82.8%, mean 68.2%), 14.6%–26.4% (mean 22.8%) of head length.

Coloration in life. Dorsal side of head and body brownish grey, mid-lateral side shallow brownish grey, and ventral side grayish white. Dorsal side of body with five distinct black crossbars (1st on back of nape, 2nd and 3rd at dorsal-fin base origin and ending respectively, 4th at vertical position above anal-fin base origin, 5th on caudal peduncle respectively). Lateral side with 8–10 different sized black blotches, some blotches sometime connect with the 3rd, 4th, and 5th crossbar on the lateral side of body; scales above lateral line black pigmented, lateral-line scales with obvious black spots, margin of first row below lateral line black pigmented, and 2nd row below lateral line slightly black pigmented. Interorbital region with a black crossbar. Operculum and suborbital region with two distinct black blotches (one between anterior margin of eye and upper lip, the other expanded from posterior orbit to opercular) and one small black blotch exist between 2nd and 3rd suborbital plate. One black blotch above pectoral-fin base. Fins membrane translucent, with numerous black pigments on some fin rays; dorsal-fin rays glittery green, with many black spots and dash lines; pectoral fin rays and pelvic fin rays glittery green, with many black spots and dash lines; anal fin rays with some black spots; caudal-fin rays with numerous black spots (Fig. 6A, B).

Coloration in preservation. Dorsal side of head and body brownish yellow, mid-lateral side shallow brownish yellow, and ventral side grayish white. Dorsal side of body with five distinct black crossbars in same position as live individual. Lateral side with 8–10 differently sized dark grey blotches; scales above lateral line black pigmented, lateral-line scales without obvious black spots, margin of first row below lateral line slightly black pigmented. Interorbital region with a black crossbar. Operculum and suborbital region with two distinct black blotches in same position as live individual, and one small black blotch exist between 2nd and 3rd suborbital plate. One black blotch above pectoral-fin base. Fins membrane pale, with numerous black pigments on some fin rays in same position as live individual, glittery green on fin rays faded.

Sexual dimorphism. No significant sexual dimorphism observed.

Distribution. According to the field collections, this species is distributed in the Guijiang and Liujiang rivers, two northern tributaries of the Xijiang River system, which belongs to the Pearl River basin. It is also found in the upper Xiangjiang River, which drains into the middle Yangtze River basin (Fig. 4).

Habitat and biology. *Microphysogobio punctatus* sp. nov. inhabits the slow flowing water of rivers approximately 30−40 meters wide. It usually appears in areas with sandy bottoms with gravel and pebbles. Co-exiting species includes e.g., *Opsariichthys bidens*, *Acheilognathus tonkinensis*, *Squalidus argentatus*, *Sarcocheilichthys* sp. *Microphysogobio zhangi*, and *Cobitis* spp.

Etymology. The new species name *punctatus* is derived from the Latin *punctum*, meaning spot. The name refers to the numerous black spots on its scales and fin rays. Suggested Chinese name for this species is "斑点小鳔鮈".

Discussion

Microphysogobio elongatus, a junior synonym of *M. tungtingensis*

Microphysogobio elongatus was originally described as a slender (body depth less than 16.7% of SL) species with six branched anal-fin rays and distribution in the Xijiang River, the tributary of the Pearl River basin (Luo et al. 1977). In its original description, it can be distinguished from "*M. tungtingensis*" (based on three non-types) only by their branched anal-fin rays (six rays in *M. elongatus* vs five rays in "*M. tungtingensis*") and their distribution. According to the subsequent studies which followed Luo et al. (1977), the key character between *M. tungtingensis* and *M. elongatus* is still basically on branched anal-fin ray count. However, after carefully checking the original descriptions of *M. tungtingensis* along with the other *Microphysogobio* species described by Nichols himself (Nichols 1926a, 1926b, 1930) and examining the X-ray photos of those types, we confirmed that the branched anal-fin rays of *M. tungtingensis* should be six. Thus, it is not easy to distinguish *M. tungtingensis* and *M. elongatus* in this situation but only by their distribution (former in the Lake Dongting system in the middle Yangtze River basin vs latter in the Xijiang River system of the Pearl River basin), causing the validity of the latter suspicious.

In order to understand the potential morphological differences between these two species, 76 specimens, including the types of both species, from a wide geographical range, were examined (Figs 1, 7). The result shows that there is no significant difference in both counts and measurable traits (Table 2). The PCA on those morphometric measurements were performed to make comparisons in detail. The first three component contributed 82.3% of the variance. Principle component 1 (PC 1) represents most on the body size of the specimens, while PC 2 and PC 3 reflected their morphology. The PCA loadings are presented in Table 4, showing that the lip papillae system pattern contributes most in PC 2 and PC 3. However, both PC1 against PC2 and PC2 against PC3 are not able to separate these two species (Fig. 8).

Molecular phylogenetic analyses were also conducted. The intraspecific distance of *M. tungtingensis* and *M. elongatus* was 0.16% and 0.04% respectively, while the interspecific distance between them is 0.13%. This value is approximate to the intraspecific distance of *M. tungtingensis*, making it hard to tell they are different. Besides, the interspecific distance is far less than any other showed in the genus *Microphysogobio*. The phylogenetic trees (Fig. 9) also demonstrate undetectable length of the branches.

Although distributed in different river basins, such distribution might be interpreted by two previously suggested hypotheses. One is that the Lingqu Canal, an

Figure 7. *Microphysogobio elongatus* (= *M. tungtingensis*), syntype, IHB 58-7-876, 77.2 mm SL **A** lateral view **B** dorsal view, and **C** ventral view.

ancient artificial canal connected in 214 B.C. during Qin Dynasty which connecting the Xiangjiang River with the Lijiang River, might cause the trans-basin gene flow between the Yangtze River basin and the Pearl River basin, which was discovered for *M. zhangi* (Huang et al. 2017). This interpretation was supported by the shared haplotype (Table 1) from both river basins. The second hypothesis is the episodic river capture events between the interwoven watersheds of the Nanling Mountains' complex landform, e.g., the Lijiang River capture (Ru 2011), causing the cross-basin distribution, which was found in *Sarcocheilichthys parvus* (Li et al. 2023). Given the low intraspecific and interspecific distances (Table 5) within the phylogenetic linage *M. tungtingensis* located (*M. tungtingensis* + *M. elongatus* + *M. fukiensis* + *M. kiatingensis*) and their broad geographical distribution (from the upper Yangtze River basin to the southeast coastal river systems), we drew the conclusion that the species within this linage performed a relatively conserved mutation in molecular. Hence, according to the trees shown in Fig. 9, it is also likely that the cross-basin distribution was caused by the very recent river capture event which was not long enough ago to accumulate a certain mutation to be detected by the current mitochondrial gene data, especially in this conserved linage.

Based on the morphological comparisons, molecular phylogenetic analyses, and its distribution, we suggest *M. elongatus* to be a junior synonym of *M. tungtingensis*. On the basis of the revision of *M. tungtingensis*, we are now able to distinguish the new species, with an overlapping distribution, discussed below.

Table 4. Loadings on the first three principal components extracted from morphometric data of *Microphysogobio tungtingensis* and *M. elongatus*.

Morphometric measurements	PC 1	PC 2	PC 3
Standard length	0.171	-0.073	0.058
Body depth	0.212	-0.108	0.213
Head length	0.181	-0.015	0.039
Head depth	0.187	-0.039	0.112
Head width	0.192	-0.017	0.135
Dorsal-fin length	0.161	-0.135	-0.009
Dorsal-fin base length	0.184	-0.106	0.119
Pectoral-fin length	0.174	-0.135	-0.043
Pectoral-fin base length	0.190	-0.073	0.112
Pelvic-fin length	0.165	-0.168	-0.048
Pelvic-fin base length	0.189	-0.114	0.210
Anal-fin length	0.168	-0.155	-0.038
Anal-fin base length	0.149	-0.122	0.033
Caudal peduncle length	0.170	-0.145	0.082
Caudal peduncle depth	0.195	-0.137	0.085
Eye diameter	0.169	-0.053	-0.034
Interorbital width	0.185	-0.086	0.012
Snout length	0.202	0.115	0.180
Pre-dorsal length	0.180	-0.040	0.052
Pre-pectoral length	0.175	-0.018	0.044
Pre-pelvic length	0.177	-0.058	0.088
Pre-anal length	0.171	-0.071	0.032
Anterior papillae length	0.229	0.115	-0.171
Anterior papillae width	0.161	**0.699**	**0.343**
Central anterior papillae width	0.155	0.105	**-0.414**
Upper jaw cutting edge width	0.117	**0.342**	-0.181
Medial pad width	0.224	0.087	**-0.322**
Mouth depth	0.237	0.160	-0.112
Mouth width	0.175	**0.332**	-0.017
Barbel length	0.187	-0.022	**-0.559**

Table 5. Genetic distances of the Cyt *b* gene computed by MEGA 6.0 amongst 14 analyzed species of *Microphysogobiol*; *Pseudogobio guilinensis* was used as the outgroup.

|		Intraspecific	1	2	3	4	5	6	7	8	9	10	11	12	13	14
1	*Microphysogobio punctatus* sp. nov.	0.0324														
2	*M. bicolor*	0.0123	0.0665													
3	*M. oujiangensis*	NA	0.1335	0.1314												
4	*M. brevirostris*	NA	0.1291	0.1328	0.0496											
5	*M. xianyouensis*	NA	0.1392	0.1377	0.0905	0.0834										
6	*M. alticorpus*	NA	0.1345	0.1407	0.1555	0.1604	0.1464									
7	*M. zhangi*	0.0263	0.1303	0.1365	0.1331	0.1218	0.1283	0.1386								
8	*M. kiatingensis*	NA	0.1290	0.1353	0.1250	0.1230	0.1106	0.1476	0.1083							
9	*M. elongatus*	0.0004	0.1206	0.1299	0.1061	0.1116	0.1102	0.1381	0.1080	0.0336						
10	*M. tungtingensis*	0.0016	0.1203	0.1290	0.1062	0.1128	0.1113	0.1388	0.1082	0.0346	0.0013					
11	*M. fukiensis*	0.0037	0.1234	0.1291	0.1106	0.1151	0.1113	0.1367	0.1068	0.0364	0.0150	0.0155				
12	*M. kachekensis*	NA	0.0980	0.1011	0.1298	0.1255	0.1298	0.1392	0.1316	0.1373	0.1289	0.1289	0.1299			
13	*M. luhensis*	NA	0.0947	0.1026	0.1330	0.1254	0.1341	0.1360	0.1314	0.1408	0.1279	0.1279	0.1306	0.0205		
14	*M. yunnanensis*	NA	0.0961	0.1023	0.1274	0.1232	0.1318	0.1339	0.1315	0.1396	0.1289	0.1289	0.1288	0.0115	0.0196	
15	*P. guilinensis* (outgroup)	NA	0.1678	0.1665	0.1686	0.1629	0.1658	0.1859	0.1634	0.1548	0.1482	0.1489	0.1528	0.1570	0.1594	0.1593
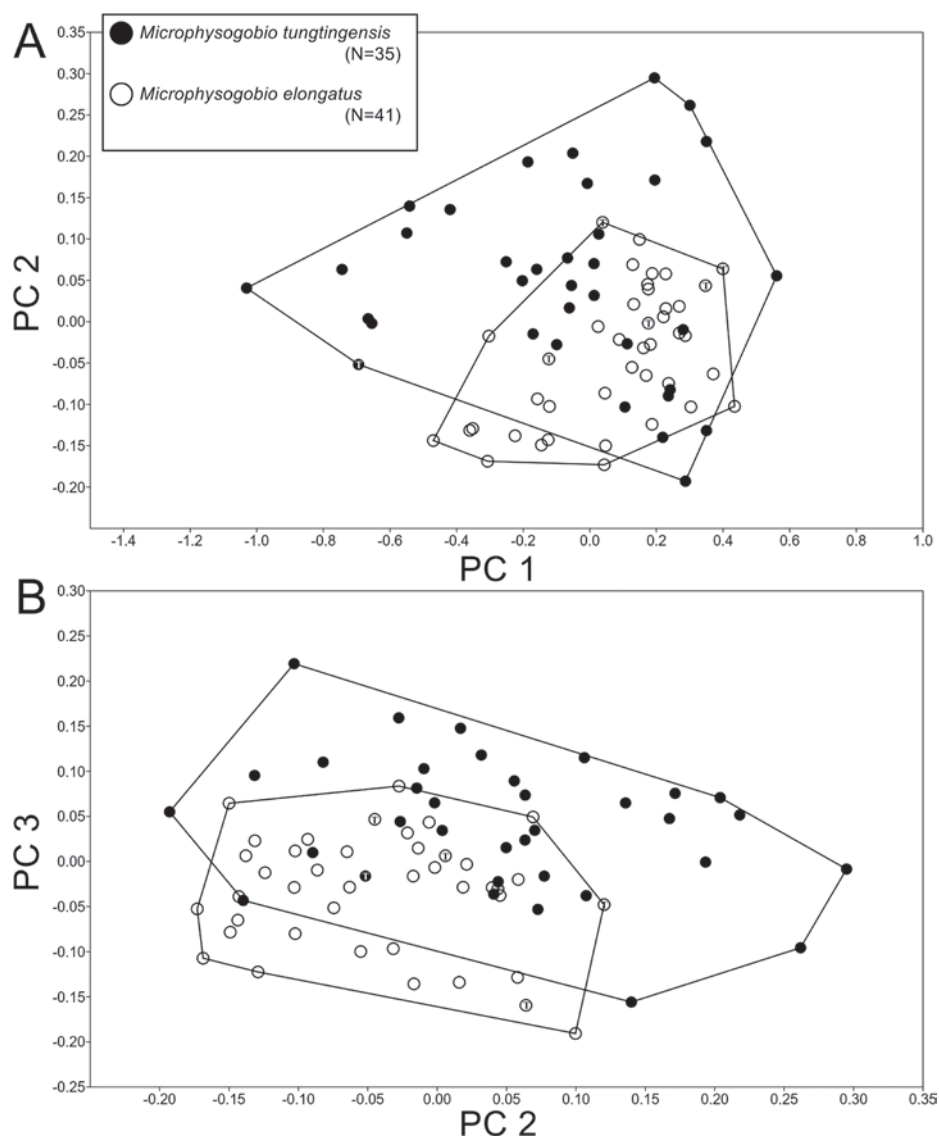
Figure 8. Scatterplot of the PC1 against PC2 (**A**) and PC2 against PC3 (**B**) extracted from 30 morphometric data of *Microphysogobio tungtingensis* and *M. elongatus*. Letter "T" marked inside the dots indicate the type specimens.

Morphological comparison of the new species

Among the 30 known *Microphysogobio* species, *M. punctatus* sp. nov. can be distinguished from *M. brevirostris* (Günther, 1868), *M. chinssuensis* (Nichols, 1926), *M. yaluensis* (Mori, 1928), *M. hsinglungshanensis* Mori, 1934, *M. koreensis* Mori, 1935, *M. longidorsalis* Mori, 1935, *M. amurensis* (Taranetz, 1937), *M. alticorpus* Bănărescu & Nalbant, 1968, *M. anudarini* Holcík & Pivnicka, 1969, *M. liaohensis* (Qin, 1987), *M. rapidus* Chae & Yang, 1999, *M. jeoni* Kim & Yang, 1999, *M. wulonghensis* Xing, Zhao, Tang & Zhang, 2011, *M. nudiventris* Jiang, Gao & Zhang, 2012, *M. xianyouensis* Huang, Chen & Shao, 2016, and *M. oujiangensis* Sun & Zhao, 2022 by having a narrower upper jaw cutting edge (width 22.0%–46.8% of mouth width vs larger than half of mouth width).

For the remaining 14 congeners, the new species can be distinguished from *M. linghensis* Xie, 1986 and *M. microstomus* Yue, 1998 by having well developed lip papillae system (vs undeveloped or less developed papillae on lips, Fig. 3E).
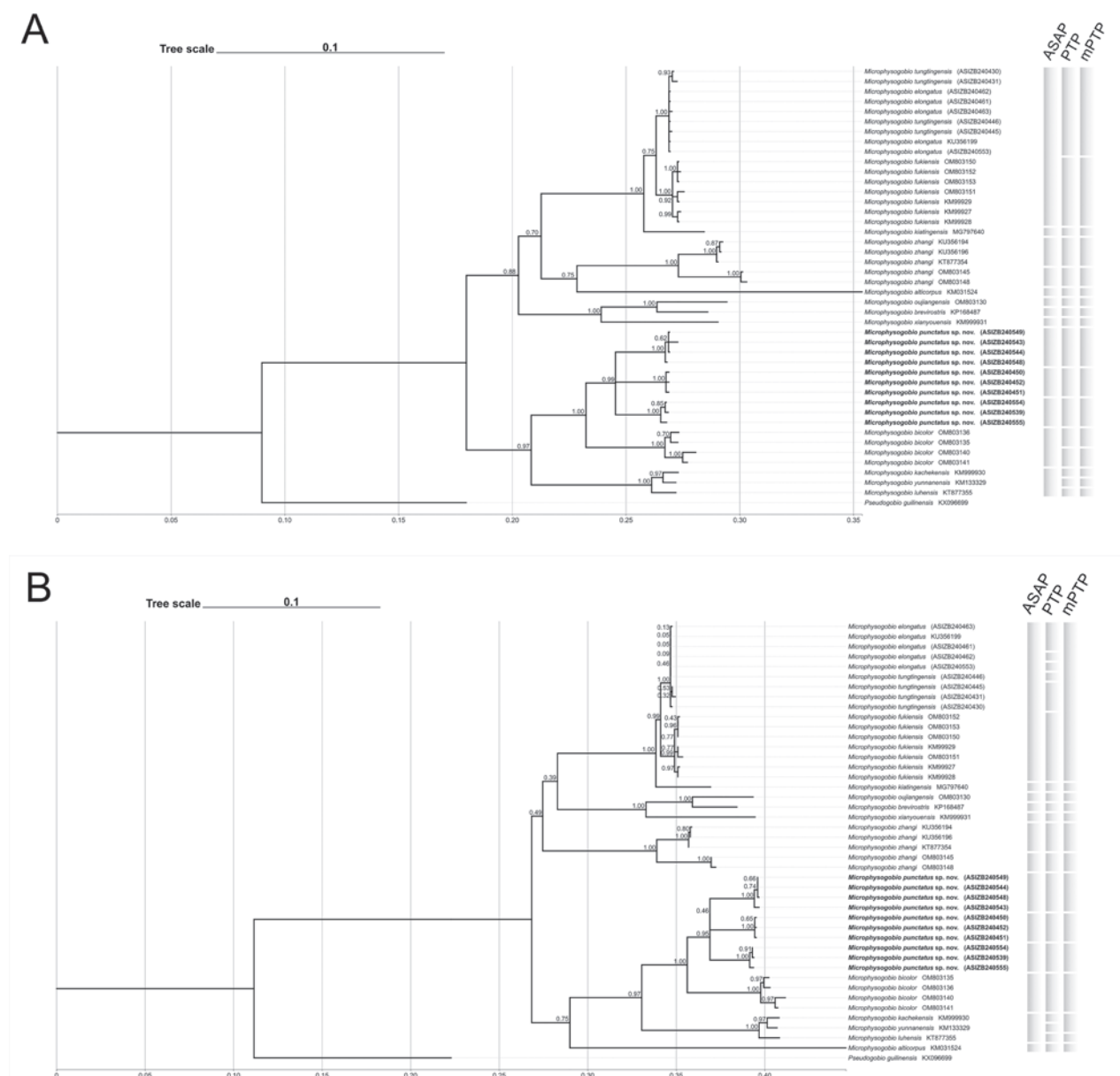
Figure 9. Molecular phylogenetic trees of *Microphysogobio punctatus* sp. nov., *M. tungtingensis*, *M. elongatus* and other phylogenetically close related congeners based on Cyt *b* sequence (1140 bp) **A** Bayesian Inference method **B** maximum likelihood method.

It can be distinguished from *M. kiatingensis* (Wu, 1930) by having a larger squamous zone on mid-ventral region (scaleless only before pectoral-fin base end vs scaleless before two-thirds of the distance from the pectoral-fin insertion to the pelvic-fin insertion). It can be distinguished from *M. bicolor* (Nichols, 1930), *M. tafangensis* (Wang, 1935), *M. zhangi* Huang, Zhao, Chen & Shao, 2017 by having more branched anal-fin rays (6 vs 5). For *M. zhangi*, the species sympatric with the new species, it can be further distinguished from the new species by having different anterior papillae pattern on upper lip (two large papillae vs two to six similar sized papillae, Fig. 3D, F) It can also be distinguished from *M. fukiensis* (Nichols, 1926), *M. tungtingensis* (Nichols, 1926) and *M. vietnamica* Mai, 1978 by having larger posterior chamber of the air-bladder (length 58.6%–82.8% of eye diameter vs length 21.9%–43.1%, 30.4%–34.9% and 35.5%–64.2% of eye diameter

respectively). Considering *M. vietnamica* has overlap on air-bladder size with the new species, it can be further distinguished from latter by having different anterior papillae pattern on upper lip (two large papillae separated from each other vs similar sized papillae tightly contacted with each other, Fig. 3D, G). The new species can be distinguished from *M. pseudoelongatus* Zhang & Zhao, 2001 by having more circumpeduncular scales (12 vs 10). For the *M. nikolskii* (Dao & Mai, 1959), the species inquirenda (Kottelat 2013), the new species can be distinguished from it by having fewer lateral-line scales (37–40 vs 43; Huang et al. 2018).

For the rest of the three congeners, they are morphologically similar with the new species by having a larger posterior chamber of the air-bladder (larger than half eye diameter and sometimes equal to eye diameter) and tightly contacted central portion of anterior papillae. The new species can be distinguished from these three species by having more black pigmentation on fin rays. In addition, the new species can be distinguished from *Microphysogobio yunnanensis* (Yao & Yang, 1977) by having fewer scales above lateral line (3.5–4 vs 4.5), from *M. luhensis* Huang, Chen, Zhao & Shao, 2018 by having a larger eye diameter (30.7%–38.5% vs 25.2%–27.9% of head length), and from *M. kachekensis* (Oshima, 1926) by having a more slender caudal peduncle (depth 34.6%–48.5% vs 48.9%–55.7% of length).

As for *Microphysogobio bicolor*, although it has already been distinguished from the new species by having fewer branched anal-fin rays (5 vs 6), it is also morphologically close to the new species by having similar size of the air-bladder (63.1%–82.0% vs 50.3%–82.8% of eye diameter in average) and lip papillae pattern (Fig. 3H). However, the new species has a slender caudal peduncle (depth 34.6%–48.5% vs 43.3%–58.4% of length; Fig. 10) and shorter preanal distance (71.5%–78.1% vs 75.5%–90.0% of SL) as compared to *M. bicolor*.

A total of 37 haplotypes from 43 *Microphysogobio* individuals for Cyt *b* gene were included in the molecular phylogeny study. Based on molecular phylogenetic analyses, the new species is sister to *M. bicolor*, and together sister to *M. luhensis*–*M. kachekensis*–*M. yunnanensis* clade. The interspecific distance between *M. punctatus* and *M. bicolor* is 6.65% for Cyt *b* based on K2P model. The intraspecific distance within *M. punctatus* is 3.24% based on K2P model, which is lower than the interspecific distance. In fact, the molecular species
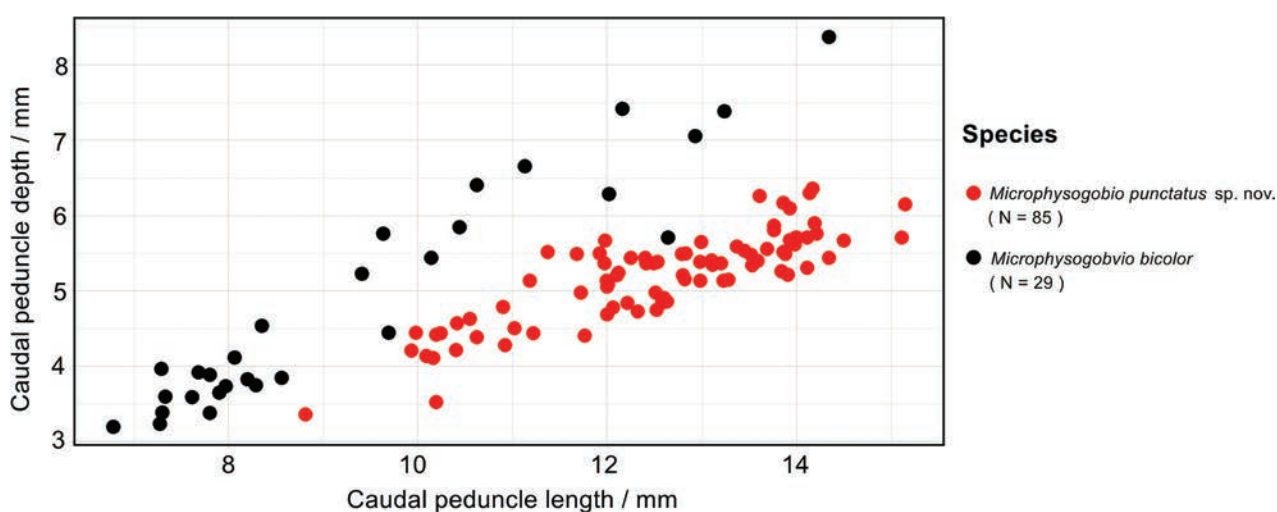
Figure 10. Morphometric measurement divergence in caudal peduncle depth between *Microphysogobio punctatus* sp. nov. and *M. bicolor*.

delineation method (ASAP and PTP) inferred that the three geographic populations (Lingchuan, Yongfu, and Guanyang counties) to be three different molecular species which forming a monophyletic lineage. However, there is no significant difference in morphology among three populations, plus the closely connected river system within their distribution, we treated them as one species.

Comparative material

***Microphysogobio bicolor*:** • AMNH 9678, holotype, 58.7 mm SL; Hekou Township, Yanshan County, Shangrao City, Jiangxi Province, from the Xinjiang River; collected by Clifford H. Pope; 22 June 1926 • ASIZB 220619−27, 9 specimens, 39.1−50.3 mm SL; Yongping Township, Yanshan County, Shangrao City, Jiangxi Province, from the Yanshanhe River (28.21615237°N, 117.79050896°E, 75 m a.s.l.); collected by Zhixian Sun and Rui Zhang; 11−12 April 2021 • ASIZB 213554, 1 specimen, 52.4 mm SL; Yongping Township, Yanshan County, Shangrao City, Jiangxi Province, from the Yanshanhe River (28.21615237°N, 117.79050896°E, 75 m a.s.l.); collected by Zhixian Sun, Rui Zhang, Chen Tian, and Xin Wang; 20 July 2021 • ASIZB 220628−35, 8 specimens, 42.1−62.2 mm SL; Taibai Township, Wuyuan County, Shangrao City, Jiangxi Province, from the Le'anhe River (29.07164455°N, 117.67277022°E, 47 m a.s.l.); collected by Junhao Li and Zhixian Sun; 16 December 2020 • ASIZB 220636−40, 220647, 220650, 220652, 220654, 9 specimens, 63.1−84.5 mm SL; bought from the Dongmen Market from the local fishermen, Wuyuan County, Shangrao City, Jiangxi Province, from the Le'anhe River; collected by Zhixian Sun and Rui Zhang; 11 April 2020 • ASIZB 229848−9, 2 specimens, 59.0−76.0 mm SL; bought from the Wangjiaba Market from the local fishermen, Guangxin District, Shangrao City, Jiangxi Province, from the Xinjiang River; collected by Zhixian Sun, Rui Zhang, Chen Tian, and Xin Wang; 21 July 2021.

***Microphysogobio fukiensis*:** • ASIZB 220660−68, 9 specimens, 50.5−64.6 mm SL; bought from the local market, Guangze County, Nanping City, Fujian Province, from the Futunxi River; collected by Zhixian Sun, Rui Zhang, Qiuju Chen and Rui Xi; 17 April 2021.

***Microphysogobio kechekensis*:** • ASIZB 240478−88, 11 specimens, 64.8−83.6 mm SL; bought from the local market, Baisha Li Autonomous County, Hainan Province, probably caught by fishermen from the Wanquanhe River; collected by Shanyu Wu; 3 April 2020 • ASIZB 69768, 1 specimen, 100.0 mm SL; Gongzheng Township, Shangsi County, Fangchenggang City, Guangxi Zhuang Autonomous Region, from a stream of Maolingjiang River; collected by Yahui Zhao; 29 April 1999.

***Microphysogobio luhensis*:** • ASIZB 204717, paratype, 55.5 mm SL; Dongkeng Township, Luhe County, Shanwei City, Guangdong Province, from the Rongjiang River (23.30165309°N, 115.71898652°E, 126 m a.s.l.); collected by Shih-Pin Huang; 2 April 2009.

***Microphysogobio microstomus*:** • SHOU 20231209017, 47.3 mm SL; Shanhu Township, Shengzhou City, Shaoxing City, Zhejiang Province, from the Shanxi River (29.63724853°N, 120.84212848°E, 12 m a.s.l.); collected by Zhixian Sun; 9 December 2023.

***Microphysogobio vietnamica*:** • ASIZB 240561−71, 11 specimens, 43.0−53.5 mm SL; Shixing County, Shaoguan City, Guangdong Province, from the Mojianghe River; collected by Zhixian Sun; 4 January 2021.

Microphysogobio yunnanensis: • IHB 645480, 645486−7, 645492, 645494−5, 645499, syntypes, 7 specimens, 73.8−82.2 mm SL; Yuanjiang Hani Yi and Dai Autonomous County, Yuxi City, Yunnan Province, from the Yuanjiang River (the Red River); May 1964 • IHB 645496, 6440132, 6440136, 6440296, 6440638, 6440648−9, 6440654, 6450063, syntypes, 9 specimens, 68.0−95.9 mm SL; Hekou Yao Autonomous County, Honghe Hani and Yi Autonomous Prefecture, Yunnan Province, from the Yuanjiang River (the Red River); April and May 1964.

Microphysogobio zhangi: • ASIZB 204677, holotype, 75.1 mm SL; Quanzhou County, Guilin City, Guangxi Zhuang Autonomous Region, from the Xiangjiang River (25.93332646N, 111.08037923E, 151 m a.s.l.); collected by Shih-Pin Huang and Jinqing Huang; 6 November 2015 • ASIZB 220669−76, 8 specimens, 48.2−63.6 mm SL; Pingle County, Guilin City, Guangxi Zhuang Autonomous Region, from the Lijiang River; collected by Zhixian Sun; 23 January 2021.

Acknowledgments

Additional information

Conflict of interest

The authors have declared that no competing interests exist.

Ethical statement

No ethical statement was reported.

Funding

Author contributions

Sun ZX contributed to the field collection, photographing, illustrating, specimens examining, data analyses and drafting of the manuscript. Tang WQ and Zhao YH was responsible for review and editing.

Author ORCIDs

Zhi-Xian Sun ⓘ https://orcid.org/0000-0003-0565-2801
Wen-Qiao Tang ⓘ https://orcid.org/0000-0001-5992-5022
Ya-Hui Zha ⓘ https://orcid.org/0000-0002-4615-596X

Data availability

All of the data that support the findings of this study are available in the main text or Supplementary Information.

References

Bănărescu P, Nalbant TT (1966) Revision of the genus *Microphysogobio* (Pisces, Cyprinidae). Věstnik Československé Společnosti Zoologické 30(3): 194–209.

Fricke R, Eschmeyer WN, Van der Laan R [Eds] (2024) Eschmeyer's catalog of fishes: genera, species, references. http://researcharchive.calacademy.org/research/ichthyology/catalog/fishcatmain.asp [Accessed 06 Apr 2024]

Hammer Ø, Harper DAT, Ryan PD (2001) PAST: Paleontological Statistics Software Package for Education and Data Analysis. Palaeontologia Electronica 4(1): 1–9.

Huang SP, Chen IS, Shao KT (2016) A new species of *Microphysogobio* (Cypriniformes: Cyprinidae) from Fujian Province, China, and a molecular phylogenetic analysis of *Microphysogobio* species from southeastern China and Taiwan. Proceedings of the Biological Society of Washington 129: 195–211. https://doi.org/10.2988/0006-324X-129.Q3.195

Huang SP, Zhao YH, Chen IS, Shao KT (2017) A new species of *Microphysogobio* (Cypriniformes: Cyprinidae) from Guangxi Province, Southern China. Zoological Studies 56: 8. https://doi.org/10.6620/ZS.2017.56-08

Huang SP, Chen IS, Zhao YH, Shao KT (2018) Description of a new species of the Gudgeon genus *Microphysogobio* Mori 1934 (Cypriniformes: Cyprinidae) from Guangdong Province, Southern China. Zoological Studies 57: 58. https://doi.org/10.6620/ZS.2018.57-58

Kalyaanamoorthy S, Minh B, Wong T, von Haeseler A, Jermiin L (2017) ModelFinder: Fast model selection for accurate phylogenetic estimates. Nature Methods 14(6): 587–589. https://doi.org/10.1038/nmeth.4285

Kapli P, Lutteropp S, Zhang J, Kobert K, Pavlidis P, Stamatakis A, Flouri T (2017) Multi-rate Poisson tree processes for single-locus species delimitation under maximum likelihood and Markov chain Monte Carlo. Bioinformatics 33(11): 1630–1638. https://doi.org/10.1093/bioinformatics/btx025

Kimura M (1980) A simple method for estimating evolutionary rates of base substitutions through comparative studies of nucleotide sequences. Journal of Molecular Evolution 16: 111–120. https://doi.org/10.1007/BF01731581

Kottelat M (2013) The fishes of the inland waters of Southeast Asia: A catalogue and core bibliography of the fishes known to occur in freshwaters, mangroves and estuaries. The Raffles Bulletin of Zoology 27: 1–663.

Leviton AE, Gibbs RH, Heal E, Dawson CE (1985) Standards in herpetology and ichthyology: Part I. Standard symbolic codes for institutional resource collections in herpetology and ichthyology. Copeia 3: 802–832.

Li MY, Yang XS, Ni XM, Fu CZ (2023) The role of landscape evolution in the genetic diversification of a stream fish *Sarcocheilichthys parvus* from Southern China. Frontiers in Genetics 13: 1075617. https://doi.org/10.3389/fgene.2022.1075617

Lunghi E, Zhao Y, Sun XY, Zhao YH (2019) Morphometrics of eight Chinese cavefish species. Scientific Data 6: 233. https://doi.org/10.1038/s41597-019-0257-5

Luo YL, Yue PQ, Chen YY (1977) Gobioninae. In: Wu XW (Ed.) The Cyprinid Fishes of China. Vol. 2. Science Press, Beijing, 439 pp. [In Chinese]

Nichols JT (1926a) Some Chinese fresh-water fishes. XV. Two apparently undescribed catfishes from Fukien. XVI. Concerning gudgeons related to *Pseudogobio*, and two new species of it. XVII. Two new Rhodeins. American Museum Novitates 214: 1–7.

Nichols JT (1926b) Some Chinese fresh-water fishes. XVIII. New species in recent and earlier Fukien collections. American Museum Novitates 224: 1–7.

Nichols JT (1930) Some Chinese fresh-water fishes. XXVI. Two New Species of *Pseudogobio*. XXVII. A New Catfish from Northeastern Kiangsi. American Museum Novitates 440: 1–5.

Nichols JT (1943) The freshwater fishes of China. Natural History of Central Asia Vol. 9. American Museum of Natural History, New York, 322 pp.

Puillandre N, Brouillet S, Guillaume A (2020) ASAP: assemble species by automatic partitioning. Molecular Ecology Resources 21(2): 609–620. https://doi.org/10.1111/1755-0998.13281

Ronquist F, Teslenko M, Mark P, Ayres D, Darling A, Höhna S, Larget B, Liu L, Suchard M, Huelsenbeck J (2012) MrBayes 3.2: Efficient Bayesian Phylogenetic Inference and Model Choice Across a Large Model Space. Systematic Biology 61(3): 539–542. https://doi.org/10.1093/sysbio/sys029

Ru JW (2011) Changes in Lijiang River System. Man and the Biosphere 5: 18–26. [In Chinese]

Sun ZX, Zhao YH (2022) Revalidation and redescription of a gobionine species *Microphysogobio bicolor* (Nichols, 1930) (Teleostei: Cypriniformes) from the Yangtze River Basin, China. Zootaxa 5092(3): 361–377. https://doi.org/10.11646/zootaxa.5092.3.7

Sun ZX, Kawase S, Zhang R, Zhao YH (2021) Taxonomic revision and redescription of *Microphysogobio hsinglungshanensis*, the type species of *Microphysogobio* Mori, 1934 (Cypriniformes: Cyprinidae). Journal of Fish Biology 99(2): 373–383. https://doi.org/10.1111/jfb.14725

Sun ZX, Li XJ, Tang WQ, Zhao YH (2022a) A new species of the gudgeon genus *Huigobio* Fang, 1938 (Cypriniformes: Cyprinidae) from the Yangtze River Basin, southern China. Zoological Research 43(1): 33–39. https://doi.org/10.24272/j.issn.2095-8137.2021.168

Sun ZX, Zhu BQ, Wu J, Zhao YH (2022b) A new species of the gudgeon genus *Microphysogobio* Mori, 1934 (Cypriniformes: Cyprinidae) from Zhejiang Province, China. Zoological Research 43(3): 356–361. https://doi.org/10.24272/j.issn.2095-8137.2021.398

Tamura K, Stecher G, Peterson D, Filipski A, Kumar S (2013) MEGA6: Molecular Evolutionary Genetics Analysis Version 6.0. Molecular Biology and Evolution 30(12): 2725–2729. https://doi.org/10.1093/molbev/mst197

Xiao S, Lan JH (2023) Taxonomic Atlas of the Freshwater Fishes in Guangxi. Henan Science and Technology Press, Zhengzhou, 420 pp. [In Chinese]

Xie JM, Chen YR, Cai GJ, Cai RL, Hu Z, Wang H (2023) Tree Visualization By One Table (tvBOT): a web application for visualizing, modifying and annotating phylogenetic trees. Nucleic Acids Research 51(1): 587–592. https://doi.org/10.1093/nar/gkad359

Yue PQ (1998) Gobioninae. In: Chen YY et al. (Eds) Fauna Sinica. Osteichthyes Cypriniformes II. Science Press, Beijing, 531 pp. [In Chinese]

Wen YC (2006) Gobioninae. In: Zhou J, Zhang CG (Eds) Freshwater Fishes of Guangxi, China. 2nd Edn. Guangxi People Publishing House, Nanning, 535 pp. [In Chinese]

Zhang CG, Zhao YH (2016) Species Diversity and Distribution of Inland Fishes in China. Science Press, Beijing, 296 pp. [In Chinese]

Supplementary material 1

Raw data of the type specimens of *Microphysogobio tungtingensis* and *M. elongatus*

Authors: Zhi-Xian Sun, Wen-Qiao Tang, Ya-Hui Zhao

Data type: xlsx

Link: https://doi.org/10.3897/zookeys.1214.127061.suppl1

ZooKeys

Short Communication

Complementary description of *Peltidium nayarit* (Copepoda, Harpaticoida, Peltidiidae) and a new record at Revillagigedo Archipelago, Mexico

José Ricardo Palomares-García[1], Jaime Gómez-Gutiérrez[1]

1 Departamento de Plancton y Ecología Marina, Centro Interdisciplinario de Ciencias Marinas, Instituto Politécnico Nacional, C.P. 23096, La Paz, BCS, Mexico
Corresponding author: Jaime Gómez-Gutiérrez (jagomezg@ipn.mx)

Abstract

Four adult females of a rare benthic/epiphytic harpacticoid copepod species of the genus *Peltidium* Philippi, 1839 were collected from insular zooplankton samples obtained at Revillagigedo National Park, Mexico. They were identified as *Peltidium nayarit* Suárez-Morales & Jarquín-González, 2013 with type location (and the single previously known distribution site) at Playa Careyeros (20°46'59.46"N, 105°30'35.48"W), Nayarit, Mexico. We provide a complementary description of this species including new details of antennules, caudal rami, legs 1 and 5, and cuticular ornamentation using scanning electron microscopy observations. *Peltidium nayarit* has a dark reddish-pink coloration allegedly mimicking the color of the macroalgae where they live, but specimens collected in the present study were obtained from sea surface zooplankton net tows. The record of *Peltidium nayarit* in the Revillagigedo Islands represents the southwestern-most record of the genus in the Americas and the second record for Mexico.

Key words: Crustacean fauna, Harpaticoida, marine copepods, range extension, taxonomy

Introduction

The copepod genus *Peltidium* currently includes 47 nominal species widely distributed in different regions of the world's oceans (Walter and Boxshall 2024). However, *Peltidium* species are typically found in low species richness in each region (Suárez-Morales and Jarquín-González 2013). Five *Peltidium* species have been reported in the Caribbean region (Varela 2005; Suárez-Morales et al. 2006; Varela and Gómez 2013). Only two species of the subfamily Peltidiinae have been reported in the Eastern Tropical Pacific (Gómez and Varela 2013; Suárez-Morales and Jarquín-González 2013). Gómez and Varela (2013) described a new Peltidiidae species, *Alteutha alsagopu* Gómez & Varela, 2013, collected on the coast of Sinaloa, Gulf of California, Mexico. *Peltidium nayarit* Suárez-Morales & Jarquín-González, 2013, is therefore the second record of Peltidiidae known in the Mexican Pacific. *Peltidium nayarit* was discovered in meiobenthic samples collected from a rocky, sandy beach in the state of Nayarit, Mexico. The original description of *P. nayarit* was based only

on optical microscopy. The goal of the present study was to complement the original morphological description with the description of females observed with scanning electron microscopy and report the offshore distribution range of this species previously known only from the neritic region of the Central Mexican Pacific.

Materials and methods

We carried out a pioneering biological survey of the insular zooplankton diversity of the four islands of the Revillagigedo National Park (San Benedicto, Roca Partida, Clarion, Socorro), Mexico, from 18−22 April 2023 on board the *L/A Quino El Guardian*. Quantitative zooplankton samples were collected with a standard zooplankton net (0.6 m mouth diameter, 2 m length, 300 µm mesh size), towed near the sea surface (<2 m depth) for 10 minutes. The net was equipped with a General Oceanic digital flowmeter (GO R2030) to estimate the filtered seawater volume and calculate standardized abundance expressed in ind./1000 m^3 (Smith and Richardson 1977). Copepods were fixed in a 4% formalin solution buffered with saturated sodium borate, then sorted from the original samples and transferred to 70% ethanol with glycerin for long-term preservation. All harpacticoid copepods were sorted out from the entire zooplankton samples. Two harpacticoid copepod specimens of a *Peltidium* species were observed with a scanning electron microscope (SEM, Hitachi S-3000N) in the Laboratory of Scanning Electron Microscopy located at Centro de Investigaciones Biológicas del Noroeste S.C., La Paz, Baja California Sur, Mexico. This methodology stands out due to its high resolution and great depth of field, which allows a three-dimensional visualization of the copepods. Each specimen was gradually dehydrated for one hour at each of the following ethanol concentrations: 70, 80 and 96%. The harpacticoid copepods were later dried to the critical point with carbon dioxide gas (CO_2) using the Polaron E3000 critical point equipment (Samdri PVT 3B). The copepods were mounted on a copper filament with sticky glue to observe the specimens from different angles in the SEM. The specimens were coated with gold ions using a Polaron E5100 sputter-coater (Denton Vacuum Desk II). The observations were made with an intensity of 20 kV capable of a maximum of 300,000 × magnification. The other two *Peltidium* harpacticoid specimens were observed using an optical stereo microscope (Carl Zeiss Stemi 2000).

Digital images of the *Peltidium* specimens were obtained in dorsal, ventral, lateral and frontal views. Taxonomic diagnostic characters of this species were described in detail from anterior to posterior appendages. The images were improved in contrast and brightness and transparency of the background using the digital analysis of layers with Photoshop CS5 (v.12.0 x64). Plates of each specimen were made with a black background to contrast the SEM images using Adobe Illustrator CS5 (v. 15.0). The copepod specimens examined in the present study (including both specimens observed with SEM) were deposited in the Zooplankton Collection, Centro Interdisciplinario de Ciencias Marinas, Instituto Politécnico Nacional, La Paz, Baja California Sur, Mexico (Curator José Ricardo Palomares-García).

Description

Peltidium nayarit Suárez-Morales & Jarquín-González, 2013
Figs 1–3

Material examined. • Four adult females, two specimens mounted on glycerin sealed with acrylic varnish for optical stereo microscope observation and two specimens used for scanning electron microscopy • Two adult females collected at Punta Norte, San Benedicto Island, Revillagigedo National Park, Mexico (19°20'10"N, 110°47'58"W); 18 April 2023, 16:10 h, zooplankton sample collected near surface < 2 m depth; collector Jaime Gómez-Gutierrez • One adult female collected at Punta Sureste, Clarion Island, Revillagigedo National Park, Mexico (18°20'50"N, 114°41'39"W); 21 April 2023, 18:47 h, zooplankton sample collected near surface < 2 m depth; collector Jaime Gómez-Gutierrez • One adult female collected at Piedra Caleta, Clarion Island, Revillagigedo National Park, Mexico (18°22'17"N, 114°41'35"W); 23 April 2023, 18:47 h, zooplankton sample collected near surface < 2 m depth; collector Jaime Gómez-Gutierrez. Standardized abundance of *P. nayarit* was typically low (average 9.7 ind./1000 m^3, range 7.2–12.5 ind./1000 m^3), found in three positive sampling stations out of a total of 10 zooplankton sampling stations.

New locality. San Benedicto and Clarion islands, Revillagigedo National Park, Mexico.

Complementary description. We describe only the observed morphological differences and details not included in the original description of *Peltidium nayarit* reported in Suárez-Morales and Jarquín-González (2013).

Copepods with dark reddish-pink coloration (Fig. 1A). Specimens measure on average 0.8 mm total length and 0.5 mm width (Fig. 1B, C). Free endopodal segment with outer row of long spinules, armed with one spine and two lateral setae plus seven distal setal elements, four of them being articulated stout setae. The same element is ornamented with inner pectinate margin (Fig. 2A, B). *Antenna.* Coxa small, allobasis with short abexopodal seta and longitudinal patch of spinules on outer margin. Exopod two-segmented, elongated, first segment with short slender seta, second segment bearing three setae distally, distal margin with row of short spinules. One exopodal seta modified, with regular pectinate ornamentation along both margins (Suárez-Morales and Jarquín-González 2013, Fig. 2C). The pectinate ornamentation of the distal margin of the antenna was not shown in the original description of *P. nayarit* (Suárez-Morales and Jarquín-González 2013).

Leg 1 (Fig. 2D). Coxa elongate, ornamented with single row of small spinules on inner and outer margins, plus single short seta on inner middle part of segment. Basis wide, inner margin and part of outer margin ornamented with spinules. Inner distal basipodal seta reaching distal margin of first endopodal segment. Outer basipodal seta reaching distal end of basis. *Exopod* three-segmented, second exopodal segment longest, about 1.5 times as long as first segment, with patch of minute spinules on outer distal margin. Two exopodal claws on distal position of third exopodal segment; outer claw half as long as inner claw. *Endopod* two-segmented, shorter than exopod. Endopodal segments wide, globose (sensu Wells 2007), ornamented with rows of short setule
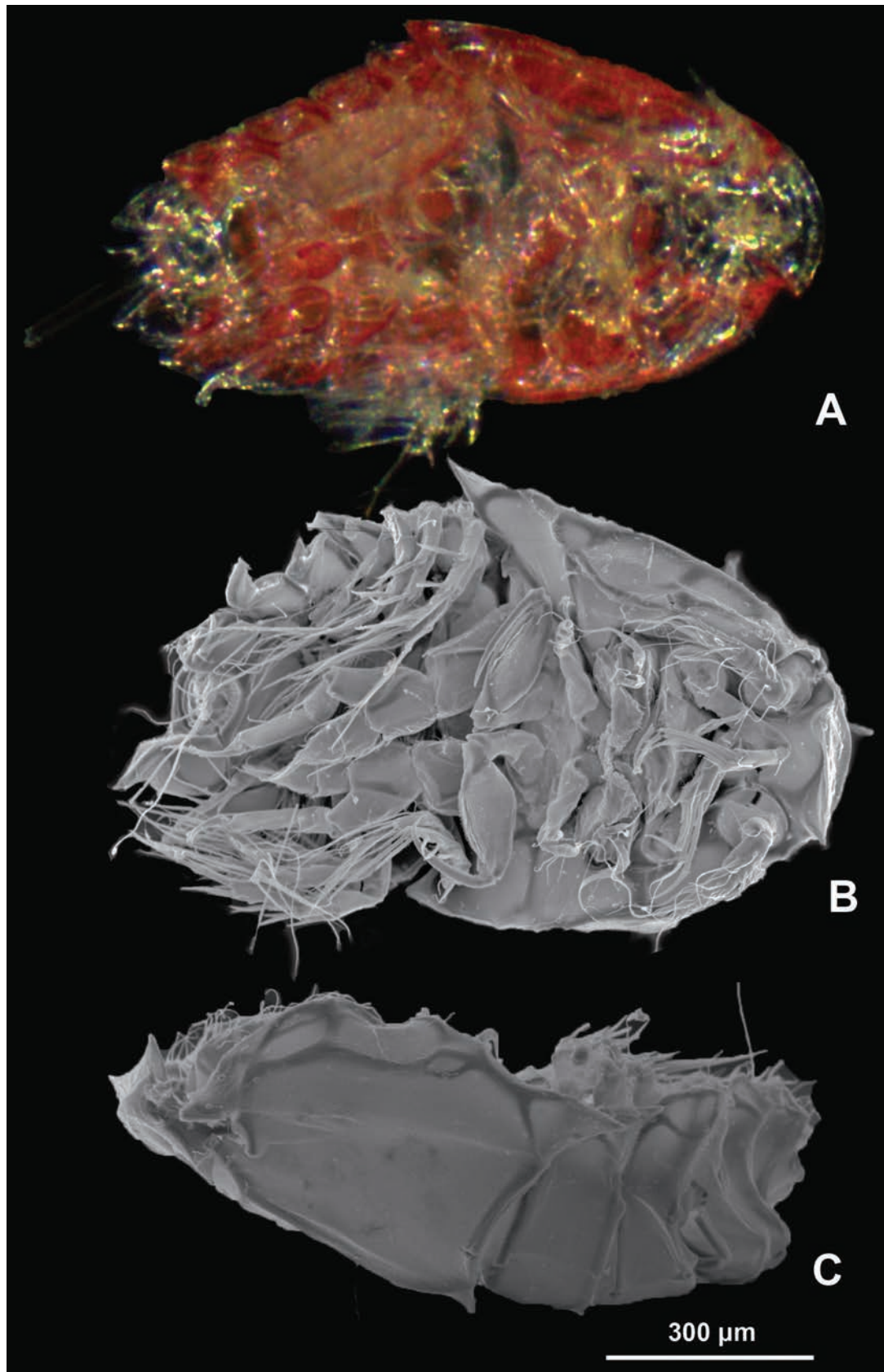
Figure 1. *Peltidium nayarit* adult females collected from San Benedicto and Clarion Islands, Revillagigedo National Park, Mexico **A** photograph of a female showing dark reddish-pink coloration in ventral view **B** SEM image of a specimen in ventral view **C** SEM image of a specimen in right lateral view.
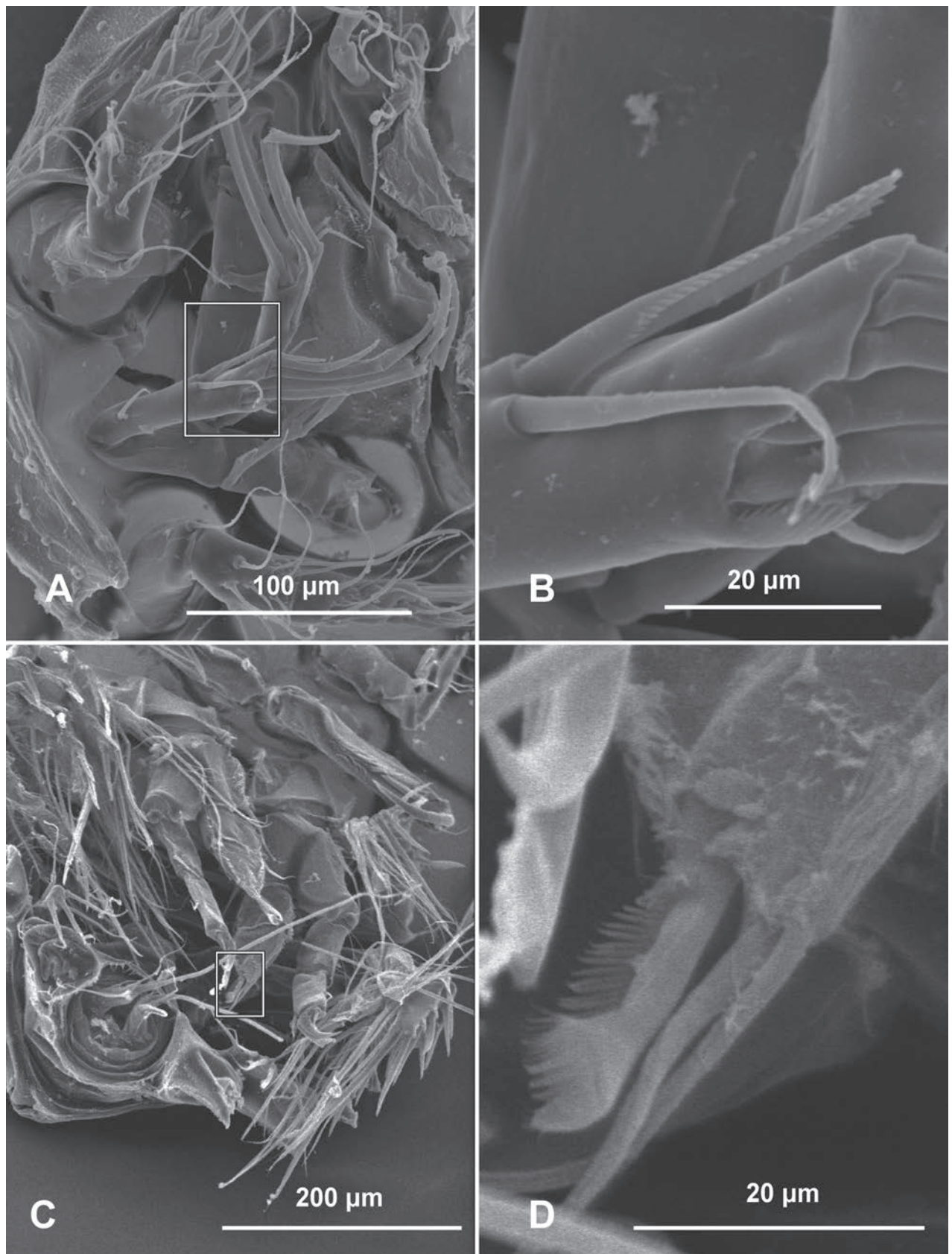
Figure 2. *Peltidium nayarit* adult female collected from San Benedicto and Clarion Islands, Revillagigedo National Park, Mexico **A** antenna with ornamented inner pectinate margin **B** detail of the pectinate margin **C** leg 1 with a pectinate fringe **D** detail of the inner margin of the second endopodite segment.
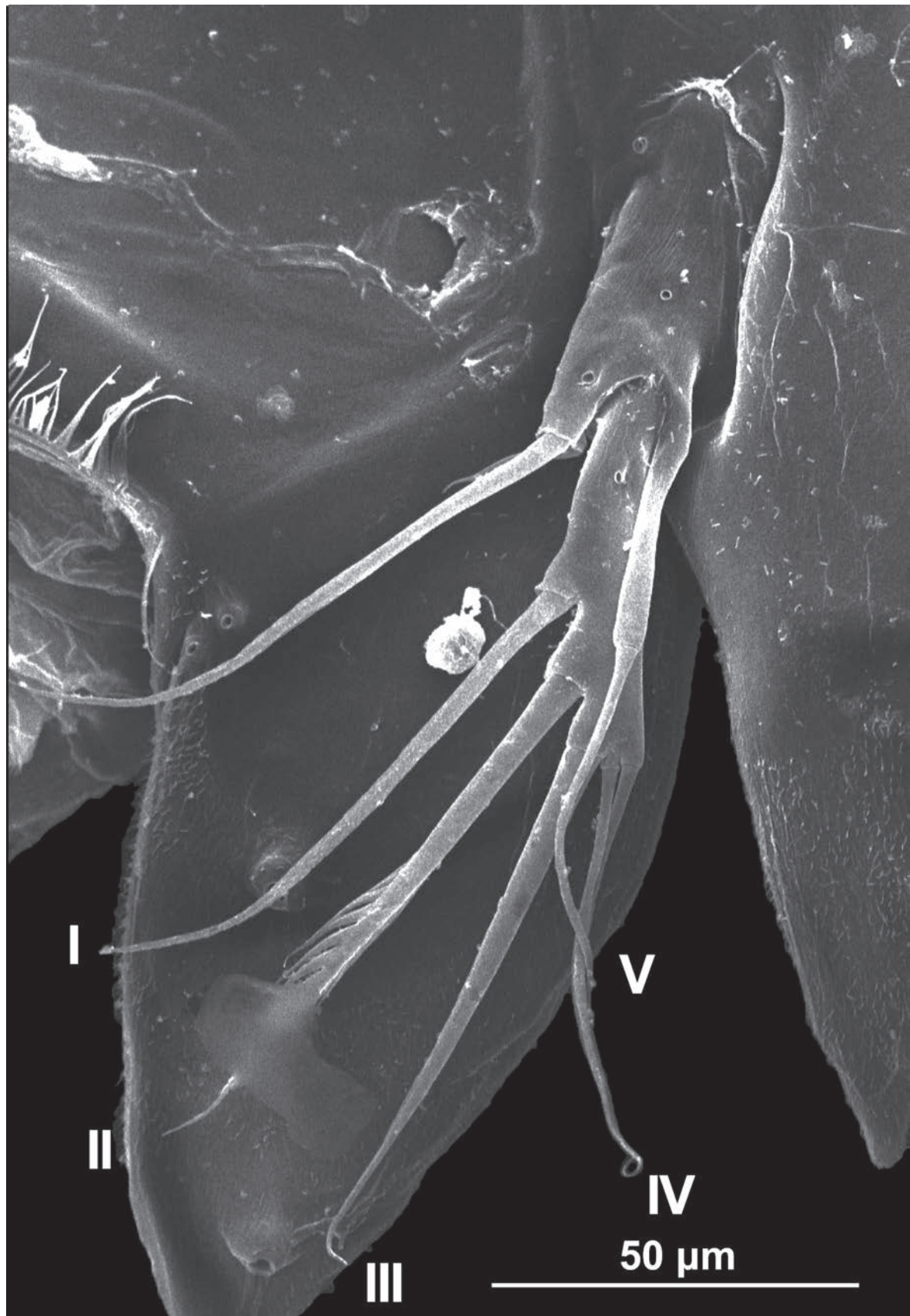
Figure 3. Leg 5 of *Peltidium nayarit*, adult female, showing exopodal setae. Setal nomenclature follows Wells (2007) and Suárez-Morales and Jarquín-González (2013). Specimen collected from San Benedicto Island, Revillagigedo National Park, Mexico.

along the inner and outer margins. Terminal elements include a spine ornamented with distal row of minute spinules and two equally long slender setae. First endopodite segment with an inner seta; second endopodite segment with an inner seta and two equally long slender terminal setae, the inner seta bears a pectinate fringe on its inner margin (Fig. 2C, D).

Remarks. In the original description of *P. nayarit* (Suárez-Morales and Jarquín-González 2013, fig. 2C) the margin of the endopodite with the pectinate fringe on its inner margin was not described (Fig. 2C, D).

Leg 5 (Fig. 3). This is the amendment of the original description exopod and baseoendopod separated. Baseoendopod with two pores bearing single inner seta; external seta long, borne on elongate cylindrical lobe of baseoendopod reaching half the length of exopodal lobe; exopodite slender, with one pore and with 5 setal elements (I–V) (sensu Wells 2007), two inserted on inner margin (I, II), and three (III–V) distally; elements I–III represented by stout, distally pinnate setae, elements IV and V possess equally long slender setae; in the specimens from the Revillagigedo Islands, the unique pinnate element observed is element III, and elements I and II were spiniform (Fig. 2E).

According to Suárez-Morales and Jarquín-González (2013), *P. nayarit* shares some diagnostic morphological characters with *P. speciosum* Thompson & Scott, 1903, including leg 5 with a very similar armature and structure except for a relatively robust exopodal segment (length/width ratio = 3.7 vs. 4.2 in *P. nayarit*) and a shorter outer baseoendopodal seta, reaching to about half the length of exopodal seta V (Nicholls 1941, see fig. 8). These morphological features differ from *P. nayarit*, in which the same seta almost reaches the distal end of seta V (Suárez-Morales and Jarquín-González 2013, fig. 3). However, we observed remarkable morphological differences with the original description, because the III element of the exopodite of the specimens of the present study bear only pinnate element and elements I and II were spiniform, while in specimens of *P. nayarit* from the Nayarit coast elements I–III have setae.

Discussion

Several harpacticoid genera have been discovered and described as meiobenthic fauna. The meiobenthic habitat is commonly exposed to strong seawater currents, where the low-profile body shape (like an isopod) helps the copepod maintain its position on the substrate's surface or remain attached to coral or macroalgae (Noodt 1971; Hicks 1980; Gheerardyn et al. 2006). Overall, sampling effort in phytal-meiobenthic habitats has been scarce and has received little attention in most regions of the world. The original discovery and single record of *Peltidium nayarit* was from a rocky beach (20°46'59.46"N, 105°30'35.48"W, Nayarit, central Pacific of Mexico) as a result of resuspension of sediments by turbulence from the meiobenthic community into the water (Suárez-Morales and Jarquín-González 2013).

We report the second record of this species from two distant oceanic islands at Revillagigedo National Park, San Benedicto and Clarion Islands. The San Benedicto record represents an unexpected distant habitat about 600 km offshore from the type locality on the Nayarit coast; Clarion Island is a further 425 km offshore from San Benedicto Island. This broad distribution range may be related to the influence of episodic storms and hurricanes caus-

ing anomalous river plumes that favor improbable zooplankton transport between the mainland (Nayarit and Colima states) and the Islas Marias Archipelago, four islands located close to the shelf-break off the central Mexican Pacific coast (Martínez-Flores et al. 2011; Gómez-Gutiérrez et al. 2014). However, other oceanographic processes, such as eddies from Cabo San Lucas and Cabo Corrientes with a typical southwest offshore trajectory (Kurczyn et al. 2012) can cause the drift of offshore zooplankton to reach the insular habitats of Revillagigedo Archipelago. *Peltidium nayarit* in its planktonic phase is allegedly a low-abundance copepod species that likely attains larger population densities in the epibenthic habitat, which will be investigated in future studies.

Acknowledgements

Additional information

Conflict of interest

The authors have declared that no competing interests exist.

Ethical statement

No ethical statement was reported.

Funding

Author contributions

Conceptualization: JRPG, JGG. Data curation: JRPG, JGG. Formal analysis: JRPG. Funding acquisition: JGG, JRPG.

Author ORCIDs

José Ricardo Palomares-García ⬤ https://orcid.org/0000-0002-0054-9656
Jaime Gómez-Gutiérrez ⬤ https://orcid.org/0000-0003-2516-897X

Data availability

All of the data that support the findings of this study are available in the main text.

References

Gheerardyn H, Fiers F, Vincx M, De Troch M (2006) *Peltidiphonte* gen. n., a new taxon of Laophontidae (Copepoda: Harpacticoida) from coral substrates of the Indo-West Pacific Ocean. Hydrobiologia 553: 171–199. https://doi.org/10.1007/s10750-005-1134-0

Gómez S, Varela C (2013) A new species of *Alteutha* Baird (Harpacticoida: Peltidiidae) from north-western Mexico. Journal of Natural History 47(5–12): 313–328. https://doi.org/10.1080/00222933.2012.747634

Gómez-Gutiérrez J, Funes-Rodríguez R, Arroyo-Ramírez K, Sánchez-Ortíz CA, Beltrán-Castro JR, Hernández-Trujillo S, Palomares-García JR, Aburto-Oropeza O, Ezcurra E (2014) Oceanographic mechanisms that possibly explain dominance of neritic-tropical zooplankton species assemblages around the Islas Marías Archipelago, Mexico. Latin American Journal of Aquatic Research 42(5): 1009–1034. https://doi.org/10.3856/vol42-issue5-fulltext-7

Hicks GR (1980) Structure of phytal harpacticoid copepod assemblages and the influence of habitat complexity and turbidity. Journal of Experimental Marine Biology and Ecology 44(2): 157–192. https://doi.org/10.1016/0022-0981(80)90151-3

Kurczyn JA, Beier E, Lavín MF, Chaigneau A (2012) Mesoscale eddies in the northeastern Pacific tropical-subtropical transition zone: Statistical characterization from satellite altimetry. Journal of Geophysical Research: Oceans 117: C10. https://doi.org/10.1029/2012JC007970

Martínez-Flores G, Nava-Sánchez EH, Zaitzev O (2011) Remote sensing of suspended matter plumes triggered by runoff in the south Gulf of California. CICIMAR Oceánides 26(1): 1–18. https://doi.org/10.37543/oceanides.v26i1.91

Nicholls AG (1941) Littoral Copepoda from South Australia. I. Harpacticoida. Records of the South Australian Museum 6(4): 381–427.

Noodt W (1971) Ecology of the Copepoda. In: Hulings HC (Ed.) Proceedings of the First International Conference on Meiofauna. Smithsonian Contributions to Zoology 76: 97–102.

Smith EP, Richardson SL (1977) Standard techniques for pelagic fish eggs and larvae surveys. FAO Fisheries Technical Papers, Rome 175: 1–100.

Suárez-Morales E, Jarquín-González J (2013) A new species of *Peltidium* Philippi, 1839 (Crustacea, Copepoda, Harpacticoida) from the Pacific coast of Mexico. ZooKeys 325: 21–32. https://doi.org/10.3897/zookeys.325.5726

Suárez-Morales E, De Troch M, Fiers F (2006) A checklist of the marine Harpacticoida (Copepoda) of the Caribbean Sea. Zootaxa 1285: 1–19. https://doi.org/10.11646/zootaxa.1285.1.1

Varela C (2005) Una nueva especie de *Peltidium* (Copepoda: Harpacticoida) de Cuba. Novitates Caribaea 6: 51–62. https://doi.org/10.33800/nc.v0i6.107

Varela C, Gómez S (2013). Dos nuevas especies de la familia Peltidiidae Boeck, 1873 (Copepoda: Harpacticoida) de Cuba. Novitates Caribaea 6: 51–62. https://doi.org/10.33800/nc.v0i6.107

Walter TC, Boxshall G (2024) World of Copepods Database. *Peltidium* Philippi, 1839. World Register of Marine Species. https://www.marinespecies.org/aphia.php?p=taxdetails&id=115430 [on 2024-07-11]

Wells JBJ (2007) An annotated checklist and keys to the species of Copepoda Harpacticoida (Crustacea). Zootaxa 1568: 1–872. https://doi.org/10.11646/zootaxa.1568.1.1

ZooKeys

Revision of the Afrotropical genus *Protoleptops* Heinrich, 1967 (Hymenoptera, Ichneumonidae, Ichneumoninae), with description of a new species from Burundi

Davide Dal Pos[1], Augustijn De Ketelaere[2], Filippo Di Giovanni[3]

1 Department of Biology, University of Central Florida, Orlando, FL 32816, USA

2 Beernem, Belgium

3 Department of Life Sciences, University of Siena, Siena, Italy

Corresponding author: Filippo Di Giovanni (aphelocheirus@gmail.com, filippo.digiovanni@unisi.it)

Abstract

This study presents a comprehensive revision of the genus *Protoleptops* Heinrich, 1967. We describe a new species, *P. nyeupe* Dal Pos & Di Giovanni, **sp. nov.**, from Burundi, marking the first documented occurrence of an Ichneumoninae species in the country. Additionally, we provide the first diagnostic description of the female *P. farquharsoni* Heinrich, 1967 and report a new occurrence of this species in KwaZulu-Natal. Furthermore, we document *P. magnificus* for Mpumalanga (South Africa) and *P. angolae* Heinrich, 1967 in Uganda, thereby extending the known range of the latter into East Africa. A detailed catalogue of all species within the genus *Protoleptops* is also included.

Key words: Biodiversity, Darwin wasps, identification key, new records, parasitoids, taxonomy

OPEN ACCESS

Introduction

Among the extant subfamilies of Darwin wasps, Ichneumoninae stands out as the most diverse, with over 4300 species in 430 genera (Yu et al. 2016; Santos et al. 2021). After a troubled past, marked by several inconsistent and paraphyletic tribal subdivisions, the subfamily Ichneumoninae is currently divided into seven monophyletic tribes, with Ichneumonini comprising the vast majority of the taxa (Santos et al. 2021). In the Afrotropics, Heinrich (1967) recognized 12 tribes of Ichneumoninae (and did not deal with Phaeogenini), of which nine have been synonymized under Ichneumonini (Santos et al. 2021). Among these dissolved tribes, Protichneumonini was recognized by having: (1) the area dentipara gradually curving down on the propodeum, almost reaching the hind coxa; (2) frons smooth, without longitudinal carina; (3) propodeum not abbreviated into a boss or arch; (4) head not cubical; (5) face and clypeus with a distinct epistomal sulcus (also called clypeal suture); and (6) mandibles not or only slightly twisted (e.g., Heinrich 1961; Heinrich 1967).

Within Protichneumonini, Heinrich (1967) described two new genera: the monotypic *Protoleptops* Heinrich, 1967, comprising only *Protoleptops heinrichi*

Heinrich, 1967, and *Apatetorops* Heinrich, which contained three new species – *Apatetorops angolae* Heinrich, 1967, *A. farquharsoni* Heinrich, 1967, and *A. magnificus* Heinrich, 1967. Heinrich (1967) proposed mainly the following characters for the separation of the two genera: the carination of the propodeum (well developed in *Protoleptops*, extremely reduced in *Apatetorops*) and the constriction of T2–T5 (constricted in *Protoleptops*). Later on, Townes and Townes (1973) recognized *Apatetorops* as a junior synonym of *Protoleptops*, without providing any reasoning for their action but probably not considering the above characters as sufficient for the separation of the two genera. Since then, the genus has never been reviewed nor recorded.

In the current contribution, we provide a review of *Protoleptops*, with an updated diagnosis of the genus, the first diagnosis of the female of *P. farquharsoni*, and the description of a new species, *P. nyeupe* Dal Pos & Di Giovanni, sp. nov. from Burundi. Additionally, a commented catalogue of the species is presented, together with some additional new distributional records.

Materials and methods

Photographs

An OPTIKA SZM-2 dissecting stereo microscope was used for observation and study. Photographs of *Protoleptops nyeupe* Dal Pos & Di Giovanni, sp. nov. were taken with a Canon EOS 7D, Canon MP-E 65 mm f/2.8 1–5 × macro lens and a Canon EF 100 mm macro lens. Zerene Stacker software ver. 1.04 was used for the stacking. Images were enhanced using Adobe Photoshop ver. 24.4.1. All the other pictures were taken using an Olympus OM-D camera mounted on a Leica M125 C binocular microscope and stacked using Helicon Focus (ver. 8).

Mapping

Maps were generated in QGIS ver. 3.2 using the ESRI Imagery plugins (https://www.esri.com), integrated into the Python console for QGIS for the main background layer, and an overlaid globe projection using the Thematic Mapping in the Thematic Mapping Engine integration. Following Dal Pos et al. (2023), the distribution for Madagascar follows the official division, which recognizes 23 regions ("faritra") instead of the former six provinces (INSTAT 2010).

List of depositories

DDPC	Davide Dal Pos private collection, Orlando, Florida, USA;
FSCA	Florida State Collection of Arthropods, Gainesville, Florida, USA (Elijah Talamas);
MNHN	Muséum national d'Histoire naturelle, Paris, France;
MZUR	Museum of Entomology, "Sapienza" University of Rome, Italy (Maurizio Mei);
OÖLM	Oberösterreichische Landesmuseen, Linz, Austria;
ZSM	Zoologische Staatssammlung München, Munich, Germany (Olga Schmidt).

Data of examined material

Label information for the type specimens is reported verbatim, using the following conventions: / = different lines; // = different labels; italic = handwriting. For non-type specimens, names of collecting localities have been standardized.

Treatment of taxa

Morphological terminology follows Broad et al. (2018) and is aligned with the Hymenoptera Anatomy Ontology (Yoder et al. 2010). However, unlike Broad et al. (2018), we used the following terms: "mesoscutellum" instead of "scutellum" [see Dal Pos et al. (2024) for more details]; and "epistomal sulcus" instead of "clypeal sulcus". We also decided to employ "propodeum" instead of the HAO-suggested term "metapectal-propodeal complex" simply because the former is more widely used. For propodeal carinae and areas, we adhered to the terminology used by Broad et al. (2018) and we did not align it with the HAO, as this terminology is almost completely absent from the database. In addition, we reported the widely used term "costula" to indicate the portion of the anterior transverse carina dividing the area externa from the area dentipara. Names of metasomal tergites are abbreviated as T1 (first metasomal tergite), T2 (second metasomal tergite), etc.

For each species, a differential diagnosis, type information, material examined, and relevant comments are provided. Type localities are reported as they appeared in the original publication with the addition of the country of origin. Unavailable names are identified in square brackets (as in Dal Pos et al. 2023).

Results

Key to the species of *Protoleptops* Heinrich, 1967

1 Carination of propodeum nearly complete (Fig. 4D, 6B): lateral portion of anterior transverse carina (i.e., costula) strong, also lateral longitudinal carina at the level of area dentipara distinct, even forming a slight ridge between area dentipara and area spiracularis (Fig. 6B). Scopa absent (Fig. 4C). T2–T5 each anteriorly constricted (Fig. 4E)................***P. heinrichi* Heinrich, 1967**
– Carination of propodeum incomplete (Figs 1D, 3B, 5D, 6E, 7B): anterior transverse carina lacking or at least incomplete (i.e., costula absent or only hinted), area dentipara confluent with area externa and area spiracularis. Scopa present (Figs 1E, 2C, 5E, 7E). T2–T5 not anteriorly constricted (Figs 1F, 2E, 3B, 3E, 5F, 6E, 7B)..**2**
2 Temples straight (not bulging) in dorsal view (Figs 1C, 7C). Hind tarsus white marked **3**
– Temples strongly bulging in dorsal view (Figs 2D, 5C). Hind tarsus brownish-black..**4**
3 T2 medially densely punctate (Fig. 1F, 3B). In females, mesoscutellum reddish-orange, mesoscutum black laterally, reddish-orange medially (Fig. 1D). Scopa small, reduced to a tuft of setae on ventro-distal area of the hind coxa (Fig. 1E). T2 black with a posterior white band (Fig. 1F, 3B). Area petiolaris not delimited, confluent with area basalis and area superomedia

(Fig. 1D, 3B). Mesopleuron densely and strongly punctate (Fig. 1A, 3A) .... ***P. angolae* (Heinrich, 1967)**

‒ T2 medially strongly longitudinally striate (Fig. 7B). In females, mesoscutellum and mesoscutum completely white (Fig. 7A). Scopa mid-sized, covering 1/3 of the ventro-distal area of the hind coxa (Fig. 7E). T2 completely reddish-brown, without posterior white band (Fig. 7B). Area petiolaris separated from area superomedia (Fig. 7B). Mesopleuron superficially and sparsely punctate ....***P. nyeupe* Dal Pos & Di Giovanni, sp. nov.**

4 T2 strongly longitudinally striate; T3‒T8 smooth and shining (Fig. 5F, 6E). Mesoscutum sparsely and superficially punctate throughout; mesoscutellum with lateral white bands, reddish-brown medially (Fig. 5C). Scopa large, covering roughly 2/3 of the ventro-distal area of the hind coxa (Fig. 5E) ....***P. magnificus* (Heinrich, 1967)**

‒ T2 medially densely punctate; T3‒T8 shagreened (Fig. 2E, 3E). Mesoscutum densely punctate anteriorly; mesoscutellum completely reddish-orange (Fig. 2D). Scopa reduced to a tuft of setae on ventro-distal area of the hind coxa (Fig. 2C) .... ***P. farquharsoni* (Heinrich, 1967)**

Taxonomy

Class Insecta Linnaeus, 1758
Order Hymenoptera Linnaeus, 1758
Superfamily Ichneumonoidea Latreille, 1802
Family Ichneumonidae Latreille, 1802
Subfamily Ichneumoninae Latreille, 1802
Tribe Ichneumonini Latreille, 1802

Genus *Protoleptops* Heinrich, 1967

Protoleptops Heinrich, 1967: 71‒72. Type species *Protoleptops heinrichi* Heinrich, 1967, by original designation.

Apatetorops Heinrich, 1967: 79‒81. Type species *Apatetorops magnificus* Heinrich, 1967, by original designation. Synonymized by Townes and Townes (1973: 226).

Diagnosis. We hereby provide a brief diagnosis of *Protoleptops* by including the traits of its junior synonym *Apatetorops*, therefore expanding the concept of the genus. We discovered a new character that separates well the former two genera that was not reported by Heinrich (1967): the presence/absence of a scopa on the ventral section of the hind coxa. The dimension of the scopa also works well in separating some of the species (see key above). A phylogenetic analysis with the inclusion of more specimens will be necessary to understand if the synonymy of the two genera proposed by Townes and Townes (1973) still stands. Since *Apatetorops* and *Protoleptops* were included by Heinrich (1967) in the now-dissolved tribe Protichneumonini, we invite the reader to either use Heinrich's (1967) key to the Afrotropical tribe or review our diagnosis in the Introduction. Within this former tribe, *Protoleptops* can easily be distinguished from all the other Afrotropical genera of Ichneumoninae by the following combination of characters: (1) carination of the propodeum not fully complete, at

least with area superomedia and area basalis confluent (divided in *Chasmopygium* Heinrich, 1967 and *Holcichneumon* Cameron, 1911); (2) postpetiole with either irregular striation or puncto-striate (uniformly and densely punctate in *Aethiamblys* Heinrich, 1967, *Afrocoelichneumon* Heinrich, 1938, *Corymbichneumon* Morley, 1919, and *Punctileptops* Heinrich, 1967); (3) hypostomal carina not lamellate nor with triangular projections (modified in *Genaemirum* Heinrich, 1936, *Leptophatnus* Cameron, 1906, *Oriphatnus* Heinrich, 1967); (4) lower tooth of the mandible lying in the same plane as the upper tooth (bent inward in *Apatetorides* Heinrich, 1938); (5) T2 with punctures (almost completely smooth and impunctate in *Apatetor* Saussure, 1892); (6) area between gastrocoeli bigger than the width of a gastrocoelus (gastrocoeli extremely enlarged in *Stenapatetor* Heinrich, 1938); (7) metascutellum not carinated or carinated only at the base; (8) mandible wide and robust (slender in *Pseudocoelichneumon* Heinrich, 1967); (9) upper tooth longer than lower tooth (shortened in *Liojoppa* Szépligeti, 1908); (10) mesoscutum longer than wide (as long as wide in *Liojoppa* Szépligeti, 1908); (11) metascutellum not globular (globular in *Coeloleptops* Heinrich, 1967); (12) first flagellar segment longer than second (shorter in *Punctileptops* Heinrich, 1967); and (13) area dentipara not well defined (bordered by carinae in *Punctileptops* Heinrich, 1967).

Protoleptops angolae (Heinrich, 1967)
Figs 1A–F, 3A–C

Apatetorops angolae Heinrich, 1967: 83–84 (original description, key); Schmidt and Schmidt 2011: 64 (type catalogue).
Protoleptops angolae; Townes and Townes 1973: 226 (catalogue, new combination); Yu and Horstmann 1997: 530 (catalogue); Yu et al. 2016 (catalogue).

Differential diagnosis. *Protoleptops angolae* can be easily distinguished from all the other known species of the genus by the following combination of characters: (1) incomplete carination of propodeum, with costulae lacking and area dentipara confluent with area externa and area spiracularis (carination almost complete in *P. heinrichi*); (2) temples straight and converging (bulging and not converging in *P. farquharsoni*, *P. heinrichi* and *P. magnificus*); (3) white hind tarsus (infuscate in *P. farquharsoni*, *P. heinrichi*, and *P. magnificus*); (4) presence of a small scopa (absent in *P. heinrichi*, bigger in *P. magnificus* and *P. nyeupe* sp. nov.); (5) mesoscutellum reddish-orange (entirely white in *P. nyeupe* sp. nov. and with white lateral marks in *P. magnificus*); (6) T2 medially densely punctate (longitudinally striate in *P. magnificus* and *P. nyeupe* sp. nov.); (7) area petiolaris not delimited (clearly separated from area superomedia in *P. nyeupe* sp. nov.); and (8) mesopleuron densely and strongly punctate (superficially and sparsely punctate in *P. nyeupe* sp. nov.).

Original type series. *Holotype* (by original designation). Angola • ♀; Cuanza Norte, Roca Canzele, 30 km north of Quiculungo, Mar. 1954; (ZSM). *Paratypes* Angola • 1♀ & 1♂; Cuanza Norte, Roca Canzele, 30 km north of Quiculungo, Mar. 1954; (ZSM).

Material examined. *Holotype.* Angola • ♀; "[White label] Roca Canzele / Angola, 30 km / nordl.Quiculungo / III. 54 // [White label] *Apatetorops* / ♀ *angolae* / det
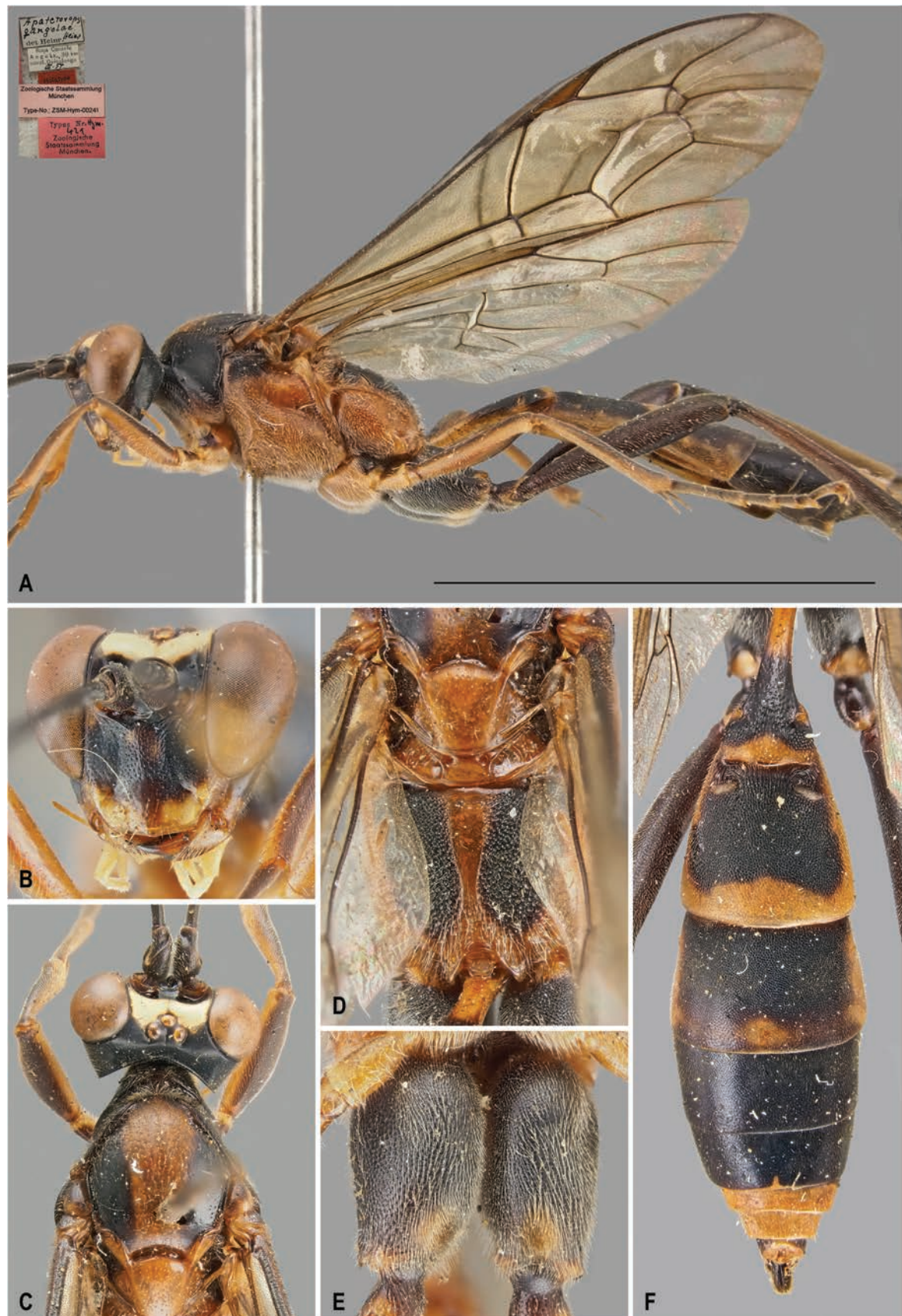
Figure 1. *Protoleptops angolae* (Heinrich, 1967), female, holotype **A** habitus, lateral view **B** face, frontal view **C** head and mesoscutum, dorsal view **D** mesoscutellum and propodeum, dorsal view **E** hind coxa, ventral view **F** metasomal tergites, dorsal view. Scale bar: 1 cm.

Heinr. *Heinr* // [Red label] Holotype // [Pink label] Zoologische Staatssammlung / München / Type-No.: ZSM-Hym-00241 // [Red label] Typus Nr. *Hym.* / *421* / Zoologische / Staatsammlung / München.”; (ZSM). **Paratype.** ANGOLA • 1♂; “[White label] Roca Canzele / Angola, 30 km / nordl.Quiculungo / III. 54 // [White label] *Apatetorops* / ♂ *angolae* / det Heinr. *Heinr* // [Red label] Allotype; (ZSM).

Non-type specimens. UGANDA • 1♀; Kibale N. P., Kanyawara Bio. Station, 00°33'54.4"N, 30°21'29.8"E, 11−18 Apr. 2010, 1509 m, Malaise trap, S. Katusabe & Co. leg. (DDPC).

Male. Described in the original description by Heinrich (1967) as “Allotype”.

Distribution. Angola: Cuanza Norte Province (Heinrich 1967); Uganda: Western Region (new record) (Fig. 8).

Remarks. *Protoleptops angolae* is hereby recorded for the first time in Uganda, expanding the range of the species from southern Africa to East Africa.

Protoleptops farquharsoni (Heinrich, 1967)
Figs 2A−E, 3D−F

Apatetorops farquharsoni Heinrich, 1967: 84−85 (original description, key); Schmidt and Schmidt 2011: 74 (type catalogue).
Protoleptops farquharsoni; Townes and Townes 1973: 226 (catalogue, new combination); Yu and Horstmann 1997: 530 (catalogue); Yu et al. 2016 (catalogue).

Diagnosis of female. The diagnosis of the female is provided here for the first time based on two females from South Africa (see below in Material examined). Compared to the male, the female has less white patterning overall. The prosternum, mesosternum, and femora are predominantly reddish-brown with only a few scattered yellow patches. In males, these body parts are mostly whitish-yellow. The face is primarily white, with a darker, infuscate area in the center. The orange of the mesoscutum is slightly reduced and the infuscation is more extensive. The posterior yellow band on T2 is smaller and the hind coxa is entirely reddish-brown without any white markings.

Differential diagnosis. *Protoleptops farquharsoni* can be easily distinguished from all the other known species of the genus by the following combination of characters: (1) incomplete carination of propodeum, with costulae lacking and area dentipara confluent with area externa and area spicularis (carination almost complete in *P. heinrichi*); (2) temple, in dorsal view, bulging (straight and converging in *P. angolae* and *P. nyeupe* sp. nov.); (3) hind tarsus brownish-black (white in *P. angolae* and *P. nyeupe* sp. nov.); (4) presence of a small scopa (absent in *P. heinrichi*, bigger in *P. magnificus* and *P. nyeupe* sp. nov.); (5) mesoscutellum reddish-orange (entirely white in *P. nyeupe* sp. nov. and with white lateral marks in *P. heinrichi* and *P. magnificus*); (6) T2 medially densely punctate (longitudinally striate in *P. magnificus* and *P. nyeupe* sp. nov.); and (7) mesoscutum densely punctate anteriorly (sparsely and superficially punctate in *P. magnificus*).

Original type series. *Holotype* (by original designation). SOUTH AFRICA • ♂; Eastern Cape, King William's Town [now Qonce], Peeree forest, 6 Mar. 1962; (ZSM).
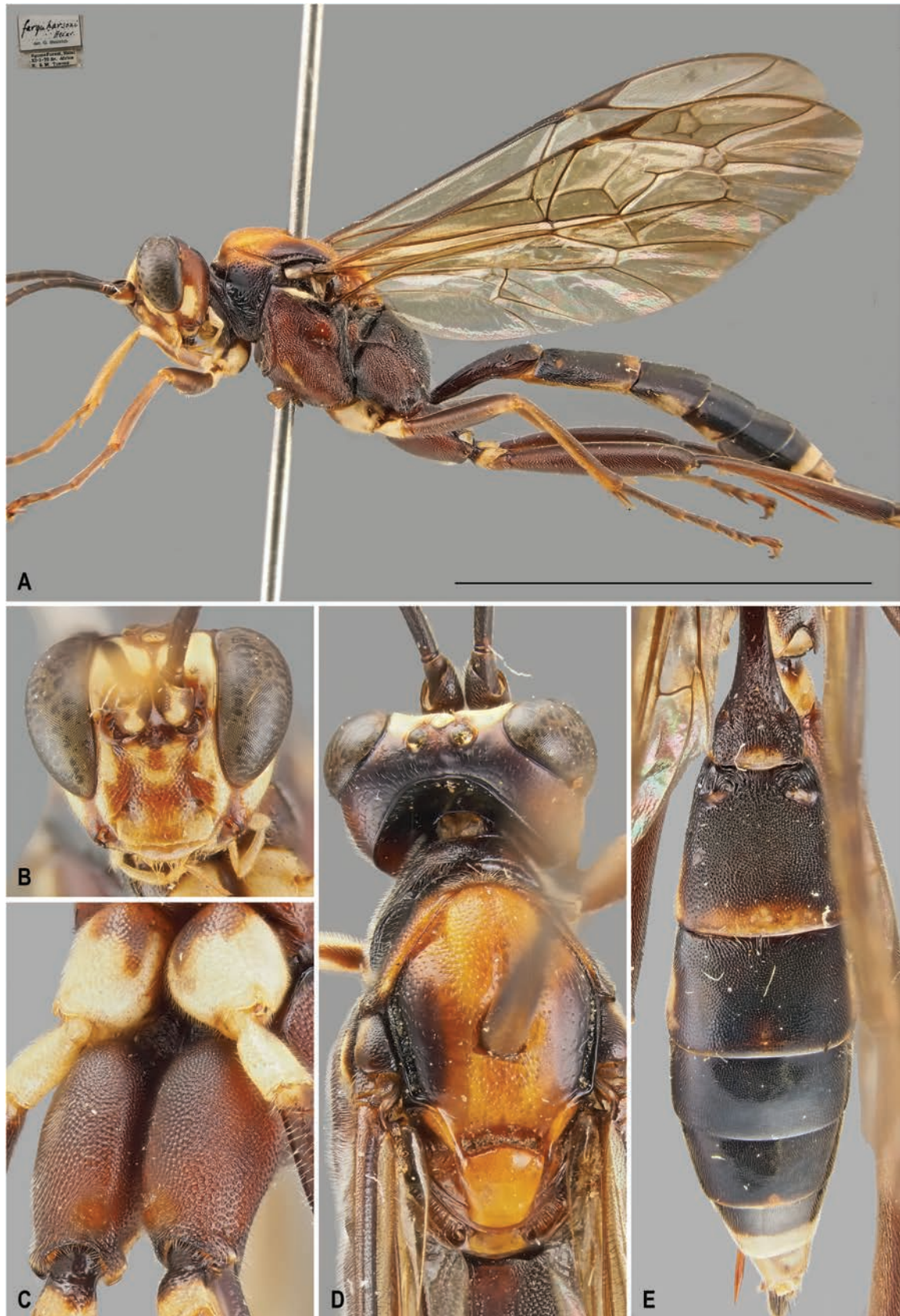
Figure 2. *Protoleptops farquharsoni* (Heinrich, 1967), female **A** habitus, lateral view **B** face, frontal view **C** hind coxa, ventral view **D** head, mesoscutum and mesoscutellum, dorsal view **E** metasomal tergites, dorsal view. Scale bar: 1 cm.
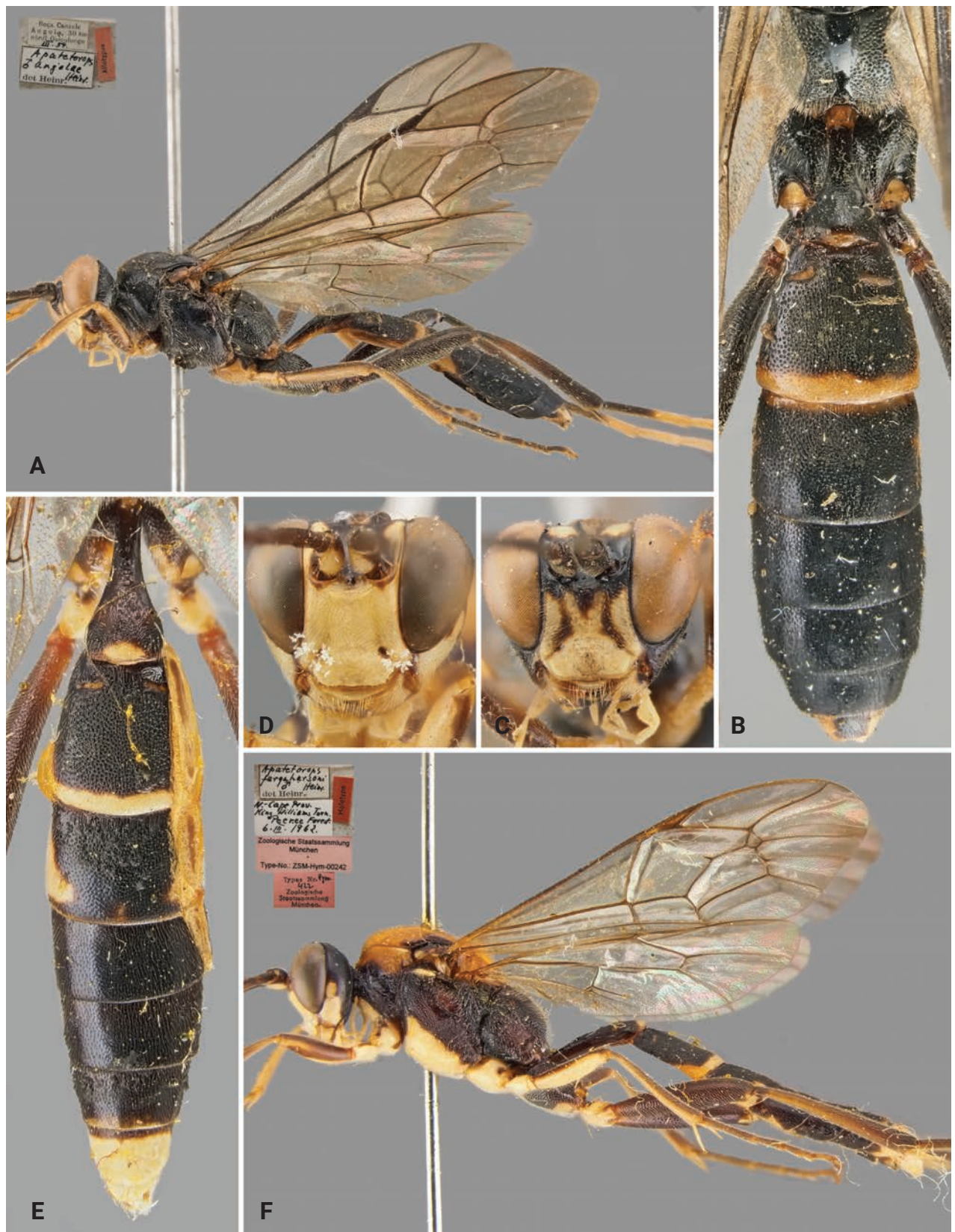
Figure 3. *Protoleptops angolae* (Heinrich, 1967), male, paratype **A** habitus, lateral view **B** propodeum and metasomal tergites, dorsal view **C** face, frontal view. *Protoleptops farquharsoni* (Heinrich, 1967), male, holotype **D** face, frontal view **E** metasomal tergites, dorsal view **F** habitus, lateral view. Scale bar: 1 cm.

Material examined. *Holotype*. SOUTH AFRICA • ♂; "[White label] *N.-Cape Prov. / King Williams Town / Peeree Forest / 6.III. 1962* // [White label] *Apatetorops / farquharsoni / ♂ Heinr.* / det Heinr. // [Red label] Holotype // [Pink label] Zoologische Staatssammlung / München / Type-No.: ZSM-Hym-00242 // [Red label] Typus Nr. *Hym. / 422* / Zoologische / Staatsammlung / München."; (ZSM).

Non-type specimens. SOUTH AFRICA • 2♀♀; KwaZulu-Natal, Ngome Forest, 1 Nov. 1970, H. & M. Townes leg.; (ZSM).

Distribution. South Africa: Eastern Cape (Heinrich 1967); KwaZulu-Natal (new record) (Fig. 8).

Remarks. The two specimens used for the first female diagnosis of the species had been identified as *Apatetorops farquharsoni* by Gerd Heinrich, but the records were never published, despite being integrated into the ZSM collection.

In the original identification key, Heinrich (1967: 81) mentioned "mesosternum uniformly white" as a trait to differentiate *farquharsoni* from *angolae*. However, in the female of the species, the mesosternum is reddish-brown and therefore, the white coloration of the mesosternum should be considered a male-specific trait.

Protoleptops heinrichi Heinrich, 1967
Figs 4A–E, 6A–C

Protoleptops heinrichi Heinrich, 1967: 72–73 (original description, key, figures); Townes and Townes 1973: 226 (catalogue); Yu and Horstmann 1997: 530 (catalogue); Yu et al. 2016 (catalogue).

Differential diagnosis. *Protoleptops heinrichi* can be easily distinguished from all the other known species of the genus by the following combination of characters: (1) almost complete carination of the propodeum (incomplete in all the other species); (2) absence of a scopa (present in all the other species); and (3) T2–T5 anteriorly constricted (not constricted in all the other species).

Original type series. *Holotype* (by original designation). MADAGASCAR • ♀; Antsiranana, Ivondro, Feb. 1940; (MNHN). ***Paratypes*.** MADAGASCAR • 1♂; Antsiranana, Ivondro, Dec. 1938; MNHN • 1♀; Antsiranana, Rogez, 1935; (ZSM).

Material examined. *Holotype*. MADAGASCAR • ♀; "[White label] MADAGASCAR // [White label] *Ivondro* // [Blue label] MUSÉUM PARIS / *II.40* / A. SEYRIG // [White label] *Apatetor / heinrichi*/ TYPE // [White label] *Protoleptops / ♀ heinrichi / Heinr.* / det Heinr. // [Red label] Holotype // [Whitel label] Muséum Paris / EY10172"; (MNHN). ***Paratypes*.** MADAGASCAR • ♂; "[White label] MADAGASCAR // [White label] *Ivondro* [Written over Rogez, Foret Cote Est] // [Blue label] MUSÉUM PARIS / *XII.38* / A. SEYRIG // [White label] *Protoleptops / heinrichi ♂ / Heinr.* / det Heinr. // [Red label] Allotypus // [Whitel label] Muséum Paris / EY10173"; (MNHN) • ♀; "[White label] MADAGASCAR / Rogez / Foret Core Est // [Blue label] MUSÉUM PARIS / *1935* / A. SEYRIG // [White label] *heinrichi / Heinr.* / det. G. Heinr. // [White label] *Protoleptops / heinrichi / ♀ Heinr.* / det Heinr. // [Yellow label] Paratypus"; (ZSM).

Male. Described in the original description by Heinrich (1967) as "Allotype".

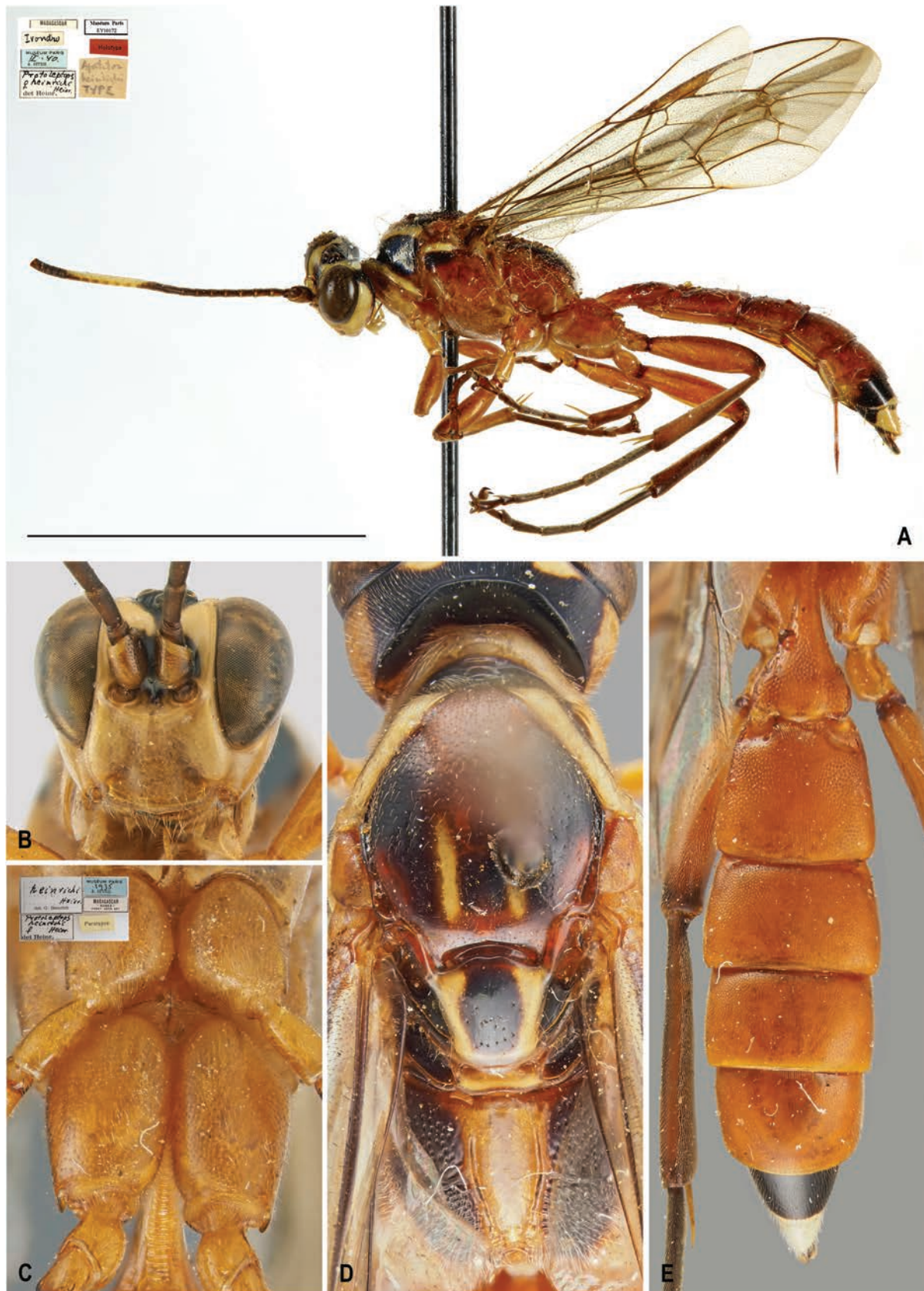**Distribution.** Madagascar: Antsiranana (Heinrich 1967) (Fig. 8).

Figure 4. *Protoleptops heinrichi* Heinrich, 1967, female, holotype **A** habitus, lateral view; female, paratype **B** face, frontal view **C** hind coxa, ventral view **D** head, mesoscutum, mesoscutellum, and propodeum, dorsal view **E** metasomal tergites, dorsal view. Images of the habitus downloaded from the public MNHN database (available at https://science.mnhn.fr/institution/mnhn/collection/ey/item/ey10172). Scale bar: 1 cm.

Remarks. The specific epithet given by Heinrich might appear to be self-glorification, as it is named after himself. However, it is actually a dedication to his friend, A. Seyrig, who was the first to recognize it as a new species and labeled it as *"Apatetor heinrichi"*, but never officially described it. When Heinrich discovered the species at the MNHN, he chose to retain the name in honor of his friend's intentions, stating: "I felt bound to carry out the will of my late friend, rather than to shrink from the possibility of being blamed for self-glorification in using this species name" (Heinrich 1967: 72).

Protoleptops magnificus (Heinrich, 1967)
Figs 5A–F, 6D–F

Apatetorops magnificus Heinrich, 1967: 81–83 (original description, key, figures); Schmidt and Schmidt 2011: 83 (type catalogue).
Protoleptops magnifica [sic]; Townes and Townes 1973: 226 (catalogue, new combination, incorrect gender agreement).
Protoleptops magnificus; Yu and Horstmann 1997: 530 (catalogue, mandatory change); Yu et al. 2016 (catalogue).

Differential diagnosis. *Protoleptops magnificus* can be easily distinguished from all the other known species of the genus by the following combination of characters: (1) incomplete carination of the propodeum, with costulae lacking and area dentipara confluent with area externa and area spiracularis (carination almost complete in *P. heinrichi*); (2) temple, in dorsal view, bulging (straight and converging in in *P. angolae* and *P. nyeupe* sp. nov.); (3) hind tarsus infuscate (white in *P. angolae* and *P. nyeupe* sp. nov.); (4) presence of a scopa taking up 2/3 of the ventral part of the coxa (absent in *P. heinrichi*, reduced in *P. angolae* and *P. farquharsoni*); (5) mesoscutellum with lateral white marks (reddish-orange in *P. farquharsoni* and *P. angolae*); (6) T2 longitudinally striate medially (densely punctate in *P. angolae* and *P. farquharsoni*); and (7) mesoscutum sparsely and superficially punctate (densely punctate anteriorly in *P. farquharsoni*).

Original type series. *Holotype* (by original designation). Tanzania • ♀; Tanga, West Usambara Mountains, Lushoto, 1700 m 19 Feb. 1962; (ZSM).

***Paratypes*.** Tanzania • 5♀♀ & 1♂; same locality as the holotype, 17 Feb. 1962; ZSM • 1♀; same locality as the holotype, 1600 m, 5 Mar. 1962; (ZSM). South Africa • 1♀; Eastern Cape, Port St. Johns, 20 Feb. 1963; (ZSM)

Material examined. *Holotype*. Tanzania • ♀; "[White label] TANGANYIKA / W Usambara Mts. / 1700 m. Lushoto / *19*.II.1962 [White label] *Apatetorops* / *magnificus* / ♀ *Heinr.* / det.Heinr. // [Red label] Holotype // [Pink label] Zoologische Staatssammlung / München / Type-No.: ZSM-Hym-00240 // [Red label] Typus Nr. *Hym. / 420* / Zoologische / Staatsammlung / München."; (ZSM). ***Paratypes*.** Tanzania • ♂; "[White label] TANGANYIKA / W Usambara Mts. / 1700 m. Lushoto / *17*.II.1962 [White label] *Apatetorops* / *magnificus* / ♂ *Heinr.* / det.Heinr. // [Red label] Allotypus"; (ZSM).

Non-type specimens. South Africa • 1♀; Mpumalanga, Waterval-Boven [=Emgwenya], Elandsrivier, 18.i.2000, J. Halada leg.; (OÖLM).

Male. Described in the original description by Heinrich (1967) as "Allotype".
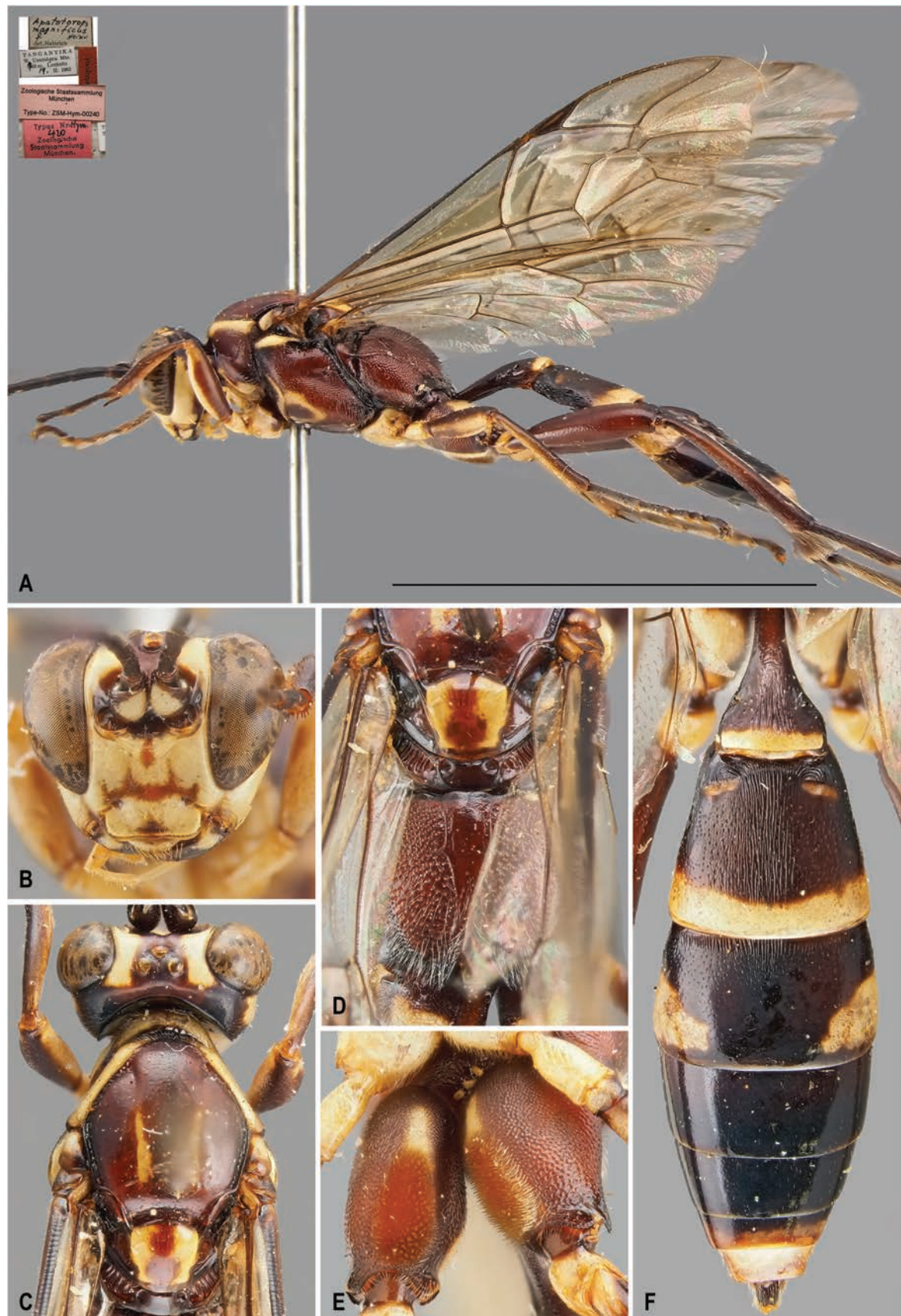
Figure 5. *Protoleptops magnificus* (Heinrich, 1967), female, holotype **A** habitus, lateral view **B** face, frontal view **C** head, mesoscutum and mesoscutellum, dorsal view **D** propodeum, dorsal view **E** hind coxa, ventral view **F** metasomal tergites, dorsal view. Scale bar: 1 cm.
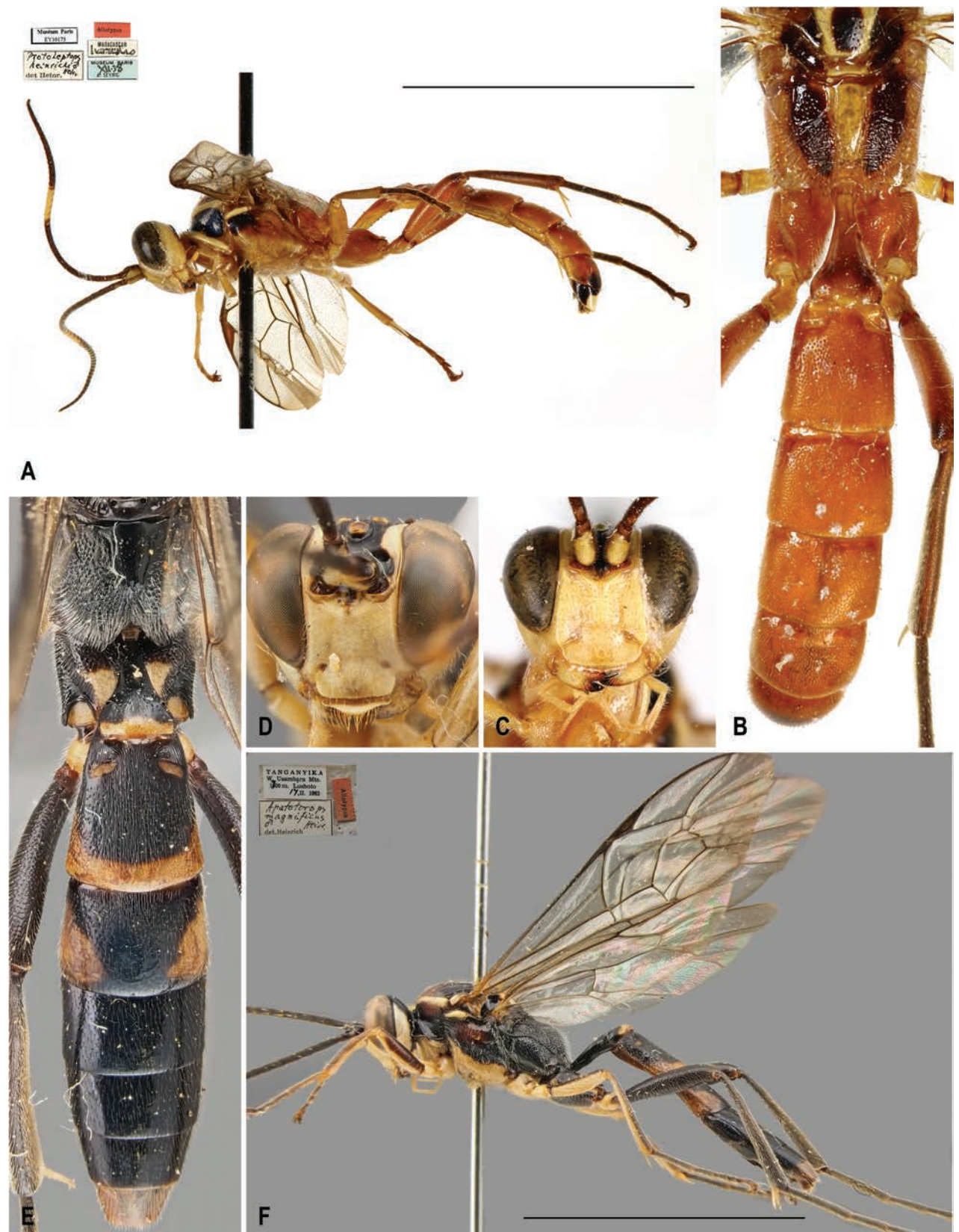
Figure 6. *Protoleptops heinrichi* Heinrich, 1967, male, paratype **A** habitus, lateral view **B** propodeum and metasomal tergites, dorsal view **C** face, frontal view. Downloaded from the public MNHN database (available at https://science.mnhn.fr/institution/mnhn/collection/ey/item/ey10173). *Protoleptops magnificus* (Heinrich, 1967), male, paratype, **D** face, frontal view **E** propodeum and metasomal tergites, dorsal view **F** habitus, lateral view. Scale bar: 1 cm.

Distribution. South Africa: Eastern Cape (Heinrich 1967); Mpumalanga (new record); Tanzania: Tanga region (Heinrich 1967) (Fig. 8).

Remarks. In their catalogue, Townes and Townes (1973: 226) provided a new combination for *Apatetorops magnificus* Heinrich, 1967, moving the species into the genus *Protoleptops*. While doing so, they referred to *Protoleptops magnifica* [sic], possibly misinterpreting the gender of the genus *Protoleptops* as feminine instead of masculine. Subsequently, Yu and Horstmann (1997: 530) correctly interpreted the gender as masculine and made the mandatory change to the suffix in accordance with ICZN (1999: article 34.2).

Protoleptops nyeupe Dal Pos & Di Giovanni, sp. nov.
https://zoobank.org/54F974F4-597C-46A2-B817-0EB76421D494
Fig. 7A−E

Type material. *Holotype* • ♀, "[White label] BURUNDI. Rwegura, Kibira / Nat. Park, 2 53 25.9S 29 27 25.4E, / 2226 m, 28-30.I.2011, M. Mei, / P. Cerretti, D. Withmore [Whitmore] leg. // [Red label] HOLOTYPE / *Protoleptops* / *nyeupe* / Dal Pos & Di Giovanni, des. 2024 // FSCA 00051872" (FSCA). The specimen is in perfect condition. ***Paratype*** • ♀, same data as the holotype. The specimen is in perfect condition (MZUR).

Differential diagnosis. *Protoleptops nyeupe* sp. nov. can be easily distinguished from all the other known species of the genus by the following combination of characters: (1) incomplete carination of the propodeum, with costulae lacking and area dentipara confluent with area externa and area spiracularis (almost complete in *P. heinrichi*); (2) temples straight and converging (bulging and not converging in *P. farquharsoni*, *P. heinrichi* and *P. magnificus*); (3) white hind tarsus (infuscate in *P. farquharsoni*, *P. heinrichi*, and *P. magnificus*); (4) presence of a scopa taking up 1/3 of the ventral part of the coxa (absent in *P. heinrichi*, reduced in *P. angolae* and *P. farquharsoni*, and taking up 2/3 of the ventral side of the coxa in *P. magnificus*); (5) mesocutellum entirely white (reddish-orange in *P. farquharsoni* and *P. angolae*; with lateral white marks in *P. heinrichi* and *P. magnificus*); (6) T2 medially longitudinally striate (densely punctate in *P. angolae* and *P. farquharsoni*); (7) area petiolaris well delimited (not well delimited in *P. angolae* sp. nov.); and (8) mesopleuron superficially and sparsely punctate (densely and strongly punctate in *P. angolae*).

Etymology. The specific epithet *nyeupe* is a noun in apposition, derived from the Swahili word "nyeupe" for white. This name refers to the extensive white coloration of the mesoscutum and mesoscutellum, which stands in stark contrast to the dark coloration of the rest of the body.

Description. Holotype female. Body length: 17.8 mm; fore wing length: 14.2 mm. ***Head***. Overall shining; face subquadrate, as wide as medially high, smooth, with very sparse and superficial punctures, medio-apically protruding in a very distinct blunt tubercle right below antennal sockets, clear delimitation between clypeus and face present; frons concave, smooth and shining; vertex matt and impunctate; ocellar triangle equilateral, elevated and proximally delimited by a shallow sulcus; ocular-ocellar distance about 1.3 × ocellus diameter, inter-ocellar distance 1.0 × ocellus diameter; occipital carina distinct and complete, meeting hypostomal carina at base of mandible; temples straight and converging in dorsal view; gena, in lateral view, not strongly inflated, matt; clypeus medially
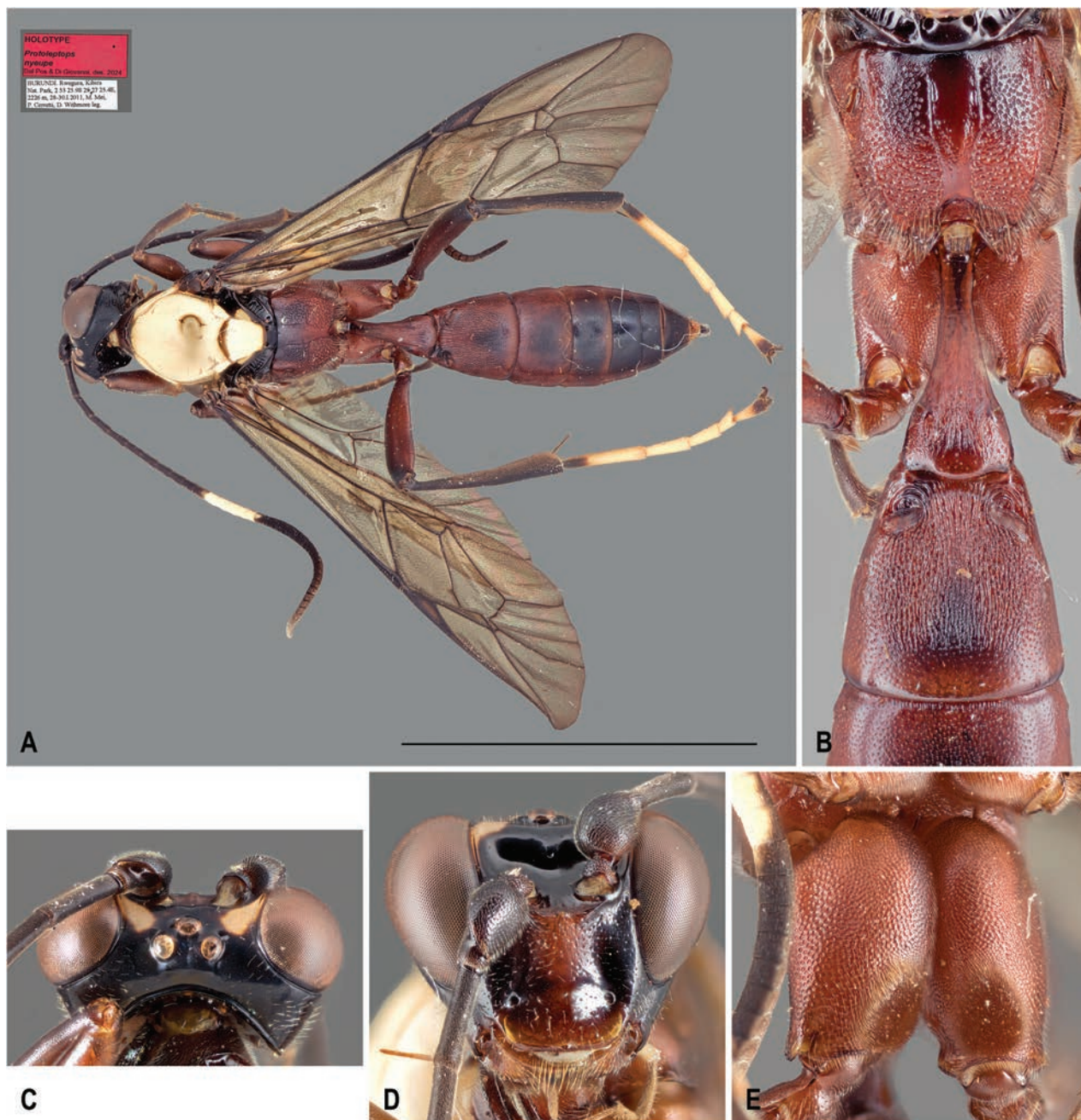
Figure 7. *Protoleptops nyeupe* Dal Pos & Di Giovanni, sp. nov., female, holotype **A** habitus, dorsal view **B** propodeum and T1-T2, dorsal view **C** head, dorsal view **D** face, frontal view **E** hind coxa, ventral view. Scale bar: 1 cm.

slightly convex in lateral view, shining with straight apical margin and almost completely impunctate; malar space about 0.7 × basal width of mandible; malar sulcus present and shagreened; mandible robust, with sparse setiferous punctures centrally, teeth rather stout and widely separated with ventral tooth shorter (about 0.5 ×) than upper tooth; maxillary palp long, reaching fore coxa, 5th segment about 1.5 × as long as 4th; antenna with 45 flagellomeres, slightly enlarged, with flagellomeres 20–38 ventrally flattened and 1.4 × as wide as long, 1st flagellomere about 1.3 × as long as 2nd, apical flagellomere distinctly longer than wide. ***Mesosoma***. Overall shining; pronotum with shallow punctures; epomia present and strong; propleuron smooth, with dense, shallow punctures and covered with setae, projected into a blunt, rounded flange ventro-apically; mesoscutum sub-
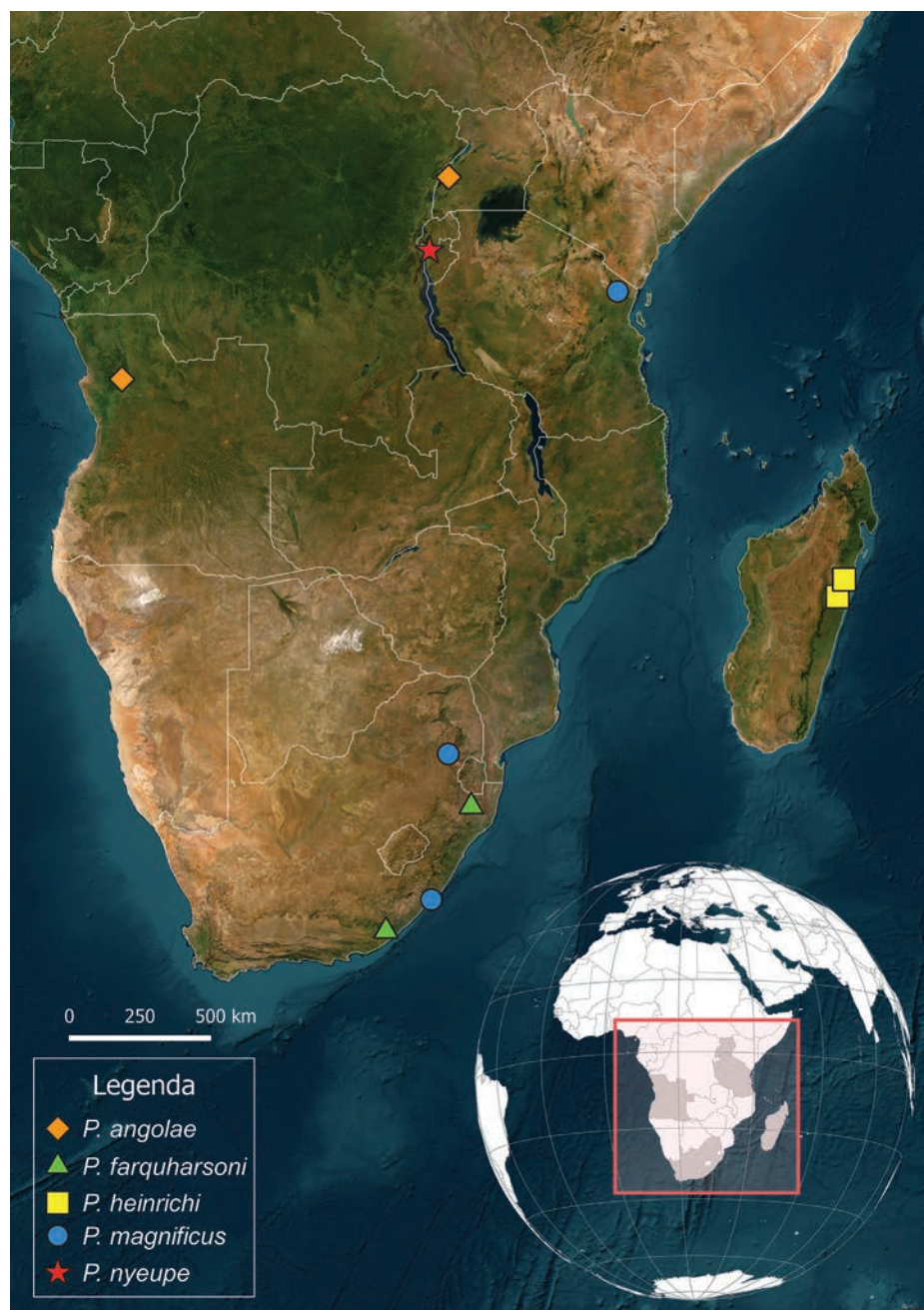
Figure 8. Distribution map of the known species of the genus *Protoleptops* Heinrich, 1967.

quadrate, smooth, impunctate, notauli absent; mesoscutellum not elevated over metascutellum, impunctate and not carinated; mesopleuron shining on upper 1/3, with shallow and sparse punctures, more densely and finely punctate ventrally, on upper-posterior section with a deep sulcus right below subtegular ridge; epicnemial carina continuous with subtegular ridge; subtegular ridge strongly projecting outwardly anteriorly; sternaulus absent; posterior transverse carina of mesosternum completely absent; metapleuron with dense, shallow punctures, juxtacoxal carina absent; propodeum short in lateral view, sloping gently with almost no horizontal portion, overall irregularly sculptured throughout except for anterior margin and for area basalis and area petiolaris, which are completely smooth and almost shining; lateral longitudinal carina present throughout length of propodeum; lateromedian longitudinal carina present; anterior transverse ca-

rina absent so that area basalis and area superomedia are continuous; posterior transverse carina present only medially, delimiting a small area petiolaris. ***Legs.*** All coxae setose; fore and middle coxae ventrally impunctate; hind coxa with dense punctures throughout; scopa present, occupying 1/3 of apico-ventral region of hind coxa. Hind femur about 5.3 × as long as medially high. Tarsal claws without pecten. ***Wings.*** Fore wing with 3rs-m present, areolet rhomboidal, with 3rs-m and 2rs-m converging; 1cu-a opposite M&RS, CU between 1m-cu&M and 2cu-a about 1.5 × as long as 2cu-a. Hind wing with distal abscissa of CU present, pigmented, CU about 3.5 × as long as cu-a. ***Metasoma.*** T1 shining throughout, with postpetiole longitudinally striate except shagreened posterior portion with sparse punctures; T2 with gastrocoeli deep and subquadrate; thyridia present, space between gastroceoli narrower than one gastrocoelus; T3 superficially and densely punctate, impunctate posteriorly; remaining tergites shagreened; terebra (i.e., external visible portion of the ovipositor) short, with densely setose ovipositor sheaths. ***Coloration.*** Head black with central area of face, clypeus and mandible (except black apical teeth) reddish-brown; two white comma-shaped patches on frons running from frontal orbit towards ocellar triangle. Scape and pedicel black with only a reddish-brown patch; flagellum black with white annulus present only on dorsal side, from 10th to 15th flagellomeres. Mesosoma reddish-brown, with dorso-lateral portion of propleuron, entire mesoscutum, and mesoscutellum white; dorsal portion of mesopleuron, metanotal trough and anterior portion of propodeum infuscate. Legs overall reddish-brown, with dorsal sides of all femora and fore and mid tibiae infuscate; hind tibia, fore and mid tarsi, black; hind tarsus white with only proximal part of basitarsus, distal portion of telotarsus and claws black. Wing entirely hyaline with pterostigma centrally light brown. Metasoma with T1–T3 reddish-brown with only an infuscate patch on postero-median portion of T2 and T3; T4 infuscate; T4–T8 black.

Male. Unknown.

Host. Unknown.

Distribution. Burundi: Cibitoke Province (Fig. 8).

Discussion

The discovery of the new species occurred in the bushes at the edge of a dirt road, where specimens of *P. nyeupe* sp. nov. were collected together with some females of an unidentified Cryptini (Ichneumonidae, Cryptinae), with which the new species shares an absolutely identical color pattern (i.e., creamy white mesoscutum in sharp contrast to the dark coloration of the rest of the body). The two species, *P. nyeupe* sp. nov. and the unidentified Cryptinae, markedly stood out from the background as small whitish moving spheres (M. Mei pers. obs.). From our observations in different museums and collections, various species and genera of both Ichneumoninae and Cryptinae share this distinctive color pattern in the Afrotropics. However, the significance of this unusual mimetic chain is likely to remain unanswered until a deeper understanding of the taxonomy and biology of Darwin wasps in the Afrotropics is achieved. Of note, the discovery of *P. nyuepe* sp. nov. also marks the first record of the subfamily Ichneumoninae for Burundi. This "surprising" finding, coupled with the first record of *P. angolae* in East Africa, shows that knowledge about the diversity and distribution of Darwin wasps in the Afrotropical region is still severely lacking.

Indeed, beyond a small number of nations that, for historical reasons, have been reasonably sampled, most ecotypes and countries in the Afrotropics have not been adequately investigated yet (Meier et al. 2024).

Acknowledgments

Additional information

Conflict of interest

The authors have declared that no competing interests exist.

Ethical statement

No ethical statement was reported.

Funding

Author contributions

Conceptualization: DDP, FDG; Writing - original draft: DDP; Writing - review & editing: DDP, ADK, FDG; Visualization: DDP, FDG; Funding acquisition: FDG.

Author ORCIDs

Davide Dal Pos ⓘ https://orcid.org/0000-0002-9122-934X
Augustijn De Ketelaere ⓘ https://orcid.org/0009-0007-0260-5483
Filippo Di Giovanni ⓘ https://orcid.org/0000-0002-9811-5599

Data availability

All of the data that support the findings of this study are available in the main text.

References

Broad GR, Shaw MR, Fitton MG (2018) Ichneumonid wasps (Hymenoptera: Ichneumonidae): their classification and biology. Handbooks for the Identification of British Insects 7: 1–418. https://doi.org/10.1079/9781800625471.0000

Dal Pos D, Claridge B, Diller E, van Noort S, Di Giovanni F (2023) Still counting: new records, nomenclatural notes, and three new species of Phaeogenini (Hymenoptera, Ichneumonidae, Ichneumoninae) from the Afrotropical region. European Journal of Taxonomy 868: 1–71. https://doi.org/10.5852/ejt.2023.868.2105

Dal Pos D, Broad GR, Martens A (2024) Small jewels: two new species of the rare genus *Masona* van Achterberg (Hymenoptera, Ichneumonoidea, Braconidae), with a cata-

logue of world species and comments on the peculiar morphology of the genus. European Journal of Taxonomy 925: 135–160. https://doi.org/10.5852/ejt.2024.925.2457

Heinrich G (1961) Synopsis of Nearctic Ichneumoninae Stenopneusticae with particular reference to the Northeastern Region (Hymenoptera). Part I. Introduction, Key to Nearctic Genera of Ichcneumoninae Stenopneusticae, and Synopsis of the Protichneumonini North of Mexico. The Canadian Entomologist 92: 1–88. https://doi.org/10.4039/entm9427fv

Heinrich G (1967) Synopsis and reclassification of the Ichneumoninae Stenopneusticae of Africa south of Sahara (Hym.). Vol. 1. Introduction; Key to Tribes and Subtribes of Ichneumoninae Stenopneusticae; Synopsis of the Protichneumonini, Ceratojoppini, Ischnojoppini, Trogini. Farmington State College Press, Altötting, Germany, 250 pp.

ICZN (1999) International code of zoological nomenclature. 4th edn. The International Trust for Zoological Nomenclature, London, UK, [xxix+]306 pp.

INSTAT [Institut Nationale de la Statistique] (2010) Présentation des résultats de la cartographie numérique en préparation du troisième recensement générale de la population et de l'habitation. Government of Madagascar [press release].

Meier N, Gordon M, van Noort S, Reynolds T, Rindos M, Di Giovanni F, Broad GR, Spasojevic T, Bennett A, Dal Pos D, Klopfstein S (2024) Species richness estimation of the Afrotropical Darwin wasps (Hymenoptera, Ichneumonidae). Plos ONE 19(7): e0307404. https://doi.org/10.1371/journal.pone.0307404

Santos BF, Wahl DB, Rousse P, Bennett AMR, Kula RR, Brady SG (2021) Phylogenomics of Ichneumoninae (Hymenoptera, Ichneumonidae) reveals pervasive morphological convergence and the shortcomings of previous classifications. Systematic Entomology 46: 704–824. https://doi.org/10.1111/syen.12484

Schmidt O, Schmidt S (2011) Primary types of Ichneumoninae described by Gerd H. Heinrich deposited in the Zoologische Staatssammlung München (Hymenoptera, Ichneumonidae). Spixiana 34(1): 59–107.

Townes HK, Townes M (1973) A catalogue and reclassification of the Ethiopian Ichneumonidae. Memoirs of the American Entomological Institute 19: 1–416.

Yoder MJ, Mikó I, Seltmann KC, Bertone MA, Deans AR (2010) A gross anatomy ontology for Hymenoptera. PLoS ONE 5: e15991. https://doi.org/10.1371/journal.pone.0015991

Yu DSK, Horstmann K (1997) A catalogue of world Ichneumonidae (Hymenoptera). Part 1: Subfamilies Acaenitinae to Ophioninae. Memoirs of the American Entomological Institute 58: 1–763.

Yu DSK, van Achterberg C, Horstmann K (2016) Taxapad 2016, Ichneumonoidea 2015. Nepean, Ontario, Canada.

ZooKeys

Research Article

Discovery of a new gall-inducing species, *Aciurina luminaria* (Insecta, Diptera, Tephritidae) via multi-trait integrative taxonomy

Quinlyn Baine[1] , Branden White[1], Vincent G. Martinson[1*] , Ellen O. Martinson[1*]

1 Department of Biology, University of New Mexico, 219 Yale Blvd, Albuquerque, NM 87131, USA
Corresponding author: Quinlyn Baine (quinbaine@gmail.com)

Abstract

Integrative taxonomic practices that combine multiple lines of evidence for species delimitation greatly improve our understanding of intra- and inter-species variation and biodiversity. However, extended phenotypes remain underutilized despite their potential as a species-specific set of extracorporeal morphological and life history traits. Primarily relying on variations in wing patterns has caused taxonomic confusion in the genus *Aciurina*, which are gall-inducing flies on Asteraceae plants in western North America. However, species display distinct gall morphologies that can be crucial for species identification. Here we investigate a unique gall morphotype in New Mexico and Colorado that was previously described as a variant of that induced by *Aciurina bigeloviae* (Cockerell, 1890). Our analysis has discovered several consistent features that distinguish it from galls of *A. bigeloviae*. A comprehensive description of *Aciurina luminaria* Baine, **sp. nov.** and its gall is provided through integrative taxonomic study of gall morphology, host plant ecology, wing morphometrics, and reduced-representation genome sequencing.

Key words: *Bigeloviae*, candle, ddRAD, *Ericameria*, flame, marshmallow, *nauseosa*, rabbitbrush, tephritid, *trixa*, wing

OPEN ACCESS

Introduction

Species delimitation is an essential step in our collective goal as biologists to calculate the total diversity of life on the planet (Dayrat 2005), and is particularly vital in the midst of ongoing decline of insects – the world's most species-rich group of animals (Dirzo et al. 2014; Stork et al. 2015; Sánchez-Bayo and Wyckhuys 2019). However, species divisions are frequently unclear, particularly where purely morphological descriptions include high levels of intra-species variation, which poses a significant challenge in taxonomy, as it can result in unreliable diagnosis of species boundaries (Gentile et al. 2021). Most descriptions of insect species are made from adult morphological characters alone and are presented as a list of traits that have some author-determined significance in recognition (e.g., coloration, wing patterns, integumental texture). This issue can be addressed by combining multiple lines of evidence, such as morphological, ecological, and geographical data, to make more accurate and robust species delimitations; a long-standing practice coined in recent decades as "integrative taxonomy"

---

* Contributed equally to this work.

(Schlick-Steiner et al. 2010). Taxonomists are also now equipped with molecular tools that can provide deep genome-wide datasets to investigate intra-taxon distinctions, even in cryptic or rare groups of arthropods (Hebert et al. 2003; Sheikh et al. 2022). An integrative taxonomy approach to species description improves our overall species estimates and identification of significant radiations in evolutionary history. By embracing a holistic approach, integrative taxonomy allows for a more nuanced understanding of biodiversity, leading to more precise species identification (Schlick-Steiner et al. 2010). This not only enhances our knowledge of the natural world but also is crucial for conservation efforts, as accurately identifying species is foundational to protecting them and their habitats.

Though many have adopted integrative taxonomic description, a potentially powerful tool for species delimitation remains under-utilized: the extended phenotype. This refers to an organism's genetic expression that can be observed beyond their own bodies, particularly in the case of animals that construct or modify unique structures such as bird nests and spider webs (Blamires 2013; Mainwaring et al. 2014). These extensions of the phenotype represent species-specific behaviors and adaptations, establishing them as a key piece of the species' ecology, and a set of additional morphological traits that can be used in species delimitation (Bailey et al. 2009; Freudenstein et al. 2016). For example, gall-inducing insects create structures that are so frequently species-specific that they can be used as a diagnostic character for identification (Raman et al. 2005; Bailey et al. 2009; Redfern 2011; Russo 2021). Integrating extended phenotypes in species description will likely enhance the resolution of taxonomic classifications, especially with ecosystem engineers like gall-inducing insects.

The genus *Aciurina* (Diptera: Tephritidae) are gall-inducing flies on Asteraceae shrubs in western North America (Foote et al. 1993). Many species in this genus are informally recognized by gall morphological characters, and, similarly to many tephritid "picture-wing" flies, formally identified with diagnostic black and transparent markings of the wings. The common and widespread species *Trypeta bigeloviae* was first described only as a "white, woolly [sic], and conspicuous" gall on the plant *Bigelovia* (Cockerell 1890a). The fly was then described in the same year as both *T. bigeloviae* and *T. bigeloviae* var. *disrupta* based on a single distinction in the postero-distal hyaline region of the wing: in *disrupta* this area is divided (disrupted) into two by a complete black marking (Cockerell 1890b). Bates (1935) later re-assigned *T. bigeloviae* to the genus *Aciurina*, including the variety *disrupta* which he did not consider distinct, citing variation of this character in specimens from the same locality. Wing marking variation led Steyskal (1984) in his revision of *Aciurina* to then synonymize the type species *Aciurina trixa* Curran, 1932 and *Aciurina semilucida* Bates, 1935 with *Aciurina bigeloviae* (Cockerell, 1890), which he characterized as being the most variable species of the genus. However, Dodson and George (1986) soon after described the likely recently diverged relationship of *A. bigeloviae* and *A. trixa* based on thorough examination of gall morphology, host plant ecology, hybrid breeding success, and genetic allelic frequencies. First Goeden and Teerink (1996) reinstated *A. semilucida*, then Headrick et al. (1997) officially reinstated *A. trixa* as a species distinct from *A. bigeloviae* and provided a larval description. The most reliable diagnostic character established between the sister species was gall morphology: *A. bigeloviae* has a white, wooly "cotton" gall and *A. trixa* has a resinous, waxy "smooth" gall. Both species form galls on

Ericameria nauseosa (Pall. ex Pursh) G.L.Nesom & G.I.Baird, however on different varieties of the species.

Dodson and George (1986) also described in detail the confusing variation in wing patterns noted by the other authors above by establishing three pattern categories among the two species: 1) the Type I pattern that included the originally described wing pattern for *A. bigeloviae* plus that of var. *disrupta*, 2) the Type II pattern which matched the description of *A. trixa*, and 3) the Type II' pattern (hereafter referred to as Type III) as a modified version of the *A. trixa* wing pattern, but from flies reared from *A. bigeloviae*-type cotton galls (Fig. 1). The authors admit that this third pattern, with its unexpected gall-wing morphological pairing, left them somewhat stumped: "Whether they belong to *bigeloviae*, *trixa*, or a third species probably will not be resolved until further studies parallel to those reported here are carried out" (Dodson and George 1986).

Here we follow this thread and using an integrative taxonomic approach that employs gall morphology, previously unexplored host plant ecology, extensive wing morphometric and character analysis, and multi-locus reduced representation genome sequencing, provide evidence that the Type III flies are a third species. We provide a name for this species, *Aciurina luminaria*, and a complete morphological description of the adult fly and its gall.

Materials and methods

We observed in previous collections of *A. bigeloviae* that "cotton" galls in New Mexico could be categorized into two groups by general gall shape: spherical and teardrop-shaped (Fig. 2). We were able to confirm from rearing haphazardly collected galls that the spherical cotton galls were induced by flies with Type I wing morphology (*A. bigeloviae*), and the teardrop-shaped galls were induced by flies with Type III wing morphology. The ability to recognize the different gall morphs in the field allowed us to perform targeted collections for each morphotype.

We systematically collected and reared *A. bigeloviae* and *A. trixa* galls in New Mexico between 2021–2022 following methods outlined in Baine et al. (2023a). Type III galls were collected haphazardly from identified populations throughout New Mexico and Colorado in April and May of 2021–2023 by clipping sections of stem with gall attached and transporting them to the University of New Mexico. In the lab, galls were placed in insect rearing cages (BugDorm) and kept at 45% relative humidity. Adult flies were removed from cages as they emerged and preserved in 100% EtOH at -20 °C for the following analyses. A subset of pinned flies and galls was examined for morphological characters and photographed using an EOS 40D camera fitted with a 65 mm MP-E macro photo lens (Canon) mounted on Stackshot macro rail with controller (Cognisys), and then focus stacked with Zerene Stacker software. Representative flies and galls of each sampled population, plus other material examined, including the holotype of *A. luminaria*, were deposited in the following collections: The Museum of Southwestern Biology, Arthropods Division, New Mexico (**MSBA**); Smithsonian Institution, National Museum of Natural History, Washington DC (**USNM**); and William F. Barr Entomological Museum, Idaho (**WFBM**).

Aciurina species are frequently documented as specialists on particular varieties of *E. nauseosa*. For example, *A. bigeloviae* is associated with *E. n.* subsp. *nauseosa* var. *graveolens*, and *A. trixa* in New Mexico is associated

with *E. n.* subsp. *nauseosa* var. *latisquamea* (Dodson and George 1986). To determine the host plant identity of Type III galls, we additionally returned to a subset of sites during the flowering season in the fall of 2022 and 2023 to obtain plant voucher specimens. Plant samples were identified using Anderson (2006) and Allred and Jercinovic (2020), and deposited in the MSB Herbarium.

Wing morphology

A total of 62 female *Aciurina* specimens of the three morphotypes from 19 populations were selected for morphological assessment. Both wings of each specimen were carefully removed by pulling at the connection point where the tegula meets the thorax. Wings were mounted on glass slides with a Euparal mounting medium (Hempstead Halide). The edges of the cover slide were then sealed with clear nail polish and slides were left to dry at room temperature for 24 hours. Images of each wing were taken using a Axiocam 208 color camera mounted on a Stemi 508 microscope (Zeiss). Measurements were taken in ZEN 3.6 blue edition (Zeiss). The methodology used to take standardized proxy measurements of the wing width (represented by distance from apex of vein R1 to junction of vein M4 and crossvein dm-m) and length (represented by distance from junction of vein M4 and crossvein bm-m to apex of vein M4) follows Baleba et al. (2019). A total of seven different measurements and three different categorical observations were made for each wing (Fig. 1A). To facilitate comparison without influence of difference in overall body size, each measurement was divided by our measurement for wing length. Finally, measurements from each wing pair were averaged. We then compared morphotype III to both morphotype I and II using each set of measurements by analysis of variance (ANOVA, *aov*) or Kruskal-Wallis where assumptions for ANOVA were not met (*kruskal.test*), and each set of categorical variables by Pearson's χ^2 test (*chi.test*) in R version 4.2.2 (R Core Team 2021).

The terminology we used for venation and cells follows Cumming and Wood (2017), and our selected measurements and categorical variables are defined as follows (Fig. 1A):

- **brL:** The maximum diameter of the subapical hyaline spot of cell br. This spot has a circular-elliptical shape, so the measurement typically follows a line from one elliptical-vertex to the other.
- **rrL:** The maximum width of the hyaline region located within cells r_1 and r_{2+3}, crossing vein R_{2+3}: measurement taken from the midpoint of the vein C to the parabolic vertex of the shape. This pattern occasionally reaches vein R_{4+5}; in this case the midpoint that borders this vein is used instead of a parabolic vertex.
- **rrH:** The maximum length of the same region hyaline in cells r_1 and r_{2+3}, measured along vein R_{2+3}.
- **mrL:** The maximum length of the subapical hyaline region in cells r_{4+5} and m: length taken from the postero-distal corner to the parabolic vertex of the region.
- **C1:** The presence or absence of a complete medial stripe within the anal lobe from veins CuA+CuP to the posterior wing margin.
- **C2:** The presence or absence of a complete medial stripe within cell m_4 from vein M_4 to the posterior wing margin.

- **C3:** The extent of black medial stripe in the large subbasal hyaline region on the posterior margin of the wing within cell m. Three conditions exist: stripe absent, stripe incomplete, and stripe completely bisecting the region (var. *disrupta* morphology).

Genomics

From three populations each of *A. bigeloviae*, *A. trixa* and Type III, we extracted whole-body DNA from three replicates (total n = 27) using the DNeasy Blood & Tissue kit and protocol (Qiagen), and quantified nucleic acid with a Qubit 3.0 fluorometer (Invitrogen). We generated genotypes for each sample from single-nucleotide polymorphisms (SNPs) derived from double digest restriction site associated DNA sequencing (ddRADseq) (Peterson et al. 2012). DNA was digested with enzymes EcoRI and MseI, and fragments were coupled with Illumina adaptors through T4 ligation. Pooled fragments were used for PCR with a proofreading enzyme (Iproof; BioRad), and fragment size selection for 300–450 bp
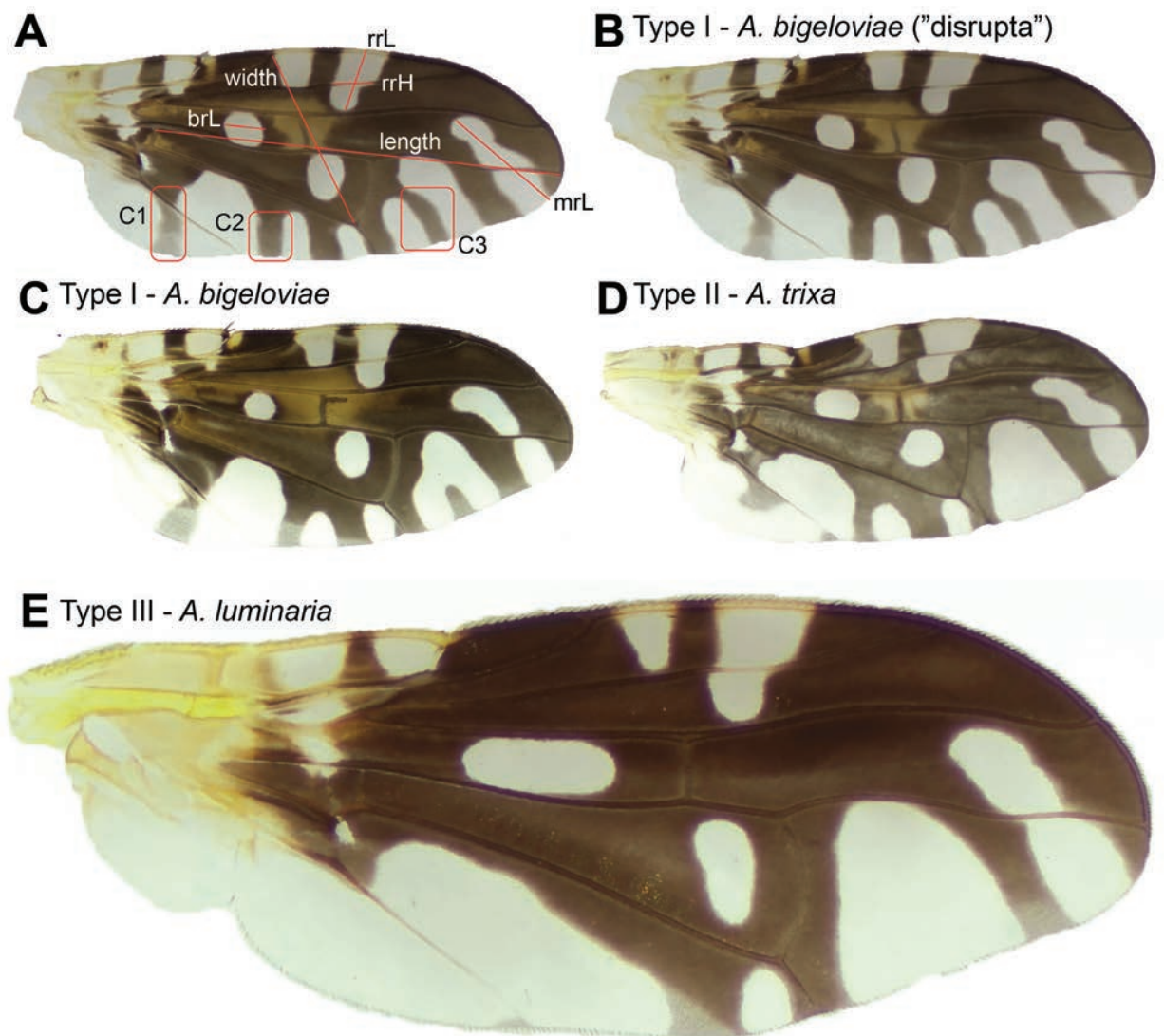
Figure 1. Wing morphotypes and measurements taken **A** diagram of characters and measurements defined and used in analysis **B** *A. bigeloviae* **C** *A. bigeloviae* **D** *A. trixa* **E** *A. luminaria* sp. nov. Not to scale.
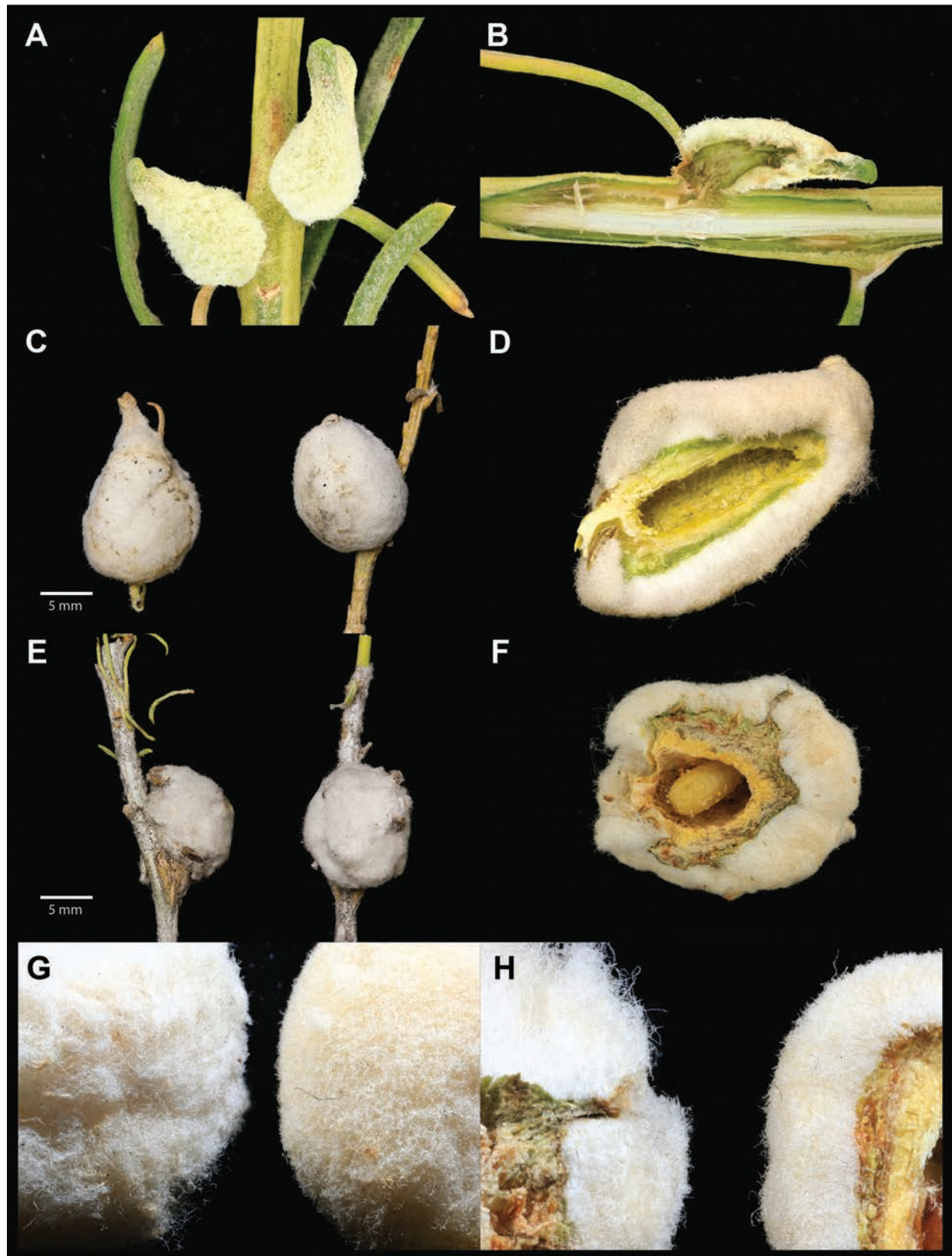
Figure 2. Galls of *A. luminaria* and *A. bigeloviae* **A** immature *A. luminaria* galls **B** internal view of immature *A. luminaria* gall with early instar larva burrowing into the stem while gall develops **C** mature *A. luminaria* galls **D** internal view of mature *A. luminaria* gall with full-sized larval chamber **E** mature *A. bigeloviae* galls **F** internal view of *A. bigeloviae* gall with a mature larva in the larval chamber. Side by side comparison of *A. bigeloviae* (left) and *A. luminaria* (right) tomentum texture and uniformity **G** external view **H** internal view.

was performed using a Pippin Prep quantitative electrophoresis unit. An Illumina NovaSeq S2 housed at the University of Texas at Austin Genomic Sequencing and Analysis Facility (Austin, TX) generated sequences of ~100 bp from input fragments. Trimmomatic 0.39 was used to truncate and filter demultiplexed single-end reads to a threshold of 85 bp (Bolger et al. 2014). Sequence files are deposited in NCBI GenBank under BioProject ID PRJNA1075688.

We mapped trimmed reads *de novo* using the Stacks 2.61 (Catchen et al. 2011) wrapper *denovo_map.pl* with the selected parameters: 5 minimum reads per stack, 3 maximum mismatches per locus, 3 maximum mismatches per stack, and minimum 80% individuals required per locus (parameter optimization was performed generally following Paris et al. 2017). We then filtered stacks in R with *SNPfiltR* (DeRaad 2022) and the settings: maximum depth of 50, maximum missing per sample 80%, minimum SNP completeness 80%, and minimum minor allele count of 1. Filtered SNP loci were used for principal component analysis (PCA) using packages *vcfR* (Knaus and Grünwald 2017), *dartR* (Gruber et al. 2018) and *adegenet* (Jombart 2008). We also calculated π for each population as a measure of nucleotide diversity. Structure was estimated using sparse non-negative matrix factorization (sNMF) with package *LEA* (Frichot and Francois 2015). For each K value, where K represents the number of clusters ranging from 1 to 9, we performed 50 iterations. We then selected and graphed the best result from the most optimal K value, as identified through the cross-entropy criterion.

SNPs per sample were concatenated to generate sequences for each individual, and sequences were aligned in Stacks. Phylogeny was inferred by maximum likelihood (ML) tree with IQ-TREE 2.2.0 (Minh et al. 2020). ModelFinder (Kalyaanamoorthy et al. 2017) was used to select the best model as determined by Akaike Information Criterion (AIC). We calculated branch support from 1000 ultrafast bootstrap (UFBoot) (Hoang et al. 2018) and 1000 Shimodaira–Hasegawa approximate likelihood ratio test (SH-aLRT) (Guindon et al. 2010) replications. We report the selected model and basal branch support values. Sequence reads used in all above genomic analyses are deposited in NCBI GenBank within BioProject PRJNA1075688.

Results

Wing morphology

Morphometric comparisons of *A. bigeloviae* and *A. trixa* with the Type III morphotype highlighted regions of the wing that differ significantly in relative size and can therefore be used as diagnostic characters. The greater length of the hyaline spot within cell br (measurement brL) in Type III is the most notably distinct wing measurement from the other two morphotypes (*A. bigeloviae* χ^2 = 20.57, p < 0.0001; *A. trixa* χ^2 = 20.83, p < 0.0001). Type III also differs in the dimensions of the hyaline spot in r_1 and r_{2+3}, being longer than in *A. bigeloviae* (measurement rrH, F = 30.61, p < 0.0001), and wider than in *A. trixa* (measurement rrL, F = 7.99, p < 0.01). Finally, the measurement mrL is slightly greater in *A. trixa* than in Type III (F = 4.44, p < 0.05).

Despite variation, *A. bigeloviae* wings had the darkened stripes represented by the selected characters consistently present, while in Type III they were absent (Table 1). The absence of the dark stripe within the hyaline region in cell

m (C3) that frequently separates *A. trixa* from *A. bigeloviae*, also separates the Type III morphotype from *A. bigeloviae*, but not from *A. trixa*. See Suppl. material 1: fig. S1 for wing character variation in each of the three morphotypes sampled.

Table 1. Significance values from χ^2 tests to compare the presence/absence of wing characters in the three morphotypes.

Wing pattern character	*A. bigeloviae* ~ Type III	*A. trixa* ~ Type III
C1	$\chi^2 = 50.22$, df = 1, p < 0.0001	$\chi^2 = 36.29$, df = 1, p < 0.0001
C2	$\chi^2 = 68$, df = 1, p <0.0001	$\chi^2 = 65.33$, df = 1, p < 0.0001
C3	$\chi^2 = 47.28$, df = 2, p < 0.0001	NS

Genomics

From the ddRAD sequencing of the three morphotypes, 42,838 SNPs were retained after filtering. A single sample was filtered out for high relative missingness, so we used 26 samples total for the following analyses. The first principal component (PC1) in the PCA performed accounted for 42.3% of the variance, splitting the morphotypes into discrete clusters that match to gall morphology (Fig. 3A). The second principal component (PC2) explained an additional 21.2% of the variance, splitting Type III from *A. bigeloviae*, and also with minimal loadings on geographic variation within *A. bigeloviae* populations (Fig. 3A). The PCA represents the greatest amount of variance exists between the three morphotypes. Average genetic diversity across all sites (π) was lower in Type III (0.0008) than in *A. bigeloviae* (0.0014) or *A. trixa* (0.0011) across all populations (0.0775, 0.1324, 0.1083, respectively across variant sites). Genetic diversity was also lower by a comparable margin in Type III across the populations at the sympatric site for all three morphotypes, "SNM" (0.0767 versus 0.12 *A. bigeloviae* and 0.1006 *A. trixa*). The most optimal K for structure-like sNMF analysis was 3, and plots reveal that there is virtually no admixture present between the morphotypes, even in the populations at the sympatric sites (Fig. 3C).

Finally, to construct the phylogeny, we selected with ModelFinder a transversion substitution model of AG=CT and empirical unequal base frequencies, plus a FreeRate model (Yang 1995; Soubrier et al. 2012) for rate heterogeneity across sites with 2 categories, and an ascertainment bias correction appropriate for SNP alignments (TVM+F+ASC+R2). The output tree supports the pattern observed in the results above, that the morphotypes are consistently distinct, and that variation is lower in *A. bigeloviae* (Fig. 3B). The tree also suggests that Type III is more closely related to *A. bigeloviae* than *A. trixa* is, which may mean that their shared gall morphological traits are ancestral.

Taxonomy

Aciurina luminaria Baine, sp. nov.
https://zoobank.org/BC9BB3A4-E1CC-4793-AC8D-B8A4E779FFBF
The Candle Flame Gall Tephritid

Type material examined. *Holotype* (Fig. 4A, C) USA • **NM**; *Santa Fe Co.*; ♀; Tesuque E arroyo crossing Road 74; 35.77686°N, 105.92904°W; 5 May 2021; Q. Baine leg.; MSBA81957. *Allotype* (Fig. 4B, D) USA • **NM**; *Santa Fe Co.*; ♂; 1 mi SE Chupadero
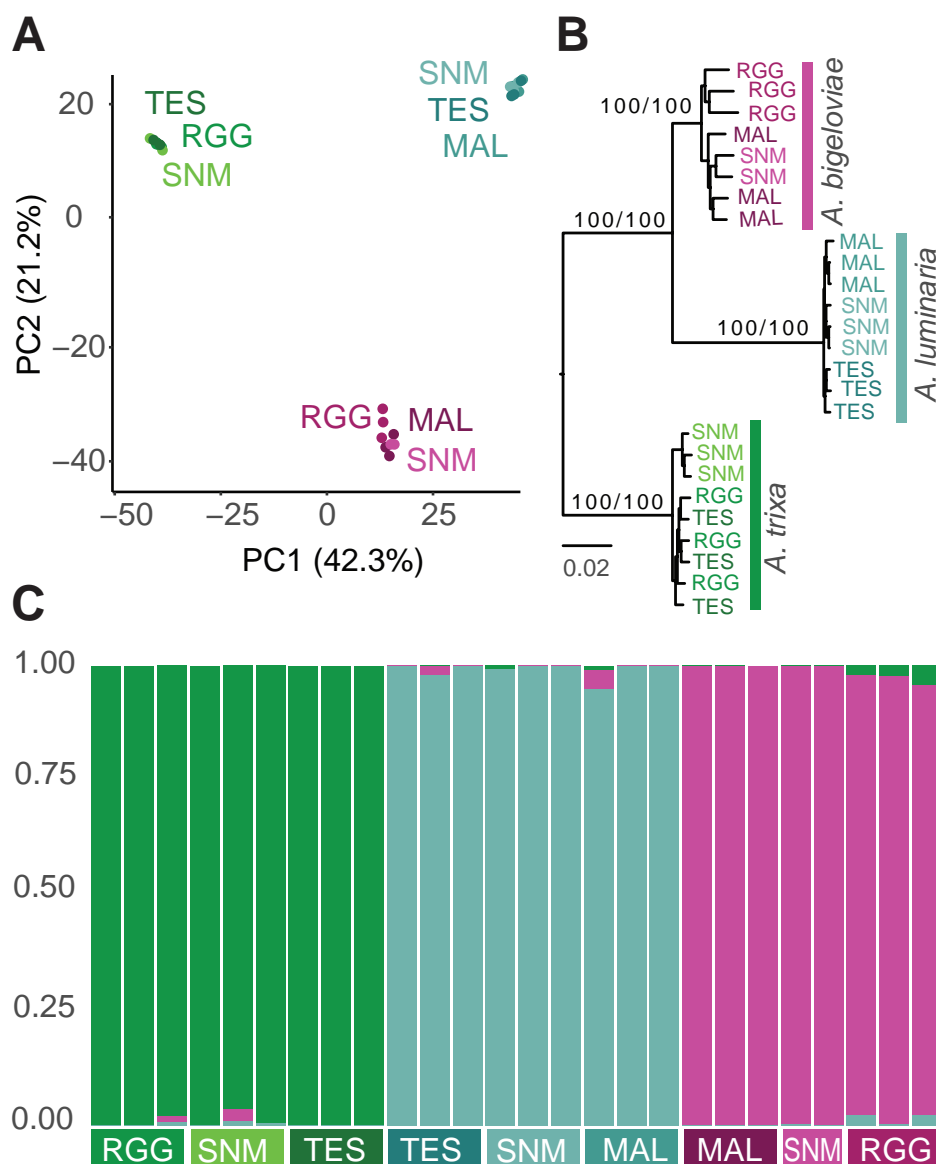
Figure 3. Results from SNP comparisons across populations (labeled as three-letter abbreviations) of the three morphotypes (labeled by color) **A** PCA plot **B** Maximum likelihood tree with basal support values UFBoot + SH-aLRT **C** sNMF structure-like admixture plot.

off St Rd 592; 35.814°N, 105.907426°W; 7 May 2023; Q. Baine leg.; MSBA81946. ***Paratypes*** USA • **CO**; *Alamosa Co.*; 2♀ 1♂; S of Mosca side of Hwy 17; 37.62534°N, 105.86636°W; 20 May 2021; V. Martinson leg.; MSBA81880–81882 • 3♀ 3♂ 1 gall; San Luis State Wildlife Area, Lane 6 N; 37.66256°N, 105.72293°W; 20 May 2021; E. Martinson & V. Martinson leg.; MSBA81892–81893, MSBA81896–81897, USNMENT02011093–USNMENT02011095 • 4♀ 4♂; San Luis State Wildlife Area, Lane 6 N; 37.66256°N, 105.72293°W; 14 May 2023; Q. Baine leg. MSBA81926–81933 • 7♀ 6♂; W of San Luis Valley Regional Airport entrance, Alamosa; 37.4442°N, 105.86753°W; 14 May 2023; Q. Baine leg.; MSBA81898–81901, USNMENT02011096–USNMENT02011097 • 2♀ 3♂; 2 mi S Zapata Falls turnoff Hwy 150; 37.59092°N, 105.6015°W; 15 May 2023; Q. Baine leg.; MSBA81909–81913. 2♀ 1♂; Road N 110 and Lane 1 N off Hwy 17; 37.59092°N, 105.6015°W; 15 May 2023; Q. Baine leg.; MSBA81914–81916 • 2♀ 1♂; Corner of Cortez Rd
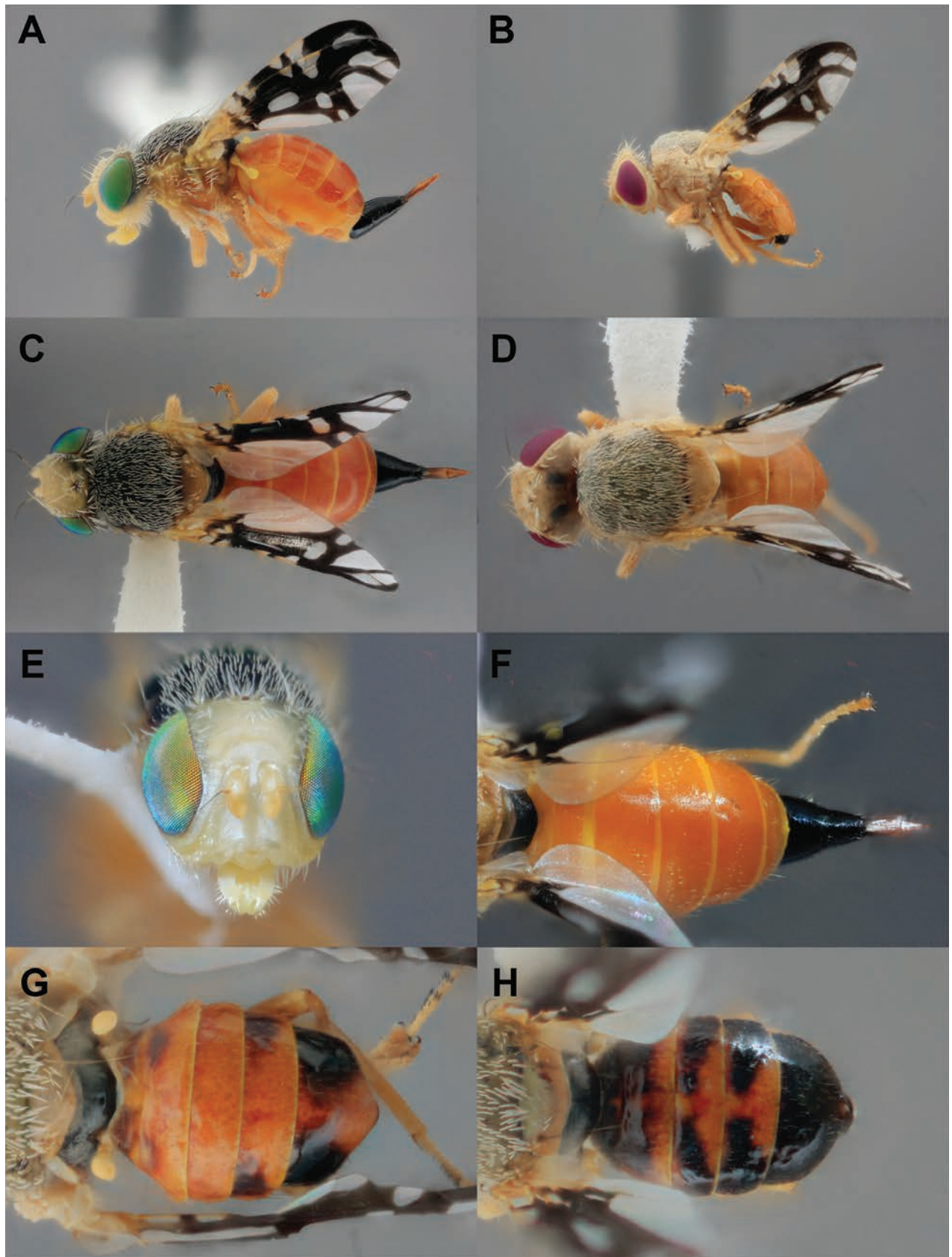
Figure 4. *Aciurina luminaria* sp. nov. **A** holotype lateral habitus **B** allotype lateral habitus. Difference in eye color is a result of the age of mounted specimen **C** holotype dorsal habitus **D** allotype dorsal habitus **E** holotype head, anterior **F** holotype abdomen, dorsal **G–H** variation in dorsal abdomen color **G** mostly orange morph **H** dark morph.

and Van Iwarden Dr, Alamosa; 37.43771°N, 105.88511°W; 14 May 2023; Q. Baine leg.; MSBA81922–81925. *Chaffee Co.* • 2♀ 2♂; Hwy 285 W of Johnson Village; 38.80956°N, 106.11603°W; 20 May 2021; E. Martinson leg.; MSBA81883–81886 • **NM**; *Cibola Co.*; 2♀ 2♂; El Malpais National Conservation Area Narrows; 34.96499°N, 107.81464°W; 15 May 2022; V. Martinson leg.; MSBA81876–81879. *San Juan Co.* • 1♂; S Bloomfield Hwy 550 Kutz Wash; 36.64524°N, 108.00264°W; 18 March 2022; E. Martinson leg.; MSBA81891. *Sandoval Co.* • 4♀; N side Hwy 550, La Jara; 36.0581873°N, 106.9749619°W; 31 May 2020; D. Hughes leg.; MSBA81887–81890. *Santa Fe Co.* • 5♀ 4♂, 1 gall; Tesuque E arroyo crossing Road 74; 35.77686°N, 105.92904°W; 7 May 2023; Q. Baine leg.; MSBA81934–81938, MSBA81941–81942, USNMENT02011090–USNMENT02011092 • 2♀; Tesuque E arroyo crossing Road 74; 35.77686°N, 105.92904°W; 5 May 2021; Q. Baine leg.; MSBA81956–81957 • 4♀ 2♂; 1 mi SE Chupadero off St Rd 592; 35.814006°N, 105.907426°W; 7 May 2023; Q. Baine leg.; MSBA81943–81948 • 3♀ 4♂; Tesuque Arroyo Ancho and Meredith Dr on Tesuque Village Rd; 35.752991°N, 105.934346°W; 7 May 2023; Q. Baine leg.; MSBA81949–81955. *Taos Co.* • 2♀ 3♂; 3 mi N Ojo Caliente off Hwy 285; 36.33046°N, 106.00581°W; 14 May 2023; Q. Baine leg.; MSBA81917–81921 • **UT**; *Kane Co.*; 1♀ 1♂; Coral Pink Sand Dunes; 3 July 1966; E.J. Allen leg.; WFBM0050980–0050981.

Other material examined. USA • **NM**; *Alamosa Co.*; 4 galls, 1 pupa; S Nageezi side of Pueblo Pintado Rd; 36.21480°N, 107.69633°W; 23 May 2024; S. Rollins leg • 4♀ 3♂; Corner of Cortez Rd and Van Iwarden Dr, Alamosa; 37.43771°N, 105.88511°W; 14 May 2023; Q. Baine leg. • 3 larvae; San Luis State Wildlife Area, Lane 6 N; 37.66256°N, 105.72293°W; 20 May 2021; E. Martinson leg.

Diagnosis. This wing pattern of the adult *A. luminaria* can be distinguished most easily from both *A. bigeloviae* and *A. trixa* by the elongate hyaline spot in cell br, consistent dark brown region surrounding crossvein r-m, and lack of dark stripe in anal cell; it further from *A. bigeloviae* by lack of dark stripe in the postero-distal region of cell m and lack of medial dark stripe in cell cua$_1$ (frequently present in *A. trixa* also). It differs from the similar-looking *A. maculata* (Cole, 1919) and *A. lutea* (Coquillett, 1899) by the hyaline cell bc and hyaline basal region of cell br. The extent of bright orange on the abdomen of many *A. luminaria* specimens also distinguishes it from *A. maculata* which has a more red abdomen, and from *A. bigeloviae* and *A. trixa* which frequently have a dark orange, brown, or black abdomen. Genitalia structures are highly similar to that of *A. bigeloviae*, except perhaps for the rounded tips of the prensisetae which differ from illustrations in Steyskal (1984). However, Steyskal describes *A. bigeloviae* (at the time synonymized with *A. trixa* and *A. semilucida*) as being highly variable in male terminalia characters, so this may or may not be reliably diagnostic. The gall can be distinguished from *A. bigeloviae* and *A. maculata* by the pointed, teardrop shape, and from all remaining galls in the genus by the thick layer of dense tomentum covering the surface (Fig. 2).

Description. Female body length (minus terminalia) 6 mm.

Head (Fig. 4E) uniformly pale yellow except for occiput and narrow interocular margin grey and moderately pilose. Compound eye bright green, drying to dull red. Three pairs of frontal setae, two pairs of orbital setae, and one pair of ocellar setae present. All setae pale yellow in color matching frons in color. Antenna yellow with black arista.

Thorax. Scutum and dorsal portions of pleura dark gray in background color with pale gray pollinosity and dense pale yellow setulae making the scutum appear pale

yellow-gray in color at a distance. Scutellum pale orange-brown at apex, narrowly gray at base. Subscutellum with anterior half pale yellow, posterior half and all of mediotergite black with pale gray pollinosity. Ventral part of pleura yellow-orange. The following setae are present, and pale yellow: basal scutellar, postalar, intra-alar, acrostichal, postsutural dorsocentral, presutural supra-alar, postsutural supra-alar, two notopleural, postpronotal, anepisternal, and katepisternal. Anepimeral seta indistinguishable from surrounding setulae. Legs wholly orange in color except for black tarsal claw and apical tarsal setae. Forefemur with elongate comb-like setae. Wing 4.2 mm in length. Costa pale orange. Setae narrowly present dorsally at junction of R_{2+3} and vein R_{4+5}. Wing coloring is dark brown to black with the following hyaline regions: cell bc, base of cell br, two vertical bands in cell c, the proximal one extending posteriorly halfway into cell bm, two marginal spots in r_1 with apical spot extending into r_{2+3}, large (2× wide as high) subapical spot in cell br, medial spot in cell bm, large basal and small apical spot in cell cua_1, subapical spot (1.5× high as wide) in cell dm, entire cell cup except for narrowly at apex, alula, anal lobe, large basal marginal spot in cell m, and subapical band extending from posterior margin in cell m into cell r_{4+5} reaching vein R_{4+5}. Halteres bright yellow.

Abdomen bright red-orange and shiny. Oviscape wholly black and shining. Eversible membrane brown, with shallowly semicircular cuticle denticles. Aculeus short (0.8 mm), notched at basal edge. Apical one third of aculeus with minute denticles covering medial edge (Fig. 5A).

Male body length (minus terminalia) 4 mm. Matching female in all respects except for terminalia. Epandrium black and shining, and proctiger pale yellow-orange. Surstylus pale brown, and prensisetae paired, bluntly rounded at the tips, and black. Phallus (1.25 mm long) and glans dark brown (Fig. 5B).

Variation. Ventral thoracic pleura (including episternum, meron, anatergite and katatergite) in darker morphs are black with gray pollinosity, as on the scutum. Abdomen color ranges from wholly orange, orange with black tergite 6 (5 in male), orange with lateral black spots on tergites 5 and 6 (4 and 5 in male), to mostly black with orange background in dark morphs of both sexes (Fig. 4F–H).

Immature. Second instar larva: Body white, elliptical-oblong and rounded on both anterior and posterior ends. Body segmented by rows of acanthae. Gnathocephalon conical and generally smooth. Mouth hook black and bidentate. Posterior spiracular plate with three pale brown rimae. Puparium: length 4.00 mm, width 1.62 mm. Dark brown, shining, elliptical-oblong, and rounded on both anterior and posterior ends. Anterior end with invagination scar and anterior thoracic spiracle. Posterior spiracular plate with spiracle darkened and flat.

Gall relatively large at maturity (7.24 mm mean latitudinal diameter), has a mostly rounded oblong to tapered teardrop shape and is covered uniformly in dense off-white cottony tomentum (Fig. 2C).

Biology. *Aciurina luminaria* is univoltine and has a life cycle and phenology similar to *A. bigeloviae* and *A. trixa* (Baine et al. 2023a; 2023b). Eggs are laid singly into the leaf bud of a distal plant stem. The gall forms at the oviposition site and the developing larva feeds on the tissue surrounding the central chamber of the gall. By fall, the gall reaches full size, and the larva reaches its final instar and chews to the outer layer of the gall to create a circular trap door. The larva ceases feeding and overwinters inside the gall, then pupates in the spring. Adults eclose in summer and push their way through the door to emerge from the gall and find a mate. The period of emergence from galls reared by these
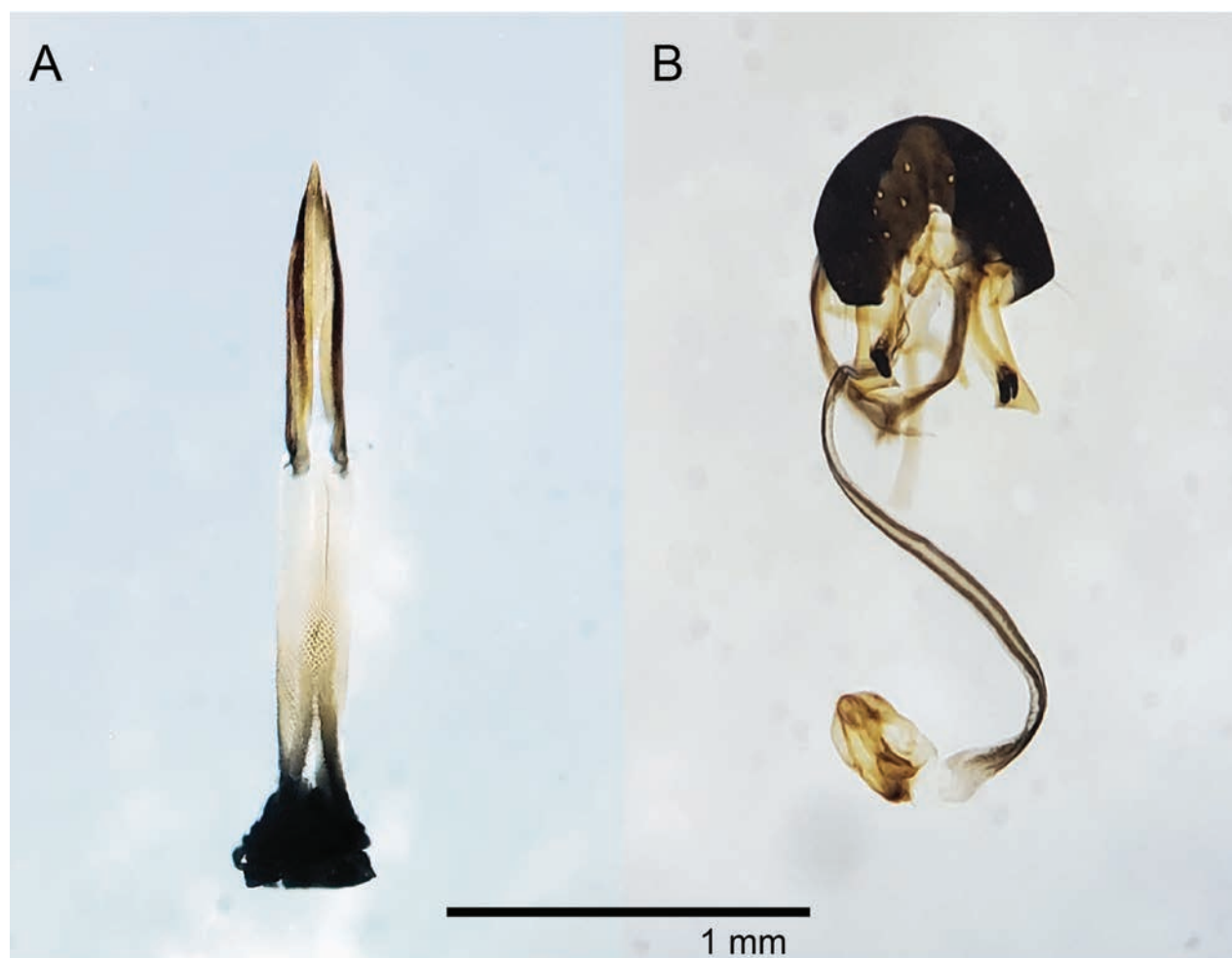
Figure 5. *Aciurina luminaria* terminalia **A** female **B** male.

authors is May 29th – June 28th. The latest date of emergence in examined material from Utah is July 18th (gall collected 3 July 1966).

Associated arthropods. The most common parasitoid by far is *Eurytoma chrysothamni* (Hymenoptera: Eurytomidae). We reared very few unidentified *Halticoptera*, *Pteromalus* (Pteromalidae), and *Torymus* (Torymidae) wasps, which may be the same species as those associated with *A. bigeloviae* (Baine et al. 2023a). We also observed and reared a small number of *Rhopalomyia* (Diptera: Cecidomyiidae) hypergalls on the surface of galls collected in northwestern New Mexico. The hypergall system has been previously documented on both *A. bigeloviae* (Baine et al. 2023b) and *A. trixa* (Russo 2021), but whether the midge species is the same is unknown. Unexpectedly, and unknown from other *Aciurina* systems, a single *Synergus* (Hymenoptera: Cynipidae) wasp was also reared.

Host plant. The known host plant is strictly *Ericameria nauseosa* subsp. *ammophila* L.C. Anderson, which was described from the San Luis Valley in Colorado (Anderson 2006). This plant is restricted to sandsheet and sand dune habitat and is known from southern Colorado (Anderson 2006) and here we add to its range northern New Mexico. Floral specimens from galled plants in New Mexico are deposited in MSB Herbarium (UNM0143677−UNM0143682). The host plant of material from Pink Sand Dunes, Utah is only identified as "*Chrysothamnus nauseosus*" [sic] and the host plants of gall observations in Arizona are unidentified.

Geographical range. Beyond the localities of the examined material above, we have confirmed the presence of this species in some locations reported by Dodson and George (1986): Great Sand Dunes National Monument, CO, and near the cities Grants and Gallup, NM. We are aware of a specimen collected from Kanab, UT (A. Norrbom, pers. comm. Aug 2024). We are also able to definitively identify from photos the distinctive tomentum and shape of this gall on iNaturalist. Thus, the following localities are added to our own observations to the range of *A. luminaria* from public user observations: Petrified Forest National Park, AZ (obs. no. 2848593 & 112933554); Porcupine Spring, AZ (170773584); Brown's Canyon, CO (151317053); Nageezi, NM (141568708); Aztec, NM (151553769); White Sands National Park, NM (199614395); and Kodachrome Basin State Park, UT (57095918).

Etymology. The species epithet is a noun derived from the Spanish word for "light" which is specifically used in the southwest United States for small decorative lanterns traditionally displayed during the winter leading up to Christmas. We chose this epithet because the shape of this species' gall is similar to that of a small flame on a candle, like those inside luminarias. Furthermore, this species' galls are easiest to find when they are mature, and after the host leaves have dropped, so they are also associated with display in wintertime in the Southwest. The tradition of luminarias is common and adored in New Mexico, the type locality of this species. We elected to use the more widespread term luminaria over northern New Mexico regionally specific "farolito" because the species' range extends into other regions in the West.

Discussion

We used multiple lines of evidence to illuminate the species boundaries in an oft-confused complex of gall-inducing flies in the southwestern United States. *Aciurina luminaria* induces galls of a distinct and diagnostic shape on a different *E. nauseosa* subspecies than its sympatric relatives, *A. bigeloviae* and *A. trixa*. It can further be consistently separated from these species by consistent differences in the adult wing pattern, and by genotyping via reduced representation genome sequencing.

We provide the following supplement, modified from that of Headrick et al. (1997) couplets to modify the key to species of *Aciurina* by Foote et al. (1993), with figure citations referencing Foote et al. (1993) except as noted. We have also removed a character from the key of Headrick et al. (1997: 419) that we found to be inconsistently present in both *A. bigeloviae* and *A. trixa* in New Mexico, and therefore not reliable as a diagnostic character: "pterostigma of at least one wing with a proximal hyaline or subhyaline incision".

Additions to the key to species of *Aciurina* by Foote et al. (1993)

10   Pterostigma along costa no more than 1.5× as long as its greatest width (fig. 121c); vein dm-cu nearly straight (fig. 121e), the lower apical angle of cell dm ~ 65° (fig. 121f); wing predominantly hyaline ....***A. notata* (Coquillett)**

–   Pterostigma along costa at least 2.0 × as long as its greatest width (fig. 124a); vein dm-cu usually bowed apicad (fig. 124b), the lower apical angle of cell dm seldom less than 90° (fig. 124c); wing with approximately equal area hyaline and brown, or predominantly brown **11**

11   Proximal marginal hyaline incision in cell m lacking median, dark mark **12**
−   Proximal marginal hyaline incision in cell m with a median, dark, often elongate mark (fig. 122), which sometimes divides the incision (Steyskal 1984: fig. 13) (Dodson and George 1986: fig. la, b); galls spheroid with cottony tomentum...***A. bigeloviae* (Cockerell)**
12   Anal cell bisected at least partially by medial brown mark from veins A1+CuA1 extending posteriorly, often reaching posterior wing margin; hyaline spot within cell br of the wing subcircular, 1−1.5 × as long as wide; brown region surrounding vein r-m paler in color than remaining dark part of wing, appearing like a diffuse orange spot; submedial dark mark usually present crossing cell cua_1 from vein CuA_1 to posterior wing margin; galls without tomentum.. ***A. trixa* Curran**
−   Anal cell without medial brown mark; hyaline spot within cell br of the wing elongated longitudinally, 1.5−2.5 × as long as wide; brown region surrounding vein r-m consistent in color, no diffuse spot present; submedial dark mark in cell cua_1 absent; galls frequently ovoid or teardrop shaped with dense cottony tomentum..........................***A. luminaria* Baine, sp. nov.**

The adaptive significance of melanized wing patterns present on tephritid fly species is unclear as studies have found evidence that these patterns could play a role in sexual communication (Benelli et al. 2014; Hippee et al. 2022), thermoregulation (Sivinski and Pereira 2005), or predator deterrence by salticid mimicry (Mather and Roitberg 1987; Whitman et al. 1988; Rao and Díaz-Fleischer 2012). From this study, it is clear that *A. luminaria* wings are not sexually dimorphic, similar to *A. bigeloviae* and *A. trixa*. However, it is also clear that *A. luminaria* wings have less melanized area on them than these species, and in combination with their usually paler abdomens, indicates that there may be an advantage to paler colors in their habitats.

The lower nucleotide diversity of *A. luminaria* suggests it is a more recently speciated group, and potentially the result of a "founder-effect" in which very few individuals from a population establish a lineage after colonizing a novel niche on a different host plant variety (Balakrishnan and Edwards 2009). This is supported by our observations of wing pattern variation, which is higher in *A. bigeloviae* and lower in *A. luminaria*. However, in the field, populations of the host plant *E. n.* subsp. *ammophila* appear largely fragmented across the range, often separated by dozens of miles, so the dispersal mechanisms of this species, if it was evolved from a single founding population, is mysterious.

Because *A. luminaria* occurs in sympatry with *A. bigeloviae* but on a unique host plant subspecies, speciation may be a result of host-race formation. Evidence of speciation via host-race formation, from a host switch specifically, is well-supported in the tephritid genus *Rhagoletis*, who display extraordinary host fidelity similar to that observed in *Aciurina* (Abrahamson and Blair 2008). Host-race formation is also documented in the closely related galling tephritid *Eurosta solidaginis* (Fitch, 1855), where two populations that are specific to distinct species of host *Solidago* (goldenrod) are reproductively isolated via assortative mating, and oviposition preference to the plant species of maternal provenance (Abrahamson and Blair 2008). Though we do not have documentation of *A. luminaria* mating or ovipositional behavior, the lack of intermediates in both our wing and genomic analyses suggest a similar level of isolation

that may be maintained by similar barriers. In both *Eurosta* and *Rhagoletis*, there is substantial evidence that host switches were advantageous for enemy escape (Brown et al. 1995; Feder et al. 1995); a new niche, like a host plant and/or altered gall form may be absent of, or inaccessible to, predators that previously had a negative impact on fitness of the fly. In rearing *A. luminaria* for this description, we observed many fewer enemy parasitoids than have been reared from *A. bigeloviae* in a similar and overlapping range (Baine et al. 2023a), suggesting a lower rate of attack and therefore the possibility of enemy escape driving differentiation.

Although evolutionary biologists frequently view species delimitation as an impossible task due to disagreement on significant characters that define species concepts (De Queiroz 2007), we can describe species with relatively high confidence if we use "integration by congruence" which delimits based on multiple, independent, taxonomic characters (e.g., ecological niche + DNA) (Padial et al. 2010). In the case of *A. luminaria*, we employ integrative taxonomy to use the combined evidence of distinction in ecological niche, diagnostic morphology, and genomic structure to recognize a new species.

Acknowledgements

Additional information

Conflict of interest

The authors have declared that no competing interests exist.

Ethical statement

No ethical statement was reported.

Funding

Author contributions

Conceptualization: VGM, EOM. Data curation: BW, QB. Formal analysis: BW, QB. Funding acquisition: EOM, VGM. Investigation: EOM, QB, BW, VGM. Methodology: QB. Resources: EOM, VGM. Supervision: EOM. Visualization: QB. Writing – original draft: BW, QB. Writing – review and editing: EOM, VGM.

Author ORCIDs

Quinlyn Baine ⬤ https://orcid.org/0000-0001-5025-3741
Vincent G. Martinson ⬤ https://orcid.org/0000-0001-5824-3548
Ellen O. Martinson ⬤ https://orcid.org/0000-0001-9757-6679

Data availability

All of the data that support the findings of this study are available in the main text or Supplementary Information. Sequence data used in phylogenetic analysis is stored in NCBI GenBank within BioProject ID PRJNA1075688.

References

Abrahamson WG, Blair CP (2008) Sequential radiation through host-race formation: herbivore diversity leads to diversity in natural enemies. In: Tilmon KJ (Ed.) Specialization, speciation, and radiation. The evolutionary biology of herbivorous insects. University of California Press, Berkeley, CA, 188–202. https://doi.org/10.1525/california/9780520251328.003.0014

Allred KW, Jercinovic EM (2020) Part 2: Dicotyledonous Plants Flora Neomexicana III: An illustrated identification manual, 2nd ed. Publisher, city, 795 pp.

Anderson LC (2006) *Ericameria nauseosa* subsp. *ammophila* (Asteraceae), a new rabbitbrush from the San Luis Valley of Colorado. SIDA, Contributions to Botany 22: 867–872.

Bailey R, Schönrogge K, Cook JM, Melika G, Csóka G, Thuróczy C, Stone GN (2009) Host niches and defensive extended phenotypes structure parasitoid wasp communities. PLOS Biology 7: e1000179. https://doi.org/10.1371/journal.pbio.1000179

Baine Q, Casares EE, Hughes DWW, Martinson VG, Martinson EO (2023a) Arthropod communities associated with gall-inducing *Aciurina bigeloviae* and *Aciurina trixa* (Diptera: Tephritidae) in New Mexico. Annals of the Entomological Society of America 117: 107–117. https://doi.org/10.1093/aesa/saad037

Baine Q, Casares EE, Carabotta E, Martinson VG, Martinson EO (2023b) Galls on galls: A hypergall-inducing midge and its parasitoid community. Ecology 104: e4018. https://doi.org/10.1002/ecy.4018

Balakrishnan CN, Edwards SV (2009) Nucleotide variation, linkage disequilibrium and founder-facilitated speciation in wild populations of the zebra finch (*Taeniopygia guttata*). Genetics 181: 645–660. https://doi.org/10.1534/genetics.108.094250

Baleba SBS, Masiga D, Torto B, Weldon CW, Getahun MN (2019) Effect of larval density and substrate quality on the wing geometry of *Stomoxys calcitrans* L. (Diptera: Muscidae). Parasites & Vectors 12: 222. https://doi.org/10.1186/s13071-019-3483-y

Bates M (1935) Notes on American Trypetidae (Diptera) III. The genus *Tephrella*. Pan-Pacific Entomologist 11: 103–114.

Benelli G, Daane KM, Canale A, Niu C-Y, Messing RH, Vargas RI (2014) Sexual communication and related behaviours in Tephritidae: current knowledge and potential applications for Integrated Pest Management. Journal of Pest Science 87: 385–405. https://doi.org/10.1007/s10340-014-0577-3

Blamires SJ (2013) Spider webs as extended phenotypes. In: Santerre M (Ed.) Spiders: morphology, behavior and geographic distribution. Nova Science Publishers, New York, NY, 47–70.

Bolger AM, Lohse M, Usadel B (2014) Trimmomatic: a flexible trimmer for Illumina sequence data. Bioinformatics 30: 2114–2120. https://doi.org/10.1093/bioinformatics/btu170

Brown JM, Abrahamson WG, Packer RA, Way PA (1995) The role of natural-enemy escape in a gallmaker host-plant shift. Oecologia 104: 52–60. https://doi.org/10.1007/BF00365562

Catchen JM, Amores A, Hohenlohe P, Cresko W, Postlethwait JH (2011) *Stacks*: Building and genotyping loci *de novo* from short-read sequences. G3 Genes|Genomes|Genetics 1: 171–182. https://doi.org/10.1534/g3.111.000240

Cockerell TDA (1890a) The evolution of insect-galls. The Entomologist 23: 73–76. https://doi.org/10.4039/Ent2276a-4

Cockerell TDA (1890b) *Trypeta bigeloviae*, n. sp. The Entomologist's monthly magazine: 324.

Cumming JM, Wood DM (2017) Adult morphology and terminology. In: Kirk-Spriggs AH, Sinclair BJ (Eds) Manual of Afrotropical Diptera Volume 1. Introduction and Family Keys. Suricata 4. SANBI Graphics & Editing, Pretoria, South Africa, 89–133.

Dayrat B (2005) Towards integrative taxonomy. Biological Journal of the Linnean Society 85: 407–415. https://doi.org/10.1111/j.1095-8312.2005.00503.x

De Queiroz K (2007) Species concepts and species delimitation. Systematic Biology 56: 879–886. https://doi.org/10.1080/10635150701701083

DeRaad DA (2022) snpfiltr: An R package for interactive and reproducible SNP filtering. Molecular Ecology Resources 22: 2443–2453. https://doi.org/10.1111/1755-0998.13618

Dirzo R, Young HS, Galetti M, Ceballos G, Isaac NJB, Collen B (2014) Defaunation in the Anthropocene. Science 345: 401–406. https://doi.org/10.1126/science.1251817

Dodson G, George SB (1986) Examination of two morphs of gall-forming *Aciurina* (Diptera: Tephritidae): ecological and genetic evidence for species. Biological Journal of the Linnean Society 29: 63–79. https://doi.org/10.1111/j.1095-8312.1986.tb01771.x

Feder JL, Reynolds K, Go W, Wang EC (1995) Intra- and interspecific competition and host race formation in the apple maggot fly, *Rhagoletis pomonella* (Diptera: Tephritidae). Oecologia 101: 416–425. https://doi.org/10.1007/BF00329420

Foote RH, Blanc FL, Norrbom AL (1993) Handbook of the fruit flies (Diptera: Tephritidae) of America north of Mexico. Comstock Pub. Associates, Ithaca, 571 pp.

Freudenstein JV, Broe MB, Folk RA, Sinn BT (2016) Biodiversity and the species concept – lineages are not enough. Systematic Biology: syw098. https://doi.org/10.1093/sysbio/syw098

Frichot E, Francois O (2015) LEA: an R package for landscape and ecological association studies. Methods in Ecology and Evolution 6: 925–929. https://doi.org/10.1111/2041-210X.12382

Gentile G, Bonelli S, Riva F (2021) Evaluating intraspecific variation in insect trait analysis. Ecological Entomology 46: 11–18. https://doi.org/10.1111/een.12984

Goeden RD, Teerink JA (1996) Life history and descriptions of adults and immature stages of *Aciurina semilucida* (Bates) (Diptera: Tephritidae) on *Chrysothamnus viscidiflorus* (Hooker) Nuttall in Southern California. Proceedings of the Entomological Society of Washington 98: 752–766.

Gruber B, Unmack PJ, Berry OF, Georges A (2018) dartr: An r package to facilitate analysis of SNP data generated from reduced representation genome sequencing. Molecular Ecology Resources 18: 691–699. https://doi.org/10.1111/1755-0998.12745

Guindon S, Dufayard J-F, Lefort V, Anisimova M, Hordijk W, Gascuel O (2010) New algorithms and methods to estimate maximum-likelihood phylogenies: assessing the performance of PhyML 3.0. Systematic Biology 59: 307–321. https://doi.org/10.1093/sysbio/syq010

Headrick DH, Goeden RD, Teerink JA (1997) Taxonomy of *Aciurina trixa* Curran (Diptera: Tephritidae) and its life history on *Chrysothamnus nauseosus* (Pallas) Britton in Southern California; with notes on *A. bigeloviae* (Cockerell). Proceedings of the Entomological Society of Washington 99: 415–428.

Hebert PDN, Cywinska A, Ball SL, deWaard JR (2003) Biological identifications through DNA barcodes. Proceedings of the Royal Society of London. Series B: Biological Sciences 270: 313–321. https://doi.org/10.1098/rspb.2002.2218

Hippee AC, Beer MA, Norrbom AL, Forbes AA (2022) Stronger sexual dimorphism in fruit flies may be favored when congeners are present and females actively search for mates. https://doi.org/10.1101/2022.05.17.492314

Hoang DT, Chernomor O, von Haeseler A, Minh BQ, Vinh LS (2018) UFBoot2: Improving the ultrafast bootstrap approximation. Molecular Biology and Evolution 35: 518–522. https://doi.org/10.1093/molbev/msx281

Jombart T (2008) *adegenet*: a R package for the multivariate analysis of genetic markers. Bioinformatics 24: 1403–1405. https://doi.org/10.1093/bioinformatics/btn129

Kalyaanamoorthy S, Minh BQ, Wong TKF, von Haeseler A, Jermiin LS (2017) ModelFinder: fast model selection for accurate phylogenetic estimates. Nature Methods 14: 587–589. https://doi.org/10.1038/nmeth.4285

Knaus BJ, Grünwald NJ (2017) vcfr: a package to manipulate and visualize variant call format data in R. Molecular Ecology Resources 17: 44–53. https://doi.org/10.1111/1755-0998.12549

Mainwaring MC, Hartley IR, Lambrechts MM, Deeming DC (2014) The design and function of birds' nests. Ecology and Evolution 4: 3909–3928. https://doi.org/10.1002/ece3.1054

Mather MH, Roitberg BD (1987) A sheep in wolf's clothing: tephritid flies mimic spider predators. Science 236: 308–310. https://doi.org/10.1126/science.236.4799.308

Minh BQ, Schmidt HA, Chernomor O, Schrempf D, Woodhams MD, von Haeseler A, Lanfear R (2020) IQ-TREE 2: New Models and Efficient Methods for Phylogenetic Inference in the Genomic Era. Molecular Biology and Evolution 37: 1530–1534. https://doi.org/10.1093/molbev/msaa015

Padial JM, Miralles A, De La Riva I, Vences M (2010) The integrative future of taxonomy. Frontiers in Zoology 7: 16. https://doi.org/10.1186/1742-9994-7-16

Paris JR, Stevens JR, Catchen JM (2017) Lost in parameter space: a road map for stacks. Methods in Ecology and Evolution 8: 1360–1373. https://doi.org/10.1111/2041-210X.12775

Peterson BK, Weber JN, Kay EH, Fisher HS, Hoekstra HE (2012) Double digest RADseq: an inexpensive method for *de novo* SNP discovery and genotyping in model and non-model species. PLoS ONE 7: e37135. https://doi.org/10.1371/journal.pone.0037135

R Core Team (2021) R: A language and environment for statistical computing. R Foundation for Statistical Computing, Vienna, Austria.

Raman A, Schaefer CW, Withers TM (2005) Biology, ecology, and evolution of gall-inducing arthropods. Science Publishers, Enfield, (NH), 817 pp.

Rao D, Díaz-Fleischer F (2012) Characterisation of predator-directed displays in tephritid flies. Ethology 118: 1165–1172. https://doi.org/10.1111/eth.12021

Redfern M (2011) Plant galls. HarperCollins, London.

Russo R (2021) Plant galls of the Western United States. Princeton University Press, Princeton, 368 pp. https://doi.org/10.1515/9780691213408

Sánchez-Bayo F, Wyckhuys KAG (2019) Worldwide decline of the entomofauna: A review of its drivers. Biological Conservation 232: 8–27. https://doi.org/10.1016/j.biocon.2019.01.020

Schlick-Steiner BC, Steiner FM, Seifert B, Stauffer C, Christian E, Crozier RH (2010) Integrative taxonomy: a multisource approach to exploring biodiversity. Annual Review of Entomology 55: 421–438. https://doi.org/10.1146/annurev-ento-112408-085432

Sheikh SI, Ward AKG, Zhang YM, Davis CK, Zhang L, Egan SP, Forbes AA (2022) *Ormyrus labotus* (Hymenoptera: Ormyridae): another generalist that should not be a generalist is not a generalist. Insect Systematics and Diversity 6: 8. https://doi.org/10.1093/isd/ixac001

Sivinski J, Pereira R (2005) Do wing markings in fruit flies (Diptera: Tephritidae) have sexual significance? Florida Entomologist 88: 321–324. https://doi.org/10.1653/0015-4040(2005)088[0321:DWMIFF]2.0.CO;2

Soubrier J, Steel M, Lee MSY, Der Sarkissian C, Guindon S, Ho SYW, Cooper A (2012) The influence of rate heterogeneity among sites on the time dependence of molecular rates. Molecular Biology and Evolution 29: 3345–3358. https://doi.org/10.1093/molbev/mss140

Steyskal GC (1984) A synoptic revision of the genus *Aciurina* Curran, 1932 (Diptera, Tephritidae). Proceedings of the Entomological Society of Washington 86: 582–598.

Stork NE, McBroom J, Gely C, Hamilton AJ (2015) New approaches narrow global species estimates for beetles, insects, and terrestrial arthropods. Proceedings of the National Academy of Sciences 112: 7519–7523. https://doi.org/10.1073/pnas.1502408112

Whitman DW, Orsak L, Greene E (1988) Spider mimicry in fruit flies (Diptera: Tephritidae): further experiments on the deterrence of jumping spiders (Araneae: Salticidae) by *Zonosemata vittigera* (Coquillett). Annals of the Entomological Society of America 81: 532–536. https://doi.org/10.1093/aesa/81.3.532

Yang Z (1995) A space-time process model for the evolution of DNA sequences. Genetics 139: 993–1005. https://doi.org/10.1093/genetics/139.2.993

Supplementary material 1

Selection of mounted wing pairs from each of the three sampled morphotypes to show variation in wing pattern

Authors: Quinlyn Baine, Branden White, Vincent G. Martinson, Ellen O. Martinson
Data type: pdf
Link: https://doi.org/10.3897/zookeys.1214.130171.suppl1

Research Article

Two new hypogean species of the genus *Triplophysa* (Osteichthyes, Cypriniformes, Nemacheilidae) from Guizhou Province, Southwest China, with underestimated diversity

Chang-Ting Lan[1*], Li Wu[2*], Tao Luo[1*], Ye-Wei Liu[3*], Jia-Jun Zhou[4,5], Jing Yu[2], Xin-Rui Zhao[1], Ning Xiao[6], Jiang Zhou[2]

1 School of Life Sciences, Guizhou Normal University, Guiyang 550025, Guizhou, China
2 School of Karst Science, Guizhou Normal University, Guiyang 550001, Guizhou, China
3 Guangxi Key Laboratory for Forest Ecology and Conservation, College of Forestry, Guangxi University, Nanning 530004, Guangxi, China
4 Zhejiang Forest Resource Monitoring Center, Hangzhou 310020, Zhejiang, China
5 Zhejiang Forestry Survey Planning and Design Company Limited, Hangzhou 310020, Zhejiang, China
6 Guiyang Healthcare Vocational University, Guiyang 550081, Guizhou, China

Corresponding authors: Jiang Zhou (zhoujiang@ioz.ac.cn); Ning Xiao (armiger@163.com)

Abstract

Two new species of the genus *Triplophysa* from southwestern Guizhou Province, China, are described. These are *Triplophysa ziyunensis* Wu, Luo, Xiao & Zhou, **sp. nov.** and *Triplophysa yaluwang* Lan, Liu, Zhou & Zhou, **sp. nov.** from Maoying Town, Ziyun County, Guizhou Province, China. *Triplophysa ziyunensis* Wu, Luo, Xiao & Zhou, **sp. nov.** is distinguished from other hypogean species of the genus *Triplophysa* by having a combination of the following characteristics: body naked, scaleless, pigmented markings on surface of body, except ventral; eyes reduced, diameter 2.4–4.9% of head length; pelvic-fin tip extending to anus; tip of pectoral fin not reaching pelvic fin origin; anterior and posterior nostrils closely set, with anterior nostril elongated to a barbel-like tip; tip of outrostral barbel extending backward, not reaching anterior margin of the eye; lateral line complete; posterior chamber of air bladder degenerated; and fin differences. *Triplophysa yaluwang* Lan, Liu, Zhou & Zhou, **sp. nov.** is distinguished from other hypogean species of the genus *Triplophysa* by having a combination of the following characteristics: body naked, scaleless, with irregular pale and dark brownish brown markings, except ventrally; eyes reduced, diameter 4.6–6.1% of head length; pelvic-fin tip reaching anus; tip of pectoral fin not reaching to pelvic fin origin; anterior and posterior nostrils closely set, with anterior nostril elongated to a barbel-like tip; tip of outrostral barbel extending backward, not reaching to anterior margin of the eye; lateral line complete; posterior chamber of air bladder degenerated; and fin differences. Mitochondrial Cyt *b* revealed relatively small genetic differences, 1.4–2.0%, between the two new species and close relatives. Nuclear gene RAG1 indicated that the two new species possessed unique haplotypes with multiple linking mutations. This study emphasizes the importance of utilizing nuclear genes to identify new species in rapidly speciation cave species, with small genetic differences due to mitochondrial introgression occurring interspecies.

Key words: Mitochondrial DNA, morphology, new species, nuclear gene, *Triplophysa*

---

* These authors contributed equally to this paper.

Introduction

The high-plateau loach fish genus *Triplophysa* Rendahl, 1933 comprises more than 184 recognized species of small loaches that are distributed on the Qinghai-Xizang Plateau and nearby regions (Luo et al. 2023; Fricke et al. 2024). Morphological characteristics that distinguish *Triplophysa* from other genera in the Nemacheilidae include closely set anterior and posterior nostrils and a posterior wall of the bony capsule of the swim bladder. Males have tubercle-bearing, elevated skin on both sides of the head and a thickened tuberculated pad or agglomerations on the dorsal surfaces of the broadened and widened pectoral-fin rays (Zhu 1989; Zheng et al. 2009; Prokofiev 2010; He et al. 2012; Ren et al. 2012; Yang et al. 2012; Wu et al. 2018a; Chen and Peng 2019; Deng et al. 2022). *Triplophysa* species are distributed from the Qinghai-Xizang Plateau at an average elevation of 4000 m to the Yunnan-Guizhou Plateau at an average elevation of 1000–2000 m (Zhu 1989; Luo et al. 2023). Their habitats include lakes, rivers, and caves (Zhu 1989; Lan et al. 2013), on the basis of which Triplophysa can be divided into two life groups: An epigean group and a hypogean or cave-dwelling group (Liu et al. 2022; Lu et al. 2022). The hypogean group is mainly distributed in underground rivers in southwest China, including Guizhou, Chongqing, Guangxi, Yunnan, and Hunan provinces (Luo et al. 2023). This group can be further subdivided into two morphological types, the stygobionts, and stygophiles (Zhao et al. 2011; Ma et al. 2019), based on the level of adaptation to the cave environment (Zhao et al. 2011; Lu et al. 2022). There are 106 species of *Triplophysa* and 39 hypogean species are distributed in Chongqing, Guangxi, Guizhou, Yunnan, and Hunan provinces in China (Table 1) (Lan et al. 2013; Zhang et al. 2020; Chen et al. 2021; Liu et al. 2022; Lu et al. 2022; Luo et al. 2023).

Guizhou Province is the region where the two major rivers of Asia, the Pearl River, and the Yangtze River, are separated (Fig. 1). The subtropical monsoon climate and paleogeology have shaped the karst landscapes and rich cave resources. This ecological background has enabled the formation of a diverse subterranean biota (Li et al. 2022; Wen et al. 2022). A total of 12 species occur in this region, eight of which have been described during the last ten years. These are *Triplophysa anlongensis* Lan, Song, Luo, Zhao, Xiao & Zhou, 2023, *T. baotianensis* Li, Liu & Li, 2018, *T. guizhouensis* Wu, He & Yang, 2018, *T. cehengensis* Luo, Mao, Zhao, Xiao & Zhou, 2023, *T. longliensis* Ren, Yang & Chen, 2012, *T. nasobarbatula* Wang & Li, 2001, *T. panzhouensis* Yu, Luo, Lan, Xiao & Zhou, 2023, *T. qingzhenensis* Liu, Zen & Gong, 2022, *T. rongduensis* Mao, Zhao, Yu, Xiao & Zhou, 2023, *T. sanduensis* Chen & Peng, 2019, *T. wudangensis* Liu, Zen & Gong, 2022, and *T. zhenfengensis* Wang & Li, 2001 (Wang and Li 2001; Ren et al. 2012; Li et al. 2018; Wu et al. 2018a; Chen and Peng 2019; Liu et al. 2022; Luo et al. 2023). Body pigmentation and pigmented markings were present in 11 of the 12 species, except for *T. cehengensis*, and the key distinguishing characteristics of these species are shown in Table 2. Four new species of *Triplophysa* were recently described in Guizhou (Luo et al. 2023), thus suggesting that additional undescribed species may exist in this region.

In August and December 2023, we collected several specimens of *Triplophysa*, identified by the closely set anterior and posterior nostrils, while

Table 1. A list of 39 species of hypogean fishes of the genus *Triplophysa* distributed in the Southwest China.

ID	Species	Province	Main drainage	Tributary	Reference
1	*T. aluensis* Li & Zhu, 2000	Yunnan	Pearl River	Nanpanjiang River	Li and Zhu 2000
2	*T. anshuiensis* Wu, Wei, Lan & Du, 2018	Guangxi	Pearl River	Hongshui River	Wu et al. 2018a
3	*T. anlongensis* Lan, Song, Luo, Zhao, Xiao & Zhou, 2023	Guizhou	Pearl River	Nanpanjiang River	Luo et al. 2023
4	*T. baotianensis* Li, Liu & Li, 2018	Guizhou	Pearl River	Nanpanjiang River	Li et al. 2018
5	*T. cehengensis* Luo, Mao, Zhao, Xiao & Zhou, 2023	Guizhou	Pearl River	Beipanjiang River	Luo et al. 2023
6	*T. erythraea* Liu & Huang, 2019	Hunan	Yangtze River	Yuanjiang River	Huang et al. 2019
7	*T. fengshanensis* Lan, 2013	Guangxi	Pearl River	Hongshui River	Lan et al. 2013
8	*T. flavicorpus* Yang, Chen & Lan, 2004	Guangxi	Pearl River	Hongshui River	Yang et al. 2004
9	*T. gejiuensis* (Chu & Chen, 1979)	Yunnan	Pearl River	Nanpanjiang River	Chu and Chen 1979
10	*T. guizhouensis* Wu, He & Yang, 2018	Guizhou	Pearl River	Hongshui River	Wu et al. 2018b
11	*T. huapingensis* Zheng, Yang & Che, 2012	Guangxi	Pearl River	Hongshui River	Zheng et al. 2012
12	*T. langpingensis* Yang, 2013	Guangxi	Pearl River	Hongshui River	Lan et al. 2013
13	*T. longipectoralis* Zheng, Du, Chen & Yang, 2009	Guangxi	Pearl River	Liujiang River	Zheng et al. 2009
14	*T. longliensis* Ren, Yang & Chen, 2012	Guizhou	Pearl River	Hongshui River	Ren et al. 2012
15	*T. luochengensis* Li, Lan, Chen & Du, 2017	Guangxi	Pearl River	Hongshui River	Li et al. 2017a
16	*T. macrocephala* Yang, Wu & Yang, 2012	Guangxi	Pearl River	Liujiang River	Yang et al. 2012
17	*T. nandanensis*Lan, Yang & Chen, 1995	Guangxi	Pearl River	Hongshui River	Lan et al. 1995
18	*T. nanpanjiangensis*Zhu & Cao, 1988	Yunnan	Pearl River	Nanpanjiang River	Zhu and Cao 1988
19	*T. nasobarbatula* Wang & Li, 2001	Guizhou	Pearl River	Liujiang River	Wang and Li 2001
20	*T. panzhouensis* Yu, Luo, Lan, Xiao & Zhou, 2023	Guizhou	Pearl River	Nanpanjiang River	Luo et al. 2023
21	*T. posterodorsalus* (Li, Ran & Chen, 2006)	Guangxi	Pearl River	Liujiang River	Ran et al. 2006
22	*T. qingzhenensis* Liu, Zen, & Gong, 2022	Guizhou	Yangtze River	Wujiang River	Liu et al. 2022
23	*T. qini* Deng, Wang & Zhang, 2022	Chongqing	Yangtze River	Yuanjiang River	Deng et al. 2022
24	*T. qiubeiensis* Li & Yang, 2008	Yunnan	Pearl River	Nanpanjiang River	Li et al. 2008
25	*T. rongduensis* Mao, Zhao, Yu, Xiao & Zhou,2023	Guizhou	Pearl River	Beipanjiang River	Luo et al. 2023
26	*T. rosa* Chen & Yang, 2005	Chongqing	Yangtze River	Wujiang River	Chen and Yang 2005
27	*T. sanduensis*Chen & Peng, 2019	Guizhou	Pearl River	Duliujiang River	Chen and Peng 2019
28	*T. shilinensis* Chen,Yang & Xu, 1992	Yunnan	Pearl River	Nanpangjiang River	Chen et al. 1992
29	*T. tianeensis* Chen, Cui & Yang, 2004	Guangxi	Pearl River	Hongshui River	Chen et al. 2004
30	*T. tianlinensis* Li, Li, Lan & Du, 2017	Yunnan	Pearl River	Hongshui River	Li et al. 2017b
31	*T. tianxingensis* Yang, Li & Chen, 2016	Yunnan	Pearl River	Nanpangjiang River	Yang et al. 2016
32	*T. wudangensis* Liu, Zen & Gong, 2022	Guizhou	Yangtze River	Wujiang River	Liu et al. 2022
33	*T. wulongensis* Chen, Sheraliev, Shu & Peng, 2021	Chongqing	Yangtze River	Wujiang River	Chen et al. 2021
34	*T. xiangshuingensis* Li, 2004	Yunnan	Pearl River	Nanpanjiang River	Li 2004
35	*T. xiangxiensis* Yang, Yuan & Liao, 1986	Hunan	Yangtze River	Yuanjiang River	Yang et al. 1986
36	*T. xichouensis* Liu, Pan, Yang & Chen, 2017	Yunnan	Red River	Red River	Liu et al. 2017
37	*T. xuanweiensis* Lu, Li, Mao & Zhao, 2022	Yunnan	Pearl River	Beipanjiang River	Lu et al. 2022
38	*T. yunnanensis* Yang, 1990	Yunnan	Pearl River	Nanpanjiang River	Chu and Chen 1990
39	*T. zhenfengensis* Wang & Li, 2001	Guizhou	Pearl River	Beipanjiang River	Wang and Li 2001

conducting a survey of cave fishes in western Guizhou Province, China. Morphological examination and molecular phylogenetic analysis indicated that these specimens were distinct from the 39 hypogean species of *Triplophysa*. We formally describe two new species, *Triplophysa ziyunensis* sp. nov., and *Triplophysa yaluwang* sp. nov., based on evidence from morphology, mitochondrial, and nuclear genes.

Table 2. Comparison of the diagnostic features of the two new species described here with those selected for the 39 recognized hypogean species of the genus *Triplophysa*. Modified from Wu et al. (2018b), Liu et al. (2022), and Luo et al. (2023). "–" indicates uncertainty.

ID	Species	Body pigmentation	Eyes	Eye diameter (% HL)	Interorbital width (% HL)	Dorsal fin distal margin	Secondary sex characteristics	Scales	Lateral line	Posterior chamber of air bladder	Dorsal fin rays	Anal fin rays	Pectoral fin rays	Pelvic fin rays	Caudal fin rays	Tip of pelvic fin reaching anus	Anterior nostril barbel-like	Vertebrae
1	*T. yaluwang* sp. nov.	Entire body	Reduced	4.6–6.1	24.3–26.0	Emarginated	Absent	Absent	Complete	Degenerated	iii, 7	iii, 5	i, 9	i, 5–6	14	Yes	Yes	4 + 36
2	*T. ziyunensis* sp. nov.	Entire body	Reduced	2.4–4.9	22.3–26.2	Truncated	Absent	Absent	Complete	Degenerated	iii, 8	iii, 5	i, 10	i, 6	16	Yes	Yes	4 + 35
3	*T. aluensis*	Absent	Reduced	5.6	22.2	Truncated	–	Absent	Complete	Degenerated	iii, 7	iii, 5	i, 9	i, 6	13	No	Yes	–
4	*T. anlongensis*	Entire body	Normal	5.1–9.3	32.1–35.6	Truncated	Absent	Absent	Complete	Degenerated	iii, 8	iii, 5	i, 11	ii, 8	16	No	Yes	4 + 37
5	*T. anshuiensis*	Dorsal	Absent	Absent	–	Truncated	Absent	Absent	Complete	Developed	iv, 7–8	ii, 6	i, 10	i, 6	14	Yes	Yes	–
6	*T. baotianensis*	Entire body	Normal	14.0–15.0	3.40–4.57	Truncated	–	Absent	Complete	Degenerated	iii, 6–7	ii, 4–5	i, 9	i, 5	11–13	No	Yes	–
7	*T. cehengensis*	Absent	Reduced	1.5–2.2	27.2–36.5	Emarginated	Absent	Absent	Complete	Developed	iv, 9	iii, 5	i, 10	ii, 8	16	Yes	Yes	4 + 35
8	*T. erythraea*	Absent	Absent	Absent	–	Truncated	Absent	Absent	Complete	Developed	ii, 8	i, 6	ii, 10	ii, 5	17	Yes	No	–
9	*T. fengshanensis*	Absent	Absent	Absent	–	Truncated	–	Absent	Complete	–	ii, 8	ii, 6	i, 8–10	i, 6–7	16	No	Yes	–
10	*T. flavicorpus*	Entire body	Normal	5.1–6.8	3.1–5.2	Emarginated	–	Present	Complete	Degenerated	iii, 10	iii, 6–7	i, 11	i, 6–7	16	Yes	No	4 + 34
11	*T. gejiuensis*	Absent	Absent	Absent	–	Truncated	–	Absent	Complete	Developed	iii, 7–8	iii, 4–6	i, 10	i, 5	14–15	Yes	Yes	–
12	*T. guizhouensis*	Entire body	Normal	9.4–12.1	20.3–24.3	Truncated	Absent	Present	Complete	Developed	iii, 8	iii, 6	i, 8–9	i, 6	14	No	Yes	–
13	*T. huapingensis*	Entire body	Normal	10.4–14.3	27.6–30.8	Truncated	Present	Present	Complete	Degenerated	iii, 8–9	iii, 5	i, 9–10	i, 5–6	16	No	No	–
14	*T. langpingensis*	Absent	Reduced	2.7–5.9	30.6–34.5	Truncated	–	Absent	Incomplete	–	iii, 7–8	iii, 5–6	i, 10–11	i, 6	14	Yes	Yes	–
15	*T. longipectoralis*	Entire body	Normal	11.8–16.4	21.2–25.3	Emarginated	Present	Present	Complete	Degenerated	iii, 8	iii, 5–6	i, 9–10	i, 6	14–15	Yes	Yes	4 + 35
16	*T. longliensis*	Entire body	Normal	9.5–11.5	31.4–37.5	Emarginated	Present	Absent	Complete	Developed	iii, 8	iii, 5	i, 10	i, 6	15–16	Yes	Yes	4 + 38
17	*T. luochengensis*	Entire body	Reduced	7.5–8.6	18.4–21.3	Truncated	Present	Present	Complete	Degenerated	iii, 8	ii, 6	i, 10	i, 6	16–17	No	Yes	4 + 33–34
18	*T. macrocephala*	Entire body	Reduced	3.6–8.0	22.9–25.8	Truncated	Present	Absent	Complete	Degenerated	iii, 7–9	iii, 5–6	i, 9–11	i, 6	15–17	Yes	Yes	–
19	*T. nandanensis*	Entire body	Normal	11.1–21.3	24.4–27.8	Emarginated	–	Present	Complete	Degenerated	iv, 8	iv, 5	i, 9–10	i, 6	14–16	No	Yes	4 + 36
20	*T. nanpanjiangensis*	Entire body	Normal	12.0–16.5	30.3–34.5	Truncated	Present	Absent	Complete	Degenerated	iii, 7–8	ii, 5	i, 9–10	i, 6	16	No	No	4 + 38
21	*T. nasobarbatula*	Entire body	Normal	9.1–13.3	27.0–33.3	Truncated	–	Present	Complete	Degenerated	iii, 8	iii, 5	i, 9	i, 6	15	Yes	Yes	4 + 36
22	*T. panzhouensis*	Entire body	Normal	7.0–11.0	22.1–31.3	Truncated	Absent	Absent	Complete	Degenerated	iv, 7–8	iii, 5	i, 11	ii, 7	16	No	Yes	4 + 35
23	*T. posterodorsalus*	Absent	Absent	Absent	–	Truncated	–	Absent	Complete	–	iii, 6	ii, 4	i, 13	i, 5	15	No	Yes	–

ID	Species	Body pigmentation	Eyes	Eye diameter (% HL)	Interorbital width (% HL)	Dorsal fin distal margin	Secondary sex characteristics	Scales	Lateral line	Posterior chamber of air bladder	Dorsal fin rays	Anal fin rays	Pectoral fin rays	Pelvic fin rays	Caudal fin rays	Tip of pelvic fin reaching anus	Anterior nostril barbel-like	Vertebrae
24	T. qingzhenensis	Entire body	Reduced	2.1–4.4	25.1–30.4	Truncated	Absent	Absent	Complete	Degenerated	iii, 7–8	iii, 5	i, 8–9	i, 5	14	No	Yes	4 + 36
25	T. qini	Absent	Absent	Absent	–	Emarginated	Present	Absent	Complete	–	ii, 8	ii, 5	–	–	14–16	Yes	No	4 + 34–35
26	T. qiubeiensis	Absent	Absent	Absent	–	Emarginated	–	Absent	Complete	Degenerated	iii, 7	iii, 5	i, 7–9	i, 5	14–15	Yes	No	4 + 35
27	T. rongduensis	Entire body	Normal	7.2–14.7	24.1–28.6	Truncated	Absent	Absent	Complete	Degenerated	iv, 9	iii, 5	i, 10	ii, 7	16	No	Yes	4 + 39
28	T. rosa	Absent	Absent	Absent	–	Emarginated	Absent	Absent	Complete	–	iii, 9	iii, 6	i, 12	i, 7	14	Yes	Yes	–
29	T. sanduensis	Entire body	Normal	11.9–15.4	31.2–40.2	Emarginated	Present	Present	Complete	Degenerated	ii, 8–9	i, 5	i, 8–9	i, 5	17–18	No	Yes	4 + 37
30	T. shilinensis	Absent	Absent	Absent	–	Truncated	–	Absent	Complete	Degenerated	iii, 7	iii, 5	i, 8–10	i, 6	14	No	Yes	–
31	T. tianeensis	Entire body	Reduced	3.0–5.9	21.3–25.6	Truncated	Present	Absent	Complete	Degenerated	iii, 6–7	iii, 6	i, 8–9	i, 5–6	15–16	No	Yes	4 + 35
32	T. tianlinensis	Absent	Reduced	Absent	Absent	Truncated	Present	Absent	Complete	Degenerated	iv, 8–9	iii, 6	i, 10	i, 6	15–16	Yes	Yes	–
33	T. tianxingensis	Entire body	Normal	4.2–6.7	17.4–24.0	Truncated	Absent	Absent	Complete	Developed	iii, 8	ii, 5	i, 9	i, 5	16	No	No	4 + 38
34	T. wudangensis	Entire body	Reduced	5.1–6.5	33.1–35.8	Truncated	Absent	Absent	Complete	Degenerated	iii, 7	iii, 5	i, 8	i, 5	14	No	Yes	4 + 34
35	T. wulongensis	Entire body	Normal	11.1–19.1	38.5–43.1	Emarginated	–	Absent	Complete	Degenerated	ii, 8–9	i, 5–6	i, 8–9	i, 5–7	18	No	Yes	4 + 38–39
36	T. xiangshuingensis	Entire body	Normal	7.5	32.3	Emarginated	–	Absent	Complete	Degenerated	iii, 6	iii, 5	i, 9	i, 6	14	No	Yes	–
37	T. xiangxiensis	Absent	Absent	Absent	–	Emarginated	–	Absent	Complete	Developed	iii, 8	iii, 6	i, 11	i, 6	16	Yes	Yes	–
38	T. xichouensis	Entire body	Reduced	Absent	–	Truncated	Absent	Absent	Complete	Developed	iii, 8	ii, 6	i, 9–10	i, 5–6	16	Yes	Yes	4 + 36
39	T. xuanweiensis	Absent	Absent	Absent	–	Emarginated	–	Absent	Complete	Well developed	iii, 7–8	iii, 5	i, 10–12	i, 7–8	17–18	Yes	No	–
40	T. yunnanensis	Entire body	Normal	7.2–8.3	27.0–27.8	Emarginated	Present	Present	Complete	Degenerated	iii, 7	iii, 5	i, 9–10	i, 7	15–16	No	Yes	–
41	T. zhenfengensis	Entire body	Normal	7.1–16.7	22.2–34.5	Truncated	–	Present	Complete	Degenerated	iii, 7	iii, 5	i, 9	i, 5–7	14–15	No	No	4 + 36

Figure 1. Sample collection localities and distributions of the two new species and 39 hypogean species of the genus *Triplophysa* in southern China. The base maps are from the Standard Map Service website (http://bzdt.ch.mnr.gov.cn/index.html).

Materials and methods

Sampling

Thirty-seven samples of six species were collected in total for morphology comparison and genetic analysis (Fig. 1). Of these five specimens representing the new species, we collected *Triplophysa ziyunensis* sp. nov., from Maoying Town, Ziyun County, Guizhou, and five specimens representing the new species, *Triplophysa yaluwang* sp. nov., from Maoying Town, Ziyun County, Guizhou. The following specimens were used for morphometric data: nine specimens were *T. rosa* from Huolu Town, Wulong County, Chongqing; three specimens were *T. wudangensis* from Wudang District, Guiyang City, Guizhou; eight specimens were *T. qingzhenensis* from Qingzhen County, Guiyang City, Guizhou; and seven specimens were *T. guizhouensis* from Baijin Town, Huishui County, Guizhou. All of the specimens were fixed in 10% buffered formalin and later transferred to 75% ethanol for preservation. Muscle samples used for molecular analysis were preserved in 95% alcohol and stored at −20 °C. All of the specimens were deposited at Guizhou Normal University (GZNU), Guiyang City, Guizhou Province, China.

DNA extraction, PCR, and sequencing

Genomic DNA was extracted from muscle tissue using a DNA extraction kit from Tiangen Biotech (Beijing) Co. Ltd. In total, six tissue samples used for molecular analysis were amplified and sequenced for mitochondrial gene cytochrome b

(Cyt *b*) using the primers L3975 (5′-CGCCTGTTTACCAAAAACAT-3′) and H4551 (5′-CCGGTCTGAACTCAGATCACGT-3′) following Xiao et al. (2001). We also amplified one nuclear gene recombinase-activating 1 protein gene (*RAG1*) for 16 tissue samples, using primer LTF1 (5′-ATCATCGATGGCCTCTCAGGTT-3′) and LTR1 (5′-ACGTGGGCTAGAGTCTTGTGTAGGT-3′). PCR amplifications were performed within a 20 µl reaction volume with the cycling conditions that follow: An initial denaturing step at 95 °C for 4 min, 35 cycles of denaturing at 95 °C for 30 s, annealing at 45 °C (for Cyt b)/ 52 °C (for *RAG1*) for 40 s, and extension at 72 °C for 1 min followed by a final extension at 72 °C for 10 min. PCR products were purified with spin columns. The products were sequenced on an ABI Prism 3730 automated DNA sequencer at Chengdu TSING KE Biological Technology Co. Ltd. (Chengdu, China). All of the newly obtained sequences were submitted to GenBank (Table 3).

Phylogenetic analyses and nuclear haplotyping

Sixty-three mitochondrial Cyt *b* sequences, including six newly sequenced and 57 downloaded from GenBank, were used for molecular analysis. We followed the phylogenetic study of Luo et al. (2023) and used *Barbatula labia*, *B. barbatula*, and *Homatula berezowskii* as outgroups (Table 3).

All of the sequences were assembled and aligned using the MUSCLE (Edgar 2004) module in MEGA v. 7.0 (Kumar et al. 2016) with default settings. Alignment results were checked visually. Phylogenetic trees were constructed via both maximum likelihood (ML) and Bayesian inference (BI) methods. The ML was conducted in IQ-TREE v. 2.0.4 (Nguyen et al. 2015) with 10,000 ultrafast bootstrap (UBP) replicates (Hoang et al. 2018), and it was performed until a correlation coefficient of at least 0.99 was reached. The BI was performed in MrBayes v. 3.2.1 (Ronquist et al. 2012), and the best-fit model was obtained based on the Bayesian information criterion computed with PartitionFinder v. 2.1.1 (Lanfear et al. 2017). The first, second, and third codons of Cyt *b* were defined in this analysis.

The analysis suggested the best partition scheme for each codon position of Cyt *b*. TRNEF+I+G, HKY+I, and TIM+I+G were selected for the first, second, and third codons, respectively. Two independent runs were conducted in the BI analysis, each of which was performed for 2×10^7 generations and sampled every 1000 generations. The first 25% of the samples were discarded as a burn-in, resulting in a potential scale reduction factor of < 0.01. Nodes in the trees were considered well-supported when Bayesian posterior probabilities (BPP) were ≥ 0.95 and the ML ultrafast bootstrap value (UBP) was ≥ 95%. Uncorrected *p*-distances (1000 replicates) based on Cyt *b* were estimated using MEGA v. 7.0.

We also used the nuclear gene (*RAG1*) in PopART v. 1.7 (Leigh and Bryant 2015) based on the Median Joining method (Bandelt et al. 1999) to obtain haplotypes for assessing differences between the new species and genetically similar species.

Morphometrics, comparisons, and statistics

Morphometric data were collected from 37 well-preserved specimens of *Triplophysa* (Suppl. material 1). Twenty measurements were recorded to the nearest 0.1 mm with digital calipers following the protocols of Tang et al. (2012) and Li et al. (2018). All of the measurements were taken on the left side when looking directly at the head end of the fish.

Table 3. Localities, voucher information, and GenBank numbers for all samples used. Numbers in bold were generated in this study.

ID	Species	Localities (* type localities)	Voucher ID	Cytb	RAG1
1	*T. guizhouensis*	Lewang Town, Wangmo County, Guzihou, China	GZNU20220313001	OQ241174	PQ117091
2	*T. guizhouensis*	Lewang Town, Wangmo County, Guzihou, China	gznu09	KU987438	PQ117092
3	*T. guizhouensis*	Baijin Town, Huishui County, Guzihou, China*	GZNU20230722007	GZ01	PQ117093
4	*T. yaluwang* sp. nov.	Maoying Town, Ziyun City, Guizhou, China*	GZNU20240118005	PQ117067	PQ117090
5	*T. yaluwang* sp. nov.	Maoying Town, Ziyun City, Guizhou, China*	GZNU20240118006	PQ117068	PQ117089
6	*T. longliensis*	/	SWU2016090300	MW582825	
7	*T. sanduensis*	Zhonghe Town, Sandu County, Guizhou, China*	SWU20170613001	MW582822	
8	*T. qini*	Houping Village, Wulong County, Chongqing, China*		ON528184	
9	*T. xiangxiensis*	Feihu Cave, Hunan, China*	/	JN696407	
10	*T. xiangxiensis*	/	IHB 2015010002	KT751089	
11	*T. nandanensis*	Hechi City, Guangxi,China	SWU20151123046	MG697588	
12	*T. nandanensis*	Liuzhai Town, Nandan County, Guangxi, China*	GZNU20230404005	OQ754126	
13	*T. nandanensis*	Liuzhai Town, Nandan County, Guangxi, China*	GZNU20230404007	OQ754128	
14	*T. tianeensis*	/	/	MW582826	
15	*T. tianeensis*	Bala Township, Tian 'e County, Guangxi, China*	GZNU20230404003	OQ754124	
16	*T. nasobarbatula*	Dongtang Township, Libo County, Guizhou, China*	GZNU20190114001	MH685911	
17	*T. nasobarbatula*	Dongtang Township, Libo County, Guizhou, China*	GZNU20220313010	OQ241175	
18	*T. nasobarbatula*	Dongtang Township, Libo County, Guizhou, China*	GZNU20220313011	OQ241176	
19	*T. macrocephala*	Lihu Town, Nandan County, Guangxi, China*	GZNU20230404002	OQ754123	
20	*T. rosa*	Huolu Town, Wulong County, Chongqing, China*	SWU10100503	JF268621	
21	*T. rosa*	/	F3911	MG697587	
25	*T. rosa*	HuoLuTown, Wulong County, Chongqing City, China*	GZNU20230404009	OQ754130	PQ117076
22	*T. rosa*	Huolu Town, Wulong County, Chongqing, China*			PQ117079
23	*T. rosa*	Huolu Town, Wulong County, Chongqing, China*			PQ117080
24	*T. rosa*	Huolu Town, Wulong County, Chongqing, China*			PQ117081
26	*T. qingzhenensis*	Qingzhen County, Guiyang City, Guizhou, China*	IHB 201911150004	MT700458	
27	*T. qingzhenensis*	Qingzhen County, Guiyang City, Guizhou, China*			PQ117082
28	*T. qingzhenensis*	Qingzhen County, Guiyang City, Guizhou, China*			PQ117083
29	*T. qingzhenensis*	Qingzhen County, Guiyang City, Guizhou, China*			PQ117084
30	*T. wudangensis*	Wudang District, Guiyang City, Guizhou, China*	IHB 201908090003	MT700460	
31	*T. wudangensis*	Wudang District, Guiyang City, Guizhou, China*	GZNU20230404010	OQ754131	PQ117085
32	*T. wudangensis*	Wudang District, Guiyang City, Guizhou, China*			PQ117086
33	*T. wudangensis*	Wudang District, Guiyang City, Guizhou, China*			PQ117087
34	*T. wudangensis*	Wudang District, Guiyang City, Guizhou, China*			PQ117071
35	*T. ziyunensis* sp. nov.	Maoying Town, Ziyun City, Guizhou, China*	GZNU20230529003	PQ117069	PQ117072
36	*T. ziyunensis* sp. nov.	Maoying Town, Ziyun City, Guizhou, China*	GZNU20230529004	PQ117069	PQ117073
37	*T. ziyunensis* sp. nov.	Maoying Town, Ziyun City, Guizhou, China*	GZNU20230529005	PQ117071	PQ117074
38	*T. ziyunensis* sp. nov.	Maoying Town, Ziyun City, Guizhou, China*			PQ117075
39	*T. erythraea*	Dalong Cave, Huayuan County, Hunan, China*	/	MG967615	
40	*T. xuanweiensis*	Tangtang Town, Xuanwei City, Yunnan, China*	ASIZB223818	OL675196	
41	*T. xuanweiensis*	Tangtang Town, Xuanwei City, Yunnan, China*	ASIZB223819	OL675197	
42	*T. xuanweiensis*	Tangtang Town, Xuanwei City, Yunnan, China*	ASIZB223820	OL675198	
43	*T. zhenfengensis*	Xinlongchang Town, Xingren City, Guizhou, China*	GZNU20220313007	OQ241177	
44	*T. zhenfengensis*	Xinlongchang Town, Xingren City, Guizhou, China*	GZNU20220313008	OQ241178	
45	*T. zhenfengensis*	Xinlongchang Town, Xingren City, Guizhou, China*	GZNU20220313009	OQ241179	
46	*T. zhenfengensis*	Xinlongchang Town, Xingren City, Guizhou, China*	GZNU20220313005	OQ241180	

ID	Species	Localities (* type localities)	Voucher ID	Cytb	RAG1
47	*T. rongduensis*	Rongbei Town, Ceheng County, Guzihou, China*	GZNU20230110001	OQ754135	
48	*T. rongduensis*	Rongbei Town, Ceheng County, Guzihou, China*	GZNU20230110002	OQ754136	
49	*T. rongduensis*	Rongbei Town, Ceheng County, Guzihou, China*	GZNU20230110003	OQ754137	
50	*T. anlongensis*	Xinglong Town, Anlong County, Guzihou, China*	GZNU20230112001	OQ754138	
51	*T. anlongensis*	Xinglong Town, Anlong County, Guzihou, China*	GZNU20230112002	OQ754139	
52	*T. anlongensis*	Xinglong Town, Anlong County, Guzihou, China*	GZNU20230112003	OQ754140	
53	*T. baotianensis*	Baotian Town, Panzhou City, Guzihou, China*	GZNU20180421005	MT992550	
54	*T. baotianensis*	Baotian Town, Panzhou City, Guzihou, China*	GZNU20180421006	OQ241181	
55	*T. panzhouensis*	Hongguo Town, Panzhou City, Guizhou, China*	GZNU20220513001	OQ754119	
56	*T. panzhouensis*	Hongguo Town, Panzhou City, Guizhou, China*	GZNU20220513002	OQ754120	
57	*T. panzhouensis*	Hongguo Town, Panzhou City, Guizhou, China*	GZNU20220513003	OQ754121	
58	*T. cehengensis*	Rongbei Town, Ceheng County, Guzihou, China*	GZNU20230109001	OQ754132	
59	*T. cehengensis*	Rongbei Town, Ceheng County, Guzihou, China*	GZNU20230109002	OQ754133	
60	*T. cehengensis*	Rongbei Town, Ceheng County, Guzihou, China*	GZNU20230109003	OQ754134	
61	*T. huapingensis*	/	F3917	MG697589	
62	*T. huapingensis*	Huaping Town, Leye County, Guangxi, China*	GZNU20230404004	OQ754125	
63	*T. langpingensis*	Longping Township, Tianlin County, Guangxi*	GZNU20230404001	OQ754122	
64	*T. qiubeiensis*	NijiaoVillage, Qiubei County, Yunnan , China*	GZNU20230404006	OQ754127	
65	*T. wulongensis*	Wulong County, Chongqing, China*	/	MW582823	
66	*T. wulongensis*	HuoLuTown, Wulong County, Chongqing City, China	GZNU20230404008	OQ754129	
67	*T. nujiangensa*	Fugong County, Yunnan, China	IHB201315814	KT213598	
68	*T. tibetana*	Mafamu lake, Xinjiang, China	NWIPB1106069	KT224364	
69	*T. tenuis*	Niutou river, Qingshui County, Gansu, China	IHB0917490	KT224363	
70	*T. wuweiensis*	Yongchang County, Gansu, China	IHB201307124	KT224365	
71	*Barbatula barbatula*	/	/	KP715096	
72	*Barbatula labiata*	Xinyuan County, Xinjiang, China	IHB201306569	KT192057	
73	*Homatula berezowskii*	Qujing City, Yunnan, China	FS-2014-Y03	NC_040302	

Comparative data for the 39 hypogean species of *Triplophysa* were obtained from the literature and specimen examination (Table 2). Specimens of 19 species from the type locality were collected and examined, and these included: *T. anlongensis*, *T. cehengensis*, *T. baotianensis*, *T. erythraea*, *T. guizhouensis*, *T. huapingensis*, *T. langpingensis*, *T. macrocephala*, *T. nasobarbatula*, *T. nandanensis*, *T. panzhouensis*, *T. qingzhenensis*, *T. qini*, *T. qiubeiensis*, *T. rosa*, *T. rongduensis*, *T. tianeensis*, *T. wudangensis*, and *T. zhenfengensis* (see Suppl. material 1). The measurements of these species were also included in the statistical analysis, taking into consideration the morphological similarity, genetic differences, and geographical distances of the two new species to *T. rosa*, *T. qingzhenensis*, *T. wudangensis*, *T. guizhouensis*, *T. sanduensis*, and *T. longliensis*.

Principal component analyses (PCAs) of size-corrected measurements and simple bivariate scatterplots were used to characterize the morphometric differences between the new species and closely related species. Mann–Whitney *U* tests were used to determine the significance of differences in morphometric characteristics between the new species and similar species. All of the statistical analyses were performed using SPSS 21.0 (SPSS, Inc., Chicago, IL, USA), and differences were considered statistically significant at $P < 0.05$. PCAs of morphological data were performed after logarithmic transformation and under nonrotational conditions. All of the pre-processing of morphological data was performed in Microsoft Excel (Microsoft Corporation 2016).

Results

Phylogenetic analyses, genetic divergence, and nuclear haplotypes

ML and BI phylogenies were constructed based on mitochondrial Cyt *b*, with the sequence length being 1140 base pairs. The BI and ML phylogenetic trees showed a highly consistent topology that strongly supported the monophyly of the genus *Triplophysa*, and indicated that *Triplophysa* could be divided into two major clades, namely, the hypogean group and the epigean group (Fig. 2A).

The hypogean group contains 24 species from the karsts of southwest China (Chongqing, Guangxi, Guizhou, Hubei, and Yunnan) and two other lineages from western Guizhou that can be further divided into three clades (Fig. 2A): Clade A, only *T. wulongensis*, mainly in the Wujiang River basin (Fig. 1); subclade B1, including *T. qiubeiensis*, *T. langpingensis*, *T. huapingensis*, *T. cehengensis*, *T. panzhouensis*, *T. baotianensis*, *T. anlongensis*, *T. rongduensis*, and *T. zhenfengensis*, mainly in the Nampanjiang, Beipanjiang, and Hongshui River basins (Fig. 2A); and subclade B2 including *T. xuanweiensis*, *T. erythraea*, *T. wudangensis*, *T. qingzhenensis*, *T. rosa*, *T. macrocephala*, *T. nasobarbatula*, *T. tianeensis*, *T. nandanensis*, *T. xiangxiensis*, *T. qini*, *T. sanduensis*, *T. longliensis*, *T. guizhouensis*, and two other lineages from western Guizhou, mostly upstream of the Pearl and Yangtze rivers (Fig. 1).

All of the samples within subclade B1 from Shuitang Village, Maoying Town, Ziyun County, Guizhou Province (samples 35–38 in Table 3), clustered together in a sister clade to *T. wudangensis*, *T. qingzhenensis*, and *T. rosa* with strong node support (BPP/UBP = 1.00/1.00). This population could be distinguished from all of the known species and other undescribed lineages in this study via distinct morphological characteristics and molecular differences, with a lower *p*-distance of 1.8–2.0% (vs *T. wudangensis*, *T. rosa*, and *T. qingzhenensis*) (Table 4). Thus, the population at this locality represents an independently evolved lineage and is described below as a new species, *Triplophysa ziyunensis* sp. nov.

All of the samples within subclade B1 from Xinzhai Village, Maoying Town, Ziyun County, Guizhou Province (samples 4 and 5 in Table 3), clustered together in a sister clade to *T. guizhouensis* with strong node support (BPP/UBP = 0.98/0.96). This population could be distinguished from all of the known species and other undescribed lineages in this study by distinct morphological characteristics and molecular differences, with a lower *p*-distance of 1.4% (vs *T. guizhouensis*) (Table 4). Thus, the population at this locality represents an independently evolved lineage and is described below as a new species, *Triplophysa yaluwang* sp. nov.

Haplotype networks based on *RAG1* showed that unique, non-shared haplotypes were observed in the two new species and multiple linking mutations occurred with closely related species (Fig. 2B). We observed shared haplotypes from among *T. qingzhenensis*, *T. rosa*, and *T. wudangensis* (Fig. 2B). More haplotype diversity was found within *T. rosa*, a pattern that may be related to higher genetic diversity and wider distribution.

Morphological analyses

Mann-Whitney U tests revealed differences in several morphological characteristics among the two new species (*T. ziyunensis* sp. nov. and *T. yaluwang* sp. nov.), and between the new species and the closely related species (Table 5).

Table 4. Uncorrected *p*-distance (%) between new species and 24 congeneric species of the genus *Triplophysa* based on mitochondrial Cyt *b*.

| ID	Species	1	2	3	4	5	6	7	8	9	10	11	12	13	14	15	16	17	18	19	20	21	22	23	24	25
1	T. ziyunensis sp. nov.																									
2	T. yaluwang sp. nov.	9.5																								
3	T. anlongensis	15.3	14.5																							
4	T. baotianensis	14.9	14.0	6.8																						
5	T. cehengensis	15.1	13.8	3.8	6.8																					
6	T. erythraea	11.5	10.3	14.6	13.8	14.6																				
7	T. guizhouensis	9.8	1.4	14.7	14.5	13.9	10.6																			
8	T. huapingensis	15.1	14.1	9.9	10.2	9.3	14.9	14.6																		
9	T. langpingensis	14.2	14.7	14.1	14.0	13.8	15.8	15.1	14.4																	
10	T. longliensis	10.0	2.5	14.6	14.2	14.2	10.6	2.8	14.6	15.0																
11	T. macrocephala	10.0	9.2	15.4	15.9	15.3	12.0	9.6	14.9	15.7	9.4															
12	T. microphthalmus	14.5	13.8	10.0	11.0	9.5	15.1	13.8	5.9	13.8	14.0	15.1														
13	T. nandanensis	10.9	9.7	16.5	16.3	16.0	12.3	10.1	16.0	16.4	10.3	5.3	16.0													
14	T. nasobarbatula	9.9	9.1	15.5	15.8	15.2	12.1	9.6	14.9	15.3	9.4	0.9	15.2	5.5												
15	T. panzhouensis	15.8	13.6	7.0	7.7	8.2	13.4	14.3	10.1	14.7	12.9	15.3	10.2	15.7	15.2											
16	T. qingzhenensis	2.0	8.5	15.4	15.1	15.3	11.3	8.9	14.6	14.4	9.1	9.7	14.3	10.2	9.5	15.2										
17	T. qini	9.5	5.1	14.7	15.5	14.5	10.7	5.0	15.1	15.6	5.3	9.1	13.9	10.5	9.4	14.3	8.8									
18	T. qiubeiensis	14.1	12.7	14.7	14.2	14.2	13.8	12.8	14.6	14.5	13.3	14.6	14.5	14.5	14.2	14.4	13.8	13.4								
19	T. rosa	1.9	8.7	15.4	15.1	15.4	11.6	9.0	15.3	14.5	9.3	10.0	14.6	10.7	9.7	15.5	1.4	9.1	13.9							
20	T. sanduensis	9.9	2.5	14.8	14.7	14.5	11.0	2.6	14.7	15.1	0.7	9.3	13.9	10.5	9.2	13.5	9.0	5.3	13.6	9.3						
21	T. tianeensis	10.6	9.8	16.6	16.5	16.5	11.6	10.2	16.1	16.2	10.5	5.1	16.3	2.0	5.3	15.8	10.0	10.0	14.6	10.6	10.6					
22	T. wudangensis	1.8	8.7	15.3	14.9	15.4	11.3	9.1	14.8	14.4	9.3	10.1	14.4	10.7	9.8	15.5	1.6	9.3	14.2	1.5	9.3	10.5				
23	T. wulongensis	13.7	14.1	16.9	16.6	16.5	15.4	13.9	17.7	15.5	13.5	15.1	16.5	14.8	15.1	16.3	13.6	13.4	15.5	13.8	13.4	14.6	13.8			
24	T. xiangxiensis	9.3	7.9	14.3	14.7	14.2	11.2	8.1	15.2	14.6	7.2	8.5	14.5	9.7	8.4	13.9	8.6	5.9	13.8	8.7	7.8	9.0	9.0	14.4		
25	T. xuanweiensis	11.3	11.1	14.8	14.2	14.8	11.9	11.6	14.4	14.0	11.8	11.5	14.5	11.7	11.4	14.1	11.5	11.4	12.3	11.6	11.7	12.0	11.2	14.2	11.4	
26	T. zhenfengensis	15.6	13.9	3.4	6.8	0.9	14.5	14.0	9.0	13.6	14.4	15.6	9.3	16.2	15.3	7.7	15.4	14.8	14.1	15.6	14.6	16.7	15.5	16.3	14.3	14.4
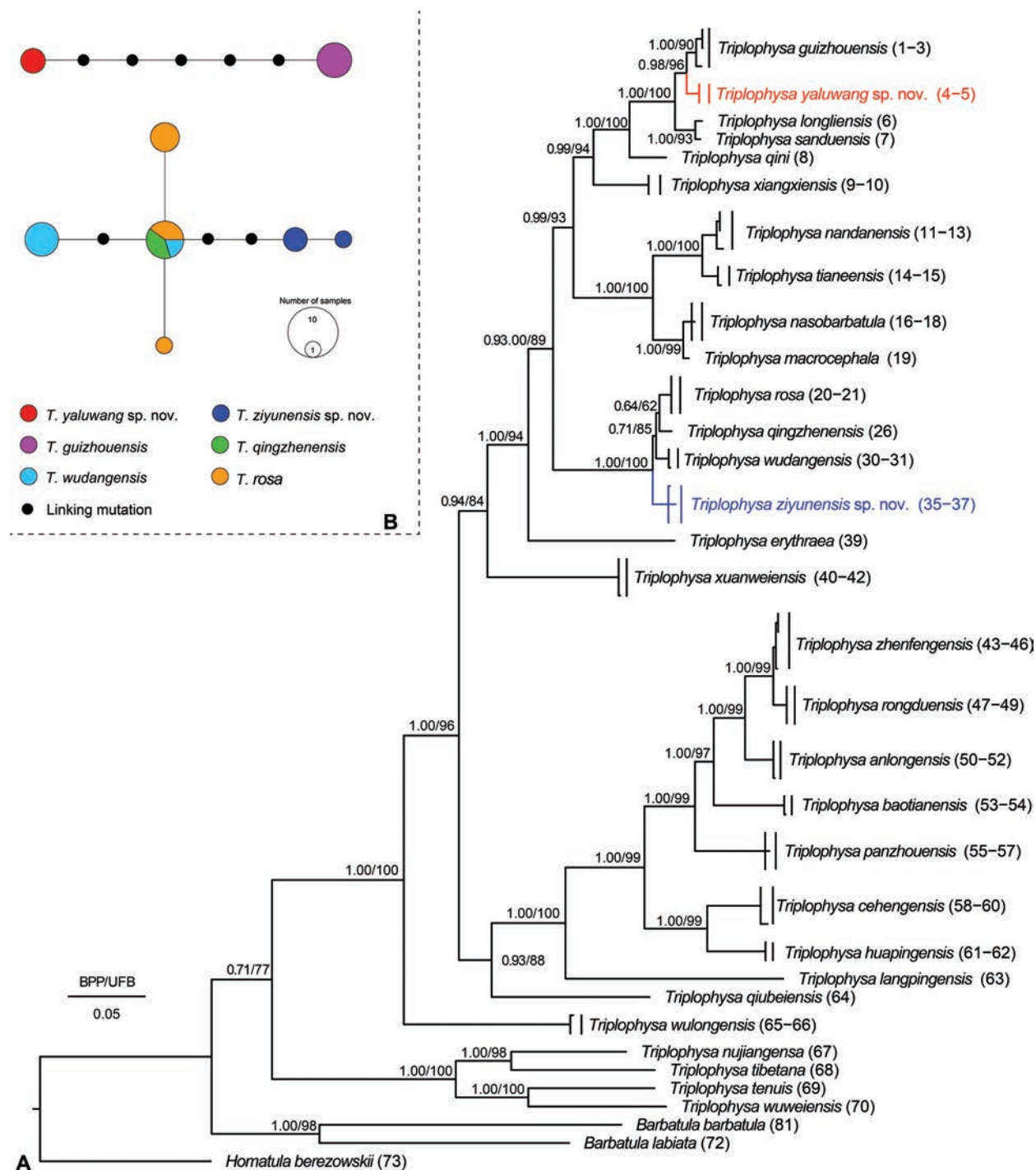
Figure 2. Phylogeny and nuclear gene haplotypes **A** phylogenetic tree based on mitochondrial Cyt *b* (1140 bp). Bayesian posterior probabilities (BPP) from BI analysis/ultrafast bootstrap supports (UBP) from ML analysis are noted beside nodes. Scale bars represent 0.05 nucleotide substitutions per site. The numbers at the tips of species name correspond to the ID numbers listed in Table 2 **B** haplotypes inferred based on the nuclear gene *RAG1*.

These significantly different measurements were concentrated on the head, barbel, fins, and tail (Table 5). There are significant morphological differences only in eye diameter and pectoral-fin ray length for *Triplophysa yaluwang* sp. nov. and *T. guizhouensis*.

Four principal component factors with eigenvalues greater than one were extracted based on the PCA of the morphological data. These factors accounted

for 83.42% and 74.86% of the total variation (Suppl. material 2). The first principal component (PC1) accounted for 38.23% and 28.77% of the variation and was positively correlated with all of the variables (eigenvalue = 3.0 and 4.1). On the two-dimensional plots of PC1 and PC2, the new species *T. ziyunensis* sp. nov. can be readily distinguished from *T. wudangensis*, *T. rosa*, and *T. qingzhenensis* (Fig. 3A). *T. yaluwang* sp. nov. can be readily distinguished from *T. guizhouensis* (Fig. 3B), while the holotype of *T. longliensis* are mosaic in the *T. yaluwang* sp. nov. The two new species are clearly distinguished by morphological characteristics from the geographical and morphological relative species based on statistical analysis of the measurements and the PCA result.
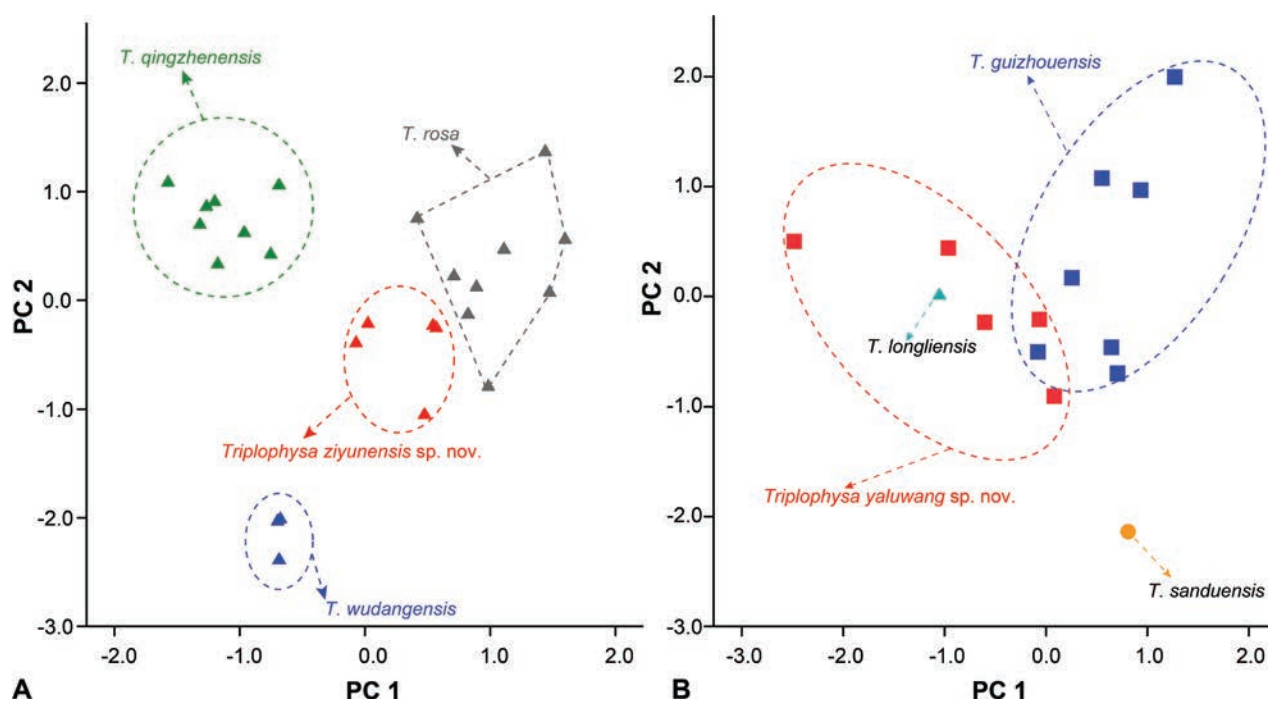
Figure 3. Plots of principal components analysis scores of **A** *T. ziyunensis* sp. nov. and **B** *T. yaluwang* sp. nov., and closely related species based on morphometric data.

Taxonomic account

Triplophysa ziyunensis Wu, Luo, Xiao & Zhou, sp. nov.

https://zoobank.org/BA4F7B39-A976-4D59-AE66-439DB9130A2E
Figs 4, 5, Table 5, Suppl. material 1

Type material. *Holotype.* GZNU20230529001 (Fig. 4), 105.1 mm total length (TL), 86.7 mm standard length (SL), collected by Li Wu and Xing-Liang Wang on 29 May 2023, at Shuitang Village, Maoying Town, Ziyun County, Guizhou Province, China (25.96846238°N, 106.13737106°E; 1228 m a.s.l.; Fig. 1).

Paratypes. Four specimens from the same locality as the holotype: GZNU20230226008-226010, and GZNU20230529002, 63.3−100.1 mm SL, collected by Tao Luo, Li Wu, Xing-Liang Wang, Xin-Rui Zhao, and Chang-Ting Lan on 26 February 2023.

Diagnosis. *Triplophysa ziyunensis* sp. nov. is distinguished from other hypogean species of the genus *Triplophysa* by the following characteristics in combination: (1) body naked, scaleless, pigmented markings on surface of
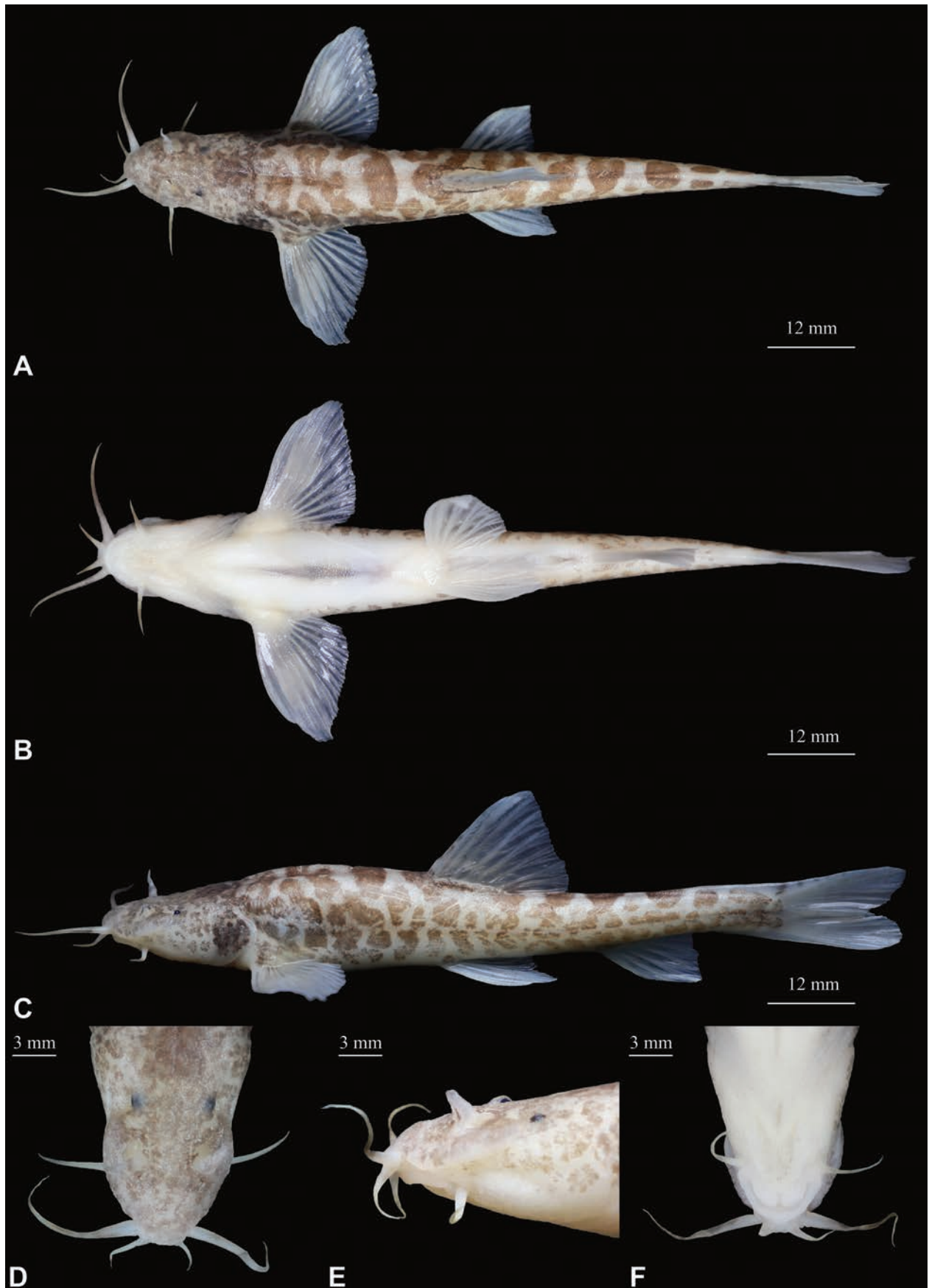
Figure 4. Morphological characteristics of holotype GZNU20230529001 of *Triplophysa ziyunensis* sp. nov. in preservative (10% formalin) **A** dorsal view **B** ventral view **C** lateral view **D** dorsal view of head **E** lateral view of head, and **F** ventral view of head.

body, except ventral; (2) eyes reduced, diameter 2.4–4.9% of head length (HL); (3) pelvic-fin tip extending to anus; (4) tip of pectoral fin not reaching pelvic fin origin; (5) anterior and posterior nostrils closely set, with anterior nostril elongated to a barbel-like tip; (6) tip of outrostral barbel extending backward, not reaching anterior margin of eye; (7) lateral line complete; (8) posterior chamber of air bladder degenerated; and (9) dorsal-fin rays iii-8, pectoral-fin rays i-10, pelvic-fin rays i-6, anal-fin rays iii-5, and 16 branched caudal-fin rays.

Description. Morphological data on the specimens of *Triplophysa ziyunensis* sp. nov. are provided in Table 5 and Suppl. material 1. Body elongated and cylindrical, posterior portion gradually compressed from dorsal fin to caudal-fin base, with deepest body depth anterior to dorsal-fin origin, deepest body depth 13–16% of standard length (SL). Dorsal profile slightly convex from snout to dorsal-fin insertion, and then straight from posterior portion of dorsal-fin origin to caudal-fin base. Ventral profile flat. Head short, length 26–27% of SL, slightly depressed and flattened, width slightly greater than depth (head width (HW)/head depth (HD) = 1.1–1.3). Snout slightly pointed, and snout length 46–50% of HL. Mouth inferior and curved, mouth corner situated below anterior nostril, upper and lower lips smooth, lower lip with V-shaped median notch. Three pairs of barbels are present: inner rostral barbel long, length 23–27% of HL, backward extending to corner of the mouth; out rostral barbel long, length 52–58% of HL, backward extending to beyond posterior margin of eyes. Maxillary barbel not extending to posterior margin of operculum, length 34–42% of HL. Anterior and posterior nostrils closely set, length 0.20–0.25 mm. Anterior nostril tube long, with an elongated short barbel-like tip, tip of posterior nostril extending backward not reaching to anterior margin of the eye. Eyes reduced, with diameter 2–5% of HL. Gill opening small, gill rakers not developed, ten inner gill rakers on first gill arch (*n* = 1).

Dorsal-fin rays iii-8, pectoral-fin rays i-10, pelvic-fin rays i-6, anal-fin rays i-5, 16 branched caudal-fin rays. Dorsal fin short, length 20–23% of SL, distal margin emarginated, origin anterior to pelvic-fin insertion and situated slightly posterior to the midpoint between snout tip and caudal-fin base, first branched ray longest, shorter than head length, tip of dorsal fin vertical to the anus. Pectoral fin moderately developed, length 22–24% of SL, tip of pectoral fin extending backward almost to midpoint between origin of pectoral and pelvic fin origins, not reaching to pelvic fin origin. Pelvic fin length 16–20% of SL, vertically aligned with third branched ray of dorsal fin, tips of pelvic fin reaching anus. Anal fin length 16–20% of SL, distal margin truncated, origin close to anus, tips of anal fin not reaching caudal-fin base, distance between tips of anal fin and anus 8.5× the eye diameter. Caudal fin forked, upper lobe equal in length to lower lobe, tips pointed, caudal peduncle length ~ 13.6 mm, caudal peduncle depth ~ 5.8 mm, with weak adipose crests along both dorsal and ventral sides. Total vertebrae: 39 (*n* = 1).

Cephalic lateral line system developed. Lateral line complete, exceeding tip of pectoral fin and reaching base of caudal fin. Two chambers of air bladder, anterior chamber dumbbell-shaped and membranous, open on both sides, slightly closed posteriorly; posterior chamber degenerated, slightly filling the body cavity, connected with anterior chamber by a long, slender tube.

Coloration. In cave water, the body of living fish is semi-translucent and pale pink, with irregular dark brownish brown patches on the head and body (Fig. 5). After fixation in 10% formalin solution, the body color was pale grey, and the dark-brown patches on the head and body were more prominent (Fig. 4).

Table 5. Morphological comparison of *Triplophysa ziyunensis* sp. nov. (*TZ*), *Triplophysa yaluwang* sp. nov. (*TY*), *T. wudangensis* (*TW*), *T. rosa* (*TR*), *T. qingzhenensis* (*TQ*), and *T. guizhouensis* (*TG*). All units in mm. *P*-values are at the 95% significance level.

	T. ziyunensis sp. nov.		*T. yaluwang* sp. nov.		*T. wudangensis*		*T. rosa*		*T. qingzhenensis*		*T. guizhouensis*		TY vs TG	TZ vs TW	TZ vs TR	TZ vs TQ
	Range	Mean ± SD	Range	Mean ± SD	Range	Mean ± SD	Range	Mean ± SD	Range	Mean ± SD	Range	Mean ± SD				
Total length	78.6–120.0	103.8 ± 16.3	66.5–99.4	77.4 ± 15.3	73.4–85.9	79.5 ± 6.3	62.3–130.8	91.8 ± 23.8	84.6–123.3	109.6 ± 14.0	54.9–88.1	75.5 ± 12.2	0.808	0.101	0.386	0.38
Standard length	63.3–100.1	85.2 ± 14.4	54.1–83.9	64.3 ± 13.7	59.8–66.8	63.7 ± 3.6	49.8–104.3	74.0 ± 19.0	72.2–103	91.7 ± 11.4	45.8–72.8	62.5 ± 9.9	0.935	0.101	0.317	0.38
Head length	17.4–26.2	22.5 ± 3.6	13.4–19.7	15.3 ± 2.8	11.5–12.9	12.3 ± 0.7	14.7–28.6	21.0 ± 4.8	15.8–24.4	21.2 ± 3.2	6.2–16.7	13.3 ± 3.7	0.372	0.025	0.463	0.464
Head depth	8.6–11.9	10.5 ± 1.5	6.1–9.8	7.4 ± 1.7	6.6–7.4	7.0 ± 0.4	6.8–16.1	10.4 ± 3.0	8.6–12.9	11.3 ± 1.7	5.8–8.3	7.2 ± 0.9	0.935	0.025	0.739	0.188
Head width	10.5–16.1	12.9 ± 2.6	6.9–12.4	9.0 ± 2.4	8.2–9.2	8.8 ± 0.5	8.8–17.2	11.8 ± 2.6	10.2–15.8	13.5 ± 2.0	7.1–10.9	9.4 ± 1.3	0.57	0.025	0.386	0.884
Snout length	8.6–12	10.4 ± 1.6	0.0–9.3	6.0 ± 3.7	6.2–7	6.6 ± 0.4	7.3–10.4	8.7 ± 1.3	7.9–12.3	10.7 ± 1.7	5.2–7.4	6.4 ± 0.8	0.935	0.025	0.142	0.941
Eye diameter	0.4–1.2	0.9 ± 0.3	0.0–1.1	0.7 ± 0.4	0.6–0.7	0.6 ± 0.1	0.0–0.4	0.0 ± 0.1	0.2–0.3	0.2 ± 0.1	1.7–2.3	1.9 ± 0.2	0.004	0.227	0.001	0.003
Interorbital distance	4.5–6.5	5.4 ± 0.9	0.0–5	3.2 ± 1.9	4.0–4.5	4.3 ± 0.2	4.7–6.8	5.7 ± 0.9	5.1–7.7	6.8 ± 1.0	2.1–4.3	3.3 ± 0.9	0.685	0.025	0.327	0.028
Body depth	9.4–14.7	12.2 ± 2.3	6.5–13.5	9.1 ± 2.8	6.6–7.3	7.0 ± 0.4	5.9–17.2	10.2 ± 3.9	11.7–17	14.8 ± 1.9	6.3–11.2	8.8 ± 1.7	0.935	0.025	0.162	0.057
Body width	7.6–13.2	10.6 ± 2.5	8.1–9.1	8.5 ± 0.4	4.8–5.4	5.1 ± 0.3	4.3–14.7	7.9 ± 3.4	10.6–15.6	13.3 ± 1.9	5.8–9.8	7.3 ± 1.4	0.062	0.025	0.096	0.057
Maxillary barbel length	6.0–9.5	8.5 ± 1.5	3.0–6.8	4.9 ± 1.4	5.2–5.9	5.6 ± 0.3	5.1–10.3	7.5 ± 2.0	5.5–9.5	7.6 ± 1.3	3.9–6.4	5.2 ± 0.8	0.745	0.025	0.549	0.188
Outrostral barbel length	10.1–14.5	12.1 ± 1.8	5.3–8.1	6.4 ± 1.3	7.2–8.0	7.6 ± 0.4	6.5–10.6	8.4 ± 1.5	6.7–10.6	8.9 ± 1.3	4.6–7.7	6.2 ± 1.0	0.935	0.025	0.006	0.008
Inrostral barbel length	4.6–7	5.7 ± 0.9	2.2–4.5	3.5 ± 1.0	3.1–3.5	3.3 ± 0.2	3.2–6.5	4.5 ± 1.1	3.8–5.4	4.7 ± 0.6	2.8–3.9	3.3 ± 0.4	0.465	0.025	0.039	0.028
Dorsal-fin length	15.0–22.6	19.2 ± 3.2	11.1–16.1	13.0 ± 2.3	28.3–31.7	30.2 ± 1.7	13.4–26.9	18.2 ± 4.3	12.3–20.1	16.8 ± 2.9	9.0–14.4	12.6 ± 1.8	0.935	0.025	0.463	0.242
Dorsal-fin base length	9.6–13.4	11.8 ± 1.6	5.9–10.3	7.8 ± 1.8	7.3–8.2	7.8 ± 0.5	7.4–15.8	10.7 ± 3.2	7.9–9.6	8.8 ± 0.6	5.6–9.5	8.1 ± 1.3	0.808	0.025	0.463	0.005
Pectoral-fin length	13.7–21.7	18.5 ± 3.0	11.3–16.8	13.6 ± 2.2	12–13.4	12.8 ± 0.7	14.4–35.9	21.0 ± 6.6	14.3–21.7	17.9 ± 2.6	7.4–12.2	10.3 ± 1.6	0.019	0.025	0.386	0.661
Anal-fin length	11.9–18.2	15.6 ± 2.6	9.2–13.5	10.7 ± 1.9	9.8–10.9	10.4 ± 0.6	9.5–25.3	15.8 ± 4.8	10.2–16.1	14.0 ± 2.0	8.0–11.5	10.2 ± 1.2	0.935	0.025	0.841	0.188
Pelvic-fin length	11.6–19.3	15.3 ± 2.8	9.0–13.3	10.5 ± 1.9	9.2–10.2	9.8 ± 0.5	8.9–24.4	15.1 ± 4.8	10.8–16.8	14.0 ± 2.1	9.0–14.7	12.0 ± 1.8	0.372	0.025	0.641	0.38
Caudal peduncle length	9.8–16.9	13.6 ± 3.0	9.8–16.5	12.0 ± 2.8	11.8–13.1	12.5 ± 0.7	8.5–17.7	11.9 ± 3.5	11.9–18.2	15.9 ± 2.4	6.6–12.8	9.9 ± 2.4	0.291	0.655	0.257	0.107
Caudal peduncle depth	4.8–6.7	5.8 ± 0.8	3.8–6.6	4.8 ± 1.2	3.9–4.4	4.2 ± 0.2	3.1–9.3	5.5 ± 2.2	6.5–9.4	7.9 ± 1.0	3.5–5.9	4.8 ± 1.0	0.871	0.025	0.205	0.005

Figure 5. Ecological photographs of *Triplophysa ziyunensis* sp. nov. and closely related species in life **A** *Triplophysa ziyunensis* sp. nov. **B** *T. rosa* **C** *T. wudangensis*, and **D** *T. qingzhenensis*, from Dr. Zhi-Xuan Zeng.

Secondary sex characteristics. No secondary sex characteristics were observed based on the present specimens of *Triplophysa ziyunensis* sp. nov.

Comparisons. Detailed comparative morphological data of *Triplophysa ziyunensis* sp. nov. with the 39 recognized hypogean species of *Triplophysa* are given in Table 2. *Triplophysa ziyunensis* sp. nov. is genetically close to *T. qingzhenensis*, *T. rosa*, and *T. wudangensis* and shares some similar morphological characters, such as reduced eye degeneration and degenerated body pigmentation, pigmented markings on the body surface, except ventral, but can still be distinguished by a combination of some morphological characters.

Triplophysa ziyunensis sp. nov. is be distinguished from *T. qingzhenensis* and *T. wudangensis* by having 10 branched pectoral fin rays (vs 8–9), 6 branched pelvic-fin rays (vs 5), 16 branched caudal fin rays (vs 14–15), and inhabiting the Pearl River basin (vs Yangtze River basin).

Triplophysa ziyunensis sp. nov. can be distinguished from *T. rosa* by having reduced body pigmentation, pigmented markings on body surface, except ventral (vs absence), eyes reduced, diameter 2.4–4.9% of HL (vs absent), 8 branched dorsal fin rays (vs 9), 10 branched pectoral fin rays (vs 12), 6 branched pelvic-fin rays (vs 7), 16 branched caudal fin rays (vs 14), and inhabiting the Pearl River basin (vs Yangtze River basin).

Ecology and distribution. *Triplophysa ziyunensis* sp. nov. has only been found in one cave in Shuitang Village, Maoying Town, Ziyun County, Guizhou Province, China, at an elevation of 1134 m. The pool where the new species was found is more than 15 m long, 13 m wide, and ~ 3 m deep, with a slow flow of water, and is located 80 m further inside the entrance of the cave. Inside the cave, another fish (*Sinocyclocheilus multipunctatus*, three individuals), bats (*Rhinolophus* sp., five individuals), and frogs (*Odorrana wuchuanensis*, 11 individuals) were found. Outside the cave, rapeseed and peppers were being grown. The population of the new species is very small and only five specimens were collected.

Remarks. The new species, *Triplophysa ziyunensis* sp. nov., inhabits the underground rivers of the type locality. Eyes are present and reduced, and with irregular dark brownish brown patches on the head and body. Therefore, this species can be considered as a stygophile fish within the hypogean group of the genus *Triplophysa*.

Etymology. The specific epithet *ziyunensis* refers to the type locality of the new species: Shuitang Village, Maoying Town, Ziyun County. We propose the common English name "Ziyun high-plateau loach" and the Chinese name "Zǐ Yún Gāo Yuán Qīu (紫云高原鳅)".

Triplophysa yaluwang Lan, Liu, Zhou & Zhou, sp. nov.

https://zoobank.org/DE306B1B-F770-4E79-9B9E-400CEC202266
Figs 6, 7, Table 5, Suppl. material 1

Type material. *Holotype.* GZNU20240118001 (Fig. 6), 87.6 mm total length (TL), 73.9 mm standard length (SL), collected by Jia-Jun Zhou on 18 January 2024, in Xinzhai Village, Maoying Town, Ziyun County, Guizhou Province, China (25.89908752°N, 106.07921141°E, 1276 m a.s.l.; Fig. 1).

Paratypes. Four specimens from the same locality as the holotype: GZNU20240118002–118005, 54.1–83.9 mm SL, collected by Jia-Jun Zhou and Ye-Wei Liu on 27 September 2023.

Figure 6. Morphological characteristics of holotype GZNU20240118001 of *Triplophysa yaluwang* sp. nov. in preservative (10% formalin) **A** dorsal view **B** ventral view **C** lateral view **D** dorsal view of head **E** lateral view of head, and **F** ventral view of head.

Diagnosis. *Triplophysa yaluwang* sp. nov. is distinguished from other hypogean species of the genus *Triplophysa* by the following characteristics in combination: (1) body naked, scaleless, with irregular pale dark brownish brown markings, except ventral; (2) eyes reduced, diameter 4.6–6.1% of head length; (3) pelvic-fin tip reaching anus; (4) tip of pectoral fin not reaching to pelvic fin

origin; (5) anterior and posterior nostrils closely set, with the anterior nostril elongated to a barbel-like tip; (6) tip of outrostral barbel extending backward, not reaching to anterior margin of eye; (7) lateral line complete; (8) posterior chamber of air bladder degenerated; and (9) dorsal-fin rays iii-7, pectoral-fin rays i-9, pelvic-fin rays i-5, anal-fin rays i-5, and 14 branched caudal-fin rays.

Description. Morphological data of *Triplophysa yaluwang* sp. nov. specimens are provided in Table 5 and Suppl. material 1. Body elongated and cylindrical, posterior portion gradually compressed from dorsal fin to caudal-fin base, with deepest body depth anterior to dorsal-fin origin, deepest body depth 12−16% of SL. Dorsal profile slightly convex from snout to dorsal-fin insertion, then straight from posterior portion of dorsal-fin origin to caudal-fin base. Ventral profile flat. Head short, length 26−27% of SL, slightly depressed and flattened, width slightly greater than depth (HW/HD = 1.1−1.3). Snout slightly pointed, and snout length 43−52% of HL. Mouth inferior and curved, mouth corner situated below anterior nostril, upper and lower lips smooth, lower lip with V-shaped median notch. Three pairs of barbels are present: inner rostral barbel long, length 16−27% of HL, backward extending to corner of mouth; out rostral barbel long, length 39−44% of HL, backward extending to beyond anterior margin of eyes. Maxillary barbel not extending to posterior margin of operculum, length 22−36% of HL. Anterior and posterior nostrils closely set, length 0.44−0.82 mm. Anterior nostril tube long, with an elongated short barbel-like tip, tip of posterior nostril extending backwards not reaching to anterior margin of eye. Eyes reduced, with diameter 5−6% of HL. Gill opening small, gill rakers not developed, nine inner gill rakers on first gill arch (*n* = 1).

Dorsal-fin rays iii-7, pectoral-fin rays i-9, pelvic-fin rays i-5−6, anal-fin rays i-5, 14 branched caudal-fin rays. Dorsal fin short, length 19−22% of SL, distal margin emarginated, origin anterior to pelvic-fin insertion and situated slightly posterior to the midpoint between snout tip and caudal-fin base, first branched ray longest, shorter than head length, tip of dorsal fin vertical to anus. Pectoral fin moderately developed, length 19−25% of SL, tip of pectoral fin extending backward almost to the midpoint between origin of pectoral and pelvic fin origins, not reaching to pelvic fin origin. Pelvic fin length 16−17% of SL, vertically aligned with second branched ray of dorsal fin, tips of pelvic fin reaching to anus. Anal fin length 16−18% of SL, distal margin truncated, origin close to anus, tips of anal fin not reaching caudal-fin base, distance between tips of anal fin and anus 2.2× the eye diameter. Caudal fin forked, upper lobe slightly longer than lower lobe, tips pointed, caudal peduncle length ~ 12 mm, caudal peduncle depth ~ 4.8 mm, with weak adipose crests along both dorsal and ventral sides. Total vertebrae: 40 (*n* = 1).

Cephalic lateral line system developed. Lateral line complete, exceeding tip of pectoral fin and reaching base of caudal fin. Two chambers of air bladder, anterior chamber dumbbell-shaped and membranous, open on both sides, slightly closed posteriorly; posterior chamber degenerated, slightly filling the body cavity, connected with anterior chamber by a long, slender tube.

Coloration. In cave water, living fish were semi-translucent with a pale pink body with irregular dark brownish brown patches on the Entire body (Fig. 7). After fixation in 10% formalin, the body color was white, and the dark brown color lightened (Fig. 6).
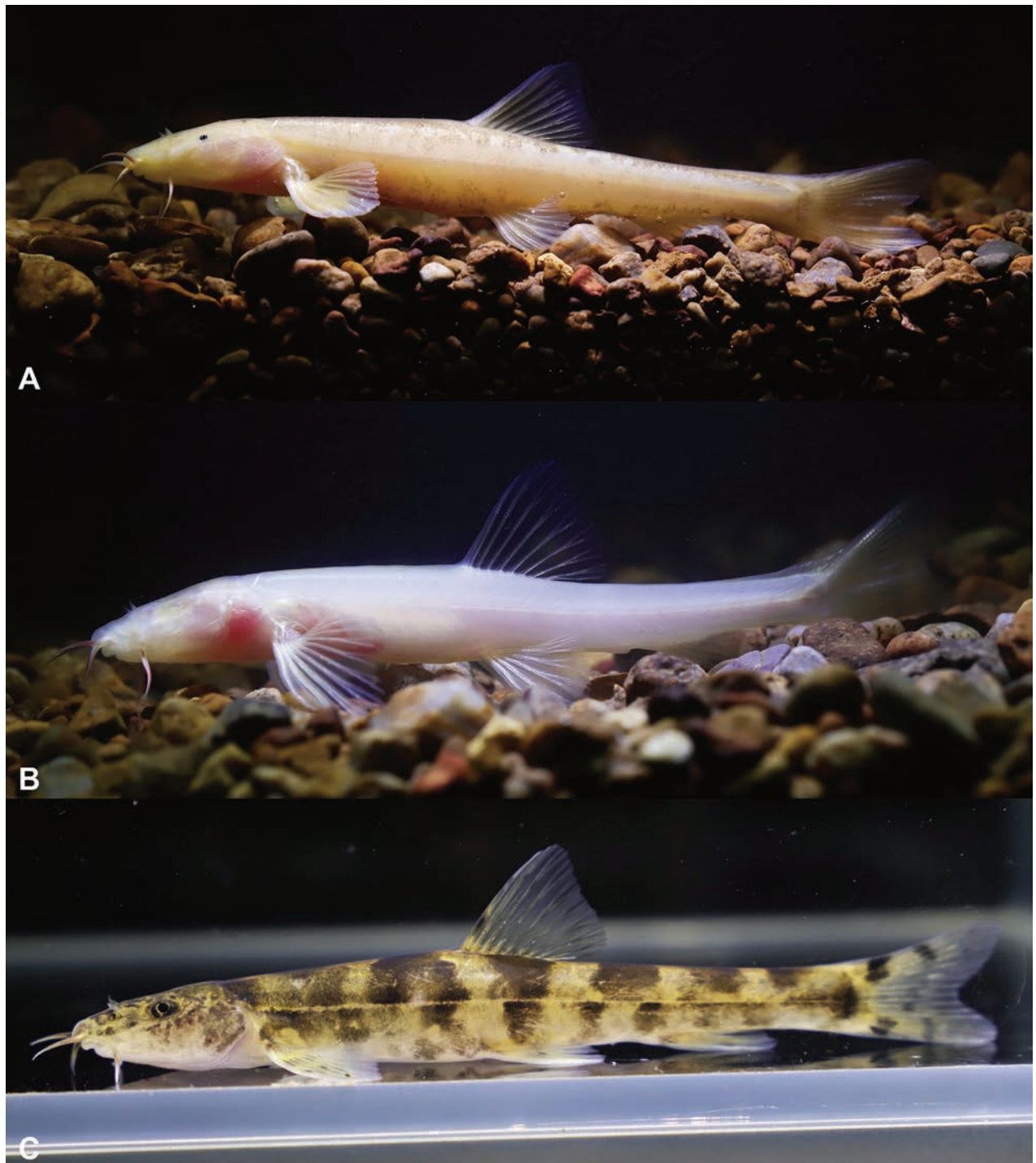
Figure 7. Ecological photographs of *Triplophysa yaluwang* sp. nov. and closely related species in life **A** *Triplophysa yaluwang* sp. nov. (paratype, GZNU20240118002) **B** *Triplophysa yaluwang* sp. nov. (paratype, GZNU20240118005), and **C** *T. guizhouensis*.

Variations. Among the five specimens collected, GZNU20240118002–118004 are essentially identical to the holotype in fin characteristics and body coloration. GZNU20240118005 differs from the holotype by the absence of body pigmentation and the absence of the eye (Fig. 7).

Secondary sex characteristics. Secondary sex characteristics were not observed in the specimens of *Triplophysa yaluwang* sp. nov.

Comparisons. Detailed morphological comparative data of *Triplophysa yaluwang* sp. nov. with *Triplophysa ziyunensis* sp. nov. and the 39 hypogean species of *Triplophysa* are given in Table 2. *Triplophysa yaluwang* sp. nov. is genetically close to *T. guizhouensis*, *T. longliensis*, and *T. sanduensis*, but it can be distinguished in combination with morphological characteristics.

Triplophysa yaluwang sp. nov. can be distinguished from *Triplophysa ziyunensis* sp. nov. by having dorsal fin distal margin being emarginated (vs truncated), total vertebrae 40 (vs 39), seven branched dorsal fin rays (vs 8), nine branched pectoral fin rays (vs 10), and 14 branched caudal fin rays (vs 16).

Triplophysa yaluwang sp. nov. is distinguished from *T. longliensis* by having eyes reduced, small diameter 4.6−6.1% of HL (vs normal, diameter 9.5−11.5% of HL), interorbital width, 24.3−26.0% of HL (vs 31.4−37.5 of HL), total vertebrae 40 (vs 42), degenerated posterior chamber of air bladder (vs developed), seven branched dorsal-fin rays (vs 8), nine branched pectoral-fin rays (vs 10), and 14 branched caudal-fin rays (vs 15−16).

Triplophysa yaluwang sp. nov. is distinguished from *T. sanduensis* by having eyes reduced, small diameter 4.6−6.1% of HL (vs normal, diameter 11.9−15.4% of HL), interorbital width, 24.3−26.0% of HL (vs 31.2−40.2 of HL), total vertebrae 40 (vs 41), dorsal-fin rays, iii, 7 (vs ii, 8−9), three unbranched anal-fin rays (vs 1), 14 branched caudal-fin rays (vs 17−18), and tip of pelvic fin reaching anus (vs not reaching anus).

Triplophysa yaluwang sp. nov. differs from *T. guizhouensis* by having eyes reduced, diameter 4.6−6.1% of HL (vs normal, diameter 9.4−12.1% of HL), dorsal fin distal margin being emarginated (vs truncated), body scaleless (vs body covered by sparse scales), degenerated posterior chamber of air bladder (vs developed), seven branched dorsal fin rays (vs 8), five branched anal-fin rays (vs 6), and tip of pelvic fin reaching anus (vs not reaching anus).

Ecology and distribution. The new species *Triplophysa yaluwang* sp. nov. was found in one cave far from the village of Xinzhai Village, Maoying Town, Ziyun County, Guizhou Province, China (Fig. 1), in a water system where the underground river is a tributary of the Hongshui River. The cave habitat is a vertical shaft with an entrance located halfway up the mountainside. The underground river is approximately 150 m deep from the entrance, and the accessible portion is around 200 m long, 3 m wide, and 1−2 m deep. In this cave, the new species is sympatric with *Sinocyclocheilus multipunctatus* and some unnamed spiders.

Remarks. The new species, *Triplophysa yaluwang* sp. nov., inhabits the underground rivers of the type locality. Eyes are present and reduced, and with irregular dark brownish brown patches on the head and body. Therefore, this species can be considered as a stygophile fish within the hypogean group of the genus *Triplophysa*.

Etymology. The specific epithet *yaluwang* comes from King Yalu, a hero to the Miao people of Ziyun County, Guizhou Province, China, where the type locality is found. He was the 18th generation leader of the Miao ancestors in western China and led the Miao people through many trials and tribulations. He eventually carved out a suitable land for his people to live in near the type locality. His deeds have been preserved in the form of a song, which has been organized into the first full-length heroic epic of the Hmong, King Yalu. We propose the common English name "King Yalu high-plateau loach" and the Chinese name "Yà Lǔ Wáng Gāo Yuán Qīu (亚鲁王高原鳅)".

Discussion

We describe two new species, *Triplophysa ziyunensis* sp. nov. and *Triplophysa yaluwang* sp. nov., based on morphological comparisons (Table 2), mitochondrial DNA sequence differences, and nuclear gene haplotypes (Fig. 2). The description of these two new species increases the number of species in the hypogean group of *Triplophysa* from 39 to 41 and the previous number of known species from Guizhou is increased to 15. The previous 13 species are *T. cehengensis*, *T. rongduensis*, *T. panzhouensis*, *T. anlongensis*, *T. baotianensis*, *T. guizhouensis*, *T. longliensis*, *T. nasobarbatula*, *T. qingzhenensis*, *T. sanduensis*, *T. wudangensis*, *T. wulongensis*, and *T. zhenfengensis* (Table 1). Our previous studies revealed that the cave-dwelling species of *Triplophysa* in Guizhou are concentrated in the south, central, and southwest (Fig. 1). Before this study, a large recording gap existed between central-southern and western Guizhou (Fig. 1), suggesting the possible presence of cryptic species in this region (Luo et al. 2023). This hypothesis was supported by the results of the present study. Similarly, discontinuities with previous records remain in northeastern and eastern Guizhou, suggesting that it would be useful to focus efforts there on the discovery of new species or new distribution areas.

The new species described here have only slight mitochondrial differences from closely related species (Table 4). For example, the new species *T. yaluwang* sp. nov. clusters with *T. guizhouensis*, both from the Hongshui River drainage basin, at a genetic distance of 1.4%. The type locality of the two new species is near the watershed between the Pearl and Yangtze rivers, i.e., the Miaoling Mountains (Fig. 1). Geological evidence suggests that the Miaoling mountains formed in the Early Pleistocene and eventually became the watershed between the Pearl River and Yangtze River systems during the mid- to late Pleistocene (Zhou and Chen 1993). Thus, the slight mitochondrial differences are associated with multiple connectivity between rivers, includes both surface and underground rivers, which leads to potential mitochondrial introgression (Yuan et al. 2023). Similar gene flow was observed among species of *Triplophysa* in the Qinghai-Tibetan Plateau region (Feng et al. 2019). This hypothesis is also supported by the mitochondrial matrilineal tree in this study, i.e., the species of the independent hydrological origin are not clustered together in the phylogenetic tree, but rather are distributed in a mosaic fashion (Figs 1, 2). However, this could also be related to short-term radial species formation. To evaluate this situation, we suggest the use of additional nuclear genetic markers or genomic evidence in the description of new species.

Acknowledgments

Additional information

Conflict of interest

The authors have declared that no competing interests exist.

Ethical statement

No ethical statement was reported.

Author contributions

All authors have contributed equally.

Author ORCIDs

Chang-Ting Lan https://orcid.org/0009-0007-2381-3601
Li Wu https://orcid.org/0000-0002-7898-7517
Tao Luo https://orcid.org/0000-0003-4186-1192
Ye-Wei Liu https://orcid.org/0000-0003-4712-1072
Jia-Jun Zhou https://orcid.org/0000-0003-1038-1540
Jing Yu https://orcid.org/0009-0004-3629-3826
Xin-Rui Zhao https://orcid.org/0000-0002-9125-6276
Ning Xiao https://orcid.org/0000-0002-7240-6726
Jiang Zhou https://orcid.org/0000-0003-1560-8759

Data availability

All of the data that support the findings of this study are available in the main text or Supplementary Information.

References

Bandelt HJ, Forster P, Röhl A (1999) Median-joining networks for inferring intraspecific phylogenies. Molecular Biology and Evolution 16(1): 37–48. https://doi.org/10.1093/oxfordjournals.molbev.a026036

Chen SJ, Peng ZG (2019) *Triplophysa sanduensis*, a new loach species of nemacheilid (Teleostei: Cypriniformes) from South China. Zootaxa 4560(2): 375–384. https://doi.org/10.11646/zootaxa.4560.2.10

Chen XY, Yang JX (2005) *Triplophysa rosa* sp. nov.: A new blind loach from China. Journal of Fish Biology 66(3): 599–608. https://doi.org/10.1111/j.0022-1112.2005.00622.x

Chen YR, Yang JX, Xu GC (1992) A new blind loach of *Triplophysa* from Yunnan stone forest with comments on its phylogenetic relationship. Zoological Research 13(1): 17–23. [In Chinese]

Chen XY, Cui GH, Yang JX (2004) A new cave dwelling fish species of genus *Triplophysa* (Balitoridae) from Guangxi, China. Zoological Research 25(3): 227–231. [In Chinese]

Chen S, Sheraliev B, Shu L, Peng Z (2021) *Triplophysa wulongensis*, a new species of cave-dwelling loach (Teleostei, Nemacheilidae) from Chongqing, Southwest China. ZooKeys 1026: 179–192. https://doi.org/10.3897/zookeys.1026.61570

Chu XL, Chen YR (1979) A new blind cobitid fish (Pisces, Cypriniformes) from subterranean waters in Yunnan, China. Dong Wu Xue Bao 25(3): 285–287. [In Chinese]

Chu XL, Chen YR (1990) The fishes of Yunnan, China. Part 2. Science Press, Beijing, 313 pp. [In Chinese]

Deng SQ, Wang XB, Zhang E (2022) *Triplophysa qini*, a new stygobitic species of loach (Teleostei: Nemacheilidae) from the upper Chang-Jiang Basin in Chongqing, Southwest China. Ichthyological Exploration of Freshwaters 1178: 1–11. https://doi.org/10.23788/IEF-1178

Edgar RC (2004) MUSCLE: Multiple sequence alignment with high accuracy and high throughput. Nucleic Acids Research 32(5): 1792–1797. https://doi.org/10.1093/nar/gkh340

Feng C, Zhou W, Tang Y, Gao Y, Chen J, Tong C, Liu S, Wanghe K, Zhao, K (2019) Molecular systematics of the *Triplophysa robusta* (Cobitoidea) complex: extensive gene flow in a depauperate lineage. Molecular Phylogenetics and Evolution 132: 275–283. https://doi.org/10.1016/j.ympev.2018.12.009

Fricke R, Eschmeyer WN, Van der Laan R (Eds) (2024) Catalog of fishes: genera, species, references. California Academy of Sciences, San Francisco. https://researcharchive.calacademy.org/research/ichthyology/catalog/fishcatmain.asp [accessed 17 January 2023]

He CL, Zhang E, Song ZB (2012) *Triplophysa pseudostenura*, a new nemacheiline loach (Cypriniformes: Balitoridae) from the Yalong River of China. Zootaxa 3586(1): 272–280. https://doi.org/10.11646/zootaxa.3586.1.26

Hoang DT, Chernomor O, von Haeseler A, Minh BQ, Vinh L (2018) UFBoot2: Improving the ultrafast bootstrap approximation. Molecular Biology and Evolution 35(2): 518–522. https://doi.org/10.1093/molbev/msx281

Huang TF, Zhang PL, Huang XL, Wu T, Gong XY, Zhang YX, Peng QZ, Liu ZX (2019) A new cave-dwelling blind loach, *Triplophysa erythraea* sp. nov. (Cypriniformes: Nemacheilidae), from Hunan Province, China. Zoological Research 40(4): 331–336. https://doi.org/10.24272/j.issn.2095-8137.2019.049

Kumar S, Stecher G, Tamura K (2016) MEGA7: Molecular evolutionary genetics analysis version 7.0 for bigger datasets. Molecular Biology and Evolution 33(7): 1870–1874. https://doi.org/10.1093/molbev/msw054

Lan JH, Yang JX, Chen YR (1995) Two new species of the subfamily Nemacheilinae from Guangxi, China (Cypriniformes: Cobitidae). Dong Wu Fen Lei Xue Bao 20(3): 366–372. [In Chinese]

Lan JH, Gan X, Wu TJ, Yang J (2013) Cave Fishes of Guangxi, China. Science Press, Beijing. [In Chinese]

Lanfear R, Frandsen PB, Wright AM, Senfeld T, Calcott B (2017) PartitionFinder 2: New methods for selecting partitioned models of evolution for molecular and morphological phylogenetic analyses. Molecular Biology and Evolution 34(3): 772–773. https://doi.org/10.1093/molbev/msw260

Leigh JW, Bryant D (2015) POPART: full-feature software for haplotype network construction. Methods in Ecology and Evolution 6(9): 1110–1116. https://doi.org/10.1111/2041-210X.12410

Li WX (2004) The three new species of Cobitidae from Yunnan, China. Journal of Jishou University 25(3): 93–96. [Natural Science Edition] [In Chinese]

Li WX, Zhu ZG (2000) A new species of *Triplophysa* from cave Yunnan. Journal of Yunnan University 22(5): 396–398. [Natural Science Edition] [In Chinese]

Li WX, Yanf HF, Chen H, Tao CP, Qi SQ, Han NF (2008) A New Blind Underground Species of the Genus *Triplophysa* (Balitoridae) from Yunnan, China. Zoological Research 29(6): 674–678. https://doi.org/10.3724/SP.J.1141.2008.06674

Li J, Lan JH, Chen XY, Du LN (2017a) Description of *Triplophysa luochengensis* sp. nov. (Teleostei: Nemacheilidae) from a karst cave in Guangxi, China. Journal of Fish Biology 91(4): 1009–1017. https://doi.org/10.1111/jfb.13364

Li J, Li XH, Lan JH, Du LN (2017b) A new troglobitic loach *Triplophysa tianlinensis* (Teleostei: Nemacheilidae) from Guangxi, China. Ichthyological Research 64(3): [1–6]: 295–300. https://doi.org/10.1007/s10228-016-0565-0

Li CQ, Liu T, Li R (2018) A new species of the genus Plateau loach from caves in Guizhou Province. Journal of Jishou University 39(4): 60–63. https://doi.org/10.13438/j.cnki.jdzk.2018.04.012 [Natural Science Edition] [In Chinese]

Li XQ, Xiang XG, Jabbour F, Hagen O, Ortiz RDC, Soltis PS, Soltis DE, Wang W (2022) Biotic colonization of subtropical East Asian caves through time. Proceedings of the National Academy of Sciences 119(34): e2207199119. https://doi.org/10.1073/pnas.2207199119

Liu SW, Pan XF, Yang JX, Chen XY (2017) A new cave-dwelling loach, *Triplophysa xichouensis* sp. nov. (Teleostei Nemacheilidae) from Yunnan, China. Journal of Fish Biology 90(3): 834–846. https://doi.org/10.1111/jfb.13201

Liu F, Zeng ZX, Gong Z (2022) Two new hypogean species of *Triplophysa* (Cypriniformes: Nemacheilidae) from the River Yangtze drainage in Guizhou, China. Journal of Vertebrate Biology 71(22062): 22062. https://doi.org/10.25225/jvb.22062

Lu ZM, Li XJ, Lü WJ, Huang JQ, Xu TK, Huang G, Qian FQ, Yang P, Chen SG, Mao WN, Zhao YH (2022) *Triplophysa xuanweiensis* sp. nov., a new blind loach species from a cave in China (Teleostei: Cypriniformes: Nemacheilidae). Zoological Research 43(2): 221–224. https://doi.org/10.24272/j.issn.2095-8137.2021.310

Luo T, Mao M-L, Lan C-T, Song L-X, Zhao X-R, Yu J, Wang X-L, Xiao N, Zhou J-J, Zhou J (2023) Four new hypogean species of the genus *Triplophysa* (Osteichthyes, Cypriniformes, Nemacheilidae) from Guizhou Province, Southwest China, based on molecular and morphological data. ZooKeys 1185: 43–81. https://doi.org/10.3897/zookeys.1185.105499

Ma L, Zhao Y, Yang JX (2019) Cavefish of China. In Encyclopedia of caves (3rd edn.). Academic Press, Pittsburgh, USA, 237–254. https://doi.org/10.1016/B978-0-12814124-3.00027-3

Microsoft Corporation (2016) Microsoft Excel. https://office.microsoft.com/excel

Nguyen LT, Schmidt HA, Von Haeseler A, Minh BQ (2015) IQ-TREE: A fast and effective stochastic algorithm for estimating maximum-likelihood phylogenies. Molecular Biology and Evolution 32(1): 268–274. https://doi.org/10.1093/molbev/msu300

Prokofiev AM (2010) Morphological classification of loaches (Nemacheilinae). Journal of Ichthyology 50(10): 827–913. https://doi.org/10.1134/S0032945210100012

Ran JC, Li WX, Chen HM (2006) A new species of blind loach of *Paracobitis* from Guangxi, China (Cypriniformes: Cobitidae). Guangxi Shifan Daxue Xuebao. Ziran Kexue Ban 24(3): 81–82. [In Chinese]

Ren Q, Yang JX, Chen XY (2012) A new species of the genus *Triplophysa* (Cypriniformes: Nemacheilidae), *Triplophysa longliensis* sp. nov., from Guizhou, China. Zootaxa 3586(1): 187–194. https://doi.org/10.11646/zootaxa.3586.1.17

Ronquist F, Teslenko M, Van Der Mark P, Ayres DL, Darling A, Höhna S, Larget B, Liu L, Suchard MA, Huelsenbeck JP (2012) MrBayes 3.2: Efficient Bayesian phylogenetic inference and model choice across a large model space. Systematic Biology 61(3): 539–542. https://doi.org/10.1093/sysbio/sys029

Tang L, Zhao YH, Zhang CG (2012) A new blind loach, *Oreonectes elongatus* sp. nov. (Cypriniformes: Balitoridae) from Guangxi, China. Environmental Biology of Fishes 93(4): 483–449. https://doi.org/10.1007/s10641-011-9943-7

Wang DZ, Li DJ (2001) Two new species of the genus *Triplophysa* from Guizhou, China (Cypriniformes: Cobitidae). Acta Zootaxonomica Sinica 16(1): 98–101. [In hinese]

Wen H, Luo T, Wang Y, Wang S, Liu T, Xiao N, Zhou J (2022) Molecular phylogeny and historical biogeography of the cave fish genus *Sinocyclocheilus* (Cypriniformes: Cyprinidae) in southwest China. Integrative Zoology 17(2): 311–325. https://doi.org/10.1111/1749-4877.12624

Wu TJ, Wei ML, Lan JH, Du LN (2018a) *Triplophysa anshuiensis*, a new species of blind loach from the Xijiang River, China (Teleostei, Nemacheilidae). ZooKeys 744: 67–77. https://doi.org/10.3897/zookeys.744.21742

Wu WJ, He AY, Yang JX, Du LN (2018b) Description of a new species of *Triplophysa* (Teleostei: Nemacheilidae) from Guizhou Province, China. Journal of Fish Biology 93(1): 88–94. https://doi.org/10.1111/jfb.13670

Xiao W, Zhang Y, Liu H (2001) Molecular systematics of Xenocyprinae (Teleostei: Cyprinidae): taxonomy, biogeography, and coevolution of a special group restricted in East Asia. Molecular Phylogenetics and Evolution 18(2): 163–173. https://doi.org/10.1006/mpev.2000.0879

Yang GY, Yuan FX, Liao YM (1986) A new blind Cobitidae fish from the subterranean water in Xiangxi, China. Huazhong Nongye Daxue Xuebao 5(3): 219–223. [In Chinese]

Yang JX, Chen XY, Lan JH (2004) Occurrence of two new Plateau indicator loaches of Nemacheilinae (Balitoridae) in Guangxi with Reference to Zoogeographical Significance. Zoological Research 25(2): 111–116. [In Chinese]

Yang J, Wu TJ, Yang JX (2012) A new cave-dwelling loach, *Triplophysa macrocephala* (Teleostei: Cypriniformes: Balitoridae), from Guangxi, China. Environmental Biology of Fishes 93(2): 169–175. https://doi.org/10.1007/s10641-011-9901-4

Yang HF, Li WX, Chen ZM (2016) A new cave species of the genus *Triplophysa* from Yunnan, China. Zoological Research 37(5): 296–300. https://doi.org/10.13918/j.issn.2095-8137.2016.5.296

Yuan Z, Wu D, Wen Y, Xu W, Gao W, Dahn HA, Liu X, Jin J, Yu C, Xiao H, Che J. (2023) Historical mitochondrial genome introgression confounds species delimitation: evidence from phylogenetic inference in the *Odorrana grahami* species complex. Current Zoology 69(1): 82–90. https://doi.org/10.1093/cz/zoac010

Zhang CG, Shao GZ, Wu HL, Zhao YH (2020) Species Catalogue of China. Vol. 2. Animals, Vertebrates (V), Fishes. Science Press, Beijing. [In Chinese]

Zhao YH, Gozlan RE, Zhang CG (2011) Out of sight out of mind: Current knowledge of Chinese cave fishes. Journal of Fish Biology 79(6): 1545–1562. https://doi.org/10.1111/j.1095-8649.2011.03066.x

Zheng LP, Du LN, Chen XY, Yang JX (2009) A new species of Genus *Triplophysa* (Nemacheilinae: Balitoridae), *Triplophysa longipectoralis* sp. nov., from Guangxi, China. Environmental Biology of Fishes 85(3): 221–227. https://doi.org/10.1007/s10641-009-9485-4

Zheng LP, Yang JX, Chen XY (2012) A new species of *Triplophysa* (Nemacheilidae: Cypriniformes), from Guangxi, southern China. Journal of Fish Biology 80(4): 831–841. https://doi.org/10.1111/j.1095-8649.2012.03227.x

Zhou QY, Chen PY (1993) Lithofacies change and palaeogeographical evolution during Late Cenozoic in Guizhou and its vicinity. Geology of Guizhou 10(3): 201–207.

Zhu SQ (1989) The loaches of the subfamily Nemacheilinae in China (Cypriniformes: Cobitidae). Jiangsu Science and Technology Publishing House, Nanjing, 150 pp. [In Chinese]

Zhu SQ, Cao WX (1988) Descriptions of two new species and a new subspecies of Noemacheilinae from Yunnan Province (Cypriniformes: Cobitidae). Dong Wu Fen Lei Xue Bao (1): 95–100. [In Chinese]

Supplementary material 1

Morphological characters and measurement data of the new species *Triplophysa ziyunensis* sp. nov., *Triplophysa yaluwang* sp. nov., *T. wudangensis*, *T. rosa*, *T. qingzhenensis*, and *T. guizhouensis*

Authors: Chang-Ting Lan, Li Wu, Tao Luo, Ye-Wei Liu, Jia-Jun Zhou, Jing Yu, Xin-Rui Zhao, Ning Xiao, Jiang Zhou

Data type: docx

Explanation note: *indicates the holotype.

Copyright notice: This dataset is made available under the Open Database License (http://opendatacommons.org/licenses/odbl/1.0/). The Open Database License (ODbL) is a license agreement intended to allow users to freely share, modify, and use this Dataset while maintaining this same freedom for others, provided that the original source and author(s) are credited.

Link: https://doi.org/10.3897/zookeys.1214.122439.suppl1

Supplementary material 2

Results and percentage of variance explained by principal component analysis

Authors: Chang-Ting Lan, Li Wu, Tao Luo, Ye-Wei Liu, Jia-Jun Zhou, Jing Yu, Xin-Rui Zhao, Ning Xiao, Jiang Zhou

Data type: docx

Copyright notice: This dataset is made available under the Open Database License (http://opendatacommons.org/licenses/odbl/1.0/). The Open Database License (ODbL) is a license agreement intended to allow users to freely share, modify, and use this Dataset while maintaining this same freedom for others, provided that the original source and author(s) are credited.

Link: https://doi.org/10.3897/zookeys.1214.122439.suppl2

Supplementary material 3

Specimens examined in this work

Authors: Chang-Ting Lan, Li Wu, Tao Luo, Ye-Wei Liu, Jia-Jun Zhou, Jing Yu, Xin-Rui Zhao, Ning Xiao, Jiang Zhou

Data type: docx

Copyright notice: This dataset is made available under the Open Database License (http://opendatacommons.org/licenses/odbl/1.0/). The Open Database License (ODbL) is a license agreement intended to allow users to freely share, modify, and use this Dataset while maintaining this same freedom for others, provided that the original source and author(s) are credited.

Link: https://doi.org/10.3897/zookeys.1214.122439.suppl3

Research Article

Integrative delimitation of a new *Epeorus* (*Caucasiron*) (Ephemeroptera, Heptageniidae) from the Caucasus with a supplement to the identification guide of Caucasian and Irano-Anatolian species

Ľuboš Hrivniak[1], Pavel Sroka[2], Gencer Türkmen[3], Alexander V. Martynov[4], Jindřiška Bojková[1]

1 Department of Botany and Zoology, Faculty of Science, Masaryk University, Kotlářská 2, 61137 Brno, Czech Republic
2 Biology Centre of the Czech Academy of Sciences, Institute of Entomology, Branišovská 31, 370 05 České Budějovice, Czech Republic
3 Department of Biology, Faculty of Science, Hacettepe University, 06800 Beytepe, Ankara, Turkiye
4 National Museum of Natural History, National Academy of Sciences of Ukraine, Bohdan Khmelnytsky str., 15, 01030, Kyiv, Ukraine

Corresponding author: Ľuboš Hrivniak (lubos.hrivniak@gmail.com)

Abstract

As part of our detailed study of the Caucasian mayfly fauna, we describe *Epeorus* (*Caucasiron*) *abditus* **sp. nov.**, a new species of the genus *Epeorus* Eaton, 1881, subgenus *Caucasiron* Kluge, 1997, based on larvae collected in Türkiye, Georgia, and Russia. We use several methodological approaches to delimit the new species by analysing COI sequence data and larval morphology. We provide a comparison with related taxa and diagnostic characters allowing determination of the larvae. We also update the identification key for the Caucasian species of *E.* (*Caucasiron*) with *E.* (*C.*) *abditus* **sp. nov.** and two recently described species, *E.* (*C.*) *hyrcanicus* Hrivniak & Sroka, 2021 and *E.* (*C.*) *tripertitus* Hrivniak & Sroka, 2022.

Key words: Aquatic insects, species delimitation, taxonomy

Introduction

The biota of the Caucasus biodiversity hotspot is extraordinarily diverse (Mittermeier et al. 2011) and mayflies (Ephemeroptera) are no exception. Currently, 130 species from 15 families and 33 genera are known from the Caucasus, almost half of which (61 species) are considered endemic (Hrivniak 2020). The genus *Epeorus* Eaton, 1881 is one of the most diversified mayfly genera in the Caucasus region. The larvae inhabit cold and well-oxygenated streams and rivers with stony substrate and are relatively common in the region (Bojková et al. 2018; Hrivniak et al. 2018). Considering the large body size of mature larvae, which can exceed 20 mm in some species, such as *E.* (*Caucasiron*) *magnus* (Braasch, 1978), they represent a charismatic and conspicuous group of mountain aquatic biota. Except for a single species, *Epeorus* (*Epeorus*) *zaitzevi* Tshernova, 1981, all Caucasian *Epeorus* species belong to the subgenus *Caucasiron* Kluge, 1997 (Hrivniak et al. 2021), which encompasses 17 species known from the Caucasus and the neighbouring mountains (Pontic, Taurus, and Zagros Mountains) (Hrivniak et al. 2022).

The geographic distribution of *E.* (*Caucasiron*) is split into two areas, the Caucasus and Central-East Asia, which includes the Tian Shan, the Himalayas, and mountain ranges in the Yunnan-Guizhou Plateau in south-west China (Braasch 2006; Chen et al. 2010; Kluge 2015; Ma et al. 2022). The latter appears to be less diversified and species-rich, although it has been studied less intensively.

Current phylogenetic analyses suggest that species richness may be even higher in the Caucasus, as cryptic diversity was detected within *E.* (*C.*) *znojkoi* Tshernova, 1938 and *E.* (*C.*) *tripertitus* Hrivniak & Sroka, 2022 (Hrivniak et al. 2020a, 2022), and some unexplored lineages were found. In this study, we investigate the identity of several specimens that were rarely found in Türkiye, Georgia, and Russia during our extensive sampling in the area in 2013–2019. To test whether they represent a new species, we use various molecular species delimitation tools and comparative morphology. Additionally, we extend an identification guide for *E.* (*Caucasiron*) larvae published by Hrivniak et al. (2020b) to include the species described after 2020 and allow correct identification of all *E.* (*Caucasiron*) species from the Caucasus and adjacent Mediterranean and Irano-Anatolian regions.

Material and methods

The material used for this study was collected in Russia (2013), Türkiye (2016), and Georgia (2016, 2019) using hydrobiological hand net. All specimens were preserved in 75–96% EtOH and are deposited in the collections of the Biology Centre of the Czech Academy of Sciences, Institute of Entomology, České Budějovice, Czech Republic (IECA). The material of other *E.* (*Caucasiron*) species used for morphological comparisons was obtained from the IECA collection.

Morphological examination

Parts of specimens were mounted on microscopic slides using HydroMatrix (MicroTech Lab, Graz, Austria) mounting medium. To remove the muscle tissue for an investigation of the cuticular structures, specimens were left overnight in a 10% solution of NaOH prior to slide mounting. Drawings were made using a stereomicroscope Olympus SZX7 and a microscope Olympus BX41, both equipped with a drawing tube. Photographs were obtained using Leica DFC450 camera fitted with macroscope Leica Z16 APO and stacked in Helicon Focus ver. 5.3 X64. All photographs were subsequently enhanced with Adobe Photoshop ver. CS5. Morphological diagnostic characters for the description of a new species were adopted from Hrivniak et al. (2020b).

DNA extraction, PCR, sequencing and alignment

Total genomic DNA of four specimens (labelled as A1–A3 and A6) was extracted from legs using the DEP-25 DNA Extraction Kit (TopBio) and DNeasy Blood & Tissue Kit (Qiagen), both according to the manufacturer's protocol. Mitochondrial cytochrome oxidase subunit I (COI) was sequenced according to Hrivniak et al. (2017). COI sequences of other *E.* (*Caucasiron*) species used for molecular comparisons were obtained from Hrivniak et al. (2017, 2019, 2020c, 2021, 2022). The PCR amplification of COI and reaction volumes was carried out as described in Hrivniak et al. (2017). Sequences were assembled

in Mega X (Kumar et al. 2018) and aligned in Jalview (Waterhouse et al. 2009) using the Mafft algorithm. Newly obtained sequences were deposited in Gen-Bank with accession numbers (GB) PP987168–PP987171.

Molecular species delimitation

Molecular delimitation of species was performed using the single threshold General Mixed Yule Coalescent model (GMYC, Pons et al. 2006; Fujisawa and Barraclough 2013), Multi-rate Poisson tree processes for single-locus (mPTP; Kapli et al. 2016) and the Assemble Species by Automatic Partitioning (ASAP; Puillandre et al. 2021). GMYC, mPTP, and ASAP were performed by the online servers https://species.h-its.org/gmyc/, https://bio.tools/mptp and https://bioinfo.mnhn.fr/abi/public/asap/, respectively. The COI gene tree for GMYC and mPTP was reconstructed using BEAST ver. 2 (Bouckaert et al. 2014) with settings described in Hrivniak et al. (2020c). The dataset included all described species from the subgenus *Caucasiron* distributed in the Caucasus and adjacent regions. Two analyses were running on CIPRES Science Gateway (Miller et al. 2010) for 200 million generations sampled every 20 000 generations. Convergence and effective sample size (ESS > 200) were verified using Tracer ver. 1.7 (Rambaut et al. 2018). The first 10% of trees from each run were discarded as burn-in. Files from both independent runs were combined using LogCombiner ver. 2.6.7. The maximum clade credibility tree was constructed using TreeAnnotator ver. 1.8.4 with default settings. The input dataset for ASAP comprised sequences aligned in a fasta file. The simple pairwise genetic distances were selected, and other settings were default. Inter- and intraspecific pairwise genetic distances were calculated in MEGA X.

Results and discussion

Molecular species delimitation

The final COI alignment contained 97 sequences, 631 base pairs and 197 parsimony informative positions. The single threshold GMYC model estimated 20 species (CI = 12–28) consisting of 19 ML clusters and one singleton. *Epeorus* (*Caucasiron*) *abditus* sp. nov. was delimited as a distinct species. The mPTP method and the distance-based ASAP analysis also delimited *E.* (*Caucasiron*) *abditus* sp. nov. as a distinct species (Fig. 2). The monophyly of all species clusters was supported (PP = 1).

Pairwise genetic distances between *E.* (*Caucasiron*) *abditus* sp. nov. and other *E.* (*Caucasiron*) species ranged from 8.33% in *E.* (*C.*) *magnus* to 15.93% in *E.* (*C.*) *shargi* Hrivniak & Sroka, 2020. Genetic distances within *E.* (*Caucasiron*) *abditus* sp. nov. varied between 0.33 and 1.64%.

Taxonomy

Epeorus (*Caucasiron*) *abditus* sp. nov. is attributed to the subgenus *Caucasiron* within the genus *Epeorus* based on the presence of projection on the costal rib of gill plates II–VII (Fig. 5G, arrow), and the presence of medio-dorsally directed hair-like setae located on the anterior margin of the head (see Kluge 2015 for a revision of the subgenus).

Epeorus (*Caucasiron*) *abditus* Hrivniak & Sroka, sp. nov.

https://zoobank.org/AF0C3D08-A97C-483C-A766-9B3F9CFE6113
Figs 4, 5

Type material. *Holotype* • female larva (GB: PP987170), Türkiye: Artvin Province, Camili Village, unnamed mountain stream, 1599 m a.s.l.; 41°24'04"N, 42°24'04"E; code: CAM 6, 25.7.2016, G. Türkmen leg.

Paratypes • 1 larva (mounted on slide), same data as holotype • 1 larva (GB: PP987171; mounted on slide), Georgia: Adjara, Kobuleti district, vicinity of Khino (Didvake) village, Kintrishi River, 792 m a.s.l.; 41°43'01"N, 42°02'41"E; code: No6, 19.4.2013, A.V. Martynov leg • 1 larva (GB: PP987168, mouthparts mounted on slide), Georgia: Kakheti Province, South of Alazani Pass, Stori River, 1514 m a.s.l.; 42°14'35.1"N, 45°29'44.5"E; code GEO60/2019, 3.5.2019; Ľ. Hrivniak leg • 1 larva, Russia: Kabardino-Balkaria, vicinity of Terskol village, left tributary of Baksan River, 2192 m a.s.l.; 43°14'31"N, 42°33'49"E; 19.5.2013, V.V. Martynov leg • 2 larvae (one barcoded, GB: PP987169), Russia: Kabardino-Balkaria, vicinity of Tyrnyauz village, right tributary of Baksan River, 1904 m a.s.l., 43°21'N, 42°52'E; 19.5.2013, V.V. Martynov leg.

Type material is deposited in IECA.

Etymology. The species name *abditus* (Latin) means hidden. It refers to rare distribution and morphological similarity with related species.

Distribution and habitat preferences of larvae. *Epeorus* (*Caucasiron*) *abditus* sp. nov. has relatively wide distribution in the Caucasus region but appears to be relatively rare due to low number of specimens obtained by extensive sampling. They were found in the Pontic Mountains and the Lesser Caucasus (northeast Türkiye and southwest Georgia), and the central (Russia: Kabardino-Balkaria) and eastern (Georgia: Kakheti) parts of the Greater Caucasus (Fig. 1). The larvae were found in low abundance in cold and clear streams and rivers between 792 and 2192 m a.s.l. on stony bed substrate in turbulent flow (Fig. 3). They were not recorded in urban and agricultural areas within the region, where many localities were investigated. Larvae co-occurred with *E*. (*C*.) *znojkoi*, *E*. (*C*.) *alpestris* (Braasch, 1979), *E*. (*C*.) *magnus*.

Description of larva. General colouration of larvae yellowish brown with dark brown maculation. Body length of late instar larvae: ca 13.3 mm (female), 11.1–11.25 mm (male). Length of cerci approximately 1.2× body length.

Head. Shape oval to trapezoidal. Anterior and lateral margin rounded, posterior margin rounded in female (Fig. 4E) and slightly rounded in male (Fig. 4D). Head dimensions of late instar larvae: length ca 4.5 mm, width ca 3.2 mm in female; length ca 4.05 mm, width 2.75–2.8 mm in male. Head width/length ratio: 1.46–1.48 in female; 1.46–1.51 in male.

Colouration of head: dorsal surface with pair of elongated maculae located along epicranial suture; pale stripes extending from lateral ocelli to lateral edges of head; blurred (or rectangular) macula between ocelli; rounded maculae anterolateral of lateral ocelli; blurred (or triangular) maculae near inner edges of compound eyes; pair of stripes (or scattered smaller maculae) located anteriorly from median ocellus (Fig. 4D, E). Compound eyes grey to brownish to black. Ocelli blackish. Antennae yellowish brown, scapus and pedicellus darkened. Hair-like setae along anterior margin of head extend to lateral margins. Dorsal surface of head covered with fine hair-like setae and
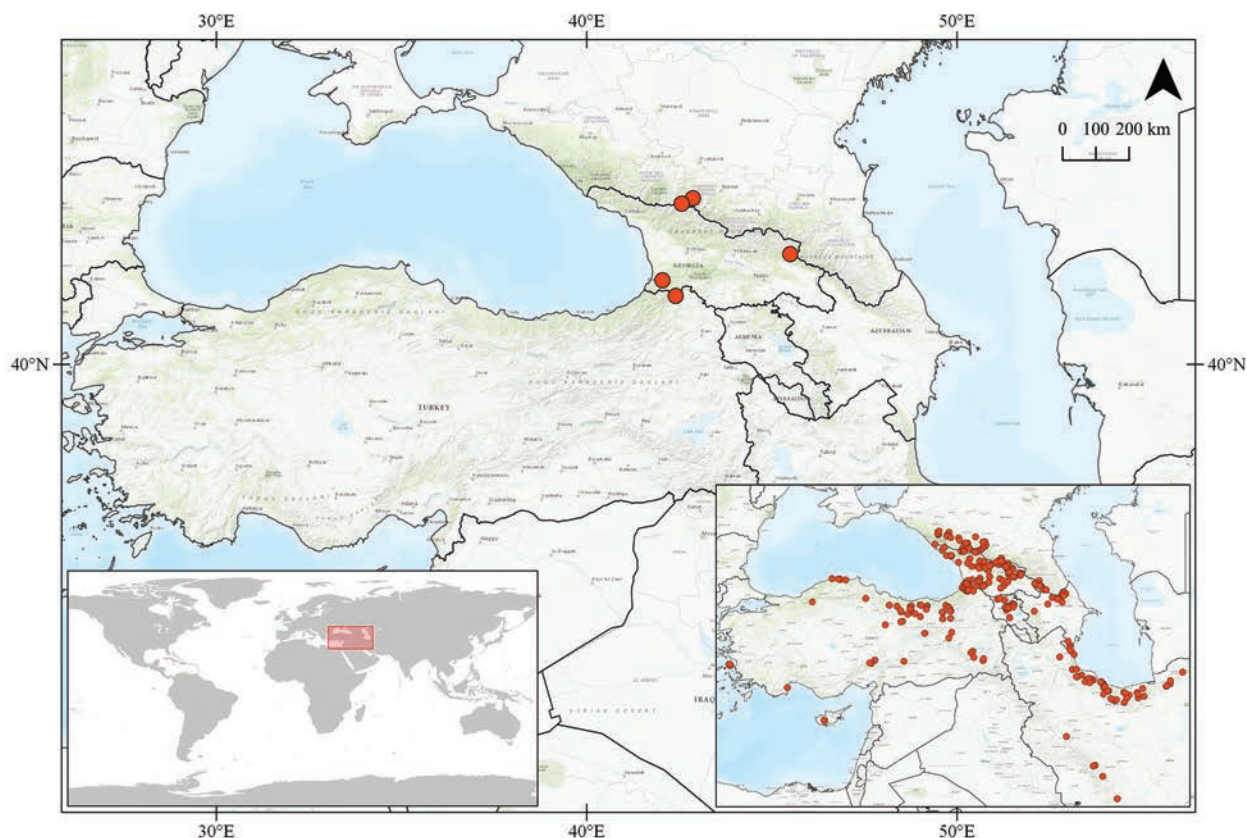
Figure 1. Distribution of *Epeorus* (*Caucasiron*) *abditus* sp. nov.; global localisation of a study area (lower left corner) and our sampling sites investigated between 2008–2019 (lower right corner).

sparsely distributed stick-like setae. Sparse longer and fine hair-like setae located posteriorly to eyes.

Mouthparts. Labrum (Fig. 5A) widened anteriorly, with anterior margin slightly rounded or nearly straight (in dorsal view), lateral angles rounded. Dorsal surface (Fig. 5A, left) sparsely covered with hair-like setae and short bristle-like setae; 5–6 longer bristle-like setae located antero-medially and two antero-laterally. Epipharynx with longer, shortly plumose bristles situated along lateral to anterior margin (Fig. 5A, right; range of setation figured as large black dots), and brush of fine hair-like setae medially (not figured); ventral surface with group of 10–16 setae of various size located medio-posteriorly. Outer incisors of both mandibles with three apical teeth (Fig. 5B, C). Inner incisor of left mandible with three apical teeth, right inner incisor bifurcated. Outer edge of both mandibular incisors with numerous setae (range of setae marked with dashed polygons).

Thorax. Pronotum anteriorly narrowed, lateral edges slightly curved. Metanotum with slight postero-medial projection. Dorsal surface with dark brown maculation as on Fig. 4A and covered with fine, hair-like setae (as on abdominal terga and head); sparse longer, hair-like setae along pro-, meso- and metanotal suture.

Legs. Colour pattern of femora as on Fig. 4F. Femora without medial hypodermal spot. Femora apically slightly darkened; patella-tibial suture darkened; tarsi proximally and distally darkened. Dorsal surface of femora covered by short (sporadically elongated) apically rounded spatulate setae (Fig. 5D). Dorsal margin of tibiae and tarsi with row of long setae; ventral margin of both with short distally accumulated spine-like setae. Tarsal claws with 3–4 denticles.
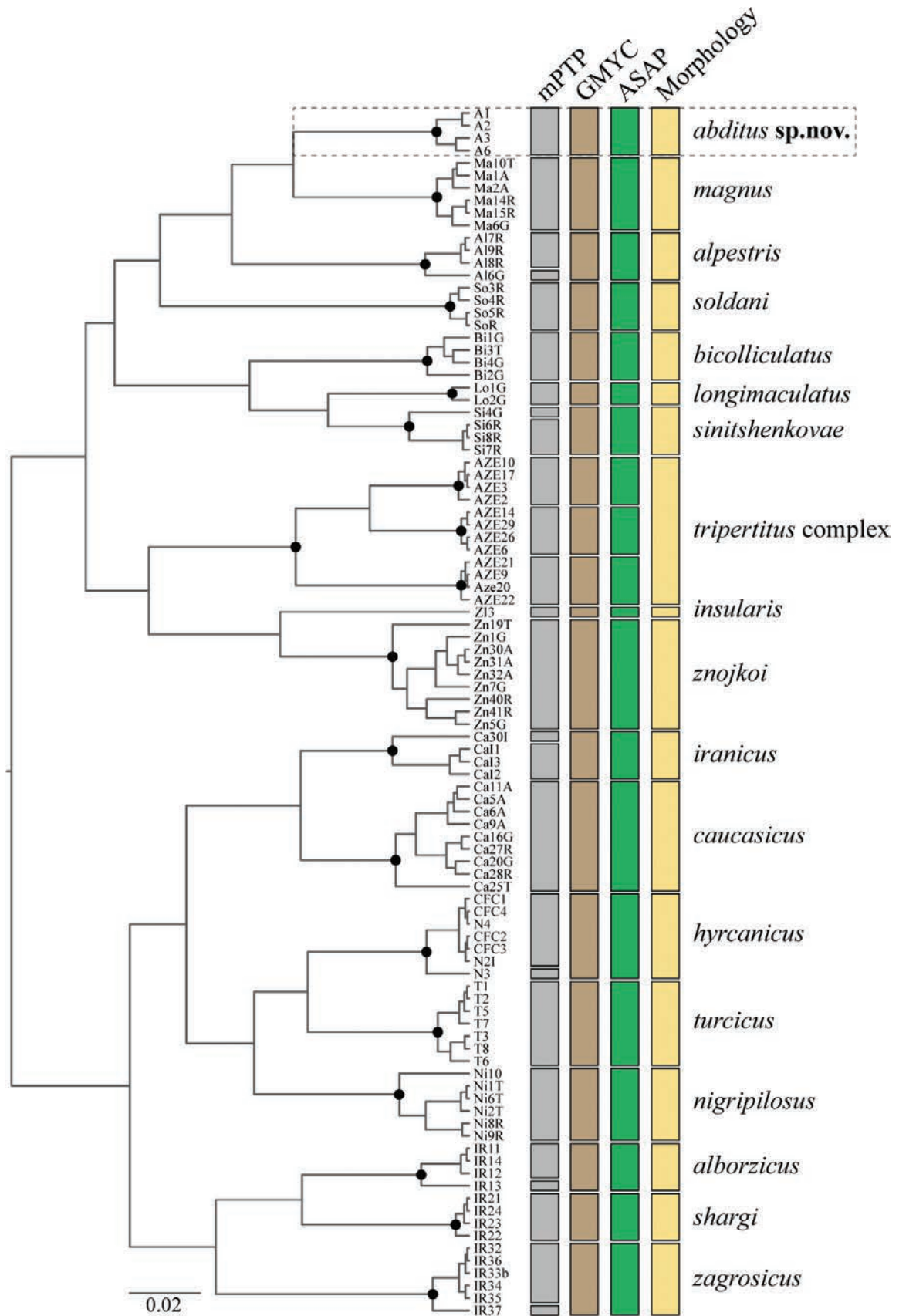
Figure 2. COI gene tree with results of molecular species delimitation tools and larval morphology according to Hrivniak et al. (2020b). Black points correspond to posterior probability 1. Delimitation of *Epeorus* (*Caucasiron*) *abditus* sp. nov. is highlighted by the dashed frame.

Figure 3. The habitat (type locality) of *Epeorus* (*Caucasiron*) *abditus* sp. nov. from north-east Türkiye (photo: G. Türkmen).

Abdominal terga. Colour pattern of abdominal terga consists of transversal stripe along anterior margin of terga I–IX, medially extending to: i) large median triangular macula on terga II–III (IV), and ii) triangular or T-shaped macula on terga V–IX (medial macula on tergum VIII and IX often widened). Median macula on terga V–VII surrounded by pale area (Fig. 4G). Tergum X without distinct maculation. Lateral margin of terga I–IX with oblique macula. Denticles along posterior margin on terga strongly sclerotised, irregular and pointed (Fig. 5E). Surface of terga covered with hair-like setae and sparsely with stick-like setae. Tergum X with short postero-lateral projections (Fig. 5J, K). Longitudinal medial row of hair-like setae along abdominal terga present.

Abdominal sterna. Yellowish, with colouration pattern on sterna I–VIII consisting of rounded median macula (Fig. 4H, arrow). In more pigmented specimens, median macula with paired pale spots located medio-posteriorly. Rounded median
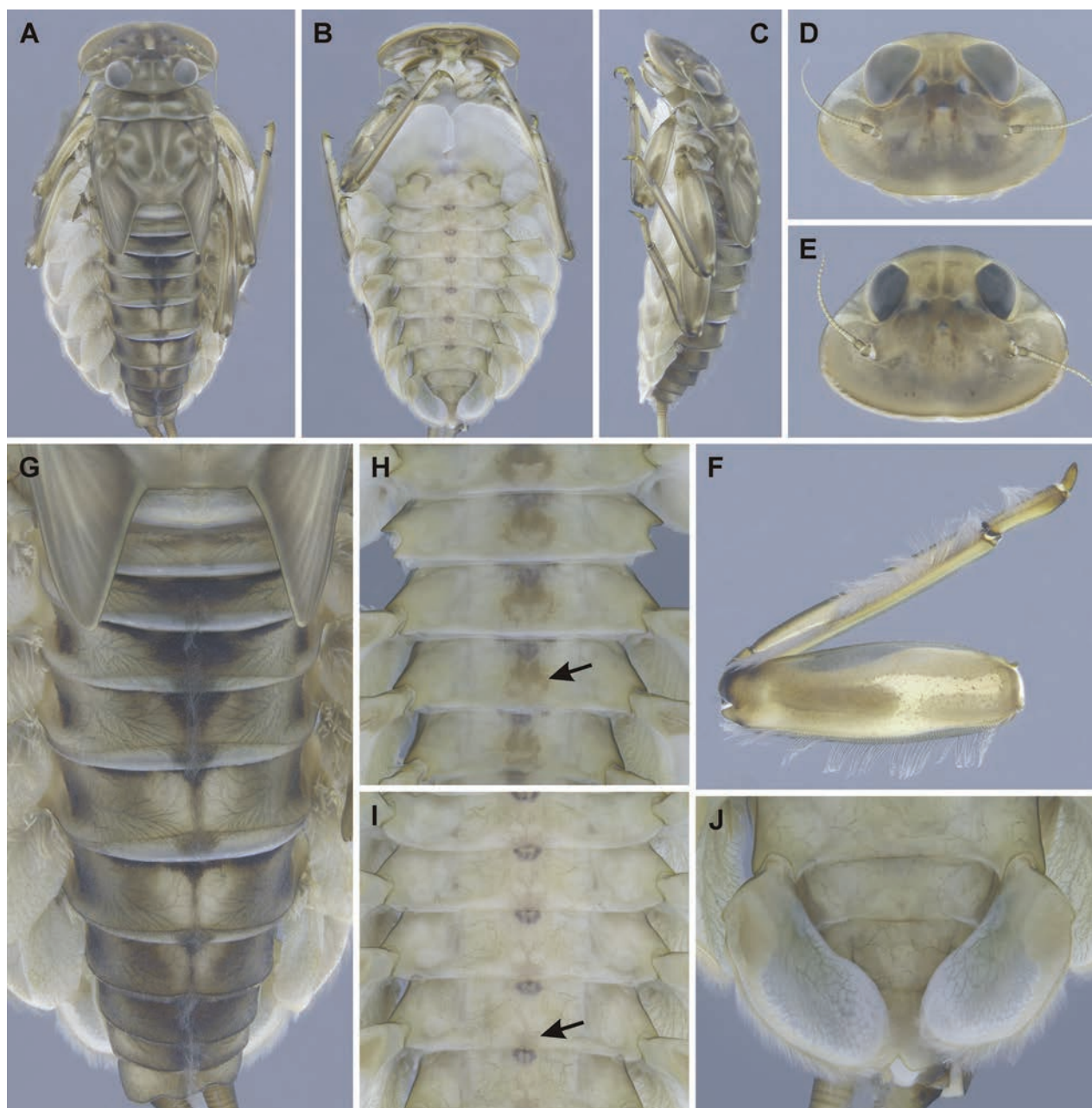
Figure 4. *Epeorus* (*Caucasiron*) *abditus* sp. nov., larva **A** habitus in dorsal view **B** habitus in ventral view **C** habitus in lateral view **D** head of male in dorsal view **E** head of female in dorsal view **F** middle leg in dorsal view **G** abdominal terga **H, I** abdominal sterna II–VI (arrow points on median maculation) **J** gills VII (in natural position from ventral view).

macula often poorly expressed and only medio-posterior edge of sterna is slightly pigmented (Fig. 4I, arrow). Colouration pattern sporadically restricted to sterna I and II or absent. Sternum IX of female with V-shaped median emargination and surface covered by setae centrally (Fig. 5L).

Gills. Dorsal surface of gill plate I yellowish; of gill plates II–VII greyish on anterior half, brownish on posterior half. Ventral margin of all gill plates yellowish. Costal projection on gill plate III well-developed (Fig. 5G, arrow). Gill plate VII wide (in natural position of ventral view; Figs 4J, 5H, I).

Cerci. Yellowish brown, basally darkened.

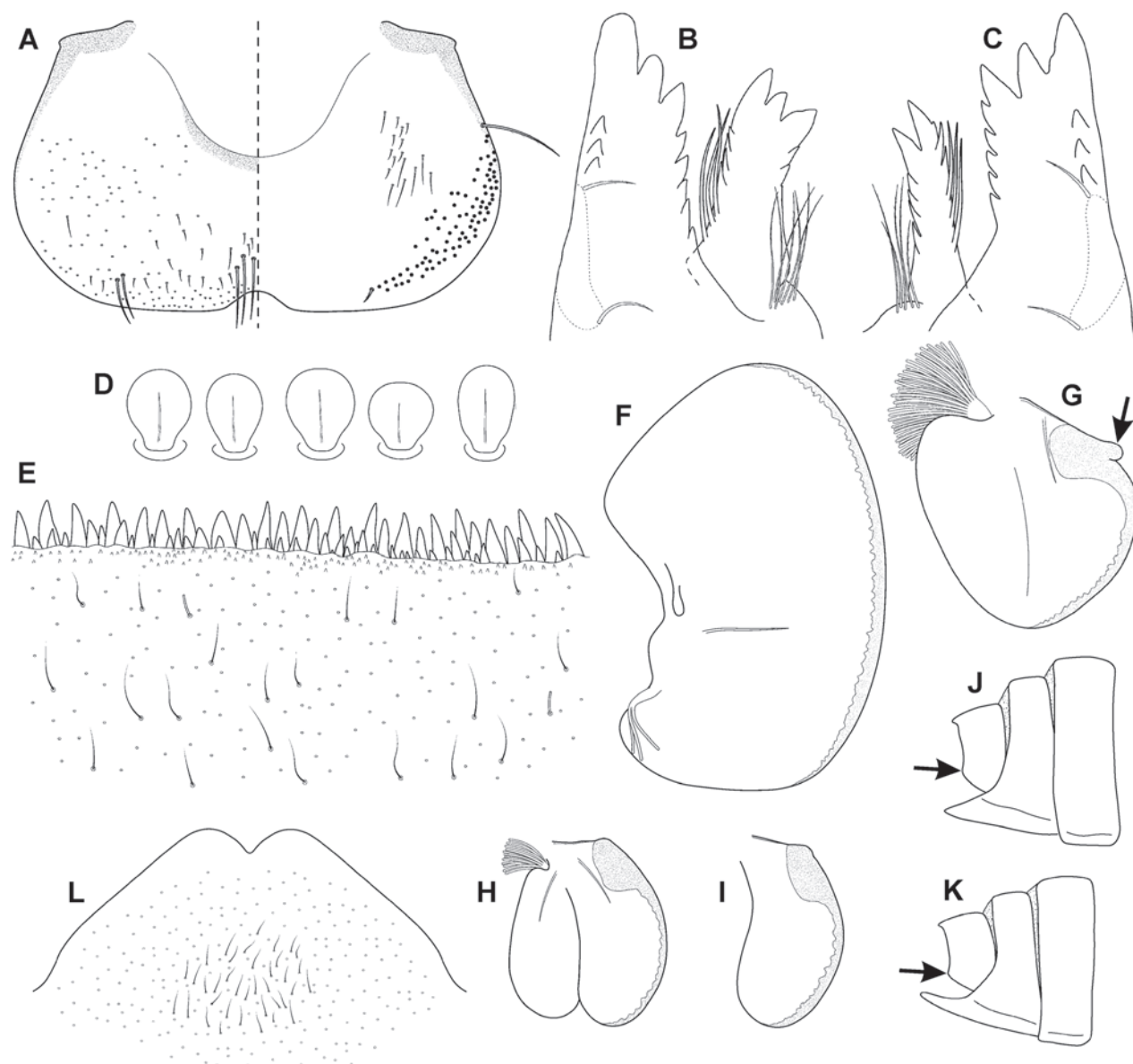**Subimagoes, imagoes, and eggs.** Unknown.

Figure 5. *Epeorus* (*Caucasiron*) *abditus* sp. nov., larva **A** labrum (left half in dorsal view, right half in ventral view; black dots refer to range of setae) **B** incisors of left mandible **C** incisors of right mandible (dashed polygons on outer edge of both mandibles refer to range of setae) **D** setae on dorsal surface of femora **E** surface and posterior margin of abdominal tergum VII **F** gill I **G** gill III (arrow points to projection on costal margin) **H** gill VII (flattened on slide) **I** gill VII (in natural position from ventral view) **J, K** abdominal segments VIII−X in lateral view (arrow points on postero-lateral projection) **L** sternum IX of female.

Morphological diagnostics of larvae. *Epeorus* (*Caucasiron*) *abditus* sp. nov. can be distinguished by the combination of the following morphological characters: i) femora without median spot (Fig. 4F); ii) abdominal sterna with circular median macula as on Fig. 4H (colouration may be restricted to medio-posterior part of sterna as on Fig. 4I); iii) abdominal terga V−VII with triangular or T-shaped macula surrounded by pale area (Fig. 4G); iv) tergum X with short postero-lateral projection (Fig. 5J, K, arrow); v) surface of abdominal terga with hair-like setae (Fig. 5E); vi) shape of gill plates VII wide (in natural position from ventral view, Figs 4J; 5H, I).

Morphological affinities. *Epeorus* (*Caucasiron*) *abditus* sp. nov. is similar to several species from the Caucasus and neighbouring Mediterranean and Irano-Anatolian ranges, namely *E.* (*C.*) *alpestris* (distributed in the Greater Caucasus),

E. (*C.*) *alborzicus* Hrivniak & Sroka, 2020 (Alborz Mountains), and *E.* (*C.*) *bicollicula-tus* Hrivniak, 2017 (Pontic Mountains, Lesser and Greater Caucasus). All of them possess abdominal sterna with a rounded median macula and femora without median spot (Hrivniak et al. 2020b).

Epeorus (*C.*) *alpestris* can be distinguished from *E.* (*C.*) *abditus* sp. nov. by the absence of postero-lateral projections on the tergum X (Hrivniak et al. 2020b, fig. 17L) present in *E.* (*C.*) *abditus* sp. nov. (Fig. 5J, K, arrow). Additionally, the rounded maculae on abdominal sterna are always present in *E.* (*C.*) *alpestris* (Hrivniak et al. 2020b, fig. 16I), whereas the colouration pattern of abdominal sterna varies from a well-defined pattern (Fig. 4H) to an indistinct (Fig. 4I) or no pattern in *E.* (*C.*) *abditus* sp. nov. Moreover, *Epeorus* (*C.*) *alpestris* is character-ised by typical maculation of abdominal terga (Hrivniak et al. 2020b, fig. 16G, H).

Epeorus (*C.*) *alborzicus* possesses abdominal sterna with a large circular me-dial macula (Hrivniak et al. 2020b, fig. 40L−N) and blurred macula (or a pair of rounded maculae) on tergum II and III (Hrivniak et al. 2020b, fig. 40H, I), in con-trast to *E.* (*C.*) *abditus* sp. nov. with relatively small rounded medial macula on abdominal sterna (Fig. 4H, I) and triangular macula on tergum II and III (Fig. 4G).

Epeorus (*C.*) *bicolliculatus* differs from *E.* (*C.*) *abditus* sp. nov. by the presence of paired postero-medial protuberances on abdominal terga II−IX (Hrivniak et al. 2020b, fig. 34H) and basally widened setae on the surface of terga (Hrivniak et al. 2020b, fig. 35E) in contrast to basally narrow setae in *E.* (*C.*) *abditus* sp. nov. (Fig. 5E).

The larvae of *E.* (*C.*) *abditus* sp. nov. with weakly pigmented abdominal sterna may be erroneously assigned to *E.* (*C.*) *magnus* (distributed in the Greater and Lesser Caucasus, Pontic and Taurus Mountains). This species differs from *E.* (*C.*) *abditus* sp. nov. by the presence of dense bristle-like setae on the dorsal surface of the labrum (Hrivniak et al. 2020b, fig. 11A) in contrast to sparse and hair-like setae in *E.* (*C.*) *abditus* sp. nov. (Fig. 5A). In addition, *E.* (*C.*) *magnus* often has clearly developed lateral projections on the tergum X (Hrivniak et al._2020b, fig. 11K−M) in contrast to only short projections in *E.* (*C.*) *abditus* sp. nov. (Fig. 5J, K).

Two species distributed in the western and central Greater Caucasus, name-ly *E.* (*C.*) *soldani* (Braasch, 1979) and *E.* (*C.*) *sinitshenkovae* (Braasch & Zim-merman, 1979), have abdominal sterna without or with weakly developed co-louration pattern and no femoral spot. *Epeorus* (*C.*) *soldani* can also be easily distinguished from *E.* (*C.*) *abditus* sp. nov. by setae on abdominal terga that are basally widened in the former species (Hrivniak et al. 2020b, fig. 20E) and narrow in the latter (Fig. 5E). *Epeorus* (*C.*) *sinitshenkovae* can be separated by a poorly developed projection on costal margin of gill plates (Hrivniak et al. 2020b, fig. 26G) from *E.* (*C.*) *abditus* sp. nov. bearing a well-developed projec-tion (Fig. 5G). Additionally, *E.* (*C.*) *sinitshenkovae* is characterised by a specific colouration of abdominal terga and femora (Hrivniak et al. 2020b, fig. 25H, F).

All other species of *E.* (*Caucasiron*) from the Caucasus, Mediterranean, and Irano-Anatolian ranges can be easily distinguished from *E.* (*C.*) *abditus* sp. nov. by the presence of specific colouration pattern of abdominal sterna and/or presence of femoral spot. These include *E.* (*C.*) *caucasicus* (Tshernova, 1938), *E.* (*C.*) *nigripilosus* (Sinitshenkova, 1976), *E.* (*C.*) *zagrosicus* Hrivniak & Sroka, 2020, *E.* (*C.*) *iranicus* (Braasch & Soldán, 1979), *E.* (*C.*) *longimaculatus* (Braasch, 1980), *E.* (*C.*) *turcicus* Hrivniak, Türkmen & Kazancı, 2019, *E.* (*C.*) *shargi*, *E.* (*C.*) *hyrcanicus*, and *E.* (*C.*) *tripertitus*.

Supplement to the identification guide to larvae of Caucasian and Irano-Anatolian species of *E*. (*Caucasiron*)

The identification guide by Hrivniak et al. (2020b) includes 15 species of *E*. (*Caucasiron*) described between 1938 and 2020 and covers the entire area of the Caucasus and adjacent Mediterranean and Irano-Anatolian mountain ranges. Since then, three more species have been described from this area, namely *E*. (*C*.) *hyrcanicus*, *E*. (*C*.) *tripertitus*, and *E*. (*C*.) *abditus* sp. nov. Therefore, we provide a supplement to the original guide that includes recently described species. For accurate identification of *E*. (*Caucasiron*) larvae, this supplement should be used prior to the original guide. When the possibility that the specimens to be identified represent one of the three recently described species is ruled out, the user can proceed with Hrivniak et al. (2020b). The abbreviations used in this key: N: north, SE: southeast, NE: northeast, SW: southwest. The geographic delimitation of the mountain ranges was given by Hrivniak et al. (2020b).

Key to species (part II)

1   Medial hypodermal femur spots present (Figs 6A, B, 7A) ....**group A**
2   Medial hypodermal femur spots absent (Fig. 4F) ....**group B**

Group A

–   Colouration pattern on abdominal sterna present (Figs 6D, E, 7D, E) **3**
–   Colouration pattern on abdominal sterna absent ....**continue to subgroup A2 in Hrivniak et al. (2020b, p. 9)**
3   Setae on abdominal terga wide at base (Fig. 6C). Sterna II–VI with rounded (or blurred) median macula and pair of medio-lateral maculae (Fig. 6D, arrows) (colouration pattern sometimes poorly expressed, Fig. 6E); gill plates VII narrow (Fig. 6F); medial hypodermal femur spot elongated, often blurred or poorly expressed (Fig. 6A, B) ....*E*. (*C*.) *tripertitus* **(Greater Caucasus; see Hrivniak et al. 2022)**
4   Setae on abdominal terga hair-like (Fig. 7B). Sterna with oblique stripes often laterally extended (Fig. 7D, E, arrows); gill plates VII relatively wide (Fig. 7C); medial hypodermal femur spot as in Fig. 7A................................. ....*E*. (*C*.) *hyrcanicus* **(N Iran, SE Azerbaijan; see Hrivniak et al. 2021)**
–   Characters differ from the combinations above .... **continue to subgroup A1 in Hrivniak (2020, p. 9)**

Group B

–   Sterna II–VI: with rounded median macula (Fig. 4H, arrow)/with darkened posterior margin (Fig. 4I, arrow)/unpatterned (sterna I–II often darkened); tergum X with short postero-lateral projections (Fig. 5J, K); gill plates VII wide (Figs 4J, 5H, I); dorsal margin of labrum with sparse setae (Fig. 5A) ... . *E*. (*C*.) *abditus* **sp. nov. (NE Türkiye, SW Georgia, Greater Caucasus)**
–   Characters differ from the combination above .... **continue to group B in Hrivniak et al. (2020b, p. 9)**
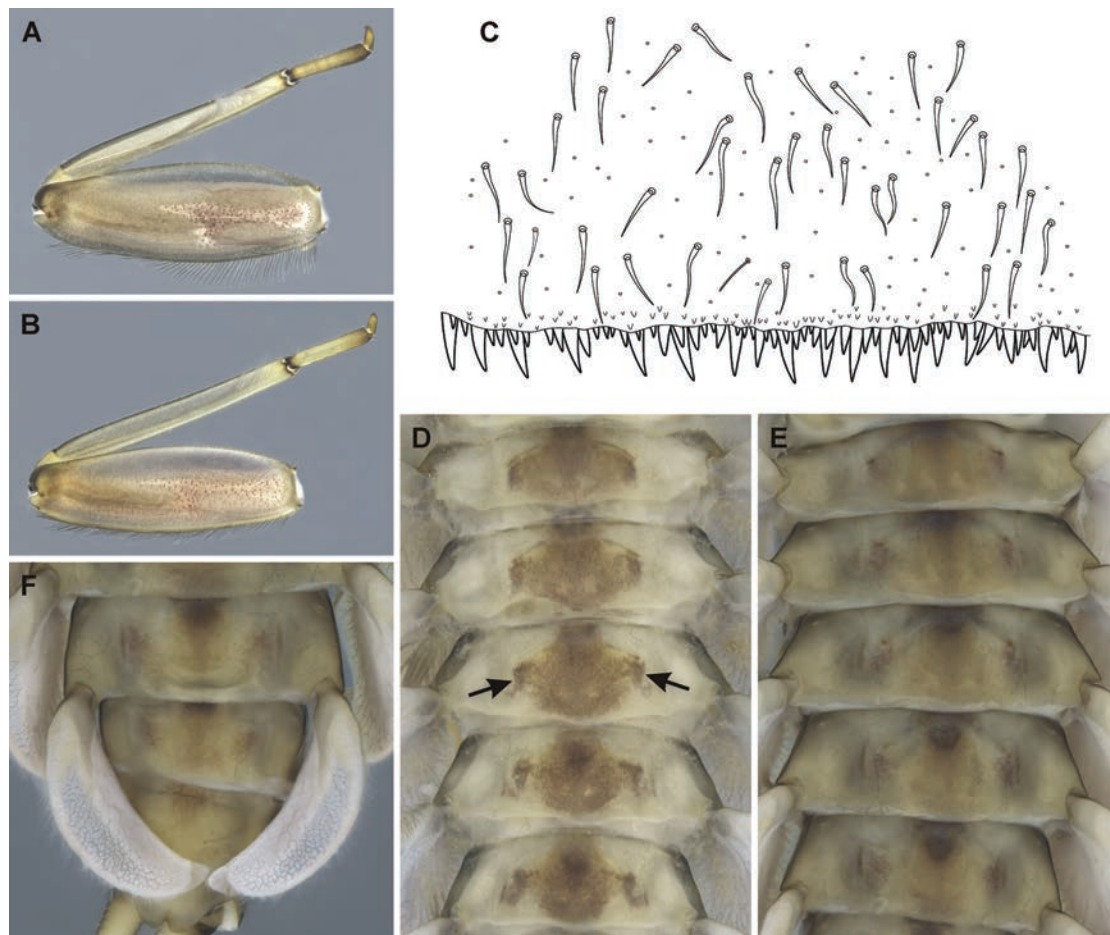
Figure 6. *Epeorus* (*Caucasiron*) *tripertitus,* larva **A, B** middle leg **C** surface and posterior margin of abdominal tergum VII **D, E** abdominal sterna II–VI (arrows point on paired medio-lateral maculae) **F** gills VII (in natural position from ventral view).
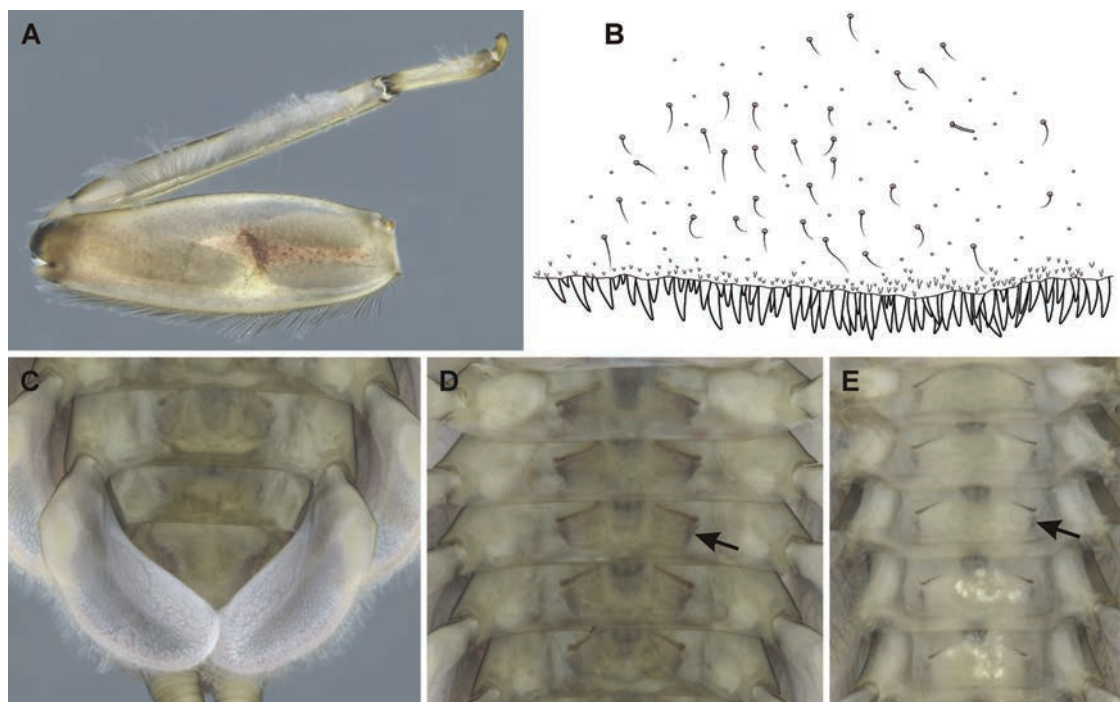

Figure 7. *Epeorus* (*Caucasiron*) *hyrcanicus,* larva **A** middle leg **B** surface and posterior margin of abdominal tergum VII **C** gills VII (in natural position from ventral view) **D, E** abdominal sterna II–VI (arrow points on lateral extension of oblique stripe).

Acknowledgements

Additional information

Conflict of interest

The authors have declared that no competing interests exist.

Ethical statement

No ethical statement was reported.

Funding

Author contributions

Conceptualization: ĽH. Formal analysis: ĽH. Investigation: ĽH. Methodology: ĽH. Resources: GT, ĽH, AVM. Visualization: PS, ĽH. Writing – original draft: PS, ĽH, JB.

Author ORCIDs

Ľuboš Hrivniak https://orcid.org/0000-0002-9327-1314
Pavel Sroka https://orcid.org/0000-0003-4367-6564
Gencer Türkmen https://orcid.org/0000-0002-1155-8275
Alexander V. Martynov https://orcid.org/0000-0002-6506-5134

Data availability

All of the data that support the findings of this study are available in the main text.

References

Bojková J, Sroka P, Soldán T, Namin JI, Staniczek AH, Polášek M, Hrivniak Ľ, Abdoli A, Godunko RJ (2018) Initial commented checklist of Iranian mayflies, with new area records and description of *Procloeon caspicum* sp. n. (Insecta, Ephemeroptera, Baetidae). ZooKeys 749: 87–123. https://doi.org/10.3897/zookeys.749.24104

Bouckaert R, Heled J, Kühnert D, Vaughan T, Wu CH, Xie D, Suchard MA, Rambaut A, Drummond AJ (2014) BEAST 2: a software platform for Bayesian evolutionary analysis. PLoS Computational Biology 10: e1003537. https://doi.org/10.1371/journal.pcbi.1003537

Braasch D (1978) *Epeorus znojkoi* and *Iron magnus* new species (Heptageniidae Ephemeroptera) from the Caucasus USSR. Entomologische Nachrichten 22(5): 65–70.

Braasch D (1979) Beitrag zur Kenntnis der Gattung Iron Eaton im Kaukasus (UdSSR) (III) (Ephemeroptera, Heptageniidae). Reichenbachia 17 (33): 283–294.

Braasch D (1980) Beitrag zur Kenntnis der Gattung Iron Eaton (Heptageniidae, Ephemeroptera) im Kaukasus (UdSSR), 2. Entomologische Nachrichten 24 (10–11): 166–173.

Braasch D (2006) Neue Eintagsfliegen der Gattungen *Epeorus* und *Iron* aus dem Himalaja (Ephemeroptera, Heptageniidae). Entomologische Nachrichten 50 (1–2): 79–88.

Braasch D, Zimmermann W (1979) Iron sinitshenkovae sp. n. – eine neue Heptageniide (Ephemeroptera) aus dem Kaukasus. Entomologische Nachrichten 23 (7): 103–107.

Chen P, Wang YY, Zhou CF (2010) A new mayfly species of *Epeorus* (*Caucasiron*) from southwestern China (Ephemeroptera: Heptageniidae). Zootaxa 2527: 61–68. https://doi.org/10.11646/zootaxa.2527.1.4

Eaton AE (1881) An announcement of new genera of the Ephemeridae. Entomologist's Monthly Magazine 18: 21–27.

Fujisawa T, Barraclough TG (2013) Delimiting species using single-locus data and the generalized mixed yule coalescent approach: a revised method and evaluation on simulated datasets. Systematic Biology 62: 707–724. https://doi.org/10.1093/sysbio/syt033

Hrivniak Ľ (2020) Diversity and speciation of mayflies (Ephemeroptera) from the Caucasus and adjacent areas. Ph.D. Thesis Series, No. 15. University of South Bohemia, Faculty of Science, School of Doctoral Studies in Biological Sciences, České Budějovice, 269 pp.

Hrivniak Ľ, Sroka P, Godunko RJ, Žurovcová M (2017) Mayflies of the genus *Epeorus* Eaton, 1881 s.l. (Ephemeroptera: Heptageniidae) from the Caucasus Mountains: a new species of *Caucasiron* Kluge, 1997 from Georgia and Türkiye. Zootaxa 4341: 353–374. https://doi.org/10.11646/zootaxa.4341.3.2

Hrivniak Ľ, Sroka P, Godunko RJ, Palatov D, Polášek M, Manko P, Oboňa J (2018) Diversity of Armenian mayflies (Ephemeroptera) with the description of a new species of the genus *Ecdyonurus* (Heptageniidae). Zootaxa 4500: 195–221. https://doi.org/10.11646/zootaxa.4500.2.3

Hrivniak Ľ, Sroka P, Türkmen G, Godunko RJ, Kazancı N (2019) A new *Epeorus* (*Caucasiron*) (Ephemeroptera: Heptageniidae) species from Turkey based on molecular and morphological evidence. Zootaxa 4550: 58–70. https://doi.org/10.11646/zootaxa.4550.1.2

Hrivniak Ľ, Sroka P, Bojková J, Godunko RJ, Soldán T, Staniczek AH (2020a) The impact of Miocene orogeny for the diversification of Caucasian *Epeorus* (*Caucasiron*) mayflies (Ephemeroptera: Heptageniidae). Molecular Phylogenetics and Evolution 146: 106735. https://doi.org/10.1016/j.ympev.2020.106735

Hrivniak Ľ, Sroka P, Bojková J, Godunko RJ (2020b) Identification guide to larvae of Caucasian *Epeorus* (*Caucasiron*) (Ephemeroptera, Heptageniidae). ZooKeys 986: 1–53. https://doi.org/10.3897/zookeys.986.56276

Hrivniak Ľ, Sroka P, Bojková J, Godunko RJ, Namin JI, Bagheri S, Nejat F, Abdoli A, Staniczek AH (2020c) Diversity and distribution of *Epeorus* (*Caucasiron*) (Ephemeroptera, Heptageniidae) in Iran, with descriptions of three new species. ZooKeys 947: 71–102. https://doi.org/10.3897/zookeys.947.51259

Hrivniak Ľ, Sroka P, Bojková J, Manko P, Godunko RJ (2021) A new species of *Epeorus* (*Caucasiron*) (Ephemeroptera: Heptageniidae) from Azerbaijan and Iran. ZooKeys 1068: 13–26. https://doi.org/10.3897/zookeys.1068.70717

Hrivniak Ľ, Sroka P, Godunko RJ, Manko P, Bojková J (2022) Diversification in Caucasian *Epeorus* (*Caucasiron*) mayflies (Ephemeroptera: Heptageniidae) follows topographic deformation along the Greater Caucasus range. Systematic Entomology 47(4): 603–617. https://doi.org/10.1111/syen.12551

Kapli T, Lutteropp S, Zhang J, Kobert K, Pavlidis P, Stamatakis A, Flouri T (2016) Multi-rate Poisson tree processes for single-locus species delimitation under maximum likelihood and Markov chain Monte Carlo. Bioinformatics 33(11): 1630–1638. https://doi.org/10.1093/bioinformatics/btx025

Kluge NJ (1997) New subgenera of Holarctic mayflies (Ephemeroptera: Heptageniidae, Leptophlebiidae, Ephemerellidae). Zoosystematica Rossica 5(2): 233–235.

Kluge NJ (2015) Central Asian mountain Rhithrogenini (Ephemeroptera: Heptageniidae) with pointed and ephemeropteroid claws in the winged stages. Zootaxa 3994: 301–353. https://biotaxa.org/Zootaxa/article/view/zootaxa.3994.3.1

Kumar S, Stecher G, Li M, Knyaz C, Tamura K (2018) MEGA X: Molecular Evolutionary Genetics Analysis across computing platforms. Molecular Biology and Evolution 35: 1547–1549. https://doi.org/10.1093/molbev/msy096

Ma Z, Li R, Zhu B, Zheng X, Zhou C (2022) Comparative mitogenome analyses of subgenera and species groups in *Epeorus* (Ephemeroptera: Heptageniidae). Insects 13: 599. https://doi.org/10.3390/insects13070599

Miller MA, Pfeiffer W, Schwartz T (2010) Creating the CIPRES Science Gateway for inference of large phylogenetic trees. In: Proceedings of the Gateway Computing Environments Workshop (GCE), 14 Nov. 2010, New Orleans, 1–8. https://doi.org/10.1109/GCE.2010.5676129

Mittermeier RA, Turner WR, Larsen FW, Brooks TM, Gascon C (2011) Global biodiversity conservation: the critical role of hotspots. In: Zachos FE, Habel JC (Eds) Biodiversity Hotspots. Distribution and Protection of Conservation Priority Areas. Springer, Berlin, Heidelberg.

Pons J, Barraclough TG, Gomez-Zurita J, Cardoso A, Duran DP, Hazell S, Kamoun S, Sumlin WD, Vogler AP (2006) Sequence-based species delimitation for the DNA taxonomy of undescribed insects. Systematic Biology 55: 595–609. https://doi.org/10.1080/10635150600852011

Puillandre N, Brouillet S, Achaz G (2021) ASAP: Assemble species by automatic partitioning. Molecular Ecology Resources 21: 609–620. https://doi.org/10.1111/1755-0998.13281

Rambaut A, Drummond AJ, Xie D, Baele G and Suchard MA (2018) Posterior summarisation in Bayesian phylogenetics using Tracer 1.7. Systematic Biology 67(5): 901–904. https://doi.org/10.1093/sysbio/syy032

Sinitshenkova ND (1976) Mayflies of the genus Iron Eaton (Ephemeroptera, Heptageniidae) in the fauna of the Caucasus. Entomological Review 55(4): 85–92.

Tshernova OA (1938) Zur Kenntnis der Ephemeropteren Ost-Transkaukasien. Trudy Azerbajdshanskogo Filiala AN SSSR, Baku 7(42): 55–64.

Tshernova OA (1981) On the systematics of adult mayflies of the genus *Epeorus* Eaton 1881 (Ephemeroptera, Heptageniidae). Revue d'Entomologie de l'URSS] 60(2): 323–336.

Waterhouse AM, Procter JB, Martin DMA, Clamp M, Barton GJ (2009) Jalview Version 2 – a multiple sequence alignment editor and analysis workbench. Bioinformatics 25: 1189–1191. https://doi.org/10.1093/bioinformatics/btp033

Research Article

New species and records of limpets (Mollusca, Gastropoda) from the Pacific Costa Rica Margin

Melissa J. Betters[1], Jorge Cortés[2], Erik E. Cordes[1]

1 *Department of Biology, Temple University, Philadelphia, PA, USA*
2 *(CIMAR) Universidad de Costa Rica, San José, Costa Rica*
Corresponding author: Melissa J. Betters (melissajbetters@gmail.com)

Abstract

The ocean remains a reservoir of unknown biodiversity, particularly in the deep sea. Chemosynthesis-based ecosystems, such as hydrothermal vents and hydrocarbon seeps, host unique and diverse life forms that continue to be discovered and described. The present study focuses on patelliform gastropods (limpets) collected from Pacific Costa Rica Margin hydrocarbon seeps during three research cruises from 2017 to 2019. Genetic and morphological analyses revealed the presence of several new lineages within the genera *Bathyacmaea* Okutani, Tsuchida & Fujikura,1992, *Cocculina* Dall, 1882, *Paralepetopsis* McLean, 1990, and the family Lepetodrilidae McLean, 1988: *Bathyacmaea levinae* **sp. nov.**, *Paralepetopsis variabilis* **sp. nov.**, *Pseudolepetodrilus costaricensis* **gen. et sp. nov.**, and *Cocculina methana* **sp. nov.** These investigations also expanded the known ranges of the species *Pyropelta corymba* McLean, 1992 and *Lepetodrilus guaymasensis* McLean, 1988 to the Costa Rica Margin. This research highlights the uniqueness of gastropod fauna at the Costa Rica Margin and contributes to our understanding of the biodiversity at chemosynthesis-based deep-sea ecosystems in the face of global biodiversity loss and increased commercial interest in deep-sea resources.

Key words: Biodiversity, chemosynthetic ecosystems, cold seeps, deep sea, systematics, taxonomy

Introduction

Despite marine species across all phyla being described at an average rate of more than 2,000 new species per year (Bouchet et al. 2023), estimates still place the unknown number of species in the ocean at approximately 0.3–2.2 million species (Mora et al. 2011; Costello et al. 2012). Species discovery in the deep ocean (defined as depths below 200 meters) tends to be slower than in other oceanic regions. Bouchet et al. (2023) examined 600 randomly selected, newly discovered marine species from around the globe and found that just 7% came from depths below 1,000 meters. Representation of the deep ocean is also consistently lower than shallow waters on biodiversity platforms like the Ocean Biodiversity Information System (OBIS; Webb et al. 2010). With increasing commercial interest in deep-sea resources (e.g., deep-sea mining; Van

Dover et al. 2020), increasing attention paid to the ocean's role in regulating climate (e.g., Levin et al. 2020), and the global threat of biodiversity loss across ecosystems (IPBES 2019), documenting marine biodiversity before it is lost is an increasingly salient issue.

Chemosynthesis-based ecosystems, such as hydrothermal vents and hydrocarbon seeps, represent biodiversity hotspots on the ocean floor (Levin et al. 2016). In the first 30 years after their initial discovery in 1977, more than 1,300 species had been described from chemosynthesis-based ecosystems (Corliss et al. 1979; German et al. 2011). Chemosynthesis, primary production fueled by fluids expelled from the seafloor through mantle dewatering processes (hydrocarbon seeps; Suess 2014) or geothermal activity (hydrothermal vents; Corliss et al. 1979), produces enough energy to support entire, diverse ecosystems (Cavanaugh et al. 1981; Levin et al. 2016). Comparatively, the rest of the deep ocean is relatively nutrient-poor (Van Dover and Trask 2000; Levin et al. 2001). Thus, many species at chemosynthesis-based ecosystems are endemic to these environments, as they are often directly or indirectly reliant on chemosynthetically derived carbon (Cordes et al. 2006; Bergquist et al. 2007; Cordes et al. 2009; German et al. 2011).

Hydrocarbon seeps at the Costa Rica Margin (CRM) host an abundance and diversity of deep-sea fauna that were extensively sampled during three cruises from 2017–2019. These sampling efforts yielded a high abundance and diversity of life, of which patelliform gastropod mollusks comprised a large portion. Patelliform gastropods (hereafter "limpets") are common denizens at chemosynthesis-based ecosystems and are often the primary biofilm grazers at these sites (Sasaki et al. 2010 in Kiel 2010). Limpets are not monophyletic; rather, this body plan has evolved many times in the deep ocean, potentially due to its versatility in adapting to highly variable habitats (Vermeij 2017; Chen and Watanabe 2020). Current consensus on gastropod taxonomy delineates six discrete subclasses: Caenogastropoda, Heterobranchia, Neomphaliones, Neritimorpha, Patellogastropoda, and Vetigastropoda (Bouchet et al. 2017). Patellogastropoda, Neomphaliones, and Vetigastropoda are all found at chemosynthesis-based ecosystems. While several genera within these subclasses were preliminarily recognized from biological samples from the CRM, the exact species present at the CRM are largely unknown.

The present study aims to characterize the diversity of limpet species at the CRM hydrocarbon seeps. We herein investigate the genetic identities of limpet species at the CRM and whether these species are new to science. The CRM is situated near the Central American Isthmus and is separated from other nearby vent and seep fields by tens to hundreds of kilometers. Furthermore, it is positioned in the path of the equatorial currents and countercurrents, which move water west and east across the Pacific, as well as the Costa Rica Thermal Dome, which brings deep water to the surface (Kessler 2006; Fiedler and Talley 2006). This geographic position leads us to hypothesize that the CRM will host endemic species that are closely related to, but distinct from, known species from nearby regions. This paper thus undertakes the identification and description of the limpet species at the CRM and contributes novel information about the biodiversity that inhabits chemosynthesis-based ecosystems in the deep sea.

Materials and methods

Materials

Limpet specimens were collected from four hydrocarbon seep sites at the Pacific Costa Rica Margin (Fig. 1) during three cruises aboard the research vessels R/V Atlantis (**AT**) and R/V Falkor (**FK**): AT37-13 (Spring 2017), AT42-03 (Fall 2018), FK19-0106 (winter 2019). Additional specimens from the same hydrocarbon seep sites collected during AT15-44 (winter 2009) and AT15-59 (winter 2010) were also examined. The human-operated vehicle (HOV) Alvin was used aboard the R/V Atlantis and the remotely operated vehicle (ROV) SuBastian was used aboard the R/V Falkor. Specimens were collected in situ using sampling tools attached to the HOV and ROV such as vacuum suction and manipulator arms. Time and date of sampling events were recorded during each dive. Upon arrival to the surface, limpets were sorted into distinct shell morphotypes, promptly placed into > 95% ethanol, and subsequently stored at room temperature. All type specimens yielded are deposited at the Scripps Institute of Oceanography Benthic Invertebrate Collection (**SIO-BIC**) in San Diego, California, USA, or at the Museo de ZoologÍa de la Universidad de Costa Rica (**MZUCR**) in San José, San Pedro, Costa Rica (see the section "New species and records" below for more details on type materials). All other specimens collected are either stored at SIO-BIC, or in the personal collections of Erik Cordes at Temple University in Philadelphia, Pennsylvania, USA.
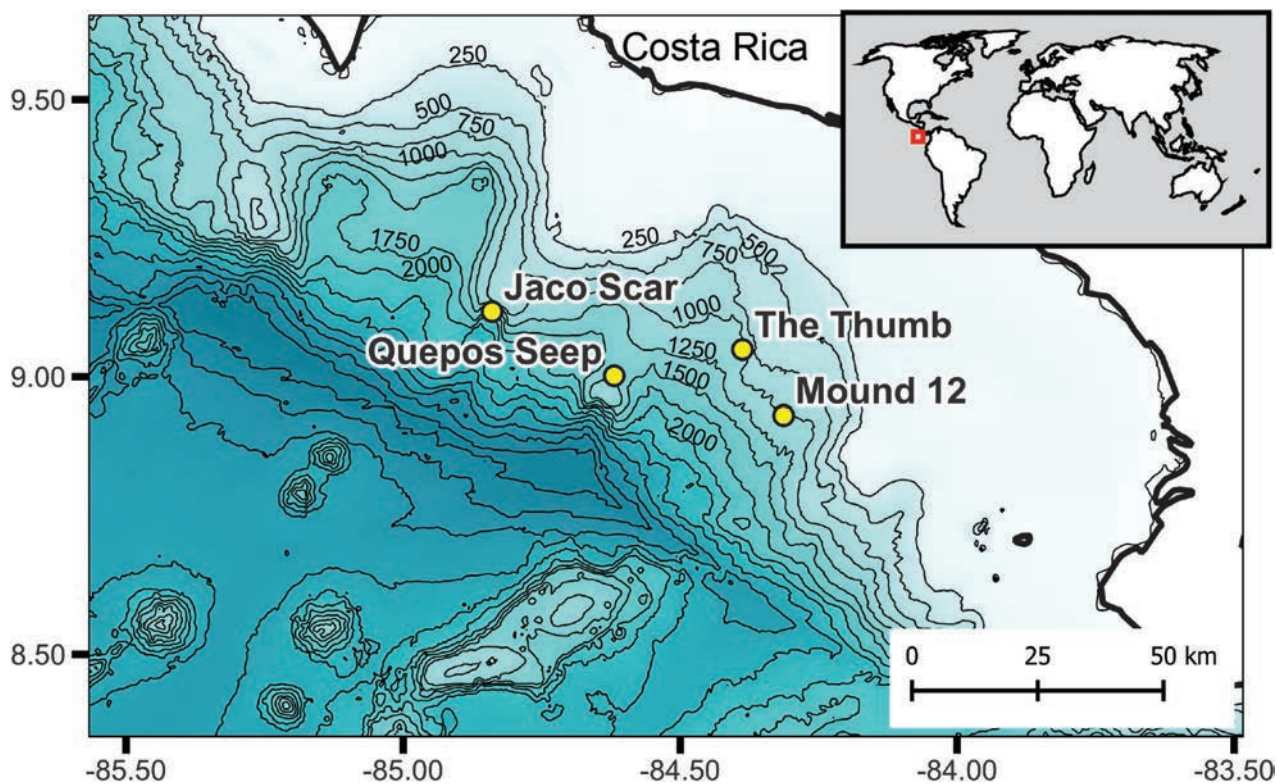

Figure 1. Map of the Pacific Costa Rica Margin. Four hydrocarbon seep locations from which patelliform gastropods were collected are depicted: Jaco Scar (9.12, -84.84), Quepos Seep (9.03, -84.6), The Thumb (9.05, -84.4), and Mound 12 (8.93, -84.3). Contour lines denote bottom seafloor bathymetry in meters and are drawn every 250 m.

Morphological characterization

Shells and soft tissues of all morphotypes were photographed using an AmScope microscope adapter camera attached to a standard dissection microscope (Leica S6D, Leica Microsystems GmbH). Each image included a standardized scalebar to allow for downstream measurements. Specimens were kept submerged in 1 cm of >95% ethanol while images were taken. To characterize the radulae of representative individuals, soft tissues were first separated from the shell and bisected latitudinally using a sharp scalpel blade. The anterior half of each specimen was then processed as follows: whole tissue was incubated in a 1.5 mL microcentrifuge tube containing a 10% solution of proteinase-k for 5–15 minutes at 56 °C. Incubation was monitored and terminated once tissue was visibly degraded, but not fully digested. The tissue was then removed from the heat source, pulse-vortexed 3 ×, and then rinsed into a clean glass petri dish using deionized (DI) water. Under a dissection scope, the radular ribbon was then extricated from any remaining soft tissue and removed to another clean glass petri dish containing DI water to further dilute the proteinase-k solution and prevent further breakdown of the radular ribbon. Silicon wafer chips cut into ~ 1 cm^3 squares were used as mounting substrate for scanning electron microscopy (SEM). To mount the radula, a drop of DI water was placed onto a chip within which the radula was then placed and manipulated into a flat, teeth-up position using forceps or a sharp probe. The radula's position was monitored and adjusted under a light microscope while the water was allowed to evaporate. Once dry, radulae naturally adhered to the chip's surface and were then stored dry until imaging.

For specimens of *Bathyacmaea*, shell cross-sections were additionally imaged as shell microstructures are considered one of the few reliable morphological characters with which to identify species in this genus (Chen et al. 2019; Sato et al. 2020). Soft tissue was removed, then a cut was made with dissection scissors on one side of the shell from the shell margin to the apex (Fig. 2). Shell pieces cleaved apart naturally during this process along radial growth lines, and additional pieces were pried away using forceps. All pieces were sorted into more recently formed shell material (those closer to the shell margin) or older shell material (those closer to the apex). Shell pieces were then soaked in 0.5% commercial bleach (sodium hypochlorite) for 12 h. Pieces were then rinsed with de-ionized water, soaked in a 2% solution of 1 M hydrochloric acid for one minute, rinsed again, then left to dry before SEM imaging.

SEM was undertaken using a Quanta™ 450 FEG scanning electron microscope (FEI 2012) in its high-vacuum setting at the Nano Instrumentation Center at Temple University's College of Engineering. High-quality images were obtained without sputter coating. For imaging, *Bathyacmaea* shell pieces were adhered to a silicon wafer chip using carbon tape. Transverse (top-down) cross sections of the shell pieces were then imaged for both newer and older shell material.

Genetic characterization

Representative individuals from each distinct shell morphotype were targeted for genetic sequencing. DNA was also extracted from the posterior half of each specimen that was bisected for radular isolation. Tissue was digested using a
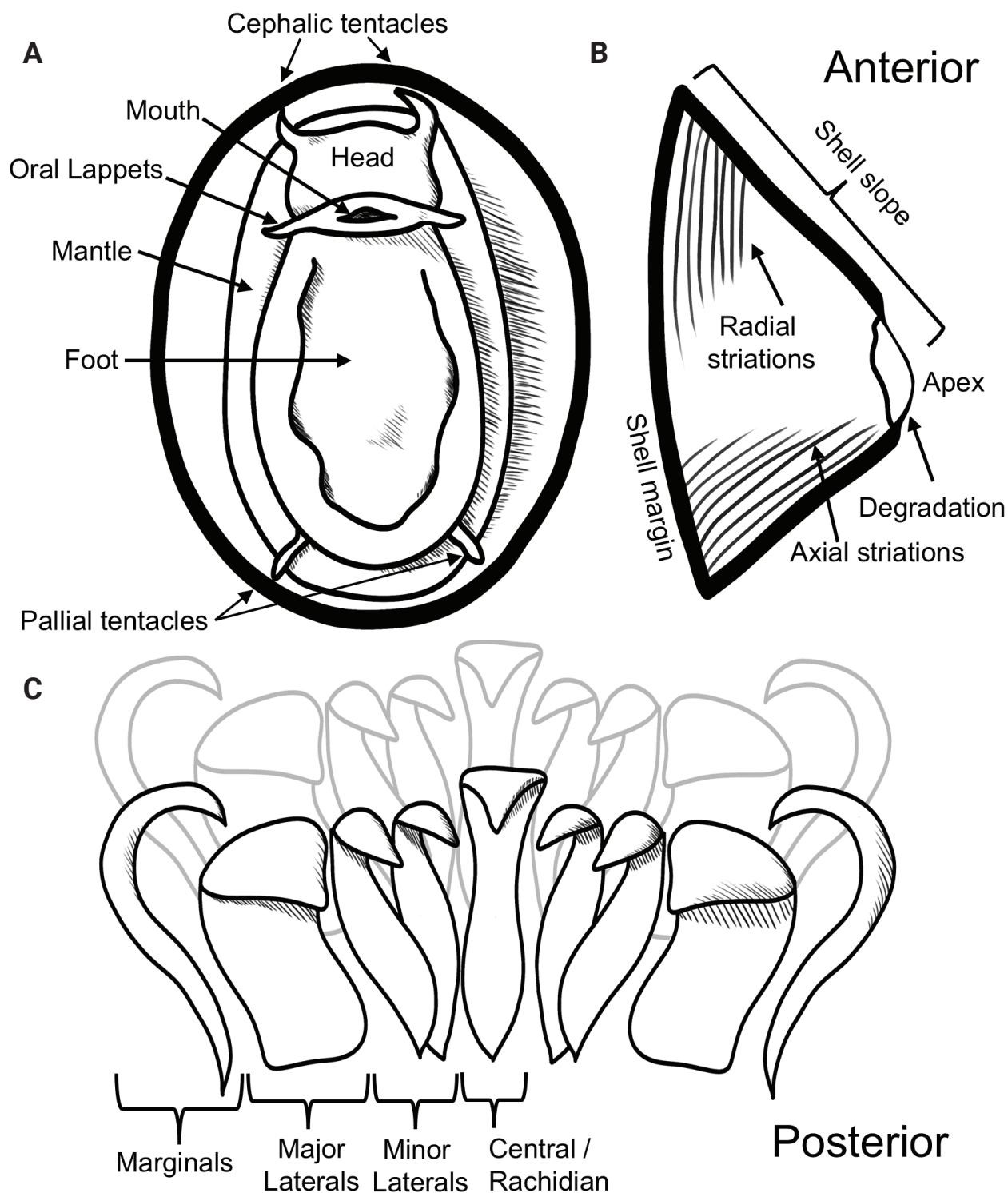
Figure 2. Selected character definitions for limpet **A** soft tissue **B** shells, and **C** radular teeth.

Qiagen Blood & Tissue DNA Extraction kit (QIAGEN, Valencia, CA). Extracts of DNA were obtained, quantitated using a Nanodrop 2000 spectrophotometer, and stored at -20 °C. A 710 base pair (bp) section of the mitochondrial cytochrome oxidase 1 (CO1) gene was targeted for sequencing using the primer pair LCO1490/HCO2198 (Folmer et al. 1994). A 275 bp section of the nuclear histone-3 (H3) gene was also targeted for sequencing using the primer pairs H3F/H3R or H3NF/H3NR (Colgan et al. 2000). Exact reaction conditions varied

across polymerase chain reactions (PCR) (Suppl. material 1). Forward and reverse sequence reads were obtained from PCR products through GeneWiz (Azenta Life Sciences, South Plainfield, NJ), then cleaned and quality-assured using BioEdit (v. 7.2.5; Hall 1999). Reverse reads were reverse-complemented in MEGA-X (v. 10.2.6; Kumar et al. 2018) before all sequences were aligned using ClustalW (Thompson et al. 2003). One consensus sequence was then generated for each individual. Sequences were then run through NCBI's nucleotide basic local alignment tool (BLAST) to find highly similar sequences. Sequences that yielded BLAST results within the same genus were grouped and investigated together.

Nesting of CRM specimens within a particular family and genus was assessed using published sequences from hypothesized sister species, genera, families, as well as representative sequences from unrelated gastropod subclasses (outgroups). For each phylogenetic investigation, novel and published sequences were aligned using ClustalW embedded within MEGA-X and the best-fit substitution model was determined using the MEGA-X model finder based on the lowest Bayesian Information Criterion. Maximum likelihood (ML) phylogenies were computed within MEGA-X using 10,000 bootstrap replicates. Bayesian phylogenies were computed within the joint programs BEAUTi and BEAST (v. 1.10.4; Suchard et al. 2018) using a strict time clock, yule speciation process (Gernhard 2008), and random starting tree in all cases. Unless otherwise stated, all other program settings were left as default. The maximum clade credibility tree was selected from the BEAST output using TreeAnnotator (v. 1.10.4) with 100,000 burn-in states. For both Bayesian and ML approaches, all base positions with less than 95% coverage were excluded from analyses. Resultant phylogenies were visualized using Fig. Tree (v. 1.4.4; Rambaut 2018) and finalized in Adobe Illustrator (v. 27.3.1). For the genus *Paralepetopsis*, which was particularly difficult to identify to species, we additionally employed the program Assemble Species by Automatic Partitioning (ASAP; Puillandre et al. 2021) to determine the number of likely species represented by our sequences. We also calculated average pairwise sequence distances between and within our sequences of *Paralepetopsis* using MEGA-X, a Jukes-Cantor substitution model, and the 95% pairwise deletion option.

Results

Morphological characterization

Nearly 4,000 limpets were collected from the Costa Rica Margin hydrocarbon seeps. All morphological characters are defined in Fig. 2. Two genera of patellogastropods were identified from the CRM: *Bathyacmaea* Okutani, Tsuchida & Fujikura, 1992 and *Paralepetopsis* McLean, 1990. Two morphotypes of *Bathyacmaea* were identified from the CRM: one inhabiting tubeworms (Fig. 3A−I), and one inhabiting mussel shells (Fig. 3J−O). Previous studies of *Bathyacmaea* have revealed substrate-dependent ecophenotypes within a single species (Chen et al. 2019), and it was thus considered a possibility that the two morphotypes identified here could constitute a single species. The specimens found on mussels most closely resembled the species *Bathyacmaea subnipponica* Sasaki, 2003 and *Bathyacmaea nipponica* Okutani, Tsuchida & Fujikura,

1992, while those found on tubeworms most closely resembled *Bathyacmaea kanesunosensis* Sasaki, 2003. Early radular teeth of this species were found to be morphologically distinct from either of the mature morphotypes (Fig. 3V).

Measurements of *Bathyacmaea* specimens (n = 52) across the entire, sampled size range at the CRM found divergent trends in growth between substrates culminating in the morphological differences observed between the two substrates (Fig. 4). Specimens from tubeworms (n = 33) grew relatively taller than those found on mussels (n = 19) as shell length increased (Fig. 4A; tubeworm specimens: m = 0.78 p < 0.001, R2 = 0.85; mussel specimens: m = 0.55, p < 0.001, R2 = 0.87). Specimens from tubeworms also became significantly more oblique as shell length increased (Fig. 4B; m = -0.02, p < 0.001, R2 = 0.33), while those from mussel shells stayed around a constant measure of roundness (0.78), regardless of size (Fig. 4B; p > 0.1).

Shell microstructures varied slightly between newer pieces of shell (Fig. 5A–C) and older pieces of shell (Fig. 5E–G). The outermost shell layers were formed of irregular spherulitic prismatic type-A (Fuchigami and Sasaki 2005; Sato et al. 2020), followed by semi-foliated structures, then by concentric crossed lamellar structures. In newer shell pieces, this concentric crossed lamellar structure was interspersed with bands of radial crossed lamellar structures (Fig. 5B,C), which were absent in older shell pieces (Fig. 5E, F).

Specimens identified as *Paralepetopsis* encompassed an abundance of individuals and a wide variety of shell morphotypes, making sorting and identification difficult. All *Paralepetopsis* at the CRM exhibited white, semi-translucent shells and apexes that were consistently degraded and anteriorly offset (Figs 6, 7). Specimens were variable in many aspects of their morphology, including their shell sculpturing, the flatness of their shell margins, their shell slopes, and the shape and coloration of their soft tissues (Figs 6, 7). Some shells displayed axial sculpturing with minute beading (Fig. 6J, K), resembling their sister genus *Neolepetopsis* McLean, 1990. However, as later reported, genetic results consistently distinguished our specimens from members of *Neolepetopsis*. While radulae were not attained for all shell morphotypes identified (Fig. 7), radulae that were successfully examined showed consistency in their tooth shape and configuration (Fig. 6S–V). Subtle variations in morphology were also observed; The first major lateral teeth were found to be set at noticeably different angles depending on the individual and potentially the substrate. The erosion of the marginal teeth also varied between individuals, potentially due to differences in age or wear.

Two genera of vetigastropods were identified from the CRM: *Pyropelta* McLean & Haszprunar, 1987 and *Lepetodrilus* McLean 1988. Specimens of *Pyropelta* were very small, with shells that were slightly ovate, semi-translucent, and that exhibited centrally located apexes of variable height (Fig. 8A). These specimens most closely resembled *P. corymba* McLean, 1992 or *P. musaica* McLean & Haszprunar, 1987, depending on their shell apex height. Soft tissue had a pinkish hue with two short, posterior epipodial tentacles and two cephalic tentacles (Fig. 8A). Radulae closely resembled those of a *P. corymba* specimen that was previously characterized from a Guaymas Basin hydrothermal vent (McLean 1992).

Morphological characterization of the vetigastropod genus *Lepetodrilus* yielded two distinct morphotypes. One morphotype matched the shell

description of *L. guaymasensis* McLean, 1988 which displayed ovate apertures, variable shell heights, anterior narrowing of the shell and apexes which were very posteriorly shifted such that some overhung the posterior margin of the shell (Fig. 9A–F). The second morphotype had rounded apertures, low shell profiles, posteriorly shifted apexes that were more diminished than the preceding morphotype, three epipodial tentacles, and brown periostraca (Fig. 9G–M); These most closely resembled the species *L. shannonae* Warén & Bouchet, 2009. Radulae obtained from this second morphotype most closely resembled those of *L. guaymasensis* but had central and first lateral teeth that were distinct in shape (Fig. 9N, O).

Finally, one morphotype within the Neomphaliones genus *Cocculina* Dall, 1882 was identified. Specimens of *Cocculina* from the CRM had ovate apertures, moderately rounded shell margins, central shell apexes, and a golden-brownish periostracum (Fig. 10A, B, D, E). These shells most closely resembled those of *Cocculina japonica* Dall, 1907. Notably, the periostracum of these specimens corroded significantly with prolonged ethanol preservation (Fig. 10G, H). Radulae of these specimens most closely resembled those of *C. cowani* McLean, 1987 but with distinct central teeth that form a narrow, defined ridge down the center of the radula (Fig. 10I, J).

Genetic characterization

Individuals representing the full diversity of morphotypes collected were genetically barcoded for the mitochondrial cytochrome oxidase I (CO1) gene (*n* = 63) and the histone-3 (H3) gene (*n* = 19) (Table 1). All CO1 sequences generated were deposited in GenBank via NCBI under the accession numbers OQ644569–OQ644631. All H3 sequences generated were deposited under the accession numbers Q658576–OQ658595.

From the Patellogastropods, specimens identified as *Bathyacmaea* Okutani, Tsuchida & Fujikura, 1992 were sequenced for CO1 (*n* = 4) and H3 (*n* = 2), evenly divided between mussel shell and tubeworm substrates (Table 1). Phylogenetic analyses supported their inclusion within the subclass Patellogastropoda (CO1: 100 (Bayesian Posterior Probability (BPP); H3: 100 (BPP)), the family Pectinodontidae (CO1: 100 (BPP)), and the genus *Bathyacmaea* (CO1: 100 (BPP), 95 (Bootstrap Likelihood (ML)); H3: 99 (BPP), 82 (ML)) (Fig. 11A, B). CO1 sequences from the tubeworm and mussel morphotypes showed minimal pairwise genetic divergence from one another (<2%). Our novel sequences were verified as being distinct from all other published *Bathyacmaea* sequences but were most similar to *B. nipponica* (GenBank Accession = MK341688; CO1 Percent Identity = 93.74%).

Specimens identified as *Paralepetopsis* McLean, 1990 were sequenced for CO1 (*n* = 33) and H3 (*n* = 6; Table 1). Phylogenetic analyses supported these specimens' inclusion within the subclass Patellogastropoda (CO1: 100 (BPP); H3: 100 (BPP)), the family Neolepetopsidae (CO1: 100 (BPP), 90 (ML)), and the genus *Paralepetopsis* (CO1: 100 (BPP), 90 (ML); H3: 100 (BPP), 91 (ML)) (Fig. 12A, B). Contrary to what was expected given their observed shell morphologies, no specimens grouped within the sister genus *Neolepetopsis* McLean, 1990. Our novel sequences were verified as being distinct from all other published *Paralepetopsis* sequences besides one (GenBank accession number

Table 1. Overview of gastropod limpet specimens collected from the Costa Rica Margin. Accession numbers refer to records in the NCBI Nucleotide Database (GenBank). Substrate abbreviations: B = Bone, C = Clams, M = Mussel, R = Rock, T = Tubeworm, W = Wood. Equipment dive number abbreviations: SD = Remotely operated vehicle SUBASTIAN dive, AD = human-operated vehicle Alvin dive. * = Locality not depicted on the region map in Fig. 1 (coordinates: 9.65, -85.88). ** = Cryptic species; only data from confirmed clade members are reported.

Genus	Total	Sites	Representative Sequence Accession Numbers			Depth	Substrate	Equipment dives
			Mound 12	Jaco Scar	Quepos Seep			
Bathyacmaea levinae sp. nov. (mussel) Holotype: SIO-BIC M22535	33	Jaco Scar	NA	CO1: OQ644573, OQ644574. H3: OQ658577.	NA	1780–1820	M, R	SD214, AD4914, AD4977
Bathyacmaea levinae sp. nov. (tubeworm) Holotype: SIO-BIC M22535	74	Jaco Scar	NA	CO1: OQ644578, OQ644584. H3: OQ658580.	NA	1720–1820	T	AD4911, AD4915, AD4971, AD4972, AD4989
Cocculina methana sp. nov. Holotype: SIO-BIC M22533	64	Mound 12, Mound Jaguar*, Jaco Scar, Quepos Seep	NA	NA	CO1: OQ644628, OQ644629. H3: OQ658592, OQ658593	992–2000	T, W, B, C	SD230, AD4508, AD4913, AD4916, AD4924, AD4974
Lepetodrilus guaymasensis	765	Mound 12, Jaco Scar, The Thumb, Quepos Seep	CO1: OQ644589, OQ644591, OQ644592, OQ644593, OQ644594, OQ644595, OQ644596, OQ644602, OQ644603, OQ644604, OQ644605, OQ644611. H3: OQ658586, OQ658587	CO1: OQ644590, OQ644606. H3: OQ658585.	CO1: OQ644607, OQ644609, OQ644610.	990–1820	T, M, R	SD214, SD217, AD4511, AD4912, AD4915, AD4917, AD4922, AD4977, AD4984, AD4987
Pseudolepetodrilus costaricensis gen. et sp. nov. Holotype: SIO-BIC M22534	10	Jaco Scar	NA	CO1: OQ644586, OQ644587, OQ644588. H3: OQ658582, OQ658583, OQ658584.	NA	1760	T	AD4989
Paralepetopsis (all specimens)	>1420	Mound 12, Jaco Scar, The Thumb, Quepos Seep	See below	See below	See below	990–1820	T, M, R, C	AD4513, AD4908, AD4915, AD4916, AD4917, AD4922, AD4923, AD4971, AD4972, AD4977, AD4978, AD4984, AD4985, AD4987
Paralepetopsis variabilis sp. nov. Clade 1** Holotype: SIO-BIC M22537	**	Mound 12, Jaco Scar	CO1: OQ644571, OQ644572, OQ644580, OQ644581, OQ644582, OQ644585, OQ644597, OQ644598, OQ644601, OQ644614, OQ644615, OQ644622, OQ644623, OQ644624. H3: OQ658589.	CO1: OQ644612, OQ644616, OQ644617.	NA	995–1741	T, M	AD4501, AD4908, AD4916, AD4922, AD4978, AD4984, AD4985, AD4987
Paralepetopsis variabilis sp. nov. Clade 2** Holotype: SIO-BIC M22537	**	Mound 12, Jaco Scar	CO1: OQ644579, OQ644569, OQ644576.	CO1: OQ644618, OQ644620, OQ644619. H3: OQ658590.	NA	998–1796	T, M	AD4915, AD4922, AD4971
Paralepetopsis variabilis sp. nov. Clade 3** Holotype: SIO-BIC M22537	**	Jaco Scar	NA	CO1: OQ644625, OQ644626, OQ644627, OQ644583, OQ644613, OQ644575. H3: OQ658578.	NA	1783–1796	T, M	AD4915, AD4971, AD4972, AD4977
Paralepetopsis sp. Clade 4**	**	Mound 12, Jaco Scar	CO1: OQ644599	CO1: OQ644570. H3: OQ658576.	NA	998–1724	T, M	AD4908, AD4971

Genus	Total	Sites	Representative Sequence Accession Numbers			Depth	Substrate	Equipment dives
			Mound 12	Jaco Scar	Quepos Seep			
Paralepetopsis sp. Clade 5**	**	Jaco Scar	NA	CO1: OQ644577, OQ644621. H3: OQ658579, OQ658591.	NA	1783–1796	M	AD4971, AD4977
Pyropelta corymba	1692	Mound 12, The Thumb	CO1: OQ644600, OQ644608, OQ644630, OQ644631. H3: OQ658588, OQ658594, OQ658595	NA	NA	995–1080	T, M, R	SD217, AD4908, AD4917, AD4922, AD4978, AD4984

KY581541; CO1 Percent Identity = 98%) obtained from an undescribed species from a Pescadero Basin hydrothermal vent.

It was difficult to discern the number of discrete species represented by our specimens of *Paralepetopsis*. To clarify this number, automatic hierarchical partitioning based on the mitochondrial CO1 gene was performed. Hierarchical clustering supported the existence of seven distinct subsets within our *Paralepetopsis* genetic dataset, with a threshold distance of 0.025 and a grouping distance of 0.043 (Fig. 13; $p < 0.01$). While this partitioning pattern was significant, two pairs of subsets could not be confidently distinguished from panmictic populations (Fig. 13; clades 4.1 and 4.2; clades 5.1 and 5.2; Puillandre et al. 2021). Notably, these four subsets were represented by only one sequence each. Thus, we collapsed these four subsets into two, conservatively designating five distinct clades from our results.

Pairwise sequence distances were then computed among these five conservative clades for both CO1 and H3 sequences. Sequence distances for CO1 fell between 5–13.6% and between 0–1.5% for H3 (Table 2). Clades 1–3 were not distinguishable based on H3 (0% for all pairs). For CO1, within-clade distances for clades 1–3 fell between 0.2–0.5% while between-clade distances fell between 5–7%. Within-clade distances for clades 4 and 5 were 4.6% and 5.4%, respectively. Thus, within-clade variation for clades 4 and 5 was comparable to the between-clade variation seen between clades 1, 2, and 3 (5% pairwise sequence divergence). These data dictate that one should either designate three distinct species (clades 1–3, 4, and 5) or designate seven distinct species (clades 1, 2, 3, 4.1, 4.2, 5.1, and 5.2). For the sake of being conservative in our delineations and given these clades' morphological flexibility, overlapping distributions, and low H3 divergence, we opt for the former option and designate

Table 2. The number of base substitutions per site from averaging over all sequences of *Paralepetopsis*. Analyses were conducted using the Jukes-Cantor substitution model, a gamma distribution rate of variation among sites, and pairwise deletion between sequence pairs. Cytochrome oxidase I distances between clades are given below the periphery ($n = 32$ sequences). Cytochrome oxidase I distances within clades are given at the periphery. Histone-3 distances between clades are given above the periphery ($n = 6$ sequences). Standard errors are given in parentheses and were estimated using 1,000 bootstrap replicates.

	Clade 1	Clade 2	Clade 3	Clade 4	Clade 5
Clade 1	0.003 (0.001)	0.000 (0.000)	0.000 (0.000)	0.006 (0.004)	0.015 (0.006)
Clade 2	0.067 (0.013)	0.005 (0.002)	0.000 (0.000)	0.006 (0.004)	0.015 (0.006)
Clade 3	0.050 (0.011)	0.050 (0.011)	0.002 (0.001)	0.006 (0.004)	0.015 (0.006)
Clade 4	0.107 (0.167)	0.111 (0.018)	0.108 (0.017)	0.046 (0.011)	0.015 (0.006)
Clade 5	0.120 (0.018)	0.136 (0.021)	0.127 (0.018)	0.121 (0.015)	0.054 (0.010)

three distinct species among our *Paralepetopsis* specimens. Unfortunately, due to a shortage of representatives for clades 4 and 5, radulae and morphological variations were unable to be fully characterized, precluding formal description.

For the vetigastropods, specimens identified as *Pyropelta* McLean & Haszprunar, 1987 were sequenced for CO1 (*n* = 4) and H3 (*n* = 3). These sequences supported these specimens' inclusion within Vetigastropoda (CO1: 100 (BPP); H3: 100 (BPP)), and within the genus *Pyropelta* (CO1: 100 (BPP), 54 (ML); H3: 66 (BPP), 54 (ML)) (Fig. 14A, B). Genetic affinity to *P. corymba* and *P. musaica*, the species that ours most morphologically resembled, could not be assessed due to a lack of available sequences on GenBank. However, our sequences were nonetheless verified as being distinct from all other published *Pyropelta* sequences and were most similar to an unidentified species from the Gulf of Mexico (GenBank Accession = FJ977753; CO1 Percent Identity = 89.4%). Our novel CO1 sequences showed minimal pairwise genetic divergence from one another (< 1%).

The two morphotypes identified as *Lepetodrilus* McLean, 1988 were genetically characterized and supported as being within the superfamily Vetigastropoda (CO1: 100 (BPP); H3: 100 (BPP)) and the family Lepetodrilidae (CO1: 100 (BPP), 93 (ML); H3: 100 (BPP), 95 (ML)). One morphotype nested within the genus *Lepetodrilus* (CO1: 100 (BPP), 99 (ML); H3: 100 (BPP), 96 (ML)) and among the species *L. guaymasensis* with high confidence (CO1: 100 (BPP), 100 (ML)) (Fig. 15A, B). *Lepetodrilus guaymasensis* is a known species from the CRM matching the physical descriptions of our specimens, and thus this genetic affinity was expected (Johnson et al. 2008; GenBank accession number EU306419; CO1 Percent Identity = 100%). These novel CO1 sequences showed minimal pairwise genetic divergence from one another (< 1%).

The second morphotype, however, nested within the family Lepetodrilidae (CO1: 100 (BPP), 93 (ML); H3: 100 (BPP), 95 (ML)), but were excluded from the genus *Lepetodrilus* (CO1: 100 (BPP), 93 (ML); H3: 100 (BPP), 95 (ML)), despite morphological similarities. They were also excluded from all other Lepetodrilid genera (Fig. 14A, B). These sequences were verified as being distinct from all other published Lepetodrilidae sequences besides one unidentified specimen on GenBank (GenBank Accession number KJ566949; CO1 Percent Identity = 94.4%). These novel CO1 sequences showed minimal pairwise genetic divergence from one another (< 1%).

Finally, the Neomphaliones genus *Cocculina* Dall, 1882 was sequenced for CO1 (*n* = 2) and H3 (*n* = 2) (Table 1). Genetic characterization of these specimens supported their inclusion within the subclass Neomphaliones (CO1: 100 (BPP), 97 (ML); H3: 72 (BPP), 57 (ML)), the family Cocculinidae (CO1: 100 (BPP), 78 (ML)), and the genus *Cocculina* (CO1: 100 (BPP), 87 (ML); H3: 97 (BPP), 67 (ML)). (Fig. 16A, B). Pairwise distances between our CO1 sequences were found to be very low (< 2%). Our novel sequences were verified as being distinct from all other published *Cocculina* sequences but were most similar to *C. japonica* (GenBank accession number OL801181; CO1 Percent Identity = 88.4%).

Institution codes

SIO-BIC	Scripps Institute of Oceanography Benthic Invertebrate Collection
MZUCR	Museo de Zoología de la Universidad de Costa Rica
EC	Erik Cordes, Personal Collection at Temple University

New species and records

Subclass Patellogastropoda
Family Pectinodontidae Pilsbry, 1891
Genus *Bathyacmaea* Okutani, Tsuchida & Fujikura, 1992

***Bathyacmaea levinae* sp. nov.**
https://zoobank.org/3ACA68B0-D822-4518-BC96-F6345718B7D9
Fig. 3

Type material examined. *Holotype.* Costa Rica • whole organism; ethanol-fixed; Original label: "*Bathyacmaea levinae* holotype, 1, whole organism, AD4971, Costa Rica Margin, Jaco Scar, 9.11785, -84.8407, 1800 m, from tubeworms."; SIO-BIC M22535. *Paratypes:* • Same data as for holotype. Original label: "*Bathyacmaea levinae* paratype, 1, whole organism, AD4971, Costa Rica Margin, Jaco Scar, 9.11785, -84.8407, 1800m, from tubeworms.". SIO-BIC M22536. Costa Rica • 2 specimens; same data as for holotype; Original label: "*Bathyacmaea levinae* paratype, 2, whole organisms, AD4971, Costa Rica Margin, Jaco Scar, 9.11785, -84.8407, 1720–1820 m, from tubeworms."; MZUCR10674-01-02. Costa Rica • 2 specimens; Costa Rica Margin, Quepos Seep, 9.03174, -84.62158; hydrocarbon seep; mussels; 1,409 m; 7 June 2017; AT37-13 ALVIN Dive 4924 leg.; Paratype; whole organism; ethanol-fixed; Original label: "*Bathyacmaea levinae* paratype, 2, whole organisms, AD4924, Costa Rica Margin, Quepos Seep, 9.03174, -84.62158, 1409 m, from mussels."; SIO-BIC M22532. Costa Rica • 2 specimens; Costa Rica Margin, Quepos Seep, 9.03174, -84.62158; hydrocarbon seep; mussels; 1,409 m; 7 June 2017; AT37-13 ALVIN Dive 4924 leg.; Paratype, whole organism; ethanol-fixed; Original label: "*Bathyacmaea levinae* paratype, 2, whole organisms, AD4924, Costa Rica Margin, Quepos Seep, 9.03174, -84.62158, 1409 m, from mussels."; MZUCR10672-02-03.

Type locality. Costa Rica • Costa Rica Margin, Jaco Scar, 9.11785, -84.8407; hydrocarbon seep; tubeworms; 1,720–1,820 m; 17 October 2018; AT42-03 ALVIN Dive 4971 leg.

Other material examined. Costa Rica • 5 specimen(s); Costa Rica Margin, Jaco Scar; 9.117375, -84.8397; 1,811 m; 26 May 2017; AT37-13 ALVIN Dive 4911 leg.; Tubeworm, Erik Cordes Personal Collection (EC) 5739 • 5 specimen(s); Costa Rica Margin, Jaco Scar; 9.117375, -84.8397; 1,794 m; 29 May 2017; AT37-13 ALVIN Dive 4914 leg.; Mussel, EC5760 • 1 specimen(s); Costa Rica Margin, Jaco Scar; 9.11753, -84.83953; 1,886 m; 29 May 2017; AT37-13 ALVIN Dive 4914 leg.; Mussel, Scripps Benthic Invertebrate Collection (SIO-BIC) M16154 • 5 specimen(s); Costa Rica Margin, Jaco Scar; 9.117368, -84.839661; 1,796 m; 30 May 2017; AT37-13 ALVIN Dive 4915 leg.; Tubeworm, EC5815 • 10 specimen(s); Costa Rica Margin, Quepos Seep; 9.03048, -84.6202; 1,409 m; 7 June 2017; AT37-13 ALVIN Dive 4924 leg.; SIO-BIC M16201 • 10 specimen(s); Costa Rica Margin, Quepos Seep; 9.03048, -84.6202; 1,409 m; 7 June 2017; AT37-13 ALVIN Dive 4924 leg.; SIO-BIC M16179 • 10 specimen(s); Costa Rica Margin, Jaco Scar; 8.97043, -84.8429167; 1,724 m; 17 October 2018; AT42-03 ALVIN Dive 4971 leg.; Tubeworm, EC7745 • 10 specimen(s); Costa Rica Margin, Jaco Scar; 8.97043, -84.8429167; 1,724 m; 17 October 2018; AT42-03 ALVIN Dive 4971 leg.; Tubeworm, EC7420 • 10 specimen(s); Costa Rica Margin, Jaco Scar; 8.97043, -84.8429167; 1,724 m; 17 October 2018; AT42-03 ALVIN Dive
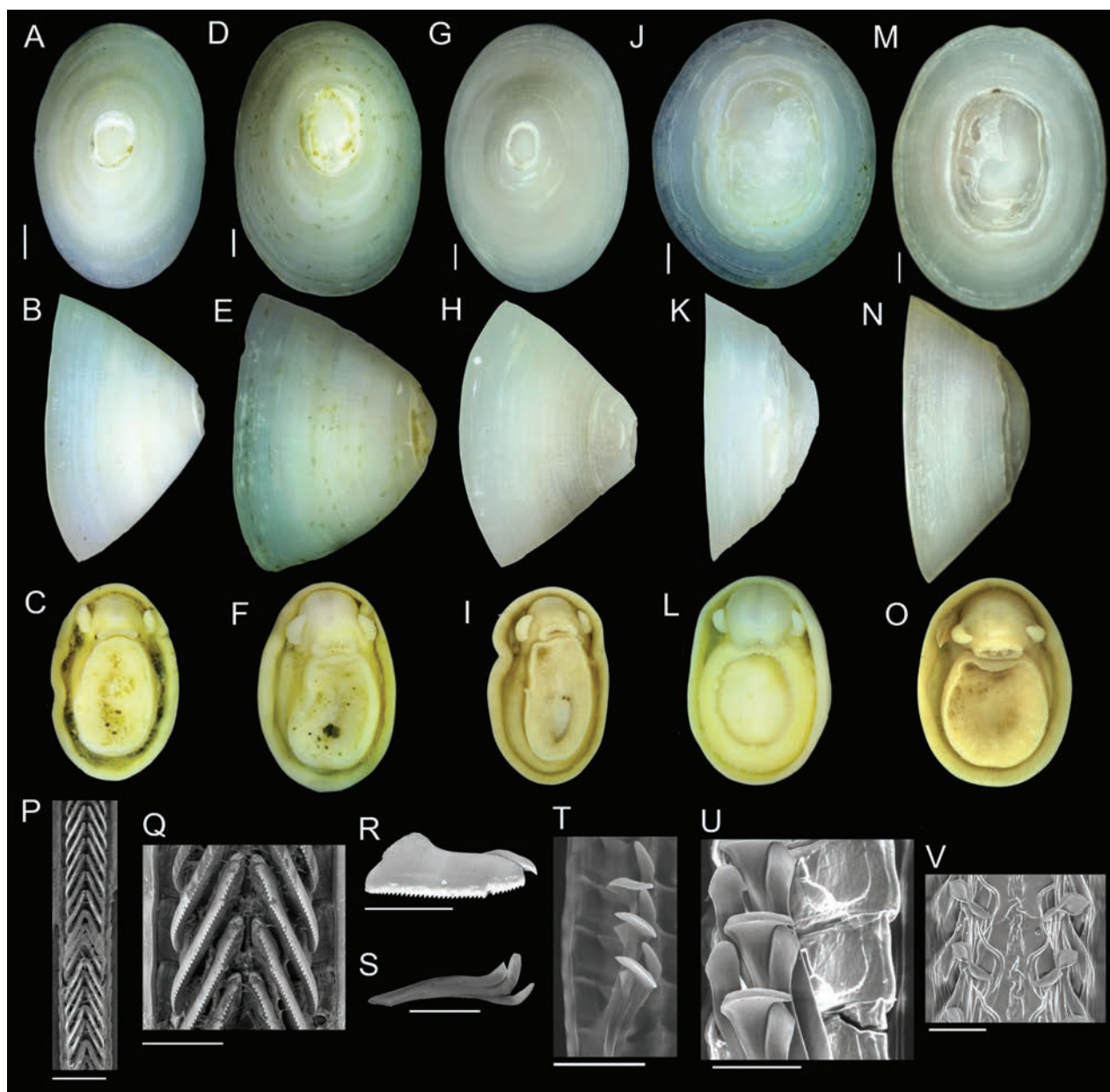
Figure 3. *Bathyacmaea levinae* sp. nov. **A–C** holotype from tubeworms at Jaco Scar, 1,724 m, AD4971, 17 October 2018 **D–F** paratype from tubeworms at Jaco Scar, 1,724 m, AD4971, 17 October 2018 **G–I** Sequenced specimen (GenBank Accession #OQ644578) from tubeworms at Jaco Scar, 1,760 m, AD4989, 4 November 2018 **J–L** paratype from mussels at Quepos Seep, 1,409 m, AD4924, 7 June 2017 **M–O** sequenced specimen (GenBank Accession #OQ644573) from mussels at Jaco Scar, 1,783 m, AD4977, 23 October 2018 **P** radula from specimen sampled from tubeworms **Q** closer view of the same radula **R** isolated radular tooth **S** isolated radular tooth from specimen sampled from mussels **T, U** radula from specimen sampled from mussels **V** under-developed (young) section of radula from the same specimen. Scale bars: 1 mm (**A–O**); 250 µm (**P**); 100 µm (**Q–T**); 50 µm (**U**);100 µm (**V**).

4971 leg.; Tubeworm, EC7419 • 1 specimen(s); Costa Rica Margin, Jaco Scar; 9.117433333, -84.83961667; 1,796 m; 17 October 2018; AT42-03 ALVIN Dive 4971 leg.; Tubeworm, SIO-BIC M16731 • 10 specimen(s); Costa Rica Margin, Jaco Scar; 8.97071, -84.8372817; 1,785 m; 18 October 2018; AT42-03 ALVIN Dive 4972 leg.; Tubeworm, EC7336 • 10 specimen(s); Costa Rica Margin, Jaco Scar; 8.97071, -84.8372817; 1,785 m; 18 October 2018; AT42-03 ALVIN Dive 4972 leg.; Tubeworm, EC7320 • 1 specimen(s); Costa Rica Margin, Jaco Scar;
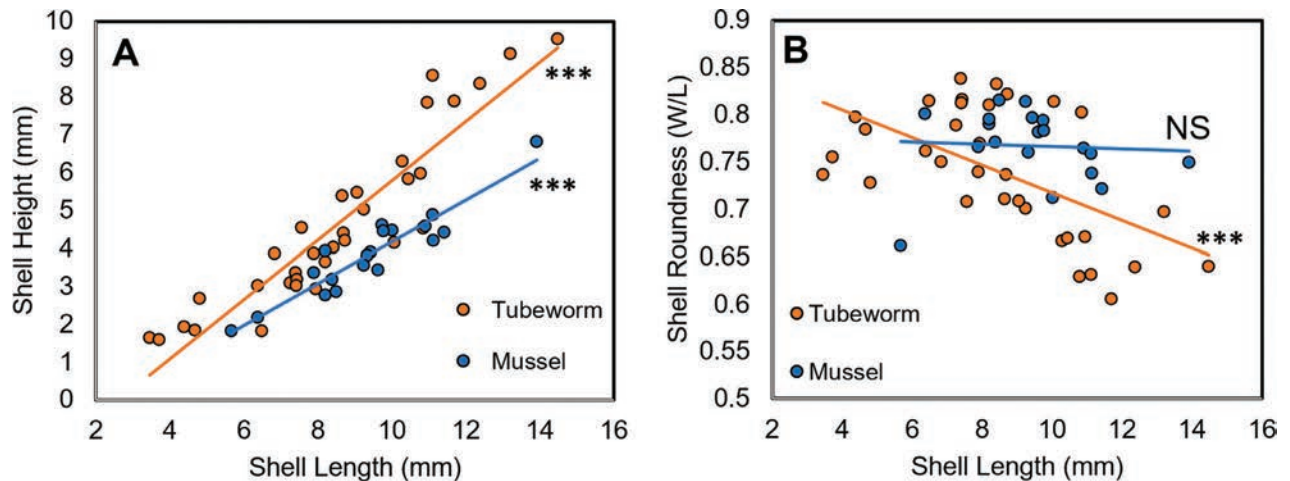
Figure 4. Divergent trends in growth among *Bathyacmaea levinae* sp. nov. Data from 52 individuals (Tubeworm, *n* = 33; Mussel, *n* = 19) are shown **A** specimens found on tubeworms become taller than those found on mussels as they grow, despite being similar in height at smaller sizes **B** specimens found on tubeworms become less round as they grow (*m* = -0.015, p < 0.001), while specimens found on mussels remain approximately the same roundness regardless of size (p > 0.1).

9.11735, -84.83958333; 1,795 m; 18 October 2018; AT42-03 ALVIN Dive 4972 leg.; Tubeworm, SIO-BIC M16795 • 1 specimen(s); Costa Rica Margin, Jaco Scar; 9.11785, -84.83952833; 1,784 m; 19 October 2018; AT42-03 ALVIN Dive 4973 leg.; Tubeworm, SIO-BIC M16748 • 10 specimen(s); Costa Rica Margin, Jaco Scar; 8.97067, -84.839533; 1,783 m; 23 10 2018; AT42-03 ALVIN Dive 4977 leg.; Mussel, EC7548 • 11 specimen(s); Costa Rica Margin, Jaco Scar; 9.117567, -84.840718; 1,760 m; 4 November 2018; AT42-03 ALVIN Dive 4989 leg.; Tubeworm, EC8894 • 1 specimen(s); Costa Rica Margin, Jaco Scar; 9.117783333, -84.83945; 1,783 m; 4 November 2018; AT42-03 ALVIN Dive 4989 leg.; Rock, SIO-BIC M16943 • 8 specimen(s); Costa Rica Margin, Quepos Seep; 9.031816667, -84.62048333; 1,400 m; 5 November 2018; AT42-03 ALVIN Dive 4990 leg.; Mussel, SIO-BIC M17001 • 4 specimen(s); Costa Rica Margin, Quepos Seep; 9.031816667, -84.62048333; 1,400 m; 5 November 2018; AT42-03 ALVIN Dive 4990 leg.; Mussel, SIO-BIC M16988 • 2 specimen(s); Costa Rica Margin, Quepos Seep; 9.031816667, -84.62055; 1,401 m; 5 November 2018; AT42-03 ALVIN Dive 4990 leg.; Combined Slurp, SIO-BIC M16920 • 1 specimen(s); Costa Rica Margin, Jaco Scar; 9.1174, -84.839855; 1,803.1 m; 7 January 2019; FK19-0106 SUBASTIAN Dive 214 leg.; Rock, EC9345 • 1 specimen(s); Costa Rica Margin, Jaco Scar; 9.117775, -84.839525; 1,803 m; 7 January 2019; FK19-0106 SUBASTIAN Dive 214 leg.; Rock, EC9338 • 1 specimen(s); Costa Rica Margin, Jaco Scar; 9.1174, -84.839855; 1,803 m; 7 January 2019; FK19-0106 SUBASTIAN Dive 214 leg.; Rock, EC9337 • 1 specimen(s); Costa Rica Margin, Jaco Scar; 9.1174, -84.839855; 1,812.41 m; 7 January 2019; FK19-0106 SUBASTIAN Dive 214 leg.; Mussel, EC9323.

Diagnosis. From tubeworms, *Bathyacmaea levinae* sp. nov. may be diagnosed by their flat, serrated radular teeth and high, conical shells lacking any obvious axial sculpturing. On mussels, *Bathyacmaea levinae* sp. nov. may be diagnosed through the combination of their ovate, evenly sloped, flattened shells lacking any obvious axial sculpturing with their radular characteristics. At the time of publication, these are the only *Bathyacmaea* species known from the Eastern Pacific Ocean.
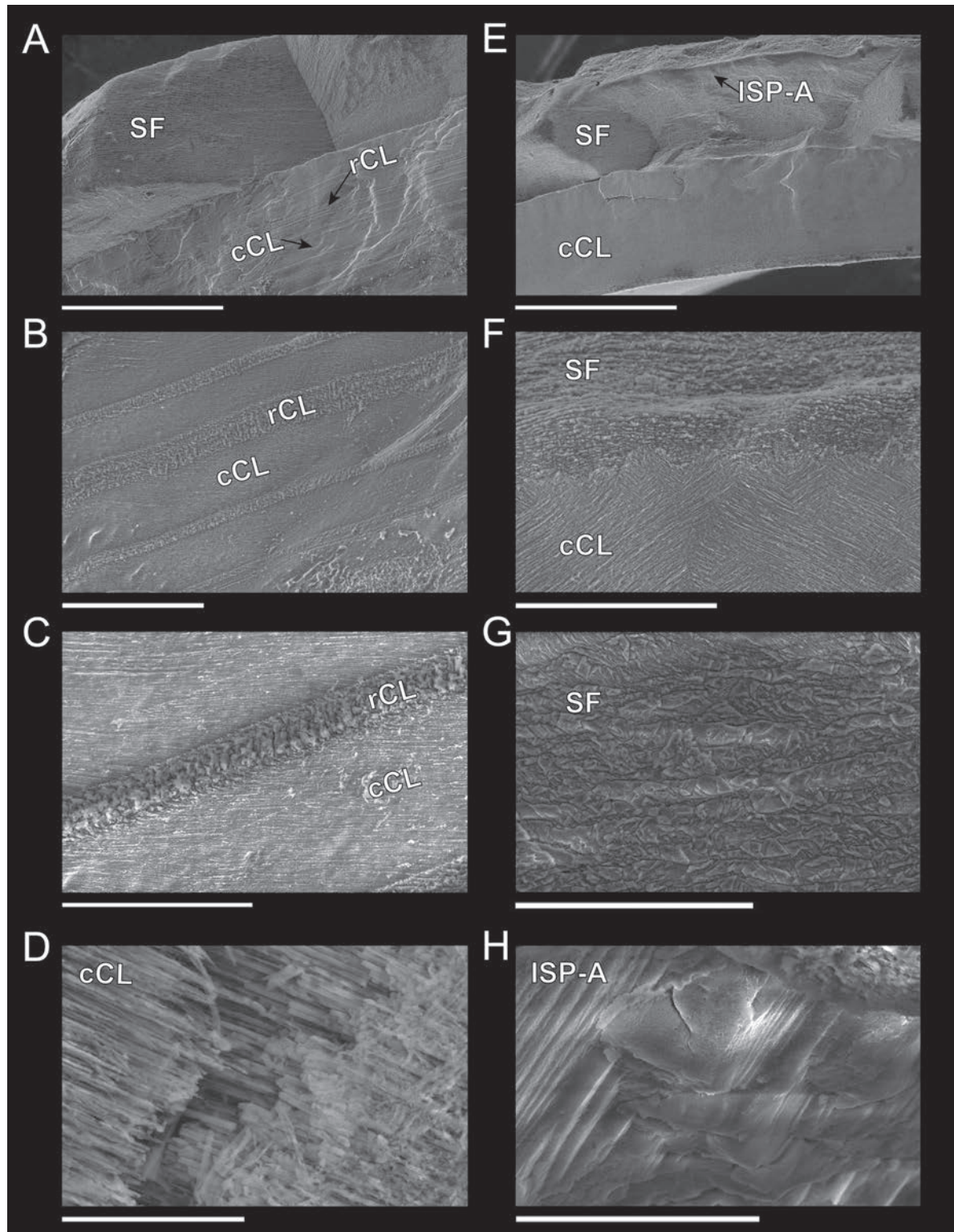
Figure 5. Shell microstructures of *Bathyacmaea levinae* sp. nov. from tubeworms at Jaco Scar, 1,785, October 2018. For all images, the outer shell is oriented to be at the top of the image, and the inner shell is at the bottom **A** cross section of newer shell (closer to the shell margin). Outermost layer shows semi-foliated structure, followed by alternating bands of crossed lamellar structure in concentric and radial orientations **B–D** close-up views of A **E** cross section of older shell (closer to the apex). Outermost layer shows irregular spherulitic prismatic type-A structure, followed by semi-foliated and concentric crossed lamellar structures **F–H** close-up views of E. Abbreviations: SF = semi-foliated structure, cCL = concentric crossed lamellar structure, rCL = radial crossed lamellar structure, ISP-A = spherulitic prismatic type-A structure. Scale bars: 300 µm (**A**); 50 µm (**B**); 20 µm (**C**); 10 µm (**D**); 300 µm (**E**); 40 µm (**F, G**); 5 µm (**H**).

Description. *Shell* (Figs 3A, B, 5): Specimens exhibit uncoiled, patelliform shells. Holotype measures 8.1 mm in length, 5.2 mm in width, and 4.7 mm in maximum height. Shell roundness (width ÷ length) is 0.65. Shell sculpturing and ornamentation lacking but fine radial growth lines are present. Very fine axial striations present but not raised. Aperture opening is ovate and aperture lip is thick and unornamented. Shell slope is flattened to mildly convex. Shell apex is degraded and centrally located. Protoconch is unknown. Shell is thick, white, and semi-translucent. Shell microstructures are (in order from the outermost shell layer to the innermost): irregular spherulitic prismatic type-A, semi-foliated, concentric crossed lamellar structures, and radial crossed lamellar structures (Fig. 5).

Soft parts (Fig. 3C): Soft tissue is white-to-yellowish in color. Mantle is thick with a flat margin. Foot follows the shape of the shell aperture in terms of its roundness. Margin of the foot sole is flat. Pallial tentacles are lacking. Operculum is absent. Two cephalic tentacles are present which are short, thick, and placed low on the head. Bipectinate gill extends from behind animal's right cephalic tentacle. Eyes are absent. Oral lappets are absent but the oral opening is lined with thickened tissue ornamented with very fine frilling.

Radula (Fig. 3P–R): Radula was obtained from the sequenced specimen (Fig. 3G–I), whose shell measured 10 mm in length, 7.0 mm in width, and 6.8 mm in height. Docoglossate radula with formula 0+1+0+1+0. Radular ribbon measures ~ 240 μm across. Rachidian teeth highly diminished and obscured by laterals. Lateral teeth are long, robust, and consisting of three distinct cusps that appear to be fused together. Lateral teeth may measure up to 400 μm in length. The first, most anterior, cusp forms a single sharp hook lacking denticle. The second cusp is longer than the first and falls in line with the third cusp such that it creates one continuous ridge. Eight or nine short, sharp denticles are present on this second cusp. The third, most posterior, cusp is the longest (~ 3 × the length of the second cusp) and forms a robust, serrated ridge with 25 or more short, sharp denticles that are indistinguishable from those on the second cusp. The third cusp's posterior end curves inward towards the radular ribbon. The connecting point of the lateral teeth to the radular ribbon is located near the posterior end of the third cusp. Marginal teeth lacking.

Variation. Two distinct morphotypes of *Bathyacmaea levinae* sp. nov. are herein identified: One inhabiting tubeworms (Fig. 3A–I), and one inhabiting mussel shells (Fig. 3J–O). Holotype description applies to specimens found on tubeworms. *Bathyacmaea levinae* sp. nov. found on mussel shells differ in that they exhibit rounder apertures, flatter shell margins, lower shell profiles, and greater apex erosion (Fig. 3J–N). Paratype specimens from mussel shells measure between 7.9–11.0 mm in length, 6.4–9.0 mm in width, and 3.0–4.5 mm in height. Measures of shell roundness (width ÷ length) for these paratypes are all between 0.81–0.85, distinguishing them from the roundness of the holotype (0.65).

Radulae of specimens found on mussels also differ (Fig. 3S–U). Formula remains 0+1+0+1+0 with tricuspid laterals, reduced rachidian teeth, and no marginals. All cusps of the lateral teeth are located at the very anterior end of a long, thin tooth shaft which connects to the radular ribbon at its far posterior end (Fig. 3S). The first, most anterior cusp of the lateral teeth is similar between morphotypes, being sharp, hooked, and lacking denticles. The second cusp of specimens found on mussels resembles the first cusp in terms of thickness, but with a blunt outer edge that lacks denticles and points forward (perpendicular to

the radular ribbon). The third, most posterior cusp is short, thick, lacking denticles, and is fused with the second cusp. This third cusp is truncated and forms a sharp barb which faces outwards when situated on the radular ribbon. Under-developed teeth of this species (Fig. 3V) further differ. Rachidian and minor lateral teeth are highly reduced; Reduced minor lateral teeth present as thin and strand-like with pointed anterior ends. Major laterals exhibit broad, un-serrated cusps whose outermost end is twisted backwards, forming a lemniscate shape. The first tooth cusp forms a sharp barb, similar to the mature radular tooth (Fig. 3S).

Distribution. *Bathyacmaea levinae* sp. nov. has been collected from the hydrocarbon seep sites "Jaco Scar" (9.12, -84.84) and "Quepos Seep" (9.03, -84.62) at the Pacific Costa Rica Margin. This species was sampled from both mussels and tubeworms between 1,400–1,890 m depth.

Remarks. Measurements of *Bathyacmaea levinae* sp. nov. across the entire, sampled size range at the CRM found divergent trends in growth between substrates culminating in the morphological differences observed (Fig. 4). These substrate-determined differences support previous studies that demonstrate radula and shell variability in *Bathyacmaea* (Chen et al. 2019). *Bathyacmaea levinae* sp. nov. found on mussels at the CRM most closely resemble the species *Bathyacmaea nipponica* Okutani, Tsuchida & Fujikura, 1992. However, *Bathyacmaea levinae* sp. nov. are genetically distinct from this species for both the mitochondrial CO1 gene and the nuclear histone-3 gene. Furthermore, the inner shell layers of *Bathyacmaea levinae* sp. nov. are comprised of concentric and radial crossed lamellar microstructures only, distinguishing them from *Bathyacmaea nipponica*, whose inner shell layers display an interspersion of semi-foliated microstructures and crossed lamellar structures (Sato et al. 2020). *Bathyacmaea levinae* sp. nov. from mussel shells also closely resemble *Bathyacmaea subnipponica* Sasaki, 2003, but lack its cancellated shell sculpture. *Bathyacmaea levinae* sp. nov. found on tubeworms most closely resemble *Bathyacmaea kanesunosensis* Sasaki, 2003, though its distribution is highly distinct from our specimens. Due to a lack of sequences published for *B. kanesunosensis*, their genetic distinction remains unknown. At the time of publication, *Bathyacmaea levinae* sp. nov. is the only *Bathyacmaea* species found in the Eastern Pacific.

Etymology. This species is named for Dr. Lisa A. Levin from Scripps Institute of Oceanography for her significant contribution to deep-sea knowledge, especially in regard to hydrocarbon seeps.

Family Neolepetopsidae McLean 1990
Genus *Paralepetopsis* McLean 1990

***Paralepetopsis variabilis* sp. nov.**
https://zoobank.org/BD92F9DD-83FD-4B3D-9883-950DDD9D0454
Fig. 6

Type material examined. *Holotype*. Costa Rica • whole organism; ethanol-fixed; Original label: "Paralepetopsis variabilis holotype, 1, whole organism, AD4987, Costa Rica Margin, Mound 12, 8.92982, -84.31167, 996 m, from tubeworms."; SIO-BIC M22537. *Paratypes*: Costa Rica • 9 specimens; same data as for holotype; Original label: "*Paralepetopsis variabilis* paratype, 9, whole organisms, AD4987, Costa Rica Margin, Mound 12, 8.92982, -84.31167, 996 m,

Figure 6. *Paralepetopsis variabilis* sp. nov. **A–C** holotype from tubeworms at Mound 12, 995 m, AD4987, 2 November 2018 **D–F** sequenced clade 3 specimen (GenBank Accession #OQ644613) from plastic chip deployment, Jaco Scar, 1,796 m, AD4915, 17 October 2018 **G–I** sequenced clade 1 specimen (GenBank Accession #OQ644624) from mussels at Mound 12, 997 m, AD4978, 24 October 2018 **J–L** sequenced clade 1 specimen (GenBank Accession # OQ644614) from unknown substrate at Mound 12, 1,008 m, AD4501, 22 February 2009 **M–O** sequenced clade 2 specimen (GenBank Accession # OQ644619) from tubeworms, Jaco Scar, 1,724 m, AD4971, 17 October 2018 **P–R** sequenced clade 1 specimen (GenBank Accession # OQ644571) from mussels at Mound 12, 995 m, AD4985, 31 October 2018 **S–V** details of radular ribbons. Scale bars: 1 mm (**A–R**); 40 µm (**S**); 20 µm (**T**); 40 µm (**U**); 50 µm (**V**).

from tubeworms."; SIO-BIC M22538. Costa Rica • 10 specimens; same data as for holotype; Original label: "*Paralepetopsis variabilis* paratype, 10, whole organisms, AD4987, Costa Rica Margin, Mound 12, 8.9298, -84.31167, 996 m, from tubeworms."; MZCR10675-01-10.

Type locality. Costa Rica • Costa Rica Margin, Mound 12, 8.92982, -84.31167; hydrocarbon seep; tubeworms; 996 m; 2 November 2018; AT42-03 ALVIN Dive 4987 leg.

Other material examined. Costa Rica • 11 specimen(s); Costa Rica Margin, Mound 11; 8.9208, -84.3054; 1,040 m; 25 February 2009; AT15-44 ALVIN Dive 4504 leg.; Tubeworm, SIO-BIC M11995 • 3 specimen(s); Costa Rica Margin, Jaco Scar; 9.1172, -84.8417; 1,866 m; 3 March 2009; AT15-44 ALVIN Dive 4509 leg.; SIO-BIC M12037 • 10 specimen(s); Costa Rica Margin, Mound 12; 8.9305, -84.3123; 1,001 m; 5 March 2009; AT15-44 ALVIN Dive 4511 leg.; SIO-BIC M12058 • 25 specimen(s); Costa Rica Margin, Mound 12; 8.93042, -84.31278; 999 m; 22 May 2017; AT37-13 ALVIN Dive 4907 leg.; SIO-BIC M16114 • 9 specimen(s); Costa Rica Margin, Jaco Scar; 9.11538, -84.83618; 1,859 m; 27 May 2017; AT37-13 ALVIN Dive 4912 leg.; SIO-BIC M16126 • 1 specimen(s); Costa Rica Margin, Jaco Scar; 9.11538, -84.83618; 1,859 m; 27 May 2017; AT37-13 ALVIN Dive 4912 leg.; SIO-BIC M16122 • 5 specimen(s); Costa Rica Margin, Jaco Scar; 9.117368, -84.839661; 1,796 m; 30 May 2017; AT37-13 ALVIN Dive 4915 leg.; Tubeworm, EC5815 • 3 specimen(s); Costa Rica Margin, Jaco Scar; 9.117368, -84.839661; 1,796 m; 30 May 2017; AT37-13 ALVIN Dive 4915 leg.; Tubeworm, EC5769 • 7 specimen(s); Costa Rica Margin, Jaco Scar; 9.117368, -84.839661; 1,796 m; 30 May 2017; AT37-13 ALVIN Dive 4915 leg.; Tubeworm, EC5731 • 49 specimen(s); Costa Rica Margin, Jaco Scar; 9.118023533, -84.84095552; 1,741 m; 31 May 2017; AT37-13 ALVIN Dive 4916 leg.; Tubeworm, EC5783 • 11 specimen(s); Costa Rica Margin, Jaco Scar; 9.1193, -84.84277; 1,854 m; 31 May 2017; AT37-13 ALVIN Dive 4916 leg.; SIO-BIC M16170 • 3 specimen(s); Costa Rica Margin, Mound 12; 8.930395, -84.3124245; 995 m; 1 June 2017; AT37-13 ALVIN Dive 4917 leg.; Tubeworm, EC5794 • 3 specimen(s); Costa Rica Margin, Mound 12; 8.9293, -84.315; 1,000 m; 1 June 2017; AT37-13 ALVIN Dive 4917 leg.; SIO-BIC M16161 • 81 specimen(s); Costa Rica Margin, Mound 12; 8.93046775, -84.31244503; 998 m; 5 June 2017; AT37-13 ALVIN Dive 4922 leg.; Mussel, EC5743 • 2 specimen(s); Costa Rica Margin, Quepos Seep; 9.03048, -84.6202; 1,409 m; 7 June 2017; AT37-13 ALVIN Dive 4924 leg.; SIO-BIC M16200 • 8 specimen(s); Costa Rica Margin, Quepos Seep; 9.03048, -84.6202; 1,409 m; 7 June 2017; AT37-13 ALVIN Dive 4924 leg.; SIO-BIC M16182 • 15 specimen(s); Costa Rica Margin, Quepos Seep; 9.03048, -84.6202; 1,409 m; 7 June 2017; AT37-13 ALVIN Dive 4924 leg.; SIO-BIC M16181 • 5 specimen(s); Costa Rica Margin, Jaco Scar; 8.97043, -84.8429167; 1,724 m; 17 October 2018; AT42-03 ALVIN Dive 4971 leg.; Tubeworm, EC7751 • 156 specimen(s); Costa Rica Margin, Jaco Scar; 8.97043, -84.8429167; 1,724 m; 17 October 2018; AT42-03 ALVIN Dive 4971 leg.; Tubeworm, EC7750 • 3 specimen(s); Costa Rica Margin, Jaco Scar; 8.97043, -84.8429167; 1,724 m; 17 October 2018; AT42-03 ALVIN Dive 4971 leg.; Tubeworm, EC7745 • 10 specimen(s); Costa Rica Margin, Jaco Scar; 8.97043, -84.8429167; 1,724 m; 17 October 2018; AT42-03 ALVIN Dive 4971 leg.; Tubeworm, EC7744 • 3 specimen(s); Costa Rica Margin, Jaco Scar; 8.97043, -84.8429167; 1,724 m; 17 October 2018; AT42-03 ALVIN Dive 4971 leg.; Tubeworm, EC10486 • 16 specimen(s); Costa Rica Margin, Jaco Scar; 8.97043, -84.8429167; 1,724 m; 17 October 2018; AT42-03 ALVIN Dive 4971 leg.; Tubeworm, EC10471 • 63 specimen(s); Costa Rica Margin, Jaco Scar; 9.117433333, -84.83961667; 1,796 m; 17 10 2018; AT42-03 ALVIN Dive 4971 leg.; SIO-BIC M16752 • 3 specimen(s); Costa Rica Margin, Jaco Scar; 9.117433333,

-84.83961667; 1,796 m; 17 October 2018; AT42-03 ALVIN Dive 4971 leg.; Rock, SIO-BIC M16733 • 123 specimen(s); Costa Rica Margin, Jaco Scar; 8.97071, -84.8373; 1,785 m; 18 October 2018; AT42-03 ALVIN Dive 4972 leg.; Tubeworm, EC7346 • 6 specimen(s); Costa Rica Margin, Jaco Scar; 8.97071, -84.8373; 1,785 m; 18 10 2018; AT42-03 ALVIN Dive 4972 leg.; Tubeworm, EC7343 • 25 specimen(s); Costa Rica Margin, Jaco Scar; 9.11785, -84.83728; 1,785 m; 18 October 2018; AT42-03 ALVIN Dive 4972 leg.; Tubeworm, EC7340 • 1 specimen(s); Costa Rica Margin, Jaco Scar; 9.11735, -84.83958333; 1,795 m; 18 October 2018; AT42-03 ALVIN Dive 4972 leg.; SIO-BIC M16796 • 37 specimen(s); Costa Rica Margin, Jaco Scar; 9.1178, -88.839533; 1,783 m; 23 October 2018; AT42-03 ALVIN Dive 4977 leg.; Mussel, EC7556 • 1 specimen(s); Costa Rica Margin, Jaco Scar; 9.11775, -84.83953333; 1,783 m; 23 October 2018; AT42-03 ALVIN Dive 4977 leg.; SIO-BIC M16805 • 64 specimen(s); Costa Rica Margin, Mound 12; 8.9308, -84.31263; 997 m; 24 October 2018; AT42-03 ALVIN Dive 4978 leg.; Mussel, EC10473 • 37 specimen(s); Costa Rica Margin, Mound 12; 8.9308, -84.31263; 997 m; 24 October 2018; AT42-03 ALVIN Dive 4978 leg.; Mussel, EC10472 • 425 specimen(s); Costa Rica Margin, Mound 12; 8.9307, -84.3128; 997 m; 30 October 2018; AT42-03 ALVIN Dive 4984 leg.; Mussel, EC8314 • 30 specimen(s); Costa Rica Margin, Mound 12; 8.9307, -84.3128; 997 m; 30 October 2018; AT42-03 ALVIN Dive 4984 leg.; Mussel, EC10477 • 20 specimen(s); Costa Rica Margin, Mound 12; 8.9307, -84.3128; 997 m; 30 October 2018; AT42-03 ALVIN Dive 4984 leg.; Mussel, EC10476 • 6 specimen(s); Costa Rica Margin, Mound 12; 8.9299, -84.31299; 995 m; 31 October 2018; AT42-03 ALVIN Dive 4985 leg.; Mussel, EC10478 • 100 specimen(s); Costa Rica Margin, Mound 12; 8.92983, -84.31167; 995 m; 2 November 2018; AT42-03 ALVIN Dive 4987 leg.; Tubeworm, EC8615 • 1 specimen(s); Costa Rica Margin, Jaco Scar; 9.117783333, -84.83944667; 1,785 m; 4 November 2018; AT42-03 ALVIN Dive 4989 leg.; SIO-BIC M16974 • 2 specimen(s); Costa Rica Margin, Jaco Scar; 9.117783333, -84.83944667; 1,785 m; 4 November 2018; AT42-03 ALVIN Dive 4989 leg.; SIO-BIC M16973 • 2 specimen(s); Costa Rica Margin, Quepos Seep; 9.031816667, -84.62048333; 1,400 m; 5 November 2018; AT42-03 ALVIN Dive 4990 leg.; Mussel, SIO-BIC M16995 • 2 specimen(s); Costa Rica Margin, Quepos Seep; 9.031816667, -84.62048333; 1,400 m; 5 November 2018; AT42-03 ALVIN Dive 4990 leg.; Mussel, SIO-BIC M16994 • 3 specimen(s); Costa Rica Margin, Quepos Seep; 9.031816667, -84.62048333; 1,400 m; 5 November 2018; AT42-03 ALVIN Dive 4990 leg.; Mussel, SIO-BIC M16991 • 1 specimen(s); Costa Rica Margin, The Thumb; 9.1174, -84.839855; 1,074 m; 7 January 2019; FK19-0106 SUBASTIAN Dive 214 leg.; Mussel, EC9348 • 10 specimen(s); Costa Rica Margin, The Thumb; 9.1174, -84.839855; 1,074 m; 7 January 2019; FK19-0106 SUBASTIAN Dive 214 leg.; Mussel, EC9328 • 1 specimen(s); Costa Rica Margin, The Thumb; 9.1174, -84.839855; 1,074 m; 7 January 2019; FK19-0106 SUBASTIAN Dive 214 leg.; Mussel, EC9327 • 1 specimen(s); Costa Rica Margin, The Thumb; 9.05, -84.4; 1,074 m; 10 January 2019; FK19-0106 SUBASTIAN Dive 217 leg.; Tubeworm, EC9480 • 1 specimen(s); Costa Rica Margin, The Thumb; 9.05, -84.4; 1,074 m; 10 January 2019; FK19-0106 SUBASTIAN Dive 217 leg.; Mussel, EC9468 • 1 specimen(s); Costa Rica Margin, The Thumb; 9.05, -84.4; 1,074 m; 10 January 2019; FK19-0106 SUBASTIAN Dive 217 leg.; Mussel, EC9451 • 1 specimen(s); Costa Rica Margin, The Thumb; 9.05, -84.4; 1,074 m; 10 January 2019; FK19-0106 SUBASTIAN Dive 217 leg.; Mussel, EC9434.

Diagnosis. *Paralepetopsis variabilis* sp. nov. may be diagnosed by their ovate, white, semi-translucent shells showing fine, radial growth rings. This species also exhibits two cephalic tentacles which are short (they do not extend past the outer shell margin) and placed low on the head. Soft tissue is whiteish-yellow in color. However, the most reliable way to diagnose *Paralepetopsis variabilis* sp. nov. is through DNA characterization, as morphology is highly variable within this species and intersects with other known species in the genus.

Description. *Shell* (Fig. 6A, B): Specimen exhibits uncoiled, patelliform shell. Holotype measures 6.8 mm in length, 4.1 mm in width, and 2.9 mm in maximum height. Shell roundness (width ÷ length) is ~ 0.61. Shell sculpturing and ornamentation lacking but fine radial growth lines are present. Aperture opening is ovate and aperture lip is thin and unornamented. Shell apex is degraded and anteriorly shifted. Anterior and posterior shell slopes are flattened to mildly convex. Shell is very thin, white, and semi-translucent.

Soft parts (Fig. 6C): Soft tissue is white to yellowish in color. Mantle is thick with a mildly crumpled margin. Foot follows the shape of the shell aperture in terms of its roundness. Margin of the foot sole is flat. Pallial tentacles are lacking. Operculum is absent. Two cephalic tentacles are present which are short, thick, and placed low on the head. Eyes are absent. Very reduced oral lappets are present, as well as thickened tissue around the mouth ornamented with very fine frilling. The animal's head has a slight brownish coloration and a high profile.

Radula (Fig. 6S): Docoglossate radula with formula 2+1+2+1+2+1+2. Rachidian teeth have long shapes, with large triangular cusps at their anterior ends lacking serration. Rachidian teeth are flanked on either side by a pair of minor lateral teeth that are similar in shape to the rachidian. These two minor laterals also have triangular cusps lacking serrations and are slightly rotated inwards. The third (major) lateral tooth is distinct from the other two laterals, in that its cusp is very broad, flat, and perpendicular to the radular ribbon with 9−13 small serrations along its edge. These serrations become less pronounced near the tooth's outer end. These major laterals are not in line with the others, being set slightly lower, approximately midway between the rows of rachidian and minor lateral teeth. There are two marginal teeth set on the outer edge and just below the major laterals. Marginals have very short, semi-lunate cusps that lack serrations. First outer marginals are ~ 2 × the size of the second outer marginals.

Variation. *Paralepetopsis variabilis* sp. nov. exhibits significant shell variation across specimens which makes distinguishing species based on morphology alone difficult. Shells may measure 5−10 mm with shell roundness varying between 0.6 and 0.8. While all specimens exhibit uncoiled, patelliform shells, specimens may exhibit axial sculpturing, radial sculpturing, both, or neither. Shell margins may vary in that they may be flat, convex, or rounded. Shell apexes were unanimously degraded and anteriorly shifted, but the degree of this erosion varies; Some shells have only the protoconch degraded, while others have the majority of their outer shell degraded. Anterior and posterior shell slopes may be flat or mildly rounded. Shells may be thickened, very thin, yellowish, white, or semi-translucent.

Radulae of this species are somewhat variable, with the third major lateral teeth being at noticeably different angles depending on the individual and, potentially, the substrate (Fig. 6S−V). The first major lateral teeth imaged
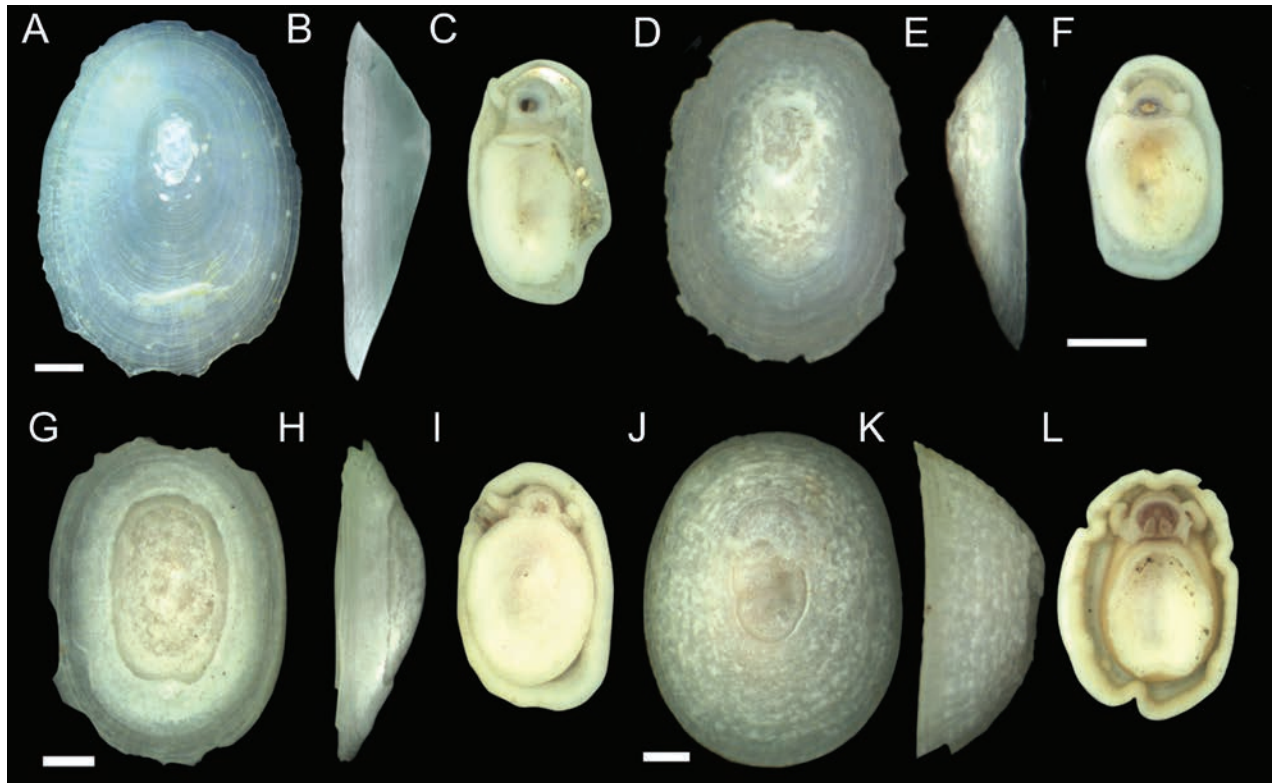
Figure 7. Specimens of *Paralepetopsis* representing clades 4 and 5 from Fig. 11 **A−C** clade 4 specimen (GenBank Accession # OQ644570) found on tubeworms, Jaco Scar, 1,724 m, AD4971, 17 October 2018 **D−F** clade 4 specimen (GenBank Accession # OQ644599) found on mussels, Mound 12, 998 m, AD4908, 23 May 2017 **G−I** clade 5 specimen (GenBank Accession # OQ644577) from mussels, Jaco Scar, 1,783 m, AD4977, 23 October 2018 **J−L** clade 5 specimen (GenBank Accession # OQ644621) from plastic chip deployments, Jaco Scar, 1,796 m, AD4971, 17 October 2018. Radulae were unattainable for all specimens. Scale bars: 1 mm.

from a specimen collected from tubeworms were perpendicular to the radular ribbon (Fig. 6S), those collected from plastic were comparatively rotated outwards (Fig. 6U), and those collected from mussels were comparatively rotated inwards (Fig. 6V). The presence or absence of marginal teeth also varies (Fig. 6T), which may be dependent on the amount of wear on the radula or the stage of radular tooth development. This hypothesis, however, requires further testing to validate.

The mantle and foot margins of specimens may vary from flat to crumpled. Coloration of soft tissues varies between specimens, with some exhibiting a distinct blue-to-purple pigmentation around the oral lappets, while others do not.

Distribution. *Paralepetopsis variabilis* sp. nov. has been collected from the hydrocarbon seep sites "Jaco Scar" (9.12, -84.84), "Quepos Seep" (9.03, -84.62), "Mound 11" (8.92, -84.31), and "Mound 12" (8.93, -84.31) from the Pacific Costa Rica Margin. This species was sampled from mussels, tubeworms, and rocks between 995−1,860 m depth. Specimens have also been found and genetically characterized from a Pescadero Basin hydrocarbon seep site (23.64, -108.39), collected by the ROV Tiburon during dive #756 from below 2000 meters depth.

Remarks. *Paralepetopsis variabilis* sp. nov. clade 1 shells resemble most closely those of *P. clementensis* (McLean 2008) but could be distinguished from them by having flat, rather than rounded, shell margins and flat, rather than convex, shell slopes. At least one specimen of clade 1 exhibited shell structuring

that fits the description of the closely related genus *Neolepetopsis* (Fig. 6J, K; McLean 1990). However, such specimens occurring within the genus *Paralepetopsis* indicates that shell sculpturing may not be as taxonomically informative as previously thought. *Paralepetopsis variabilis* sp. nov. clade 2 specimens most closely resembled *P. clementensis* (McLean 2008); however, the axial striations exhibited by these individuals are distinct and are instead most like *P. tunnicliffae* (McLean 2008). Clade 2 specimens may be distinguished from *P. tunnicliffae* in that their shell margins are rounded, rather than flat. Radulae obtained from *Paralepetopsis* clade 2 appears most like *P. tunnicliffae* in their reduced lateral marginal teeth. *Paralepetopsis variabilis* sp. nov. clade 3 specimens most closely resembled *P. clementensis* (McLean 2008); however, they lack the convex shell slopes typical of this species. Radulae of this species, overall, resembled those of *P. ferrugivora*, but have a distinct major lateral tooth shape (Warén and Bouchet 2001).

Etymology. The species name *variabilis* is Latin for variable, referring to the notable and confounding shell variation observed in this species.

Subclass Vetigastropoda
Family Pyropeltidae McLean & Haszprunar, 1987
Genus *Pyropelta* McLean & Haszprunar, 1987

***Pyropelta corymba* McLean & Haszprunar, 1987**
Fig. 8

New records. Costa Rica • 13 specimen(s); Costa Rica Margin, Mound 12; 8.93075, -84.31252; 998 m; 23 May 2017; AT37-13 ALVIN Dive 4908 leg.; Mussel, 4908_MP_12 • 4 specimen(s); Costa Rica Margin, Mound 12; 8.930395, -84.3124245; 995 m; 1 June 2017; AT37-13 ALVIN Dive 4917 leg.; Rock, EC5803 • 213 specimen(s); Costa Rica Margin, Mound 12; 8.93046775, -84.31244503; 998 m; 5 June 2017; AT37-13 ALVIN Dive 4922 leg.; Mussel, EC5741 • 973 specimen(s); Costa Rica Margin, Mound 12; 8.9308, -84.31263; 997 m; 24 October 2018; AT42-03 ALVIN Dive 4978 leg.; Mussel, EC7743 • 425 specimen(s); Costa Rica Margin, Mound 12; 8.9307, -84.3128; 997 m; 30 October 2018; AT42-03 ALVIN Dive 4984 leg.; Mussel, EC8314 • 7 specimen(s); Costa Rica Margin, Mound 12; 8.9307, -84.3128; 997 m; 30 October 2018; AT42-03 ALVIN Dive 4984 leg.; Tubeworm, EC10475 • 1 specimen(s); Costa Rica Margin, The Thumb; 9.05, -84.4; 1,072 m; 10 January 2019; FK19-0106 SUBASTIAN Dive 217 leg.; Mussel, EC9480 • 1 specimen(s); Costa Rica Margin, The Thumb; 9.05, -84.4; 1,072 m; 10 January 2019; FK19-0106 SUBASTIAN Dive 217 leg.; Mussel, EC9451 • 1 specimen(s); Costa Rica Margin, The Thumb; 9.05, -84.4; 1,072 m; 10 January 2019; FK19-0106 SUBASTIAN Dive 217 leg.; Mussel, EC9468 • 1 specimen(s); Costa Rica Margin, The Thumb; 9.05, -84.4; 1,072 m; 10 January 2019; FK19-0106 SUBASTIAN Dive 217 leg.; Mussel, EC9434.

Remarks. Specimens of *Pyropelta corymba* are herein confirmed from the hydrocarbon seep sites "Jaco Scar" (9.12, -84.84), "Mound 12" (8.93, -84.31), and "The Thumb" (9.05, -84.39) from the Pacific Costa Rica Margin. This species was sampled from mussels, tubeworms, rocks, and wood between 995–1,887 m depth. This extends the known range of this species southward from the Californian coast and Gulf of California.
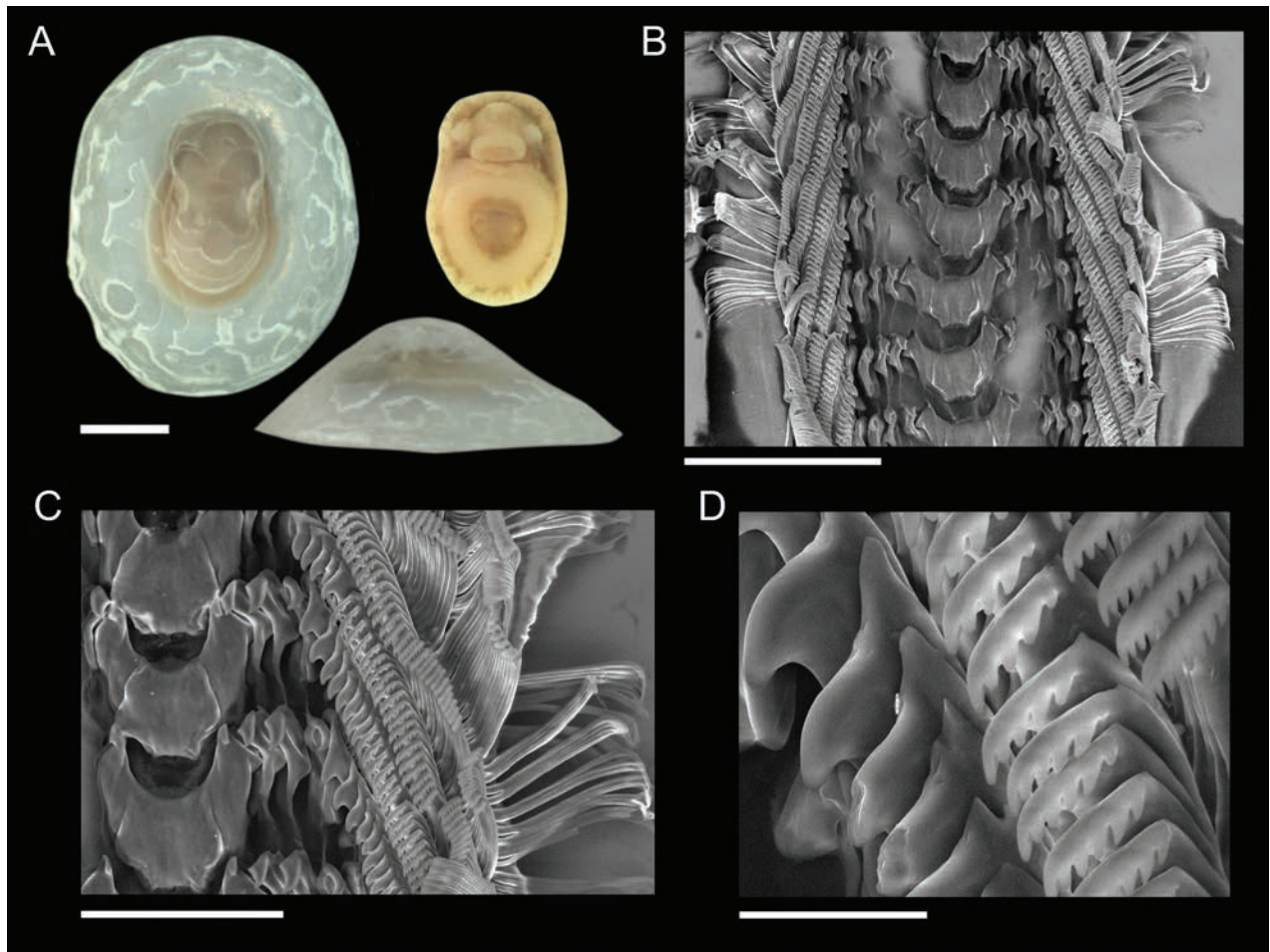
Figure 8. Specimen of *Pyropelta corymba* **A** sequenced specimen (GenBank Accession # OQ644631) found on mussel shells, Mound 12, 997 m, AD4978, 24 October 2018 **B–D** details of radula and major and minor lateral teeth. Scale bars: 1 mm (**A**); 100 µm (**B**); 50 µm (**C**); 10 µm (**D**).

Family Lepetodrilidae McLean, 1988
Genus *Lepetodrilus* McLean, 1988

***Lepetodrilus guaymasensis* McLean, 1988**
Fig. 9

New records. Costa Rica • 13 specimen(s); Costa Rica Margin, Jaco Scar; 9.117323, -84.839671; 1,795 m; 27 May 2017; AT37-13 ALVIN Dive 4912 leg.; Tubeworm, EC5737 • 3 specimen(s); Costa Rica Margin, Jaco Scar; 9.117368, -84.839662; 1,796 m; 30 May 2017; AT37-13 ALVIN Dive 4915 leg.; Tubeworm, EC5811 • 10 specimen(s); Costa Rica Margin, Mound 12; 8.930395, -84.3124245; 995 m; 1 June 2017; AT37-13 ALVIN Dive 4917 leg.; Tubeworm, EC5798 • 48 specimen(s); Costa Rica Margin, Mound 12; 8.93046775, 84.31244503; 998 m; 5 June 2017; AT37-13 ALVIN Dive 4922 leg.; Mussel, EC5746 • 2 specimen(s); Costa Rica Margin, Jaco Scar; 8.97067, -84.839533; 1,783 m; 23 October 2018; AT42-03 ALVIN Dive 4977 leg.; Mussel, EC7553 • 247 specimen(s); Costa Rica Margin, Mound 12; 8.9307, -84.3128183; 997 m; 30 October 2018; AT42-03 ALVIN Dive 4984 leg.; Mussel, EC8313 • 5 specimen(s); Costa Rica Margin, Mound 12; 8.92983, -84.3131; 995 m; 2 November 2018; AT42-03 ALVIN
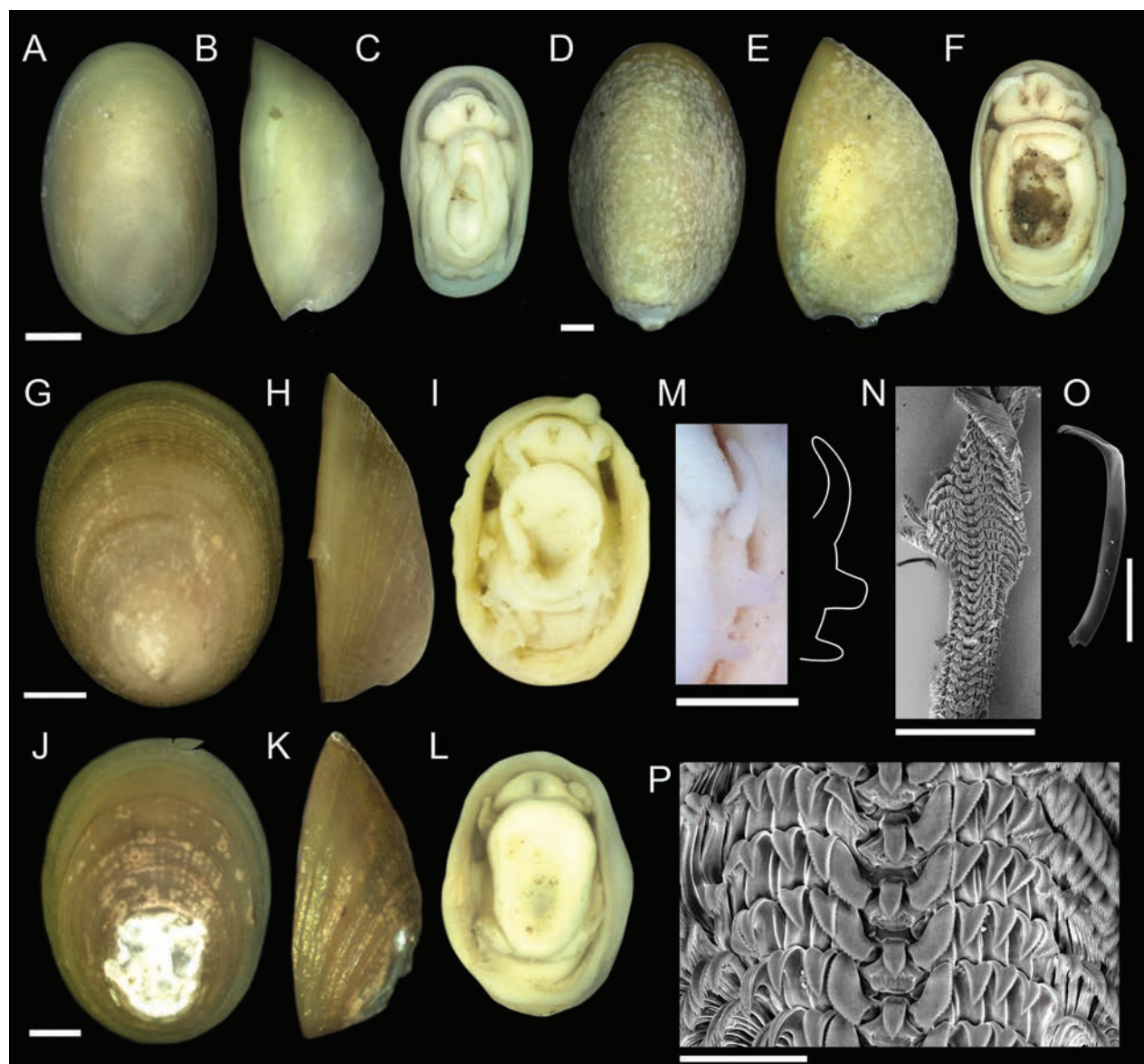
Figure 9. Specimens of *Lepetodrilus guaymasensis* and *Pseudolepetodrilus costaricensis* gen. et sp. nov. **A−C** sequenced *L. guaymasensis* specimen (GenBank Accession # OQ644591) from Mound 12, 998 m, AD4917, 1 June 2017 **D−F** additional *L. guaymasensis* specimen from Jaco Scar, 1,811 m, AD4912, 27 May 2017 **G−I** *Pseudolepetodrilus costaricensis* sp. nov. holotype (**G−I**) and sequenced specimen (**J−L**) (GenBank Accession #OQ644586), both from tubeworms, Jaco Scar, 1,760 m, AD4989, 4 November 2018 **M** close up view of *P. costaricensis* epipodial tentacles, with tracing **N−P** radula morphology representative of this new genus **O** isolated marginal lateral tooth. Scale bars: 1 mm (**A−M**); 300 µm (**N**); 50 µm (**O**); 30 µm (**P**).

Dive 4987 leg.; Tubeworm, EC8562 • 1 specimen(s); Costa Rica Margin, Jaco Scar; 9.117775, -84.839525; 1,803 m; 7 January 2019; FK19-0106 SUBASTIAN Dive 214 leg.; Rock, EC9336 • 319 specimen(s); Costa Rica Margin, Jaco Scar; 9.11741, -84.839632; 1,812.41 m; 7 January 2019; FK19-0106 SUBASTIAN Dive 214 leg.; Mussel, EC9330 • 2 specimen(s); Costa Rica Margin, The Thumb; 9.048849447, -84.39383397; 1,071.5 m; 10 January 2019; FK19-0106 SUBASTIAN Dive 217 leg.; Mussel, EC9500 • 1 specimen(s); Costa Rica Margin, The Thumb; 9.048835323, -84.39417277; 1,075 m; 10 January 2019; FK19-0106 SUBASTIAN Dive 217 leg.; Mussel, EC9488 • 1 specimen(s); Costa Rica Margin, The Thumb; 9.048821, -84.394156; 1,074 m; 10 January 2019; FK19-0106

SUBASTIAN Dive 217 leg.; Tubeworm, EC9480 • 1 specimen(s); Costa Rica Margin, The Thumb; 9.048871, -84.393744; 1,073 m; 10 January 2019; FK19-0106 SUBASTIAN Dive 217 leg.; Mussel, EC9468 • 1 specimen(s); Costa Rica Margin, The Thumb; 9.048836, -84.393773; 1,072 m; 10 January 2019; FK19-0106 SUBASTIAN Dive 217 leg.; Mussel, EC9451 • 1 specimen(s); Costa Rica Margin, The Thumb; 9.048866, -84.394112; 1,073 m; 10 January 2019; FK19-0106 SUBASTIAN Dive 217 leg.; Mussel, EC9434.

Remarks. Specimens of *Lepetodrilus guaymasensis* are herein confirmed from the hydrocarbon seep sites "Jaco Scar" (9.12, -84.84), "Quepos Seep" (9.03, -84.62), "Mound 12" (8.93, -84.31), and "The Thumb" (9.05, -84.39) from the Pacific Costa Rica Margin. This species was sampled from mussels, tubeworms, and rocks between 995–1,800 m depth.

Pseudolepetodrilus gen. nov.
https://zoobank.org/CD35F6A5-6AAA-45CF-9D10-1B38CA8A20D6
Fig. 9

Type species. *Pseudolepetodrilus costaricensis* sp. nov.
Diagnosis. *Pseudolepetodrilus* gen. nov. have a complete shell with fine radial and concentric sculptures, penis originating at the right side of the head, and three pairs of posterior epipodial tentacles.
Description. *Shell* (Fig. 9G, H): Specimens exhibit patelliform shells with moderate elevation. Apex of shell is located at the posterior end of the shell. Fine concentric radial sculpturing and axial sculpturing present. The aperture and shell margin are ovate and unornamented. Shell is robust with a thick, greenish brown periostracum covering the outer shell and wrapping over the aperture lip.
Soft parts (Fig. 9I, M): One pair of short cephalic tentacles are located on the head. One pair of epipodial tentacles are located approximately midway down the foot, with one tentacle present on either side of the organism. Three pairs of epipodial tentacles are present at the posterior end of the organism. These posterior tentacles are short and thin; They do not extend past the shell margin. A thick, triangular penis extends from beneath the right cephalic tentacle. Mouth is V-shaped. Oral lappets are lacking.
Radula (Fig. 9N, O): Radula is rhipidoglossate in configuration and is symmetrical. Rachidian tooth is sharp and triangular, lacking denticles. One broad, major lateral tooth on either side of the rachidian flanked by four minor lateral teeth all with triangular cusps: Numerous (15+) marginal teeth flank the minor lateral teeth on either side, each exhibiting spatulate cusps with short denticles.
Remarks. *Pseudolepetodrilus* gen. nov. have a complete shell, penis originating at the right side of the head, and three pairs of posterior epipodial tentacles. *Lepetodrilus* have a complete shell, penis originating at the right side of the head, and two pairs of posterior epipodial tentacles. *Gorgoleptis* have a complete shell, penis originating from the left side of the head, and two pairs of posterior epipodial tentacles. *Clypeosectus* McLean, 1989 has a slit shell and three pairs of posterior epipodial tentacles. *Pseudorimula* McLean, 1989 has a slit shell and four pairs of posterior epipodial tentacles.

The radulae of this new genus most closely resembles that of *Lepetodrilus* in that they both have a broad, oblique, first major lateral followed by laterals that

rise to a peak at the third tooth and then descend away from the short, triangular rachidian. However, while the major laterals of *Lepetodrilus* have variable, irregular edges, the major lateral teeth of *Pseudolepetodrilus* gen. nov. have an even, outer slope without any notches or grooves.

Etymology. The generic name means false (*pseudo*) *Lepetodrilus*, given its close physical resemblance to species of the genus *Lepetodrilus.*

Pseudolepetodrilus costaricensis sp. nov.
https://zoobank.org/019D87DB-0CA1-4785-9E4E-7D9306AF0592
Fig. 9

Type material examined. *Holotype:* Costa Rica • whole organism; ethanol-fixed; Original label: *"Pseudolepetodrilus costaricensis* holotype, 1, whole organism, AD4989, Costa Rica Margin, Jaco Scar, 9.11785, -84.8407, 1760 m, from tubeworms."; SIO-BIC M22534. *Paratypes:* Costa Rica • 1 specimen; same data as for holotype; Original label: *"Pseudolepetodrilus costaricensis* paratype, 1, whole organism, AD4989, Costa Rica Margin, Jaco Scar, 9.11785, -84.8407, 1760 m, from tubeworms."; MZCR10673-01.

Type locality. Costa Rica • Costa Rica Margin, Jaco Scar, 9.11785, -84.8407; hydrocarbon seep; tubeworms; 1,760 m; 4 November 2018; AT42-03 ALVIN Dive 4989 leg.

Other material examined. Costa Rica • 4 specimen(s); Costa Rica Margin, Jaco Scar; 9.11785, -84.8407; 1,760 m; 4 November 2018; AT42-03 ALVIN Dive 4989 leg.; Tubeworm; EC10483.

Diagnosis. *Pseudolepetodrilus costaricensis* sp. nov. can be diagnosed by their unique "wing-shaped" first major lateral tooth on their radula and through genetic characterization of the mitochondrial CO1 gene.

Description. *Shell* (Fig. 9G, H): Specimens exhibit patelliform shells with very small, truncated whorl at the posterior end of the shell. Holotype measures 3.7 mm in length, 2.8 mm in width, and 1.3 mm in maximum height. Shell roundness (width ÷ length) is ~ 0.75. Sinuous, concentric radial sculpturing present on shell with fine axial striations which intersect the radial sculpture to form very small, raised bumps. The aperture opening is ovate and unornamented. The aperture lip is thick and unornamented. The shell margin is flat. Posterior shell slope is flattened while the anterior shell slope is rounded. Shell apex is posteriorly shifted. Shell is robust with a thick, greenish brown periostracum covering the outer shell and wrapping over the aperture lip.

Soft parts (Fig. 9I, M): Soft tissue is light greenish-to-yellowish in color. Mantle margin is thick and irregular and envelopes the body tissue. Three pairs of posterior epipodial tentacles are present. These tentacles descend in length, with the most anterior one being the longest and the most posterior one being the shortest. Posterior tentacles do not extend past the mantle margin. Two broad, fleshy, anterior tentacles are located approximately midway up and on either side of the foot margin. Two cephalic tentacles are present that are fleshy and triangular in shape and thicker than the epipodial tentacles. The mouth has a distinctive Y-shaped opening lacking thickened tissue. Elongated oral lappets are present. The penis originates from below the right cephalic tentacle. Operculum is absent.

Radula (Fig. 9N, O): Rhipidoglossate radula. Rachidian teeth have very short shafts and sharp, triangular cusps. The anterior end of each cusp is flat while the pointed ends lack denticles. Rachidian teeth are flanked by one major lateral tooth on each side. Major laterals have broad, wing-shaped cusps that extend higher than the rachidian teeth. The outer edges of these cusps are serrated with ~ 16 short denticles. Three minor laterals follow which have long, sharp, triangular cusps whose outer edge is serrated with short denticles, but whose inner edges are not. The anterior edge of these minor laterals is slightly convex. The fourth, minor lateral teeth also have long, sharp, triangular cusps like the preceding three, but with serrations along both their inner and outer edges. Marginal teeth number ≥ 15 and exhibit rounded, spatulate cusps that are lined with ~ 40 denticles each. Denticles on each marginal tooth are elongated posteriorly and shorten as one moves anteriorly. Marginal cusps are located at the anterior end of a long, thin tooth shaft which connects to the radular ribbon at its base. Morphological transitions between major laterals, minor laterals, and marginal teeth are continuous.

Distribution. *Pseudolepetodrilus costaricensis* sp. nov. is confirmed from the hydrocarbon seep sites "Jaco Scar" (9.12, -84.84) at the Pacific Costa Rica Margin. This species was sampled from tubeworms at 1,760 m depth.

Remarks. Shells of this species notably do not narrow at their anterior ends, similar to *L. shannonae* (Warén and Bouchet 2009). Radulae most closely resembled those of *L. guaymasensis*. However, unlike this species, the central teeth of *P. costaricensis* are larger and lack denticles on their cusps. Further, their first lateral teeth have a shape that is distinct from *L. guaymasensis*, exhibiting an even, sloping outer ridge.

Etymology. The species name *costaricensis* refers to the Pacific Costa Rica Margin, the geographic location where this species, and its genus, was first discovered.

Subclass Neomphaliones
Family Cocculinidae Dall 1882
Genus *Cocculina* Dall 1882

***Cocculina methana* sp. nov.**
https://zoobank.org/C1481891-E0FF-4F55-8EE3-619ADE850CC4
Fig. 10

Type material examined. *Holotype:* Costa Rica • whole organism; ethanol-fixed; Original label: "*Cocculina methana* holotype, 1, whole organism, AD4924, Costa Rica Margin, Quepos Seep, 9.03174, -84.62158, 1408 m, from clams."; SIO-BIC M22533. *Paratypes:* Costa Rica • 1 specimen; same data as for holotype; Original label: "*Cocculina methana* paratype, 1, whole organism, AD4924, Costa Rica Margin, Quepos Seep, 9.03174, -84.62158, 1408 m, from clams."; MZCR10672-01.

Type locality. Costa Rica • Costa Rica Margin, Quepos Seep, 9.03174, -84.62158; hydrocarbon seep; clams; 1,408 m; 7 June 2017; AT37-13 ALVIN Dive 4924 leg.

Other material examined. Costa Rica • 4 specimens; Costa Rica Margin, Quepos Seep; 9.03174, -84.62158; 1,408 m; 7 June 2017; AT37-13 ALVIN Dive 4924 leg.; Clams; Erik Cordes Personal Collection (EC) 5752 • 2 specimen(s);
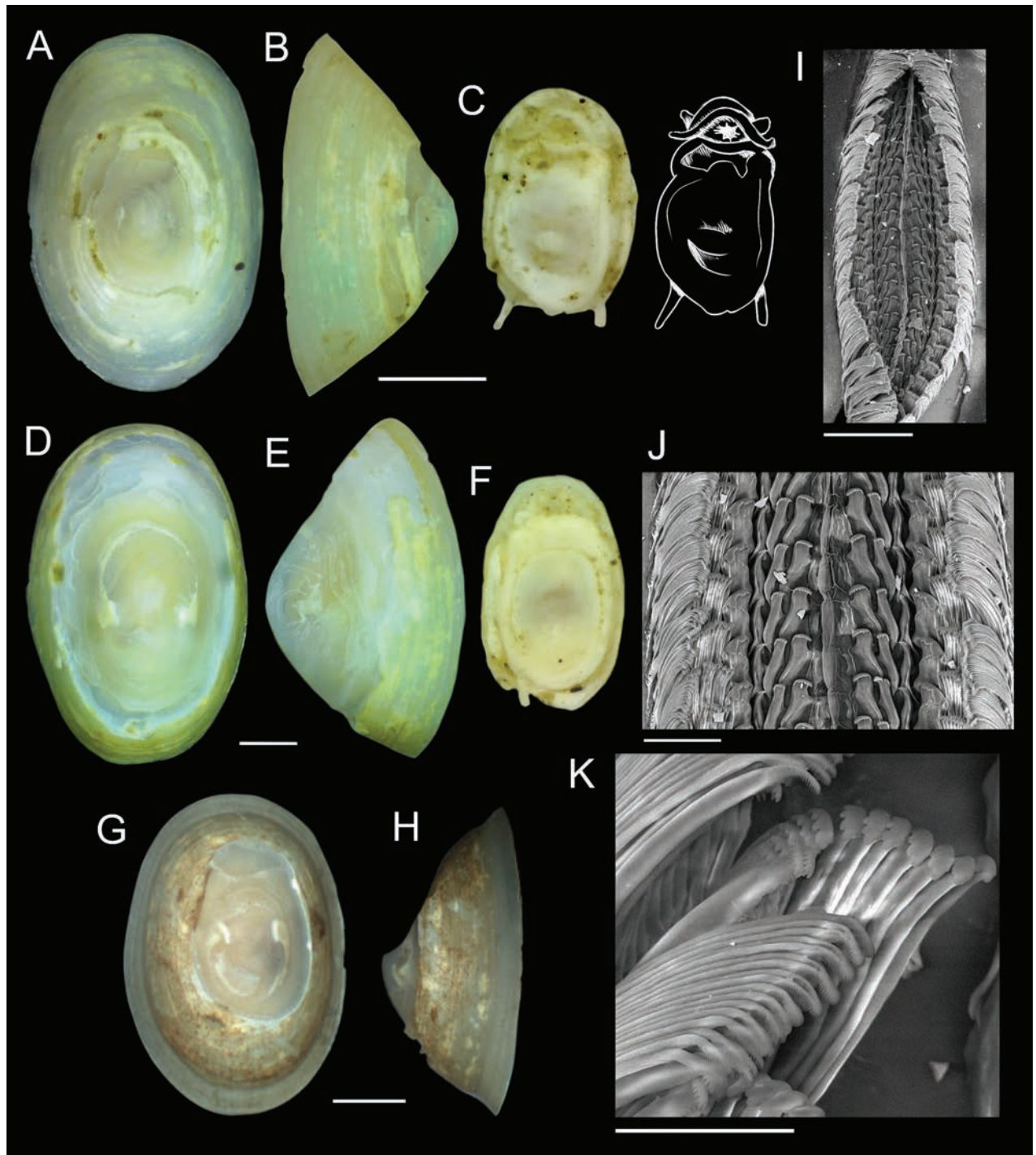
Figure 10. Specimens of *Cocculina methana* sp. nov. **A, B** holotype from clam shells, Quepos Seep, 1,408 m, AD4924, 7 June 2017 **C** holotype soft tissue with tracing **D–F** paratype from tubeworms, Quepos Seep, 1064 m, AD4923, 7 June 2017 **G, H** sequenced specimen (GenBank Accession # OQ644629) from same location as previous showing intact periostracum prior to erosion with ethanol preservation. White dotted line denotes obstruction of image by forceps used to position the specimen **I–K** details of radula **K** details of marginal teeth. Scale bars: 1 mm (**A–H**); 150 μm (**I**); 50 μm (**J**); 20 μm (**K**).

Costa Rica Margin, Mound 12; 8.929983333, -84.31167667; 992 m; 20 October 2018; AT42-03 ALVIN Dive 4974 leg.; Bone, SIO-BIC M16788 • 3 specimen(s); Costa Rica Margin, Jaco Scar; 9.11562, -84.84005; 1,908 m; 28 May 2017; AT37-13 ALVIN Dive 4913 leg.; Wood, SIO-BIC M16149 • 15 specimen(s); Costa Rica Margin, Jaco Scar; 9.1193, -84.84277; 1,854 m; 31 May 2017; AT37-13

ALVIN Dive 4916 leg.; Tubeworm, SIO-BIC M16171 • 30 specimen(s); Costa Rica Margin, Quepos Seep; 9.0303, -84.623; 1,433 m; 1 March 2009; AT15-44 ALVIN Dive 4508 leg.; SIO-BIC M12024 • 3 specimen(s); Costa Rica Margin, Jaco Scar; 9.1172, -84.8417; 1,866 m; 3 March 2009; AT15-44 ALVIN Dive 4509 leg.; SIO-BIC M12037 • 6 specimen(s); Costa Rica Margin, Mound Jaguar; 9.651755802, -85.88211866; 2,000 m; 25 January 2019; FK19-0106 SUBASTIAN Dive 230 leg.; Wood, SIO-BIC M17106 • 3 specimen(s); Costa Rica Margin, Mound Jaguar; 9.65876081, -85.88259157; 1,896 m; 25 January 2019; FK19-0106 SUBASTIAN Dive 230 leg.; Wood, SIO-BIC M17105.

Diagnosis. *Cocculina methana* sp. nov. may be diagnosed by its distinct golden-brown periostracum. It may be most reliably distinguished from its sister species, *Cocculina japonica*, through mitochondrial CO1 barcoding.

Description. *Shell* (Fig. 10A−C): Specimens exhibit uncoiled, patelliform shells. Holotype measures 3.4 mm in length, 2.3 mm in width, and 1.7 mm in maximum height. Shell roundness (width ÷ length) is ~ 0.66. Fine, concentric, radial sculpturing present on shell. The aperture opening is ovate and unornamented. The aperture lip is thin, fragile, and unornamented. The shell margin is flat. Posterior shell slope is flattened while the anterior shell slope is rounded. Shell apex is posteriorly shifted. Protoconch is unknown. Shell is robust with a thick, greenish brown periostracum covering the outer shell and wrapping over the aperture lip.
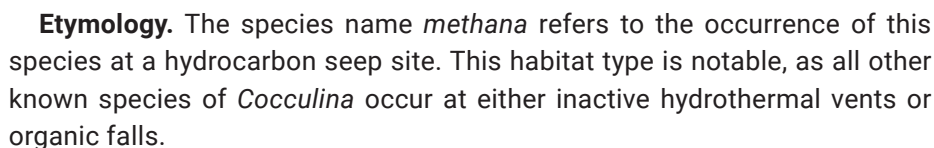
Soft parts (Fig. 10C): Soft tissue is light yellow to white in color. Mantle margin is thin and irregular. One pair of posterior epipodial tentacles present. Posterior tentacles are thin, elongated, and do not taper in width towards their distal ends. Two, short, blunt cephalic tentacles are present that are slightly thicker than the epipodial tentacles. The mouth has well-developed oral lappets surrounding a starburst-shaped oral opening. External reproductive structures were not observed. Foot margin is ovate and slightly irregular. Operculum is absent.

Radula (Fig. 10I−K): Radula is rhipidoglossate. Rachidian teeth are highly diminished, lacking cusps; The rachidian teeth form a continuous, raised ridge down the center of the radula. Rachidian are flanked by three major lateral teeth on each side. Lateral teeth have spatulate cusps that decrease in size from the first to third tooth. First major lateral teeth are the broadest, having 6−8 rounded denticles on their cusps. Second major lateral teeth are slightly thinner, having 3−5 denticles on their cusps. Finally, the third major laterals are thinner than the other two, and have two or fewer denticles on their cusps. These three major laterals are followed by one minor lateral tooth, which is broader than any of the other teeth preceding it. This minor lateral tooth has a short cusp that is angled outwards with four or five blunt, rounded denticles. Each minor lateral tooth has one or two short denticles on their innermost side (raised the highest), followed by one broad, elongated denticle, and finally followed by another short denticle on its outermost, lowest side. Two sets of numerous, marginal teeth follow, set at different angles. Sets of inner marginal teeth are more or less parallel to the radular ribbon, and number 10−12 teeth. Each tooth has a very thin and long tooth shaft (thinner than any of the preceding teeth) and a spatulate cusp with 5−7 short, rounded denticles. Sets of outer marginals are set at ~ 45° angle to the radular ribbon, and number between 15−20 teeth. These outer marginals also have a thin and long tooth shaft with spatulate cusps. These cusps, however, are decorated with ~ 24 thin, bristle-like denticles (~ 12 on each side of the cusp).

Figure 11. Bayesian phylogenies of *Bathyacmaea* and related genera **A** topology based on a 420-bp region of the mitochondrial CO1 gene and the HKY+G+I substitution model **B** topology based on a 258-bp region of the nuclear H3 gene and the GTR+G+I substitution model. Numbers above branch nodes represent Bayesian posterior probabilities. Numbers below branch nodes represent the proportion of replicate trees in which the associated taxa clustered together in the bootstrap test (10,000 replicates for CO1; 5,000 replicates for H3). Only values above 50 are shown. Novel sequences are bolded and highlighted. The trees are drawn to scale, with branch lengths representing the number of base substitutions accumulated over time.

Distribution. *Cocculina methana* sp. nov. is confirmed from the hydrocarbon seep sites Quepos Seep (9.03, -84.62), Mound 12 (8.93, -84.31), Jaco Scar (9.12, -84.84), and Mound Jaguar (9.66, -85.88) at the Pacific Costa Rica Margin. This species was sampled from clam shells, wood, tubeworms, and bone between 1,408–2,000 m depth. These are among the deepest-known *Cocculina*.

Remarks. The shells of *Cocculina methana* sp. nov. most closely resemble those of *C. japonica* (Dall 1907). Radulae of these specimens most closely resembled that of *C. cowani* (McLean 1987) but with distinct central teeth that form a narrow, defined ridge down the center of the radula (Fig. 9J). The shell apex of this species notably lacks the hooked "sail fin" appearance of other *Cocculina* species. The periostracum of these specimens was observed to significantly corrode with prolonged ethanol preservation (Fig. 10G, H). This should be considered when examining museum specimens.
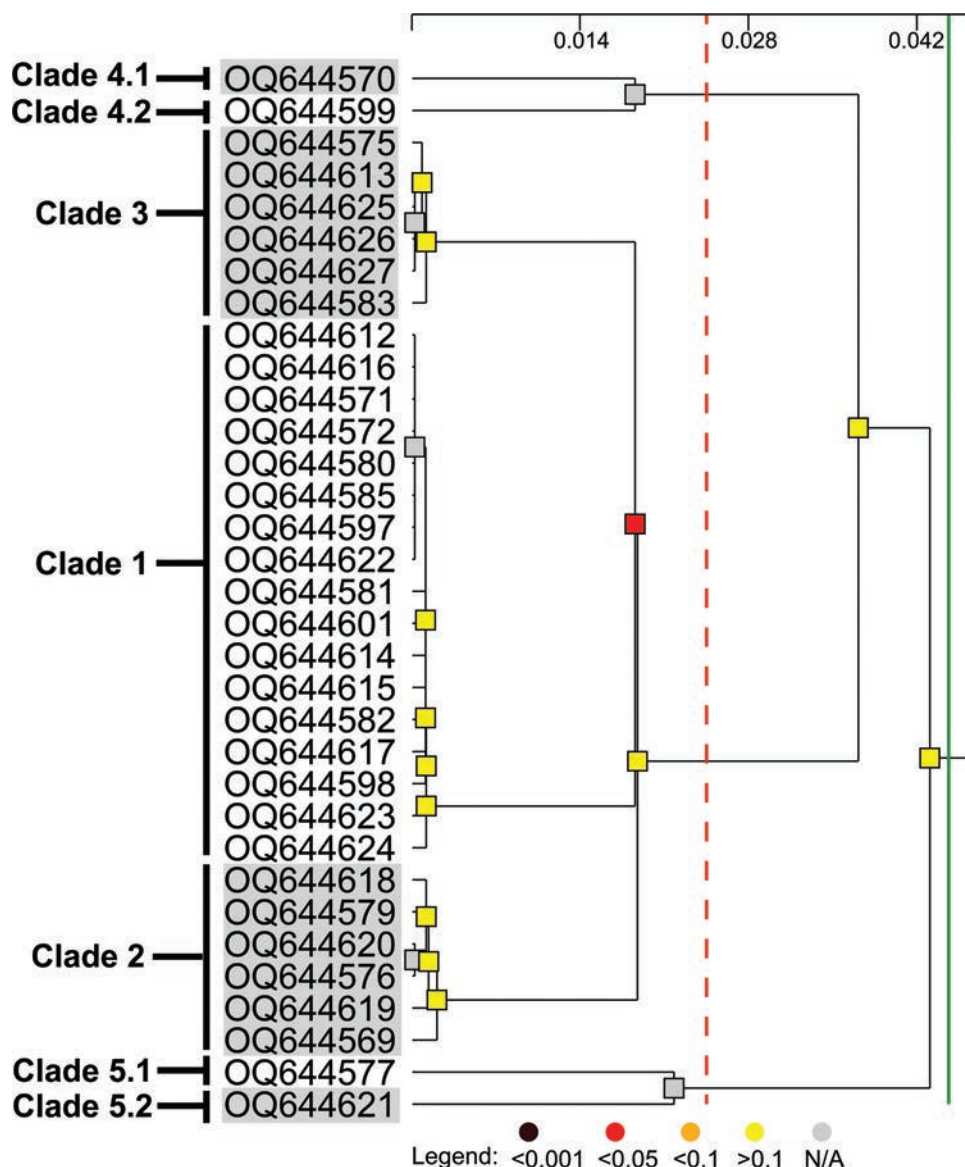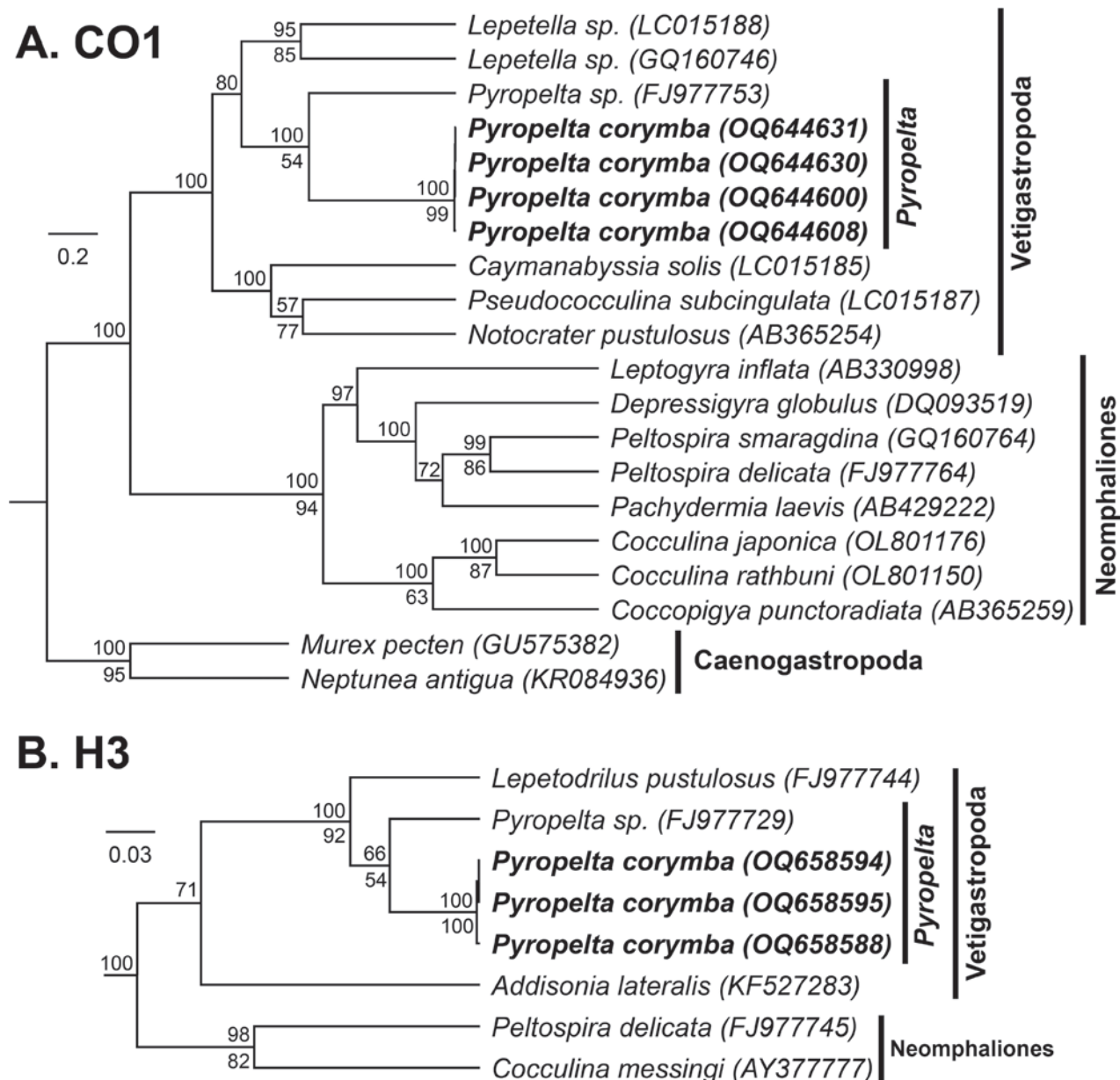
Figure 12. Bayesian phylogeny of *Paralepetopsis* and related genera **A** topology based on a 438-bp region of the mitochondrial CO1 gene and the GTR+G+I substitution model **B** topology based on a 247-bp region of the nuclear H3 gene and the GTR+G+I substitution model. Numbers above branch nodes represent Bayesian posterior probabilities. Numbers below branch nodes represent the proportion of replicate trees in which the associated taxa clustered together in the bootstrap test (10,000 replicates for CO1; 5,000 replicates for H3). Only values above 50 are shown. Novel sequences are bolded and highlighted. The tree is drawn to scale, with branch lengths representing the number of base substitutions accumulated over time.

Etymology. The species name *methana* refers to the occurrence of this species at a hydrocarbon seep site. This habitat type is notable, as all other known species of *Cocculina* occur at either inactive hydrothermal vents or organic falls.

Figure 13. Automatic hierarchical partitioning of novel *Paralepetopsis* CO1 sequences. Dendrogram shown was generated by ASAP (Puillandre et al. 2021. The red dotted line denotes the distance threshold (Dt), and the solid green line denotes the grouping distance (Dc). Colored nodes represent the likelihood that each subset is distinct from a panmictic population. The scalebar at the top represents the relative barcode gap width (W).

Discussion

The present study aimed to investigate the diversity of gastropod limpets at the Pacific Costa Rica Margin (CRM) hydrocarbon seeps. Given the CRM's unique geographic situation among multiple oceanic currents and its separation from other chemosynthetic regions, it was hypothesized that this region would host species that were related to, but distinct from, nearby chemosynthesis-based ecosystems. Using the informative genetic loci CO1 and H3, as well as shell and radular characters, four species and one new genus across three gastropod subclasses were identified from more than 4,000 limpet specimens. This study also confirmed the presence of *Lepetodrilus guaymasensis* at the CRM and expands the known range of *Pyropelta corymba* southward to include CRM hydrocarbon seeps.
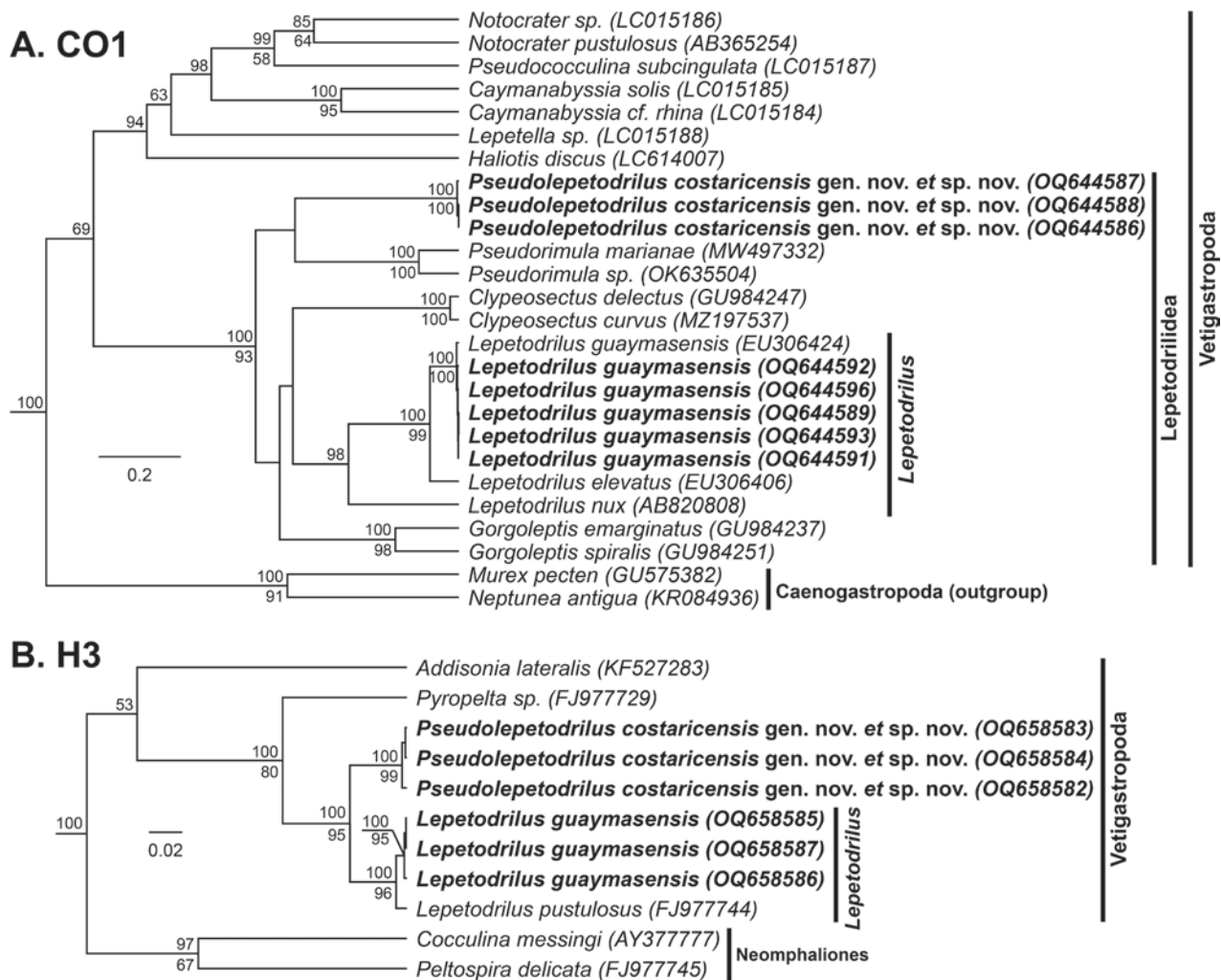
Figure 14. Bayesian phylogeny of *Pyropelta* and related genera **A** topology based on a 440-bp region of the mitochondrial CO1 gene and the GTR+G+I substitution model **B** topology based on a 321-bp region of the nuclear H3 gene and the GTR+G+I substitution model. Numbers above branch nodes represent Bayesian posterior probabilities. Numbers below branch nodes represent the proportion of replicate trees in which the associated taxa clustered together in the bootstrap test (10,000 replicates for CO1; 5,000 replicates for H3). Only values above 50 are shown. Novel sequences are bolded and highlighted. The tree is drawn to scale, with branch lengths representing the number of base substitutions accumulated over time.

New species

Bathyacmaea levinae sp. nov. found at the CRM is notably the first of its genus to be confirmed in the Eastern Pacific; all other species appear to be endemic to the Western Pacific (e.g., Okutani et al. 1992; Sasaki 2003; Zhang and Zhang 2020; Chen and Sigwart 2023). Thus, the present study expands the known range of this genus across the Pacific Ocean. This CRM species is most notable in its exhibiting distinct ecotypes depending on the substrate from which it was sampled. While studies of other marine gastropod groups have identified
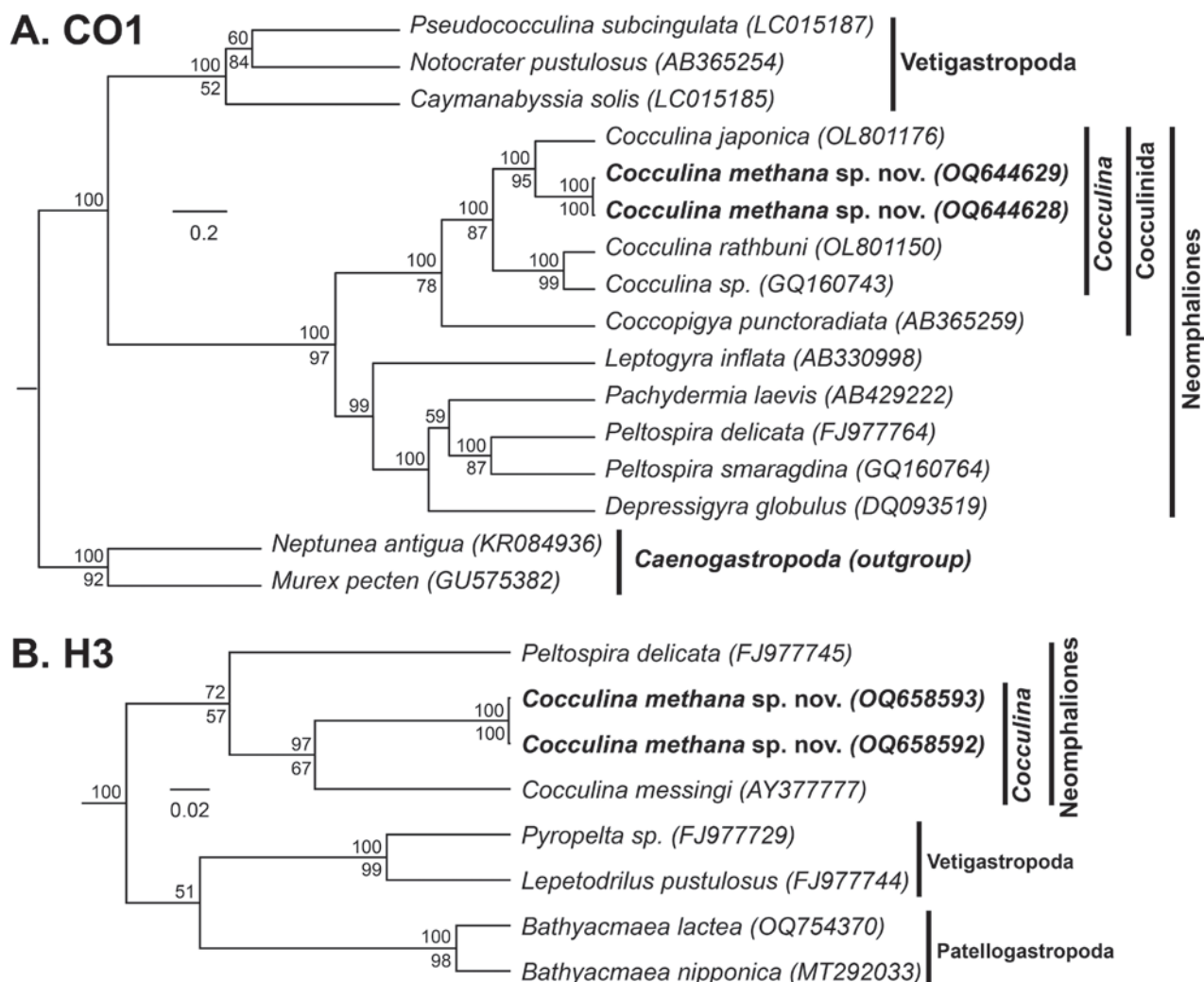
Figure 15. Bayesian phylogeny of *Lepetodrilus* and related genera **A** topology based on a 440-bp region of the mitochondrial CO1 gene and the GTR+G+I substitution model **B** topology based on a 308-bp region of the nuclear mitochondrial CO1 gene and the GTR+G+I substitution model. Numbers above branch nodes represent Bayesian posterior probabilities. Numbers below branch nodes represent the proportion of replicate trees in which the associated taxa clustered together in the bootstrap test (10,000 replicates for CO1; 5,000 replicates for H3). Only values above 50 are shown. Novel sequences are bolded. The tree is drawn to scale, with branch lengths representing the number of base substitutions accumulated over time.

substrate-dependent morphology as being the result of disruptive selection exerted by predators (Hollander and Butlin 2010), other chemosynthesis-based gastropods have been found to display similar patterns of phenotypic plasticity across these or similar substrates (e.g., *Lepetodrilus* (Chen and Watanabe 2020), *Bathyacmaea* (Chen et al. 2019)). In agreement with previous studies of *Bathyacmaea*, little to no genetic distinction between our distinct morphotypes was found (Chen et al. 2019; Zhang and Zhang 2020). These previous findings support our conclusion of a single, phenotypically plastic species at the CRM. Despite these well-documented phenotypic differences across substrate, however, little is yet known approximately the functional purpose of these changes, or what metabolic drivers are behind it.

Another group exhibiting highly variable and confounding shells is the genus *Paralepetopsis*. Individuals within this genus were highly cryptic, with little to no discernible features with which to distinguish the species under examination from one another. There also appears to be no clear environmental separation

Figure 16. Bayesian phylogeny of *Cocculina* and related genera **A** topology based on a 436-bp region of the mitochondrial CO1 gene and the GTR+G+I substitution model **B** topology based on a 258-bp region of the nuclear H3 gene and the GTR+G+I substation model. Numbers above branch nodes represent Bayesian posterior probabilities. Numbers below branch nodes represent the proportion of replicate trees in which the associated taxa clustered together in the bootstrap test (10,000 replicates for CO1; 5,000 replicates for H3). Only values above 50 are shown. Novel sequences are bolded. The tree is drawn to scale, with branch lengths representing the number of base substitutions accumulated over time.

within this group, with three of the five genetic clades identified being found at both the shallower site Mound 12 and the deeper site Jaco Scar (Table 1). All but one clade was identified from both mussels and tubeworms (Table 1). Furthermore, *Paralepetopsis*, as a genus, was present at all four sites examined in this study. Thus, the genetic diversity documented in this investigation was difficult to predict. Such sympatric speciation may be the result of cryptic mate choice or niche divergence that has not been fully characterized by the variables currently under investigation. Regardless, our investigation supports genetic barcoding as the most reliable way to identify *Paralepetopsis* species from the CRM. Furthermore, as more than 1,300 individuals from this genus were collected, it is highly likely that even more cryptic species may be hidden within this genus that remain to be described.

The new species *Paralepetopsis variabilis* sp. nov. from the CRM seems to have been first collected from the Pescadero Basin in the Gulf of California,

with one representative sequence on GenBank (KY581541, Fig. 12A). This species is described herein with permission from the corresponding author of that sequence (pers. corr. Shannon Johnson). This connectivity is notable, as the CRM and the Pescadero Basin are located more than 3,500 km apart from one another, yet may be connected through the California or West Mexican currents (Kessler 2006). Our species most closely resembled *P. tunnicliffae*; unfortunately, no published barcodes for CO1 nor H3 exist for *P. tunnicliffae* with which to compare our specimens. However, *P. tunnicliffae* was first described from hydrothermal vents at the Juan de Fuca Ridge, which may be consequential; species turnover and genetic structuring has been observed between hydrothermal vent fields in the Northeastern Pacific and the equatorial Eastern Pacific across multiple invertebrate taxa (Tunnicliffe et al. 1996) including *Lepetodrilus* limpets (Matabos and Jollivet 2019), aplacophorans (Scheltema 2008), and alvinellid worms (Chevaldonne et al. 2002). Such differences are ascribed to the subduction of the Farallon Plate beneath the North American Plate approximately 28 million years ago (Tunnicliffe et al. 1996; Vrijenhoek 2013). Furthermore, the distinction between vent and seep environments also tends to correlate with species turnover (e.g., Tunnicliffe et al. 1996). While we propose that this geological context, along with morphological differences, makes it unlikely that our Costa Rican specimens are *P. tunnicliffae*, genetic characterization of, and comparison with, *P. tunnicliffae* would still be warranted.

This study identified a single species of *Cocculina* limpets from the CRM, *Cocculina methana* sp. nov. (Table 1). While species in this genus are typically found at organic falls, such as wood or whale carcasses in both shallow and deep water, the species identified here was found at the hydrocarbon seep site Quepos Seep, which is a soft-bottom, low productivity mud volcano at the CRM. The relatively low level of hydrocarbons and sulfides at this site may have made it ideal for the settlement of *Cocculina* limpets. Furthermore, the holotype of this species was obtained from a "Bushmaster" quantitative sample that also contained foundational seep species such as the mussel *Bathymodiolus billschneideri* McCowin, Feehery & Rouse, 2020 and the tubeworm *Lamellibrachia* sp. (Webb 1969), suggesting the presence, tolerance, and potential reliance on hydrocarbon seepage in its environment.

Pyropelta corymba and *Lepetodrilus guaymasensis* were the two known species identified from the CRM. *Lepetodrilus guaymasensis* has been previously collected and genetically characterized from both the Guaymas Basin (from which it was originally described) and the CRM. Thus, it was not surprising that this species was found here and displayed the expected genetic affinity to these previously obtained sequences. *Pyropelta corymba*, however, has not been identified from the CRM before, and thus these represent novel records of occurrence for this group. Specifically, *P. corymba* from the CRM represent the most southerly population of this species known to date. While *P. corymba* has been morphologically identified from vents and seeps in the Gulf of California (McLean 1992) as well as from whale bone in the Catalina Basin (McLean and Haszprunar 1987), there are no associated gene sequences that have been published from these populations. Thus, it is impossible to assess the relatedness between our samples and these more northerly populations.

Finally, this study identifies a new genus within the family Lepetodrilidae, *Pseudolepetodrilus* gen. nov. The other genera within this family (*Lepetodrilus*,

Pseudorimula, *Gorgoleptis*, and *Clypeosectus*) are all endemic to chemosynthesis-based ecosystems and have been extensively studied over the past 50 years. This is particularly true for *Lepetodrilus*, which are highly abundant and well-characterized from the East Pacific Rise hydrothermal vents, in particular. Therefore, the identification of a wholly new genus within this family was unexpected. These specimens were relatively rare in our collections, having only been collected during one dive at Jaco Scar with a total of ten individuals identified. Morphologically, this new genus undoubtedly most closely resembles *Lepetodrilus* out of the Lepetodrilids. However, genetically, it is placed as sister to *Pseudorimula* (Fig. 14A), and has three pairs of posterior epipodial tentacles, like *Cylpeosectus*. Further research is needed to understand when and where this new genus likely originated, and whether it is represented by any additional species elsewhere.

Data availability

While results from our genetic investigations support the species herein described from the CRM, we nonetheless draw attention to the relatively small sample sizes of several genera investigated. *Pyropelta*, for instance, is only represented on GenBank by three published and one unpublished mitochondrial CO1 sequence outside of the novel sequences herein generated from the CRM. Similarly, *Paralepetopsis* is represented by just seven published mitochondrial gene sequences outside of the novel sequences generated from the CRM. Several species that were close morphological matches to our own, such as *Bathyacmaea kanesunosensis*, *Paralepetopsis tunnicliffae*, *Pyropelta corymba*, and *Pyropelta musaica*, had no associated gene sequences on public repositories, precluding genetic comparison. This shortage of sequences may lead to an overestimation of exclusivity and may mask consequential connections between the CRM and other regions. These data deficiencies highlight one of the core challenges of conducting deep-sea taxonomic work: Genetic samples are often scarce. This scarcity may arise from a lack of specimens (e.g., the general inaccessibility of these environments, the differing sampling regimes employed by expeditions), a lack of useable genetic material (e.g., preserved specimens fixed in formalin), or a lack of taxonomic work being conducted (e.g., personal, private, and museum collections awaiting genetic characterization). Furthermore, the present article only describes deceased specimens, as notes and photographs of live specimens were not obtained prior to ethanol preservation. Information regarding the morphological characters and behaviors of live specimens thus represents an avenue for future characterization and research.

Conclusions

This study conducted genetic and morphological investigations of limpets from the hydrocarbon seeps at the CRM. These investigations found support for the novelty of several limpet species at the CRM including *Bathyacmaea levinae* sp. nov., *Paralepetopsis variabilis* sp. nov., *Pseudolepetodrilus costaricensis* gen. et sp. nov., and *Cocculina methana* sp. nov. This study also presents new occurrence records for the known species *Lepetodrilus guaymasensis* and *Pyropelta corymba*. This study contributes to the growing body of knowledge surrounding the biodiversity of the deepwater off Costa Rica. Future investigations

examining the diversity of other deep-sea animal groups at the Costa Rica Margin may reveal additional novel species that should be of interest to regional and global conservation efforts.

Acknowledgements

Additional information

Conflict of interest

The authors have declared that no competing interests exist.

Ethical statement

No ethical statement was reported.

Funding

Author contributions

Conceptualization: MJB, EEC. Data curation: MJB. Formal analysis: MJB. Funding acquisition: EEC. Methodology: MJB. Supervision: EEC, JC. Validation: JC. Visualization: MJB. Writing - original draft: MJB. Writing - review and editing: JC.

Author ORCIDs

Melissa J. Betters ⬤ https://orcid.org/0000-0002-8975-257X
Jorge Cortés ⬤ https://orcid.org/0000-0001-7004-8649
Erik E. Cordes ⬤ https://orcid.org/0000-0002-6989-2348

Data availability

Gene sequences generated in this study are accessible on GenBank under the accession numbers OQ644569−OQ644631 and Q658576−OQ658595. Occurrence records may be accessed from the Global Biodiversity Information Facility at https://ipt.pensoft.net/resource?r=crm_limpets&v=1.0. This publication and associated nomenclatural acts are registered with Zoobank at LSID urn:lsid:zoobank.org:pub:487E305B-E2EF-4D96-8940-4C4141C0BA91.

References

Bergquist D, Eckner J, Urcuyo I, Cordes E, Hourdez S, Macko S, Fisher C (2007) Using stable isotopes and quantitative community characteristics to determine a local hydrothermal vent food web. Marine Ecology Progress Series 330: 49–65. https://doi.org/10.3354/meps330049

Bouchet P, Rocroi JP, Hausdorf B, Kaim A, Kano Y, Nützel A, Parkhaev P, Schrödl M, Strong E (2017) Revised classification, nomenclator and typification of gastropod and monoplacophoran families. Malacologia 61(1–2): 1–526. https://doi.org/10.4002/040.061.0201

Bouchet P, Decock W, Lonneville B, Vanhoorne B, Vandepitte L (2023) Marine biodiversity discovery: the metrics of new species descriptions. Frontiers in Marine Science 10: 929989. https://doi.org/10.3389/fmars.2023.929989

Cavanaugh C, Gardiner S, Jones M, Jannasch H, Waterbury J (1981) Prokaryotic cells in the hydrothermal vent tube worm *Riftia pachyptila* Jones: possible chemoautotrophic symbionts. Science 213(4505): 340–342. https://doi.org/10.1126/science.213.4505.340

Chen C, Sigwart JD (2023) The lost vent gastropod species of Lothar A. Beck. Zootaxa 5270(3): 401–436. https://doi.org/10.11646/zootaxa.5270.3.2

Chen C, Watanabe H (2020) Substrate-dependent shell morphology in a deep-sea vetigastropod limpet. Marine Biodiversity 50: 1–5. https://doi.org/10.1007/s12526-020-01135-y

Chen C, Watanabe H, Nagai Y, Toyofuku T, Xu T, Sun J, Qiu JW, Sasaki T (2019) Complex factors shape phenotypic variation in deep-sea limpets. Biology Letters 15(10): 20190504. https://doi.org/10.1098/rsbl.2019.0504

Chevaldonne P, Jollivet D, Desbruyeres D, Lutz R, Vrijenhoek R (2002) Sister-species of eastern Pacific hydrothermal vent worms (Ampharetidae, Alvinellidae, Vestimentifera) provide new mitochondrial COI clock calibration. Cahiers de Biologie Marine 43(3–4): 367–370. https://archimer.ifremer.fr/doc/00000/895/

Colgan D, Ponder W, Eggler P (2000) Gastropod evolutionary rates and phylogenetic relationships assessed using partial 28S rDNA and histone H3 sequences. Zoologica Scripta 29(1): 29–63. https://doi.org/10.1046/j.1463-6409.2000.00021.x

Cordes E, Bergquist D, Predmore B, Jones C, Deines P, Telesnicki G, Fisher C (2006) Alternate unstable states: convergent paths of succession in hydrocarbon-seep tubeworm-associated communities. Journal of Experimental Marine Biology and Ecology 339(2): 159–176. https://doi.org/10.1016/j.jembe.2006.07.017

Cordes E, Bergquist D, Fisher C (2009) Macro-ecology of Gulf of Mexico cold seeps. Annual Review of Marine Science 1: 143–168. https://doi.org/10.1146/annurev.marine.010908.163912

Corliss JB, Dymond J, Gordon LI, Edmond JM, von Herzen RP, Ballard RD, Green K, Williams D, Bainbridge A, Crane K, van Andel TH (1979) Submarine thermal springs on the Galapagos Rift. Science 203(4385): 1073–1083. https://doi.org/10.1126/science.203.4385.1073

Costello M, Wilson S, Houlding B (2012) Predicting total global species richness using rates of species description and estimates of taxonomic effort. Systematic Biology 61(5): 871–883. https://doi.org/10.1093/sysbio/syr080

Dall W (1882) On certain limpets and chitons from the deep waters off the eastern coast of the United States. Proceedings of the United States National Museum 4(246): 400–414. https://doi.org/10.5479/si.00963801.4-246.400

Dall W (1907) Descriptions of new species of shells, chiefly Buccinidae, from the dredgings of the U.S.S. "Albatross" during 1906, in the northwestern Pacific, Bering, Okhotsk, and Japanese Seas. Smithsonian Miscellaneous Collections 50(2): 139–173.

Fiedler P, Talley L (2006) Hydrography of the eastern tropical Pacific: A review. Progress in Oceanography 69(2–4): 143–180. https://doi.org/10.1016/j.pocean.2006.03.008

Folmer O, Black M, Hoeh W, Lutz R, Vrijenhoek R (1994) DNA primers for amplification of mitochondrial cytochrome c oxidase subunit I from diverse metazoan invertebrates. Molecular Marine Biology and Biotechnology 3(5): 294–299. https://pubmed.ncbi.nlm.nih.gov/7881515/

Fuchigami T, Sasaki T (2005) The shell structure of the recent Patellogastropoda (Mollusca: Gastropoda). Paleontological Research 9(2): 143–168. https://doi.org/10.2517/prpsj.9.143

German C, Ramirez-Llodra E, Baker M, Tyler P, ChEss Scientific Steering Committee (2011) Deep-water chemosynthetic ecosystem research during the census of marine life decade and beyond: a proposed deep-ocean road map. PLOS ONE 6(8): e23259. https://doi.org/10.1371/journal.pone.0023259

Gernhard T (2008) The conditioned reconstructed process. Journal of Theoretical Biology 253(4): 769–778. https://doi.org/10.1016/j.jtbi.2008.04.005

Hall T (1999) BioEdit: a user-friendly biological sequence alignment editor and analysis program for Windows 95/98/NT. In Nucleic Acids Symposium Series: 95–98. https://d1wqtxts1xzle7.cloudfront.net/29520866/1999hall1-libre.pdf?1390876715=&response-content-disposition=inline%3B+filename%3DBioEdit_a_user_friendly_biological_seque.pdf&Expires=1725641870&Signature=RPZ-J6NUsP6z7hJoyrrl0No4qDfTNfa~AxarCQQJafkX52XhQP3ei56HvZKeYNfNAss~Sz-5RaXSDbVtUKvQORIUgkp8WnXiuFBUcXFcCmy672afVhGtMTt~n96OBJHvZ7n-Cu82P9PE8WubEzeI8ve9I8zshUVYpo5oc-IVFNiOjL3d~bhk0ACDa0HJPcba4zw7L-ET~iQcrEoIrapwATHQbdUx2WMXePvRqzrXkDwtWme6aIVy3FxXUuv1~7jnFY~-fRzbz8wL11xIwqbPX0VJg6C6QV4gk17PwY9AUqSMNgRHkh~BKEijsFqz7xL0O-3jIQPqEEpXbAwCDCC3Lu-QZxog__&Key-Pair-Id=APKAJLOHF5GGSLRBV4ZA

Hollander J, Butlin R (2010) The adaptive value of phenotypic plasticity in two ecotypes of a marine gastropod. BMC Evolutionary Biology 10: 1–7. https://doi.org/10.1186/1471-2148-10-333

IPBES (2019) Summary for policymakers of the global assessment report on biodiversity and ecosystem services of the Intergovernmental Science-Policy Platform on Biodiversity and Ecosystem Services. Díaz S, Settele J, Brondízio ES, Ngo HT, Guèze M, Agard J, Arneth A, Balvanera P, Brauman KA, Butchart SHM, Chan KMA, Garibaldi LA, Ichii K, Liu J, Subramanian SM, Midgley GF, Miloslavich P, Molnár Z, Obura D, Pfaff A, Polasky S, Purvis A, Razzaque J, Reyers B, Chowdhury R, Shin YJ, Visseren-Hamakers IJ, Willis KJ, Zayas CN (Eds) IPBES secretariat, Bonn, Germany. https://www.de-ipbes.de/files/20220516%20Sustainable%20Use%20Primer%20FINAL%20GERMAN.pdf

Johnson S, Warén A, Vrijenhoek R (2008) DNA barcoding of *Lepetodrilus* limpets reveals cryptic species. Journal of Shellfish Research 27(1): 43–51. https://doi.org/10.2983/0730-8000(2008)27[43:DBOLLR]2.0.CO;2

Kessler W (2006) The circulation of the eastern tropical Pacific: A review. Progress in Oceanography 69(2–4): 181–217. https://doi.org/10.1016/j.pocean.2006.03.009

Kiel S (2010) The Vent and Seep Bota: Aspects from Microbes to Ecosystems. Topics in Geobiology 33. Springer Science & Business Media, Dordrecht, Netherlands, 490 pp. https://doi.org/10.1007/978-90-481-9572-5

Kumar S, Stecher G, Li M, Knyaz C, Tamura K (2018) MEGA X: molecular evolutionary genetics analysis across computing platforms. Molecular Biology and Evolution 35(6): 1547. https://doi.org/10.1093/molbev/msy096

Levin L, Etter R, Rex M, Gooday A, Smith C, Pineda J, Stuart C, Hessler R, Pawson D (2001) Environmental influences on regional deep-sea species diversity. Annual Review of Ecology and Systematics 32(1): 51–93. https://doi.org/10.1146/annurev.ecolsys.32.081501.114002

Levin L, Baco A, Bowden D, Colaco A, Cordes E, Cunha M, Demopoulos A, Gobin J, Grupe B, Le J, Metaxas A (2016) Hydrothermal vents and methane seeps: rethinking the sphere of influence. Frontiers in Marine Science 3: 72. https://doi.org/10.3389/fmars.2016.00072

Levin L, Wei CL, Dunn D, Amon D, Ashford O, Cheung W, Colaço A, Dominguez-Carrió C, Escobar EG, Harden-Davies HR, Drazen JC (2020) Climate change considerations are fundamental to management of deep-sea resource extraction. Global Change Biology 26(9): 4664–4678. https://doi.org/10.1111/gcb.15223

Matabos M, Jollivet D (2019) Revisiting the *Lepetodrilus elevatus* species complex (Vetigastropoda: Lepetodrilidae), using samples from the Galápagos and Guaymas hydrothermal vent systems. Journal of Molluscan Studies 85(1): 154–165. https://doi.org/10.1093/mollus/eyy061

McCowin MF, Feehery C, Rouse GW (2020) Spanning the depths or depth-restricted: Three new species of *Bathymodiolus* (Bivalvia, Mytilidae) and a new record for the hydrothermal vent *Bathymodiolus thermophilus* at methane seeps along the Costa Rica margin. Deep Sea Research Part I: Oceanographic Research Papers 164: 103322. https://doi.org/10.1016/j.dsr.2020.103322

McLean J (1987) Taxonomic descriptions of cocculinid limpets (Mollusca, Archaeogastropoda): two new species and three rediscovered species. Zoologica Scripta 16(4): 325–333. https://doi.org/10.1111/j.1463-6409.1987.tb00078.x

McLean J (1988) New archaeogastropod limpets from hydrothermal vents; superfamily Lepetodrilacea I. Systematic descriptions. Philosophical Transactions of the Royal Society of London B, Biological Sciences 319(1192): 1–32. https://doi.org/10.1098/rstb.1988.0031

McLean J (1989) New slit-limpets (Scissurellacea and Fissurellacea) from hydrothermal vents. Part 1. Systematic descriptions and comparisons based on shell and radular characters. Contributions in Science 407: 1–29. https://doi.org/10.5962/p.208131

McLean J (1990) Neolepetopsidae, a new docoglossate limpet family from hydrothermal vents and its relevance to patellogastropod evolution. Journal of Zoology 222(3): 485–528. https://doi.org/10.1111/j.1469-7998.1990.tb04047.x

McLean J (1992) Cocculiniform limpets (Cocculinidae and Pyropeltidae) living on whale bone in the deep sea off California. Journal of Molluscan Studies 58(4): 401–414. https://doi.org/10.1093/mollus/58.4.401

McLean J (2008) Three new species of the family Neolepetopsidae (Patellogastropoda) from hydrothermal vents and whale falls in the northeastern Pacific. Journal of Shellfish Research 27(1): 15–20. https://doi.org/10.2983/0730-8000(2008)27[15:TNSOTF]2.0.CO;2

McLean J, Haszprunar G (1987) Pyropeltidae, a new family of cocculiniform limpets from hydrothermal vents. The Veliger 30(2): 196–205. https://www.biodiversitylibrary.org/page/42468094

Mora C, Tittensor D, Adl S, Simpson A, Worm B (2011) How many species are there on Earth and in the ocean? PLOS Biology 9(8): e1001127. https://doi.org/10.1371/journal.pbio.1001127

Okutani T, Tsuchida E, Fujikura K (1992) Five bathyal gastropods living within or near the Calyptogena-community of the Hatsushima Islet, Sagami Bay. Venus (Japanese Journal of Malacology) 51(3): 137–148. https://doi.org/10.18941/venusjjm.51.3_137

Puillandre N, Brouillet S, Achaz G (2021) ASAP: assemble species by automatic partitioning. Molecular Ecology Resources 21(2): 609–620. https://doi.org/10.1111/1755-0998.13281

Rambaut A (2018) FigTree, a graphical viewer of phylogenetic trees (Version 1.4. 4). Institute of Evolutionary Biology, University of Edinburgh. http://tree.bio.ed.ac.uk/software/figtree/

Sasaki T (2003) New taxa and new records of patelliform gastropods associated with chemoautosynthesis-based communities in Japanese waters. The Veliger 46: 189–210. https://biostor.org/reference/132695

Sasaki T, Warén A, Kano Y, Okutani T, Fujikura K (2010) Gastropods from recent hot vents and cold seeps: systematics, diversity and life strategies. In: Kiel S (Ed.) The Vent and Seep Biota: Aspects from Microbes to Ecosystems, vol 33. Springer, Dordrecht, 169–254. https://doi.org/10.1007/978-90-481-9572-5_7

Sato K, Watanabe HK, Jenkins RG, Chen C (2020) Phylogenetic constraint and phenotypic plasticity in the shell microstructure of vent and seep pectinodontid limpets. Marine Biology 167(6): 79. https://doi.org/10.1007/s00227-020-03692-z

Scheltema A (2008) Biogeography, diversity, and evolution through vicariance of the hydrothermal vent aplacophoran genus *Helicoradomenia* (Aplacophora, Mollusca). Journal of Shellfish Research 27(1): 91–96. https://doi.org/10.2983/0730-8000(2008)27[91:BDAETV]2.0.CO;2

Suchard M, Lemey P, Baele G, Ayres D, Drummond A, Rambaut A (2018) Bayesian phylogenetic and phylodynamic data integration using BEAST 1.10. Virus Evolution 4(1): vey016. https://doi.org/10.1093/ve/vey016

Suess E (2014) Marine cold seeps and their manifestations: geological control, biogeochemical criteria and environmental conditions. International Journal of Earth Sciences 103: 1889–1916. https://doi.org/10.1007/s00531-014-1010-0

Thompson J, Gibson T, Higgins D (2003) Multiple sequence alignment using ClustalW and ClustalX. Current protocols in Bioinformatics(1): 2–3. https://doi.org/10.1002/0471250953.bi0203s00

Tunnicliffe V, Fowler C, Mcarthur A (1996) Plate tectonic history and hot vent biogeography. Geological Society, London, Special Publications 118(1): 225–238. https://doi.org/10.1144/GSL.SP.1996.118.01.14

Van Dover C, Trask J (2000) Diversity at deep-sea hydrothermal vent and intertidal mussel beds. Marine Ecology Progress Series 195: 169–178. https://doi.org/10.3354/meps195169

Van Dover C, Colaço A, Collins P, Croot P, Metaxas A, Murton B, Swaddling A, Boschen-Rose R, Carlsson J, Cuyvers L, Fukushima T (2020) Research is needed to inform environmental management of hydrothermally inactive and extinct polymetallic sulfide (PMS) deposits. Marine Policy 121: 104183. https://doi.org/10.1016/j.marpol.2020.104183

Vermeij G (2017) The limpet form in gastropods: evolution, distribution, and implications for the comparative study of history. Biological Journal of the Linnean Society 120(1): 22–37. https://doi.org/10.1111/bij.12883

Vrijenhoek R (2013) On the instability and evolutionary age of deep-sea chemosynthetic communities. Deep Sea Research Part II: Topical Studies in Oceanography 92: 189–200. https://doi.org/10.1016/j.dsr2.2012.12.004

Warén A, Bouchet P (2001) Gastropoda and Monoplacophora from hydrothermal vents and seeps; new taxa and records. The Veliger 44: 116–231.

Warén A, Bouchet P (2009) New gastropods from deep-sea hydrocarbon seeps off West Africa. Deep Sea Research Part II: Topical Studies in Oceanography 56(23): 2326–2349. https://doi.org/10.1016/j.dsr2.2009.04.013

Webb M (1969) *Lamellibrachia barhami*, gen. nov. sp. nov. (Pogonophora), from the Northeast Pacific. Bulletin of Marine Science 19(1): 18–47. https://www.ingentaconnect.com/content/umrsmas/bullmar/1969/00000019/00000001/art00002#

Webb TJ, Vanden Berghe E, O'Dor R (2010) Biodiversity's big wet secret: the global distribution of marine biological records reveals chronic under-exploration of the deep pelagic ocean. PLOS ONE 5(8):e10223. https://doi.org/10.1371/journal.pone.0010223

Zhang S, Zhang S (2020) Two new species of genus *Bathyacmaea* from deep-sea chemosynthetic areas in the western Pacific (Gastropoda: Pectinodontidae). Nautilus 134(1): 45–50.

Supplementary material 1

PCR Reaction conditions used to successfully amplify loci

Authors: Melissa J. Betters, Jorge Cortés, Erik E. Cordes
Data type: docx
Explanation note: PCR components were used at the following concentrations: MgCl (25 mM), BSA (10 mg/mL), DNTPs (2.5 mM each), Primers (10 uM each). PCR Protocols are as follows: 1 = { 4 min at 94 °C, 35 × (1 min at 95 °C, 1 min at 40 °C, 1.5 min at 72 °C), 7 min at 72 °C}, 2 = { 5 min at 94 °C, 35 × (30 sec at 94 °C, 1 min at 45 °C, 1 min at 72 °C), 5 min at 72 °C}, 3 = same as 2 but 30 cycles instead of 35, 4 = {2 min at 94 °C, 40 × (20 sec at 94 °C, 20 sec at 55 °C, 1 min at 68 °C)}, 5 = {2 min at 94 °C, 40 × (20 sec at 94 °C, 20 sec at 65 °C, 1 min at 72 °C)}. Accession numbers refer to identities within NCBI GenBank. "" = Same value as the cell above.

Link: https://doi.org/10.3897/zookeys.1214.128594.suppl1

Research Article

Three new species of the genus *Rhogadopsis* Brèthes (Hymenoptera, Braconidae, Opiinae) from South Korea

Yunjong Han[1*] , Cornelis van Achterberg[2*] , Hyojoong Kim[1]

1 Animal Systematics Laboratory, Department of Biological Science, Kunsan National University, Gunsan, 54150, Republic of Korea

2 Naturalis Biodiversity Center, P.O. 9517, 2300 RA Leiden, Netherlands

Corresponding author: Hyojoong Kim (hkim@kunsan.ac.kr)

Abstract

Three new species of *Rhogadopsis* Brèthes, 1913 (*R. clausulata* **sp. nov.**, *R. obliqoides* **sp. nov.** and *R. setosipunctata* **sp. nov.**) are described and illustrated. *Rhogadopsis unicarinata* (Fischer, 1959) is a new combination and a new synonym of *R. mediocarinata* (Fischer, 1963), **syn. nov.** An identification key to the species of *Rhogadopsis* known from South Korea is provided.

Key words: Identification, key, new combination, new species, new synonym, parasitoid wasp, South Korea

Introduction

The cosmopolitan subfamily Opiinae Blanchard, 1845, comprises 39 genera and approximately 2100 described valid species, consisting generally of small (1–5 mm body length) parasitoid wasps (Yu et al. 2016). It contains koinobiont parasitoid wasps that mainly parasitize leaf-mining and fruit-infesting cyclorrhaphous dipterous larvae. The classification of Opiinae genera is still under discussion and fluctuating, primarily due to uncertainties regarding some genera like *Opius* Wesmael, 1835, and *Eurytenes* Foerster, 1863 (Wharton 1987, 1988, 1997; Li et al. 2013; Wharton and Norrbom 2013). Papp (1989) reported *Opius* (*Rhogadopsis*) *parvungula* (Thomson) from North Korea (a junior synonym of *R. reconditor* (Wesmael, 1835)). Han and Kim (2023) reported *R. obliqua* Li & van Achterberg from South Korea. However, the Korean specimen of *R. obliqua* differs from the holotype by having the second and third metasomal tergites distinctly sculptured medially, the vein CU1b of the fore wing comparatively short, and vein the m-cu of the hind wing absent. In addition, *Opius mediocarinatus* (Fischer, 1963), reported from the Korean Peninsula, has been recombined into the genus *Rhogadopsis* (Chen et al. 2016) and should be included in this study.

We treat the genus *Rhogadopsis* Brèthes, 1913, as a valid genus separate from *Opius* Wesmael, 1835, as was proposed by Li et al. (2013). Three new species are described and illustrated, and an identification key to the Korean *Rhogadopsis* is provided below.

---

* These authors contributed equally to this work.

Material and methods

Specimens of *Rhogadopsis clausulata* sp. nov., *R. setosipunctata* sp. nov. and the holotype of *R. obliqoides* sp. nov. were collected in a Malaise trap, while the paratype of *R. obliqoides* sp. nov. was collected by using a net to sweep the herbal vegetation. For identification of the subfamily Opiinae, see van Achterberg (1990, 1993, 1997); for references to Opiinae, see Yu et al. (2016).

Morphological terminology follows van Achterberg (1988, 1993), including the abbreviations for the wing venation. Measurements were taken as indicated by van Achterberg (1988): the maximum length and width of a body part were taken unless otherwise indicated. The length of the mesosoma was measured from the anterior border of the mesoscutum to the apex of the propodeum and of the first tergite from the posterior border of the adductor to the medio-posterior margin of the tergite.

Observations, photographic images, and descriptions were made either with a Leica DMC2900 digital camera or with a Leica M205 C microscope (Leica Geosystems AG) or with a digital camera on a Zeiss Stereo Discovery V12 with AxioVision SE64 Rel. 49.1 software for stacking. The photos from the Leica system were stacked with Helicon Focus v. 7 software (Helicon Soft, Kharkiv, Ukraine). After stacking, illustrations were created using Adobe Photoshop CS5.1.

The holotype and paratype of *Rhogadopsis clausulata* sp. nov. are deposited in the Naturalis Biodiversity Center (**RMNH**) at Leiden, and the type specimens of *R. obliqoides* sp. nov. and *R. setosipunctata* sp. nov. are deposited in the Kunsan National University (**KSNU**) at Gunsan.

Systematics

Genus *Rhogadopsis* Brèthes, 1913

Rhogadopsis Brèthes, 1913: 44; Shenefelt 1975: 1212; Wharton 1987: 66 (as subgenus *Lissosema*). Type species (by monotypy): *Rhogadopsis miniacea* Brèthes, 1913.

Lissosema Fischer, 1972: 359. Type species (by original designation): *Opius parvungula* Thomson, 1895 (= *Opius reconditor* Wesmael, 1835; Broad et al. 2016: 291).

Diagnosis. Propodeum with a distinct (but often short) medio-longitudinal carina anteriorly (Figs 5, 11, 34); hypoclypeal depression variable; mandible symmetrical or nearly so (Figs 7, 8, 19, 32); dorsope absent; vein m-cu of fore wing usually gradually merging into vein 2-CU1, and linear with vein 2-M or nearly so (Fig. 14); if angled then hind wing comparatively wide, vein 1r-m of hind wing less oblique and 0.6–1.0× as long as vein 1-M (Figs 2, 15, 27); medio-posterior depression of mesoscutum variable (Figs 4, 17, 29); anterior groove of metapleuron usually crenulate (Figs 12, 16, 28); precoxal sulcus largely present, crenulate (Figs 12, 16, 28); vein CU1b of fore wing completely present (Figs 2, 14, 26).

Distribution. Palaearctic, Oriental, Nearctic and Afrotropical regions.

Biology. Parasitoids of mining dipterous larvae of the family Agromyzidae (*Agromyza* Fallen, 1810, *Amauromyza* Hendel, 1931, *Calycomyza* Hendel, 1931, *Cerodontha* Rondani, 1861, *Liriomyza* Mik, 1894, *Metopomyza* Enderlein, 1936, *Napomyza* Westwood, 1840, *Phytomyza* Fallen, 1810).

Key to Korean species of the genus *Rhogadopsis* Brèthes

Notes. The number of included species for Korea is based on the National Institute of Biological Resources (2019), Chen et al. (2016) and this study.

1 Medio-posterior depression of mesoscutum present (Figs 17, 29); antenna of ♀ with 23−26 segments and of ♂ with 26 segments; first metasomal tergite more widened posteriorly and 0.7−0.9× as long as its apical width (Figs 18, 30); second tergite variable **2**
– Medio-posterior depression of mesoscutum absent (Fig. 4); antenna of both sexes with 28−41 segments; first metasomal tergite less widened posteriorly and 1.0−1.6× longer than its apical width; second tergite smooth **3**
2 Mesoscutum and scutellum finely punctate (Fig. 29); antero-dorsal area of mesopleuron brown; second metasomal suture and second metasomal tergite smooth (Fig. 31); vein m-cu of fore wing interstitial or nearly so; vein m-cu of hind wing present (Fig. 27).. .... ***R. setosipunctata* Han & van Achterberg, sp. nov.**
– Mesoscutum and scutellum smooth; mesopleuron entirely black; second metasomal suture distinct crenulate dorsally; second tergite at least basally distinctly sculptured (Fig. 18); vein m-cu of fore wing distinctly postfurcal; vein m-cu of hind wing absent (Fig. 15) ....***R. obliqoides* Han & van Achterberg, sp. nov.**
3 Hypoclypeal depression absent (Figs 7, 8); first tergite about as long as wide apically (Fig. 5); vein m-cu of fore wing angled with vein 2-CU1 (Fig. 2) ....***R. clausulata* Han & van Achterberg, sp. nov.**
– Hypoclypeal depression present; first tergite 1.2−1.6× as long as wide apically; vein m-cu of fore wing gradually merging in vein 2-CU1 ....**4**
4 Clypeus nearly parallel-sided, slightly narrowed laterally, approximately 4.0× wider than high and largely smooth; first tergite 1.2−1.3× longer than wide apically; face finely punctate .... ***R. reconditor* (Wesmael, 1835)**
– Clypeus trapezoid or narrow semi-circular, distinctly narrowed laterally, 2.5−3.0× wider than high and punctate; first tergite 1.3−1.6× longer than its apical width; face rather coarsely punctate; [antenna of both sexes with 32−41 segments] ....***R. unicarinata* (Fischer, 1959), comb. nov. [= *R. mediocarinata* (Fischer, 1963), syn. nov.]**

Rhogadopsis clausulata Han & van Achterberg, sp. nov.

https://zoobank.org/9C9127E9-34AA-4F65-865A-776AAB870CB9
Figs 1−12

Type material. *Holotype*, • ♀ (RMNH), "South Korea: Kangwondo, Cuncheon, Nam-myeon, Hudong-li, MT [= Malaise trap], 17.viii.−5.ix.2003, 37°44'N

127°35'E, P. Tripotin, RMNH'12". ***Paratype:*** • 1 ♀ (RMNH), "South Korea: Kang-wondo, Cuncheon, Magogli, along Hongchen river, 70 m, 12.vi.–11.vii.2004, 37°44'N 127°35'E, P. Tripotin, RMNH'12".

Diagnosis. Antennal scape and pedicel yellowish-brown, but flagellum dark brown (Figs 9, 10); hypoclypeal depression absent (Figs 7, 8); mandible with a rather basal lamella below at base (Fig. 8; invisible in anterior view); notauli largely absent on disc (Fig. 4); mesoscutum and scutellum shiny, smooth and largely glabrous; medio-posterior depression of mesoscutum absent (Fig. 4); pterostigma wide triangular and narrowed apically (Fig. 2); vein m-cu of fore wing distinctly postfurcal; second and following tergites dark brown, except light pattern posteriorly (Fig. 5); setose part of ovipositor sheath shorter than first metasomal tergite and hardly protruding beyond apex of metasoma (Fig. 6).

Description. Holotype, female; length of body 3.9 mm, of fore wing 3.6 mm.

Head. Antenna with 33 segments and 1.1× longer than body; third antennal segment 3.0× longer than its width (Figs 9, 10); eye 1.3× longer than temple in dorsal view; vertex smooth and frons glabrous, punctate, setose; median keel on face smooth and shiny; clypeus 2.0× wider than its maximum height, moderately setose, rather flat in lateral view and its ventral margin slightly protruding medio-apically; hypoclypeal depression absent (Fig. 7); maxillary palp 1.1× longer than height of head; malar sulcus present (Figs 7, 8); occipital carina absent dorsally; mandible symmetrical with a rather basal lamella below at base in lateral view (Fig. 8).

Figure 1. *Rhogadopsis clausulata* Han & van Achterberg, sp. nov., holotype, ♀, South Korea, habitus, lateral.
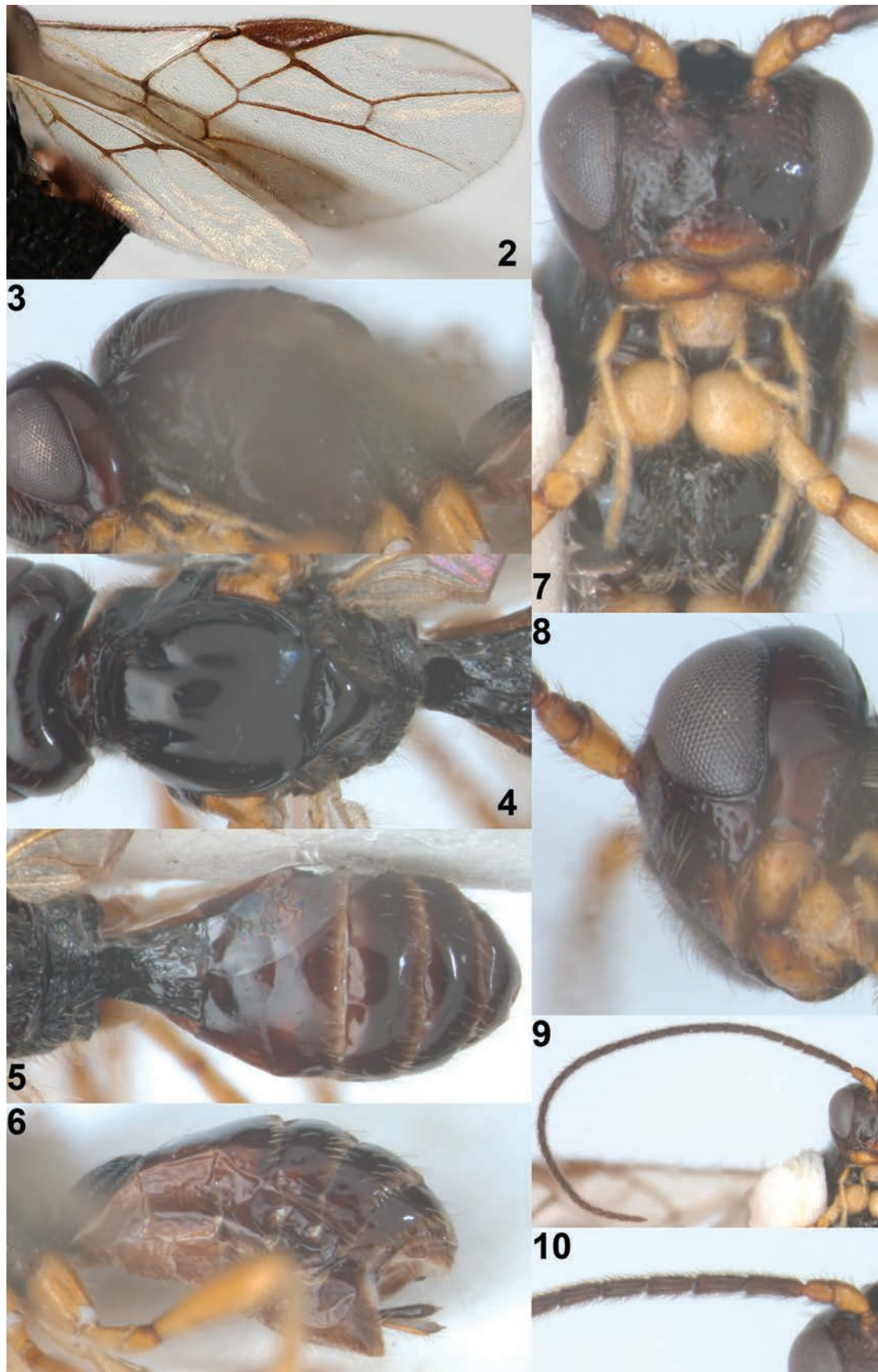
Figures 2–10. *Rhogadopsis clausulata* Han & van Achterberg, sp. nov., holotype, ♀, South Korea **2** wings **3** mesosoma, lateral **4** mesosoma, dorsal **5** propodeum and metasoma, dorsal **6** metasoma, lateral **7** head anterior and mesonotum, antero-ventral **8** mandible, latero-ventral **9** antenna **10** base of antenna.

Mesosoma. Mesosoma in lateral view 1.3× longer than its height; pronope large and elliptical (Fig. 4); propleuron shiny and smooth; pronotal side largely shiny and smooth, but postero-ventral area sculptured; mesopleuron smooth, including narrow precoxal sulcus (Fig. 12); epicnemial area crenulate ventrally, remaining area smooth; mesopleural sulcus crenulate; anterior groove of metapleuron crenulate; metapleuron shiny, reticulate-rugose and moderately setose; notauli absent on disc but with pair of short deep impressions anteriorly (Fig. 4); mesoscutum and scutellum shiny, smooth and sparsely setose; medio-posterior depression of mesoscutum absent (Fig. 4); scutellar sulcus widened medially and distinctly crenulate; propodeum coarsely reticulate-rugose with a short medio-longitudinal carina and diverging oblique two transverse carinae (Figs 4, 5).

Wings. Fore wing (Fig. 2): pterostigma wide, triangular and gradually narrowed apically; vein 1-M almost straight; vein 1-SR+M straight; vein 3-SR linear with vein r, 1.5× longer than vein 2-SR; vein 2-SR oblique; vein SR1 nearly straight; r:3-SR:SR1 = 3:29:57; vein m-cu distinctly postfurcal and 4× longer than vein 2-SR+M; vein cu-a postfurcal; vein CU1b short (Fig. 2). Hind wing: vein m-cu only pigmented basally; vein 1r-m 0.6× as long as vein 1-M; vein 2-M pigmented.

Legs. Length of hind femur 3.4× its maximum width (Fig. 1).

Metasoma. First tergite as long as its apical width, its surface shiny, reticulate-rugose and convex medially in lateral view (Figs 5, 6); dorsope absent, but dorsal carinae strongly developed and separated posteriorly (Figs 4, 5); following tergites smooth and moderately setose posteriorly (Fig. 5); second metasomal suture obsolescent dorsally; setose part of ovipositor sheath 0.3× as long as first tergite and 0.05× as long as fore wing, and slightly protruding beyond apex of metasoma (Fig. 6).

Colour. Generally black or blackish-brown (Fig. 1); scape and pedicel of antenna and ventral half of clypeus yellowish-brown; mandible, tegulae and legs light brown; palpi pale yellowish; posterior bands of third to seventh tergites yellowish; pterostigma and veins of wings brown; wings hyaline.

Variation. The paratype is very similar to the holotype, but antenna with 36 segments, length of body 4.1 mm, and of fore wing 3.6 mm, medio-longitudinal carina of propodeum distinct and half as long as propodeum.

Distribution. South Korea.

Biology. Unknown.

Etymology. Named after the closed hypoclypeal depression: "*clausus*" is Latin for shut or closed.

Figures 11, 12. *Rhogadopsis clausulata* Han & van Achterberg, sp. nov., ♀, South Korea **11** holotype mesosoma, lateral **12** paratype mesosoma, lateral.

Remarks. This new species runs to *Rhogadopsis* Brèthes by having a distinct medio-longitudinal carina on the propodeum, a complete vein CU1b of fore wing, a symmetrical mandible and a wide hind wing with less oblique vein 1r-m of hind wing, 0.6× as long as vein 1-M (van Achterberg 2023). It is similar to *Rhogadopsis unicarinata* (Fischer) because of the lack of the medio-posterior depression of the mesoscutum, the short vein r of the fore wing and the distinct medio-longitudinal carina of the propodeum (Chen et al. 2016). It differs from the latter by the robust first tergite (slender in *R. unicarinata*), lack of the hypo-clypeal depression (wide), head mainly black (more or less yellow), absence of precoxal sulcus (present medially), vein m-cu of fore wing straight (curved) and the very large pronope (absent).

Rhogadopsis obliqoides Han & van Achterberg, sp. nov.

https://zoobank.org/9B8F875A-A596-4A8B-B946-6E7C0B21F713

Figs 13−24

Type material. *Holotype*, · ♀ (KSNU), "South Korea: Baekgye-ro, Okryong, Gwang-yang, Jeonnam, 10.ix.−24.ix.2019, 35°01'41"N 127°36'51"E, MT [= Malaise trap], Hyojoong Kim leg., KSNU". *Paratype*, · 1 ♂ (KSNU), "South Korea: Yeoseo-ri, Cheongsan-myeon, Wando, Jeonnam, 2.vii.2020, 33°59'15.1"N 126°55'04.6"E, SW [=collected by sweeping], Hyojoong Kim leg., KSNU".

Figure 13. *Rhogadopsis obliqoides* Han & van Achterberg, sp. nov., holotype, ♀, South Korea, habitus, lateral.

Diagnosis. Second and third metasomal tergites largely smooth except for some faint sculpture anteriorly of both tergites (Fig. 18); hypoclypeal depression distinct (Fig. 19); precoxal sulcus crenulate (Fig. 16); medio-posterior depression of mesoscutum present (Fig. 17); first tergite reticulate-rugose without transverse carinae (Fig. 18); vein m-cu of fore wing linear with veins 2-CU1 and 2-M (Fig. 14); vein 1r-m of hind wing 0.7× as long as vein 1-M; vein m-cu of hind wing absent.

Description. Holotype, female; length of body 2.1 mm, of fore wing 2.2 mm.

Head. Antenna with 23 segments and as long as body; third segment 2.8× longer than its width, 1.1× longer than fourth segment (Fig. 24); eye in dorsal view 3.2× longer than temple (Fig. 20); vertex and frons shiny, smooth and sparsely setose; clypeus 2.1× wider than its maximum height (Fig. 19); clypeus rather convex with setae and its ventral margin almost straight; hypoclypeal depression distinct (Fig. 19); maxillary palp 0.8× longer than height of head; malar sulcus present; occipital carina interrupted dorsally; mandible triangular and gradually widened basally (Fig. 19).

Mesosoma. Mesosoma in lateral view 1.3× longer than its height; pronope deep, large and round (Figs 17, 20); mesopleuron smooth but precoxal sulcus oblique and crenulate (Fig. 16); epicnemial area smooth dorsally; mesopleural sulcus smooth; anterior groove of metapleuron crenulate, ventral area faintly rugose and remainder area smooth; notauli absent on disc except for both deep and short impressions anteriorly (Fig. 17); mesoscutum shiny, smooth and sparsely setose along imaginary notaulic courses and around medio-posterior depression; scutellum shiny and smooth; medio-posterior depression of mesoscutum round (Fig. 17); scutellar sulcus widened and distinctly crenulate; propodeum coarsely reticulate-rugose with a medio-longitudinal carina and two oblique transverse carinae (Fig. 21).

Wings. Fore wing (Fig. 14): pterostigma triangular, gradually narrowed apically; veins 1-M and SR1 curved; veins 1-SR+M and 2-SR straight; vein 3-SR 1.7× longer than vein 2-SR; r:3-SR:SR1 = 5:36:57; vein m-cu distinctly postfurcal and twice as long as vein 2-SR+M; vein CU1b rather long (Fig. 14); first discal cell closed. Hind wing (Fig. 15): vein m-cu absent; vein 1r-m 0.7× as long as vein 1-M.

Legs. Length of hind femur 4.1× its maximum width (Fig. 22); hind femur with rather long and tibia with medium-sized setae.

Metasoma. First tergite 0.9× as long as its apical width, its surface shiny, irregularly and densely rugose and convex medially in lateral view (Fig. 18); dorsope absent, but dorsal carinae strongly developed (Fig. 18); second metasomal suture distinct; second tergite largely smooth but anteriorly striate-rugose; third tergite largely smooth but densely and shortly striate-rugose anteriorly; following tergites smooth and with few setae posteriorly; setose part of ovipositor sheath 0.7× as long as first tergite and 0.1× as long as fore wing, slightly protruding beyond apex of metasoma (Fig. 23).

Colour. Generally black (Fig. 13); scape and pedicel of antenna brown; antenna, ventral half of clypeus and mandible dark brown; palpi pale yellowish; legs and tegular yellowish-brown; veins and pterostigma greyish; wings subhyaline.

Distribution. South Korea.

Biology. Unknown.

Etymology. The name is a combination of the specific name "*obliqua*" and "*oides*" (Latin for resembling) because the new species is similar to *R. obliqua* Li & van Achterberg.
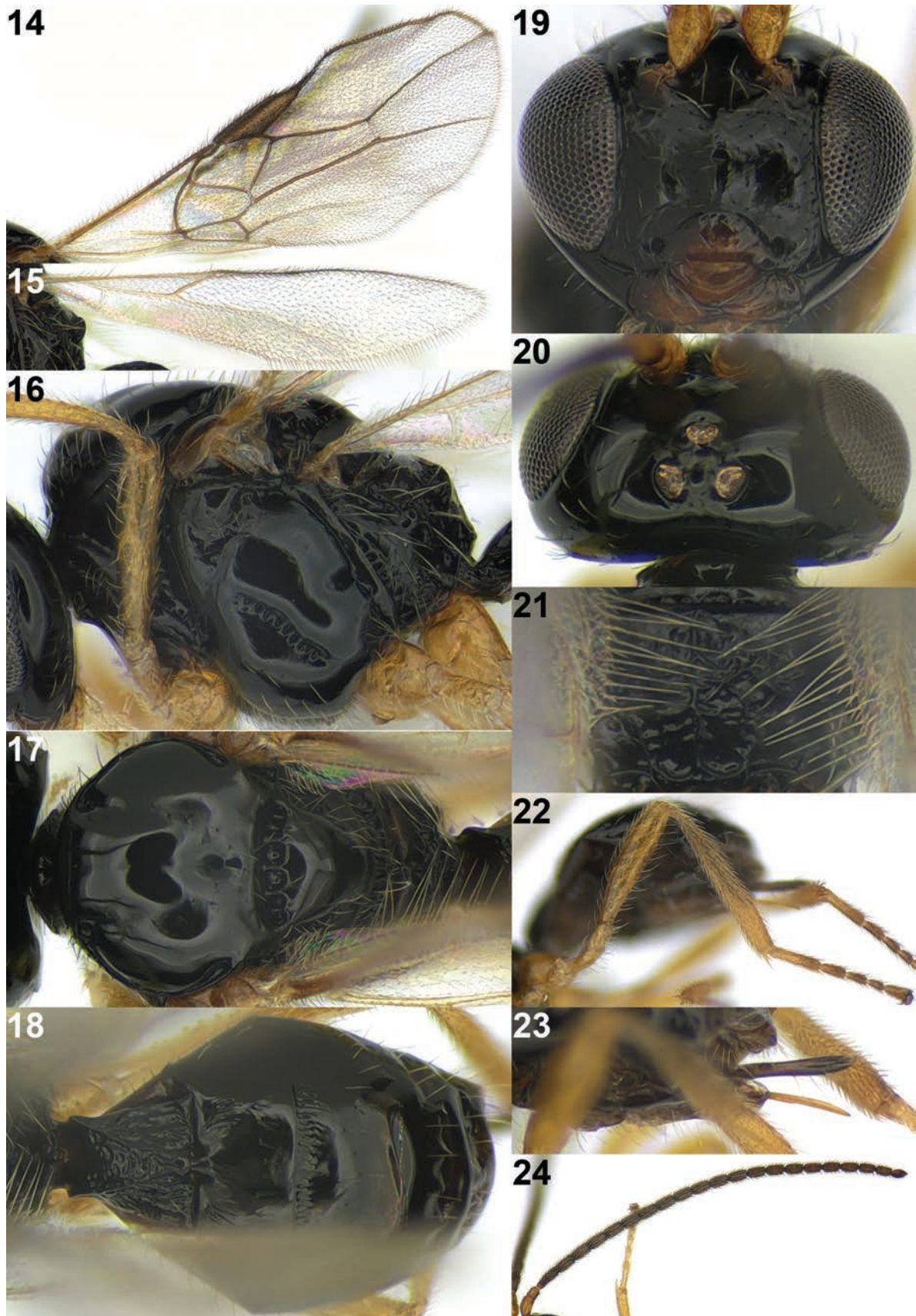
Figures 14–24. *Rhogadopsis obliqoides* Han & van Achterberg, sp. nov., holotype, ♀, South Korea **14** fore wing **15** hind wing **16** mesosoma, lateral **17** mesosoma, dorsal **18** metasoma, dorsal **19** head, anterior **20** head, dorsal **21** propodeum **22** hind leg **23** ovipositor and sheath **24** antenna.

Remarks. This species runs to *Rhogadopsis obliqua* Li & van Achterberg in the key of Li et al. (2013), because of having the antenna of ♀ with only about 23 segments, clypeus 2.1× wider than its maximum height, the medio-posterior depression of mesoscutum distinctly impressed, the propodeum with a short medio-longitudinal carina, the wide hind wing with less oblique vein 1r-m of hind wing, 0.7× as long as vein 1-M, the third metasomal tergite largely smooth, ventro-posterior crenulate groove of pronotal side, the medio-posterior depression of mesoscutum distinctly developed and the precoxal sulcus crenulated. However, it differs by having the second metasomal tergite more or less sculptured (smooth in *R. obliqua*), the lack of vein m-cu of hind wing (presented as unpigmented trace), vein 1-M of fore wing distinctly curved (slightly curved), vein m-cu of fore wing twice as long as vein 2-SR+M (1.5 times longer) and hind tibia of female wider and conspicuously setose (narrower and sparse setose).

***Rhogadopsis setosipunctata* Han & van Achterberg, sp. nov.**
https://zoobank.org/A5B24C03-7A2D-4F9D-B580-CBC6B6842796
Figs 25–37

Type material. *Holotype*, • ♀ (KSNU), "South Korea: Gonggeun-ri, Gonggeun, Hoengseong, Gangwon, 19.vii.–6.viii.2019, 37°33'58.3"N 127°57'54.9"E, MT [= Malaise trap], Hyojoong Kim leg., KSNU".

Diagnosis. Mesoscutum and scutellum finely punctate and setose (Fig. 29); antenna of ♀ with 26 segments; hypoclypeal depression distinct (Fig. 32);

Figure 25. *Rhogadopsis setosipunctata* Han & van Achterberg, sp. nov., holotype, ♀, South Korea, habitus, lateral.

precoxal sulcus crenulate (Fig. 28); antero-dorsal area of mesopleuron brown; medio-posterior depression of mesoscutum present (Fig. 29); vein m-cu of fore wing interstitial (Fig. 26) or nearly so; first metasomal tergite 0.7× as long as its apical width (Fig. 30) and smooth as following metasomal tergite.

Description. Holotype, female; length of body 2.4 mm, of fore wing 2.4 mm.

Head. Antenna with 26 segments and as long as body (Fig. 37); third segment 2.7× longer than its width, 1.1× longer than fourth segment; eye in dorsal view 2.2× longer than temple (Fig. 33); vertex and face shiny, punctate and densely setose; clypeus 2.3× wider than its maximum height (Fig. 32); clypeus in lateral view rather convex with long setae and its ventral margin slightly concave; hypoclypeal depression distinct (Fig. 32); maxillary palp 0.7× as long as height of head; occipital carina interrupted dorsally; mandible triangular and gradually widened basally (Fig. 32).

Mesosoma. Mesosoma in lateral view 1.3× longer than its height; pronope deep, large and round; mesopleuron smooth but precoxal sulcus oblique, robust and crenulate (Fig. 28); epicnemial area crenulate ventrally; mesopleural sulcus smooth; anterior groove of metapleuron crenulate; metapleuron area coarsely rugose ventrally with setae and remaining area smooth; notauli absent on disc except deep and short impressions anteriorly (Fig. 29); mesoscutum and scutellum shiny, punctate and densely setose; medio-posterior depression of mesoscutum elliptical (Fig. 29); scutellar sulcus robust and distinctly crenulate; propodeum reticulate-rugose, with a short medio-longitudinal carina anteriorly and two oblique transverse carinae, remaining area shiny and smooth (Figs 29, 34).

Wings. Fore wing (Fig. 26): pterostigma triangular, gradually narrowed apically; veins 1-M and SR1 curved; vein 1-SR 0.3× as long as vein 1-M; vein 1-SR+M sinuate; vein r 0.7× as long as vein 1-SR; vein 3-SR 1.3× longer than vein 2-SR; r:3-SR:SR1 = 7:32:54; veins m-cu, cu-a interstitial; first subdiscal cell closed. Hind wing (Fig. 27): wide; vein m-cu faintly pigmented; vein 1r-m 0.7× as long as vein 1-M.

Legs. Length of hind femur 3.6× its maximum width (Fig. 36).

Metasoma. First tergite 0.7× as long as its apical width, its surface shiny, smooth and convex medially in lateral view; dorsope absent, dorsal carinae strongly developed and reaching apex of tergite (Figs 29, 30); second metasomal suture absent; second tergite shiny, smooth, with a pair of oblique depressions anteriorly; following tergites shiny, smooth with posterior row of setae; setose part of ovipositor sheath 0.7× as long as first tergite and 0.09× as long as fore wing, slightly protruding beyond apex of metasoma (Fig. 35).

Colour. Generally black to dark brown (Fig. 25); scape of antenna, mandible and legs yellowish-brown; antenna, face, tegulae and mesopleuron antero-dorsally brown; palpi pale yellowish; veins and pterostigma brown to dark brown; wing membrane subhyaline.

Distribution. South Korea.

Biology. Unknown.

Etymology. Named after the uniformly punctate and setose face, mesoscutum and scutellum; "*punctus*" is Latin for "point", and "*setosus*" is Latin for "with setae".

Remarks. This new species fits well in the genus *Rhogadopsis* because of the short medio-longitudinal carina on the propodeum anteriorly, the symmetrical mandible, the complete vein CU1b of fore wing, the wide hind wing with less oblique vein 1r-m of hind wing 0.7× as long as vein 1-M and anterior groove of
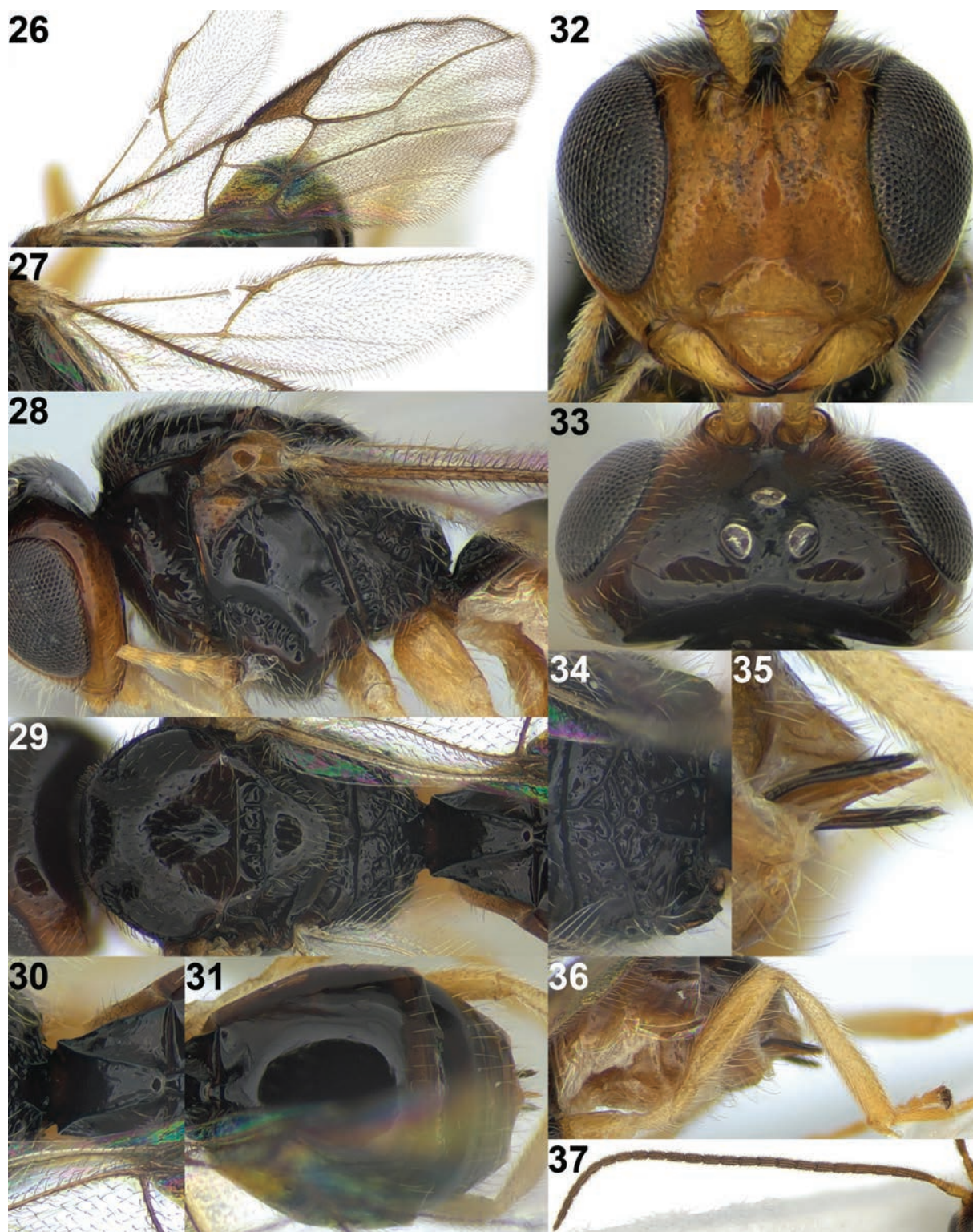
Figures 26–37. *Rhogadopsis setosipunctata* Han & van Achterberg, sp. nov., holotype, ♀, South Korea **26** fore wing **27** hind wing **28** mesosoma, lateral **29** mesosoma, dorsal **30** first metasomal tergite, dorsal **31** metasoma, dorsal **32** head, anterior **33** head, dorsal **34** propodeum **35** ovipositor and sheath **36** hind leg **37** antenna.

metapleuron crenulated. The species is unique among the East Palaearctic and Northeast Oriental species because of the punctate mesoscutum and scutellum, the smooth first tergite with coarse dorsal carinae up to the apex of the tergite and the lack of vein 2-SR+M of the fore wing (a result of the subinterstitial vein m-cu).

Acknowledgements

Additional information

Conflict of interest

The authors have declared that no competing interests exist.

Ethical statement

No ethical statement was reported.

Funding

Author contributions

Supervision: HK. Writing – original draft: YH. Writing – review and editing: CA.

Author ORCIDs

Yunjong Han https://orcid.org/0000-0003-2757-7785
Cornelis van Achterberg https://orcid.org/0000-0002-6495-4853
Hyojoong Kim https://orcid.org/0000-0002-1706-2991

Data availability

All of the data that support the findings of this study are available in the main text.

References

Brèthes J (1913) Hymenópteros de la América meridional. Anales del Museo Nacional de Historia Natural de Buenos Aires 24: 35–165.

Broad GR, Shaw MR, Godfray HCJ (2016) Checklist of British and Irish Hymenoptera - Braconidae. Biodiversity Data Journal 4: e8151. [334 pp] https://doi.org/10.3897/BDJ.4.e8151

Chen M, van Achterberg C, Tan J-L, Tan Q-q, Chen X-X (2016) Four new species of *Rhogadopsis* Brèthes from NW China (Hymenoptera, Braconidae, Opiinae). Journal of Hymenoptera Research 52: 37–60. https://doi.org/10.3897/jhr.52.9806

Fischer M (1972) Hymenoptera Braconidae (Opiinae I). (Paläarktische Region). Das Tierreich 91(1973): 1–620.

Han Y, Kim H (2023) A new record of parasitic wasp, *Rhogadopsis obliqua* (Hymenoptera: Braconidae: Opiinae), from South Korea. Korean Journal of Applied Entomology 62: 1–4.

Li X-Y, van Achterberg C, Tan J-C (2013) Revision of the subfamily Opiinae (Hymenoptera, Braconidae) from Hunan (China), including thirty-six new species and two new genera. ZooKeys 268: 1–186. https://doi.org/10.3897/zookeys.326.5911

National Institute of Biological Resources (2019) National species list of Korea. III. Insects(Hexapoda). Designzip Incheon, 988 pp.

Papp J (1989) Braconidae (Hymenoptera) from Korea X. Acta Zoologica Hungarica 35: 81–103.

Shenefelt RD (1975) Braconidae, 8. Hymenopterorum Catalogus (nov. ed.) 12: 1115–1262.

van Achterberg C (1988) Revision of the subfamily Blacinae Foerster (Hymenoptera, Braconidae). Zoölogische Verhandelingen 249: 1–324.

van Achterberg C (1990) Illustrated key to the subfamilies of the Holarctic Braconidae (Hymenoptera: Ichneumonoidea). Zoologische Mededelingen Leiden 64(1): 1–20.

van Achterberg C (1993) Illustrated key to the subfamilies of the Braconidae (Hymenoptera: Ichneumonoidea). Zoölogische Verhandelingen 283: 1–189.

van Achterberg C (1997) Revision of the Haliday collection of Braconidae (Hymenoptera). Zoölogische Verhandelingen 314: 1–115.

van Achterberg C (2023) Illustrated key to the European genera of Opiinae (Hymenoptera, Braconidae), with the description of two new Palaearctic genera and two new species. ZooKeys 1176: 79–115. https://doi.org/10.3897/zookeys.1176.104850

Wharton RA (1987) Changes in nomenclature and classification of some opiine Braconidae (Hymenoptera). Proceedings of the Entomological Society of Washington 89(1): 61–73.

Wharton RA (1988) Classification of the braconid subfamily Opiinae (Hymenoptera). Canadian Entomologist 120(4): 333–360. https://doi.org/10.4039/Ent120333-4

Wharton RA (1997) Generic relationships of opiine Braconidae (Hymenoptera) parasitic on fruit-infesting Tephritidae (Diptera). Contributions of the American Entomological Institute 30(3): 1–53.

Wharton RA, Norrbom A (2013) New species and host records of new world, mostly Neotropical, opiine Braconidae (Hymenopotera) reared from flower-infesting, stem-galling, and stem-mining Tephritidae (Diptera). Zookeys 349: 11–72. https://doi.org/10.3897/zookeys.349.5914

Yu D, van Achterberg C, Horstmann K (2016) Taxapad 2016. Ichneumonoidea 2015. Taxapad Interactive Catalogue Database on flash-drive. Ottawa.